Competing Orders in
Strongly Interacting Electron Systems:
local and non-local correlations

Habilitationsschrift

Fakultät für Physik und Astronomie
der Bayerischen Julius-Maximilians-Universität
Würzburg

vorgelegt von

MIKHAIL KISELEV

aus

Moskau

Würzburg, Januar 2003

Contents

INTRODUCTION

The interest in the studies of systems with strong electron-electron correlations considerably increased after the discovery of two classes of such systems, namely heavy fermions (see for review [1]) and high- temperature superconductors (see excellent recent review [2]). Both the heavy fermions and the cuprate high-T_c superconductors demonstrate many unusual properties which can not be explained in terms of the theory of weakly coupled electrons. For example, the cuprate high- T_c superconductors are highly correlated "bad metals" with normal state properties that are not at all those of a Fermi liquid. There is compelling evidence that they are better thought of as doped Mott insulators, rather than as strongly interacting versions of conventional metals. Practically all experiments, e.g., angle-resolved photoemission [3]-[7], NMR [8] -[10], infra-red conductivity [11], [12], transport properties [13], thermopower [14], Raman spectroscopy [15] etc provide an evidence for an anomalous metallic state above superconduction transition temperature T_c in the underdoped high-T_c cuprates. The anomalies take place below some characteristic temperature $T^*(\delta)$ depending on carrier concentration δ. The cuprates also exhibit numerous types of low temperature order which interact strongly with the superconductivity, the most prominent being antiferromagnetism and the charge and the spin density wave order. These orders can compete and coexists with superconductivity.

On the other hand, most of the heavy fermion compounds are famous for their unusual electronic and magnetic properties, including giant effective masses observed in thermodynamic and the de Haas-van Alphen measurements [16], unconventional superconductivity [17] and a fascinating variety of magnetic properties [18]. The great majority of the metallic Kondo lattice (KL) systems demonstrate antiferromagnetic (AFM) correlations and all types of the AFM order may be found in these compounds. There are localized spins in $U_2Zn_{17}, UCd_{11}, CeIn_3$ [18], quadrupole ordering in CeB_6 [19], interplay between localized and itinerant excitations in several U- and Ce-based compounds [20], puzzling magnetic order of tiny moments in $UPt_3, URu_2Si_2, UNi_2Al_3$ [21], quantum phase transition in $CeCu_{6-x}Au_x$ [22], fluctuation-type dynamical ordering in $U(Pt_{1-x}Pd_x)_3$ [23], short-range magnetic correlations in an astonishingly wide temperature interval of critical behavior in $CeCu_6$ and $CeRu_2Si_2$ [24]. This list is by no means exhaustive. The superconducting state in most cases coexists with antiferromagnetism, and, apparently, Cooper pairing itself is mediated by magnetic fluctuations [17, 25].

Heavy fermions

The most remarkable feature of Heavy Fermion (HF) compounds is a dramatically sharper scattering resonance near the Fermi level [26]. This narrow resonance appears due to the many-body effects which lead, within the framework of Landau's Fermi-liquid theory, to strongly renormalized electronic quasiparticles with, e.g., very heavy masses [1]. The formation of the heavy quasiparticles takes place at a low temperature. In the dilute alloys the characteristic energy scale $\epsilon \sim T_K$ related to the resonance at ϵ_F is commonly con-

nected with the Kondo effect [27] - the resonance scattering of an electron on a magnetic impurity with a simultaneous change of the spin projection. This "Kondo temperature" T_K typically lies in the range of a few degrees Kelvin. In many respects, concentrated heavy-fermion systems show striking similarities with the dilute Kondo systems. Most of the properties may be understood via one characteristic energy scale T^*, which could be surprisingly close to the value of T_K of the corresponding dilute system. As in the dilute case the electrical resistivity of the heavy fermion compounds has a negative temperature coefficient above T^*. Hence, the concentrated Kondo systems can be considered as a periodic structure of Kondo impurities which scatter conduction electrons coherently. The behavior of such a systems is described by the periodic Anderson model (PAM) [28] which contains a localized f band of strongly correlated electrons interacting with a d band of free conduction electrons. In some HF systems, e.g. most of the U-based HF compounds, the f states contribute to the crystal binding via hybridization with delocalized band states whereas, e.g., in most of Ce - based compounds, the contribution of the f states to the energy is negligible due to large valence-excitation energy. These materials have been labeled as "Kondo lattices". In these compounds, the direct exchange and the crystal field effects determine the low-temperature state, which mostly involves a magnetic order.

In a lattice - periodic system the ground state, even if not magnetic or superconducting, should be coherent, and the low lying excitations should obey the well known laws of Landau's Fermi liquid (FL) theory. In many systems a FL behavior is observed at low temperatures $T < T_{coh}$ with a specific heat $C_v \sim T$, a magnetic susceptibility $\chi \approx const$ and a resistivity $\rho \approx \rho_0 + AT^2$, where $T_{coh} < T^*$ is a "coherence temperature". However, in several heavy fermion systems, a pronounced deviation from FL behavior had been found in a number of physical properties. Most such non-Fermi-liquid (NFL) materials share two characteristics: a proximity to the magnetic region of the appropriate phase diagram (usually temperature vs. pressure or chemical composition), and disorder due to chemical substitution. Recent experiments show that disorder is very important to produce the NFL behavior. Therefore, the NFL properties of these compounds are the consequence of the competition between the one-site Kondo interaction and the inter-site Ruderman - Kittel - Kasuya - Yosida (RKKY) [29] interaction in a disordered environment [30, 31].

In addition, the surprisingly high effective masses of the quasiparticles and the NFL behavior, in particular the exotic properties of the cooperative states of the heavy fermion systems stimulate the new theoretical concepts for highly correlated electron systems. A variety of interesting magnetic phenomena, e.g., modulated structures, Spin Density Waves (SDW), reduced moments, strong deviation from Bardin-Cooper-Schrieffer (BCS) theory in the superconducting state and even the coexistence of magnetic order with unconventional superconductivity have been observed in the heavy fermion compounds. Thus, the HF behavior demonstrates, in a particularly pronounced fashion, the impact of strong correlations on classical condensed matter physics.

In the phase diagram of the disordered KL more exotic possibilities such as non Fermi liquid regimes arise, which were observed, for example, near the $T = 0$ quantum critical point in $Y_{1-x}U_xPd_3$ (see, e.g., Ref. [32]). In this family of ternary alloys, the spin glass (SG) behavior was discovered in a U concentration range given by $0.3 < x < 0.5$ with

a freezing temperature T_f growing monotonically with x (see Ref.[33]). Among other U-based heavy fermion compounds with SG behavior, URh_2Ge_2 [34], $U_2Rh_3Si_5$ [35], U_2PdSi_3 [36] should be mentioned. The effects of "Kondo disorder" were reported for $UCu_{5-x}Pd_x$ in Ref. [37]. Later on the competition between RKKY and Kondo exchange for disordered Ce alloys was discovered experimentally (see Refs. [38] - [40]). The magnetic phase diagram of $CeNi_{1-x}Cu_x$ exhibits a change of magnetic ordering from AFM to FM at $x = 0.8$, whereas for $0.2 < x < 0.8$ the SG state appears only at high temperatures above the FM order. Apparently, the Kondo interaction could be considered as the mechanism leading to the reduction of magnetic moments because increasing the Ni contents effectively reduces the strength of the indirect exchange interaction, and then, a larger temperature stability range of the SG phase appears (see Refs. [38] - [39]).

Cuprate high-T_c superconductors

In cuprates, the ground state of the undoped perovskite oxide is an antiferromagnetic Mott insulator, with nearest-neighbor $Cu^{2+} - Cu^{3+}$ antiferromagnetic exchange interaction in the CuO_2 plane [41], [42]. Depending on doping with either electrons or holes into CuO_2 planes, the Néel temperature for the antiferromagnetic-paramagnetic transition decreases with increasing doping level. Upon further doping of carriers, long range antiferromagnetism vanishes and is replaced by superconductivity. As shown in the phase diagram for the hole-doped (p-type) and electron doped (n-type) cuprates in Fig.1, the superconducting transition temperature (T_c) first increases with increasing the doping level δ reaching a maximum T_c at an optimal doping level, then decreases and finally vanishes with further increase of doping. Although the phase diagram appear similar for both p-type and n-type cuprates, they are not truly symmetric. For p-type cuprates in the underdoped and optimally doped regime, the normal state properties below a crossover temperature T^* are significantly different from those of Fermi liquid. These unconventional normal state properties are referred as the pseudogap phenomenon [44].

Concerning the competing orders in the ground state of the cuprates, besides the obvious SU(2) broken symmetry associated with the occurrence of antiferromagnetism and U(1) broken symmetry associated with the superconducting phase transition, other competing orders include the crystalline symmetry (C) and time-reversal symmetry (T) [45]-[46]. A concept of d-density wave (DDW) state as ground state of optimally doped cuprates has been proposed in [47]. This state is also known as orbital antiferromagnetism, which involves alternating orbital currents from one plaque to the adjacent plague [47]. The DDW state is a broken T- symmetry state, which in principle, can be verified experimentally [47], although to date no conclusive empirical evidence has been found. Other possible ground states based on the simplified mean-field and two-dimensional square-lattice approximations include spin-Peierls state, Wigner crystal state, spin density waves, charge density waves and complex pairing symmetries of $(d_{x^2-y^2} + id_{xy})$ or $(d_{x^2-y^2} + is)$, depending on the doping level and the Coulomb and exchange interaction strengths [45]-[46].

There has been no consensus to date for the mechanism of cuprate superconductivity

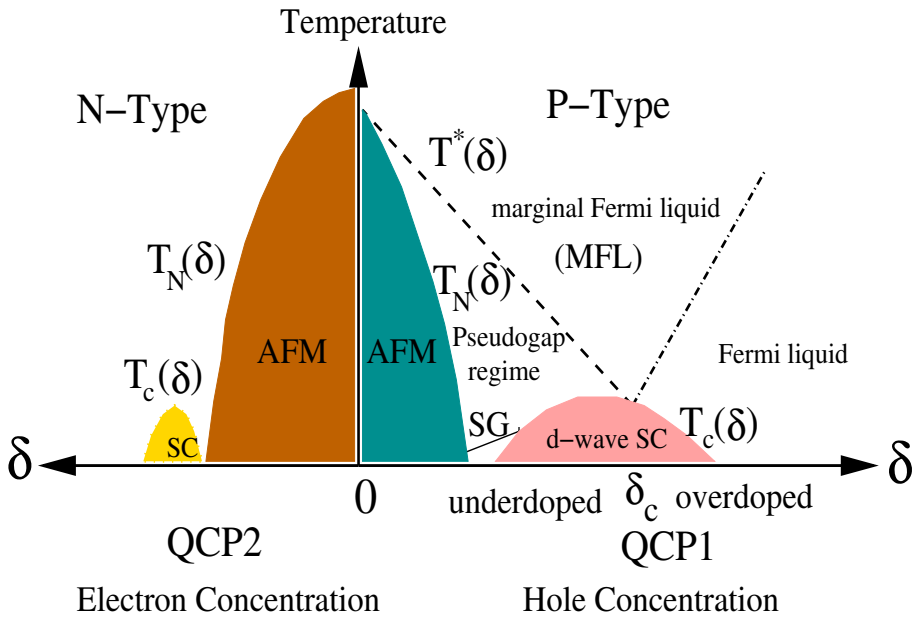

Figure 1: Generic temperature (T) vs. doping level (δ) phase diagrams of p-type and n-type cuprates in zero magnetic field. (AFM: antiferromegnetic phase; SC: superconducting phase; SG: spin glass phase; T_N and T_c are the Néel and superconducting transition temperatures, respectively; T^* is a pseudogap crossover temperature.)

[45]-[58], and the theoretical status of the field has been largely phenomenological and controversial. In general, the ground state of cuprates depends sensitively on the doping level, the type of carriers, the electronic coupling between adjacent CuO_2 layers, and the degree of disorder. The large varieties of ground states are indicative of the complex nature of competing orders in the cuprates. It is therefore imperative to identify universal characteristics among all cuprates and to develop understanding for the differences.

Lifshitz transition in 2D electron gas

In the first part of this volume we show that many of the unusual properties of the underdoped cuprates, observed experimentally in Refs.[8]-[15], can be naturally understood within the concept of the proximity of the underdoped regime to an Electronic topological transition (ETT). This concept was firstly introduced by Lifshitz [59] as "electron transition" and was subsequently called ETT [60] (see also [61] for review) due to change of the topology of the Fermi Surface (FS). It is known that the corrections to the energy of an electron gas in three dimensions at $T = 0$, associated with ETT, as a function of a change of the chemical potential μ, is proportional to $|\mu - \mu_c|^{5/2}$. Therefore, in accordance with a standard classification of the phase transitions, the ETT was attributed to so-called 2.5 - order phase transition. We emphasize, however, the difference between the Lifshitz transition and the standard second-order phase transition. The latter is related to the change of the symmetry and occurs along the curve in a plane temperature vs. pressure. The Lifshitz transition, in turn, takes place (even without any electron-electron interaction!) only at $T = 0$ and is smoothed out at finite temperatures. In papers [P5, P6, P8,

P9] the general approach to ETT as a Quantum Phase Transition (QPT) associated with an existence of a Quantum Critical Point (QCP) is developed. Since the ETT quantum critical point becomes "more singular" in low dimensions, the application of ETT concept to two-dimensional (2D) electron gas has a particular interest.

As it has been shown in [P6] and [62] - [64] that a 2D electron system on a square lattice with hopping beyond nearest neighbors undergoes an ETT at a positive hole concentrations δ ($\delta = 1-n$ where n is an electron concentration). It is true for noninteracting electrons. It is also true for a strongly correlated system with quasiparticles with a dispersion law determined by the symmetry of the square lattice. For high-T_c cuprates such quasiparticles appear in $t - t' - J$ model after taking into account the kinematic interactions.

In publications [P8, P9], various ordered states appearing in the vicinity of ETT point in the presence of interactions have been considered. It has been shown that the ordered "excitonic" phase formed in a proximity of quantum critical point (QCP) corresponding to ETT, [1] is characterized by an electron spectrum strikingly similar to that observed in the underdoped cuprates. The mentioned ETT corresponds to the electron concentration $n_c = 1-\delta_c$ at which the Fermi level (FL) crosses the saddle point (SP) energy in the bare spectrum. As shown in [63], in the case of hopping between more than nearest neighbors (or, in other words, of electron - hole asymmetry) the existence of the ETT QCP leads to a very asymmetric behavior of the noninteracting and interacting system on two sides of ETT, being quite anomalous on the side $\delta < \delta_c$. On the other hand, for realistic high-T_c cuprates with the ratio of hopping parameters between nearest and next nearest neighbors t'/t, δ_c is given by: $\delta_c = 0.27$ for $t'/t = -0.3$ and $\delta_c = 0.17$ for $t'/t = -0.2$, i.e., the anomalous regime $\delta < \delta_c$ occurs in the doping range where the experimentally observed normal metal anomalies take place. Moreover, $\delta = \delta_c$ corresponds to a maximum of $T_{sc}(\delta)$ (as discussed in [63]) and therefore the latter regime can be considered as an underdoped regime.

In the presence of a dynamic interaction between the quasiparticles with an appropriate sign, the spin density wave (SDW), the charge density wave (CDW) with different types of the order parameter symmetries (s-wave, d-wave) and the superconducting (SC) instabilities develop around the ETT point. Despite the different symmetries, the properties of such DW-ordered states resembling an "excitonic" states [65]-[71] are quite similar. For example it has been shown in [P6, P8] that the electron spectrum in the ordered phase is characterized by a gap on Fermi level for wavevectors belonging to some part of Brillouin zone which always covers the SP wavevectors $(0, \pi)$, $(\pi, 0)$ irrespective of the doping concentration. This remarkable feature is related to a quite nontrivial aspect of ETT: it is the end point of two critical lines for the "polarization operator" characterizing a behavior of the free electron system. The other aspect of the same effect is an increase of the amplitude of the order parameter (and of the gap) with increasing the deviation from the QCP on the underdoped side. Thus, the existence of a quantum critical point associated with the electronic topological transition is shown to be responsible for normal

[1] It has been shown in [63] that the ETT point is an isolated QCP. The properties of this QCP have been studied in detail in [63]

state anomalies observed in high-T_c cuprates.

Magnetic instabilities in perfect and disordered Kondo lattices

The second class of problems considered in this volume is related to the behavior of periodic Kondo systems (Kondo lattices) in the vicinity of a magnetic (spin glass) transition. In this case there are two possibilities: the compound will have a long range magnetic order when the RKKY interaction is sufficiently large compared to the Kondo interaction, or the compound will be paramagnetic due to the quenching of magnetic moments of the rare earth atoms [72] and the ground state has the features of a Kondo-singlet state. The simple Doniach dichotomy [72] predicts that either Kondo screening or the trend of magnetic order should win depending on the value of parameter α, the ratio of the single ion Kondo temperature T_K to the RKKY interaction scale T_{RKKY}. When this ratio exceeds a critical value $\alpha > \alpha_c$, the magnetism would vanish, but magnetic correlations modify the properties of the Kondo singlet state. Thus, there are several manifestations of the influence the antiferromagnetic (AF) fluctuations on the electron and spin subsystems.

i) The first one is associated with the NFL behavior of conduction electrons due to the scattering with the antiferromagnetic fluctuations [73]-[75], especially in the quantum critical regime [76]-[79].
Antiferromagnetic quantum critical behavior occurs in many heavy fermion metals, including $CePd_2Si_2$ [25], $CeIn_3$ [25], $CeNi_2Ge_2$ [80], $CeCu_{6-x}R_x$ ($R = Au, Ag$) [81], $CeRu_2Si_2$ and $U_2Pt_2In_2$. Either by pressure [82], doping or a magnetic field [83], these components can be reproducibly brought to a quantum critical point (QCP) where Néel temperature vanishes. At this point various non-Fermi liquid properties develop, such as

- Anomalous power-law temperature dependence of the resistivity (see, e.g [78]). In $CePd_2Si_2$, e.g., a power law is $\rho \sim T^{1.2}$ is seen in both the antiferromagnetic and the paramagnetic side of the transition.
- Non Curie temperature dependence of the susceptibility [84].
- Anomalous logarithmic temperature dependence of the specific heat $C_v/T \sim \ln(T^*/T)$.

Moreover, in the case of $CePd_2Si_2$ and $CeGe_2Ni_2$, superconductivity is found to develop at low temperatures in the vicinity of the QCP.

The hypothesis based on the assumption of the quasi two-dimensional magnetic fluctuations coupled with the conduction electrons was proposed in [73]-[75] for the explanation of NFL behavior in $CeCu_{6-x}Au_x$. Nevertheless, the influence of critical AFM fluctuations on the Kondo effect were not considered in this theory.

Besides, the question whether the Kondo effect happens to fail to influence the antiferromagnetic transition point (and QCP) as it is the case for an almost ferromagnetic metal, where the impurity spins magnetize the conduction electrons in the regions which are much larger than the interatomic distances [85], still remains. At present, there is no theory for the Kondo effect at the antiferromagnetic QCP. However, the break-down of the Kondo effect at a quantum critical point has been considered in other context,

particularly in quantum spin-glasses (QSG) [86]. Beyond this QCP and deep inside the quantum spin glass phase even more interesting phenomena may occur due to the presence of low–lying excitations present in the full Parisi solution.

Unconventional (p- or d- wave) superconductivity is assumed to exist in HF systems and its special symmetry offers particular conditions for its coexistence with a magnetic order. The existing disorder-averaged theory of local pairing superconductivity, in principle, well-suited to describe HF systems, requires a nonlocal extension to incorporate this symmetry. Its equivalence with the $d = \infty$-method, whose field of application is not limited to clean systems, should be employed to achieve this goal.

ii) The second manifestation of AF fluctuations in Kondo lattices is related to the behavior of interacting localized spin subsystems. In the mean-field approach, proposed by Coleman and Andrei [87], the Doniach dichotomy was supplemented by the possibility of forming the spin liquid of resonating valence bond (RVB) [88] type with Fermi statistics for the elementary excitations (spinons). This nonmagnetic spin liquid state was shown to be stabilized by the Kondo scattering, but the $s-f$ exchange interaction between spinons and electrons was treated in a mean field approximation which implies the charging RVB due to the momentary escape of a valence bond into the conduction sea. In this naive mean-field approach, the local constraint for the "pseudofermions", introduced to describe the spins, is replaced by a global one and, besides, the additional efforts are necessary to include the magnetic fluctuations into this picture.

Another interesting aspect of HF physics is related to the behavior of disordered magnets and especially the spin glasses (SG) [89, 90]. Recent experiments in HF compound like $Y_{1-x}U_xPd_3$ [32, 91] show a paramagnet to spin-glass transition within the metallic regime as the doping (x) exceeds a critical value. In this case, the ground state can either be a spin glass, in which each spin has an infinite-time memory of its spatially random moment, or a quantum paramagnet, in which the spin correlations decay to zero in the long-time limit. It is interesting to analyze the highly nontrivial relationship between Kondo effect, RKKY interaction, and Quantum Parisi Phase.

Previously, Sengupta and Georges [92] (see also [93]) found NFL behavior in an effective field theory, derived by integrating out conduction electrons, whose spins were coupled to localized ones by a Kondo interaction. In the original paper [92] the simplifying assumptions ($d = \infty$, separate electron bath for each localized spin) were made. Thus, the form of the spin-spin correlator was predetermined, and all these assumptions allowed the authors to obtain an exact solution in the framework of dynamical mean-field theory. NFL behavior was observed in this quantum critical regime spreading out from the QCP.

In publications [P10, P13] an alternative approach based on a mapping of Kondo lattice model with quenched disorder onto a single impurity Kondo model in replica-dependent magnetic field. This approach allowed to take into account the Kondo screening effects and demonstrate that the competition between Kondo and spin-glass correlations results in suppression of the spin-glass transition. Thus, the concept of competing orders applied to imperfect Kondo lattice model allowed to formulate a new class of Doniach diagrams describing a competition between Kondo scattering and effects of disorder.

Summarizing, both high temperature superconductors and heavy fermion compounds demonstrate variety of anomalous properties which can not be explained in the framework of standard BCS superconductivity theory and standard theory of localized and itinerant magnetism. Both classes of these strongly correlated systems are characterized by at least two common features:

- existence of several competing local and non-local orders
- quantum critical fluctuations associated with the existence of the quantum critical points.

In this manuscript, we demonstrate several possibilities of a microscopic description of competing orders in the high temperature cuprate superconductors and the heavy fermion compounds and discuss the origin of quantum criticality determining the anomalous properties of these materials.

In this volume, we discuss 15 publications dealing with the different aspects of strongly correlated physics. The primary goal is to give a summary and connections between these publications. Details of the calculations are, in general, not reported here and deferred to the enclosed reprints. These publications can be separated into three groups.

- The first group of publications [P5, P6, P8, P9] aims at studying the competition between d - wave superconductivity and Spin (Charge) density waves in 2-dimensional electron gas on a lattice in the vicinity of an Electron Topological Transition (ETT). The concept of two quantum critical points associated with change of geometry of Fermi surface has been introduced in [P5]. The influence of ETT on the properties of the normal state of high-T_c cuprate superconductors in the underdoped regime have been investigated in [P6]. The mean-field theory of hidden "excitonic" state associated with the ETT has been developed in [P8]. It was shown that the spectrum of excitations and angle dependence of "excitonic" order parameter have a striking similarity with the features observed in the normal state of the underdoped high-T_c cuprates. An interplay between various ordered states in the vicinity of the ETT is considered in [P9]. The summary of results is given in Section I.

- In another group of publications [P1-P4, P7, P10, P13] we study the competition between the local (magnetic, spin-glass) and the non-local (Resonance Valence Bonds) correlation in the presence of Kondo scattering. The scenario of interplay between local and non-local correlations in Kondo lattices (KL) and its application to heavy fermion compounds has been formulated in [P1]. The theory of critical antiferromagnetic fluctuations in the presence of Kondo screening has been constructed in [P2]. The diagrammatic approach to mode-mode coupling theory of the critical phenomena in Heisenberg antiferromagnet was introduced in [P3]. A self-consistent microscopic theory of the relaxation of Crystalline Electric Field levels of an impurity ion, implanted in a normal metal, is devised in [P4]. The theory successfully explained experiments in Pr - doped $CeAl_3$ and $LaAl_3$. A new approach for Kondo lattices based on semi-fermionic (SF) representation of spin has been proposed in [P7]. The Ginzburg- Landau theory of nearly antiferromagnetic Kondo lattices has been developed in [P13] with the help of SF formalism. The problem of the influence of Kondo screening on the spin glass transitions in disordered Kondo lattices has been formulated in [P10]. The effective action and replica symmetric saddle point solution has been found for KL model with infinite range Ising-like spin-spin interaction (fully connected lattice) in [P10] and for Edwards-Anderson model of disorder in [P13]. These works are summarized in Section II.

- In the third group of publications [P7, P10-P12, P14, P15] a new concept of semi-fermions is introduced. A mathematical theory of semi-fermionic representation for the generators of SU(N) group has been constructed in [P12]. Based on this theory, the minimal semi-fermionic representation for SU(2) group has been obtained in [P12] in imaginary-time formalism. A new Schwinger-Keldysh approach for quantum spin systems based on SF concept has been developed in [P11, P12, P15]. The

generalization of SF approach for the group with dynamic symmetries has been discussed in [P15]. As an example, the SO(4) group was considered. An application of SF formalism to mesoscopic system such as double quantum dot allowed to make a prediction for the Kondo effect induced by an external electric field [P14]. In this paper the competition between finite-bias and Kondo effect similar to the interplay between Kondo effect and magnetism in heavy fermion compounds is discussed in great details. The summary of mathematical aspects of the semi-fermionic representation and its application to various problems of strongly correlated physics is given in the Section III.

A summary of new results obtained in [P1-P15] is given in the Epilogue.

Summaries of publications

1. Electronic Topological Transition

Many experiments performed for high T_c cuprates provide an evidence for the existence of a pseudogap in the underdoped regime above T_c and below some temperature $T^*(\delta)$ which increases with increasing the departure from the optimal doping, $\delta_{opt} - \delta$ [8]-[15]. The pseudogap is observed directly by the angle-resolved photoemission spectroscopy (ARPES) measurements [3]-[7]. The striking feature about this gap is its increase with increasing $\delta_{opt} - \delta$ [6] while the critical temperature of superconducting (SC) transition, T_{sc}, decreases. Another prominent feature is the so-called $(\pi, 0)$ feature discovered by ARPES: the electron spectrum around the saddle-point (SP) is flat and disappears above some threshold value of wavevector [3]. Several hypotheses exist about possible origin of the pseudogap [94]-[97]. In papers [P5-P6, P8-P9] we present another explanation of this phenomenon in the framework of the model developed in [62], [P6]. In these works, the concept of the Electronic Topological Transitions in 2D system is introduced and applied to the understanding of various effects experimentally observed in high - T_c cuprates.

In papers [P5, P6, P8, P9], we focus on 2D electron systems in direct application to the high-T_c cupretes. We show that in the case of a 2D electron system on a square lattice with isotropic hopping beyond nearest neighbors, ETT is very rich, the corresponding QCP is a multi-critical point combining the different aspects of the criticality.

A starting point is a 2D system of free fermions on a square lattice with hopping between nearest (t) and next nearest (t') neighbors

$$\epsilon_{\mathbf{k}} = -2t(\cos k_x + \cos k_y) - 4t' \cos k_x \cos k_y \tag{1}$$

The dispersion law (1) is characterized by two different saddle points (SP's) located at $(\pm\, \pi, 0)$ and $(0, \pm\pi)$ (in the first Brillouin zone $(-\pi, 0)$ is equivalent to $(\pi, 0)$ and $(0, -\pi)$ is equivalent to $(0, \pi)$) with the energy $\epsilon_s = 4t'$. When we vary the chemical potential μ or the energy distance from the SP, Z, determined as

$$Z = \mu - \epsilon_s = \epsilon_F - 4t', \tag{2}$$

the topology of the Fermi surface changes when Z goes from $Z < 0$ to $Z > 0$ through the critical value $Z = 0$, see Fig.2. For $t'/t \neq 0$ which is the case of our interest, the FS does not satisfy the perfect nesting condition [98], [99] and has a different shape for different signs of t'/t. In our paper, we discuss $t'/t < 0$ that corresponds to the proper fit of ARPES experimental data. The FS's corresponding to $Z > 0$ and $Z < 0$ are shown on Fig.2.

According to Fig.2, the FS can be classified as follows. For arbitrary filling factor (depending on doping), the FS can have either 8 points which can be connected by vector $Q = (\pm\pi, \pm\pi)$ (see Fig.2), or 4 points, or do not have any such a points. These points are called "hot spots" (HS) (see [17]). The 8 hot spots are the intersection points between the Fermi Surface (FS) and the umklapp surface (US) $k_x \pm k_y = \pm\pi$. The two quantum critical points QCP1 and QCP2 correspond to critical hole doping δ_{c1} and δ_{c2}. For $\delta_{c2} < \delta < \delta_{c1}$ there are 8 hot spots. When $\delta \to \delta_{c1}$, they become 4 hot spots located at the 4 saddle points ($k_x = \pm\pi, k_y = 0$ and $k_y = \pm\pi, k_x = 0$), then for $\delta > \delta_{c1}$ they disappear. When

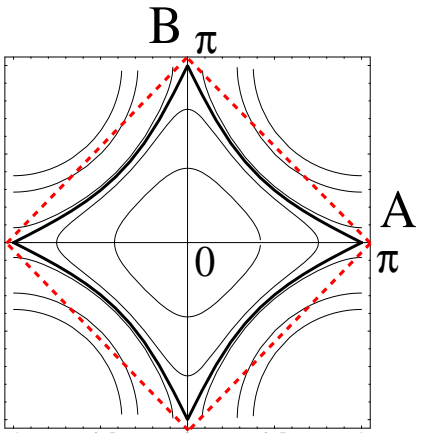

Figure 2: Fermi surface of the electron system with the dispersion law (1) for different doping. The thick line correspond to ETT.

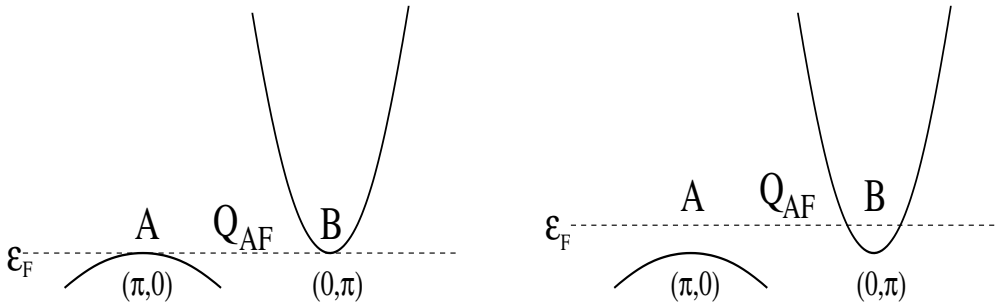

Figure 3: Schematic presentation of the electron spectrum in a vicinity of two saddle points a) at the ETT point $Z = 0$, b) in the vicinity of the ETT point $Z < 0$.

$\delta \to \delta_{c2}$ they coincide with the 4 points located at the FS along the diagonals $k_x = \pm k_y$; for $\delta < \delta_{c2}$ they disappear. The schematic presentation of the electron spectrum for $\delta_{c2} < \delta < \delta_{c1}$ is shown in Fig.3. The calculated susceptibility $\chi^0(\mathbf{Q}_{AF}, 0)$ is shown in Fig.4 as a function of hole doping δ. It reveals two singularities: a logarithmic singularity at QCP1, $\delta = \delta_{c1}$ ($\mu = 4t'$), and a square-root singularity at QCP2, $\delta = \delta_{c2}$ ($\mu = 0$), for each negative value of t'/t ($|t'/t| < 1/2$). In turn, the Cooper polarization loop is practically symmetric in the vicinity of log-singularity associated with QCP1 and is not sensible to QCP2.

It has been shown in [63], that such a system undergoes a fundamental ETT at the electron concentration corresponding to $Z = 0$. The corresponding quantum critical point is quite rich. It combines several aspects of criticality. The first standard one is related to the singularities in thermodynamic properties, in density of states at $\omega = 0$ (Van Hove singularity), to additional singularity in the superconducting (SC) response function, all reflect a local change in the topology of FS. This aspect is not important for the properties we are interested in the present paper. Important aspects which reflect a mutual change in the topology of FS in the vicinities of two SP's are the following. First of all, it is a

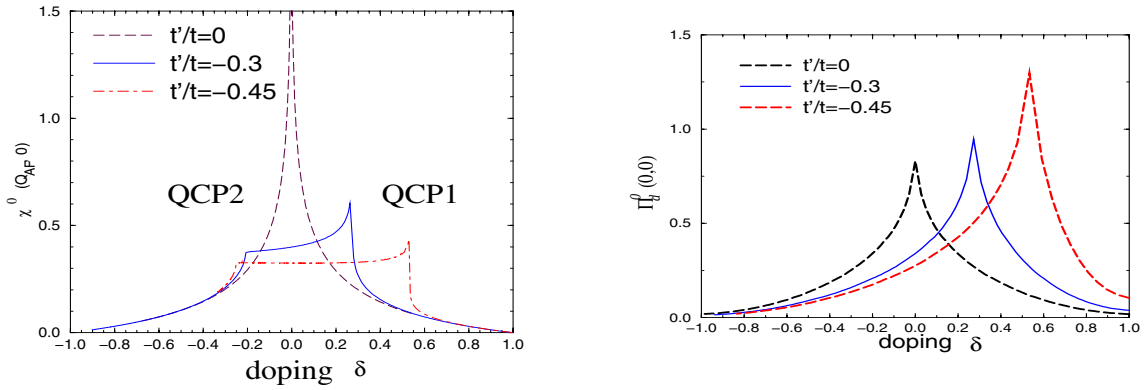

Figure 4: Electron-hole susceptibility and superconducting polarization operator (Cooper loop) around two quantum critical points QCP1 and QCP2.

logarithmic divergence of the polarizability of noninteracting electrons

$$\chi^0(\mathbf{k},\omega) = \frac{1}{N}\sum_{\mathbf{q}} \frac{n^F(\tilde{\epsilon}_{\mathbf{q}}) - n^F(\tilde{\epsilon}_{\mathbf{q}+\mathbf{k}})}{\tilde{\epsilon}_{\mathbf{q}+\mathbf{k}} - \tilde{\epsilon}_{\mathbf{q}} - \omega - i0^+}, \tag{3}$$

as $\mathbf{k} = \mathbf{Q} = (\pi,\pi)$, $\omega = 0$ and $Z \to 0$:

$$\chi^0(\mathbf{Q},0) \propto \ln\frac{\omega_{max}}{|Z|}. \tag{4}$$

which has an "excitonic" origin ($\omega_{max} \sim t$ is a cutoff energy). By "excitonic" origin we mean that two branches of the spectrum in the vicinities of two SP's ($a = t - 2t'$, $b = t + 2t'$)

$$\tilde{\epsilon}_1(\mathbf{k}) = \epsilon_1(\mathbf{k}) - \mu = -Z + ak_x^2 - bk_y^2,$$
$$\tilde{\epsilon}_2(\mathbf{k}) = \epsilon_2(\mathbf{k}) - \mu = -Z + ak_y^2 - bk_x^2 \tag{5}$$

have such a form (see Fig.3) that at $Z = 0$ the chemical potential lies on the bottom of one "band" and on the top of the another for the given directions $(0,\pi) - (\pi,\pi)$ and $(\pi,0) - (0,0)$, (see Fig.3). Therefore, no energy is needed to excite the electron-hole pair. It is this divergence that is at the origin of density wave (DW) instability. The DW instability can be of Spin Density Wave (SDW), Charge Density Wave (CDW), Spin Current Density Wave (SCDW) or Orbital Current Density Wave (OCDW) instability [71]) of the interacting electron system depending on the nature of interaction.

The non-triviality stems from the aspect of criticality related to the effect of Kohn singularity [100] in 2D system: the point $Z = 0$, $T = 0$ is the end of the critical line $Z < 0$ each point of which is a point of static Kohn singularities in polarizability of noninteracting electrons. As shown in [63], the latter aspect is a motor for the anomalous behavior of the system on the other side of ETT $Z > 0$. One among the anomalies found in [63] concerns the ordered DW phases. We have obtained that the line of DW "excitonic" instability $T_{DW}(Z)$ has the anomalous form on the side $Z > 0$: it grows from QCP instead of having the form of a bell around QCP as it usually happens in the case of ordinary QCP. Below we show that this latter aspect is also at the origin of anomalous behavior of the order parameter and of some other anomalies in the ordered state in the same regime $Z > 0$. As

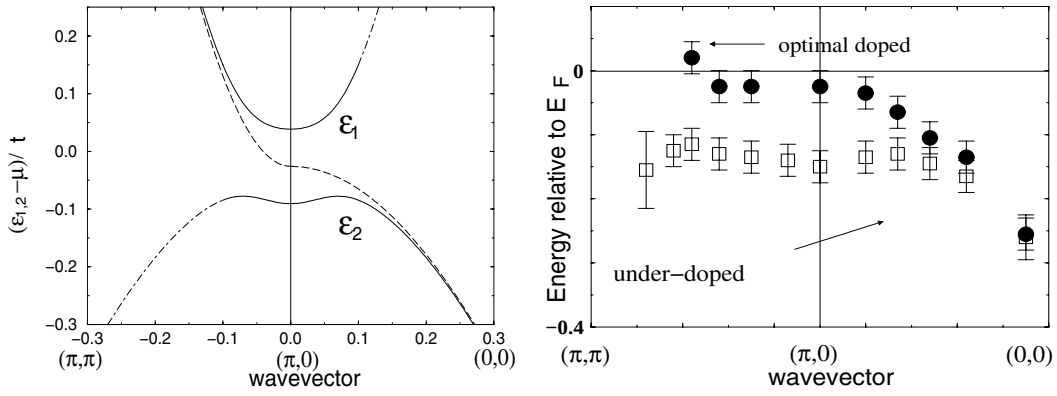

Figure 5: One-particle spectra along $(\pi, pi) - (\pi, 0)$ and $(\pi, 0) - (0, 0)$ lines. (a) calculated from $t - t' - J$ model $t'/t = -0.3$, $t/J = 1.8$, $Z/t = 0.03$. Long dashed line is the bare spectrum, dot-dashed line corresponds to the spectrum when the residue of the Green's function is less than 0.1. (b) Experimental one-particle spectra measured in the underdoped regime of BSCO.

shown in [63], on the $Z > 0$ side of the electronic topological transition point, a maximum of the static electron - hole susceptibility occurs at the wavevector $\mathbf{q} = \mathbf{Q}$. Therefore in the presence of $\mathbf{q}$ independent interaction or a $\mathbf{q}$ dependent interaction negative for $\mathbf{q} = \mathbf{Q}$, the DW instability occurs at $\mathbf{q} = \mathbf{Q}$ and this is the wavevector of ordering in the DW phase.

Let's analyze now the form of the spectrum in the DW phase (Fig.5). The spectrum in close to the SP has the following prominent features: The first is a characteristic "flat" shape which is a consequence of the hybridization of the two branches of the bare spectrum in the vicinity of two different SP's with the opposite curvatures, (see Fig.5). The second: the spectrum in the direction $(\pi, \pi) - (0, \pi)$ "disappears" above some threshold value of wavevector since the residue of Green's function tends to zero (that is also an ordinary consequence of the hybridization). The third: *the chemical potential always lies in the gap* for the part of Brillouin zone (BZ) around SP wavevectors since

$$\varepsilon_1(\mathbf{k}_{SP}) = -Z + \Delta,$$

$$\varepsilon_2(\mathbf{k}_{SP}) = -Z - \Delta$$

and the gap Δ always satisfies the condition $\Delta > Z$.

This is a consequence of the existence of the critical line $\Delta = \Delta_c$ related to the aspect of criticality of the QCP, as discussed above. The obtained theoretical spectrum has a striking similarity with the anomalous experimental electron spectrum observed by ARPES [3] in the underdoped cuprates below the characteristic line $T^*(\delta)$, we reproduce it in Fig.5b. (Let us remind that ARPES measures a spectral function only below FL.) For the direction $(0, 0) - (\pi, \pi)$, Fermi level crosses the lower branch of the spectrum, (see Fig.5), i.e. the system remains metallic. In fact, the chemical potential gets out of the gap for directions extending from the diagonal $(0, 0) - (\pi, \pi)$ to some limit direction. This corresponds to an arc of FS shown in the insert of Fig.6 which is the lower part of a pocket (the upper part corresponding to a low residue is not shown). The limit points of the arc are located on the umklapp surface away from the hot spots of the unperturbed Fermi surface. As the gap value Δ is large than Z, the FS is destroyed starting from the hot

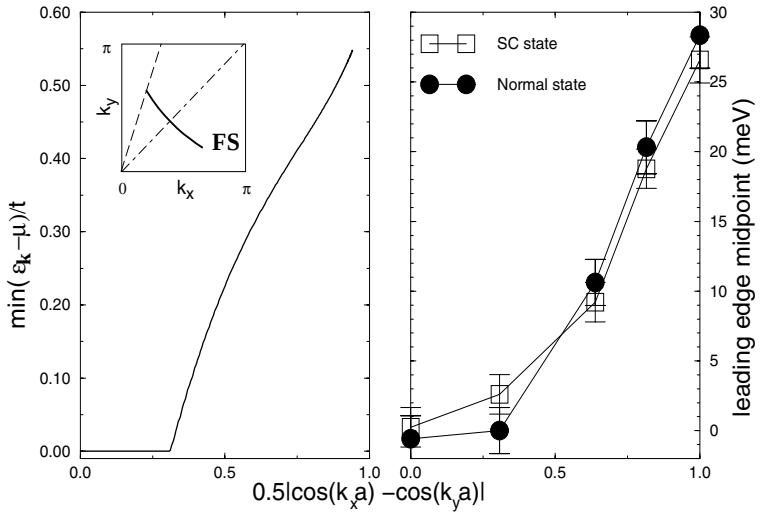

Figure 6: Theoretical angle dependence of the SDW gap calculated from FL in the underdoped regime $Z > 0$ ($t'/t = -0.3$, $t/J = 1.7$, $Z/t = 0.3$, typical shape of FS is shown on inset) (a) and the experimental leading edge midpoint measured by ARPES in the underdoped BSCO (b).

spots in both directions up to the saddle points on the side and up to limit points on the other side (the position depends on the position of the hot spots and on the strength of the interaction V). For large Z and large J, the Fermi surface pockets may fully disappear and the system becomes an insulator. The angle dependence of the value of $\epsilon_{\mathbf{k}} - \mu$, i.e. of the gap *calculated from FL*, in the same way as it is done in ARPES experiments [4] is presented in the Fig.6. Namely we plot the minimal value of $|\varepsilon_{\mathbf{k}} - \mu|$ for each given direction from the diagonal $(0,0)$ – (π,π) to the direction $(0,0)$ – $(0,\pi)$. The dependence is of a "d-wave type" in a sense that the gap increases with increasing the argument $(\cos k_x - \cos k_y)$ almost linearly in the proximity of SP. However, the dependence is flat (not linear as it happens in the d-wave case) when approaching the direction $(1,1)$. Such a behavior is also close to the experimentally found behavior above T_c [4] reproduced in Fig.6(b). [Although the authors of [4] claim that the behavior observed above and below T_c is the same, what one sees in the experimental plot is not exactly this : the behavior above and below T_c is similar in the vicinity of SP and different when approaching the $(1,1)$ direction and this occurs quite systematically, see also the plots in [4] for other samples.]

We considered the particular case of SDW as an example of ordered "excitonic" state. Nevertheless, all aforesaid is true for any other type of ordered state since the existence of such states is determined only by topology of FS.

Let us discuss the phase diagram Fig.7. In our calculations [P8, P9] we assumed $t-t'-J$ model. For such interactions, both the instabilities d-wave SC (see details in [63], [P8, P9]) and SDW take place around QCP1. Due to the symmetry of the SC response function in Z, $T_{sc}(\delta)$ is symmetrical on either sides of δ_c with a maximum at $\delta = \delta_c$, see Fig.7a. Therefore the regimes $\delta < \delta_c$ and $\delta > \delta_c$ can be considered as underdoped and overdoped, respectively. On the contrary, the line of SDW instability, $T_{SDW}(\delta)$, given by $\chi^0(\mathbf{q}, 0) = -1/J_{\mathbf{q}}$ ($\mathbf{q} = \mathbf{Q}$ for $\delta < \delta_c$ and $\mathbf{q} = \mathbf{q}_m$ for $\delta > \delta_c$) has an anomalous form in the

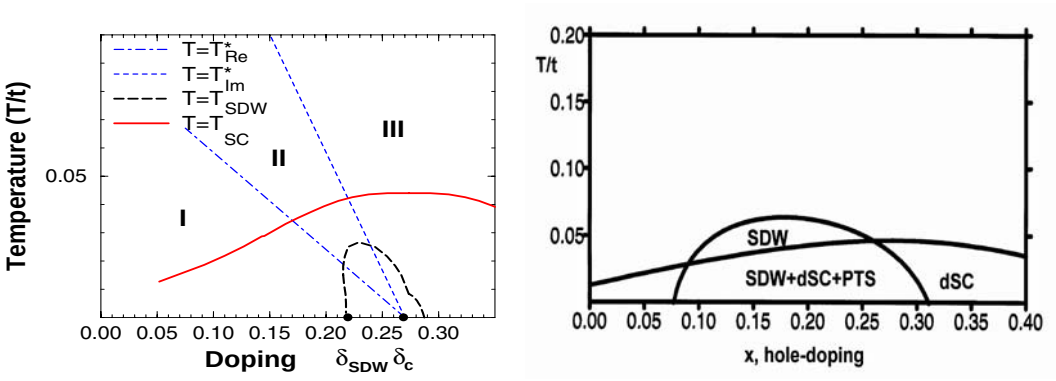

Figure 7: Phase diagram with the lines of SDW and dSC instabilities. (a) $t'/t = -0.3$, $t/J = 1.9$ (b) $t'/t = -0.3$, $t/J = 1.5$. Only metallic part of the phase diagram is considered.

regime $\delta < \delta_c$: it develops rather around the lines $T^*_{Re}(\delta)$ and $T^*_{Im}(\delta)$ than around QCP (see Fig.7) reproducing the form of lines, $\chi^0(\mathbf{Q}, 0) = const$, discussed above.

The first possibility (Fig.7a) is that the ordered SDW phase is a "hidden" phase being always below the line of the superconducting transition. When at certain doping, δ=δ_{SDW}, the ordered SDW solution disappears, it is the disordered metallic state which keeps this type of behavior: the regime $T^*_{Re}(\delta) < T < T^*_{Im}(\delta)$ (II) turns out to be a regime of a *minimum disorder* and the regime $T < T^*_{Re}(\delta)$ (I) a regime of *a reentrant in temperature quantum SDW liquid*. Indeed, two most important parameters characterizing SDW liquid: $\kappa^2 = 1 - |J_{\mathbf{Q}}|\chi^0(\mathbf{Q}, 0)$ describing a "proximity" to the SDW instability and $\Gamma_{\mathbf{Q}} = \kappa^2/C(0)$ describing a relaxation energy behave in a reentrant way in increasing T: κ^2 decreases (slightly) with T until $T^*_{Re}(\delta)$ and $\Gamma_{\mathbf{Q}}$ decreases (strongly) until $T^*_{Re}(\delta) < T^*_{\Gamma} < T^*_{Im}(\delta)$ as if the system would move towards an ordered phase. However, it does not reach it, the reentrancy stops and the system passes to the regime II of a minimum disorder above which a standard disordered state behavior is restored (regime III). On the other hand, the quantum SDW liquid state in the regime I is practically *frozen in doping* due to the very weak dependence of κ^2 on doping. As a result the disordered metal state in the regime $\delta < \delta_c$ keeps a strong memory about the ordered SDW phase (and therefore develops strong critical SDW fluctuations) very far in doping and in temperature. On the contrary, in the regime $\delta > \delta_c$ the memory about SDW instability and the corresponding fluctuations disappear rapidly due to the sharp decrease of $\chi^0(\mathbf{q}, 0)$ with increasing $\delta - \delta_c$ and T. The same is valid in both regimes $\delta > \delta_c$ and $\delta < \delta_c$ for SC fluctuations due to the discussed in the first part behavior of SC RF as a function of T and $|Z|$. Therefore, although the SDW phase itself is energetically unfavorable with respect to the SC phase (except of the case of very high J/t), the metal state above T_{sc} in the underdoped regime is a precursor of the SDW phase rather than of the SC phase.

The second possibility of SDW state surviving above superconducting state is shown on Fig.7b. This phase diagram demonstrates the results of solution of a self-consistent system of four coupled equations [P9] for DW and SC order parameters. The ordered SDW phase starting from the QCP1 at $\delta = \delta_c$ develops toward the underdoped region. Its increases with increasing the interaction J and eventually leans out the superconducting phase as

in this figure. SDW and dSC results in a mixed phase where π-triplet order predicted by $SO(5)$ theory [53]-[54] is also present.

Summarizing, we have studied the DW phase which is formed around QCP1 (associated with ETT) and we have shown that this phase is characterized by the following prominent features:

- the specific "flat" shape of the spectrum in the vicinity of SP,
- "disappearance" of the spectrum above some threshold value of wavevector in the direction $(\pi, 0)$ - (π, π),
- pseudogap in DOS with FL lying inside it,
- increasing of the gap in the spectrum around SP wavevectors and of the pseudogap in DOS with decreasing doping for $\delta < \delta_c$
- angle dependence of the gap calculating from the FL, which is of a d-wave type close to SP and flat close to the direction $(1, 1)$.

We analyzed the possibility of coexistence of various Density Wave phases with d-wave superconductivity in the framework of $t - t' - J$ model. It is shown that competing orders are possible in the vicinity of the quantum critical point associated with the Electronic Topological Transition.

All these features have a striking similarity with the experimental features revealed by ARPES in the normal state of the underdoped hole-doped cuprates.

2. Magnetic correlations in nearly AFM Kondo lattices

The problem of competition between the Ruderman-Kittel-Kasuya-Yosida (RKKY) magnetic exchange and the Kondo correlations is one of the most interesting problem of the heavy fermion physics. The recent experiments [16]-[25] unambiguously show, that such a competition is responsible for many unusual properties of the integer valent heavy fermion compounds e.g., the quantum critical behavior, the unusual antiferromagnetism and superconductivity (see review [1]).

The competition between the one-site Kondo type correlations and the indirect inter-site exchange is visualized in Doniach's diagram. where the possible phase transition and crossover energies are plotted as functions of a "bare" coupling parameter $\alpha = J/\varepsilon_F$ characterizing the exchange interaction between the spin and electron subsystems in KL [72]. Only the Kondo screening and the RKKY coupling were competing in the original Doniach diagram. Later on it was noticed that the trend to spin liquid (SL) ordering is the third type of correlation which modifies essentially the magnetic phase diagram of KL in a critical region $T_K \sim I$ of the Doniach diagram [101]-[109].

The Hamiltonian of the Kondo lattice (KL) model is given by

$$H = \sum_{k\sigma} \varepsilon_k c^\dagger_{k\sigma} c_{k\sigma} + J \sum_j \left(\mathbf{S}_j \mathbf{s}_j + \frac{1}{4} N_j n_j \right). \tag{6}$$

Here the local electron and spin density operators for conduction electrons at site j are defined as

$$n_j = \sum_{j\sigma} c^\dagger_{j\sigma} c_{j\sigma}, \quad \mathbf{s}_j = \frac{1}{2} \sum_\sigma c^\dagger_{j\sigma} \hat{\tau}_{\sigma\sigma'} c_{j\sigma'}, \tag{7}$$

where $\hat{\tau}$ are the Pauli matrices and $c_{j\sigma} = \sum_k c_{k\sigma} \exp(ikj)$. The spin glass (SG) freezing is possible if an additional quenched randomness of the inter-site exchange I_{jl} between the localized spins arises. This disorder is described by

$$H' = \sum_{jl} I_{jl} (\mathbf{S}_j \mathbf{S}_l). \tag{8}$$

We start with a perfect Kondo lattice. The spin correlations in KL are characterized by two energy scales, i.e., $I \sim J^2/\varepsilon_F$, and $\Delta_K \sim \varepsilon_F \exp(-\varepsilon_F/J)$ (the inter-site indirect exchange of the RKKY type and the Kondo binding energy, respectively). At high enough temperature, the localized spins are weakly coupled with the electron Fermi sea having the Fermi energy ε_F, so that the magnetic response of a rare-earth sublattice of KL is of paramagnetic Curie-Weiss type. With decreasing temperature either a crossover to a strong-coupling Kondo singlet regime occurs at $T \sim \Delta_K$ or the phase transition to an AFM state occurs at $T = T_N \sim zI$ where z is a coordination number in KL. If $T_N \approx \Delta_K$, the interference between two trends results in the decrease of both characteristic temperatures or in suppressing one of them. The mechanism of suppression is based on the screening effect due to the Kondo interaction. The Kondo correlations screen the local order parameter, but leave nonlocal correlations intact. The mechanism of the Kondo screening for a single-impurity Kondo problem is illustrated on Fig.8.

As a result, the magnetization of local impurity in the presence of Kondo effect is determined in terms of Green's functions $\mathcal{G}(\omega)$ of semi-fermions given by the following

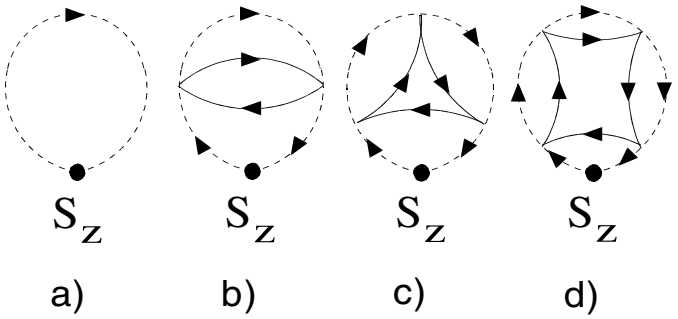

Figure 8: Kondo screening of the local moment in single-impurity Kondo problem. Dashed line denotes semi-fermions, solid line stands for conduction electrons.

expression [110]:

$$\mathcal{M}(H) = S(g\mu_B)T\sum_{\omega}(\mathcal{G}_{\uparrow}(\omega) - \mathcal{G}_{\downarrow}(\omega)) =$$

$$= S(g\mu_B)\tanh\left(\frac{H\beta}{2}\right)\left[1 - \frac{1}{\ln(T/T_K)} - \frac{\ln(\ln(T/T_K))}{2\ln^2(T/T_K)} + ...\right].$$

As we have already mentioned, the competition between the AFM and the spin liquid states takes place when the magnetic (RKKY) and the Kondo interactions are of the same order of magnitude. Thus, the critical AFM fluctuations are shown to be important in the interplay between local and non-local correlations. A scenario of RVB spin liquid crossover driven by critical AFM fluctuations was firstly proposed in [P1]. It has been shown that the relaxation regime in the vicinity of the Néel phase transition is extended in temperature in comparison to the standard critical regime for the localized moments and can even persist as $T \to 0$. The theory predicted the presence of inelastic neutron scattering corresponding to the AFM wavevector at the energies $E \sim \hbar\Omega_0$ where Ω_0 characterizes the gap in two-spinon continuum.

A complete theory of critical AFM fluctuations in Kondo lattices has been constructed in [P2]. For this sake a new version of the Feynman diagram technique has been developed to describe interaction between spin fluctuations and resonance valence bonds in self-consistent manner. It has been shown that the spin fluctuations stabilize the spin liquid against the AFM only in strongly anisotropic situation, whereas the inclusion of antiferromagnetic fluctuations in the mean-field approach in isotropic 3D case leads to the suppression of the spin liquid state. On the other hand, as it is shown in [P2], the spin liquid correlations modify spin diffusion and relaxation in antiferromagnets. The theory of AFM fluctuations in spin liquid in the presence of Kondo scattering has been applied fro explanation of anomalous properties of $CeCu_6$ and $CeRu_2Si_2$.

A simple diagrammatic version of a mode-mode coupling theory was proposed in [P3] to describe the critical dynamics of the Heisenberg antiferromagnets. In this paper the spin-current correlators has been evaluated for "diffuson"-"diffuson" and "diffuson"-"relaxon"

two-quasiparticle intermediate states. The analysis of the Ward identities for a many-particle spin-current vertices allowed to find a simple route for the calculation of the dynamical critical exponents and the scaling dimensions of the kinetic coefficients.

Yet another possibility of inelastic processes associated with the relaxation of the Crystalline Electric Field (CEF) level of an impurity ion implanted into a heavy fermion compound has been analyzed in [P4]. In this paper, a microscopic approach based on the Coqblin-Schrieffer-Copper formalism has been developed. This approach, being more general than those based on sf-exchange interaction, makes it possible to take into account the specific details of both the crystal-field states of the impurity ion and the electronic band spectrum of the metal. It is shown that the proposed approach should be useful for analyzing systems in which the crystal-field states transform into the more complicated objects as a result of strong electron correlations. Such systems include the concentrated Kondo systems, in which the rare-earth ions form a coherent lattice. Thus, the competition between the *local* CEF excitations and non-local spin-liquid correlations are shown to be responsible for the anomalous relaxation of the magnetic states. The theory of paramagnetic labeling was applied for the quantitative analysis of the relaxation of crystal-field levels of the paramagnetic ion Pr^{3+} implanted in $CeAl_3$ and $LaAl_3$. The results of calculations are in quantitative agreement with the experimental data.

A Ginzburg-Landau theory for nearly antiferromagnetic perfect and disordered lattices has been constructed in [P13]. In this theory, the microscopic Ginzburg-Landau equations are derived from the microscopic effective action written in three-mode representation (Kondo scattering, antiferromagnetic correlations, and spin liquid correlations). The new modified Doniach diagram has been constructed.

- Kondo screening of the Néel order

The new mean-field equation determining the Néel order parameter $\mathcal{N}$ in the presence of Kondo scattering reads as follows

$$\mathcal{N} = \tanh\left(\frac{I_{\mathbf{Q}}\mathcal{N}}{2T}\right)\left[1 - \frac{a_N}{\ln\left(T/T_K\right)}\frac{\cosh^2(\beta I_{\mathbf{Q}}\mathcal{N}/2)}{\cosh^2(\beta I_{\mathbf{Q}}\mathcal{N})}\right]. \tag{9}$$

As a result, the Kondo corrections to the molecular field equation reduce the Néel temperature. Such a reduction is associated with the Kondo screening effect similarly to those in single-impurity Kondo model (see Fig.8)

- Kondo enhancement of RVB correlations

A new self-consistent equation to determine the non-local semi-fermion correlator responsible for a crossover to the spin liquid state is found as

$$\Delta = -\sum_{\mathbf{q}}\frac{I_{\mathbf{q}}}{I_0}\left[\tanh\left(\frac{I_{\mathbf{q}}\Delta}{T}\right) + a_{sl}\frac{I_{\mathbf{q}}\Delta}{T\ln(T/T_K)}\right]. \tag{10}$$

It is seen that unlike the case of local magnetic order, the Kondo scattering favors transition into the spin-liquid state, because the scattering means the involvement of the itinerant electron degrees of freedom into the spinon dynamics.

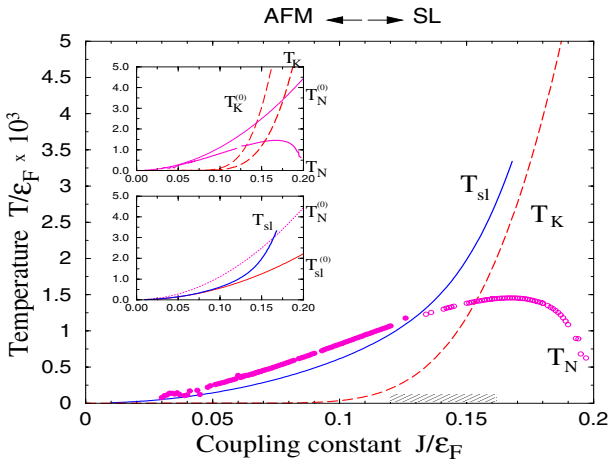

Figure 9: Doniach's diagram with modifications due to Kondo screening

The results of numerical solution of Eqs. (9) and (10) are summarized in a revised Doniach diagram shown in Fig.9. Here the renormalized transition temperatures are plotted as functions of dimensionless coupling constant $\alpha = J/\varepsilon_F$ The reduced T_N and enhanced T_{sl} are presented by circles and full line, respectively. The filled circles correspond to the region where the AFM order overcomes the SL phase, and the light circles show unphysical "suppressed" AFM solutions obtained beyond the region of validity of the mean-field equation (9 - 10). The upper inset shows the renormalized T_N in comparison to the bare mean field Neel temperature $T_N^0 = z\varepsilon_F\alpha^2/2$, and the renormalized Kondo temperature T_K in comparison to the single-impurity Kondo temperature $T_K^{(0)} = \varepsilon_F \exp(-\alpha^{-1})$. The lower inset illustrates the renormalization of T_{sl} in comparison to its mean field value $T_{sl}^{(0)}$.

As is seen from the modified Doniach's diagram, the interplay between three modes becomes significant in a critical region where the exchange coupling constant is close to the point $\alpha_c = 0.13$ where $I = \Delta_K$ in the conventional Doniach's diagram. If the Kondo screening is not taken into account, then $T_{sl}^{(0)}(\alpha) < T_N^{(0)}(\alpha)$ (thin solid and dotted lines in the lower inset). The Kondo screening changes this picture radically, and as a result a sufficiently wide interval of the values of parameter α just to the right of the critical value α_c arises, where the enhanced transition temperature T_{sl} exceeds both the reduced Neel temperature T_N and the Kondo temperature T_K. The calculations of T_{sl} presented in Fig.8 are performed for $d = 2$. The similar picture exists for $d = 3$, although the domain of stable SL state is more narrow (for a given value of zI). This means that in this region the stable magnetic phase is, in fact, the spin liquid phase. If one descends from high temperatures in a hatched region of Doniach's diagram where $T_K \sim T_N$, the Kondo scattering suppresses the AFM correlations, but the SL correlations quench Kondo processes at some temperature $T_{sl} > T_K$. As a result the Kondo-type saddle point is not realized in the free energy functional in agreement with the assumption used above in our derivation of Ginzburg-Landau expansion.

- Kondo effect and quenched disorder

Let's assume that the RKKY interactions are random (e.g. due to the presence of non-

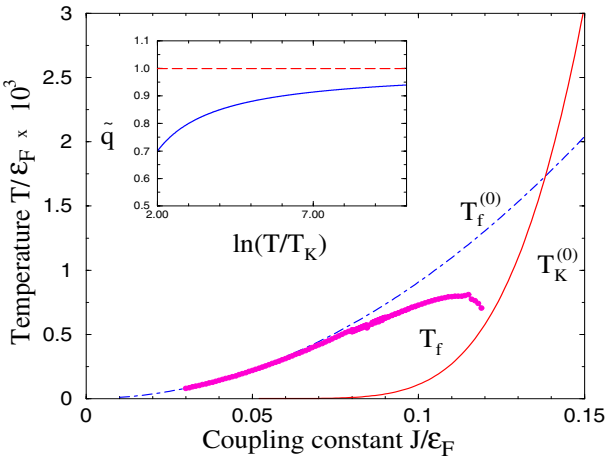

Figure 10: Doniach's diagram for spin glass transition in disordered KL.

magnetic impurities resulting in appearance of random phase in the RKKY indirect exchange). In this case, the spin glass phase should be considered. As it has been shown in [P10] and [P13], the influence of static disorder on Kondo effect in models with Ising exchange on fully connected lattices (Sherrington-Kirkpatrick model) can be taken into account by the mapping KL model with quenched disorder onto the single impurity Kondo model in random (depending on replicas) magnetic field. It allows for the self-consistent determination of the Edwards-Anderson q_{EA}order parameter given by the following set of self-consistent equations

$$\tilde{q} = 1 - \frac{2c}{\ln(T/T_K)} - O\left(\frac{1}{\ln^2(T/T_K)}\right),$$

$$q = \int_x^G \tanh^2\left(\frac{\beta I x\sqrt{\tilde{q}}}{1 + 2c(\beta I)^2(\tilde{q}-q)/\ln(T/T_K)}\right) + O\left(\frac{q}{\ln^2(T/T_K)}\right) . \qquad (11)$$

Here $q = q_{EA}$ and $\tilde{q}$ are non-diagonal and diagonal elements of Parisi matrix respectively. Therefore, the Kondo-scattering results in the depression of the freezing temperature due to the screening effects in the same way as the magnetic moments and the one-site susceptibility are screened in the single-impurity Kondo problem (c.f. Fig.8) when Ising and Kondo interactions are of the same order of magnitude (see Fig.10).

The suppression of spin glass correlations with T approaching T_K is illustrated in the insert of Fig.10 where the temperature dependence of the diagonal element of Parisi matrix is plotted. Like in the case of perfect KL, the screening effect becomes noticeable in the critical region of the phase diagram where $T_f^0 \sim T_K^0$, but the real freezing temperature *exceeds* the Kondo temperature. The latter is also reduced in comparison to T_K^0 near the spin glass transition [111]. In this paper the interplay between T_K and T_f was considered in a mean field approximation where Kondo screening is treated as a true phase transition.

Our theory shows that the reduction of T_K due to spin polarization exist even in the absence of Kondo "condensation" (see eq.), and the mutual depression of Kondo and magnetic correlations in a critical region of the Doniach phase diagram is a common feature of the ordered and the disordered Kondo lattices.

3. Semi-fermions in quantum spin systems

Since a long time [112] physicists are aware of the fact that spin operators satisfy neither Fermi nor Bose commutation relations. For example, the Pauli matrices for $S = 1/2$ operator commute on different sites and anticommute on the same site. The commutation relations for spins are determined by $SU(2)$ algebra, leading to the absence of a Wick theorem for the generators. Less convergent opinions exist on whether fermionizations or bosonizations or none of those should be used to take care of spin statistics in many body quantum theory. At least the answers appear to be linked to the kind of physical problem considered. Widely accepted is the view that path integral representations and diagrammatic expansions for the spin systems are thus substantially more complicated than those of the purely fermion/boson systems. Many variants of diagram technique [121] that are based on different representation of spins have been proposed. The first class of approaches is based on representation of spins as bilinear combination of Fermi or Bose operators [112]-[122], whereas the representations belonging to the second class deal with more complex objects like, e.g. the Hubbard operators, the nonlinear sigma model etc. However, in all cases the fundamental problem which is at the heart of the difficulty is the local constraint problem. To illustrate it, let's consider e.g., first class of representations. Introducing the auxiliary Fermi or Bose fields makes the dimensionality of the Hilbert space, where these operators act, greater than the dimensionality of the Hilbert space for the spin operators. As a result, the spurious unphysical states should be excluded from the consideration which leads in turn to some restrictions (constraints) on bilinear combinations of Fermi/Bose operators, resulting in a substantial complication of the corresponding rules of the diagrammatic technique. The representations from the second class suffer from the same kind of problem, transformed either into a high nonlinearity of the resulting model (non-linear sigma model, see, e.g., [122]) or a hierarchical structure of the perturbation series in the absence of a Wick theorem [123] (Hubbard operators). The exclusion of double occupied and empty states for a $S = 1/2$ impurity interacting with conduction electron bath (single impurity Kondo model [110]), is controlled by fictitious chemical potential (Lagrange multiplier) of Abrikosov pseudofermions [115]. At the end of calculations this "chemical potential" λ should be put $\lambda \to -\infty$ to "freeze out" all unphysical states. In other words, there exists an additional $U(1)$ gauge field which freezes the charge fluctuations associated with this representation. The method works for dilute systems where all the spins can be considered independently. Unfortunately, attempts to generalize this technique to the lattice of spins results in the replacement of the local constraint (the number of particles on each site is fixed) by the so-called global constraint where the number of particles is fixed only on an average for the whole crystal. There is no reason to believe that such an approximation is a good starting point for the description of the strongly correlated systems. Another possibility to treat the local constraint rigorously is based on Majorana fermion representation (see, e.g. [122], [124]). In this case fermions are "real" and corresponding gauge symmetry is Z_2. The difficulty with this representation is mostly related to the physical regularization of the fluctuations associated with the discrete symmetry group.

An alternative approach for spin Hamiltonians, free from local constraint problem, has been proposed in the pioneering paper of Popov and Fedotov [125]. Based on the exact fermionic representation for $S = 1/2$ and $S = 1$ operators, where the constraint is controlled by purely imaginary Lagrange multipliers, these authors demonstrated the power and simplification of the corresponding Matsubara diagram technique [126]-[127]. For these two special cases the Matsubara frequencies are ω_n=$2\pi T(n + 1/4)$ for S=1/2 and ω_n=$2\pi T(n + 1/3)$ for S=1 providing a rigorous description of (and restricted to) the equilibrium situation. The semi-fermionic representation used by PF is neither fermionic, nor bosonic, but reflects the fundamental Pauli nature of spins (see also [128]-[132]). An attempt to generalize the Popov-Fedotov imaginary time formalism for higher spins has been done in [128]. A theorem, saying that for arbitrary $S > 1$ the partition function of spin problem corresponds to the partition function of semi-fermion problem integrated with some distribution function of "imaginary chemical potentials" of semi-fermions, has been proven. Nevertheless, several questions remained open, for example

- whether the semi-fermionic representation of SU(2) group found in [128] corresponds to a minimal set of imaginary Lagrange multipliers
- how to construct the "minimal" representation and find the distribution function of imaginary Lagrange multipliers
- how to derive the semi-fermionic representation for higher SU(N) groups
- whether the semi-fermionic representation exists for the groups with dynamic symmetries
- what is the "bridge" between semi-fermionic and standard fermion/boson representations of spins
- how to work with semi-fermions in real time

The answer to these and many other related questions is given in papers [P11, P12, P15]. As it has been shown in [P12], the partition function of $SU(N)$ [133] model is related to the partition function of corresponding fermion model through the following equation:

$$Z_S = \int \prod_j d\mu(j) P(\mu(j)) Tr \exp\left(-\beta(H_F - \mu(j) n_F)\right) = \int \prod_j d\mu(j) P(\mu(j)) Z_F(\mu(j)), \tag{12}$$

here $P(\mu_j)$ is the distribution function of imaginary Lagrange multipliers. To derive the distribution function, the following identity for the constraint expressed in terms of Grassmann variables has been used

$$\delta_{n_j,m} = \frac{1}{N} \sin\left(\pi(n_j - m)\right) / \sin\left(\frac{\pi(n_j - m)}{N}\right). \tag{13}$$

As a result, the distribution function for fully antisymmetric representation of SU(N) group described by the single column Young Tableau with a filling factor m is found as

$$P_{N,m}(\mu(j)) = \frac{2i}{N} \sum_{k=1}^{\lfloor N/2 \rfloor} \sin\left(\pi m \frac{2k-1}{N}\right) \delta(\mu(j) - \mu_k), \tag{14}$$

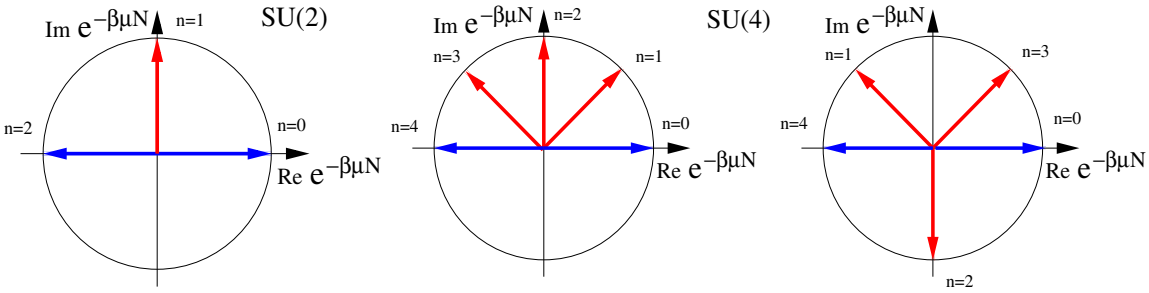

Figure 11: Graphical representation of exclusion principle for SU(N) semi-fermionic representation with even N, $n_c = 1$ (we use $\mu = i\pi T/2$ for SU(2) and $\mu_1 = i\pi T/4$, $\mu_2 = 3i\pi T/4$ for SU(4)).

where $\mu_k = -i\frac{i\pi T}{N}(2k-1)$. This partition function is proved to contain the minimal set of imaginary Lagrange multipliers and satisfy the exact particle-hole symmetry of SU(N) problem.

The exclusion principle for this case is illustrated in Fig.11, where the $S = 1/2$ representation for the first two groups SU(2) and SU(4) are shown. The first point to observe is that the spin Hamiltonian does not distinguish the n particle and the n hole (or $N-n$ particle) subspace. For this reason two phase factors $\exp(\beta\mu n)$ and $\exp(\beta\mu(N-n))$ accompanying these subspaces in Eq. (14) add up to a purely imaginary value within the same Lagrange multiplier, and the empty and the fully occupied states are always canceled. In the case of $N \geq 4$, where we have multiple Lagrange multipliers, the distribution function $P(\mu)$ linearly combines these imaginary prefactors to select out the desired physical subspace with particle number $n = m$.

In Fig.11, we note that on each picture, the empty and fully occupied states are canceled in their own unit circle. For SU(2), there is a unique chemical potential $\mu = \pm i\pi T/2$ which results in the survival of single occupied states. For SU(4), there are two chemical potentials (see also Fig.12). The cancellation of single and triple occupied states is achieved with the help of proper weights for these states in the distribution function whereas the states with the occupation number 2 are doubled according to the expression (15). In general, for SU(N) group with $n_c = 1$ there exists $N/2$ circles providing the realization of the exclusion principle.

Particularly interesting for even N is the case when the SU(N) orbital is half–filled, $m = N/2$. Then all Lagrange multipliers carry equal weight

$$P_{N,N/2}(\mu(j)) = \frac{2i}{N}\sum_{k=1}^{N/2}(-1)^{k+1}\delta\left(\mu(j) - \mu_k\right). \tag{15}$$

Taking the limit $N \to \infty$, the following limiting distribution function is obtained:

$$P_{N,N/2}(\mu(j)) \overset{N\to\infty}{\longrightarrow} \frac{\beta}{2\pi i}\exp\left(-\beta\mu(j)\frac{N}{2}\right) \tag{16}$$

resulting in the usual continuous representation of the local constraint for the simplest case $n_c = 1$

$$Z_S = Tr(\exp\left(-\beta H_F\right)\delta\left(n_j - \frac{N}{2}\right)) \tag{17}$$

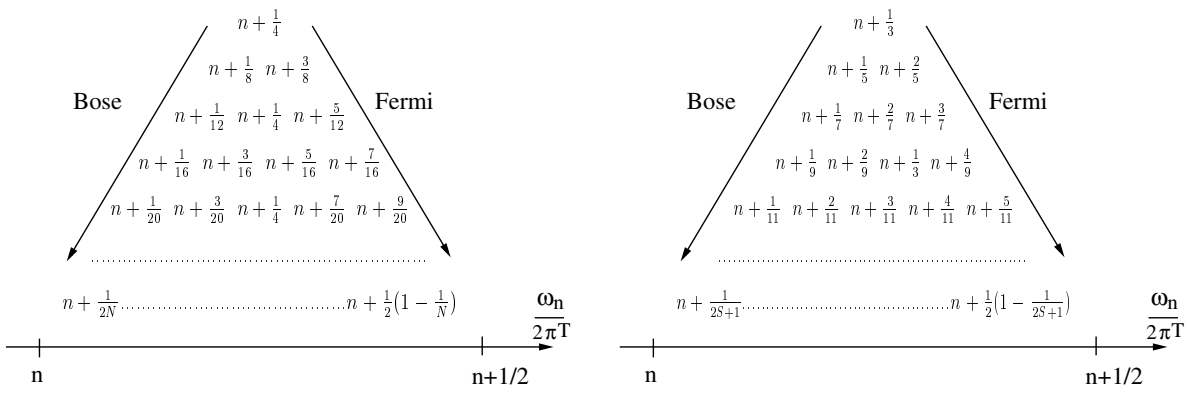

Figure 12: The minimal set of Matsubara frequencies for a) $SU(N)$ representation with even N/ $SU(2)$ representation for half-integer value of the spin. b) $SU(2)$ representation for integer values of the spin and $l = 1$.

Applying the gauge transformation to auxiliary Grassmann fields representing SU(N) generators, we arrive at generalized Grassmann boundary conditions for semi-fermions

$$a_k(j,\beta) = a_k(j,0)\exp\left(i\pi\frac{2k-1}{N}\right), \quad \bar{a}_k(j,\beta) = \bar{a}_k(j,0)\exp\left(-i\pi\frac{2k-1}{N}\right). \tag{18}$$

This leads to a temperature diagram technique for the Green's functions

$$\mathcal{G}^{\alpha\beta}(j,\tau) = -\langle T_\tau a_\alpha(j,\tau)\bar{a}_\beta(j,0)\rangle \tag{19}$$

of semi-fermions with Matsubara frequencies different from both Fermi and Bose representations (see Fig.12).

Following the same routine as for SU(N) generators and using the occupancy condition to have $l = 1$ (or $2S$) states of the $(2S+1)$ states filled, one gets the following distribution function, after using the particle–hole symmetry of the Hamiltonian H_S:

$$P_{2S+1,1}(\mu(j)) = \frac{2i}{2S+1}\sum_{k=1}^{\lfloor S+1/2\rfloor}\sin\left(\pi\frac{2k-1}{2S+1}\right)\delta(\mu(j)-\mu_k) \tag{20}$$

where the Lagrange multipliers are $\mu_k = -i\pi T(2k-1)/(2S+1)$ and $k = 1, ..., \lfloor S+1/2\rfloor$.

In the particular case of the SU(2) model for some chosen values of spin S the distribution functions are given by the following expressions

$$P_{2,1}(\mu(j)) = i\,\delta\left(\mu(j)+\frac{i\pi T}{2}\right), \tag{21}$$

for $S = 1/2$

$$P_{3,1}(\mu(j)) = P_{3,2}(\mu(j)) = \frac{i}{\sqrt{3}}\,\delta\left(\mu(j)+\frac{i\pi T}{3}\right), \tag{22}$$

for $S = 1$.

This result corresponds to the original Popov-Fedotov description restricted to the $S = 1/2$ and $S = 1$ cases.

The exclusion principle for SU(2) in the large spin limit can be also understood with the help of Fig.11 and Fig.13. One can see that the empty and the fully occupied states are canceled in each given circle similarly to even-N SU(N) algebra. The particle-hole

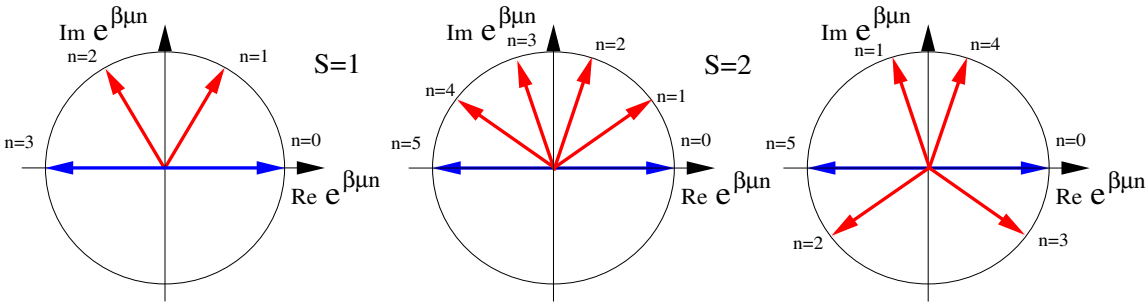

Figure 13: Graphical representation of exclusion principle for SU(2) semi-fermionic representation for $S = 1$ and $S = 2$. For any arbitrary integer value of spin there exists S circle diagrams corresponding to the S different chemical potentials and providing the realization of the exclusion principle.

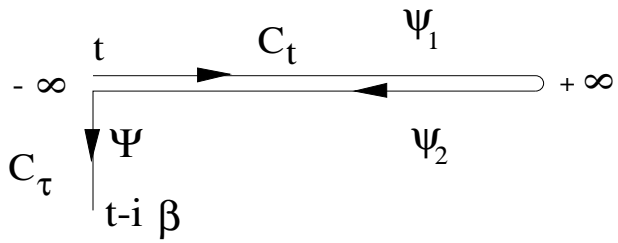

Figure 14: The Keldysh contour going from $-\infty \to \infty \to -\infty$ in real time. The boundary conditions on the imaginary time segment determine the generalized distribution functions for quasiparticles.

(PH) symmetry of the representation results in an equivalence of single occupied and $2S$ occupied states whereas all the other states are canceled due to proper weights in the distribution function (20). In accordance with PH symmetry being preserved for each value of the chemical potential, all circle diagrams (see Fig.11, Fig.13) are invariant with respect to simultaneous change $\mu \leftrightarrow -\mu$ and $n_{particle} \leftrightarrow n_{holes}$.

A long time ago Keldysh [134], [135] proposed a novel approach for the description of kinetic phenomena in metals (see also [136]-[139]). This approach was found especially fruitful for normal metals [137], and, in many recent applications, for superconductors [138], for disordered interacting (normal or superconducting) electron liquids [139] for example. The previous application of the real-time formalism to the quantum theory of Bose-Einstein condensation (BEC) [140] allowed the derivation of a Fokker-Planck equation, which describes both kinetic and coherent stages of BEC. Moreover a recent work [141] developed the closed-time path integral formalism for aging effects in quantum disordered systems being in contact with the environment. The Keldysh formalism in application to the disordered systems (see [142] -[143]) also attracted interest some time ago as an alternative approach to the replica technique. The main advantage of closed-time contour calculations (see [134]-[144]) is an automatic normalization (disorder independent) of the partition function.

In the papers [P11, P12, P15] the real time (Schwinger-Keldysh) formalism based on SF approach is constructed. The key result of [P11, P12] is that the Keldysh Green's

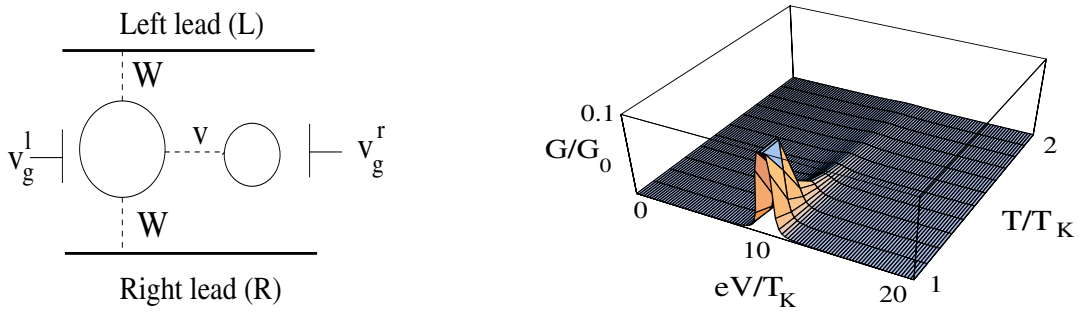

Figure 15: Double quantum dot in a side-bound configuration (a). The Kondo conductance as a function of dc-bias.

functions of free semi-fermions assumes the form

$$G_0^{\alpha}(\epsilon) = G_0^{R,\alpha} \begin{pmatrix} 1-f_\epsilon & -f_\epsilon \\ 1-f_\epsilon & -f_\epsilon \end{pmatrix} - G_0^{A,\alpha} \begin{pmatrix} -f_\epsilon & -f_\epsilon \\ 1-f_\epsilon & 1-f_\epsilon \end{pmatrix},$$

where the retarded and advanced GF's are

$$G_0^{(R,A)\alpha}(\epsilon) = (\epsilon \pm i\delta)^{-1}, \quad f_\epsilon = f^{(N,k)}(\epsilon), \tag{23}$$

with equilibrium distribution functions

$$f^{(N,k)}(\epsilon) = T\sum_n \frac{e^{i\omega_{n_k}\tau|_{+0}}}{i\omega_{n_k}-\epsilon} = \frac{1}{e^{i\pi(2k-1)/N}\exp(\beta\epsilon)+1}. \tag{24}$$

Particularly simple are the cases of $S = 1/2$ and $S = 1$,

$$f^{(2,1)}(\epsilon) = n_F(2\epsilon) - i\frac{1}{2\cosh(\beta\epsilon)}$$

$$f^{(3,1)}(\epsilon) = \frac{1}{2}n_B(\epsilon) - \frac{3}{2}n_B(3\epsilon) - i\sqrt{3}\frac{\sinh(\beta\epsilon/2)}{\sinh(3\beta\epsilon/2)} \tag{25}$$

Here, the standard notations for Fermi/Bose equilibrium distribution functions (EDF) $n_{F/B}(\epsilon) = [\exp(\beta\epsilon) \pm 1]^{-1}$ are used. For $S = 1/2$ the semi-fermionic EDF satisfies the obvious identity $|f^{(2,1)}(\epsilon)|^2 = n_F(2\epsilon)$. Both, for $S = 1/2$ and $S = 1$ the off-diagonal element (Keldysh component) is expressed in equilibrium in terms of the Brillouin function, containing correct information about occupied states.

In general the EDF for half-integer and integer spins can be expressed in terms of Fermi and Bose EDF respectively. We note that since auxiliary Fermi fields introduced for the representation of SU(N) generators do not represent the true quasiparticles of the problem, helping only to treat properly the constraint condition, the distribution functions for these objects in general do not have to be real functions. Nevertheless, one can prove that the imaginary part of the EDF does not affect the physical correlators and can be eliminated by introducing an infinitesimally small real part for the chemical potential. In spin problems, a uniform/staggered magnetic field usually plays the role of such real chemical potential for semi-fermions.

The generalization of SF formalism for the groups with dynamic symmetries has been given in [P15]. As an example, the SF representation of SO(4) group has been constructed.

The meaning of the off-diagonal constraints and correspondence between Casimir operators of SO(4) group and diagonal constraints is discussed. The non-equilibrium solution of the spin-rotator model [145]-[146] describing the double quantum dot in parallel geometry [147] with the help of SF representation of SO(4) group is given in [P14]. A competition between finite-bias effects and Kondo effect is described in a framework of SF approach. The internal singlet/triplet structure of two-electron excitations in a dot and its interplay with Kondo scattering of the electrons from the leads makes it possible to predict a Kondo effect induced by external electric field. This effect might be observed as a finite bias anomaly in double quantum dot with parallel orientation with respect to leads (see Fig.15).

In paper [P14] we demonstrated yet another application of semi-fermionic approach to the mesoscopic system with strong electron-electron correlations. The competition between local (Kondo) and nonlocal (two-electron states in a dot) exchanges has many similarities with interplay between magnetic and Kondo correlations in heavy fermion compounds. The semi-fermionic approach being a promising alternative to existing field-theoretical methods in a description of competition of various orders in heavy fermion compounds is shown to be also an useful tool for an adequate description of a nonequilibrium phenomena [148] in mesoscopic systems.

Epilogue

In this section we summarize the new results reported in the publications [P1-P15].

- A theory of the quantum phase transition related to the change of topology of Fermi surface of 2D electron gas on a square lattice is constructed. It is shown that the Electronic Topological Transition is responsible for the anomalous properties of the Fermi-liquid. A mean-field theory of competing instabilities in the vicinity of the quantum critical point associated with electron topological transition is proposed.

- A theory of stabilization of spin liquid in almost antiferromagnetic perfect Kondo lattices has been constructed. The Kondo screening effects are found to be responsible for the suppression of magnetic (Néel) transition. The influence of Kondo effect and critical antiferromagnetic fluctuations on the properties of RVB spin liquids are investigated.

- A self-consistent theory of the relaxation of the crystal-field levels of a paramagnetic ion implanted into heavy fermion metals has been developed.

- A mean-field theory of disordered Kondo lattices with a long-range magnetic interaction has been constructed. A mapping of the KL problem with quenched disorder on a fully connected lattice onto a set of independent Kondo scatters in external replica-dependent magnetic field is established. It is shown that the Kondo screening affects the Edwards-Anderson order parameter and suppresses the temperature of spin-glass transition when the spin-spin and the Kondo interactions are of the same order of magnitude.

- A mathematical background for the semi-fermionic representation of the generators of SU(N) groups is developed. It includes the circle diagram representation of the exclusion principle in the imaginary time (Matsubara) formalism and also real-time (Schwinger-Keldysh) diagrammatic approach based on semi-fermionic concepts and semi-fermionic representations of the groups with hidden symmetries.

- A finite-bias anomaly corresponding to the resonance Kondo tunneling induced by external electric field in a double quantum dot in a parallel geometry is predicted. The theory of this anomaly, based on the solution of the self-consistent renormalization group equations for SO(4) - invariant spin-rotator model, is constructed.

Acknowledgments

I would like to thank Prof. Reinhold Oppermann for fruitful and enjoyable collaborations, constant support to my research and providing a stimulating atmosphere that inspired several of our joint publications.

A special thank to Prof. Konstantin Kikoin for his generous advises, support and encouragement during many years of our fruitful collaboration.

I owe special gratitude to my co-authors Frederic Bouis (France) and Andrey Mishchenko (Japan) for collaborations and inspiring exchange of scientific ideas.

I gratefully acknowledge numerous fruitful discussions with my colleagues in the University of Würzburg: Enrico Arrigoni, Michael Bechmann, Hartmut Buhmann, Heiko Feldmann, Charles Gould, Laurens Molenkamp. Many thanks especially to Prof. Werner Hanke and all members of his group for stimulating and enjoyable discussions.

My particular thanks also to my colleagues around the globe: Dimitry Aristov and Alan Luther (Nordita), Bernard Coqblin, Flora Onufrieva and Pierre Pfeuty (Paris), Natan Andrei, Valerii Pokrovskii, Nikolai Prokof'ev and Valerii Vinokur (USA), Anne de Visser (Amsterdam), Yuval Gefen and Alexander Finkel'stein (Israel), Yuri Kagan, Leonid Keldysh and Serguei Maleev (Russia) with whom I discussed most of the results contained in this volume.

My special thanks to Amit Dutta for a careful reading of this manuscript and many useful suggestions.

My work profited considerably from the computer facilities of the Institute for Theoretical Physics and Astrophysics. I am grateful to Andreas Vetter and Christopher Dahnken for their helpfulness in resolving computer problems I had. A special thank to the secretaries Christine Schmeißer and Bridgitte Wehner for their friendly helpfulness.

I thank the Alexander von Humboldt Foundation for the support of my research project in 2000 and for the help provided during my first year of stay in Germany.

I gratefully acknowledge financial support by Deutsche Forschunggemeinschaft through the project Sonder Forschungsbereich SFB-410 of my research in the University of Würzburg.

Finally, I want to thank my wife Marina for her comprehension, helpfulness and encouragement in periods of hard work.

List of Enclosed Publications

[$P1$]. Kikoin, K.A., Kiselev, M.N., and Mishchenko, A.S. (1997): Stabilization of spin liquid in Kondo lattice: High temperature regime., Physica B 230-232, 490-492.

[$P2$]. Kikoin, K.A., Kiselev, M.N. and Mishchenko, A.S. (1997): Spin liquid in an almost antiferromagnetic Kondo - lattice., Soviet JETP 85, 399-414.

[$P3$]. Kikoin, K.A., Kiselev, M.N. (1997): Spin diffusion and relaxation in 3D isotropic Heisenberg antiferromagnets., Soviet JETP 85, 994-1000.

[$P4$]. Kiselev, M.N. and Mishchenko, A.S. (1998): Paramagnetic labeling as a method for the soft spectroscopy of electronic states., Soviet JETP 86, 1008-1019.

[$P5$]. Onufrieva, F.P., Pfeuty, P. and Kiselev, M.N. (1998): Electronic topological transition in 2D electron system on a square lattice as a motor for the "strange-metal" behaviour in high - T_c cuprates. J.Phys. and Chem. of Solids. Vol. 59, 1853-1857.

[$P6$]. Onufrieva, F., Pfeuty, P. and Kiselev, M. (1999): New scenario for High- T_c Cuprates: Electronic Topological Transition as a Motor for Anomalies in the Underdoped Regime. Physical Review Letters 82, 2370 - 2373.

[$P7$]. Bouis, F. and Kiselev, M.N. (1999): Effective action for the Kondo lattice model. New approach for S=1/2. Physica B 259-261, 195 - 197.

[$P8$]. Kiselev, M.N., Bouis, F., Onufrieva, F. and Pfeuty, P., (2000): Some consequences of electronic topological transition in 2D system on a square lattice: Excitonic ordered states., Eur. Phys. J. B 16, 601-611.

[$P9$]. Bouis, F., Kiselev, M.N., Onufrieva, F. and Pfeuty, P., (2000): Various ordered states in a 2D interacting electron system close to electronic topological transition. Physica B 284-288, 677-678.

[$P10$]. Kiselev, M.N., Oppermann, R., (2000): Spin-glass transition in Kondo lattice with quenched disorder. JETP Letters 71, 359 - 365.

[$P11$]. Kiselev, M.N., Oppermann, R. (2000): Schwinger-Keldysh semionic approach for quantum spin systems. Physical Review Letters 85, 5631 - 5635.

[$P12$]. Kiselev, M.N., Feldmann, H., Oppermann, R. (2001): Semi-fermionic representation of SU(N) Hamiltonians. Eur.Phys. J B22, 53-63.

[$P13$]. Kiselev, M.N., Kikoin, K. and Oppermann, R. (2002): Ginzburg-Landau functional for nearly antiferromagnetic perfect and disordered Kondo lattices. Physical Review B 65, 184410.

[$P14$]. Kiselev, M.N., Kikoin, K.A and Molenkamp, L.W. (2003): Resonance Kondo tunneling through a double quantum dot at finite bias. Physical Review B 68, 155323.

[$P15$]. Kiselev, M.N. (2003): Semi-fermionic approach for quantum spin systems. Extended version of the talk given at Theoretical Physics 2002 Conference, TH-2002 Paris, July 22-27 2002. Proceedings TH2002 Supplement (2003) 155-180. Birkhäuser Verlag, Basel.

References

[1] N.Grewe and F.Steglich, in *Handbook of the Physics and Chemistry of Rare Earths*, vol.**14**, ed. by K.A. Gschneider Jr. and L.Eyring (Amsterdam: Elsevier), p.343 (1991).

[2] E.W.Carlson. V.J.Emery, S.A.Kivelson, and D.Orgad, in *The Physics of Conventional and Unconventional Superconductors"*, ed. by K.H.Bennemann and J.BKetterson (Springer-Verlag) 2000, cond-mat/0206217.

[3] D.S. Marshall, D.S. Dessau, A.G. Loeser, C-H. Park, A.Y. Matsuura, J.N. Eckstein, I. Bozovic, P. Fournier, A. Kapitulnik, W.E. Sicer and Z.-X. Shen, Phys. Rev. Lett. **76**, 4841 (1996)

[4] J.M. Harris, Z.-X. Shen, P.J. White, D.S. Marshall, M.C. Schabel, J.N. Eckstein and I. Bozovic, Phys. Rev. **B54**, 15 665 (1996)

[5] H. Ding, T. Yokoya, J.C. Campuzano, T. Takahashi, M. Randeria, M.R. Norman, T. Mochiku, K. Kadowaki and J. Giapintzakis, Nature (London), **382**, 51 (1996)

[6] H. Ding, J.C. Campuzano, M.R. Norman, cond-mat/9712100

[7] H. Ding, M.R. Norman, T. Yokoya, T. Takeuchi, M. Randeria, J.C. Campuzano, T. Takahashi, T. Mochiku, and K. Kadowaki, Phys. Rev. Lett. **78**, 2628 (1997)

[8] H. Alloul, T. Ohno, P. Mendels, Bull. Am. Phys. Soc. **34**, 633 (1989), H. Alloul, T. Ohno, P. Mendels, Phys. Rev. Lett. **63**, 1700 (1989);

[9] M. Takigawa, Phys. Rev.B **49**, 4158 (1994)

[10] G.V.M. Williams, J.L. Tallon, E.M. Haines, R. Michalak and R. Dupree, Phys. Rev. Lett. **78**, 721 (1997);

[11] S.L. Cooper, G.A. Thomas, J. Orenstein, D.H. Rapkine, M. Capizzi, T. Timusk, A.J. Millis, L.F. Schneemeyer and J.V. Waszczak, Phys. Rev. B **40**, 11358 (1989)

[12] A.V. Puchkov, P. Fournier, D.N. Basov, T. Timusk, A. Kapitulnik and N.N. Kolesnikov, Phys. Rev. Lett. **77**, 3212 (1996)

[13] H.Y.Hwang, B.Batlog, H.Takagi, H.L.Kao, J,Kwo, R.J.Cava, J.J. Krajewski, and W.F.Peck, Jr., Phys.Rev.Lett **72**, 2636 (1994)

[14] J.L. Talon, J.R. Cooper, P.S.I.P.N. de Silva, G.V.M. Williams and J.W. Loram, Phys. Rev. Lett. **75**, 4114 (1995)

[15] R. Nemetschek, M. Opel, C. Hoffmann, P.F. Müller, R. Hackl, H. Berger, L. Forró, A. Erb and E. Walker, Phys. Rev. Lett. **78**, 4837 (1997)

[16] G.G. Lonzarich, J. Magn. Magn. Mat. **76-77**, 1 (1988); M. Springford, Physica B **171**, 151 (1990); Y. Onuki and A. Hasegawa, J. Magn. Magn. Mat. **108**, 19 (1992).

[17] M. Sigrist and K. Ueda, Rev. Mod. Phys. **63**, 239 (1991); R.H. Heffner and M.R. Norman, Comments Cond. Mat. Phys. **17**, 361 (1996).

[18] Rauchschwalbe U (87) Physica B **147**. 1 (1987); H.R. Ott, in *Progress in Low Temperature Physics*, Vol. XI, ed. D.F. Brewer (Elsevier, Amsterdam, 1987).

[19] J.M. Effantin, J. Rossat-Mignod, P. Burlet, H. Bartholin, S. Kunii, and T. Kasuya, J. Magn. Magn. Mater. **47-48**, 145 (1985).

[20] A. Loidl, A. Krimmel, K. Knorr, G. Sparn, M. Lang, C. Geibel, S. Horn, A. Grauel, F. Steglich, B. Welslau, N. Grewe, H. Nakotte, F. de Boer, and A.P. Murani, Ann. Physik, **1**, 78 (1992); A. Bernasconi, M. Mombelli, Z. Fisk,and H.R.Ott, Z. Phys. B **94**, 423 (1994).

[21] A. de Visser, J.J.M. France, J. Magn. Magn. Mat. **100**, 204 (1991).

[22] H. von Löhneysen, A. Neubert, T. Pietrus, A. Schröder, O. Stockert, U. Tutsch, M. Löwenhaupt, A. Rosch, and P. Wölfle. Eur. J. Phys. B **5**, 447 (1998).

[23] A. de Visser, M.J. Graf, P. Estrela, A. Amato, C. Baines, D. Andreica, F.N. Gygax, and A. Schenk, Phys. Rev. Lett. **85**, 3005 (2000).

[24] J. Rossat-Mignod, L.P. Regnauld, J.L. Jacoud, C. Vettier, P. Lejay, J. Flouquet, E. Walker, D. Jaccard, and A. Amato, J. Magn. Magn. Mat., **76&77**, 376 (1988).

[25] N.D. Mathur, F.M. Groschke, S.R. Julian, J.R. Walker, D.M. Freye, R.K.W. Haselwimmer, and G.G. Lonzarich, Nature **394**, 39 (1998).

[26] C.M. Varma in *Theory of Heavy Fermions and Valence Fluctuations*, Springer Series in Solid State Sciences, T. Kasuya and T. Saso (eds), Vol.62 (Springer: Berlin, Heidelberg), p.277

[27] J.Kondo. Progr. Theor. Phys. **32**, 37 (1964).

[28] P.W.Anderson. Phys.Rev. **124**, 41 (1961).

[29] C.Kittel. *Quantum Theory of Solids.* Willey, New York (1963).

[30] A.Yu.Zyuzin and B.Z.Spivak. Sov.Phys.JETP Lett. **43**, 234 (1986).

[31] L.N.Bulaevskii and S.V.Panyukov. Sov.Phys.JETP Lett. **43**, 240 (1986).

[32] M.B. Maple, M.C. de Andrade, J. Herrmann, Y. Dalichaouch, D.A. Gajewski, C.L. Seaman, R. Chau, R. Movshovich, M.C. Aronson, and R. Osborn, J. Low Temp. Phys, **99** 314 (1995).

[33] L.Z. Liu, J.W. Allen, C.L. Seaman, M.B. Maple, Y. Dalichaouch, J.S. Kang, M.S. Torikachvili, and M.A. Lopez de la Torre, Phys. Rev. Lett. **68**, 1034 (1992).

[34] S. Süllow, G.J. Nieuwenhuys, A.A. Menovsky, J.A. Mydosh, S.A.M. Mentink, T.E. Mason, W.J.L. Buyers, Phys. Rev. Lett **78**, 354 (1997).

[35] B. Becker, S. Ramakrishnan, A.A. Menovsky, G.J. Nieuwenhuys, and J.A.Mydosh. Phys. Rev. Lett. **78**, 1347 (1997).

[36] D.X. Li, Y. Shiokawa, Y. Homma, A. Uesawa, A. Dönni, T. Suzuki, Y. Haga, E. Yamamoto, T. Homma, Y. $\bar{O}$nuki. Phys.Rev. B **57**, 7434 (1998).

[37] O.O. Bernal, D.E. MacLaughlin, H.G. Lukefahr and A. Andraka. Phys.Rev.Lett **75**, 2023 (1995).

[38] J.C. Gomez Sal, J. Garcia Soldevilla, J.A. Blanco, J.I. Espeso, J. Rodriguez Fernandez, F. Luis, F. Bartolome, and J. Bartolome. Phys. Rev B**56**, 11747 (1997).

[39] J. Garcia Soldevilla, J.C. Gomez Sal, J.A. Blanco, J.I. Espeso, J. Rodriguez Fernandez, Phys. Rev. B**61**, 6821 (2000).

[40] D. Eom, M. Ishikawa, J. Kitagawa, and N. Takeda, J. Phys. Soc. Jpn. **67**, 2495 (1998).

[41] N.-C.Yeh, Bulletin AAPPS, Vol.12 (2002), cond-mat/0210656

[42] M.A.Kastner, R.J.Birgeneau, G.Shirane, and Y.Endoh, Rev.Mod.Phys **70**, 897 (1998)

[43] M.B.Maple, MRS Bulletin, Vol.**15**, No.6, 60 (1990)

[44] T.Timusk and B.Statt, Rep.Prog.Phys. **62**, 61 (1999)

[45] S.Sachdev, Science **288**, 475 (2000)

[46] M.Vojta, Y.Zhang, and S.Sachdev, Phys.Rev.**B 62**, 6721 (2000)

[47] S.Chakravarty and H.-Y.Kee, Phys.Rev. **B 61**, 14821 (2000)

[48] P.W.Anderson, Science **235**, 1196 (1987)

[49] P.W.Anderson, Science **268**, 1154 (1995)

[50] J.R.Schrieffer, X.G.Wen and S.-C.Zhang, Phys.Rev. **B 39**, 11663 (1989)

[51] D.Pines, Physica C **235**, 113 (1994)

[52] D.Scalapino, Phys.Rep. **250**, 329 (1995)

[53] S.-C.Zhang, Science **275**, 1089 (1997)

[54] S.-C.Zhang, J.-P.Hu, E.Arrigoni, W.Hanke, and A.Auerbach, Phys.Rev **B 60**, 13070 (1999)

[55] A.J.Leggett, J.Phys. (Paris), Colloq. **41**, C7 (1980)

[56] C.M.Varma, Phys.Rev. **B 55**, 14554 (1997); *ibid* **B 61**, R3804 (2000).

[57] V.J.Emery, S.A.Kivelson, and O.Zachar, Phys.Rev. **B 56**, 6120 (1997)

[58] T.Senthil and M.P.A.Fisher, Phys.Rev.Lett. **86**, 292 (2001); Phys.Rev. **B 62**, 7850 (2000)

[59] I.M.Lifshitz, Soviet JETP 11, 1130 (1960)

[60] A.A.Varlamov, V.S.Egorov and A.V.Pantsulaya, Adv in Phys, 38, 469 (1989)

[61] Ya.M.Blanter, M.I.Kaganov, A.V.Pantsulaya, A.A.Varlamov, Phys.Rep. 245, 159 (1994)

[62] F. Onufrieva, P. Pfeuty. Phys. Rev. Lett. 82, 3136 (1999)

[63] F. Onufrieva, P. Pfeuty. Phys. Rev. **B 61**, 799 (2000).

[64] F.Onufrieva and P.Pfeuty. Journal of Low Temp.Phys. **117**, 229 (1999).

[65] L.V.Keldysh, Yu.V. Kopaev, Sov. Phys. Solid State **6**, 2219 (1965)

[66] A.N. Kozlov, L.A. Maksimov, Sov. Phys. JETP **21**, 790 (1965)

[67] J. De Cloiseaux, Phys. & Chem. Solids **26**, 259 (1965)

[68] B.I. Halperin, T.M. Rice, Solid.State Phys., **21**, 115 (1968)

[69] T.M. Rice. Phys. Rev. **B2**, 3619 (1970)

[70] T.M. Rice, G.K. Scott, Phys. Rev. Lett **35**, 120 (1975)

[71] V.V. Tugushev, in *Electronic Phase Transitions*, ed. by W. Hanke and Yu. Kopaev. Elsevier (1992).

[72] S.Doniach, Physica **B91**, 231 (1977).

[73] A.Rosch, A.Schröder, O.Stockert, and H.v.Löhneysen, Phys.Rev.Lett. **79**, 159 (1997).

[74] A.Rosch, Phys.Rev.Lett. **82**,4280 (1999).

[75] O.Stockert, H.V.Löhneysen, A.Rosch, N.Pyka, and M.Loewenhaupt. Phys.Rev.Lett. **80**, 5627 (1998).

[76] J.Hertz. Phys.Rev. **B 14**, 1165 (1976).

[77] A.Millis. Phys.Rev **B 48**, 7183 (1993).

[78] T.Moriya and T.Takimoto. J.Phys.Soc.Jpn. **64**, 960 (1995).

[79] S.Sachdev. *Quantum Phase Transitions*. Cambridge University Press. (1999)

[80] F.Steglich, B.Buschinger, P.Gegenwart, M.Lohmann, R.Helfrich, C.Laughammer, P.Hellmann, L.Donnevert, S.Tomas, A.Link, C.Geibel, M.Lang, G.Sparn and W. Assmus. J. Phys.: Cond. Matt. **8**, 9909 (1996).

[81] H. v. Löhneysen., J.Phys.:Cond.Matter, **8**, 9698 (1996).

[82] S.R.Julian, C.Pfeiderer, F.M.Grosche, N.D.Mathur, G.J.McMullan, A.J.Diver, I.R.Walker and G.G.Lonzarich. J.Phys.:Cond Matter **8**, 0675 (1996).

[83] K.Heuser, E.-W.Scheidt, T.Schreiner, and G.R.Stewart. Phys.Rev. **B 57**, R4198 (1998).

[84] A.Schröder, G.Aeppli, E.Bucher, R.Ramazashvili, and P.Coleman. Phys.Rev.Lett. **80**, 5623 (1998).

[85] A.I.Larkin and V.I.Melnikov. Sov.Phys.-JETP **34**, 656 (1972).

[86] O.Parcollet and A.Georges, cond-mat/9806119.

[87] P.Coleman and N.Andrei, J.Phys.:Cond.Matt, **1**, 4057 (1989).

[88] G.Bascaran, Z.Zou, and P.W.Anderson. Solid State Comm. **63**, 973 (1987).

[89] J.A.Mydosh. *Spin Glasses: An Experimental Introduction.* Taylor and Francis, London (1993).

[90] J.A.Mydosh. JMMM **157/158**, 606 (1996).

[91] W.D.Wu, A.Keren, L.P.Lee, G.M.Luke, B.J.Sternlieb, and Y.J.Uemura, Phys.Rev.Lett. **72**, 3722 (1994).

[92] A.Sengupta and A.Georges. Phys.Rev. **B 52**, 10 295 (1995).

[93] S.Sachdev, N.Read, and R.Oppermann. Phys.Rev. **B 52**, 10286 (1995).

[94] A.P. Kampf and J.R. Schrieffer, Phys. Rev. **B42**, 7967 (1990)

[95] V.J. Emery and S.A. Kivelson, Nature (London) **374**, 434 (1995)

[96] S. Doniach and M. Inui, Phys. Rev **B41** 6668,(1990)

[97] B.L. Altshuler, L.B. Ioffe and A.J. Millis, Phys. Rev. **B53**, 415 (1996)

[98] J.E. Hirsch, D.Scalapino, Phys.Rev.Lett. **56**, 2732 (1986)

[99] A.Virosztek, J.Ruvalds, Phys.Rev.B **42**, 4064 (1990)

[100] W.Kohn, Phys.Rev.Lett. **2**, 393 (1959)

[101] K.A.Kikoin, M.N.Kiselev and A.S.Mishchenko. Sov.Phys.-JETP Lett. **60**, 358 (1994).

[102] K.A.Kikoin, M.N.Kiselev and A.S.Mishchenko, Physica B 206-207, 129 (1995)

[103] K.A.Kikoin, M.N.Kiselev and A.S.Mishchenko, Czech. J of Phys. 46, 1899 (1996)

[104] M.N.Kiselev and K.A.Kikoin. *Proceedings of SCES-98*, Physica B 259-261, 913 (1999).

[105] K.A.Kikoin, M.N.Kiselev, A.S.Mishchenko and A. de Visser. *Proceedings of SCES-98*, Physica B 259-261, 296 (1999).

[106] K.A.Kikoin, M.N.Kiselev, A.S.Mishchenko and A. de Visser. Phys.Rev. **B 59**, 15070 (1999).

[107] M.Kiselev and F.Bouis, Phys.REv.Lett **82**, 5172 (1999)

[108] M.Kiselev and K.Kikoin, *Proceedings of SCES-01*, Physica B 312-313, 169 (2002)

[109] M.Kiselev and R.Oppermann, *Proceedings of SCES-01*, Physica B 312-313, 167 (2002)

[110] A.Tsvelik and P.B.Wiegmann, Adv.Phys. **32**, 453 (1983).

[111] A. Theumann, B. Coqblin, S.G. Magalhães, and A.A. Schmidt, Phys. Rev. **B 63**, 054409 (2001).

[112] T. Holstein and H. Primakoff, Phys. Rev. B **58**, 1098 (1940).

[113] F. Dyson, Phys. Rev. **102**, 1217 (1956).

[114] S.V.Maleev., Sov.Phys.-JETP **6**, 776 (1958).

[115] A.Abrikosov., Physica **2**, 21 (1965).

[116] V.G.Vaks, A.I.Larkin and S.A.Pikin., Sov.Phys.-JETP **26**, 188 (1967).

[117] J.Hubbard., Proc.Roy.Soc. **A 276**, 238 (1963).,ibid **277**, 237 (1964), ibid **281**, 401 (1964).

[118] V.G.Bar'yakhtar, V.N.Krivoruchko and D.A.Yablonskii., Sov.Phys.-JETP **58**, 351 (1984).

[119] V.I.Belinicher and V.S.L'vov. Sov.Phys.-JETP **59**, 564 (1984).

[120] P. Coleman, C. Pepin, and A. M. Tsvelik, Phys. Rev. B **62**, 3852 (2000).

[121] A.Auerbach, *Interacting electrons and quantum magnetism.* Springer -Verlag (1994)

[122] A.M.Tsvelik, *Quantum field theory in condensed matter physics.* Cambridge (1995)

[123] M.Gaudin, Nucl.Phys. **15**, 89 (1960)

[124] A.Tsvelik. Phys.Rev.Lett. **69**, 2142 (1992).

[125] V.N.Popov and S.A.Fedotov. Sov.Phys.-JETP **67**, 535 (1988).

[126] V.N.Popov. *Functional Integral in Quantum Field Theory and Statistical Physics.* D.Reidel Publishing Company. Dordrecht (1983).

[127] A.A.Abrikosov, L.P.Gor'kov, and I.E.Dzyaloshinskii. *Methods of Quantum Field Theory in Statistical Physics.* Dover. New York (1975).

[128] O.Veits, R.Oppermann, M.Binderberger and J.Stein. J.Phys. I France. **4**, 493 (1994).

[129] J.Stein and R.Oppermann. Z.Phys. **B 83**, 333 (1991).

[130] C. Gros and M. D. Johnson, Physica B **165-166**, 985 (1990).

[131] S.Azakov, M.Dilaver, A.M.Oztas. Int. Journal of Modern Phys. **B 14**, 13 (2000).

[132] P.Coleman and W.Mao cond-mat/0203001,cond-mat/0205004.

[133] E. Cartan, *Leçons sur la theorie des spineurs* (Hermann, Paris, 1938).

[134] L.V.Keldysh. Sov. Phys. JETP **20**, 1018 (1965)

[135] J.Schwinger. J.Math.Phys. **2**, 407 (1961)

[136] V. S. Babichenko and A. N. Kozlov. Sol. St. Comm. **59**, 39 (1986).

[137] J.Rammer, H.Smith, Rev.Mod.Phys **58**, 323 (1986)

[138] M.V.Feigel'man, A.I.Larkin, M.A.Skvortsov, Phys.Rev. **B 61**, 12 361 (2000).

[139] A.Kamenev, A.Andreev, Phys.Rev. **B 60**, 2218 (1999), C.Chamon, A.Ludwig, C.Nayak, *ibid* p.2239 (1999)

[140] H.T.C.Stoof, Phys.Rev.Lett **78**, 768 (1997)

[141] L.Cugliandolo and G.Lozano, Phys.Rev.**B 59**, 915 (1999)

[142] R.Kree, Z.Phys, B **65**, 505 (1987)

[143] H.Sompolinski,A.Zippelius, Phys.Rev.Lett **47**,359 (1981)

[144] M.Reizer, Phys.Rev. **B 39**, 1602 (1989), *ibid*, **B 40**, 11571 (1989)

[145] K.Kikoin and Y.Avishai, Phys.Rev.Lett. **86**, 2090 (2001).

[146] K.Kikoin and Y.Avishai, Phys.Rev. **B65**, 115329 (2002).

[147] L.W.Molenkamp, K.Flensberg, and M.Kemerink, Phys. Rev. Lett. **75**, 4282 (1995)

[148] I.Aleiner, P.Brouwer, and L.Glazman, Phys. Rep. **358**, 309 (2002).

Original publications

Electronic Topological Transition

Pergamon PII: S0022-3697(98)00118-8

J. Phys. Chem Solids Vol 59, No. 10–12, pp. 1853–1857, 1998
0022-3697/98/$ - see front matter

ELECTRONIC TOPOLOGICAL TRANSITION IN 2D ELECTRON SYSTEM ON A SQUARE LATTICE AS A MOTOR FOR THE 'STRANGE-METAL' BEHAVIOUR IN HIGH-T_c CUPRATES

F. ONUFRIEVA[a], P. PFEUTY[a] and M. KISSELEV[a,b]

[a]Laboratoire Leon Brillouin, CE-Saclay 91191 Gif-sur-Yvette, France
[b]Russian Research Center 'Kurchatov Institute' 123 182 Moscow, Russia

Abstract—We show that a 2D system of free electrons on a square lattice with hoping between more than nearest neighbours is characterised by two quantum critical points associated with a change in topology of Fermi surface as a function of electron concentration. This simple model (when taking into account a positive interaction in a triplet channel) allows us to consistently explain some crucial experiments in the underdoped regime of hole-doped high-T_c cuprates (ARPES, neutron scattering). © 1998 Elsevier Science Ltd. All rights reserved

Keywords: quantum critical proof, Fermi surface topology

1. TWO QUANTUM CRITICAL POINTS IN A 2D FREE ELECTRON SYSTEM ON A SQUARE LATTICE

We study a 2D system of noninteracting electrons on a square lattice with hoping between nearest neighbours (t) and next nearest neighbours (t'). We show that it is characterised by two quantum critical points, QCP1 and QCP2, associated with a change in topology of Fermi surface (FS) as a function of electron concentration, $1-\delta$. Their criticality shows up in the electron polarisability, $\chi^0(\mathbf{k},\omega)$, at $T=0$. The calculated $\chi^0(\mathbf{Q}_{AF}=(\pi,\pi),0)$ is shown in Fig. 1 as a function of hole doping δ. It reveals two singularities: a logarithmic one at QCP1, $\delta=\delta_{c1}$ ($\mu=4t'$), and a square-root one at QCP2, $\delta=\delta_{c2}$ ($\mu=0$), for each negative value of t'/t ($|t'/t|<1/2$).

The character of these two quantum critical points appears when $\chi^0(\mathbf{k},\mathbf{0})$ is analysed as a function of $\mathbf{k}$ for different δ, see Fig. 2. Around QCP2: for both $\delta<\delta_{c2}$ and $\delta>\delta_{c2}$ there is a closed (in the extended BZ) line of static Kohn (square-root) singularities (KS's), $\mathbf{k}=\mathbf{Q}_{s2}$ which reduces into the point $\mathbf{k}=\mathbf{Q}_{AF}$ at $\delta=\delta_{c2}$. An absolute value of $\mathbf{Q}_{s2}$ along a fixed direction is given by $Q_{s2}\propto|\delta-\delta_{c2}|$. Around QCP1: at $\delta>\delta_{c1}$ and $\delta<\delta_{c1}$ the line of KS's $\mathbf{k}=\mathbf{Q}_{s2}$ related to QCP2 is preserved; in addition there is a new closed line $\mathbf{k}=\mathbf{Q}_{s1}$ at $\delta>\delta_{c1}$ which is ended at $\delta=\delta_{c1}$ being reduced into the point $\mathbf{k}=\mathbf{Q}_{AF}$. An absolute value of $\mathbf{Q}_{s1}$ along a fixed direction is given by $Q_{s1}\propto\sqrt{\delta-\delta_{c1}}$. Exactly at QCP2 and QCP1 one has respectively: $\chi^0(\mathbf{k},0)\approx A-B\sqrt{|\mathbf{k}-\mathbf{Q}_{AF}|}$ and $\chi^0(\mathbf{k},0)\propto\ln|\mathbf{k}-\mathbf{Q}_{AF}|$.

The criticality of QCP1 from another point of view is seen as a Lifshitz's electronic topological transition [1] in a 2D system with a saddle point (SP) in the electron spectrum resulting in singularities in thermodynamic properties, and an additional singularity in superconducting response function. The critical exponents associated with QCP1 and QCP2 are respectively: $\nu_1=1/2$, $z_1=2$, $s_1=\nu_1 z_1=1$, $\alpha_1=2-[(D=2)+z_1]\nu_1=0$ (logarithmic singularity in the density of states) and $\nu_2=1$, $z_2=1$, $s_2=\nu_2 z_2=1$, $\alpha_2=2-[(D=2)+z_2]\nu_2=-1$ (no singularity in the density of states).

The distance between QCP1 and QCP2 diminishes with decreasing $|t'/t|$ and the two points coincide when $t'/t=0$. In the latter case (nesting) we arrive at a quantum multicritical point with a $(\ln)^2$ singularity.

As $\delta_{c1}>0$ and $\delta_{c2}<0$ (for any t'/t), it is a doping range around QCP1 which is actual for the hole doped cuprates and around QCP2 for the electron doped. As we are interested here in the former we consider below only properties around QCP1 which are also influenced by QCP2. We assume $|t'/t|$ to be not small in order to correspond to the experimental FS observed by ARPES.

One can check that $Re\chi^0$ and $Im\chi^0$ behave in a strongly anomalous way in the regime $\delta_{c2}<\delta<\delta_{c1}$. First of all taken at the characteristic for this regime wavevector $\mathbf{q}=\mathbf{Q}_{AF}$, $Re\chi^0(\mathbf{q},0)$ changes very weakly with doping starting from some threshold value of δ (see Fig. 1) as a consequence of the interplay between QCP1 and QCP2. Secondly, energy dependences of $Re\chi^0$ and $Im\chi^0/\omega$ for $T=0$ and their temperature dependences for $\omega\to 0$ are characterised by a characteristic energy $\omega=\omega_c\propto\delta_{c1}-\delta$ and a characteristic temperature $T=T^*\propto\delta_{c1}-\delta$ both being scaled with the doping distance from QCP1. The behaviour is anomalous in the regimes $\omega<\omega_c$, $T<T^*$. For example, $Re\chi^0(\mathbf{Q}_{AF},0)$ taken at fixed δ increases with increasing T for $T<T^*$. Thirdly, $Re\chi^0(\mathbf{q},0)$ exhibits a plateau as a function of $|\mathbf{q}|$ (see Fig. 1c) until very high temperature, $T<T^*_{\mathbf{q}}\propto\delta-\delta_{c2}$, which scales with the distance from QCP2. These and other anomalies are discussed in more detail in [2].

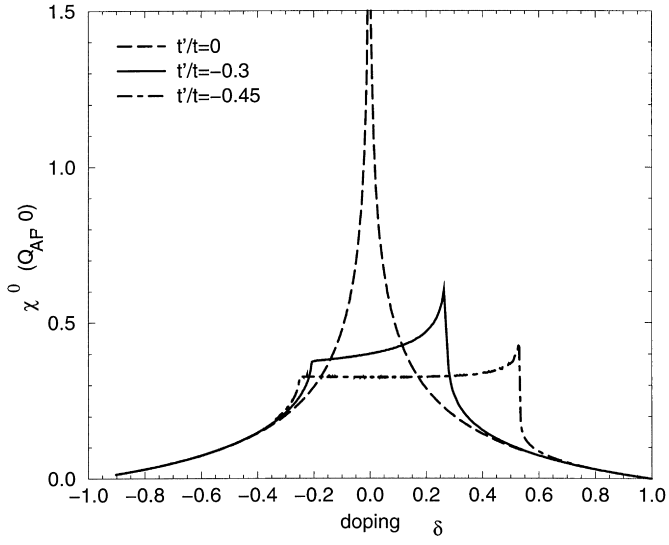

Fig. 1. Electron-hole susceptibility $\chi^0(\mathbf{Q}_{AF},0)$ around two quantum critical points, QCP1 and QCP2.

2. 2D INTERACTING SYSTEM: PROPERTIES OF CUO_2 PLANE

The anomalous behaviour of the free electron system in the presence of the two QCP is at the origin of an anomalous behaviour of interacting system. We concentrate below on properties related to long-range and short-range density wave (DW) order. (Obviously, in the presence of interactions of a certain sign, QCP1 gives rise to DW and superconducting (SC) instabilities around it due to logarithmic divergences of the corresponding response functions. What is important is that a positive interaction in a triplet channel (exchange interaction) is enough to create *both* instabilities. Such an interaction exists in the t–J model.)

A phase diagram is shown in Fig. 3. As T_{sc} is maximum at $\delta = \delta_{c1}$ (see [3]), the regime $\delta < \delta_{c1}$ is underdoped and $\delta > \delta_{c1}$ is overdoped. Although the DW phase for realistic values of t/J is hidden under the SC phase, it is DW critical fluctuations which determine a fundamentally anomalous metal behaviour below T^* and above T_{sc} (regime I) (the temperature $T = T^*(\delta)$ discussed above for the non-interacting system appears as a characteristic

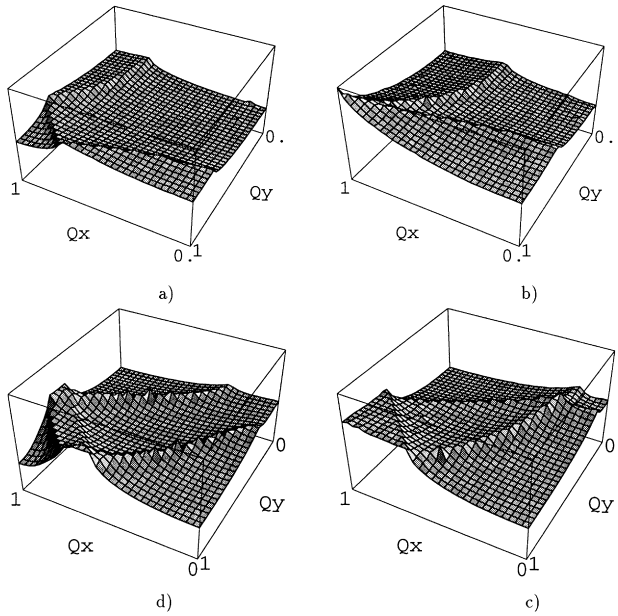

Fig. 2. Wavevector dependences of $\chi^0(\mathbf{q},0)$ for increasing doping (a) $\delta < \delta_{c2}$, (b) $\delta = \delta_{c2}$, (c) $\delta_{c2} < \delta < \delta_{c1}$ and (d) $\delta > \delta_{c1}$ ($Q_x = q_x/\pi$, $Q_y = q_y/\pi$, $t'/t = -0.3$).

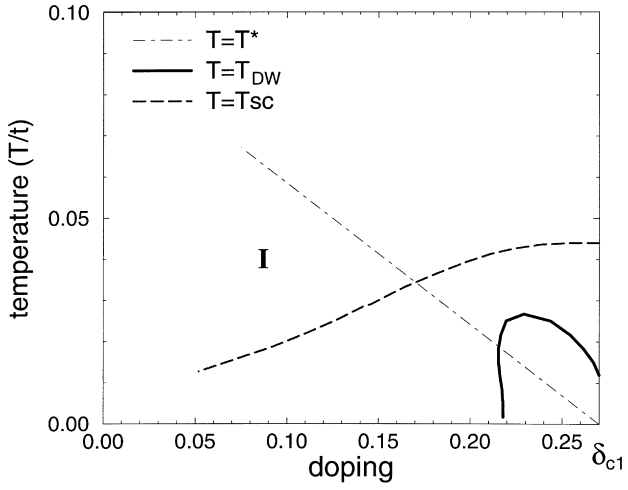

Fig. 3. Phase diagram with the lines of DW and SC instabilities and the line $T^*(\delta)$ ($t'/t = -0.3$, $t/J = 1.9$).

temperature for the interacting system). The state in regime I is reentrant in temperature and frozen in doping rigid DW liquid [2]: the correlation length slightly *increases* with T (being maximal at $T = T^*(\delta)$) and *almost does not change with doping*. Moreover, the parameter determining a proximity to the ordered DW phase does not practically change along the line $T = T^*(\delta)$, therefore remaining quite low in regime I. (All this stems from the properties of χ^0 discussed at the end of the previous section and is valid when the interaction J/t is not too small.) The ordered DW phase is also 'reentrant': T_{DW} increases with increasing $\delta_{c1} - \delta$.

All properties in the metal DW phase and in the metal regime I are anomalous. Below we show several examples.

First in Fig. 4 we show the electron spectrum in the long-range ordered DW phase. Prominent features of the spectrum are:

1. *flat shape around SP;*
2. *'disappearance' of the spectrum* in the direction $(k,\pi) - (\pi,\pi)$ above some threshold value of wavevector k (the residue tends to zero), both features being consequences of the hybridisation of the two parts of the bare spectrum around two SP's with a different curvature;
3. existence of the gap in a vicinity of SP $\Delta \propto \delta_{c1} - \delta$ *(the increase of the gap with decreasing doping* is the other side of the reentrant behaviour of DW phase). Details are given in [4].

The density of states (DOS) is shown in Fig. 5. It deviates from the bare DOS in two parts, A and B, related to QCP1 (A) and QCP2 (B). For the doping range around $\delta = \delta_{c1}$ it is the A-feature which determines properties of the system. It is characterised by a logarithmic singularity at ϵ^0 and by two jumps at ϵ^+ and ϵ^- instead of the

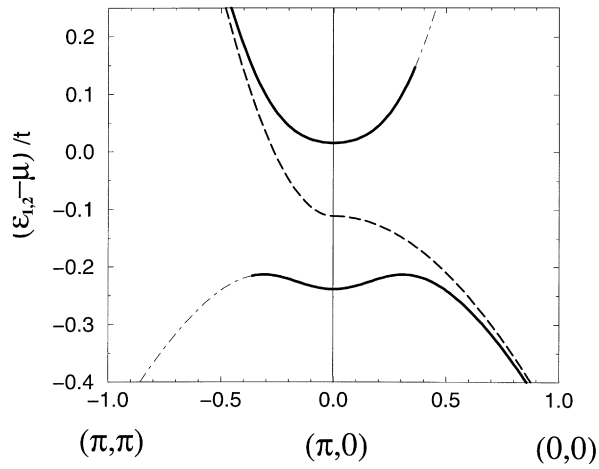

Fig. 4. Electron spectrum in DW phase around SP. The thin dot–dash line corresponds to the spectrum with residue < 0.1, and the dashed line to the bare spectrum ($t'/t = -0.3$, $t/J = 1.85$, $\delta = 0.19$).

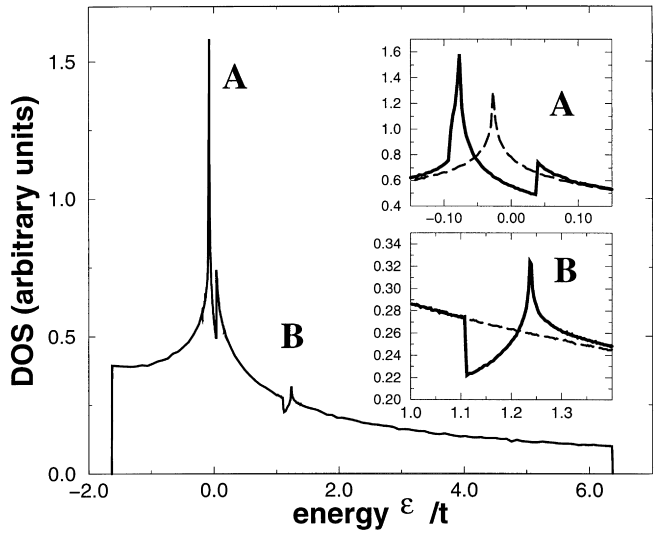

Fig. 5. Density of states with renormalised spectrum. The dashed line corresponds to the bare spectrum ($t'/t = -0.3$, $t/J = 1.8, \delta = 0.25$).

logarithmic singularity in the bare spectrum. There is a pseudogap on Fermi level.

The electron spectral function $A(\boldsymbol{k},\epsilon)$ in regime I calculated in a standard way based on the loop containing the electron Green function and the boson Green function corresponding to the susceptibility is shown in Fig. 6. The 'spectrum' deduced from it has the same shape as in Fig. 4 for $\omega < 0$. The pseudogap Δ is also proportional to $\delta_{c1} - \delta$. The difference is that for regime I the spectral function has a characteristic damped form for $\omega < 0$. The form of the 'spectrum', of the spectral function and the trend of increasing Δ with decreasing doping are in very good agreement with ARPES data above T_c [5].

The dynamic spin properties are also unusual. In Fig. 7a we show how $Im\chi(\mathbf{Q}_{AF},\omega)$ changes with decreasing T when one crosses the line $T = T^*$. One can clearly see the existence in the regime $T < T^*$ of the characteristic energy $\omega = \omega_0 \propto \delta_{DW}(0) - \delta$ (unchanging with T) at which $Im\chi$ is strongly peaked. For $T \gg T^*$ the curves lose a maximum and resemble $Im\chi^0$. In Fig. 7b we see that for low $\omega, \omega \ll \omega_c$, $Im\chi$ peaks at $\mathbf{k} = \mathbf{Q}_{AF}$. For larger ω, $Im\chi^0$ becomes flat and then even 'incommensurate' with a maximum determined by the wavevector $\mathbf{Q}_{s2}(\omega)$ related to QCP2 (a dispersion like effect). These results are in good agreement with recent INS data [6].

Summarising, a simple model taking into account the existence of two QCP's in a 2D electron system on a square lattice consistently explains certain experimental

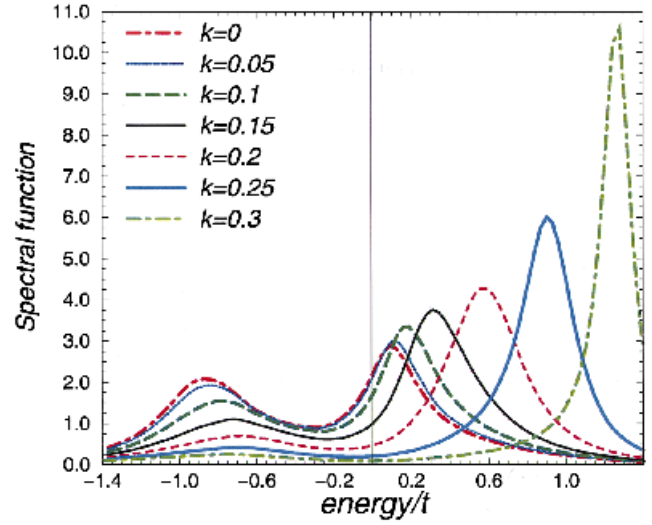

Fig. 6. Spectral function $A(\boldsymbol{k},\epsilon)$ in regime I calculated for the direction $(q,\pi) - (\pi,\pi)$. ($k = q/\pi, t'/t = -0.3$, $t/J = 1.8$, $T/t = 0.12$, $\delta = 0.1$).

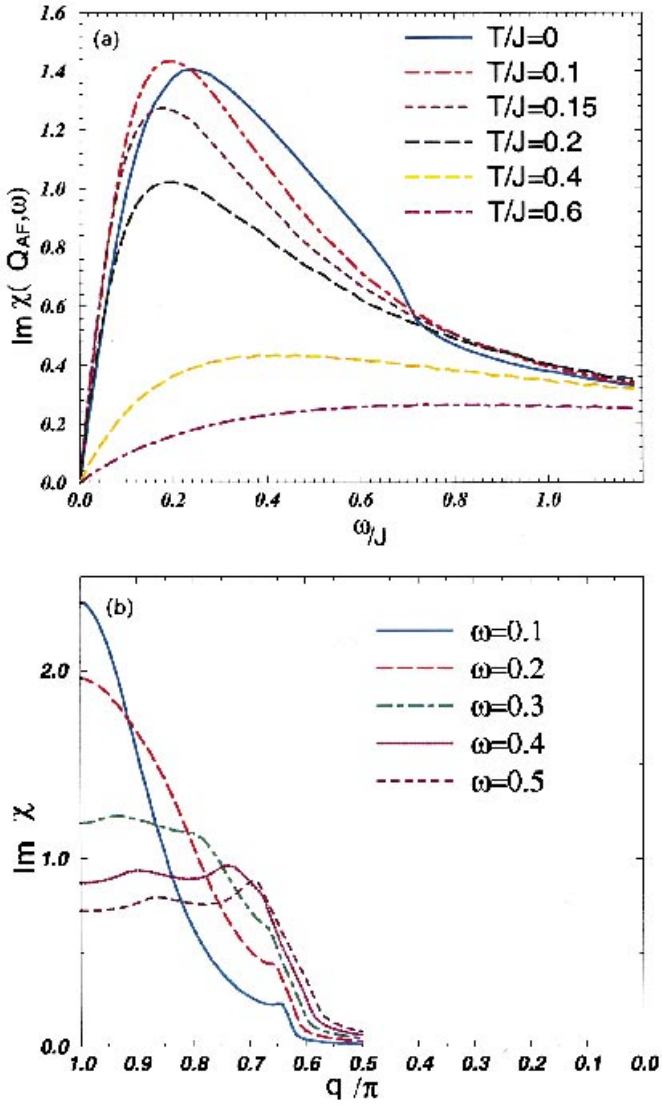

Fig. 7. *Im*χ for the underdoped regime at fixed doping $t/J = 1.83$, $t'/t = -0.3$, $\delta = 0.1$: (a) as a function of ω for different temperatures ($T^*/J = 0.2$); (b) as a function of q in the direction (q,π) for different values of ω/J (the existence of SC state is ignored).

facts considered today as crucial for understanding high-T_c cuprates.

REFERENCES

1. Lifshitz, I., *Sov. Phys. JETP*, 1960, **11**, 1130.
2. Onufrieva F. and Pfeuty P., *Phys. Rev.*, cond-mat/9804181.
3. Onufrieva, F., Petit, S. and Sidis, Y., *Phys. Rev. B*, 1996, **54**, 12464.
4. Kisselev M., Dessau, D. S., Loeser, A. G., Park, C. H., Matsuura, A. Y., Eckstein, J. N., Bozovic, J., Fournier, P., Kapitalnik, A., Spicer, W. E. and Shen, Z. X., *Phys. Rev.*, cond-mat/9804263.
5. Marshall D. S., *Phys. Rev. Lett*. **76,** 4841 (1996); Ding H., Yokoya, T., Compuzano, J. C., Takahashi, T., Ramderia, M., Norman, M. R., Moctuitzu, T., Kadowaki, K. and Giapintzaki, J., *Nature* **382,** 51 (1996); condmat/ 9712100.
6. Bourges, P., Fong, H. F., Piegnault, L. P., Bossy, J., Vettier, C., Milius, D. L., Aksay, I. A. and Keirner, B., *Phys. Rev. B*, 1997, **56**, R11439.

New Scenario for High-T_c Cuprates: Electronic Topological Transition as a Motor for Anomalies in the Underdoped Regime

F. Onufrieva, P. Pfeuty, and M. Kiselev
Laboratoire Leon Brillouin, CE-Saclay, 91191 Gif-sur-Yvette, France
(Received 2 March 1998)

We have discovered a new nontrivial aspect of electronic topological transition (ETT) in a 2D free fermion system on a square lattice. The corresponding exotic quantum critical point, $\delta = \delta_c$, $T = 0$ ($n = 1 - \delta$ is the electron concentration), is at the origin of anomalous behavior in the interacting system on one side of ETT, $\delta < \delta_c$. Most important is the appearance of the line of characteristic temperatures, $T^*(\delta) \propto \delta_c - \delta$. Application of the theory to high-T_c cuprates reveals a striking similarity to the behavior observed experimentally in the underdoped regime. [S0031-9007(99)08666-4]

PACS numbers: 74.20.Mn, 74.25.–q, 74.72.–h

This is a particularly exciting time for high-T_c. The experimental knowledge converges. Almost all experiments, nuclear magnetic resonance (NMR) [1,2], angle-resolved photoemission spectroscopy (ARPES) [3], infrared conductivity [4], etc., provide evidence for the existence of a characteristic energy scale $T^*(\delta)$ in the underdoped regime (δ is hole doping). Below and around the line $T^*(\delta)$, the "normal" state (i.e., above T_c) has properties fundamentally incompatible with the present understanding of metal physics. The field has reached the point where a consistent theory is necessary to understand this exotic from theoretical point of view (but quite well defined from an experimental point) metallic behavior. The issue has a significance beyond the field of high-T_c superconductivity—the fundamental question arises: What kind of metallic behavior is there, in addition to the well-understood Fermi liquid?

In this paper we propose our variant of the answer. We reexamine a free electron 2D system on a square lattice with hopping beyond nearest neighbors. We show that, when varying the electron concentration defined as $1 - \delta$, the system undergoes an electronic topological transition (ETT) [5] at a critical value $\delta = \delta_c$. The corresponding $T = 0$ quantum critical point (QCP) combines two aspects of criticality. The first standard one is related to singularities in thermodynamic properties, in density of states at $\omega = 0$ (Van Hove singularity), to additional singularity in the superconducting (SC) response function (RF) [6]. The second nontrivial aspect is that the same QCP *is the end of the critical line* $T = 0$, $\delta > \delta_c$, each point δ of which is characterized by static Kohn singularity (KS) in polarizability of 2D free fermions. [What we mean as a static KS is a singularity at the wave vector connecting two points of Fermi surface (FS) with parallel tangents [7]]. The two aspects of criticality are not related. It is the latter aspect (never considered before) which, as we will show, is a motor for anomalous behavior in the regime $0 < \delta < \delta_c$ of the system of noninteracting and interacting electrons (or of any fermionlike quasiparticles, e.g., of those [8] appearing in the $t - t' - J$ model describing the strongly correlated CuO_2 plane responsible for the main physics in the cuprates). The found anomalies have a striking similarity to anomalies in the underdoped high-T_c cuprates. The effect exists in all cases $t' \neq 0$ or/and $t'' \neq 0, \ldots$, except for special sets of the parameters corresponding to the perfect nesting in FS (including $t' = t'' = \ldots \to 0$) studied in many papers (see, e.g., Ref. [9]). For such sets, the QCP loses the latter aspect of criticality and the anomalies disappear.

A starting point is a 2D electron system on a square lattice with hopping beyond nearest neighbors,

$$\epsilon_{\mathbf{k}} = -2t(\cos k_x + \cos k_y) - 4t' \cos k_x \cos k_y - \cdots . \tag{1}$$

For any set of the parameters t, t', t'', ..., the dispersion law is characterized by two different saddle points (SP's) located at $(\pm\pi, 0)$ and $(0, \pm\pi)$ with the energy ϵ_s. When we vary the chemical potential μ or the energy distance from the SP, $Z = \mu - \epsilon_s$, the topology of the FS changes when Z goes from $Z > 0$ to $Z < 0$ through the critical value $Z = 0$. In vicinity of SP's the dispersion law is

$$\tilde{\epsilon}(\mathbf{k}) = \epsilon_{\mathbf{k}} - \mu = -Z + ak_\alpha^2 - bk_\beta^2 , \tag{2}$$

where $\mathbf{k}$ is measured from $(0, \pi)$ ($\alpha = x, \beta = y$) or from $(\pi, 0)$ ($\alpha = y, \beta = x$). Explicit expressions for a and b depend on t, t', ... We consider the following general case: $a \neq 0$, $b \neq 0$, $a \neq b$. We choose $a > b$ corresponding to $t'/t < 0$.

The $T = 0$ ETT has two characteristic aspects. The first (trivial) one is related to the *local change of FS topology* in the vicinity of SP. This leads to divergences in thermodynamic properties, in density of states at $\omega = 0$, etc. From this point of view the corresponding QCP is of a Gaussian-type with the dynamic exponent $z = 2$.

The nontrivial aspect is related to *mutual change* in the topology of FS in vicinities of two different SP's and reveals itself when considering the electron polarizability,

$$\chi^0(\mathbf{q}, \omega) = \frac{1}{N} \sum_{\mathbf{k}} \frac{n^F(\tilde{\epsilon}_{\mathbf{k}}) - n^F(\tilde{\epsilon}_{\mathbf{q}+\mathbf{k}})}{\tilde{\epsilon}_{\mathbf{q}+\mathbf{k}} - \tilde{\epsilon}_{\mathbf{k}} - \omega - i0^+} . \tag{3}$$

We show that the latter has a square-root singularity at

 0031-9007/99/82(11)/2370(4)$15.00

$\omega = 0$ and wave vector $\mathbf{q} = \mathbf{q}_m$ in a vicinity of $\mathbf{Q} = (\pi, \pi)$ *for any* Z *on the semiaxis* $Z < 0$: $\chi^0(\mathbf{q}, 0) - \chi^0(\mathbf{q}_m, 0) \propto \sqrt{|\mathbf{q}_m - \mathbf{q}|}$ for $|\mathbf{q}| > |\mathbf{q}_m|$. It is a static KS in the 2D electron system. The locus of the wave vectors $\mathbf{q}_m$ in the Brillouin zone (BZ) is a closed curve around $\mathbf{Q}$ with $|\mathbf{Q} - \mathbf{q}_m| \propto \sqrt{|Z|}$. With decreasing $|Z|$ the closed curve shrinks and is reduced to the point $\mathbf{q} = \mathbf{Q}$ at $Z = 0$, where $\chi^0(\mathbf{q}, 0)$ diverges logarithmically. The curve of the static KS's with $\mathbf{q}$ close to $\mathbf{Q}$ does not reappear for $Z > 0$: $\chi^0(\mathbf{q}, 0)$ is peaked at $\mathbf{q} = \mathbf{Q}$ in an intimate vicinity of ETT and it exhibits a wide plateau around $\mathbf{q} = \mathbf{Q}$ for larger Z. To illustrate this we show in Fig. 1 the $\mathbf{q}$ dependence of $\chi^0(\mathbf{q}, 0)$ calculated based on (3) and (1). [We use the model with only $t' \neq 0$ being a generic model for the family: $a \neq 0$, $b \neq 0$, $a \neq b$.] The curve discussed above is the curve of singularities in Fig. 1a closest to $\mathbf{q} = \mathbf{Q}$. In the plot, one sees only a quarter of the picture around $\mathbf{q} = \mathbf{Q}$; to see the *closed* curve around (π, π), one has to consider the extended BZ. (Few other curves of KS's seen in Fig. 1 are not sensitive to ETT; we discuss them elsewhere.)

As a result, the point $Z = 0$, $T = 0$ turns out to be the end point of the critical line $Z < 0$, $T = 0$.

Paradoxically, the *absence* of the discussed curve of static KS's for $Z > 0$ leads to an anomalous behavior of the system on this side of QCP. To see this, let us calculate ω dependencies of $\mathrm{Re}\,\chi^0(\mathbf{q}, \omega)$, $\mathrm{Im}\,\chi^0(\mathbf{q}, \omega)$ and $C(\omega) = \mathrm{Im}\,\chi^0(\mathbf{q}, \omega)/\omega$ for the characteristic for this regime wavevector $\mathbf{q} = \mathbf{Q}$. The results are shown in Fig. 2a. One can see that all functions are singular at some energy ω_c. Analytical calculations with the hyperbolic spectrum (2) give the following expression: $\mathrm{Im}\,\chi^0(\mathbf{Q}, \omega) = F(\omega/\omega_c, b/a)/2\pi t$, $\mathrm{Re}\,\chi^0(\mathbf{Q}, \omega) = \mathrm{Re}\,\chi^0(\mathbf{Q}, \omega_c) - \Phi(\omega/\omega_c, b/a)/t$ with

$$F(x, y) = \begin{cases} \ln \dfrac{\sqrt{1+xy}+\sqrt{1+x}}{\sqrt{1-xy}+\sqrt{1-x}}, & 0 \le x \le 1 \\ \ln \dfrac{\sqrt{1+xy}+\sqrt{1+x}}{\sqrt{x(1-y)}}, & x \ge 1 \end{cases},$$

$$\Phi(x, y) = \begin{cases} \gamma_1(y)(1 - x^2), & x - 1 < 0 \\ \gamma_2(y)\sqrt{x - 1}, & 0 \le x - 1 \ll 1 \end{cases} \quad (4)$$

[$\gamma_1(y) \ll 1$]. The *new energy scale* which appears and corresponds to the singularities in Fig. 2a is given by

$$\omega_c = Z(1 + b/a).$$

The singularities at $\omega = \omega_c$ are dynamic 2D KS's.

The dynamic KS's at $T = 0$ transform into static Kohn anomalies at finite temperatures (see Fig. 2b). When comparing with Fig. 2a, one can see that the behavior is similar to being smoothed by the effect of finite T. The important difference is that the characteristic temperatures of the Kohn anomalies for $\mathrm{Re}\,\chi^0(\mathbf{Q}, 0)$ and for $\lim_{\omega \to 0} \mathrm{Im}\,\chi^0(\mathbf{Q}, \omega)/\omega$ being both scaled with Z,

$$T^*_{\mathrm{Re}} = AZ, \qquad T^*_{\mathrm{Im}} = BZ, \qquad A < B,$$

are different; that is a usual effect of finite T.

Another remarkable signature of *asymmetry in* Z is the following. Taken for the characteristic for each regime

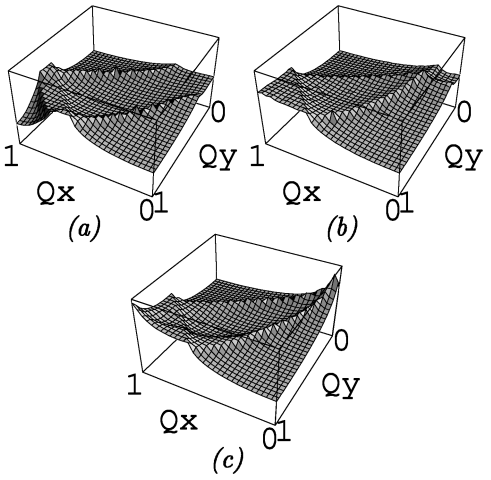

FIG. 1. $\mathbf{q}$ dependence of $\chi^0(\mathbf{q}, 0)$ through the BZ for (a) $Z < 0$, (b) $Z > 0$, (c) $Z = 0$. $Q_x = q_x/\pi$, $Q_y = q_y/\pi$. The point $\mathbf{q} = \mathbf{Q}$ corresponds to the left corner. ($t'/t = -0.3$.)

wave vector, $\mathbf{q} = \mathbf{q}_m$ for $Z < 0$ and $\mathbf{q} = \mathbf{Q}$ for $Z > 0$, $\chi^0(\mathbf{q}, 0)$ decreases rapidly with $|Z|$ for $Z < 0$ while for $Z > 0$ it remains *practically constant* (and quite high) for not too small Z. Moreover, for finite T, $\chi^0(\mathbf{Q}, 0)$ has a maximum at $Z = Z^*(T) > 0$. As a result of the described T and Z dependencies of $\chi^0(\mathbf{Q}, 0)$ in the regime $Z > 0$, the lines $\chi^0(\mathbf{Q}, 0) = \mathrm{const}$ have an unusual form in the $T - Z$ plane: They develop rather around the "critical" lines $T^*_{\mathrm{Re}}(Z)$ and $T^*_{\mathrm{Im}}(Z)$ than around the QCP, $T = 0$, $Z = 0$.

On the contrary, the behavior of SC RF (in both cases isotropic s-wave or d-wave symmetry) is symmetrical in Z being related to the first aspect of ETT. For the same reason, the SC RF decreases quite rapidly with increasing a distance from QCP, i.e., with increasing T and $|Z|$.

Above we considered a system of noninteracting electrons. In fact, the same picture takes place for any system of fermion or fermionlike quasiparticles when the dispersion law is determined by the topology of 2D square

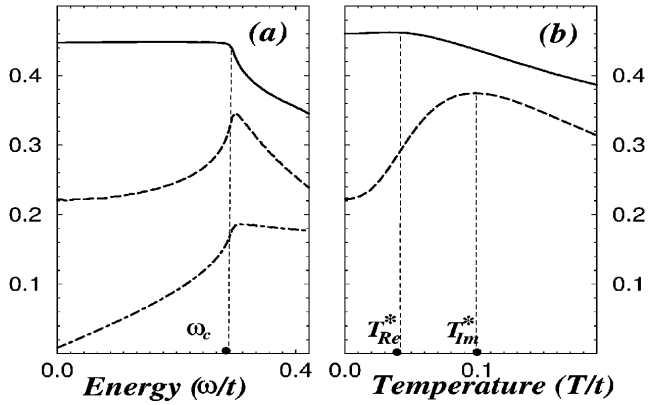

FIG. 2. $\mathrm{Re}\chi^0(\mathbf{Q}, \omega)$ (solid line), $\mathrm{Im}\,\chi^0(\mathbf{Q}, \omega)$ (dot-dashed line), and $C(\omega) = \mathrm{Im}\,\chi^0(\mathbf{Q}, \omega)/\omega$ (dashed line) in the regime $Z > 0$ (a) as a function of ω for $T = 0$ and (b) as a function of T for $\omega \to 0$. Here $t'/t = -0.3$ and $Z/t = 0.21$.

lattice and has a form (1). In [8], where we discuss some problems of strongly correlated systems, we show that such quasiparticles (with spin and charge) do exist in the $t - t' - J$ model describing the strongly correlated CuO_2 plane. On the other hand, the shape of FS observed by ARPES does imply the existence of *nnn* hopping $t' \neq 0$, so that the condition of the asymmetry $a \neq b$ necessary for the existence of the discussed ETT is fulfilled. Moreover, this shape implies $t'/t < 0$, the case for which the critical doping δ_c is positive. Below we will pass from the energy distance from ETT Z to the doping distance $\delta_c - \delta$, using a large FS condition: $1 - \delta = 2\sum_{\mathbf{k}} n^F(\tilde{\epsilon}_{\mathbf{k}})$ [8].

Let us now consider the system in the presence of interaction. A quite trivial consequence of the ETT is a developing of density wave (DW) and SC instabilities around the point $\delta = \delta_c, T = 0$. [The effects are related to the logarithmic divergence of $\chi^0(\mathbf{Q}, 0)$ and $\ln Z \ln T$ divergence of the SC RF as $T \to 0, Z \to 0$.] Nontrivial consequences concerning the DW degrees of freedom and related to the Kohn singularity aspect of ETT are (*i*) strong asymmetry between regimes $\delta < \delta_c$ and $\delta > \delta_c$, and (ii) very long (in doping and temperature) memory about DW instability in the disordered state on one side of ETT, $\delta < \delta_c$. To see this, let us consider the electron-hole RF which in the random-phase approximation is given by $\chi(\mathbf{q}, \omega) = \chi^0(\mathbf{q}, \omega)/[1 + V_{\mathbf{q}}\chi^0(\mathbf{q}, \omega)]$. In the case of interaction $V_{\mathbf{q}}$ in a triplet (singlet) channel the instability and normal state fluctuations are of spin-density wave (SDW) [charge-density wave (CDW)] type. We will consider the former interaction: $V_{\mathbf{q}} = J_{\mathbf{q}} = 2J(\cos q_x + \cos q_y)$ $(J > 0)$ as strongly supported by neutron scattering and NMR experiments for the cuprates and on the other hand, as an interaction between the above discussed quasiparticles in the $t - t' - J$ model [8]. For such interaction both instabilities d-wave SC (see details in [8]) and SDW take place around QCP. Because of the symmetry of SC RF in Z, $T_{SC}(\delta)$ is symmetrical on two sides of δ_c with a maximum at $\delta = \delta_c$ (see Fig. 3). Therefore the regimes $\delta < \delta_c$ and $\delta > \delta_c$ can be considered as underdoped and overdoped, respectively. On the contrary, the line of SDW instability, $T_{SDW}(\delta)$, given by $\chi^0(\mathbf{q}, 0) = -1/J_{\mathbf{q}}$ ($\mathbf{q} = \mathbf{Q}$ for $\delta < \delta_c$ and $\mathbf{q} = \mathbf{q}_m$ for $\delta > \delta_c$) has an anomalous form in the regime $\delta < \delta_c$: It develops rather around the lines $T^*_{\mathrm{Re}}(\delta)$ and $T^*_{\mathrm{Im}}(\delta)$ than around QCP (see Fig. 3), reproducing the form of lines $\chi^0(\mathbf{Q}, 0) = \text{const}$ discussed above.

When, at certain doping, $\delta = \delta_{SDW}$, the ordered SDW solution disappears, it is the disordered metallic state which retains this type of behavior: the regime $T^*_{\mathrm{Re}}(\delta) < T < T^*_{\mathrm{Im}}(\delta)$ (II) turns out to be a regime of a *minimum disorder* and the regime $T < T^*_{\mathrm{Re}}(\delta)$ (I) is a regime of *a reentrant in temperature quantum SDW liquid.* Indeed, the two most important parameters characterizing SDW liquid, $\kappa^2 = 1 - |J_{\mathbf{Q}}|\chi^0(\mathbf{Q}, 0)$ describing a "proximity" to the SDW instability and $\Gamma_{\mathbf{Q}} = \kappa^2/C(0)$ describing a relaxation energy, behave in a reentrant way in increasing

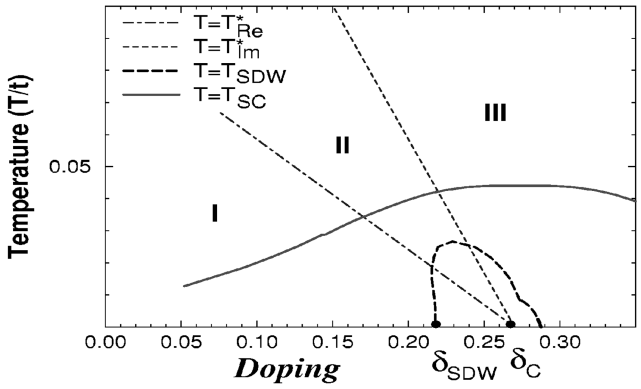

FIG. 3. Phase diagram with the lines of SDW and d-wave SC instabilities and the lines $T^*_{\mathrm{Re}}(\delta)$, $T^*_{\mathrm{Im}}(\delta)$ ($t'/t = -0.3$, $t/J = 1.9$). We consider only the metallic part of the phase diagram (for a discussion about a passage from the AF localized-spin state at low doping to the metallic state with large FS for intermediate doping, see Ref. [8]).

T: κ^2 decreases (slightly) with T until $T^*_{\mathrm{Re}}(\delta)$ and $\Gamma_{\mathbf{Q}}$ decreases (strongly) until $T^*_{\mathrm{Re}}(\delta) < T^*_{\Gamma} < T^*_{\mathrm{Im}}(\delta)$ as if the system would move towards an ordered phase. However, it does not reach it; the reentrancy stops and the system passes to the regime II of a minimum disorder above which a standard disordered state behavior is restored (regime III). On the other hand, the quantum SDW liquid state in the regime I is practically *frozen in doping* due to the very weak dependence of κ^2 on doping. As a result the disordered metal state in the regime $\delta < \delta_c$ keeps a strong memory of the ordered SDW phase (and therefore develops strong critical SDW fluctuations) very far in doping and in temperature. On the contrary, in the regime $\delta > \delta_c$ the memory of SDW instability and the corresponding fluctuations disappear rapidly due to the sharp decrease of $\chi^0(\mathbf{q}, 0)$ with increasing $\delta - \delta_c$ and T. The same is valid in both regimes $\delta > \delta_c$ and $\delta < \delta_c$, for SC fluctuations due to the above discussed behavior of SC RF as a function of T and $|Z|$. Therefore, although the SDW phase itself is energetically unfavorable with respect to the SC phase (except in the case of very high J/t), the metal state above T_{SC} in the underdoped regime is a precursor of the SDW phase rather than of the SC phase.

The lines $T^*_{\mathrm{Re}}(\delta)$ and $T^*_{\mathrm{Im}}(\delta)$ are basic lines for anomalies in the disordered metallic state. To demonstrate how the anomalies appear for different properties we consider some examples. In Fig. 4a we show calculated quasistatic magnetic characteristics corresponding to these measured by NMR $1/T_1T$ and $1/T_{2G}$ on copper as functions of T. The physical reason for a slight increase of $1/T_{2G}$, extending until $\approx T^*_{\mathrm{Re}}$, and a much stronger increase of $1/T_1T$, extending until $T \approx T^*_{\Gamma}$, is the reentrant behavior of κ^2 and $\Gamma_{\mathbf{Q}}$ with T discussed above. The theoretical behavior is very close to that observed experimentally (Fig. 4b) and explains it in fact for the first time.

In Fig. 5 we show an electron spectrum calculated for the ordered SDW phase (a) and for the disordered metal state (namely, for the regime II) (b). For the ordered

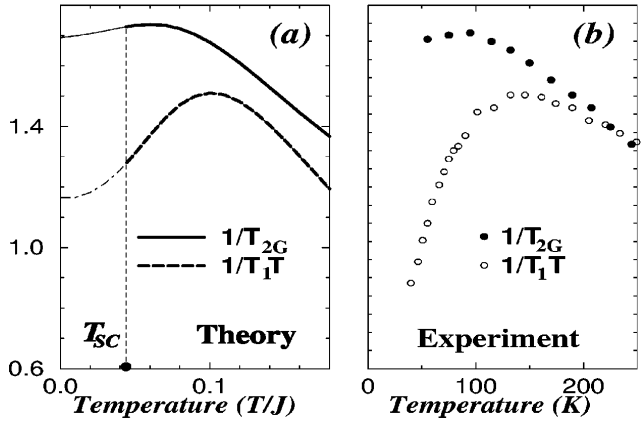

FIG. 4. $1/T_1T$ and $1/T_{2G}$ (a) calculated for $\delta = 0.15$ ($t'/t = -0.3$, $t/J = 1.9$) (should be considered only above T_{SC}) and (b) taken from NMR for $YBCO_{6.6}$ [2].

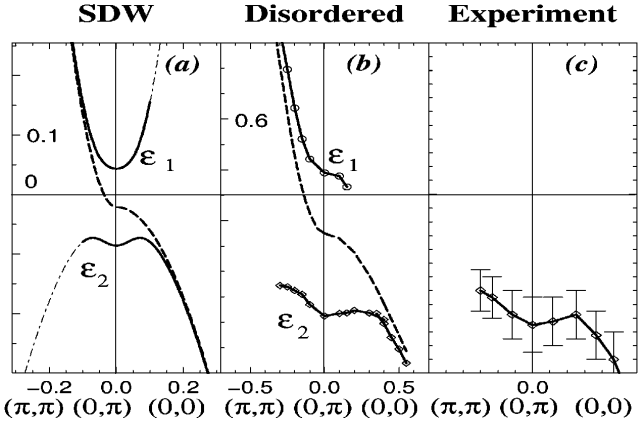

FIG. 5. Electron spectrum $\varepsilon(\mathbf{k})/t$ along Γ-X symmetry lines, (a) in SDW phase [$Z/t = 0.03$ ($\delta = 0.25$), $T = 0$], (b) in the metallic state above T_{SC} [$Z/t = 0.3$ ($\delta = 0.1$), $T/t = 0.15$], (c) ARPES data [10] for underdoped $Bi_2Sr_2CaCu_2O_{8+5}$ above T_{SC}. The dashed lines correspond to the bare spectrum, and the thin line in (a) corresponds to the spectrum with the spectral weight less than 0.1. $t'/t = -0.3$, $t/J = 1.8$; wave vectors are taken in units of π.

phase the spectrum is given by $\varepsilon_{1,2} = (\epsilon_A + \epsilon_B)/2 \pm \sqrt{[(\epsilon_A - \epsilon_B)/2]^2 + \Delta^2}$ [$\epsilon_A(\mathbf{k}) \equiv \epsilon(\mathbf{k}), \epsilon_B(\mathbf{k}) \equiv \epsilon(\mathbf{k} + \mathbf{Q})$] with the gap Δ determined self-consistently in the usual way. For the disordered state the "spectrum" is obtained from the maxima of electron spectral functions strongly renormalized due to the interaction with the above described SDW fluctuations. The characteristic form of the spectrum in both cases is a result of a hybridization of two parts of the bare spectrum in the vicinity of two different SP's $(0, \pi)$ and $(\pi, 0)$. The hybridization is static for the ordered SDW phase and is dynamic for the disordered state. (Details about the pseudogap opening in the disordered state and its behavior with T and δ will be the subject of a separate paper.) The spectrum is in excellent agreement with ARPES data (see Fig. 5c) (ARPES measures only the part corresponding to $\epsilon < 0$). The effect of splitting into two branches, and of the pseudogap, disappears quite rapidly in the regime $\delta > \delta_c$ due to the rapid weakening of SDW fluctuations. It disappears roughly above $T^*_{\mathrm{Im}}(\delta)$ for the same reason. Both facts agree with experiments for the cuprates.

We will now discuss the behavior of $\mathrm{Im}\,\chi(\mathbf{q}, \omega)$, the characteristics measured by inelastic neutron scattering (INS). As follows from the previous analysis, below T^*_{Im} it has a maximum at $\omega = \omega_0 \propto \kappa^2$ (being peaked at $\mathbf{q} = \mathbf{Q}$). Since κ^2 almost does not change with δ, the position of the peak does not as well. This agrees with INS data and explains (for the first time) the existence of the characteristic energy ($\sim$30 MeV) above T_{SC} for all δ; see, e.g., the summarizing picture in Fig. 25 in [11]. As was emphasized before, strong SDW fluctuations disappear in the overdoped regime $\delta > \delta_c$. In the underdoped regime they disappear (or strongly diminish) above $T^*_{\mathrm{Im}}(\delta)$. Both facts are in good agreement with INS.

Summarizing, the simple picture arising from the effect of ETT in a 2D electron system on a square lattice gives a unified vision of normal state anomalies in the underdoped high-T_c cuprates for both magnetic and electronic properties. We succeed in explaining the temperature anomalies in $1/T_1T$ and $1/T_{2G}$ NMR characteristics, some crucial features of INS in the normal state, the disappearance of magnetic fluctuations in the overdoped regime, an opening of a pseudogap in the electron spectrum, the shape of the latter in a vicinity of $(0, \pi)$, and the disappearance of the pseudogap in the overdoped regime. All of these are most nontrivial experimental results. Regarding that the theory does not use any external phenomenological hypothesis and only two microscopical parameters t'/t and t/J, the similarity between the theoretical results and experiments seems quite remarkable. We emphasize that the effect exists for any t'/t, $t''/t, \ldots$, except for two limit cases: (i) isotropic $a = b$ in Eq. (2) ($t' = t'' = \ldots = 0$) and (ii) extreme anisotropic one $a = 0$ or $b = 0$. Although ETT exists in both cases, the corresponding QCP's belong to different classes of universality. For $a = b$ (nesting) the behavior is symmetrical in Z, the anomalous regime discussed in this paper disappears.

[1] H. Alloul *et al.*, Phys. Rev. Lett. **63**, 1700 (1989).
[2] M. Takigawa, Phys. Rev. B **49**, 4158 (1994).
[3] H. Ding *et al.*, Nature (London) **382**, 51 (1996).
[4] S. L. Cooper *et al.*, Phys. Rev. B **40**, 11 358 (1989).
[5] I. M. Lifshitz, Sov. Phys. JETP **11**, 1130 (1960).
[6] J. E. Hirsch *et al.*, Phys. Rev. Lett. **56**, 2732 (1986).
[7] W. Kohn, Phys. Rev. Lett. **2**, 393 (1959).
[8] F. Onufrieva *et al.*, Phys. Rev. B **54**, 12 464 (1996).
[9] A. Virosztek *et al.*, Phys. Rev. B **42**, 4064 (1990).
[10] D. S. Marshall *et al.*, Phys. Rev. Lett. **76**, 4841 (1996).
[11] F. Onufrieva *et al.*, Phys. Rev. B **52**, 7572 (1995).

ELSEVIER

Physica B 284–288 (2000) 677–678

PHYSICA B

www.elsevier.com/locate/physb

Various ordered states in a 2D interacting electron system close to an electronic topological transition

F. Bouis[a,*], M.N. Kiselev[b,1], F. Onufrieva[a], P. Pfeuty[a]

[a]*Laboratoire Léon Brillouin, CE-Saclay, 91191 Gif-sur-Yvette, France*
[b]*Russian Research Center "Kurchatov Institute", 123 182 Moscow, Russia*

Abstract

We consider a 2D electron system on a square lattice with hopping beyond nearest neighbors. The existence of the quantum critical point associated with an electronic topological transition in the noninteracting system results in density wave (DW) and high-temperature d-wave superconducting (dSC) instabilities in the presence of an exchange interaction J. We analyse different DW ordering such as isotropic Spin DW (SDW), d-wave SDW, isotropic Charge DW (CDW) and d-wave CDW. The coexistence of dSC and SDW orders leads necessarily to the existence of a third order which is a π triplet superconducting (PTS) order. A new phase diagram with a mixed phase of SDW, dSC and PTS order is found. The theory is applied to high-T_c cuprates.

PACS: 74.20. − z; 74.72. − h; 75.30.Mb

Keywords: CDW; d-wave superconductivity; SDW

A strong opinion exists in the physical community that the anomalous properties of high-T_c cuprates can reflect the existence of some hidden quantum critical point (QCP). It has been suggested recently [1,2] that such a QCP could be due to an electronic topological transition (ETT) in a 2D system. As was shown, the existence of this QCP results in DW and dSC instabilities of the normal state. In the present paper we study DW states of different natures and the mixed state with both DW and dSC ordering.

The starting point is a 2D model of interacting fermions on a square lattice with hopping between nearest (t) and next nearest (t') neighbors (while $t'/t < 0$ which corresponds to the situation experimentally observed [3])

$$H = \sum_{\boldsymbol{k}} \varepsilon_{\boldsymbol{k}} c^{+}_{\boldsymbol{k}\sigma} c_{\boldsymbol{k}\sigma} + \sum_{i} U n_{i\uparrow} n_{i\downarrow} + \sum_{\langle i,j \rangle} \left[J^{z} \boldsymbol{S}^{z}_{i} \boldsymbol{S}^{z}_{j} + J^{\perp} \boldsymbol{S}^{+}_{i} \boldsymbol{S}^{-}_{j} + \frac{b}{4} n_i n_j \right], \quad (1)$$

where $n_i = n_{i\uparrow} + n_{i\downarrow}$ ($n_{i\sigma} = c^{+}_{i\sigma} c_{i\sigma}$) and $\boldsymbol{S}_i = c^{+}_{i\alpha} \sigma_{\alpha\beta} c_{i\beta}$ are the charge and spin densities. The Fermi surface (FS) of noninteracting quasiparticles with the dispersion law $\varepsilon_{\boldsymbol{k}} = -2t(\cos k_x + \cos k_y) - 4t' \cos k_x \cos k_y$ changes from closed to open at the critical doping x_c resulting in the 2D ETT which is at the origin of two types of instabilities: dSC and DW. Calculations show that the superconducting temperature is highest at x_c, thus the regimes $x < x_c$ and $x > x_c$ could be seen, respectively, as underdoped and overdoped. The shape of the FS in the underdoped regime favors the DW instabilities with the antiferromagnetic wave vector $\boldsymbol{Q} = (\pi, \pi)$. The DW order parameter is $\psi_{\boldsymbol{k}} = \langle c^{+}_{\boldsymbol{k}+\boldsymbol{Q}\uparrow} c_{\boldsymbol{k}\uparrow} \pm c^{+}_{\boldsymbol{k}+\boldsymbol{Q}\downarrow} c_{\boldsymbol{k}\downarrow} \rangle$. On the one hand, it could be of the spin (−) or charge (+) type and on the other, it could be isotropic or have a certain dependence on $\boldsymbol{k}$. The $\boldsymbol{k}$-dependent case corresponds to the so-called unconventional DW order which was considered for example in Ref. [4] (see also Ref. [5]). Below, we consider four different types of DW order: isotropic spin or charge density wave (SDW or CDW), d-wave spin or charge density wave (dSDW or dCDW). For all of them the spectrum is given by

$$E^{\pm}_{\boldsymbol{k}} = \frac{\varepsilon_{\boldsymbol{k}} + \varepsilon_{\boldsymbol{k}+\boldsymbol{Q}}}{2} \pm \sqrt{\left(\frac{\varepsilon_{\boldsymbol{k}} - \varepsilon_{\boldsymbol{k}+\boldsymbol{Q}}}{2} \right)^2 + \Delta^2_{\boldsymbol{k}}} \quad (2)$$

* Corresponding author. Tel.: + 33-1-69-089685; fax: + 33-1-69-088261.

E-mail address: bouis@llb.saclay.cea.fr (F. Bouis)

[1] Present address: Institut für Theoret. Physik, Univ. Würzburg, D-97074 Würzburg, Germany.

0921-4526/00/$ - see front matter
PII: S0921-4526(99)02355-8

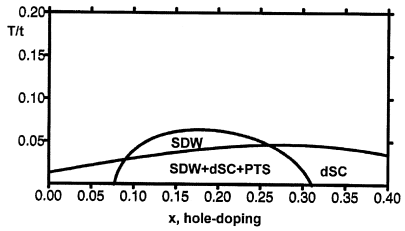

Fig. 1. Phase diagram for $t/J = 1.5$ and $t'/t = -0.3$. T is the temperature. The ordered SDW phase starting from the QCP at $x = x_c$ develops toward the underdoped region. Its size increases with increasing J and eventually leans out the superconducting phase as in this figure. SDW and dSC result in a mixed phase where PTS order is also present.

with $\Delta_k = \Delta_0$ for SDW and CDW orders, and $\Delta_k = \Delta_0[\cos k_x - \cos k_y]$ for dSDW and dCDW orders. The effective coupling constants are given respectively, by

$$g_{\mathrm{SDW}} = 2U + 2J^z, \quad g_{\mathrm{dSDW}} = b + J^z - 2J^\perp,$$

$$g_{\mathrm{CDW}} = -2U + 2b, \quad g_{\mathrm{dCDW}} = b + J^z + 2J^\perp.$$

In the case of the t–J model ($J^z = J^\perp = -b$ and $U = 0$) which we use below to describe the high-T_c cuprates, only two instabilities, dCDW and SDW, are possible, being determined by equal effective constants, $g_{\mathrm{SDW}} = g_{\mathrm{dCDW}}$.

On the second stage we write a set of coupled equations for different order parameters. We show that the mixed state with both SC and DW order parameters is favorable in the underdoped regime at low temperature (see Fig. 1). Moreover, the coexistence of DW and dSC order parameters results in the appearance of a third ordering. In the case when DW order is of the isotropic SDW type[2] this third order parameter (π triplet superconducting [6,7] (PTS) one) is related to the π operator introduced in the framework of the SO(5) theory which creates triplet Cooper pairs with total momentum $\boldsymbol{Q}$. The resulting phase diagram is shown in Fig. 1 for the t–J model with realistic parameters for high-T_c cuprates.

Notice that the pure DW order develops in the region where the pseudogap behavior in the normal state is experimentally observed, see e.g. Ref. [3]. The admixture of SDW order in the dSC state could be responsible for the anomalous spin dynamics observed by neutron scattering inside the superconducting phase. If the dSC order is suppressed, the underdoped regime could be insulating due to the DW order while the overdoped one will remain metallic in good agreement with experiment [8] where superconductivity is suppressed by a pulsed magnetic field.

References

[1] F. Onufrieva et al., Phys. Rev. Lett. 82 (1999) 2370.
[2] F. Onufrieva, P. Pfeuty, Phys. Rev. B 61 (2000) 799.
[3] D.S. Marshall et al., Phys. Rev. Lett. 76 (1996) 4841.
[4] H. Ikeda, Y. Ohashi, Phys. Rev. Lett. 81 (1998) 3723.
[5] M. Kiselev, F. Bouis, Phys. Rev. Lett. 82 (1999) 5172.
[6] E. Demler et al., Phys. Rev. Lett. 75 (1995) 4126.
[7] M. Murakami et al., J. Phys. Soc. Japan 67 (1998) 41.
[8] G.S. Boebinger et al., Phys. Rev. Lett. 77 (1996) 5417.

[2] The interplay of dSC, dCDW and the resulting third order belongs to another class of symmetry.

Eur. Phys. J. B **16**, 601–611 (2000)

THE EUROPEAN PHYSICAL JOURNAL B

EDP Sciences

Some consequences of electronic topological transition in 2D system on a square lattice: Excitonic ordered states

M. Kiselev[1,2,a], F. Bouis[1], F. Onufrieva[1], and P. Pfeuty[1]

[1] Laboratoire Léon Brillouin, CE-Saclay, 91191 Gif-sur-Yvette, France
[2] Russian Research Center "Kurchatov Institute", 123 182 Moscow, Russia

Received 9 June 1999

Abstract. We study in a mean-field approximation the ordered "excitonic" states which develop around the quantum critical point (QCP) associated with the electronic topological transition (ETT) in a 2D electron system on a square lattice. We consider the case of hopping beyond nearest neighbors when ETT has an unusual character. We show that the amplitude of the order parameter (OP) and of the gap in the electron spectrum increase with increasing the distance from the QCP, $\delta_c - \delta$, where $\delta = 1 - n$ and n is an electron concentration. Such a behavior is different from the ordinary case when OP and the gap decrease when going away from the point which is a motor for instability. We show that the chemical potential lies always inside the gap for wavevectors $\mathbf{k}$ in a proximity of $(0, \pi)$ whatever is the doping concentration. The spectrum gets a characteristic flat shape as a result of hybridization effect in the vicinity of two different SP's. The shape of the spectrum as a function of $\mathbf{k}$ and the angle dependence of the gap have a striking similarity with the features observed in the normal state of the underdoped high-T_c cuprates. We discuss also details about the phase diagram and the behaviour of the density of states.

PACS. 74.25.-q General properties; correlations between physical properties in normal and superconducting states – 74.72.-h High-T_c compounds – 74.25.Dw Superconductivity phase diagrams – 74.25.Ha Magnetic properties

Many experiments performed for high T_c cuprates provide an evidence for the existence of a pseudogap in the underdoped regime above T_c and below some temperature $T^*(\delta)$ which value increases with increasing the doping distance from the optimal doping, $\delta_{opt} - \delta$ [1–8]. The pseudogap is observed directly by angle-resolved photoemission spectroscopy (ARPES) measurements [9–13]. The striking about this gap is its increase with increasing $\delta_{opt} - \delta$ [12] while the critical temperature of superconducting (SC) transition, T_{sc}, decreases. Another prominent feature is the so-called $(\pi, 0)$ feature discovered by ARPES: the electron spectrum around the saddle-point (SP) is flat and disappears above some threshold value of wavevector [9]. Several hypotheses exist about possible origin of the pseudogap [14–17]. In this paper we present another explanation of this phenomenon in the framework of the model developed in [18–20]. In these works the concept of the Electronic Topological Transition in 2D system is developed and applied for the explanation of various effects experimentally observed in high-T_c cuprates.

In the present paper we consider various ordered states appearing in the vicinity of ETT point in the presence of interaction. We show that the ordered "excitonic" phase formed in a proximity of quantum critical point QCP corresponding to ETT[1] is characterized by the electron spectrum strikingly similar to that observed in the underdoped cuprates. The mentioned ETT corresponds to the electron concentration $n_c = 1 - \delta_c$ at which Fermi level (FL) crosses saddle point (SP) energy in the bare spectrum. As shown in [19], in the case of hopping between more than nearest neighbors (or, by other words of electron-hole asymmetry) the existence of the ETT QCP leads to a very asymmetric behaviour of the noninteracting and interacting system on two sides of ETT being quite anomalous on the side $\delta < \delta_c$. On the other hand, for realistic for the high-T_c cuprates ratios of hopping parameters between nearest and next nearest neighbors t'/t, δ_c is given by: $\delta_c = 0.27$ for $t'/t = -0.3$ and $\delta_c = 0.17$ for $t'/t = -0.2$, *i.e.* the anomalous regime $\delta < \delta_c$ occurs in the doping range where the experimentally observed normal metal anomalies take place. Moreover, $\delta = \delta_c$ corresponds to a maximum of $T_{sc}(\delta)$ (as discussed in [19]) and therefore the latter regime can be considered as an underdoped regime.

[a] *Present address*: Institüt für Theoretische Physik, Universität Würzburg, 97074 Würzburg, Germany
e-mail: kiselev@physik.uni-wuerzburg.de

[1] It has been shown in [19] that the ETT point is an isolated QCP. The properties of this QCP have been studied in detail in [19].

Some anomalies concerning the ordered "excitonic" phase have been discussed in [18]. Namely, it was shown that the line of the "excitonic" instability grows from the ETT QCP to the side $\delta < \delta_c$ instead of having the form of a bell around the QCP as it usually happens for an ordinary QCP. Other anomalies which exist in the ordered phase are considered in the present paper. (We call this phase "excitonic" ordered phase because the discussed instability has the same origin as the classical "excitonic" instability intensively discussed in the 60-70 [21–26]. Namely it is related to the opposite curvature of two parts of electron spectrum in a proximity of FL. In the case considered they correspond to spectra in vicinities of two SP's.)

We consider various possibilities for the ordered state, namely, Spin and Charge Density Wave orderings with different types of the order parameter symmetries (s-wave, d-wave) depending on the effective interaction between the quasiparticles. Despite of the different symmetries, the properties of such ordered states resembling an "excitonic" states [21–26] are quite similar. For example we show that the electron spectrum in the ordered phase is characterized by a gap on FL for wavevectors belonging to some part of Brillouin zone which always covers the SP wavevectors $(0, \pi)$, $(\pi, 0)$ whatever is the doping concentration. This remarkable feature is related, as we show in the paper, to a quite nontrivial aspect of ETT: it is the end point of two critical lines for the "polarization operator" characterizing a behaviour of the free electron system. The other side of the same effect is an increase of the amplitude of the order parameter (and of the gap) with increasing the doping distance from QCP on the underdoped side. We show also that the electron spectrum in a vicinity of SP wavevectors gets a specific "flat" form as a function of $\mathbf{k}$ that on one hand is typical for an "excitonic" phase (see for example [24]) being a result of a hybridization of two parts of the bare spectrum with the opposite curvature and on the other hand has a striking similarity with the form of the spectrum observed by ARPES [9–13]. We show that the spectrum "disappears" above some threshold value of wavevector in the direction $(\pi, 0) - (\pi, \pi)$ that is also an effect of the same hybridization. We briefly discuss also features related to strong-coupling limit of the model and effects of strong electron correlations.

A starting point is a 2D system of free fermions on a square lattice with hopping between nearest (t) and next nearest (t') neighbors

$$\epsilon_{\mathbf{k}} = -2t(\cos k_x + \cos k_y) - 4t' \cos k_x \cos k_y. \quad (1)$$

The dispersion law (1) is characterized by two different saddle points (SP's) located at $(\pm\ \pi, 0)$ and $(0, \pm\pi)$ (in the first Brillouin zone $(-\pi, 0)$ is equivalent to $(\pi, 0)$ and $(0, -\pi)$ is equivalent to $(0, \pi)$) with the energy $\epsilon_s = 4t'$. When we vary the chemical potential μ or the energy distance from the SP, Z, determined as

$$Z = \mu - \epsilon_s = \epsilon_{\mathrm{F}} - 4t', \quad (2)$$

the topology of the Fermi surface changes when Z goes from $Z < 0$ to $Z > 0$ through the critical value $Z = 0$, see Figure 1. For $t'/t \neq 0$ which is the case of our interest,

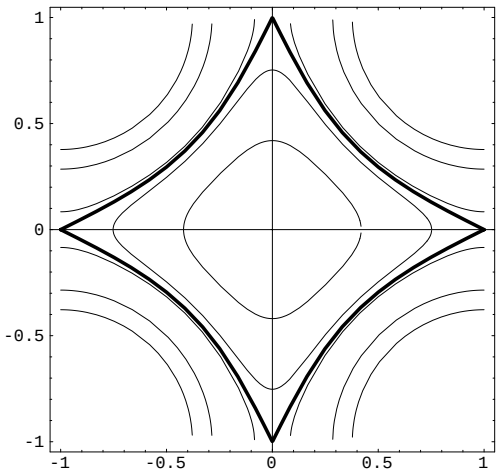

Fig. 1. Fermi surface of the electron system with the dispersion law (1) for different Z and $t'/t = -0.3$. The thick line stands for $Z = 0$. Open and close FS correspond to $Z > 0$ and $Z < 0$ respectively.

the FS does not satisfy the perfect nesting condition [27] and has a different shape for different signs of t'/t. In our paper we discuss $t'/t < 0$ that corresponds to proper fit of ARPES experimental data. The FS's corresponding to $Z > 0$ and $Z < 0$ are shown in Figure 1.

According to Figure 1, the FS can be classified as follows. For arbitrary filling factor (depending on dopings), the FS can have either 8 points which can be connected by vector $Q = (\pm\pi, \pm\pi)$ (see Fig. 1), or 4 points, or do not have any such a point. These points are called "hot spots" (HS) (see [17]). The 8 hot spots are the intersection points between the Fermi Surface (FS) and the umklapp surface (US) $k_x \pm k_y = \pm\pi$. The two quantum critical points QCP1 and QCP2 correspond to critical hole dopings δ_{c1} and δ_{c2}. For $\delta_{c2} < \delta < \delta_{c1}$ there are 8 hot spots. When $\delta \to \delta_{c1}$ they become 4 hot spots located at the 4 saddle points ($k_x = \pm\pi, k_y = 0$ and $k_y = \pm\pi, k_x = 0$), then for $\delta > \delta_{c1}$ they disappear. When $\delta \to \delta_{c2}$ they coincide with the 4 points located at the FS along the diagonals $k_x = \pm k_y$; for $\delta < \delta_{c2}$ they disappear.

It has been shown in [19] that such a system undergoes a fundamental ETT at the electron concentration corresponding to $Z = 0$. The corresponding quantum critical point is quite rich. It combines several aspects of criticality. The first standard one is related to singularities in thermodynamic properties, in density of states at $\omega = 0$ (Van Hove singularity), to additional singularity in the superconducting (SC) response function, all reflect a local change in the topology of FS. This aspect is not important for the properties we are interested in the present paper. Important aspects which reflect a mutual change in the topology of FS in the vicinities of two SP's are the following. First of all, it is a logarithmic divergence of the polarizability of noninteracting electrons

$$\chi^0(\mathbf{k}, \omega) = \frac{1}{N} \sum_{\mathbf{q}} \frac{n^{\mathrm{F}}(\tilde{\epsilon}_{\mathbf{q}}) - n^{\mathrm{F}}(\tilde{\epsilon}_{\mathbf{q}+\mathbf{k}})}{\tilde{\epsilon}_{\mathbf{q}+\mathbf{k}} - \tilde{\epsilon}_{\mathbf{q}} - \omega - \mathrm{i}0^+}, \quad (3)$$

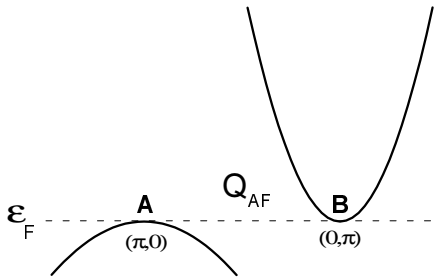

Fig. 2. Schematic presentation of the electron spectrum in a vicinity of two SP's for $Z = 0$

as $\mathbf{k} = \mathbf{Q} = (\pi, \pi)$, $\omega = 0$ and $Z \to 0$:

$$\chi^0(\mathbf{Q}, 0) \propto \ln \frac{\omega_{\max}}{|Z|}, \tag{4}$$

which has an "excitonic" origin ($\omega_{\max} \sim t$ is a cutoff energy). By "excitonic" origin we mean that two branches of the spectrum corresponding to vicinities of two SP's ($a = t - 2t'$, $\quad b = t + 2t'$)

$$\tilde{\epsilon}_1(\mathbf{k}) = \epsilon_1(\mathbf{k}) - \mu = -Z + ak_x^2 - bk_y^2,$$

$$\tilde{\epsilon}_2(\mathbf{k}) = \epsilon_2(\mathbf{k}) - \mu = -Z + ak_y^2 - bk_x^2 \tag{5}$$

have such a form (see Fig. 2) that at $Z = 0$ the chemical potential lies on the bottom of one "band" and on the top of the another for the given directions $(0, \pi) - (\pi, \pi)$ and $(\pi, 0) - (0, 0)$, (see Fig. 2). Therefore, no energy is needed to excite the electron-hole pair. It is this divergence that is at the origin of density wave (DW) instability. The DW instability can be of Spin Density Wave (SDW), Charge Density Wave (CDW), Spin Current Density Wave (SCDW) or Orbital Current Density Wave (OCDW) instability [28]) of interacting electron system depending on a nature of interaction.

The nontriviality stems from the aspect of criticality related to the effect of Kohn singularity in 2D system: the point $Z = 0$, $T = 0$ is the end of the critical line $Z < 0$ each point of which is a point of static Kohn singularities in polarizability of noninteracting electrons. As shown in [19], the latter aspect is a motor for the anomalous behaviour of the system on the other side of ETT $Z > 0$. One among the anomalies found in [19] concerns the ordered DW phases. We have obtained that the line of DW "excitonic" instability $T_{\rm DW}(Z)$ has the anomalous form on the side $Z > 0$: it grows from QCP instead of having the form of a bell around QCP as it usually happens in the case of ordinary QCP. Below we show that this latter aspect is also at the origin of anomalous behaviour of the order parameter and of some other anomalies in the ordered state in the same regime $Z > 0$.

As shown in [19], on the side $Z > 0$ of the electronic topological transition point, a maximum of the static electron-hole susceptibility occurs at the wavevector $\mathbf{q} = \mathbf{Q}$. Therefore in a presence of $\mathbf{q}$ independent interaction or $\mathbf{q}$ dependent interaction negative for $\mathbf{q} = \mathbf{Q}$, the DW instability happens at $\mathbf{q} = \mathbf{Q}$ and this is the wavevector of ordering in the DW phase. As usual for such phases, one should consider a matrix electron Green function containing as components the normal and anomalous Green functions in terms of operators $a^+_{\mathbf{k},\sigma}$ and $a_{\mathbf{k}\sigma}$ which are the creation and annihilation electron's operators respectively:

$$K_{11}(\mathbf{k}, \mathrm{i}\omega_n) = -\int_0^\beta \mathrm{d}\tau\, \mathrm{e}^{\mathrm{i}\omega_n \tau} \langle T_\tau a_{\mathbf{k}\sigma}(\tau) | a^+_{\mathbf{k}\sigma}(0) \rangle$$

$$K_{22}(\mathbf{k}, \mathrm{i}\omega_n) = -\int_0^\beta \mathrm{d}\tau\, \mathrm{e}^{\mathrm{i}\omega_n \tau} \langle T_\tau a_{\mathbf{k}+\mathbf{Q}\sigma}(\tau) | a^+_{\mathbf{k}+\mathbf{Q}\sigma}(0) \rangle$$

$$K^{\sigma\sigma'}_{12}(\mathbf{k}, \mathrm{i}\omega_n) = -\int_0^\beta \mathrm{d}\tau\, \mathrm{e}^{\mathrm{i}\omega_n \tau} \langle T_\tau a_{\mathbf{k}+\mathbf{Q}\sigma}(\tau) | a^+_{\mathbf{k}\sigma'}(0) \rangle. \tag{6}$$

(Below we will omit spin indices in the Green functions keeping in mind that $K_{12} = K^{\sigma,-\sigma}_{12}$ for CDW and OCDW states and $K_{12} = K^{\sigma\sigma}_{12}$ for SDW and SCDW states.)

If the anomalous Green function K_{12} is nonzero (that should be found selfconsistently) the explicit expressions for the two Green functions are as follows

$$K_{11}(\mathbf{k}, \mathrm{i}\omega_n) = \left[\frac{u^2(\mathbf{k})}{\mathrm{i}\omega_n - \varepsilon_1} + \frac{v^2(\mathbf{k})}{\mathrm{i}\omega_n - \varepsilon_2} \right],$$

$$K_{22}(\mathbf{k}, \mathrm{i}\omega_n) = \left[\frac{u^2(\mathbf{k})}{\mathrm{i}\omega_n - \varepsilon_2} + \frac{v^2(\mathbf{k})}{\mathrm{i}\omega_n - \varepsilon_1} \right],$$

$$K_{12}(\mathbf{k}, \mathrm{i}\omega_n) = K_{21}(\mathbf{k}, \mathrm{i}\omega_n) = u(\mathbf{k})v(\mathbf{k}) \left[\frac{1}{\mathrm{i}\omega_n - \varepsilon_1} - \frac{1}{\mathrm{i}\omega_n - \varepsilon_2} \right], \tag{7}$$

where u, v-coefficients have a standard form:

$$u^2(\mathbf{k}) = \frac{1}{2} \left[1 + \frac{\epsilon_{\rm A}(k) - \epsilon_{\rm B}(k)}{2E(\mathbf{k})} \right],$$

$$v^2(\mathbf{k}) = \frac{1}{2} \left[1 - \frac{\epsilon_{\rm A}(k) - \epsilon_{\rm B}(k)}{2E(\mathbf{k})} \right],$$

$$E(\mathbf{k}) = \sqrt{\left(\frac{\epsilon_{\rm A} - \epsilon_{\rm B}}{2} \right)^2 + |\Delta(\mathbf{k})|^2}. \tag{8}$$

The spectrum in the ordered state is given by

$$\varepsilon_{1,2} = \frac{\epsilon_{\rm A} + \epsilon_{\rm B}}{2} \pm \sqrt{\left(\frac{\epsilon_{\rm A} - \epsilon_{\rm B}}{2} \right)^2 + |\Delta(\mathbf{k})|^2},$$

$$\epsilon_{\rm A}(\mathbf{k}) \equiv \epsilon(\mathbf{k}) \qquad \epsilon_{\rm B}(\mathbf{k}) = \epsilon(\mathbf{k} + \mathbf{Q}), \tag{9}$$

where $\epsilon(\mathbf{k})$ is defined by (1). The equation for the gap is

$$\Delta(\mathbf{k}) = -T \sum_{\omega_n} \frac{1}{N} \sum_{\mathbf{p}} \Gamma_{12}(\mathbf{k}, \mathbf{k} + \mathbf{Q}, \mathbf{p}) K_{12}(\mathbf{p}, \mathrm{i}\omega_n) \tag{10}$$

where Γ_{12} is a vertex which in mean field approximation coincides with the bare interaction:

$$\Gamma_{12}(\mathbf{k},\mathbf{k}+\mathbf{Q},\mathbf{p}) = V_{\mathbf{Q}}, \quad \text{for SDW (CDW)}$$
$$\Gamma_{12}(\mathbf{k},\mathbf{k}+\mathbf{Q},\mathbf{p}) = V_{\mathbf{k}-\mathbf{p}}, \text{ for OCDW (SCDW)} \quad (11)$$

where $V_{\mathbf{k}} = 2V(\cos(k_x)+\cos(k_y))$. The type of the interaction and therefore, type of the excitonic phase depend on the model. The SDW and OCDW instabilities occur in the case of a positive interaction in the triplet channel (exchange interaction), the CDW and SCDW instabilities take place for positive interaction in the singlet channel (density-density interaction). We will not fix for the moment a type of interaction and therefore a nature of the ordered phase assuming that there exists either the first or the second interaction.

The equation (10) is reduced to the following equation

$$1 = 4|V|\Pi^{\mathrm{DW}}_{\mathbf{k}=\mathbf{0}}(\mathbf{Q},Z,\Delta) \quad (12)$$

where the "polarization operators" $\Pi^{\mathrm{DW}}(\mathbf{Q},Z,\Delta)$ are given by one of the following equations [30]:

$$\Pi^{\mathrm{SDW,CDW}}(\mathbf{Q},Z,\Delta) = \frac{1}{4N}\sum_p \frac{1}{E(\mathbf{p})}\left[\tanh\left(\frac{\varepsilon_1}{2T}\right) - \tanh\left(\frac{\varepsilon_2}{2T}\right)\right]. \quad (13)$$

$$\Pi^{\mathrm{OCDW,SCDW}}(\mathbf{Q},Z,\Delta) = \frac{1}{4N}\sum_p \frac{(\cos p_x - \cos p_y)^2}{4E(\mathbf{p})}\left[\tanh\left(\frac{\varepsilon_1}{2T}\right) - \tanh\left(\frac{\varepsilon_2}{2T}\right)\right]. \quad (14)$$

The expressions (12) are the equation for the SDW, CDW, OCDW or SCDW gap which should be solved selfconsistently. We emphasis that for $V > 0$ only SDW (OCDW) solution is possible whereas CDW (SCDW) solution takes place for $V < 0$.

The solution of (12–14) is given by one of the following expressions

$$\Delta = \Delta^{\mathrm{SDW}}(\mathbf{k}) = \Delta_0^{\mathrm{SDW}},$$
$$\Delta = \Delta^{\mathrm{CDW}}(\mathbf{k}) = \Delta_0^{\mathrm{CDW}},$$
$$\Delta = \Delta^{\mathrm{OCDW}}(\mathbf{k}) = \Delta_0^{\mathrm{OCDW}}(\cos k_x - \cos k_y)/2,$$
$$\Delta = \Delta^{\mathrm{SCDW}}(\mathbf{k}) = \Delta_0^{\mathrm{SCDW}}(\cos k_x - \cos k_y)/2. \quad (15)$$

The equations (10–15) are quite standard. A nontriviality, as we show below, is related to the behaviour of the "polarization operator" in a proximity of ETT. As we have shown in [19], the effect that the point of ETT is the end point of the critical line $Z < 0$ leads to the anomalous behaviour of the electron-hole susceptibility $\chi^0(\mathbf{Q},Z,\omega)$ on the side $Z > 0$. Below we show that a similar effect takes place for the "polarization operator" (14). The two functions coincides in the limit cases: $\chi^0(\mathbf{Q},Z,\omega=0) = \Pi^{\mathrm{DW}}(\mathbf{Q},Z,\Delta=0)$. (It is important to emphasize that the behaviour of the "polarization operator" depends only on properties of the system of noninteracting electrons, namely on the topology of FS.)

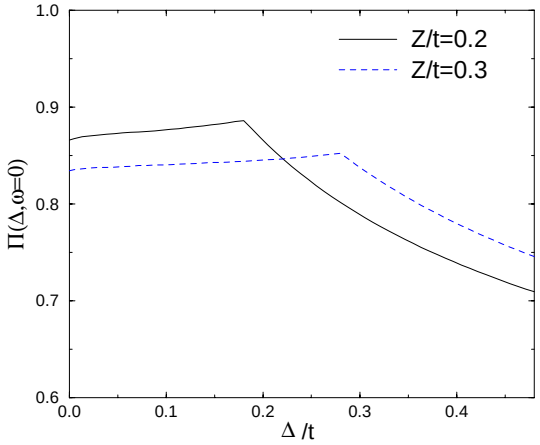

Fig. 3. Calculated "polarization operator" $\Pi(\mathbf{Q},Z,\Delta(Q))$ as a function of Δ_0 for fixed Z and $T = 0$.

Calculated for $T = 0$ "polarization operators" $\Pi^{\mathrm{DW}}(\mathbf{Q},Z,\Delta_0)$ as a function of Δ_0 for fixed Z (in the regime $Z > 0$) are shown in Figure 3. Since the properties of the "polarization operators" are similar in many aspects we shall omit later the indices (SDW, CDW, OCDW or SCDW) except for the cases when it will be necessary to emphasize the difference.

One can see that there is a singularity at some point $\Delta_0 = \Delta_{\mathrm{c}}(Z)$. The value of $\Delta_{\mathrm{c}}(Z)$ increases with increasing Z. The situation is quite similar to that analyzed in [19] for χ^0 as a function of ω for fixed Z and $T = 0$. In the latter case we have found a square-root singularity at

$$\omega = \omega_{\mathrm{c}} = \frac{2Z}{1-2t'/t},$$

which is the dynamic Kohn singularity. As we see in Figure 3, for the polarization operator $\Pi(\mathbf{Q},Z,\Delta)$ the singularity is weaker, while $\Delta_{\mathrm{c}}(Z)$ also scales with Z.

Analytical estimations show that $\Delta_{\mathrm{c}}(Z)$ is given by

$$\Delta_{\mathrm{c}}(Z) = Z \quad (16)$$

while the asymptotic form of $\Pi(\mathbf{Q},Z,\Delta)$ near the singularity is given by:

$$t\Pi(\mathbf{Q},Z,\Delta) = \begin{cases} A_1|1-\Delta/\Delta_{\mathrm{c}}| + B, & \Delta < \Delta_{\mathrm{c}} \\ A_2|1-\Delta/\Delta_{\mathrm{c}}| + B, & \Delta > \Delta_{\mathrm{c}}. \end{cases} \quad (17)$$

The jump in the derivative, $A_1 - A_2$, depends only on t'/t [31] and is proportional to

$$A_1 - A_2 \propto \frac{1}{|t'/t|}\left(\ln\left|\frac{4}{t'/t}\right| - A_0\right), \quad (18)$$

where A_0 is a constant (for the spectrum (5) $A_0 = \pi/8$). The critical line (16) is clearly seen in Figure 4 where we present the calculated $\Pi(\mathbf{Q},Z,\Delta_0)$ as a function of Z and Δ_0. From the point of view of the behaviour

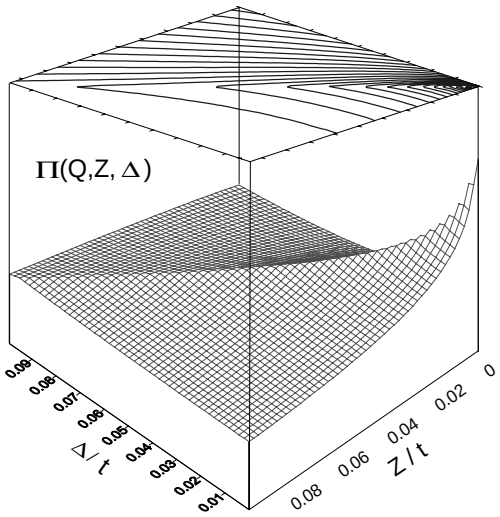

Fig. 4. $\Pi(\mathbf{Q}, Z, \Delta_0)$ as a function of Δ_0 and Z at $T = 0$ and lines $\Pi^{zz}(\mathbf{Q}) = \text{const}$ in $Z - \Delta_0$ coordinates.

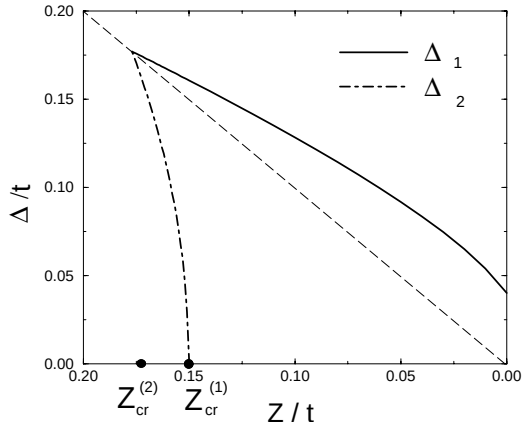

Fig. 5. Gap Δ obtained by solving equations (12), (14) as function of Z (t/V=1.8, $t'/t = -0.3$). The solid line corresponds to $\Delta_1(Z)$, the dot-dashed line to $\Delta_2(Z)$, the dashed line to $\Delta_c(Z)$.

of the "polarization operator", the ETT point is the end point of two critical lines. The first is the semi-axis $Z < 0$ each point of which corresponds to the square-root singularity in $\Pi(\mathbf{q}, Z, \Delta)$ occurring as $\Delta_0 \to 0$ and $\mathbf{q} \to \mathbf{q}_m$, where the latter is the characteristic for this regime wavevector of incommensurability (see [19] where the $\mathbf{q}$ dependence of $\Pi(\mathbf{q}, Z, 0) = \chi^0(\mathbf{q}, Z)$ is analyzed in details.) The second is the line $Z = \Delta_0$ each point of which corresponds to the kink in $\Pi(\mathbf{q}, Z, \Delta(q))$ occurring at $T = 0$ as $\mathbf{q} \to \mathbf{Q}$ where the latter is the characteristic wavevector for the regime $Z > 0$. At the point of intersection of these lines, $Z = 0$, the two types of singularities are transforming into the logarithmic singularity; $\Pi(\mathbf{q}, 0, \Delta) \propto \ln|\max(\mathbf{q} - \mathbf{Q}, \Delta)|$.

The existence of the critical line growing with increasing Z determines a quite unusual form of the lines $\Pi(\mathbf{Q}, Z, \Delta) = \text{const}$ which develop around the critical line $\Delta_c(Z)$ and grow with increasing Z (see the contour plot Fig. 4).

In preceding discussion we presented some general analysis which does not depend on details of interaction considered but only on the topology of the FS. To provide the calculations, let us consider a particular case of interaction resulting in spin density wave (11, 13). The solution of corresponding equation (12) for $t/V = 1.8$ is shown in Figure 5. Two branches of the solution have an anomalous dependence of the gap on Z reproducing the form of the lines $\Pi(\mathbf{Q}, Z, \Delta_0) = \text{const}$ in the contour plot in Figure 4. The anomaly is that for both solutions gap increases with increasing the distance from the quantum critical point, *i.e.* from the point which is at the origin of the ordered phase. (For an ordinary QCP the gap is maximum at the electron concentration corresponding to QCP and decreases monotonously with increasing the distance from QCP. For example such a picture takes place for DW phase on both sides from QCP in the case of $t' = t'' = ... = 0$; as we discussed in [19] in the latter case all anomalies in the regime $\delta < \delta_c$ disappear. In the case considered in the paper it happens on the overdoped side of the QCP.)

The difference between two solutions for the gap presented in Figure 5 is that

$$\Delta_1(Z) > Z \tag{19}$$

while

$$\Delta_2(Z) < Z \tag{20}$$

for any Z, any t/V, any t'/t since the two lines, $\Delta_1(Z)$ and $\Delta_2(Z)$ are attached to the critical line $\Delta = \Delta_c(Z) = Z$ from above and from below. For the most range of the existence of the ordered phase $Z < Z_{cr}^{(1)}$, see Figure 5, only one solution exists, the one corresponding to equation (12). In the hyperbolic approximation and under the condition $|t'/t|$ not too small $Z_{cr}^{(1)}$ is given by:

$$Z_{cr}^{(1)} \propto \omega_{\max} \exp(-\pi^2 t/(V \ln|t/t'|)).$$

For this solution one has

$$\Delta_1(Z) \equiv \Delta_0(Z) = f(Z) + \Delta(0) \tag{21}$$

where $\Delta(0)$ is given by

$$\Delta(0) \propto |t'| \exp\left(-\frac{2\pi^2|t'/V|}{\sqrt{1-(2t'/t)^2}}\right), \tag{22}$$

and $f(Z)$ is an increasing function of Z, linear under the condition $\Delta(Z) \gg \Delta(0)$. The expression (22) is valid under condition $\pi^2|t'/V|/\sqrt{1-(2t'/t)^2} \gg 1$. For the narrow Z range of the coexistence of the two solutions $Z_{cr}^{(1)} < Z < Z_{cr}^{(2)}$ it is the solution Δ_1 which is favorable (see Appendix). Therefore, the value of the gap increases with increasing Z being always larger than Z. As we have shown, this is a consequence of the effect that the point of ETT is the end point of two critical lines.

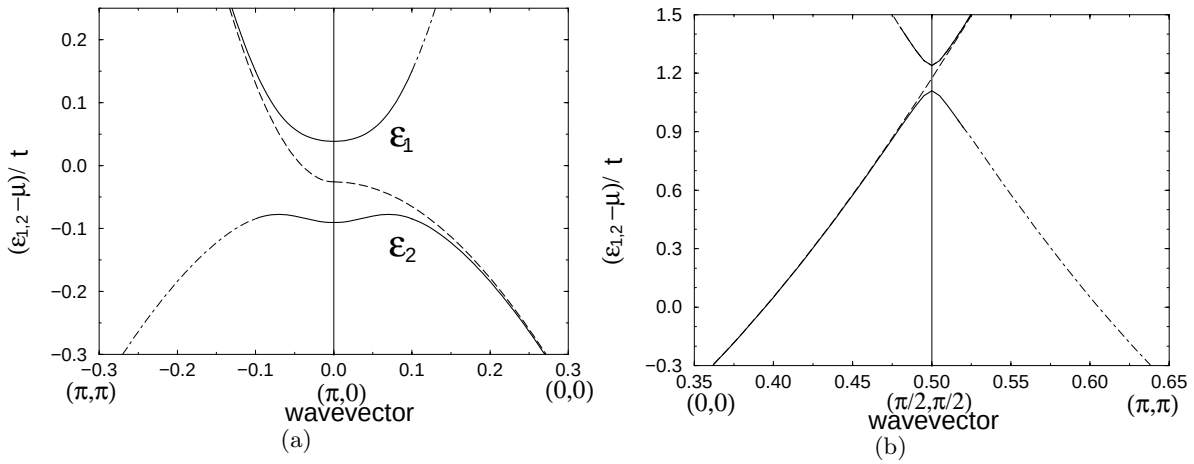

Fig. 6. One particle spectra along $(\pi,\pi)-(\pi,q_y/\pi)$ and $(\pi-q_x/\pi,0)-(0,0)$ symmetry lines (a) and in $(0,0)$ - (π,π) direction (b), $t'/t=-0.3, t/V=1.8, Z/t=0.03$. Long dashed line is the bare spectrum, dot-dashed line corresponds to the spectrum when the residue of the Green function (7) less than 0.1.

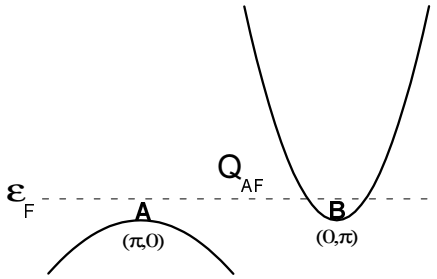

Fig. 7. Schematic representation of the bare spectrum in the vicinity of the two saddle points for $Z\neq 0$.

Let's analyze now the form of the spectrum in the DW phase. The spectrum given by (9) is plotted in Figure 6. for three important directions: $(\pi,\pi)-(\pi,0)-(0,0)$ and $(0,0)-(\pi,\pi)$. The spectrum in the vicinity of SP has the following prominent features: The first is a characteristic "flat" shape being a consequence of the hybridization of the two branches of the bare spectrum in the vicinity of two different SP's with the opposite curvatures, (see Fig. 7). The second: the spectrum in the direction $(\pi,\pi)-(0,\pi)$ "disappears" above some threshold value of wavevector since the residue $v_{\mathbf{k}}^2$ tends to zero (that is also an ordinary consequence of the hybridization). The third: the chemical potential always lies in the gap for the part of Brillouin zone (BZ) around SP wavevectors since

$$\varepsilon_1(\mathbf{k}_{\rm SP})=-Z+\Delta,$$

$$\varepsilon_2(\mathbf{k}_{\rm SP})=-Z-\Delta$$

(see, *e.g.* Eq. (9)) and $\Delta>Z$.

This is a consequence of the existence of the critical line $\Delta=\Delta_{\rm c}$ related to the discussed above aspect of criticality of the QCP. The obtained theoretical spectrum has a striking similarity with the anomalous experimental electron spectrum observed by ARPES [9] in the underdoped cuprates below the characteristic line $T^*(\delta)$, we reproduce it in Figure 8. (We remind that ARPES measures a spectral function only below FL.) For the direction $(0,0)-(\pi,\pi)$, Fermi level crosses the lower branch of the spectrum, (see Fig. 6b), *i.e.* the system remains metallic. In fact, the chemical potential gets out of the gap for directions extending from the diagonal $(0,0)$ – (π,π) to some limit direction. This corresponds to an arc of FS shown in the insert of Figure 9 which is the lower part of a pocket (the upper part corresponding to a low residue is not shown). The limit points of the arc are located on the umklapp surface away from the hot spots of the unperturbed Fermi surface. As the gap value Δ is larger than Z, the FS is destroyed starting from the hot spots in both directions up to the saddle points on the side and up to limit points on the other side (the position depends on the position of the hot spots and on the strength of the interaction V). For large Z and large V the Fermi surface pockets may fully disappear and the system becomes an insulator.

The angle dependence of the value of $\epsilon_{\mathbf{k}}-\mu$, *i.e.* of the gap calculated from FL, in the same way as it is done in ARPES experiments [10] is presented in Figure 9. Namely we plot the minimal value of $|\varepsilon_{\mathbf{k}}-\mu|$ for each given direction from the diagonal $(0,0)$ – (π,π) to the direction $(0,0)$ – $(0,\pi)$. The dependence is of a "d-wave type" in a sense that the gap increases with increasing the argument $(\cos k_x-\cos k_y)$ almost linearly in the proximity of SP. However the dependence is flat (not linear as it happens in the d-wave case) when approaching the direction $(1,1)$. Such a behaviour is also close to the experimentally found behaviour above $T_{\rm c}$ [10] reproduced in Figure 9b. (Although the authors of [10] claim that the behaviour observed above and below $T_{\rm c}$ is the same, what one sees in the experimental plot is not exactly this: the behaviour above and below $T_{\rm c}$ is similar in the vicinity of SP and different when approaching the $(1,1)$ direction and this occurs quite systematically, see also the plots in [10] for other samples.)

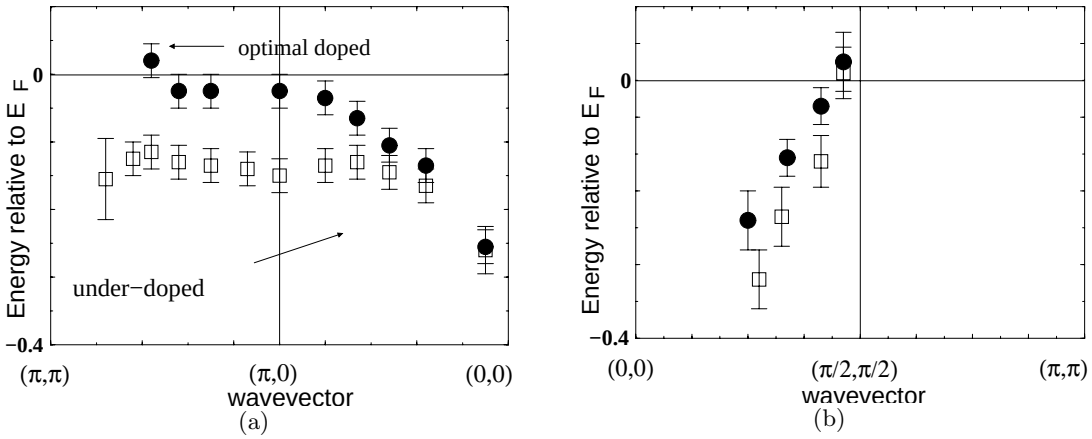

Fig. 8. Experimental one particle spectra along $(\pi,\pi)-(\pi,0)-(0,0)$ symmetry lines (a) and in $(0,0)$ -(π,π) direction (b) measured in the overdoped regime of BSCO. The data are taken from [10].

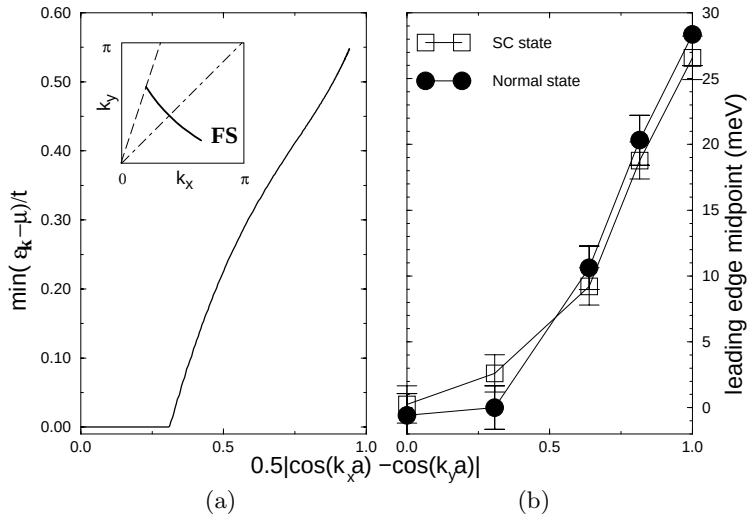

Fig. 9. Theoretical angle dependence of the SDW gap calculated from FL in the underdoped regime $Z>0$ ($t'/t=-0.3$, $t/V=1.7$, $Z/t=0.3$, typical shape of FS is shown on inset) (a) and the experimental leading edge midpoint measured by ARPES in the underdoped BSCO [11] (b).

We considered the particular case of SDW as an example of ordered "excitonic" state. Nevertheless, all aforesaid is true for any other types of ordered states since the existence of such states is determined only by topology of FS.

Let us study now a one particle density of states (DOS) given by the expression

$$\mathcal{N}(\varepsilon)=-\frac{1}{\pi}\frac{1}{N}\sum_{\mathbf{p}}[\mathrm{Im}\,K_{11}^{R}(\mathbf{p},\varepsilon)+\mathrm{Im}\,K_{22}^{R}(\mathbf{p},\varepsilon)]$$
$$=\frac{1}{N}\sum_{\mathbf{p}}[\delta(\varepsilon-\varepsilon_1(\mathbf{p}))+\delta(\varepsilon-\varepsilon_2(\mathbf{p}))]. \qquad (23)$$

Numerical calculations with the spectrum (1) give the picture shown in Figure 10. The density of states of SDW (CDW) states deviates from the DOS in the initial metallic state in two ε ranges notated as **A** and **B**. For OCDW (SCDW) states only feature **A** survives. Analytical calculations show that the **A**-feature is related to the existence of the discussed above QCP (which we call below QCP1). Calculations of the integral in (23) performing with the hyperbolic spectrum (5) valid in the vicinities of SP's show that in the **A** range DOS is characterized by three singularities (instead of one logarithmic singularity in the bare density of states $\mathcal{N}_0(\varepsilon)$ as $\varepsilon\to -Z$). Those are a logarithmic singularity at $\varepsilon_1=-Z-\Delta_0\sqrt{1-4(t'/t)^2}$ [32]

$$\mathcal{N}(\varepsilon\to\varepsilon_1)\sim\frac{1}{t\sqrt{1-4(t'/t)^2}}\ln\left(\frac{\omega_{\max}}{|\varepsilon-\varepsilon_1|}\right) \qquad (24)$$

and jumps at two energies

$$\varepsilon_{2,3}=-Z\pm\Delta_0.$$

The distance between two jumps is equal to 2Δ.

The **B** feature is related to the existence of the second quantum critical point in the system (QCP2) discussed

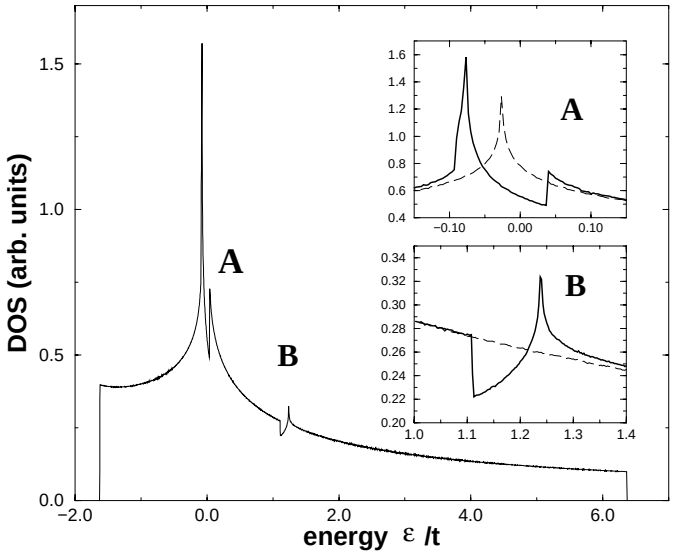

Fig. 10. Density of states in the ordered "excitonic" phase calculated for $Z/t = 0.03$ ($t/V = 1.8, t'/t = -0.3$). Dashed line corresponds to the DOS in the initial metallic state.

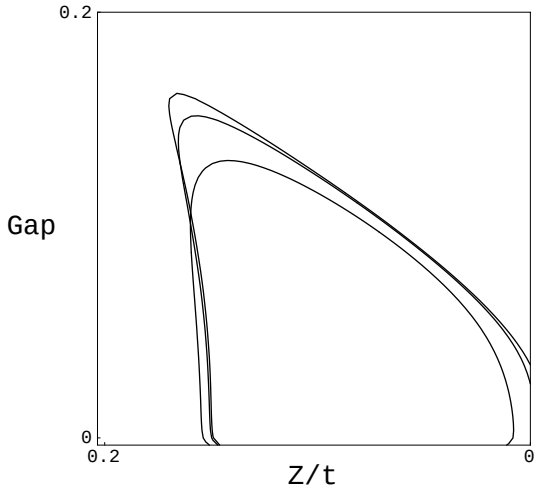

Fig. 11. The DW gap in t units as a function of Z for increasing temperature: $T/t = 0.005, 0.1, 0.2$ ($t'/t = -0.3$, $t/V = 1.8$).

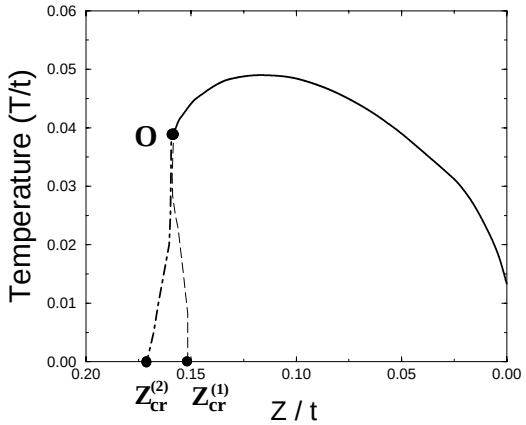

Fig. 12. Phase diagram around QCP1 in T-Z coordinates ($t/V = 1.8$, $t'/t = -0.3$). We show only the regime $Z > 0$ corresponding to the anomalous behavior. The solid line is a line of second-order phase transition, the dot-dashed is a line of first-order phase transition and the dashed line is a line of instability of the disordered metal state (spinodal). The point O is a tricritical point.

in [29]. This point corresponds to the electron concentration when the chemical potential is equal: $\mu = \mu_{c2} = 0$ or by other words when the wavevector connecting two parts of FS in the direction $(1,1)$ is equal to $\mathbf{Q}_{\rm AF} = (\pi, \pi)$. In this case two "hot spots" on FS come together at the singular position $(\pm\pi/2, \pm\pi/2)$ before disappearing. The calculations of the integral in (23) with the spectrum taken around $(\pi/2, \pi/2)$ give a logarithmic divergence at the point $\varepsilon_4 = -Z - 4t' + \Delta(\pi/2, \pi/2)$:

$$\mathcal{N}(\varepsilon \to \varepsilon_4) - \mathcal{N}_0(\varepsilon_4) \sim \frac{1}{t}\sqrt{\frac{\Delta(\pi/2,\pi/2)}{|t'|}} \ln\left(\frac{\omega_{\max}}{|\varepsilon - \varepsilon_4|}\right) \tag{25}$$

and a jump at the point $\varepsilon = -Z - 4t' - \Delta(\pi/2, \pi/2)$. This feature does not exist for OCDW (SCDW) states since $\Delta(\mathbf{k}) = 0$ along the diagonal of BZ.

The **B** feature is important in the case when the chemical potential lies close to the pseudogap in the **B** part that should take place in the electron-doped cuprates. For the hole-doped cuprates we are interested in the present paper, it is QCP1 which determines properties of the system. In this case the chemical potential lies in the "pseudo-gap" **A** according to the properties of the electron spectrum in the vicinity of SP discussed above.

Let's analyze now the range of the existence of the ordered phase in the $T-Z$ plane. For this sake let's analyze the behaviour of $\Pi(\mathbf{Q}, Z, \Delta_0)$ as a function of Z at finite temperature. (We again consider SDW state for certainty.) Results of calculations are presented in Figure 11. The first observation is that the gap changes only little with T at low T. The second is that the behaviour at finite temperature as a function of Z is qualitatively the same as for $T = 0$ and it is anomalous: the value of the gap increases with increasing Z.

The phase diagram in $T - Z$ plane obtained for SDW (CDW) instability based on the analysis of the gap behaviour at finite T is presented in Figure 12. It is worthwhile to note that the polarization operator $\Pi(\mathbf{Q}, Z, \Delta)$ (14) calculated for OCDW (SCDW) ordered states has essentially more abrupt behavior as a function of Z in comparison with those for $\Pi^{\rm SDW,CDW}(\mathbf{Q}, Z, \Delta)$ (13). Such behavior appears due to additional factor $(\cos(p_x) - \cos(p_y))^2$ in the integral (12). As a result, the domain of existence of OCDW (SCDW) solutions for equation (12) at various doping concentrations is substantially narrower than for SDW (CDW) case. Nevertheless, it does not affect the qualitative shape of phase diagram of Figure 12.

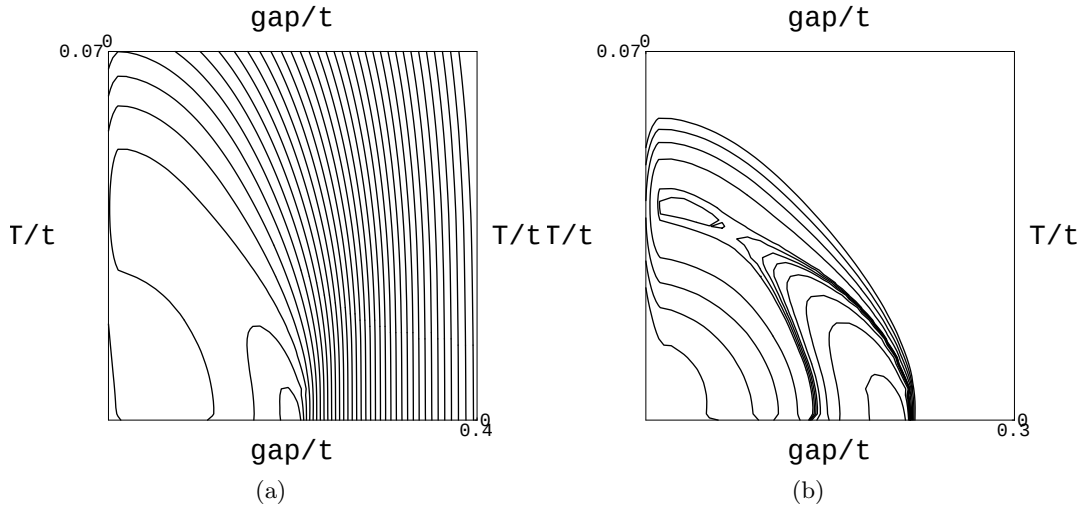

Fig. 13. Lines of $\Pi(\mathbf{Q}, Z, \Delta) = \text{const}$ for fixed $t/V = 1.8$ and different Z. The plot (b) is a zoom of the plot (a) corresponding to the coexistence of the two solutions for the gap.

The solid line on the phase diagram is the line where $\Delta_1(T) = 0$. The dashed line is the line where $\Delta_2(T) = 0$. These two lines are at the same time the lines of instabilities of the undistorted metallic state. The line $\Delta_2(T) = 0$ is not however a line of a phase transition since the nonzero solutions for the gap exist on the left of this line until the dot-dashed line. Along the latter line corresponding to the disappearance of the "ordered" solution, the gap is finite and the two solutions coincide: $\Delta_0(T) = \Delta_1(T) = \Delta_2(T)$. The situation is clearly seen from Figure 13 where we present the lines $\Pi(\mathbf{Q}, Z, \Delta) = \text{const}$ for different Z and fixed t/J which in fact give the full picture of the behaviour of the DW gap as a function of Z and T.

As we discuss in the Appendix, in the region between the dot-dashed and dashed line, where three solutions $\Delta_0 = \Delta_1$, $\Delta_0 = \Delta_2$ and $\Delta = 0$ coexist, it is the solution $\Delta_0 = \Delta_1$ which is energetically favorable.

Thus, the dot-dashed line in the phase diagram in Figure 12 is the line of the first-order phase transition. The gap along this line changes only little at low temperature and tends to zero rapidly in the vicinity of the point O. The latter is a tricritical point. The range in $T - Z$ plane in the vicinity of this point corresponds to a strongly fluctuating regime which we will consider elsewhere. It is important to add also that at the point $Z = Z_{\rm cr}^{(2)}$ of the appearance of the ordered phase at $T = 0$, the gap is exactly equal to Z that means that the upper branch of the spectrum in Figure 6a touches FL. Then when moving inside the ordered phase the gap Δ becomes larger than Z and this branch goes up leaving the FL.

Above we have considered the critical temperatures and the gap behaviour as functions of the energy distance from the QCP, Z. It is worth for applications to cuprates to change the description and to consider physical properties as functions of electron concentration $n_{\rm e}$ or of hole doping $\delta = 1 - n_{\rm e}$. To do this we use the relation between Z (or the chemical potential μ) and the hole doping which for $T = 0$ is given by:

$$1 - \delta = \int_{\omega} N(\omega) \mathrm{d}\omega. \tag{26}$$

So far as

$$Z \propto \delta_{\rm c} - \delta, \tag{27}$$

all dependencies considered above can be rewritten as functions of doping distance from QCP. For example, the phase diagram in the plane $T - \delta$ calculated for $t'/t = -0.3$ for which $\delta_{\rm c} = 0.27$ gets the form shown in Figure 14.

One can easily obtain values of doping for all plots presented in Figures 4–11 when comparing the phase diagram in $T - Z$ plane in Figure 12, and in $T - \delta$ plane in Figure 14.

Obviously, the gap $\Delta_0(\delta)$ increases with $\delta_{\rm c} - \delta$ in the same way as it increases with Z, see Figures 5 and 11 for $\Delta_0 = \Delta_1$.

All features discussed above do not depend on the nature of the ordered phase, SDW, CDW, OCDW or SCDW since they reflect the topological aspects of ETT. The type of the excitonic phases developing around ETT point depend on the type of interaction. It is the SDW or OCDW state in the case of a positive interaction in the triplet channel (exchange interaction) and the CDW or SCDW state in the case of a positive interaction in a singlet channel (density-density interaction). The ordered SDW phase is characterized by spin ordering with momentum $\langle S_Q^z \rangle = 1/2(\langle n_{\sigma\sigma}(Q) \rangle - \langle n_{\bar{\sigma}\bar{\sigma}}(Q) \rangle) = \Delta_0$ and the CDW phase by the charge ordering. In the SCDW (OCDW) the staggered magnetization (density) is equal to zero. Nevertheless, the spin-current (charge-current) correlation functions survive.

In our opinion for the case of high-$T_{\rm c}$ cuprates it is the interaction in the triplet channel which determines the behaviour of the system and the nature of DW phase.

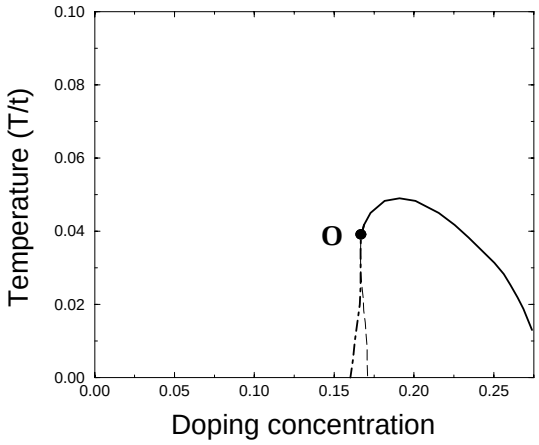

Fig. 14. Phase diagram around QCP1 in T-δ coordinates ($t/V = 1.8$, $t'/t = -0.3$).

From the theoretical point of view it is this situation which corresponds to the strong-coupling limit models: the Hubbard model and the $t-J$ model. For example for the latter with the J term written as $H_J = \sum_{ij} J_{ij}\{a\mathbf{S}_i\mathbf{S}_j - (b/4)n_in_j\}$ one has $V_{\mathbf{q}}^{\mathrm{SDW}} = aJ_{\mathbf{q}}$ while $V_{\mathbf{q}}^{\mathrm{CDW}} = -\frac{b}{4}J_{\mathbf{q}}$, *i.e.* the interaction in the triplet channel is positive while in the singlet channel is negative. This version is supported also by experiments in the high-T_c cuprates: observed experimentally (by neutron scattering, see for example [33] and NMR) strong magnetic response around $\mathbf{q} = \mathbf{Q}$ is a phenomenological argument in a favor of a strong momentum dependent interaction in a triplet channel, *i.e.* of $V_{\mathbf{q}} = J_{\mathbf{q}}$ ($J > 0$). However, we can not exclude an importance of an interaction leading to the CDW (SCDW) order.

Another point concerning the interaction is its strength. Depending on the ratio $|V|/W$ (where W is an energy bandwidth), maximal $T_{\mathrm{DW}}^{\max}$ can be high or low. Respectively, the DW phase can lean out of SC state or can be hidden under it. (In the presence of the interaction in the triplet channel, $J_{\mathbf{q}}$, both SDW and SC instabilities occur around QCP1 under the same condition: $J > 0$, for the SC instability see [34].) It is tempting to identify the properties obtained for the DW state with the properties observed experimentally in the underdoped cuprates above $T_{\mathrm{sc}}(\delta)$ and below $T^*(\delta)$. Indeed they have a striking resemblance, as one can see when comparing Figure 6 and Figure 8, Figure 9a and Figure 9b and when comparing the behaviour of the gap as a function of Z (or doping, $\delta_c - \delta$) with the experimental behaviour [12]. Our calculations (when considering both d-wave SC and DW instabilities in the presence of interaction J in the triplet channel) show that the answer is quite subtle [36]. When $t'/t = -0.2$ the ordered DW phase leans out of the SC phase for $t/J < 1.90$, for $t'/t = -0.3$ this happens when $t/J < 1.55$. So far as realistic value of t/J for cuprates is estimated to be in the interval $t/J = 1-3$, both variants when the DW phase takes place above SC phase and when it is hidden under the SC phase are possible [36,37].

Even in the latter case the study of properties of the ordered DW state performed here is important since the normal metallic state above $T_{\mathrm{sc}}(\delta)$ keeps a strong memory about the ordered phase. Therefore, electron properties in this state should be close to those in the DW ordered state being however characterized by strong damping. (By the way it is exactly what is observed by ARPES. The experimental electron spectrum has a form shown in Figure 8, being however characterized by a spectral function of a very damped form.) It should be emphasized that the calculations performed for ordered state are very important. The form of the spectrum is a solid basis to understand the physics of the precursor state. Calculations for the ordered state are in general more neat than for the precursor state.

Summarizing, we have studied the DW phase which is formed around QCP1 (associated with ETT) and we have shown that this phase is characterized by the following prominent features:

(i) the specific "flat" shape of the spectrum in the vicinity of SP,
(ii) "disappearance" of the spectrum above some threshold value of wavevector in the direction $(\pi,0)-(\pi,\pi)$,
(iii) pseudogap in DOS with FL lying inside it,
(iv) increasing of the gap in the spectrum around SP wavevectors and of the pseudogap in DOS with decreasing doping for $\delta < \delta_c$,
(v) angle dependence of the gap calculating from FL which is of a d-wave type close to SP and flat close to the direction $(1,1)$.

All these features have a striking similarity with the experimental features revealed by ARPES in the normal state of the underdoped hole-doped cuprates.

Appendix A

The free energy density in the approximation corresponding to considered in the paper is given by:

$$F = -T\frac{1}{N}\sum_{\mathbf{k}}\sum_{\alpha=1,2}\left[\ln\left(2\cosh\left(\frac{\varepsilon_\alpha(\mathbf{k},\Delta_{\mathbf{k}})}{2T}\right)\right) + \frac{\Delta_{\mathbf{k}}^2}{4V}\right] + \mu n. \tag{A.1}$$

(Note that the equation (10) corresponds to $\partial F/\partial\Delta = 0$.) Therefore, the difference between free energies corresponding to $\Delta = \Delta_1$ and $\Delta = \Delta_2$ is given by

$$F_1 - F_2 = \frac{\Delta_1^2 - \Delta_2^2}{4V} - T\frac{1}{N}\sum_{\mathbf{k}}\sum_{\alpha=1,2}\ln\left(\frac{\cosh\left(\frac{\varepsilon_\alpha(\mathbf{k},\Delta_1)}{2T}\right)}{\cosh\left(\frac{\varepsilon_\alpha(\mathbf{k},\Delta_2)}{2T}\right)}\right). \tag{A.2}$$

One can check by numerical calculations that $F_1 - F_2 < 0$ for the whole range of the coexistence of the two solutions.

Some analytical estimations can be also done for low T based on the well-known expression [35] for the difference between thermodynamic potentials of the ordered and disordered states:

$$\delta\Omega = \Omega(\Delta_1) - \Omega(0) = \int_0^{\Delta_1} \frac{\mathrm{d}(1/V)}{\mathrm{d}\Delta}\Delta^2 \mathrm{d}\Delta. \qquad (A.3)$$

When substituting the expressions for Δ_1 (21), (22) one gets

$$\delta F/t = \delta\Omega/t \sim -\frac{\sqrt{1-4|t'/t|^2}}{|t'/t|}\frac{\Delta_1^3}{t^2\Delta(Z=0)} \sim -\frac{(Z_{\mathrm{cr}}^{(1)})^3}{t^2\Delta(Z=0)}. \qquad (A.4)$$

One can see that this correction is negative. Therefore, the solution $\Delta = \Delta_1$ is favorable with respect to the solution $\Delta = 0$ for any $Z_{\mathrm{cr}}^{(1)} < Z < Z_{\mathrm{cr}}^{(2)}$.

References

1. H. Alloul, T. Ohno, P. Mendels, Bull. Am. Phys. Soc. **34**, 633 (1989); H. Alloul, T. Ohno, P. Mendels, Phys. Rev. Lett. **63**, 1700 (1989).
2. G.V.M. Williams, J.L. Tallon, E.M. Haines, R. Michalak, R. Dupree, Phys. Rev. Lett. **78**, 721 (1997).
3. M. Takigawa, Phys. Rev. B **49**, 4158 (1994).
4. S.L. Cooper, G.A. Thomas, J. Orenstein, D.H. Rapkine, M. Capizzi, T. Timusk, A.J. Millis, L.F. Schneemeyer, J.V. Waszczak, Phys. Rev. B **40**, 11358 (1989).
5. A.V. Puchkov, P. Fournier, D.N. Basov, T. Timusk, A. Kapitulnik, N.N. Kolesnikov, Phys. Rev. Lett. **77**, 3212 (1996).
6. J.L. Talon, J.R. Cooper, P.S.I.P.N. de Silva, G.V.M. Williams, J.W. Loram, Phys. Rev. Lett. **75**, 4114 (1995).
7. J.W. Loram, K.A. Mirza, J.R. Cooper, W.Y. Liang, Phys. Rev. Lett. **71**, 1740 (1993).
8. R. Nemetschek, M. Opel, C. Hoffmann, P.F. Müller, R. Hackl, H. Berger, L. Forró, A. Erb, E. Walker, Phys. Rev. Lett. **78**, 4837 (1997).
9. D.S. Marshall, D.S. Dessau, A.G. Loeser, C-H. Park, A.Y. Matsuura, J.N. Eckstein, I. Bozovic, P. Fournier, A. Kapitulnik, W.E. Sicer, Z.-X. Shen, Phys. Rev. Lett. **76**, 4841 (1996).
10. J.M. Harris, Z.-X. Shen, P.J. White, D.S. Marshall, M.C. Schabel, J.N. Eckstein, I. Bozovic, Phys. Rev. B **54**, 15 665 (1996).
11. H. Ding, T. Yokoya, J.C. Campuzano, T. Takahashi, M. Randeria, M.R. Norman, T. Mochiku, K. Kadowaki, J. Giapintzakis, Nature (London), **382**, 51 (1996).
12. H. Ding, J.C. Campuzano, M.R. Norman, `cond-mat/9712100`.
13. H. Ding, M.R. Norman, T. Yokoya, T. Takeuchi, M. Randeria, J.C. Campuzano, T. Takahashi, T. Mochiku, K. Kadowaki, Phys. Rev. Lett. **78**, 2628 (1997).
14. A.P. Kampf, J.R. Schrieffer, Phys. Rev. B **42**, 7967 (1990).
15. V.J. Emery, S.A. Kivelson, Nature (London) **374**, 434 (1995).
16. S. Doniach, M. Inui, Phys. Rev B **41**, 6668 (1990).
17. B.L. Altshuler, L.B. Ioffe, A.J. Millis, Phys. Rev. B **53**, 415 (1996).
18. F. Onufrieva, P. Pfeuty, Phys. Rev. Lett. **82**, 3136 (1999).
19. F. Onufrieva, P. Pfeuty, Phys. Rev. B **61**, 799 (2000).
20. F. Onufrieva, P. Pfeuty, M. Kisselev, Phys. Rev. Lett. **82**, 2370 (1999).
21. L.V. Keldysh, Yu.V. Kopaev, Sov. Phys. Solid State **6**, 2219 (1965).
22. A.N. Kozlov, L.A. Maksimov, Sov. Phys. JETP **21**, 790 (1965).
23. J. des Cloiseaux, Phys. Chem. Solids **26**, 259 (1965).
24. B.I. Halperin, T.M. Rice, Solid State Phys. **21**, 115 (1968).
25. T.M. Rice, Phys. Rev. B **2**, 3619 (1970).
26. T.M. Rice, G.K. Scott, Phys. Rev. Lett **35**, 120 (1975).
27. For $t'/t = 0$ and half-filling ($Z = 0$) one can recover perfect nesting spectrum when the FS for 2D electron gas is completely determined by nesting wavevectors $\mathbf{Q} = (\pm\pi, \pm\pi)$.
28. V.V. Tugushev, in *Electronic Phase Transitions*, edited by W. Hanke, Yu. Kopaev (Elsevier, 1992).
29. F. Onufrieva, P. Pfeuty, M. Kiselev, J. Phys. Chem. Sol. **59**, 1853 (1998).
30. We write down the expression for SDW and OCDW polarization operator just as an example. The pair of equations for CDW and SCDW is different only due to definition of Π^{DW}.
31. This is true under the condition of $|t'/t|$ not too small.
32. We are grateful to D.N. Aristov for paying our attention to the complicated structure of DOS in the vicinity of ε_1.
33. J. Rossat-Mignod, L.P. Regnault, C. Vettier, P. Burlet, J.Y. Henry, G. Lapertot, Physica B **169**, 58 (1991).
34. F. Onufrieva, S. Petit, Y. Sidis, Phys. Rev. B **54**, 12 464 (1996).
35. A.A. Abrikosov, L.P. Gorkov, I.E. Dzyaloshinskii, *Methods of Quantum Field Theory in Statistical Physics* (Prent ice-Hall, Englewood Cliffs, 1963).
36. F. Bouis, M. Kiselev, F. Onufrieva, P. Pfeuty, Physica B (in press).
37. F. Onufrieva, P. Pfeuty, J. Low Temp. Phys. **117**, 229 (1999).

Magnetic correlations in nearly AFM Kondo lattices

ELSEVIER

Physica B 230–232 (1997) 490–492

PHYSICA B

Stabilization of spin liquid in Kondo lattice: High temperature regime

K.A. Kikoin*, M.N. Kiselev, A.S. Mishchenko

RRC Kurchatov Institute, Kurchatov sq. 46, Moscow 123182, Russian Federation

Abstract

The mechanism explaining the key role of AFM correlations in formation of the heavy fermion state is offered. It is shown that in the case of $(T^* - T_N)/T_N \ll 1$, the critical spin fluctuations transform the mean-field second-order transition to RVB state into the crossover from high-temperature paramagnetic behavior of localized spins to strongly correlated spin liquid with quasi itinerant character of susceptibility. Thus the spin-liquid state *by its origin* is close to magnetic instability, so either short-range or long-range AFM order should arise at low T.

Keywords: Spin liquid; Magnetic instability

It was shown in [1] that the spin-liquid state of resonating valence bond (RVB) type can be stabilized by the Kondo scattering against the antiferromagnetic (AFM) ordering in 3D Kondo lattices at high enough temperatures $T^* > T_K$, provided the Kondo temperature T_K is close to the mean-field (MF) Neel temperature T_N. This stabilization is due to the fact that the Kondo scattering screens dynamically the local moments and, thus, suppresses the magnetic order, whereas the spin-liquid correlations which result in the singlet RVB are left intact by this scattering. The theory was based on the MF description of RVB state which, as is known [2], results in second-order-type transition from paramagnetic state to RVB phase. However, since the transition to the spin-liquid state takes place close to the point of AFM instability, the critical fluctuations influence essentially the character of spin-liquid transition. The description of this influence is the main subject of the present paper.

* Corresponding author.

We start with a standard Kondo lattice Hamiltonian

$$H_{\text{eff}} = \sum_{k\sigma} \varepsilon_k c^+_{k\sigma} c_{k\sigma} + J_{\text{sf}} \sum_i c^+_{i\sigma} c_{i\sigma} f^+_{i\sigma} f_{i\sigma}. \tag{1}$$

Here ε_k is the band level of conduction electron $c_{k\sigma}$, and the operator of localized f-spin is represented via fermionic operators, $S_i = \frac{1}{2} f^+_{i\sigma} \hat{\sigma} f_{i\sigma'}$, where $\hat{\sigma}$ is the Pauli matrix. At $T > T_K$ the non-crossing approximation for the Kondo scattering processes is valid, and this Hamiltonian can be transformed into effective RKKY-type Hamiltonian for spin variables only,

$$\mathrm{H}_{\text{RKKY}} = I_{\text{ss}} \sum_{ij} f^+_{i\sigma} f_{j\sigma} f^+_{i\sigma'} f_{i\sigma'}, \tag{2}$$

where $I_{\text{ss}} \sim \tilde{J}^2_{\text{sf}}(T^*)/\varepsilon_F$ is the indirect RKKY exchange interaction with the sf-vertices $\tilde{J}_{\text{sf}}(T^*)$ enhanced by the Kondo scattering which is taken into account in a high-temperature approximation of perturbation theory [1]. The Kondo processes are "quenched" at some temperature $T^* > T_K$ which characterizes the onset of spin-liquid RVB state described by the variables $b_{ij} = \sum_\sigma f^+_{i\sigma} f_{j\sigma}$ under the constraint $\sum_\sigma f^+_{i\sigma} f_{i\sigma} = 1$. If one introduces the

PII S0921-4526(96)00623-0

MF parameter $\Delta = \langle b_{ij} \rangle$ in the Hamiltonian (2), the temperature T^* is determined as $T^* = I_{ss}(2zN)^{-1}\sum_k \varphi^2(\boldsymbol{k})$, where $\varphi(\boldsymbol{k})$ is a lattice structure factor with the coordination number z. Just this temperature was shown in [1] to become higher then T_N in a critical region $T_K \sim T_N$ of the Doniach state diagram.

Since the inequality $(T^* - T_N)/T_N \ll 1$ is valid for the MF solution, the closeness to AFM instability should be taken into account. This closeness enriches the phase diagram of 3D spin-liquid in comparison with the MF scenario of homogeneous RVB state formation [1]. We consider here the Kondo lattice with AFM-type RKKY interaction for the nearest neighbors which could result in commensurate ordering with AFM wave vector $\boldsymbol{Q}$ at $T = T_N$ provided the RVB state was not realized at higher temperature T^*. This means that the denominator of the static susceptibility

$$\chi_{\boldsymbol{Q}} = \chi_0(T)[1 - \chi_0(T)I(\boldsymbol{Q})]^{-1} \tag{3}$$

is close to zero at $T \approx T^*$. Here $\chi_0(T) = \langle \boldsymbol{S}_{\boldsymbol{Q}} \cdot \boldsymbol{S}_{-\boldsymbol{Q}} \rangle_{\omega=0} = C/T$ is the Curie susceptibility of free localized spin. Below T^* the latter acquires dispersion, begins to deviate gradually from Curie law, and finally takes the form

$$\chi_{0\boldsymbol{Q}}(T) = N^{-1}\sum_{\boldsymbol{k}}(n_{\boldsymbol{k}} - n_{\boldsymbol{k}+\boldsymbol{Q}})(t_{\boldsymbol{k}+\boldsymbol{Q}} - t_{\boldsymbol{k}})^{-1}, \tag{4}$$

where $n_{\boldsymbol{k}}$ is the Fermi distribution function for the RVB excitations which are characterized by the dispersion law $t_{\boldsymbol{k}}$. This deviation is shown schematically by the solid curves in Fig. 1. The zero-temperature limit of these curves can be estimated as $f\chi_{0\boldsymbol{Q}}^{-1}(0) = \alpha T^*$, where α is the numerical coefficient whose value depends on the character of phase transition. This value can be either lower or higher then $T_N = CI(\boldsymbol{Q})$.

In the first case (curve 1 in Fig. 1), the point $\tilde{T}_N$ where $\chi_{0\boldsymbol{Q}}^{-1}$ crosses the dotted line, corresponds to AFM transition. However, the character of this transition differs from that of the localized spins. According to our scenario, the spin subsystem in the Kondo lattice bypasses the magnetic instability at $T = T_N$ to order at essentially lesser temperature $\tilde{T}_N$. However, within the interval $T_N > T > \tilde{T}_N$ the localized spins are transformed into spin liquid,

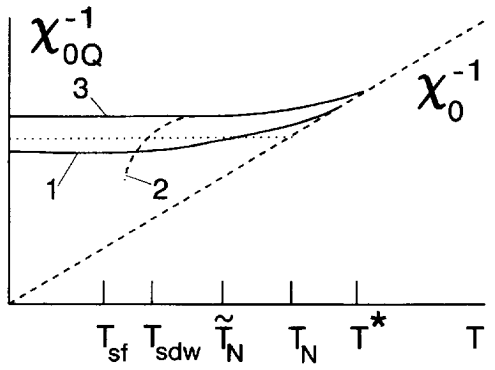

Fig. 1. Static magnetic susceptibility of RVB spin liquid.

and, as a result, the magnetic order reminds rather the itinerant AFM of conduction electrons with modulated spin density and small moments.

Since the spinon band is always half-filled because of the constraint, the nesting condition with the same wave vector $\boldsymbol{Q}$ can be realized for some geometries of the Fermi surface. In this case, $\chi_{0\boldsymbol{Q}}^{-1}$ logarithmically diverges, $\chi_{0\boldsymbol{Q}} \sim \Delta^{-1}\ln \Delta/T$, so the SDW-type magnetism appears at T_{SDW} (curve 2).

Next possibility occurs when the curve $\chi_{0\boldsymbol{Q}}^{-1}$ does not intersect T_N but comes close enough to it (curve 3). In this case we meet the peculiar situation when the paramagnon-type excitations can develop in the absence of itinerant electrons because the spin excitations have their own Fermi-type continuum in a spin-liquid state. Then, the spin-fluctuation order which reminds that for itinerant electrons [3] can occur at some temperature T_{sf}. If these fluctuations are too weak to provide the long-range order, the short-range magnetic correlations characterized by the vector $\boldsymbol{Q}$ persist at low temperatures. Thus, we see that the model grasps the whole variety of peculiar magnetic states with tiny itinerant-like moments which are known for the heavy-fermion materials.

The AFM spin fluctuations also influence the character of transition from the paramagnetic state to the RVB state. It is known that the second-order transition at $T = T^*$ is the artifact of the MF approximation, which violates the gauge invariance of the Hamiltonian (1), and the real situation is that of crossover type. Our approach demonstrates

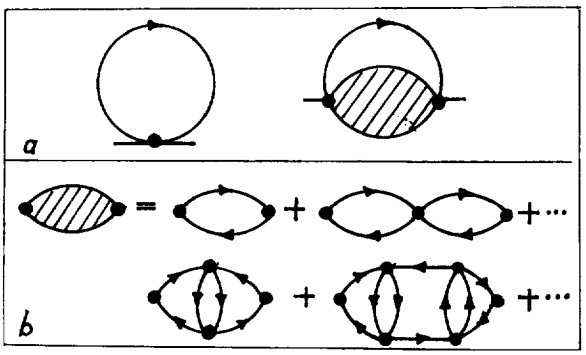

Fig. 2. Self-energy part of spinon Green's function (a) and dynamic susceptibility with vertex corrections (b).

that the real phase transition in Kondo lattice is *always* magnetic phase transition, and the spin-liquid-type correlations only change the character of this transformation.

To show this, we consider the MF self-energy $\sum_{ij}$ of the temperature spinon Green's function $G_{ij}(\tau) = -\langle T_\tau f_{i\sigma}(\tau) f^+_{j\sigma}(0)\rangle$ corrected by the critical AFM fluctuations (Fig. 2(a)). Here the lines stand for the Fourier-transformed G_{ij}, full dots correspond to $I(\boldsymbol{Q})$, the loop means spin susceptibility, $\chi_Q(\varepsilon_n)$, whose static part is given by (3). The latter correction, $\delta\Sigma_p$, inserts retardation into $G_p(\omega_m)$ and "opens" the system of equations which determine the spinon correlators for the influence of critical fluctuations. The correction $\delta\Sigma_p$ corresponds to the mode–mode coupling term in the free energy functional, $\delta\mathcal{F}_Q = J^2(\boldsymbol{Q}) M_Q^{\mathrm{AFM}} M_Q^{\mathrm{RVB}}$ where M_Q^X means the spin density fluctuations of localized (X = AFM) and itinerant (X = RVB) type.

To find $\chi_q(\varepsilon_n)$ for $\boldsymbol{q}$ close to $\boldsymbol{Q}$ one should take into account that the RVB continuum exists at temperature $T > T^* > T_N$ but still in the critical region of AFM instability as a "virtual" continuum of spinon, particle–hole pairs with the gap Ω_0 and nonzero damping γ. These excitations give both static ($\delta\chi_{0q}$) and dynamical ($\delta\chi_q(\varepsilon_n)$) contributions in a simple spinon loop and, correspondingly, in the RPA equation for $\chi_Q(\varepsilon_n)$. The vertex corrections in γ/Ω_0 should be also taken into account (Fig. 2(b)). The static contribution is responsible for initial deviation of $\chi_{0Q}(T)$ (Fig. 1) from the Curie law, and the calculation of dynamics reminds formally that was offered in Ref. [4] for the 2D Heisenberg model at finite temperatures. Our spinon-pair excitations with the gap play the same role as the Schwinger bosons in [4]. So, we come to the similar result: the relaxation mode appears in $\chi_q(\Omega)$ (Ω is the frequency analytically continued to the real axis),

$$\chi^{-1}(\boldsymbol{q}, \Omega) \sim \gamma + (qD\gamma^{-1/2})^2 - \mathrm{i}\Omega, \qquad (5)$$

where D is a sort of diffusion coefficient.

In conclusion, we have found that the RVB-type excitations appear in the Kondo lattice at high temperature, first, as a relaxation mode in susceptibility due to closeness of T^* to T_N. These excitations evolve into fermi-type particle–hole pairs with lowering temperature, and, eventually, the magnetic order of itinerant-like character arises at $\tilde{T}_N \ll T^*$, T_K. The relaxation regime is extended in T in comparison with standard critical regime for the localized moments, and even can persist at $T \to 0$. The theory predicts the presence of inelastic neutron scattering at $\Omega \approx \Omega_0$ and $\boldsymbol{q} \approx \boldsymbol{Q}$. The small magnetic moments correspond to modulation of spin-liquid density. This picture correlates with the experimental observations for $CeRu_2Si_2$ and $CeCu_6$ [5].

The support of the grants NWO 5-16501, INTAS 93-2834 and RFBR-95-02-04250 is acknowledged.

References

[1] K.A. Kikoin et al., JETP. Lett. 60 (1994) 358.
[2] P.W. Anderson et al., Phys. Rev. Lett. 58 (1987) 2790.
[3] K. Nakayama and T. Moriya, J. Phys. Soc. Japan 56 (1987) 2918.
[4] A. Chubukov, Phys. Rev. B 44 (1991) 12319.
[5] J. Rossat-Mignod, et al., J. Magn. Magn. Mater. 76, 77 (1988) 376.

Spin liquid in an almost antiferromagnetic Kondo lattice

K. A. Kikoin, M. N. Kiselev, and A. S. Mishchenko

Kurchatov Institute, 123182 Moscow, Russia
(Submitted 2 January 1997)
Zh. Éksp. Teor. Fiz. **112**, 729–759 (August 1997)

A theory of stabilization of a spin liquid in a Kondo lattice at temperatures close to the temperature of antiferromagnetic instability has been developed. Kondo exchange scattering of conduction electrons leads to emergence of a state of the spin liquid of the resonating valence bonds (RVB) type at $T > T_K$. Owing to this stabilization, low-energy processes of Kondo scattering with energies below T_K are frozen so that the ''singlet'' state of the Kondo lattice is not realized; instead a strongly correlated spin liquid with developed antiferromagnetic fluctuations occurs. A new version of the Feynman diagram technique has been developed to describe interaction between spin fluctuations and resonant valence bonds in a self-consistent manner. Emergence of a strongly anisotropic RVB spin liquid is discussed. [S1063-7761(97)02508-0]

1. INTRODUCTION

One of the most extraordinary properties of heavy-fermion compounds is the transition of a system of weakly interacting spins, which manifests paramagnetic properties at high temperatures, to a strongly correlated quantum liquid with thermodynamic and magnetic properties typical of Fermi systems at $T < T_{\rm coh} \ll T^*$. This ''dissolution'' of localized spins is usually interpreted in terms of the Kondo lattice model, and the basic mechanism which determines thermal transformation of the spin subsystem is assumed to be Kondo screening of spins by conduction electrons. This screening can be modeled in essentially the same way as a one-impurity lattice, so that the Kondo lattice can be treated as a periodic structure of Kondo impurities coherently scattering conduction electrons.[1,2] The characteristic temperature T^* at which the system switches to another regime is the Kondo temperature T_K, and the ground state in the mean-field approximation is the so-called Kondo singlet.

This simple model, however, ignores spin correlations, whose close relation to heavy fermions is beyond doubt. It is well known that formation of a heavy fermion is in all cases without exception due either to long-range antiferromagnetic order or short-range magnetic correlations. In its interpretation of this relation, the Kondo lattice theory invokes indirect exchange between localized spins via conduction electrons (RKKY exchange), which occurs in the Kondo lattice model in the second order of perturbation theory. Thus, nonlocal spin correlations compete with local effects of spin screening.[3] This naive dichotomy of Doniach's, which takes place in the mean-field approximation, predicts a tendency to antiferromagnetic ordering at small values of the effective coupling constant

$$\alpha = J_{sf}\mathcal{N}(\varepsilon_F)\Omega_0,$$

where J_{sf} is the sf-exchange integral, $\mathcal{N}(\varepsilon_F)$ is the electron density of states at the Fermi surface, Ω_0 is the elementary cell volume. At large α, Kondo screening suppresses the magnetic moment, and the ground state is the Kondo singlet. Then, for α slightly higher than α_c determined by the equation $\alpha_c^2 \exp(1/2\alpha_c) \approx 1$, the RKKY interaction can be calculated by perturbation theory, and magnetic correlations modify properties of the singlet phase.[4,5]

An alternative approach to the problem of competition between the one-site screening and magnetic intersite correlations was suggested by Coleman and Andrei.[6] The two options described by Doniach's simple model were supplemented with a third one, namely, formation of a nonmagnetic spin liquid of the resonant valence bonds (RVB) type with the Fermi statistics of elementary excitation in the spin system (spinons). They demonstrated that the spin liquid state is stabilized by Kondo scattering, but calculated both spin intersite correlations and the single-site sf-exchange between spinons and electrons in the mean-field approximation. Introduction of anomalous one-site averages of the Kondo type is, in reality, equivalent to the assumption that full dynamic spin screening takes place, and the assumption that Kondo singlets are formed at each site owing to multiple ''switching'' of RVB bonds between localized spins and conduction electron spins is equivalent to a translation of electron charge to spin degrees of freedom. Thus, in this scenario, as well as in the mean-field theory of the Kondo lattice,[7] spin degrees of freedom, which manifest themselves at high temperatures as weak paramagnetic, noncharged correlations, have a charge at $T < T_K$ and transform to charged heavy fermions (a critical discussion of this scenario was given in Ref. 8). Naturally, interpretation of the existence of magnetic correlations in the Kondo lattice requires more theoretical effort.[9]

This paper suggests an alternative scenario of formation of a spin liquid in the Kondo lattice described by the Hamiltonian

$$H_{\rm eff} = \sum_{\mathbf{k}\sigma} \varepsilon_k c^+_{\mathbf{k}\sigma} c_{\mathbf{k}\sigma} + J_{sf} \sum_{\mathbf{i}} \left(\mathbf{s_i}\cdot\mathbf{S_i} + \frac{1}{4} \right). \tag{1}$$

Here ε_k is the dispersion relation for conduction electrons, $\mathbf{S_i}$ and $\mathbf{s_i} = (1/2) c^+_{\mathbf{i}\sigma} \hat{\sigma} c_{\mathbf{i}\sigma}$, are operators of a spin localized in the f-shell and of a delocalized conduction electron spin, respectively, and $\hat{\sigma}$ are Pauli matrices. Our approach is based on an understanding that in the critical region, where all

three characteristic temperatures (the Kondo temperature $T_K \sim \varepsilon_F \exp(-1/2\alpha)$, Néel temperature $T_N \sim \varepsilon_F \alpha^2$, and the temperature T^* of the transition to the spin-liquid state) are of the same order, and the Kondo scattering is favorable to the transition to the spin-liquid state so that $T^* > T_N > T_K$, the very existence of spin-liquid correlations impedes the formation of a singlet ground state, since screening of localized spins by the Kondo scattering is, in fact, frozen at temperatures $T \sim T^* > T_K$, and at lower temperatures the system properties are controlled by nonlocal spin-liquid correlations, rather than one-site Kondo scattering. In other words, spin correlations suppress the Kondo effect in both the ordered (magnetic) and disordered (spin-liquid) phases, so Doniach's simple phase diagram should be revised.

Since the spin-liquid state emerges in the critical region $\alpha \sim \alpha_c$ at temperatures close to T_N, the coexistence of heavy fermions and magnetic correlations has a natural interpretation in the proposed model. Moreover, it is obvious that critical spin fluctuations should play an important role in the mechanism of spin-liquid formation. In this study, we have limited our calculations to the range of high temperatures $T > T_K$, where the perturbation theory in the parameter $\alpha \ln(\varepsilon_F/T_K)$ applies. We use the diagram technique for spin operators in the pseudofermion representation[10] in the approximation of noncrossing graphs (or noncrossing approximation, NCA) for the description of the Kondo scattering. The results of high-temperature expansions, which take one-site and intersite correlations into account concurrently, will be extrapolated to the range of temperatures where paramagnetic fluctuations are important. However, when the pseudofermion technique is applied to nonlocal spin-liquid correlations, the problem of nonphysical states arises, and hence the breaking of local spin symmetry.[11–15] With this circumstance in view, we have constructed a Feynman diagram technique for spin Hamiltonians, which allows us, in principle, not only to get rid of nonphysical states, but also to take into account fluctuations of calibration fields.

In Sec. 2 this technique is applied to a spin liquid of the homogeneous RVB phase type[16,17] described in terms of the Heisenberg model; in Sec. 3 the technique is applied to the Kondo lattice, and the mechanism of RVB phase stabilization by Kondo scattering in the mean-field approximation is described.[1)] The mean-field theory for the RVB phase, taking into account critical fluctuations, is generalized in Sec. 4, and Sec. 5 shows how this diagram technique can be used in describing local critical and hydrodynamic fluctuations around the antiferromagnetic instability point.

2. PROJECTION DIAGRAM TECHNIQUE FOR THE HEISENBERG LATTICE

Along with standard perturbation theory techniques developed for Fermi and Bose operators, one can find in the literature a number of diagram techniques for noncommuting operators in terms of which one can write the Hamiltonians of the spin or strongly correlated electrons systems (see, for example, Refs. 19–21 and references therein). Most of these techniques are based on Hubbard's projection operators $X_{\mathbf{j}}^{\lambda\mu} = |\mathbf{j}\lambda\rangle\langle\mathbf{j}\mu|$, where $|\mathbf{j}\lambda\rangle$ is a ket vector corresponding to state λ at site j, and the Hamiltonian in the zeroth order of perturbation theory is diagonalized in this approximation.

Diagram techniques for noncommuting operators are harder to handle than the standard Feynman technique. Only in some cases do they allow a self-consistent form of closed equation systems for skeleton diagrams. Goden's procedure factorizing the average of n operators, unlike Wick's procedure, which plays a similar role in the usual diagram technique, is ambiguous, and a successful choice of the hierarchy of couplings largely depends on the theorist's intuition (see, for example, Ref. 22).

For this reason, it is natural to attempt to express Hubbard's operators (and spin operators, which are a special case of these operators) as products of Fermi and Bose operators, and thus restore conditions for using the machinery of the Feynman and Matsubara techniques. Such attempts have been undertaken many times since the 1960s,[10,23–25] up through recent times.[22,26–28] It is clear, however, that these procedures are by no means universal or unambiguous. Moreover, each factorization leads to multiplication and complication of vertices and emergence of local constraints, whose introduction is necessary for the preservation of local gauge invariance, which is a trait of the Hamiltonian in question.

Additional problems arise due to attempts to describe nonlocal spin-liquid RVB excitation. In this case, problems arise on the level of the mean-field approximation for the self-energy part of the one-particle propagator. The usual techniques of self-consistent perturbation theory break the local gauge invariance,[11] and its restoration is quite a difficult physical and mathematical problem.[13,14]

In this section we formulate a version of the diagram technique integrating the two approaches mentioned above, and apply it to Hamiltonians with local SU(2) symmetry. With a view toward using this technique in the description of spin liquid in terms of Hamiltonian (1), we start with the simpler case of the Heisenberg Hamiltonian for spin 1/2 with antiferromagnetic interaction:

$$H = h\sum_{\mathbf{i}} S_{\mathbf{i}}^z + J\sum_{\mathbf{i}} \sum_{\mathbf{j}}^{\langle nn\rangle} \left(\mathbf{S_i}\cdot\mathbf{S_j} - \frac{1}{4} \right); \tag{2}$$

we then pass to a description of the Kondo lattice at high temperatures $T > T_K$, for which the noncrossing approximation (NCA) applies, and the system can be treated as a periodic lattice of independent Kondo scatterers interacting via the RKKY mechanism.[3]

Let us introduce a pseudofermion representation[10] for spin operators:

$$S^+ = f_\uparrow^+ f_\downarrow, \quad S^- = f_\downarrow^+ f_\uparrow, \quad S^z = \frac{1}{2}(f_\uparrow^+ f_\uparrow - f_\downarrow^+ f_\downarrow). \tag{3}$$

These operators satisfy the local constraint condition

$$n = f_\uparrow^+ f_\uparrow + f_\downarrow^+ f_\downarrow = 1 \tag{4}$$

at each site. The first term in Eq. (2) describes Zeeman splitting in an infinitesimal magnetic field $h = g\mu_B H$, and the antiferromagnetic sign of the exchange constant J is taken into account explicitly.

The SU(2) invariance means that the spin operators $\{S^+,S^-,S^z\}$ can be expressed as arbitrary linear combinations of spin-fermions $\{f_\uparrow,f_\downarrow,f_\uparrow^+,f_\downarrow^+\}$:

$$S_{\mathbf{i}}^+=(\cos\,\theta f_{\mathbf{i}\uparrow}^+ +\sin\,\theta f_{\mathbf{i}\downarrow}\,)(\cos\,\theta f_{\mathbf{i}\downarrow}-\sin\,\theta f_{\mathbf{i}\uparrow}^+\,),$$

$$S_{\mathbf{i}}^-=(\cos\,\theta f_{\mathbf{i}\downarrow}^+ -\sin\,\theta f_{\mathbf{i}\uparrow})(\cos\,\theta f_{\mathbf{i}\uparrow}+\sin\,\theta f_{\mathbf{i}\downarrow}^+), \tag{5}$$

$$S^z=\frac{1}{2}(f_{\mathbf{i}\uparrow}^+ f_{\mathbf{i}\uparrow}-f_{\mathbf{i}\downarrow}^+ f_{\mathbf{i}\downarrow}).$$

In particular, for pseudofermion filling factors, we have complete particle–hole symmetry,

$$f_{\mathbf{i}\sigma}^+ f_{\mathbf{i}\sigma}=f_{\mathbf{i}-\sigma}f_{\mathbf{i}-\sigma}^+, \tag{6}$$

which directly follows from condition (4) or from Eqs. (5) for $\theta = 0,\pi/2$. Thus, Hamiltonian (2) can be expressed in the pseudofermion representation as

$$H=H_0+H_{\rm int}=-\frac{h}{2}\sum_{\mathbf{i}\sigma}\,\sigma f_{\mathbf{i}\sigma}^+ f_{\mathbf{i}\sigma}+\frac{J}{2}\sum_{\mathbf{ij}\sigma}\,f_{\mathbf{i}\sigma_1}^+ f_{\mathbf{j}\sigma_1}f_{\mathbf{j}\sigma_2}^+ f_{\mathbf{i}\sigma_2}. \tag{7}$$

The local constraint places significant limits on the feasibility of using standard diagrammatic techniques, or in any case, makes more difficult practical description of the spin dynamics in the fermion representation, since the functional space in which the spin and fermion operators act has finite dimensionality. One of the most convenient techniques for including the spin kinetamics in the fermion representation was suggested by Abrikosov.[10] $2S+1$ spins (projections) correspond to a localized spin $\mathbf{S_i}$, whereas in its description in terms of pseudofermion operators $2^{(2S+1)}$ orthogonal states emerge, in accordance with the filling numbers (0,1) for all $2S+1$ spin projections. In a specific case of spin $S = 1/2$, there are four fermion states:

$$|0\rangle=|0,0\rangle;\quad |+\rangle=|1,0\rangle;\quad |-\rangle=|0,1\rangle;\quad |2\rangle=|1,1\rangle \tag{8}$$

and only two of them, namely states $|\pm\rangle$, correspond to physical states of the spin operator. Abrikosov suggested ascribing energy $\lambda \gg T$ to each state occupied by a pseudofermion. Then the nonphysical state $|2\rangle$ from set (8) is frozen out after averaging owing to the additional factor $\exp(-\lambda/T)$ in the partition function $\mathcal{Z}(T)$. In order to get rid of the other nonphysical state $|0\rangle$, one must introduce an additional factor $(1/2)\exp(\lambda/T)$ to $\mathcal{Z}(T)$ and take the limit $\lambda/T\to\infty$ in averaging over spin states. As a result, physical states $|\pm\rangle$ become states with the lowest ''energy'', and the final result is independent of λ. Abrikosov's prescription applies to local spin states in the case of a one-impurity Hamiltonian of sf-exchange. In a Kondo lattice it can be used only in the limit of large spin with degeneracy $N\to\infty$, for which NCA becomes an asymptotically exact approximation,[29] but this technique cannot be used in describing spin-liquid correlations.

The starting point of the proposed method is the well known similarity between the Heisenberg and Hubbard Hamiltonians in the limit of strong interaction U in the case of half-filled states. Let us express pseudofermion operators in the form of sums,

$$f_{\mathbf{i}\sigma}^+=f_{\mathbf{i}\sigma}^+(1-n_{\mathbf{i}-\sigma})+f_{\mathbf{i}\sigma}^+ n_{\mathbf{i}-\sigma},$$

$$n_{\mathbf{i}\sigma}=n_{\mathbf{i}\sigma}(1-n_{\mathbf{i}-\sigma})+n_{\mathbf{i}\sigma}n_{\mathbf{i}-\sigma}, \tag{9}$$

and introduce Hubbard's projection operators for pseudofermions, as was done by Hubbard for the real electron operators[30]:

$$X_{\mathbf{i}}^{\sigma 0}=f_{\mathbf{i}\sigma}^+(1-n_{\mathbf{i}-\sigma}),\quad X_{\mathbf{i}}^{2\sigma}=-\sigma f_{\mathbf{i}-\sigma}^+ n_{\mathbf{i}\sigma},$$

$$X_{\mathbf{i}}^{\sigma\sigma}=n_{\mathbf{i}\sigma}(1-n_{\mathbf{i}-\sigma})=n_{\mathbf{i}\sigma}n_{\mathbf{i}-\sigma},\quad X_{\mathbf{i}}^{22}=n_{\mathbf{i}\uparrow}n_{\mathbf{i}\downarrow},$$

$$X_{\mathbf{i}}^{00}=(1-n_{\mathbf{i}\uparrow})(1-n_{\mathbf{i}\downarrow}), \tag{10}$$

$$X_{\mathbf{i}}^{\sigma-\sigma}=f_{\mathbf{i}\sigma}^+ f_{\mathbf{i}-\sigma}=X_{\mathbf{i}}^{\sigma 2}X_{\mathbf{i}}^{2-\sigma}=X_{\mathbf{i}}^{\sigma 0}X_{\mathbf{i}}^{0-\sigma}.$$

These operators form a normalized basis for the group SU(4) with the obvious completeness condition

$$\sum_\mu X_{\mathbf{i}}^{\mu\mu}=1. \tag{11}$$

The second line of Eq. (9) can be rewritten in the form

$$n_{\mathbf{i}\sigma}=X_{\mathbf{i}}^{\sigma 0}X_{\mathbf{i}}^{0\sigma}+X_{\mathbf{i}}^{\sigma 2}X_{\mathbf{i}}^{2\sigma}. \tag{12}$$

As a result, Hamiltonian (2), (7) takes the form

$$H=H_0+H_{\rm int},$$

$$H_0=-\frac{h}{2}\sum_{\mathbf{i}\sigma}\,\sigma X_{\mathbf{i}}^{\sigma\sigma}+\frac{U}{2}\sum_{\mathbf{i}}\,(X_{\mathbf{i}}^{00}+X_{\mathbf{i}}^{22}), \tag{13}$$

$$H_{\rm int}=\frac{J}{2}\sum_{\mathbf{ij}\sigma}\,(X_{\mathbf{i}}^{\sigma-\sigma}X_{\mathbf{j}}^{-\sigma\sigma}-X_{\mathbf{i}}^{\sigma\sigma}X_{\mathbf{j}}^{-\sigma-\sigma})$$

$$=\frac{J}{2}\sum_{\mathbf{ij}\sigma\sigma'}\,\phi_{\mathbf{ij}}^{\sigma}\phi_{\mathbf{ji}}^{\sigma'}.$$

Here

$$\phi_{\mathbf{ij}}^{\sigma}=(\sigma X_{\mathbf{i}}^{2-\sigma}+X_{\mathbf{i}}^{\sigma 0})(\sigma X_{\mathbf{j}}^{-\sigma 2}+X_{\mathbf{j}}^{0\sigma}), \tag{14}$$

and the fictitious Hubbard repulsion parameter U for pseudofermions is introduced so as to preserve the particle–hole symmetry of the Heisenberg Hamiltonian.

Instead of using diagram techniques for the X-operators (see, for example, Refs. 19, 22, 31, and 32), we try to remain within the standard Feynman approach, but use the properties of the projection operators $X_{\mathbf{i}}^{\lambda\mu}$ in explicit form. We take for a basis of the diagram expansion the eigenstates of the Hamiltonian H_0 under the condition $U/T \equiv \beta U\to\infty$. As a result, we have the reduced Hamiltonian

$$\widetilde{H}=\widetilde{H}_0+H_{\rm int},\quad \widetilde{H}_0=-\frac{h}{2}\sum_{\mathbf{i}\sigma}\,\sigma f_{\mathbf{i}\sigma}^+ f_{\mathbf{i}\sigma} \tag{15}$$

with the partition function $\hat{\mathcal{Z}} = \mathrm{Tr}[\exp(-\beta\widetilde{H})]$, which includes only physical states $|\sigma\rangle = |\pm\rangle$ from set (8). The Hamiltonian H_0 reduces to $\widetilde{H}_0$ since the operators $X_{\mathbf{i}}^{\sigma\sigma}$ and $f_{\mathbf{i}\sigma}^+ f_{\mathbf{i}\sigma}$ have identical matrix elements in the reduced (physical) space. Now we can use $\widetilde{H}$ in the form (15) as a zero-approximation Hamiltonian for the Matsubara diagram technique.[2)]

Selection of one of the two forms of Hamiltonian (13) depends on which of the spin system states we are going to describe. Whereas the most convenient representation for the high-temperature paramagnetic phase or a state with long-

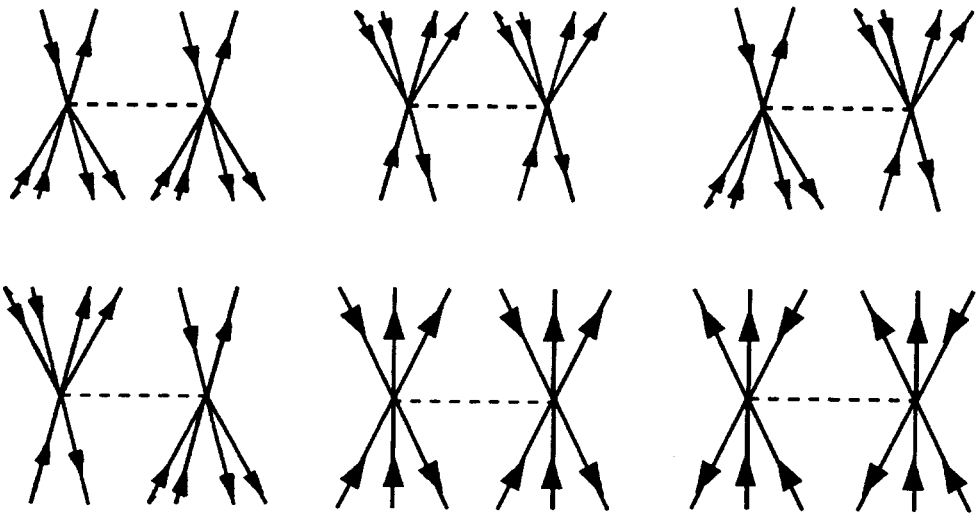

FIG. 1. Bare exchange vertices with due account of projection operators.

range magnetic order is $H_{\rm int}$ in terms of spin operators $X_{\mathbf{i}}^{\sigma\sigma'}$, it is natural to describe the RVB spin-liquid state in terms of operators $\phi_{\mathbf{ij}}^{\sigma}$.

Let us first consider the temperature Green's function

$$\mathscr{K}_{\mathbf{ij}}^{\perp}(\tau)=\langle T_{\tau}S_{\mathbf{i}}^{+}(\tau)S_{\mathbf{j}}^{-}(0)\rangle_{\tilde{H}}, \tag{16}$$

which describes elementary excitations in the standard theory of magnetism ($i\tau$ is the imaginary ''time''). To zeroth-order in the interaction, the function has the form

$$\mathscr{K}_{\mathbf{ij}}^{0}(\tau)=\frac{\delta_{\mathbf{ij}}}{4}\langle T_{\tau}f_{\mathbf{i}\uparrow}^{+}(\tau)f_{\mathbf{i}\downarrow}(\tau)f_{\mathbf{i}\downarrow}^{+}(0)f_{\mathbf{i}\uparrow}(0)\rangle_{\tilde{H}_0}. \tag{17}$$

Averaging is performed with the partition function $\mathscr{Z}=2\cosh(\beta h)$, $\beta=1/kT$. In accordance with Wick's theorem, this average can be presented in the form of a two-fermion loop and reduces to the simple expression

$$\mathscr{K}_{\mathbf{ij}}^{0}(\tau)=\frac{\delta_{\mathbf{ij}}}{4}e^{-h\tau}\begin{cases}\langle n_{\mathbf{i}\uparrow}(1-n_{\mathbf{i}\downarrow})\rangle_{\tilde{H}_0} & (\tau>0)\\ \langle n_{\mathbf{i}\downarrow}(1-n_{\mathbf{i}\uparrow})\rangle_{\tilde{H}_0} & (\tau<0)\end{cases}. \tag{18}$$

One can see that by virtue of Eq. (4), fermion states are generated in pairs, and the emergence of filling factors in the form of averages of projection operators $\langle X^{\sigma\sigma}\rangle_{\tilde{H}_0}$ [see Eq. (10)] shows that spin operators do not drive the system from the space of ''physical'' states $|\pm\rangle$.

Thus, the limit $U\to\infty$ for effective Hamiltonian (13) is equivalent to the limit $\lambda\to\infty$ in Abrikosov's procedure described above, which ''freezes out'' nonphysical pseudofermion states $|0\rangle$ and $|2\rangle$ without breaking the particle–hole symmetry.

The perturbation theory series for the function $\mathscr{K}^{\perp}$ can be constructed in accordance with the usual rules for calculating two-time Green's functions. This procedure leads to Larkin's equation[34]

$$\mathscr{K}=\Sigma+J\Sigma.\mathscr{K}. \tag{19}$$

Here Σ is the irreducible polarization operator, which is not separable with respect to the interaction. In Sec. 5 we will use this version of the diagram technique to calculate the spin diffusion coefficient near the Néel point.

Let us proceed to nonlocal spin-liquid correlations. We consider as an example an RVB homogeneous spin liquid described by the correlator

$$\mathscr{L}_{\mathbf{ij}}=\sum_{\sigma}\langle\phi_{\mathbf{ij}}^{\sigma}\phi_{\mathbf{ji}}^{\sigma}\rangle, \tag{20}$$

i.e., we use the second version of $H_{\rm int}$ in Eq. (13). Thus, the nonphysical states $|0\rangle$ and $|2\rangle$ are eliminated by the Hubbard procedure, since each fermion creation event at each site involves a projection operation in accordance with Eq. (14). This makes exchange vertex (13) more complicated; it can be described in the projection techniques by diagrams with twelve tails, as is shown by Fig. 1.

The role of projectors is to automatically eliminate a state with an opposite projection in creating a fermion with a given spin projection, and this guarantees that the creation operator acts on a state from the physical subspace $|\pm\rangle$. But, although correlator (20) is diagonal in subspace $|\pm\rangle$, the nonphysical states $|0\rangle$ and $|2\rangle$ manifest themselves as intermediate states in any attempt to describe the spin liquid in terms of fermion operators.

In Refs. 11 and 13 it was noted that introduction of a homogeneous RVB state in the mean-field approximation[16] violates the local gauge invariance due to constraint (4), (6), and long-wave fluctuations of gauge fields significantly change the character of RVB excitations in a two-dimensional Heisenberg lattice (see also Refs. 14, 35, and 36). In this paper, we do not consider the problem of long-wave fluctuations in gauge fields. We are interested primarily in nonlocal high-temperature magnetic fluctuations, which are also related, however, to the violation of the constraint.

As was shown in the fundamental study by Baskaran, Zou and Anderson,[16] the description of a uniform RVB state requires ''anomalous'' coupling between pseudofermions at different sites. It is clear that such a procedure drives the system beyond the physical space $|\pm\rangle$. The gauge theory of a spin liquid demonstrates that free propagation of a spinon is impossible. The complex shape of vertices in the projection technique (Fig. 1) indicates the same thing. Nonetheless,

we start construction of our scheme with a demonstration of how far this technique applies in the mean-field approximation; we then consider the possible effect of fluctuations on the mean-field solution.

Let us introduce an anomalous one-particle (one-fermion) temperature Green's function. In order to preserve particle–hole symmetry, let us express it in matrix form:

$$\hat{\mathscr{G}}_{\mathbf{ij}\sigma}(\tau)=-\langle T_\tau \hat{X}_{\mathbf{i}\sigma}(\tau)\hat{X}^+_{\mathbf{j}\sigma}(0)\rangle_{\tilde{H}}, \tag{21}$$

where

$$\hat{X}_{\mathbf{i}\sigma}=\begin{pmatrix} X_{\mathbf{i}}^{0\sigma} & X_{\mathbf{i}}^{\sigma 0} \\ \sigma X_{\mathbf{i}}^{-\sigma 2} & \sigma X_{\mathbf{i}}^{2-\sigma}\end{pmatrix}, \quad \hat{X}^+_{\mathbf{i}\sigma}=\begin{pmatrix} X_{\mathbf{i}}^{\sigma 0} & \sigma X_{\mathbf{i}}^{2-\sigma} \\ X_{\mathbf{i}}^{0\sigma} & \sigma X_{\mathbf{i}}^{-\sigma 2}\end{pmatrix}. \tag{22}$$

This Green's function has the structure

$$\hat{\mathscr{G}}_{\mathbf{ij}\sigma}(\tau)=-\begin{pmatrix} \langle T_\tau(X_{\mathbf{i}}^{0\sigma}(\tau)X_{\mathbf{j}}^{\sigma 0}(0) & \sigma\langle T_\tau(X_{\mathbf{i}}^{0\sigma}(\tau)X_{\mathbf{j}}^{2-\sigma}(0) \\ +X_{\mathbf{i}}^{\sigma 0}(\tau)X_{\mathbf{j}}^{0\sigma}(0))\rangle & +X_{\mathbf{i}}^{\sigma 0}(\tau)X_{\mathbf{j}}^{-\sigma 2}(0)\rangle \\ \sigma\langle T_\tau(X_{\mathbf{i}}^{-\sigma 2}(\tau)X_{\mathbf{j}}^{\sigma 0}(0) & \langle T_\tau(X_{\mathbf{i}}^{-\sigma 2}(\tau)X_{\mathbf{j}}^{2-\sigma}(0) \\ +X_{\mathbf{i}}^{2-\sigma}(\tau)X_{\mathbf{j}}^{-0\sigma}(0)\rangle & +X_{\mathbf{i}}^{2-\sigma}(\tau)X_{\mathbf{j}}^{-\sigma 2}(0)\rangle \end{pmatrix}. \tag{23}$$

The zero (one-site) matrix Green's function

$$\hat{g}_{\mathbf{i}\sigma}(\tau)=-\langle T_\tau \hat{X}_{\mathbf{i}\sigma}(\tau)\hat{X}^+_{\mathbf{i}\sigma}(0)\rangle_{\tilde{H}_0} \tag{24}$$

is diagonal, and its elements are

$$\begin{aligned} g^{(11)}_{\mathbf{i}\sigma}(\tau)&=-\langle T_\tau(X_{\mathbf{i}}^{0\sigma}(\tau)X_{\mathbf{i}}^{\sigma 0}(0)+X_{\mathbf{i}}^{\sigma 0}(\tau)X_{\mathbf{i}}^{0\sigma}(0))\rangle_0, \\ g^{(22)}_{\mathbf{i}\sigma}(\tau)&=-\langle T_\tau(X_{\mathbf{i}}^{-\sigma 2}(\tau)X_{\mathbf{i}}^{2-\sigma}(0) \\ &\quad +X_{\mathbf{i}}^{2-\sigma}(\tau)X_{\mathbf{i}}^{-\sigma 2}(0))\rangle_0. \end{aligned}$$

As in the previous case, the averaging $\langle\ldots\rangle_0\equiv\langle\ldots\rangle_{\tilde{H}_0}$ leaves the one-site Green's function in the physical sector of the Fock space. In particular,

$$\begin{aligned} g^{(11)}_{\mathbf{i}\sigma}(\tau_1-\tau_2)&=-\langle X_{\mathbf{i}}^{\sigma 0}(\tau_1)X_{\mathbf{i}}^{0\sigma}(\tau_2)\rangle_0 \\ &=-\langle X_{\mathbf{i}}^{\sigma\sigma}\rangle_0\ \exp[-i\sigma h(\tau_1-\tau_2)/2] \\ &\quad\times(\tau_1>\tau_2), \\ g^{(11)}_{\mathbf{i}\sigma}(\tau_1-\tau_2)&=\langle X_{\mathbf{i}}^{\sigma 0}(\tau_2)X_{\mathbf{i}}^{0\sigma}(\tau_1)\rangle_0 \\ &=\langle X_{\mathbf{i}}^{\sigma\sigma}\rangle_0\ \exp[-i\sigma h(\tau_1-\tau_2)/2](\tau_2>\tau_1). \end{aligned} \tag{25}$$

Unlike spin Green's functions (17), matrix elements of the function $\hat{g}_{\mathbf{i}\sigma}(\tau)$ formally represent the three-fermion loops containing one particle (spin up) and two hole (spin down) propagators, or one hole and two particle propagators. This function, however, can be simplified using the idempotence property of operator $b^\dagger b$, conditions (4) and (6), and Wick's theorem. By substituting the Hubbard operators in the interaction picture into Eq. (25), we obtain expressions for the elements of the one-site propagator,

$$g^{(11)}_{\mathbf{i}\uparrow}=\frac{1}{2}e^{-h\tau}\begin{cases} -\langle(1-n_{\mathbf{i}\downarrow})\rangle_0 & (\tau>0) \\ \langle n_{\mathbf{i}\downarrow}\rangle_0 & (\tau<0), \end{cases}$$

and a similar expression for the spin-down state.

One can easily check that the Green's function $\mathscr{G}^{(\alpha\alpha)}_{\mathbf{i}\sigma}$ is periodic, $\mathscr{G}_{\mathbf{ii}\sigma}(\tau<0)=-\mathscr{G}_{\mathbf{ii}\sigma}(\tau+1/T)$, so that by introducing the Matsubara frequencies $\omega_n=(2n+1)\pi T$ in the usual manner, we obtain

$$g^{(\alpha\alpha)}_{\mathbf{i}\sigma}(\omega_n)=\frac{1}{2}\,\frac{1}{i\omega_n+(-1)^\alpha\sigma h/2}. \tag{26}$$

The mean-field approximation[16] is based on the introduction of anomalous averages $\langle f^+_{\mathbf{i}\sigma}f_{\mathbf{j}\sigma}\rangle$. For the anomalous matrix Green's function (21), we must introduce four components:

$$\begin{aligned} \Delta^{11}_{ij\sigma}&=\langle X_{\mathbf{i}}^{\sigma 0}(\tau)X_{\mathbf{j}}^{0\sigma}(\tau'\to\tau)\rangle, \\ \Delta^{22}_{ij\sigma}&=\langle X_{\mathbf{i}}^{-\sigma 2}(\tau)X_{\mathbf{j}}^{2-\sigma}(\tau'\to\tau)\rangle, \\ \Delta^{12}_{ij\sigma}&=\langle X_{\mathbf{i}}^{\sigma 0}(\tau)X_{\mathbf{j}}^{-\sigma 2}(\tau'\to\tau)\rangle, \\ \Delta^{21}_{ij\sigma}&=\langle X_{\mathbf{i}}^{2-\sigma}(\tau)X_{\mathbf{j}}^{0\sigma}(\tau'\to\tau)\rangle, \end{aligned} \tag{27}$$

where $\Delta^{11}_{ij\sigma}=\Delta^{22}_{ij\sigma}$. Then one can easily check that the anomalous Green's function also satisfies a periodic condition like that in Eq. (21) on the inverse temperature. Thus, we can use the projection diagram technique in calculating the anomalous average $\Delta=\Sigma_\sigma\langle\phi^\sigma_{\mathbf{ij}}\rangle$, which characterizes a uniform RVB state. This ''order parameter'' can be derived from the relation

$$\Delta=\mathrm{Tr}(\hat{1}+\hat{\tau}_1)\hat{\mathscr{G}}_{\mathbf{ij}}(\tau\to-0), \tag{28}$$

where $\hat{1}$ and $\hat{\tau}_1$ are the Pauli matrices.

Let us rewrite Hubbard operators (10) in the particle–hole representation, $f_{\mathbf{i}\uparrow}\equiv a_{\mathbf{i}}$, $f_{\mathbf{i}\downarrow}\equiv b^+_{\mathbf{i}}$:

$$X_{\mathbf{i}}^{\uparrow 0}=a^+_{\mathbf{i}}b^+_{\mathbf{i}}b_{\mathbf{i}}, \quad X_{\mathbf{i}}^{2\downarrow}=a^+_{\mathbf{i}}b_{\mathbf{i}}b^+_{\mathbf{i}}, \quad X_{\mathbf{i}}^{\uparrow\downarrow}=a^+_{\mathbf{i}}b^+_{\mathbf{i}}\ldots$$

The mean-field approximation (28) corresponds to the following splitting of the interaction Hamiltonian H_{int}:

$$H_{\mathrm{MF}}=J\Delta\sum_{\mathbf{i}}\sum_{\mathbf{j}}^{\langle nn\rangle}(Y^{(h)}_{\mathbf{ij}}+Y^{(p)}_{\mathbf{ij}}), \tag{29}$$

where

$$\begin{aligned} Y^{(p)}_{\mathbf{ij}}&=a^+_{\mathbf{i}}b^+_{\mathbf{i}}b_{\mathbf{i}}b^+_{\mathbf{j}}b_{\mathbf{j}}a_{\mathbf{j}}+a^+_{\mathbf{i}}b_{\mathbf{i}}b^+_{\mathbf{i}}b_{\mathbf{j}}b^+_{\mathbf{j}}a_{\mathbf{j}}+a^+_{\mathbf{i}}b_{\mathbf{i}}b^+_{\mathbf{i}}b^+_{\mathbf{j}}b_{\mathbf{j}}a_{\mathbf{j}} \\ &\quad+a^+_{\mathbf{i}}b^+_{\mathbf{i}}b_{\mathbf{i}}b_{\mathbf{j}}b^+_{\mathbf{j}}a_{\mathbf{j}}, \\ Y^{(h)}_{\mathbf{ij}}&=b_{\mathbf{i}}a_{\mathbf{i}}a^+_{\mathbf{i}}a_{\mathbf{j}}a^+_{\mathbf{j}}b^+_{\mathbf{j}}+b_{\mathbf{i}}a^+_{\mathbf{i}}a_{\mathbf{i}}a^+_{\mathbf{j}}a_{\mathbf{j}}b^+_{\mathbf{j}}+b_{\mathbf{i}}a_{\mathbf{i}}a^+_{\mathbf{i}}a^+_{\mathbf{j}}a_{\mathbf{j}}b^+_{\mathbf{j}} \end{aligned}$$

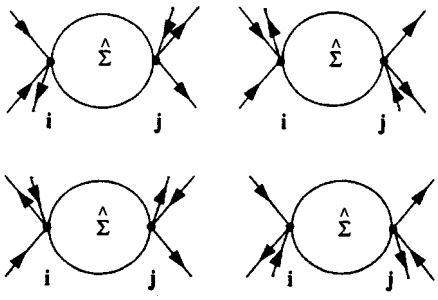

FIG. 2. Components of $\hat{\Sigma}$ matrix for the one-particle Green's function $\mathscr{G}_{\mathbf{ij}}$.

$$+ b_{\mathbf{i}} a_{\mathbf{i}}^{+} a_{\mathbf{i}} a_{\mathbf{j}} a_{\mathbf{j}}^{+} b_{\mathbf{j}}^{+} .$$

In terms of perturbation theory, this approximation can be described by the diagrams for the self-energy component $\hat{\Sigma}_{\mathbf{ij}}$ of Green's function (23) shown in Fig. 2. The four diagrams correspond to the four elements of $\hat{\Sigma}$. The Dyson matrix equation in this approximation is expressed by the diagrams in Fig. 3, in which double lines denote the one-site matrices $g_{\mathbf{i}\sigma}$, the dashed line denotes the Heisenberg exchange constant, and thick lines with two arrows denote the anomalous Green's function $\hat{\mathscr{G}}_{\mathbf{ij}\sigma}$. The Dyson equation

$$\hat{\mathscr{G}}_{\mathbf{ij}\sigma}(\omega_n) = \hat{g}_{\mathbf{i}\sigma}(\omega_n)\left(\delta_{\mathbf{ij}} + \sum_{\mathbf{l}} \hat{\Sigma}_{\mathbf{il}} \hat{\mathscr{G}}_{\mathbf{lj}\sigma}(\omega_n) \right) \tag{30}$$

is Fourier transformed to (as $h \to 0$)

$$2 i\omega_n \mathscr{G}_{\mathbf{k}\sigma}^{(\alpha\beta)}(i\omega_n) = \delta_{\alpha\beta} + J\Delta\varphi(\mathbf{k}) \sum_{\gamma} \mathscr{G}_{\mathbf{k}\sigma}^{(\gamma\beta)}(i\omega_n). \tag{31}$$

A solution of this equation system is

$$\mathscr{G}_{\mathbf{k}\sigma}^{(11)}(i\omega_n) = \frac{1}{2} \frac{i\omega_n - \epsilon_{\mathbf{k}}/2}{i\omega_n (i\omega_n - \epsilon_{\mathbf{k}})},$$

$$\mathscr{G}_{\mathbf{k}\sigma}^{(12)}(i\omega_n) = \frac{1}{2} \frac{\sigma\epsilon_{\mathbf{k}}/2}{i\omega_n (i\omega_n - \epsilon_{\mathbf{k}})}. \tag{32}$$

Here $\epsilon_{\mathbf{k}}$ is the spinon dispersion relation in the mean-field approximation in the form

$$\epsilon_{\mathbf{k}} = J\Delta\varphi(\mathbf{k}) \tag{33}$$

in the case of antiferromagnetic exchange only between nearest neighbors; $\varphi(\mathbf{k})$ is the corresponding form factor:

$$\varphi(\mathbf{k}) = \sum_{\mathbf{l}}^{(nn)} e^{i\mathbf{k}\cdot\mathbf{l}}. \tag{34}$$

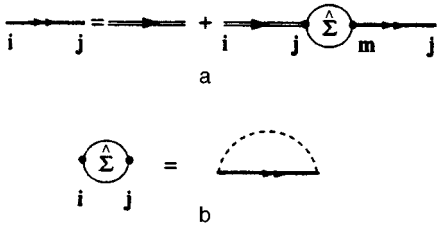

FIG. 3. (a) Dyson equation and (b) self-energy part of the Green's function $\mathscr{G}_{\mathbf{ij}}$ in the mean-field approximation.

By substituting Green's functions (32) into Eq. (28), we obtain a self-consistent equation for Δ:

$$\Delta = (ZN)^{-1} \sum_{\mathbf{k}} \varphi(\mathbf{k}) \tanh \frac{\beta[J\Delta\varphi(\mathbf{k}) - \mu]}{2}, \tag{35}$$

where Z is the coordination number. The chemical potential μ is treated as a Lagrange multiplier when constraint (4) is substituted into the Hamiltonian. This operation corresponds to substitution of $i\omega_n + \mu$ for $i\omega_n$. As usual, the local constraint can be replaced with a global one in the mean-field approximation:

$$N^{-1} T \sum_{\mathbf{k}} \sum_{\omega_n} \mathrm{Tr}(\hat{1} + \hat{\tau}_1) \hat{\mathscr{G}}_{\mathbf{k}}(i\omega_n) = 0. \tag{36}$$

By substituting Green's function (32) into Eq. (36), we obtain another self-consistency condition, which fixes μ at the mid-position of the spinon ''band,'' in accordance with particle–hole symmetry.

The ''phase transition'' temperature T^* at which a nontrivial solution for Δ emerges is given by

$$T^* = \frac{J}{2} (ZN)^{-1} \sum_{\mathbf{k}} \varphi^2(\mathbf{k}), \tag{37}$$

which is usually derived in the mean-field approximation using the functional integration technique (see, for example, Refs. 6, 37, and 38).

Thus, we have found that kinematic constraints on the pseudofermion representation of spin operators taken into account through Hubbard projection operators do not affect the mean-field solution for the RVB state as long as particle–hole symmetry is preserved at each step of the calculation. In this respect, the situation is different from that in which the same problem is solved by the Hubbard operator technique for the $t-J$ model with a finite density of holes,[39] where this symmetry is violated from the outset, since only doubly filled states $|2\rangle$ are excluded. In Ref. 22 another symmetry-based approach to elimination of nonphysical states is suggested, in which the ''fermion'' set $|0\rangle$, $|2\rangle$ is replaced with a unified ''boson'' vacuum $|V\rangle$.

Although the projection technique does not contribute any new features to the mean-field solution for the uniform RVB liquid, it offers, in principle, new opportunities for taking gauge fluctuations into account, which inevitably occur in spinon propagation. Moreover, as will be shown in the next section, in a three-dimensional Kondo lattice, spin liquid is formed in the neighborhood of the antiferromagnetic instability, because magnetic fluctuations are a decisive factor for both the transition temperature to the RVB state and the mechanism of this transition.

3. STABILIZATION OF SPIN LIQUID IN THE KONDO LATTICE AT HIGH TEMPERATURES. MEAN-FIELD APPROXIMATION

It is well known[40] that in the three-dimensional Heisenberg lattice the ground state energy of the RVB phase, E_{SL}, is higher than the antiferromagnetic state energy E_{AFM}. It has also been shown, however, that in the Kondo lattice described by the Hamiltonian (1), spin-flip scattering processes

can lead to stabilization of the RVB phase with respect to the magnetically ordered phase.[6,18] Since antiferromagnetic and spin-liquid correlations in the sf-exchange model are governed by the same coupling constant J_{RKKY}, the temperature at which the spin liquid is formed is close to the point of magnetic instability, $T^*-T_N<T_N$, so that antiferromagnetic correlations can significantly alter the character of a transition to the RVB phase, as compared to the results obtained in the mean-field approximation.

In order to describe formation of spin liquid in the Kondo lattice, we take Hamiltonian (1) in the original form

$$H_{\mathrm{eff}}=\sum_{\mathbf{k}\sigma}\ \varepsilon_k c^+_{\mathbf{k}\sigma}c_{\mathbf{k}\sigma}+\frac{1}{4}J_{sf}\sum_{\mathbf{i}}\ c^+_{\mathbf{i}\sigma}c_{\mathbf{i}\sigma'}f^+_{\mathbf{i}\sigma'}f_{\mathbf{i}\sigma}. \tag{38}$$

As mentioned in the Introduction, we operate in the range of parameters $\alpha\approx\alpha_c$ of Doniach's diagram,[3] in which all characteristic temperatures ($T_K\sim\varepsilon_F\exp(-1/2\alpha)$, $T_{N0}\sim\varepsilon_F\alpha^2$, and T^*, which is to be calculated) are of the same order of magnitude, so that in constructing the real phase diagram one must take into account the mutual effects of all three types of correlation—in particular, the change in the Néel temperature with respect to T_{N0} as given by simple perturbation theory in the parameter α.

As noted above, in this study we limit discussion to the range of high temperatures $T>T_K,T_{N0}$, in which the magnetic subsystem is a lattice of paramagnetic spins immersed in the Fermi sea of conductance electrons, and NCA applies to the one-site paramagnetic sf-scattering, i.e., each spin localized at a lattice site scatters conduction electrons independently of other spins. As the temperature is reduced, both Kondo scattering and correlations among lattice sites due to the indirect RKKY interaction are intensified.

The problem of competition between the indirect exchange among lattice sites and one-site sf-scattering has been discussed in literature many times, largely in terms of the Kondo problem with two impurities. In particular, Varma[41] analyzed the mutual influence of Kondo scattering and RKKY interaction at high temperatures by perturbation theory and concluded that the mutual influence of these two processes is small, at least in the leading logarithmic approximation in $\alpha\ \ln(\varepsilon_F/T)$. In this section, we will show that in the Kondo lattice, the effect of spin-flip scattering on magnetic correlations is a decisive factor for stabilization of the RVB phase in the critical region of Doniach's diagram, $\alpha\sim\alpha_c$.

In describing the intersite magnetic interaction under conditions of Kondo scattering in the noncrossing approximation (NCA), the effective vertex of the RKKY exchange $\tilde{J}_{\mathbf{ij}}(T,\epsilon)$ is determined by the diagram in Fig. 4a. In this diagram, dashed lines denote electron Green's functions, and the ingoing and outgoing lines correspond to pseudofermion operators. The one-site sf-exchange vertices Γ include loops corresponding to the leading logarithmic approximation in $\alpha\ \ln(\varepsilon_F/T)$ for the Kondo problem[3)] (Fig. 5). As a result, the effective interaction is given by

$$\tilde{J}_{\mathbf{ij}}(T,\varepsilon_m)=\Pi(R,\varepsilon_m)\Gamma^2, \tag{39}$$

where $\varepsilon_m=2m\pi T,\ R=|R_{\mathbf{i}}-R_{\mathbf{j}}|$.

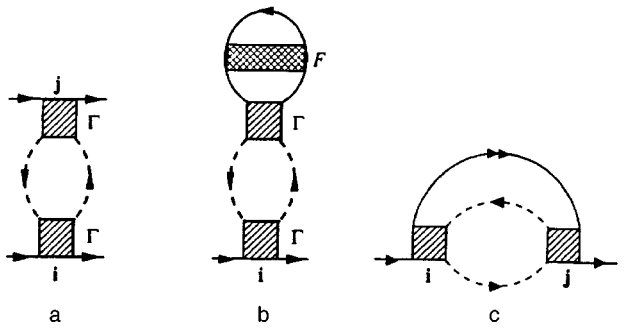

FIG. 4. (a) Effective vertex of renormalized RKKY interaction; self-energy part of the one-particle Green's function in the mean-field approximation (b) for the Néel and (c) RVB phase.

In the spirit of the logarithmic perturbation theory,[10] the argument of vertex Γ should contain only the highest input frequency, which is determined in our case by energies of electronic Green's functions included in the polarization loop $\Pi(R,\varepsilon_m)$ in the integral $\hat{J}_{\mathbf{ij}}(T,\varepsilon_m)$ (Eq. (39)). The polarization operator in the coordinate representation has the form

$$\Pi(\mathbf{R},\varepsilon_m)=T\sum_n\ D(-\mathbf{R},\omega_n+\varepsilon_m)D(\mathbf{R},\omega_n). \tag{40}$$

Since all heavy-fermion systems are characterized by large lattice constants, we use for electronic Green's functions $D(\mathbf{R},\omega_n)$ an expression asymptotic in p_FR:

$$D(R,\omega_n)=-\frac{p_F}{2\pi v_F R}\exp\left(-\frac{|\omega_n|}{2\varepsilon_F}p_FR+ip_FR\ \mathrm{sign}\ \omega_n\right), \tag{41}$$

so that the polarization operator takes the form

$$\Pi(R,\varepsilon_m)=\left(\frac{p_F}{2\pi v_F R}\right)^2 T\sum_{n=-\infty}^{n=\infty}\exp\left(-\frac{|\omega_n|}{v_F}R-\frac{|\omega_n+\varepsilon_m|}{v_F}R+ip_FR[\mathrm{sign}\omega_n+\mathrm{sign}(\omega_n+\varepsilon_m)]\right). \tag{42}$$

In the static limit,

$$\tilde{J}_R(T,0)=T\sum_n\ D^2(R,\omega_n)\Gamma^2(\omega_n,T). \tag{43}$$

The temperature dependence in Eq. (43) is largely determined by one-site vertices, and in the polarization loop one can use the condition $2\pi TR/v_f\ll 1$ and change summation over discrete frequencies to integration (see Appendix I). Then the exchange integral takes the form

FIG. 5. Parquet diagrams for effective vertex Γ.

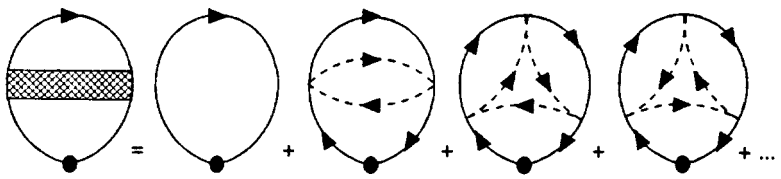

FIG. 6. Single-site diagrams describing Kondo screening of a localized spin.

$$\widetilde{J}_R(T,0)=2\left(\frac{p_F}{2\pi v_F R}\right)^2\cos(2p_FR)\times\int_{T\to 0}^{\infty}\frac{d\varepsilon}{2\pi}\exp\left(-\frac{\varepsilon}{\varepsilon_F}p_FR\right)\Gamma^2(\varepsilon,T). \quad (44)$$

This equation transforms to the standard RKKY exchange integral when modified vertices are replaced with the ''bare'' integrals, $\Gamma\to J_{sf}\Omega_0$, where Ω_0 is the elementary cell volume:

$$J_R^0=(J_{sf}\Omega_0)^2\Pi(R,0)=(J_{sf}\Omega_0)^2\frac{mp_F^4}{\pi^3}\times\left[\frac{\cos(2p_FR)}{(2p_FR)^3}+O\left(\frac{1}{(2p_FR)^4}\right]\right.$$
$$\equiv\left(\frac{J_{sf}^2}{\varepsilon_F}\right)\frac{(p_Fa_0)^6}{2\pi^3}\Phi(2p_FR). \quad (45)$$

Let us substitute into $\widetilde{J}_R(T,0)$ the vertex $\Gamma(\varepsilon,T)$ calculated in the leading logarithmic approximation, in accordance with diagrams given in Fig. 5 with the input frequency ε satisfying the condition $\ln(\varepsilon_F/\overline{\varepsilon})\gg 1$. For the characteristic energy $\overline{\varepsilon}\gg 1$, which determines integral (44) (see Appendix II), we find that the exchange parameter can be approximated by the function

$$\widetilde{J}_R(T,0)\approx\epsilon_F\frac{(p_Fa_0)^6}{2\pi^3}\left(\frac{J_{sf}}{\varepsilon_F}\right)^2\Phi(2p_FR)\times\left(1+2\alpha\,\ln\frac{T}{\varepsilon_F}\right)^{-n}. \quad (46)$$

The exponent n in this function depends on α and the argument of the oscillating function $\Phi(p_FR)$ (see the insert in Fig. 11). Thus, one can see that Kondo scattering has little influence on the form and spatial periodicity of the indirect exchange integral for $T>T_K$.[41] But this integral can be larger, and the larger the separation R between magnetic f-ions, the greater the increase.

In calculating the polarization operator and RKKY integral (46), we assumed that the electron Fermi surface was spherical. Note, however, that the exponent n in Eq. (46) is sensitive to the asymptotic behavior of the function $\Phi(2p_FR)$, so that the role of Kondo processes in intensification of the exchange turns out to be important in the case of a highly anisotropic Fermi surface. In the limiting case of a cylindrical Fermi surface,

$$\Phi(2p_FR)=-\left[\frac{\sin(2p_FR)}{(2p_FR)^2}+O\left(\frac{1}{(2p_FR)^3}\right)\right] \quad (47)$$

(see Appendix I), so that at the same value of p_FR, the integral $\widetilde{J}_R(T,0)$ is larger in the case of a cylindrical Fermi surface than in the case of a spherical surface.

Thus, the spin system can be described at $T>T_K$ by the effective RKKY Hamiltonian with the vertex shown in Fig. 4a in the nearest-neighbor approximation and under the assumption that the RKKY nearest-neighbor coupling has the antiferromagnetic sign. In the mean-field approximation, we treat the problem of stabilization of the spin liquid as a comparison between temperatures of transitions to the RVB state $[T^*(\alpha)]$ and to the antiferromagnetic state $[T_N(\alpha)]$ under conditions of sufficiently strong Kondo scattering, $\alpha\to\alpha_{c0}-0$, and the stabilization criterion is the inequality $T^*(\alpha)>T_N(\alpha)$. The function $T_N(\alpha)$ deviates from the quadratic function prescribed by the bare RKKY vertex. Along with the intensification of one-site vertices described by Eq. (46) and discussed above, there is a dynamic Kondo screening of localized spins, which is the reason for the suppression of antiferromagnetic order as $\alpha\to\alpha_{c0}$.

In the mean-field approximation, the transition temperatures $T_N(\alpha)$ and $T^*(\alpha)$ can be derived from the exchange vertex in Fig. 4a by closing spin-fermion lines, as shown in Figs. 4b and 4c, respectively. The first of these diagrams determines the molecular field for commensurate magnetic ordering characterized by the antiferromagnetic vector $\mathbf{Q}$ such that $\mathbf{Q}\cdot\mathbf{R}_{ij}=\pi$. The suppression of magnetic correlation by Kondo scattering is described by the vertex $F(T)$ in the diagram of Fig. 4b.[42,43] Summation of the set of logarithmic diagrams, the first of which are shown in Fig. 6, yields

$$F(T)=1-2\alpha\,\ln\frac{\varepsilon_F}{T}\Big/\ln\frac{T}{T_K}. \quad (48)$$

Although the function $F(T)$ deviates from this formula as $T\to T_K$,[44] and complete screening occurs only at $T=0$, the suppression of magnetic correlations compensates for the exchange intensification and thus reduces T_N as $\alpha\to\alpha_{c0}$.

The self-energy part of the one-site Green's function $\mathcal{G}_{\mathbf{ii}}$ (Eq. (21)), corresponding to the diagram of Fig. 4b, is

$$\Sigma_N(T)=\lambda\widetilde{J}(R,T)\langle S_z\rangle_T \quad (49)$$

(the factor λ is determined by the lattice configuration). Hence we derive for the mean spin

$$\langle S_z\rangle_T=\frac{1}{2}(\langle a_{\mathbf{i}}^+a_{\mathbf{i}}\rangle+\langle b_{\mathbf{i}}^+b_{\mathbf{i}}\rangle-1)$$

a self-consistent equation

$$\langle S_z\rangle_T=\frac{1}{2}F(T)\tanh\frac{\Sigma_N(T)}{2T}, \quad (50)$$

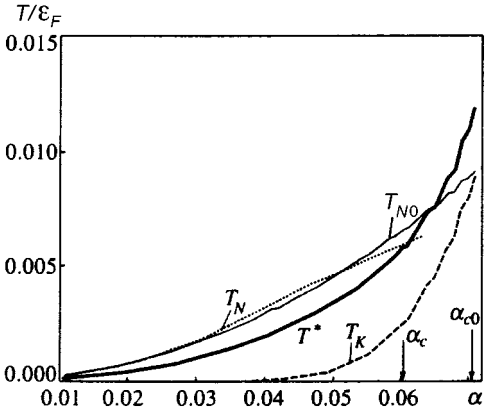

FIG. 7. Generalized Doniach diagram taking the RVB phase into account.

which is, naturally, the standard Brillouin equation for Weiss' molecular field taking Kondo screening into account.

The mean-field equation for Δ (Eq. (28)) is determined by the self-energy part of the anomalous Green's function $\hat{G}_{\mathbf{ij}}(\tau)$ (Eq. (23)) shown in Fig. 4c. This diagram can be substituted into the Dyson equation (Fig. 3), which in this case takes the form

$$\hat{G}(\mathbf{p},\omega_n)=g_0(\omega_n)\Bigg[1-2T\sum_m\sum_{\mathbf{q}}\tilde{J}(\mathbf{p}-\mathbf{q},\omega_n-\omega_m)\times\hat{G}(\mathbf{q},\omega_m)\hat{G}(\mathbf{p},\omega_n)\Bigg]. \tag{51}$$

Here $g_0(\omega_n)$ is the zero one-site Green's function with components (26), and $\tilde{J}(\mathbf{p}-\mathbf{q},\omega_n)$ is a Fourier transform of the indirect exchange integral (39), which in the nearest-neighbor approximation takes the form

$$\tilde{J}(\mathbf{q},\varepsilon_m)=\sum_{\mathbf{l}=0,\langle\mathbf{l}\rangle_{nn}}\tilde{J}_R(\varepsilon_m)e^{-i\mathbf{qr}}=\tilde{J}_0(\varepsilon_m)+\tilde{J}_R(\varepsilon_m)\varphi(\mathbf{q}). \tag{52}$$

The one-site integral $\tilde{J}_0(T,0)$ is estimated as $\alpha^2 T\ln(\varepsilon_F/T)$. Since this integral contains an additional small factor α at $T\sim T^*$, as compared to the intersite integral (46), it can be omitted.

By neglecting, as usual, the frequency dependence of the RKKY interaction, we obtain the mean-field equation (35) for Δ with the coupling constant $J=\tilde{J}_R(T,0)$. As follows from the configuration of the anomalous self-energy part (Fig. 4c), the screening effect responsible for suppression of local magnetic moments does not affect the mean-field parameter Δ, which can be naturally attributed to the singlet nature of the RVB-coupling. The Kondo ''screening'' radius can be estimated by high-temperature perturbation theory to be $\hbar v_F/2T_K$, which is much larger than the correlation radius of the singlet RVB pair, since electron scattering by these pairs is inefficient.

Calculations of the temperatures T^* and T_N by Eqs. (35), (46), (49), and (50) are given in Fig. 7 (see also Ref. 18). This graph shows that as $\alpha\to\alpha_{c0}$, these temperatures become closer, a new critical point α_c emerges in Doniach's diagram, on the right of which the RVB phase is stable with respect to the antiferromagnetic phase, and this stabilization takes place in the logarithmic neighborhood of the Kondo temperature. A calculation of T_N for $\alpha>\alpha_c$ makes no sense, because magnetic ordering in this region should follow another scenario.

Thus, we conclude that stabilization of a homogeneous RVB spin liquid in a three-dimensional Kondo lattice can occur only near the magnetic instability point under conditions of sufficiently strong Kondo screening of localized spins by conduction electrons. This result, obtained in the mean-field approximation, indicates that stabilization of the spin-liquid phase is incompatible with formation of Kondo singlet states characterized by anomalous averages $\langle c_i^+ f_i\rangle$,[6,45] since anomalous Kondo scattering is frozen at $T\approx T^*>T_K$. This resolves Nozières' well-known paradox[46] about the impossibility of screening all spins in the Kondo lattice by electrons from a thin layer of width T_K near the Fermi surface. In the scheme proposed above, the screening vanishes at sufficiently high temperatures above T_K, the Kondo temperature itself is not a singular point of the theory, renormalization of the sf-exchange integral is frozen at about $\tilde{J}(T^*)$, and at $T<T_K$, T^* electrons interact not with localized spins, but with spin-liquid excitations of the spinon type (see also Ref. 47).

In addition to the disadvantages related to violation of local gauge invariance, however, the mean-field approximation in the case of RVB coupling has another flaw, namely, it does not take into account the proximity of the spin system to the antifferomagnetic instability. In the following sections, we discuss possible consequences of this proximity for the RVB state, first in the self-consistent field approximation, then beyond this model.

4. EFFECT OF SPIN FLUCTUATIONS AND MAGNETIC ANISOTROPY ON RVB PHASE STABILIZATION

In the previous section, we determined that antiferromagnetic fluctuations inevitably turn out to be strong in an RVB spin liquid in the three-dimensional Kondo lattice at high temperatures $T\sim T^*$, and can lead, in principle, to magnetic ordering at $T\ll T^*$. Leaving this issue for subsequent studies, let us consider now the effect of spin fluctuations on features of the transition to the spin-liquid state in the mean-field approximation, but using its modification obtained through the projection technique, in which the order parameter is defined by Eq. (28). The diagram technique using Hubbard operators and developed in Sec. 2 allows us to take into consideration long-wave fluctuations of gauge fields due to the U(1) noninvariance of the RVB order parameter. Terms that take the phase of function Δ into account can be introduced into the effective Hamiltonian in standard fashion.[13,14] It is known that long-wave fluctuations in calibration fields do not lead to divergences destabilizing RVB averages in three-dimensional systems. Therefore, the introduction of such fluctuations reduces to the usual Fermi-liquid renormalizations with due account of the particle–hole symmetry condition. In two-dimensional Heisenberg lattices, however, fluctuations are important and must be taken into consideration.[13,14] In what follows, we do not discuss the

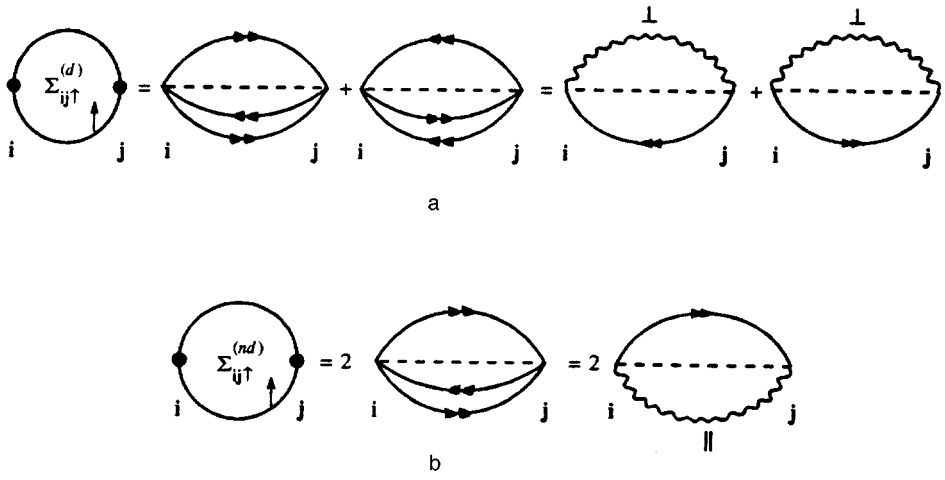

FIG. 8. Self-energy part for the anomalous propagator $\mathscr{G}_{ij}$, including the contribution of critical fluctuations in the mean-field approximation.

issue of long-wave fluctuations in gauge fields, and our analysis is limited to the mean-field approximation in a fixed calibration.

Having expressed the mean-field Hamiltonian in the form of Eq. (29), we considered in the subsequent calculations additional operators in $Y^{(p,h)}_{ij}$ as purely static projection operators, eliminating nonphysical states in thermodynamic averages. We now consider the fluctuation component of this ''kinematic'' interaction by transforming the effective mean-field spinon Hamiltonian for the Kondo lattice as follows:

$$H^{(\mathrm{RKKY})}_{\mathrm{MF}}=\tilde{J}\Delta\sum_{ij\sigma}\phi^{\sigma}_{ij}\equiv\tilde{J}\Delta\sum_{ij}\,(a^{+}_{i}K_{ij}a_{j}-a_{j}K^{+}_{ji}a^{+}_{i}+b_{i}K^{+}_{ij}b^{+}_{j}-b^{+}_{j}K_{ji}b_{i}). \tag{53}$$

Here $\tilde{J}$ is the renormalized constant of the RKKY interaction given by Eq. (46),

$$K_{ij}=S^{-}_{i}S^{+}_{j}-S^{z}_{i}S^{z}_{j}+\frac{1}{4},$$

and $K^{+}_{ij}=K_{ij}$. In the vicinity of the magnetic instability point, it is natural to consider operator K_{ij} as an operator describing critical excitations due to spinon propagation at temperatures close to T_N.

In order to obtain an expression for the spinon Green's function corresponding to this approximation, we reconsider the definition of its self-energy part. In the standard mean-field theory (Fig. 3), projection operators were included in the static approximation. The diagrams in Fig. 8 show how the diagonal and off-diagonal components of the self-energy part of the Green's function $\mathscr{G}_{ij}$, including transverse and longitudinal spin correlators, can be constructed from the vertices shown in Fig. 1. The lines with two arrows in Fig. 8 denote anomalous propagators

$$g^{\uparrow}_{ij}=-\langle T_{\tau}a_{i}(\tau)a^{+}_{j}(\tau')\rangle,$$
$$g^{\downarrow}_{ij}=-\langle T_{\tau}b_{i}(\tau)b^{+}_{j}(\tau')\rangle, \tag{54}$$

and wavy lines denote transverse and longitudinal correlation functions

$$\mathscr{K}^{\pm}_{ij}(\tau\to 0)=\langle T_{\tau}a^{+}_{j}(\tau+0)b^{+}_{j}(\tau+0)b_{i}(0)a_{i}(0)\rangle=\langle T_{\tau}S^{+}_{j}(\tau+0)S^{-}_{i}(0)\rangle,$$
$$\mathscr{K}^{zz}_{ij}(\tau\to 0)=\langle T_{\tau}b^{+}_{j}(\tau+0)b_{j}(\tau+0)b^{+}_{i}(0)b_{i}(0)\rangle=\frac{1}{4}-\langle T_{\tau}S^{z}_{j}(\tau+0)S^{z}_{i}(0)\rangle. \tag{55}$$

Unlike the fully anomalous Green's function (23), the anomalous functions (54) are one-particle propagators, while intersite spin correlators (55) are formed from projection operators. Now the sum of diagonal elements

$$\Sigma^{(d)}_{ij\uparrow}=\Sigma^{(11)}_{ij\uparrow}+\Sigma^{(22)}_{ij\uparrow}$$

in Eq. (28) is determined by the diagrams in Fig. 8a, while the contribution of off-diagonal elements

$$\Sigma^{(nd)}_{ij\uparrow}=\Sigma^{(12)}_{ij\uparrow}+\Sigma^{(21)}_{ij\uparrow}$$

corresponds to the diagrams in Fig. 8b. In deriving these expressions, we have used definition (3) and condition (6). Similar diagrams can be obtained for $\Sigma_{ij\downarrow}$. Summation of all these contributions in the mean-field approximation yields the effective Hamiltonian (53).

In the critical region $T_N<T<T^*$, the main contribution to spin correlators (53) is due to long-wave excitations with $\mathbf{k}\to 0$ and short-wave excitations with $\mathbf{k}\to\mathbf{Q}$ (see, for example, Ref. 48 and Sec. 5). The behavior of the response function $K(\mathbf{k})$ in the long-wave (hydrodynamic) limit $k\to 0$ is determined by fluctuations of the total magnetization of sublattices (which is zero in antiferromagnetic systems) and is diffusive in nature:

$$K^{R}(\mathbf{k},\omega)=K_{0}(\mathbf{k})\frac{iDk^{2}}{\omega+iDk^{2}}, \tag{56}$$

where

$$K_{0}(\mathbf{k})=\mathscr{K}(\mathbf{k},\omega=0)=\frac{\chi_{0}}{\tau+[1-J(\mathbf{k})/J(\mathbf{Q})]}\approx\frac{1}{2}\chi_{0}(T_N),$$

$$J(\mathbf{k})=J\sum_{\langle \mathbf{g}\rangle} e^{i\mathbf{kg}},\quad \chi_0(T)=\frac{S(S+1)}{3T},\quad \tau=\frac{T-T_N}{T_N} \tag{57}$$

(in Eq. (56) we have passed to the retarded Green's function for real frequency ω).

Near the antiferromagnetic vector $\mathbf{Q}$, the response function behavior is relaxation-like:

$$K^R(\mathbf{q},\omega)=\frac{1}{-i\omega/\Gamma\chi_0+K_0^{-1}(\mathbf{q})},\quad \mathbf{q}=\mathbf{k}-\mathbf{Q}, \tag{58}$$

where

$$K_0(\mathbf{q})=\mathscr{K}(q,\omega=0)=\frac{\chi_0}{\tau+(ql_0)^2} \tag{59}$$

is the Ornstein–Zernike static correlation function, and l_0 is the elementary excitation mean free path, which is comparable to the lattice constant.

In the mean-field approximation, we ignore the retardation of the RKKY interaction, and the diagrams in Fig. 8 yield for the self-energy

$$\tilde{\epsilon}_{\mathbf{k}}=\Sigma(\mathbf{k})=2\tilde{J}T^2\sum_{n,m\mathbf{q}}\sum_s \varphi(\mathbf{k}-\mathbf{q})g_{\mathbf{k}}(i\omega_n)\mathscr{K}^s_{\mathbf{q}}(i\varepsilon_m)$$

$$\approx\tilde{J}\Delta\left(\frac{\varphi(\mathbf{k})}{2}+2T\sum_{\mathbf{q}}\varphi(\mathbf{k}-\mathbf{q})K_0(\mathbf{q})\right). \tag{60}$$

Here s is the polarization index, while the anomalous Green's function $g_{\mathbf{k}}$ is expressed as $g_{\mathbf{k}}(i\omega_n)=(i\omega_n-\tilde{\epsilon}_{\mathbf{k}})^{-1}$. At high temperatures, we retain only the term with $\varepsilon_m=0$ in the sum over even Matsubara frequencies; then the spin Green's function $\mathscr{K}^s(\mathbf{q},0)$ in Fig. 8 has the same form in both the hydrodynamic and critical regions,[48] so that the main contribution to the spinon spectrum renormalization is due to the static susceptibility $K_0(\mathbf{q})$ (Eq. (59)).

The order parameter Δ defined by Eq. (28) and corresponding to the approximation of Eq. (53) and diagrams of Fig. 8 is given by

$$\Delta=\frac{1}{z}\sum_{\mathbf{pq}}\varphi(\mathbf{p}-\mathbf{q})\left[\frac{1}{2}\delta_{\mathbf{q},0}+2TK_0(\mathbf{q})\right]\tanh\frac{\tilde{\epsilon}_{\mathbf{p}}}{2T}. \tag{61}$$

Self-consistent equations (35) and (61) have been derived for the simplest case of isotropic exchange, which is, generally speaking, never realized in Kondo lattices. Therefore, before analyzing the effect of spin fluctuations on T^*, we generalize the mean-field theory to the case of anisotropic exchange. Let us introduce an exchange integral $J_{\mathbf{ij}}=\{J_\parallel,J_\perp\}$, where $J_\parallel$ and $J_\perp$ are the coupling constants for nearest neighbors in the basal plane and in the perpendicular direction, respectively. The degree of exchange anisotropy is measured by the parameter $\gamma=J_\perp/J_\parallel$. Now, instead of Hamiltonian (29) or (53), we must write the anisotropic mean-field Hamiltonian

$$H_{\mathrm{MF}}=\sum_{\mathbf{i},\rho_\perp}J_\perp\Delta_\perp Y_{\mathbf{i},\mathbf{i}+\rho_\perp}+\sum_{\mathbf{i},\rho_\parallel}J_\parallel\Delta_\parallel Y_{\mathbf{i},\mathbf{i}+\rho_\parallel}. \tag{62}$$

Here the anomalous averages $\langle Y_{\mathbf{i},\mathbf{i}+\rho_u}\rangle$, where $u=\perp,\parallel$, are derived from the equation system

$$\Delta_u=\frac{1}{z_u}\sum_{\mathbf{p}}\phi_u\left(\mathbf{p},\frac{T}{T_N},\gamma\right)\tanh\frac{\tilde{\epsilon}^u_{\mathbf{p}}(T/T_N,\gamma)}{2T} \tag{63}$$

with the dispersion relation

$$\tilde{\epsilon}^u_{\mathbf{p}}(T/T_N,\gamma)=J_u\Delta_u\phi_u(\mathbf{p},T/T_N,\gamma). \tag{64}$$

The structure factor $\phi_u(\mathbf{p},T/T_N,\gamma)$ renormalized by spin fluctuations can be expressed in terms of a structure factor $\varphi_u(\mathbf{p})$ like that in Eq. (33), where summation over nearest neighbors $\mathbf{l}$ is performed only in the basal plane ($\gamma<1$) or in the perpendicular direction ($\tilde{\gamma}=\gamma^{-1}<1$):

$$\phi_u\left(\mathbf{p},\frac{T}{T_N},\gamma\right)=\frac{1}{2}\varphi_u(\mathbf{p})+2T\sum_{\mathbf{q}}\varphi_u(\mathbf{p}-\mathbf{q})K_0(\mathbf{q}). \tag{65}$$

Index γ on the left-hand side of Eq. (65) is due to the anisotropic nature of correlator $K_0(\mathbf{q})$. Thus, the character of the transition to the spin-liquid state is determined by the degree of anisotropy: in the case of $\gamma<1$ spin-liquid correlations emerge first in the basal plane, and if $\gamma>1$ in the z-direction. At lower temperatures, the spin liquid naturally takes on three-dimensional properties, given that $\gamma\neq(0,\infty)$.

The transition temperature to the spin-liquid state, when spin fluctuations are taken into account, is determined by solving the equation

$$T_u^*=\frac{1}{2}\max\{J_\parallel,J_\perp\}\theta_u\left(\frac{T_u^*}{T_N},\gamma\right), \tag{66}$$

where

$$\theta_u\left(\frac{T_u^*}{T_N},\gamma\right)=(z_uN)^{-1}\sum_{\mathbf{p}}\phi_u^2\left(\mathbf{p},\frac{T}{T_N},\gamma\right), \tag{67}$$

$z_\parallel$ is the coordination number in the basal plane, and $z_\perp=2$.

In estimating the role of spin fluctuations for establishing the spin-liquid regime, it is convenient to introduce the temperature

$$T_u^{*(0)}=\frac{1}{2}\max\{J_\parallel,J_\perp\}\theta_u^{(0)} \tag{68}$$

of the transition to the RVB state in the anisotropic lattice without taking spin fluctuations into account. In this case,

$$\theta_u^{(0)}=(z_uN)^{-1}\sum_{\mathbf{p}}\varphi_u^2(\mathbf{p}). \tag{69}$$

Then the condition that the transition occurs by virtue of the spin-fluctuation mechanism is

$$\Upsilon_u(\gamma,T_u^{*(0)}/T_N)=\theta_u(T_u^{*(0)}/T_N,\gamma)/\theta_u^{(0)}>1. \tag{70}$$

The parameter $\Upsilon_u(\gamma)$ ($\Upsilon_u(\tilde{\gamma})$) for a simple cubic lattice is calculated in Appendix III. Critical values of the anisotropy parameters $\gamma_{1,2}$ at which the spin-liquid state stabilizes in almost one-dimensional and almost two-dimensional magnetic lattices are given for the case $T_u^{*(0)}/T_N=1$ in Fig. 9 for different values of τ. It is clear that only in a strongly anisotropic situation, almost one- or two-dimensional (see Eqs. (A.III.7) and (A.III.8)) spin correlations help formation of the spin liquid, and in the anisotropic case, inclusion of antiferromagnetic fluctuations in the mean-field approximation leads to suppression of the spin-liquid phase.

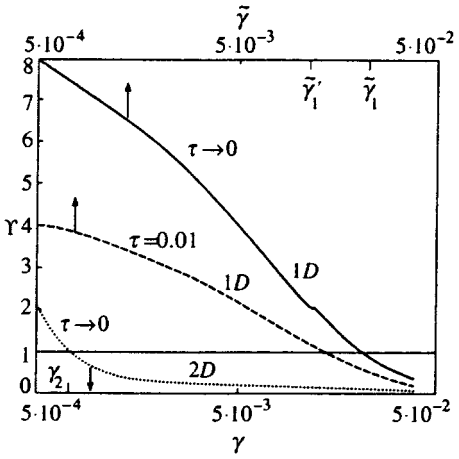

FIG. 9. Parameter Υ describing the effect of critical spin fluctuations on the transition temperature to the RVB phase for the quasi-one-dimensional ($1D$) and quasi-two-dimensional ($2D$) Kondo lattices. Parameter τ characterizes the proximity to the antiferromagnetic instability. The RVB state emerges at $\gamma<\gamma_1$ and $\tilde{\gamma}<\tilde{\gamma}_2$ in the cases of axial and plane magnetic anisotropy, respectively.

The analysis in this section once again indicates that the mean-field approximation is insufficient for the description of the spin liquid. In particular, even the diagrams of Fig. 8 indicate that the static approximation, generally speaking, does not apply to the critical region, since antiferromagnetic fluctuations define their own time and energy scales, which determine the real character of transition from the paramagnetic state to the spin-liquid state.

5. CRITICAL ANTIFERROMAGNETIC FLUCTUATIONS AND SPIN DIFFUSION

As mentioned in Sec. 4, in antiferromagnets critical fluctuations have differing properties in the long-wave ($k\to0$) and short-wave ($k\to Q$) regions, and the spin response function in these regions takes the form of Eqs. (56) and (58), respectively. The critical dynamics of antiferromagnets is usually analyzed using renormalization-group techniques applied to phenomenological models.[49,50] Chubukov[48] calculated the dynamic susceptibility of a two-dimensional antiferromagnet in the diffusion and relaxation regions using a diagram technique in the Schwinger boson representation. We investigate the dynamic susceptibility as a function of frequency and momentum in the thee-dimensional configuration using the pseudofermion technique.

In order to calculate the spin diffusion factor D and the relaxation constant Γ, we need to know, in addition to the spin correlators defined by the Larkin equation (19), the low-frequency behavior of the current correlator:

$$K_{\dot{S}\dot{S}}^{\alpha\beta}(\mathbf{k},\tau)=\delta_{\alpha\beta}\sum_{\mathbf{k}_1\mathbf{k}_2}V(\mathbf{k},\mathbf{p}_1)V(-\mathbf{k},-\mathbf{p}_2)\times\langle T_\tau(S^\mu_{\mathbf{p}_1+\mathbf{k}/2}S^\rho_{-\mathbf{p}_1+\mathbf{k}/2})_\tau(S^\mu_{-\mathbf{p}_2-\mathbf{k}/2}S^\rho_{\mathbf{p}_2-\mathbf{k}/2})_0\rangle, \tag{71}$$

where

$$V(\mathbf{k},\mathbf{p})=J(\mathbf{k}+\mathbf{p}/2)-J(-\mathbf{k}+\mathbf{p}/2).$$

FIG. 10. Self-energy part of the Green's function $\mathscr{G}_{\mathbf{ii}}$ including the contribution of critical fluctuations in the Born approximation.

There is an exact solution for the Fourier transform of correlator $K_{\dot{S}\dot{S}}$ continued to the upper half-plane expressed in terms of irreducible (noncuttable along the interaction line) self-energy parts of the spin and current correlation functions:

$$K^R_{\dot{S}\dot{S}}(\omega)=\Sigma^R_{\dot{S}\dot{S}}+\omega^2\frac{\Sigma^R_{SS}\mathscr{V}\Sigma^R_{SS}}{1-\Sigma^R_{SS}\mathscr{V}}. \tag{72}$$

Here $\mathscr{V}=(\Sigma^R)^{-1}-(K_0)^{-1}$ is the vertex part determined by the static response in the critical region.[19,51]

Using the Kramers–Kronig dispersion relations for retarded and advanced correlation functions, and the analytic properties of irreducible self-energy parts, one can derive from Eqs. (19) and (72) the expression

$$K^R_{SS}(\omega)=K_0\frac{\Gamma_{\mathbf{k},\omega}}{-i\omega+\Gamma_{\mathbf{k},\omega}}, \tag{73}$$

which holds as both $\mathbf{k}\to0$ and $\mathbf{k}\to\mathbf{Q}$.

The spin correlation functions can be expressed in terms of the pseudofermion Green's functions. For example, the expression for the one-site susceptibility has the form

$$\mathscr{K}^\perp_{\mathbf{i}}(\varepsilon_m)=T\sum_m\mathscr{G}_{\mathbf{ii}}(\omega_n+\varepsilon_m)\mathscr{G}_{\mathbf{ii}}(\omega_n), \tag{74}$$

(see Eq. (16)). Here $\mathscr{G}_{\mathbf{ii}}(\omega_n)$ is a Fourier component of the pseudofermion Green's function $\mathscr{G}_{\mathbf{ii}}(\tau)=\langle T_\tau f_{\mathbf{i}}(\tau)f^\dagger_{\mathbf{i}}(0)\rangle$. Since nonphysical states do not appear when calculating single-site averages for $S=1/2$, there is no need to introduce projection operators. As $T\to T_N$, scattering by the relaxation mode contributes a component described by the diagram in Fig. 10 to the self-energy part of the Green's function $\Sigma(\omega_n)$. Unlike the diagram of Fig. 8, here solid lines correspond to one-site propagators $\mathscr{G}_{\mathbf{ii}}$, and points to exchange vertices $\tilde{J}(\mathbf{q})$. The wavy line in this diagram corresponds to the spin Green's function (16) determined by the Larkin equation (19). In the absence of spin-liquid correlations, let us substitute into the self-energy part $\Sigma(\omega_n)$ of the pseudofermion Green's function the ''bare'' function $g_{i\sigma}$ from Eq. (26) and a spin function $\mathscr{K}(\varepsilon_m,\mathbf{q})$ in the form of a relaxator:

$$\Sigma(\omega_n)=\tilde{J}^2T\sum_m N^{-1}\sum_{\mathbf{q}}\varphi(\mathbf{q})^2\frac{1}{i(\varepsilon_m-\omega_n)}\frac{\Gamma\chi_0(T)}{|\varepsilon_m|+b(q)}, \tag{75}$$

where $b(q)=\Gamma[\tau+(ql_0)^2]$, and Γ should be calculated independently using the Dyson and Larkin equations. By calculating the sum over frequencies in Eq. (75) and continuing it analytically to the complex z plane, we obtain the following equation for poles of the pseudofermion Green's function:

$$z-\Sigma(z)=0,$$

$$\Sigma(z)=\sum_{\mathbf{q}} \frac{J^2\varphi^2(\mathbf{q})\mathscr{A}}{\pi}\frac{z}{z^2+b_{\mathbf{q}}^2}\left[\psi\left(-\frac{iz}{2\pi T}\right)-\psi\left(\frac{b_{\mathbf{q}}}{2\pi T}\right)-\frac{\pi T}{b_{\mathbf{q}}}+\frac{i\pi T}{z}\right], \tag{76}$$

where $\mathscr{A}=\Gamma\chi_0(T)$, and $\psi(y)$ is the digamma function. Hence, it is clear that the pseudofermion Green's function in this approximation is $\mathscr{G}^R_{\mathbf{ii}}(\omega)\sim[\omega+i\Gamma(T)]^{-1}$. By substituting this into Eq. (74), we find the one-site susceptibility

$$K^R_{\mathbf{i}}=\frac{\overline{\chi_0}}{1-i\omega/\Gamma}, \tag{77}$$

which is, in turn, can be substituted into the Larkin equation (which also includes, generally speaking, vertex corrections[48]), and thus the equation system for Γ and I_0 is closed.

The spin-liquid effects on the behavior of the spin correlation functions in the critical region can be accounted for by introducing anomalous intersite contributions into $\Sigma(\omega)$ (Fig. 10). Nonlocal fermion correlations lead to emergence of a new characteristic length characterizing short-range order, and change the temperature dependence of the static spin susceptibility and dynamic response functions. As a result, we have changes in the scaling behavior and in the frequency and momentum dependence of the spin susceptibility.

The spin diffusion factor is also determined by the self-energy part of the current correlator:[51]

$$D=\lim_{k\to 0,\omega\to 0}\frac{1}{k^2}\frac{\mathrm{Im}\Sigma^R_{\dot{S}\dot{S}}(\mathbf{k},\omega)}{\omega}K_0^{-1}(\mathbf{k}). \tag{78}$$

Since the behavior of the current correlator is fully determined by relaxation processes, effects of nonlocal spin correlations should also change scaling characteristics of the spin susceptibility in the hydrodynamic region.

The calculations described in this section are not considered a complete description of critical phenomena in antiferromagnets. These are instead illustrations given with the following aims: first, to demonstrate applicability of the suggested diagram technique to traditional problems of the theory of magnetic phase transition and, second, to outline feasible methods for taking into account the effect of spin-liquid correlations on antiferromagnetic fluctuations in the critical region.

6. CONCLUSIONS

In this paper, we have demonstrated that the spin-liquid state in the Kondo lattice can be more stable than the Kondo singlet state, owing to the same processes as those responsible for Kondo screening in the case of sufficiently strong antiferromagnetic sf-exchange. This rather paradoxical result can be explained by the fact that strong competition between Kondo scattering and spin-liquid correlations occurs at temperatures near the Néel point. Since all correlation effects at such temperatures have the same order of magnitude, the simple mean-field approximation cannot be used in describing the spin subsystem in a three-dimensional Kondo lattice.

The projection diagram technique suggested in the paper and based on the similarity between the Hubbard Hamiltonian for electrons and Heisenberg Hamiltonian for pseudofermions allows one, in principle, to go beyond the standard mean-field model of the homogeneous RVB phase.[6,16] Attempts to include antiferromagnetic fluctuations in the mean-field approximation (Sec. 4) do not produce any trustworthy results. Preliminary analysis, however, indicates[52] that the diagram technique suggested in the paper may allow one to manage without the mean-field approximation in describing effects which occur in the region of critical antiferromagnetic fluctuations and devise a more realistic scenario of emergence of the spin liquid in the Kondo lattice.

The investigation of spin diffusion near the Néel point reported in Section 5 indicates that the diagram techniques used in describing critical antiferromagnetic correlations at high temperatures may yield new physical results in the hydrodynamic region.

The authors are indebted to Yu. Kagan, N. V. Prokof'ev, G. G. Khaliullin, D. E. Khmel'nitskiĭ, and D. I. Khomskiĭ for helpful discussions and critical remarks. This work was supported by the Russian Fund for Fundamental Research (Project 95-02-04250a), INTAS (Project 93-2834), and Netherlands Organization for Support of Scientific Research (NWO, Project 07-30-002).

APPENDIX I

In calculating the polarization operator $\Pi(\mathbf{R})$ (Eq. (40)), we use the asymptotic form of the Green's function (41). Substituting it into Eq. (42), we obtain the expression for a spherical Fermi surface:

$$\Pi(R,\varepsilon_m)=T\left(\frac{m}{2\pi R}\right)^2\exp\left(-\frac{2|\varepsilon_m|}{v}R\right)\times\frac{\cos(2p_FR+i\varepsilon_mR/v)}{\sinh(2\pi TR/v)}+T\left(\frac{m}{2\pi R}\right)^2\times\exp\left(-\frac{|\varepsilon_m|}{v}R\right)\left[\frac{|\varepsilon_m|}{2\pi T}+\frac{\sinh(|\varepsilon_m|R/v)}{\sinh(2\pi TR/v)}\times\exp\left(-\frac{|\varepsilon_m|}{v}R+2ip_FR\ \mathrm{sign}\ \varepsilon_m\right)\right]. \tag{AI.1}$$

In the static limit, it reduces to

$$\Pi(R,0)=T\left(\frac{m}{2\pi R}\right)^2\frac{\cos(2p_FR)}{\sinh(2\pi TR/v)}=\frac{mp_F^4}{8\pi^3}\frac{\cos(2p_FR)}{(p_FR)^3}\left[1-\frac{\pi^2}{6}\left(\frac{T}{\varepsilon_F}p_FR\right)^2+\ldots\right], \tag{AI.2}$$

hence we have Eq. (45) at $T=0$.

In the case of a quasi-two-dimensional cylindrical Fermi surface

$$g(\mathbf{R},z,\omega_n)=\int\frac{d^3p}{(2\pi)^3}\frac{1}{i\omega_n-\xi(\mathbf{p})}\exp(i\mathbf{p}\cdot\mathbf{R}+ip_zz)$$

$$= \int_{-p_{z0}}^{p_{z0}} \frac{dp_z}{2\pi} e^{ip_z z} \int \frac{pdpd\varphi}{(2\pi)^2} \frac{1}{i\omega_n - \xi(\mathbf{p})} e^{i\mathbf{p}\cdot\mathbf{R}},$$

$$g(\mathbf{R},z,\omega_n) = \frac{\sin(p_{z0}z)}{\pi z} G(\mathbf{R},\omega_n). \tag{AI.3}$$

For $p_{z0} \gg p_F$ the effective RKKY interaction is independent of p_{z0},

$$J_{\mathrm{RKKY}}(\mathbf{R}) = \left(\frac{J}{\widetilde{n}_0}\right)^2 \Pi(\mathbf{R},0) = \left(\frac{J}{\widetilde{n}_0}\right)^2 \int \frac{d\omega}{2\pi} g^2(\mathbf{R},\omega)$$

$$= \left(\frac{J}{n_0}\right)^2 \int \frac{d\omega}{2\pi} G^2(\mathbf{R},\omega). \tag{AI.4}$$

Here $\widetilde{n}_0 = 4\pi p_F^2 p_{z0}/(2\pi)^3 = p_{z0}p_F^2/2\pi^2 = p_{z0}n_0/\pi$, $n_0 = p_F^2/2\pi$ is the two-dimensional density of electronic states, and $G(R,\omega_n)$ is the two-dimensional Green's function

$$G(R,\omega_n) = \int \frac{pdpd\varphi}{(2\pi)^2} \frac{1}{i\omega_n - \xi(\mathbf{p})} \exp(ipR\cos\varphi). \tag{AI.5}$$

Let us use the integral representation of the Bessel function

$$J_0(z) = \frac{1}{2\pi} \int_0^{2\pi} d\varphi \exp(iz\cos\varphi) \tag{AI.6}$$

in the asymptotic limit for large $|z|$:

$$J_0(z) \approx \sqrt{\frac{2}{z\pi}} \cos\left(z - \frac{\pi}{4}\right). \tag{AI.7}$$

Then we have

$$G(R,\omega_n) = -i\,\mathrm{sign}\,\omega_n \frac{m}{\sqrt{2\pi p_F R}} \exp\left(-\frac{|\omega_n|}{2\varepsilon_F} p_F R + i\left(p_F R - \frac{\pi}{4}\right)\mathrm{sign}\,\omega_n\right). \tag{AI.8}$$

Substituting this expression into Eq. (AI.4), we obtain

$$\Pi(R,\varepsilon_m) = -T\frac{m^2}{2\pi p_F R} \exp\left(-\frac{2|\varepsilon_m|}{v} R\right) \times \frac{\sin(2p_F R + i\varepsilon_m R/v)}{\sinh(2\pi TR/v)} - T\frac{m^2}{2\pi p_F R} \times \exp\left(-\frac{|\varepsilon_m|}{v} R\right) \left\{ \frac{|\varepsilon_m|}{2\pi T} - \frac{\sinh(|\varepsilon_m|R/v)}{\sinh(2\pi TR/v)} \exp\left[-\frac{|\varepsilon_m|}{v} R + 2i \times \left(p_F R - \frac{\pi}{4}\right)\mathrm{sign}\,\varepsilon_m\right]\right\}. \tag{AI.9}$$

In the low-temperature limit this expression becomes

$$\Pi(R,0) = -T\frac{m^2}{2\pi p_F R} \frac{\sin(2p_F R)}{\sinh(2\pi TR/v)}$$

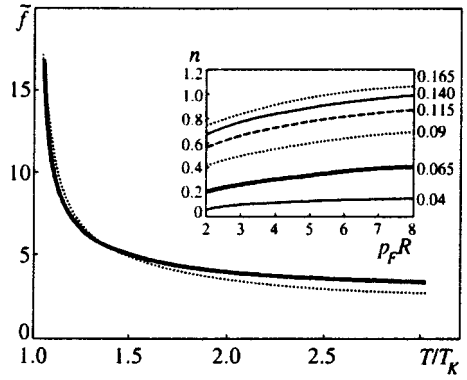

FIG. 11. Numerical values of integral $\widetilde{f}(p_F R)$ (solid line) and of the approximating function $f(p_F R)$ (see text).

$$= -\frac{mp_F^2}{4\pi^2} \frac{\sin(2p_F R)}{(p_F R)^2} \left[1 - \frac{\pi^2}{6}\left(\frac{T}{\varepsilon_F} p_F R\right)^2 + \ldots\right], \tag{AI.10}$$

and at $T=0$ to Eq. (47).

APPENDIX II

Intensification of the RKKY interaction due to Kondo renormalization of the single-site sf-exchange vertex, which is taken into account in the logarithmic approximation,

$$\Gamma(\varepsilon,\alpha) = \frac{1}{(1 + 2\alpha\,\ln(\varepsilon/\varepsilon_F))^2}, \tag{AII.1}$$

is described by the expression

$$f\left(p_F R, \alpha, \frac{T}{\varepsilon_F}\right) = \int_{T/\varepsilon_F}^{\infty} \frac{\exp(-p_F R x)dx}{(1 + 2\alpha\,\ln(x))^2}. \tag{AII.2}$$

The temperature dependence of this integral is determined by both Doniach's parameter α and the separation between neighboring Kondo centers (parameter $p_F R$).

If we neglect logarithmic renormalization (AII.1), the integral in (A.II.2) equals $1/p_F R$ for $T \ll \varepsilon_F/k_B$, and the integral in (44) reduces to the usual RKKY formula (45). When Kondo processes are taken into account, the function f defined by Eq. (A.II.2) can be approximated in the temperature range of interest, $[T_K, 3T_K]$, by the expression

$$f\left(p_F R, \alpha, \frac{T}{\varepsilon_F}\right) \approx \frac{1}{p_F R} \frac{1}{(1 - 2\alpha\,\ln(T/\varepsilon_F))^{n(p_F R,\alpha)}}, \tag{AII.3}$$

where the exponent $n = n(p_F R, \alpha)$ is independent of temperature. As a result, the high-temperature behavior of the RKKY interaction is determined by the function $\widetilde{f}(p_F R, \alpha, T/\varepsilon_F) = f(p_F R, \alpha, T/\varepsilon_F) p_F R$, which can be approximated as

$$\widetilde{f}\left(p_F R, \alpha, \frac{T}{\varepsilon_F}\right) \approx \frac{1}{(1 + 2\alpha\,\ln(T/\varepsilon_F))^{n(p_F R,\alpha)}}. \tag{AII.4}$$

Figure 11 shows the temperature dependence of the exact function $\widetilde{f}(p_F R = 5.0, \alpha = 0.09)$ calculated numerically (solid line) and the approximate function $\widetilde{f}(p_F R = 0.5, \alpha = 0.09)$ (dotted line) in the temperature range

$T_K<T<3T_K$. The exponent $n=n(p_FR,\alpha)$ of approximate function (AII.4) is shown in the insert as a function of p_FR in the range $2<p_FR<8$ for several values of α in the interval $0.04<\alpha<0.165$. The exponent was determined using the least-square fit in the temperature range $1.2T_K<T<3T_K$.

APPENDIX III

In this Appendix, we calculate the parameter Υ defined by Eq. (70), which characterizes the effect of spin correlations on the transition temperature to the RVB phase for a simple cubic lattice with anisotropic RKKY interaction due, for example, to a nonspherical Fermi surface. Let us introduce $J_\parallel \equiv J_x = J_y$ and $J_\perp \equiv J_z$. Then we must substitute into Eq. (57) for the spin correlator $K_0(\mathbf{q},\gamma)$ the parameter

$$j_q \equiv J_q/|J_Q| = -j_\parallel(\varphi_\parallel + \gamma\varphi_\perp), \tag{AIII.1}$$

where $\varphi_\parallel(q)=2(\cos q_x+\cos q_y)$, $\varphi_\perp(q)=2\cos q_z$, and $j_\parallel = J_\parallel/J_{\mathbf{Q}}$ $(a=1)$. To calculate sums in Eq. (65) like

$$T\sum_{\mathbf{q}} \varphi_u(\mathbf{p}-\mathbf{q})K_0(\mathbf{q},\gamma) = \frac{S(S+1)T}{6T_N j_0}\sum_{\mathbf{q}} \frac{\varphi_u(\mathbf{p}-\mathbf{q})}{T/T_N j_0 - j_{\mathbf{q}}/j_0}, \tag{AIII.2}$$

we use the integral representation for the spin correlator

$$K_0(\mathbf{q},\gamma) = \frac{S(S+1)j_{\mathbf{q}}}{6T_N j_0}\int_0^\infty dt\ \exp\left\{-\left(\frac{T}{T_N j_0}-\frac{j_q}{j_0}\right)t\right\}. \tag{AIII.3}$$

When the interaction in the basal plane is dominant $(\gamma<1)$, the spectrum of spin-liquid excitations has the form

$$\tilde{\epsilon}^{\parallel}_{\mathbf{p}}(T/T_N,\gamma) = \frac{1}{2}J_\parallel\Delta_\parallel\left[1-(2+\gamma)\frac{T}{T_N}A(\gamma,T/T_N)\right]\varphi_\parallel(q), \tag{AIII.4}$$

where the function $A(\gamma,T/T_N)$ can be expressed in terms of integrals of Bessel functions:

$$A(\gamma,\tau) = \int_0^\infty dt\ \exp\{-(2+\gamma)(1+\tau)t\}I_1(t)I_0(t)I_0(\gamma t). \tag{AIII.5}$$

Given that $\theta^{(0)}_\parallel = \theta^{(0)}_\perp = 1$ for the simple cubic lattice, we obtain

$$\Upsilon_\parallel(\gamma, T^{*(0)}_u/T_N) = [1-(2+\gamma)(1+\tau)A(\gamma,\tau)]^2/4. \tag{AIII.6}$$

When the interaction perpendicular to the basal plane is dominant $(\tilde{\gamma}<1)$, we have instead of Eqs. (A.III.4)–(A.III.6)

$$\tilde{\epsilon}^{\perp}_{\mathbf{p}}\left(\frac{T}{T_N},\gamma\right) = J_\perp\Delta_\perp\left[1-(1+2\tilde{\gamma})\frac{T}{T_N}\tilde{A}\left(\gamma,\frac{T}{T_N}\right)\right]\cos p_z, \tag{AIII.4$'$}$$

$$\tilde{A}(\tilde{\gamma},\tau) = \int_0^\infty dt\ \exp\{-(1+2\tilde{\gamma})(1+\tau)t\}I_1(t)I_0^2(\tilde{\gamma}t), \tag{AIII.5$'$}$$

$$\Upsilon_\perp(\tilde{\gamma}, T^{*(0)}_u/T_N) = [1-(1+2\tilde{\gamma})(1+\tau)\tilde{A}(\tilde{\gamma},\tau)]^2/4. \tag{AIII.6$'$}$$

Using asymptotic expressions for the integrals:

$$A(\gamma,\tau)|_{\gamma,\tau\to 0} \propto -\ln\max(\gamma,\tau),$$

$$\tilde{A}(\tilde{\gamma},\tau)|_{\tilde{\gamma},\tau\to 0} \propto [\max(\tilde{\gamma},\tau)]^{-1/2},$$

we obtain for the neighborhood of T_N in the case of strong anisotropy

$$\Upsilon_\parallel(\gamma, T^{*(0)}_u/T_N) \propto -\ln\max(\gamma,\tau), \tag{AIII.7}$$

$$\Upsilon_\perp(\tilde{\gamma}, T^{*(0)}_u/T_N) \propto [\max(\tilde{\gamma},\tau)]^{-1/2}, \tag{AIII.8}$$

and as a result, strong spin fluctuations stabilize the spin liquid.

[1)] Preliminary results of this study were given in the short note.

[2)] A procedure similar to that suggested below was described in Ref. 33 in the cases of the Anderson impurity and Anderson lattice. But since the Anderson Hamiltonian, unlike spin Hamiltonians (1) and (2), does not have local SU(2) symmetry, and the requirement of exact particle-hole symmetry is not imposed, there are many differences between formulations of rules of the diagram techniques.

[3)] Since in the case $S=1/2$ for one-site processes the constraint condition is satisfied automatically,[10] it is unnecessary to introduce projection operators.

[1] G. Zwicknagl, Adv. Phys. **41**, 203 (1992).
[2] A. C. Hewson, *The Kondo Problem to Heavy Fermions*, Cambridge University Press, Cambridge (1993).
[3] S. Doniach, Physica B **91**, 231 (1977).
[4] F. J. Ohkawa, Prog. Theor. Phys. Suppl. No. 108, 209 (1992).
[5] Y. Kuramoto and K. Miyake, Prog. Theor. Phys. Suppl. No. 108, 199 (1992).
[6] P. Coleman and N. Andrei, J. Phys.: Condens. Matter **1**, 4057 (1989).
[7] J. A. Millis and P. A. Lee, Phys. Rev. B **35**, 3394 (1987).
[8] Yu. Kagan, K. A. Kikoin, and N. V. Prokof'ev, Physica B **182**, 201 (1992).
[9] J. Gan, P. Coleman, and N. Andrei, Phys. Lett. **68**, 3476 (1992).
[10] A. A. Abrikosov, Physics **2**, 21 (1965).
[11] I. Affleck and J. B. Marston, Phys. Rev. B **37**, 3774 (1988).
[12] I. Affleck, Z. Zou, T. Hsu, and P. W. Anderson, Phys. Rev. B **38**, 745 (1988).
[13] L. B. Ioffe and A. I. Larkin, Phys. Rev. B **39**, 8988 (1989).
[14] P. A. Lee and N. Nagaosa, Phys. Rev. B **46**, 5621 (1992).
[15] S. Elitzur, Phys. Rev. D **12**, 3978 (1975).
[16] G. Baskaran, Z. Zou, and P. W. Anderson, Solid State Commun. **63**, 973 (1987).
[17] A. Ruckenstein, P. Hirschfeld, and J. Appel, Phys. Rev. B **36**, 857 (1987).
[18] K. A. Kikoin, M. N. Kiselev, and A. S. Mishchenko, JETP Lett. **60**, 358 (1994).
[19] Yu. A. Izyumov and Yu. N. Skryabin, *Statistical Mechanics of Magnetically Ordered Systems* [in Russian], Nauka, Moscow (1987).
[20] V. G. Bar'yakhtar, V. N. Krivoruchko, and D. A. Yablonskii, *Green's Functions in the Theory of Magnetism* [in Russian], Naukova Dumka, Kiev (1984).
[21] H. Keiter and G. Morandi, Phys. Rep. **109**, 227 (1984).
[22] F. Onufrieva and J. Rossat-Mignod, Phys. Rev. B **52**, 7572 (1995).
[23] D. C. Mattis, *The Theory of Magnetism*, Harper and Row, New York (1965).
[24] W. W. Lewis and R. B. Stinchcombe, Proc. Phys. Soc. London **92**, 1002 (1967).
[25] S. E. Barnes, J. Phys. F **6**, 1375 (1976).
[26] G. Kotliar and A. E. Ruckenstein, Phys. Rev. Lett. **57**, 1362 (1986).
[27] P. Coleman, E. Miranda, and A. M. Tsvelik, Phys. Rev. Lett. **70**, 2960 (1993).
[28] X.-G. Wen and P. A. Lee, Phys. Rev. Lett. **76**, 503 (1996).
[29] Y. Ono, T. Matsuura, and Y. Kuroda, Physica C **159**, 878 (1989).
[30] J. Hubbard, Proc. R. Soc. London, Ser. A **285**, 542 (1965).

[31] R. O. Zaitsev, Zh. Éksp Teor. Fiz. **70**, 1100 (1976) [Sov. Phys. JETP **43**, 574 (1976)].
[32] T. Yanagisawa, Phys. Rev. B **40**, 6666 (1989).
[33] J. Brinckmann, Europhys. Lett. **28**, 187 (1994).
[34] A. I. Larkin, Zh. Éksp. Teor. Fiz. **37**, 264 (1960) [Sov. Phys. JETP **10**, 186 (1960)].
[35] K. Kuboku, J. Phys. Soc. Jpn. **62**, 420 (1993).
[36] C. Mudry and E. Fradkin, Phys. Rev. B **49**, 5200 (1994).
[37] D. R. Grempel and M. Lavagna, Solid State Commun. **83**, 595 (1992).
[38] T. Tanamoto, H. Kohno, and H. Fukuyama, J. Phys. Soc. Jpn. **62**, 617 (1993).
[39] I. S. Sandalov and M. Richter, Phys. Rev. B **50**, 12855 (1994).
[40] P. W. Anderson, Mater. Res. Bull. **8**, 153 (1973).
[41] C. M. Varma, in *Theory of Heavy Fermions and Valence Fluctuations*, Springer Series in Solid-State Sciences, T. Kasuya and T. Saso (eds.), Vol. 62, Springer-Verlag, Berlin (1985), p. 277.
[42] K. Yosida and A. Okiji, Prog. Theor. Phys. **34**, 505 (1965).
[43] A. A. Abrikosov and A. A. Migdal, J. Low Temp. Phys. **3**, 519 (1970).
[44] A. M. Tsvelik and P. B. Wiegmann, Adv. Phys. **32**, 453 (1983).
[45] K. Miura, T. Ono, and K. Kuboku, Physica C **179**, 411 (1991).
[46] F. Nozières, Ann. de Phys. **10**, 1 (1985).
[47] K. A. Kikoin, J. Phys.: Condens. Matter **8**, 3601 (1996).
[48] A. Chubukov, Phys. Rev. B **44**, 392 (1991).
[49] B. I. Halperin and P. C. Hohenberg, Rev. Mod. Phys. **49**, 435 (1977).
[50] S. Chakraverty, B. I. Halperin, and D. Nelson, Phys. Rev. B **39**, 2344 (1989).
[51] S. V. Maleyev, Sov. Sci. Rev. A, I. M. Khalatnikov (ed.), Harwood Press, New York (1987), Vol. 8, p. 323.
[52] K. A. Kikoin, M. N. Kiselev, and A. S. Mishchenko, E-prints archive, Cond-Matt/96 08 121.

Translation was provided by the Russian Editorial office.

Spin diffusion and relaxation in three-dimensional isotropic Heisenberg antiferromagnets

K. A. Kikoin

Kurchatov Institute Russian Scientific Center, 123182 Moscow, Russia

M. N. Kiselev

Kurchatov Institute Russian Scientific Center, 123182 Moscow, Russia; Laboratoire Léon Brillouin, CEA-CNRS, CE Saclay, 91191 Gif-sur-Yvette Cedex, France

(Submitted 3 April 1997)
Zh. Éksp. Teor. Fiz. **112**, 1816–1829 (November 1997)

A theory is proposed for kinetic effects in isotropic Heisenberg antiferromagnets at temperatures above the Néel point. The scaling behavior of the generalized coefficient of spin diffusion and relaxation constant in the paramagnetic phase is studied in terms of the approximation of interacting modes. It is shown that the kinetic coefficients in an antiferromagnetic system are singular in the fluctuation region. The corresponding critical indices for diffusion and relaxation processes are calculated. The scaling dimensionality of the kinetic coefficients agrees with the predictions of dynamic similarity theory and a renormalization group analysis. The proposed theory can be used to study the momentum and frequency dependence of the kinetic parameters, and to determine the form of the scaling functions. The role of nonlocal correlations and spin-fluid effects in magnetic systems is discussed. © *1997 American Institute of Physics.* [S1063-7761(97)02111-2]

1. INTRODUCTION

Recent heightened interest in the critical dynamics of antiferromagnetic materials[1–6] has been stimulated by active experimental and theoretical research on quasi-two-dimensional magnetic correlations in high-temperature superconductors, and on the anomalous magnetic properties of heavy-fermion compounds.[6–8] In particular, critical spin fluctuations have been invoked to explain the non-Fermi fluid behavior of the specific heat and resistance at low temperatures in the compounds[7,8] $CeCu_{6-x}Au_x$ and $Ce_{1-x}La_xRu_2Si_2$ near the concentration critical point. In addition, a proposed[9,10] spin-fluid approach to the Heisenberg model, based on introducing resonating valence bonds with Fermi statistics for excitations in the magnetic sublattice (spinons), may, in turn, also serve as a scenario for describing the behavior of cerium compounds with heavy fermions.[11,12] Here it turns out that critical spin fluctuations play an important role in the formation mechanism of a spin fluid. The behavior of the kinetic coefficients in this case can deviate substantially from that predicted by dynamic similarity theory.[13]

In this paper we develop a microscopic approach for studying the scaling behavior of the spin diffusion coefficient and the relaxation constant of an isotropic Heisenberg antiferromagnet in the fluctuation region above the Néel temperature. The scaling dimensionality of the kinetic coefficients in magnets was predicted by Halperin and Hohenberg,[14,15] who developed a hypothesis of scale invariance based on the idea that the values of the dynamic critical indices are conserved on both sides of the phase transition. Maleev then made a microscopic study of spin diffusion in the paramagnetic phase of ferromagnets.[16,17] He, in particular, established the approximations required to satisfy the requirements of the hypothesis of scale invariance, and studied the momentum and frequency dependence of the spin diffusion coefficient. The analogous problem for antiferromagnets will be examined in the present paper.

It is known[14] that in the neighborhood of a phase transition, two regions can be distinguished in the momentum-temperature plane: a hydrodynamic region determined by long-wavelength fluctuations in the ordering parameter $\mathbf{N}=\mathbf{N}_1-\mathbf{N}_2$, the difference in the moments of the sublattices, with characteristic wave vectors $q\xi\ll 1$, where $q=|\mathbf{k}-\mathbf{Q}|$ describes the deviation of the moment from the antiferromagnetic vector $\mathbf{Q}$ and ξ is the correlation length, and a critical region, with wave vectors $q\xi\gg 1$. Here the concept of a correlation length is related to the characteristic behavior of the ordering parameter $\mathbf{N}$. In an antiferromagnet, however, there is an additional conserved quantity, the vector $\mathbf{M}=\mathbf{M}_1+\mathbf{M}_2$, the sum of the moments of the sublattices. Nevertheless, we shall also refer to the long-wavelength fluctuation region for the vector $\mathbf{M}$, $k\xi\ll 1$, as hydrodynamic. In this paper we examine the behavior of the spin correlation functions in the paramagnetic phase and establish the relationship between the kinetic coefficients in the fluctuation region of the phase diagram.

In the hydrodynamic regime, the dynamics of the fluctuations in the magnetization have a diffusive character, i.e., the variation in the magnetic moment with time obeys the macroscopic van Hove diffusion equation:

$$\frac{\partial \mathbf{M}}{\partial t}=D_0\nabla^2\mathbf{M}, \tag{1}$$

where D_0 is the spin diffusion coefficient. This behavior of the fluctuations is related to the conservation of the magnetic moment; the operator corresponding to it commutes with the Hamiltonian.

A different pattern is observed in the critical region. The nonconservation of the ordering parameter determines the

relaxation character of the time variation in the vector **N**, i.e., the dynamics of this vector obey the relaxation equation:

$$\frac{\partial \mathbf{N}}{\partial t} = -\frac{\Gamma_0}{\chi}\mathbf{N}, \tag{2}$$

where χ is the susceptibility and the kinetic coefficient $\Gamma_0 > 0$. We note also that, in contrast to the diffusion equation (1), relaxation (2) can be uniform; the gradient corrections omitted from Eq. (2) are proportional to q^2 in this case. Although the average value of the magnetization vector **M** is zero on both sides of the phase transition point, fluctuations occur in the magnetization vector near the zero value. Unlike in a ferromagnet, however, the diffusion mode is not critical.

In the following we shall be interested in the dynamic susceptibility of a cubic Heisenberg antiferromagnet located in zero magnetic field above the Néel temperature:

$$H = -\sum_{\langle i,j\rangle} V_{ij}\mathbf{S}_i \cdot \mathbf{S}_j . \tag{3}$$

We also neglect dipole forces.[17]

The susceptibility is known to be related to the retarded spin Green function by the equation

$$\lambda(\mathbf{k},\omega) = (g\mu_0)^2 K^R_{SS}(\mathbf{k},\omega), \tag{4}$$

where g is the Landé g factor, μ_0 is the Bohr magneton, and

$$K^R_{SS}(\mathbf{k},\omega) = i\int_0^\infty dt\ e^{i\omega t}\langle [S^z_{\mathbf{k}}(t), S^z_{-\mathbf{k}}(0)]\rangle,$$

$$\mathbf{S}_{\mathbf{k}} = \frac{1}{\sqrt{N}}\sum_i e^{-i\mathbf{k}\cdot\mathbf{R}_i}\mathbf{S}_i ,$$

$$\mathbf{M} = \langle \mathbf{S}_0\rangle, \quad \mathbf{N} = \langle \mathbf{S}_{\mathbf{Q}_{\mathbf{AFM}}}\rangle. \tag{5}$$

Proceeding from Eqs. (1) and (2), we can obtain the form of the correlation functions K^R in the diffusion

$$K^R_{SS}(\mathbf{k}\to\mathbf{0},\omega) = \mathscr{K}(\mathbf{k},\omega) = G_0(k)\ \frac{iDk^2}{\omega + iDk^2} \tag{6}$$

and relaxation regions

$$K^R_{SS}(\mathbf{q} = (\mathbf{k}-\mathbf{Q}) \to 0, \omega) = \mathscr{L}(\mathbf{q},\omega) = \frac{1}{-i\omega/\Gamma + G_0^{-1}(q)}. \tag{7}$$

Here G_0 is the static susceptibility.

In the fluctuation region $\tau = |T - T_c|/T_c \ll Gi$ (Gi is the Ginzburg number, which characterizes the limits of applicability of the Landau theory), when the fluctuations become large, the fluctuation dynamics obey the Halperin–Hohenberg similarity law, according to which the dynamic susceptibility χ and, therefore, the function K^R_{SS} can be expressed in terms of the scaling function F:

$$K^R_{SS}(\mathbf{k},\omega) = G_0(\mathbf{k})F\left(k\xi, \frac{\omega}{T_c\tau^{\nu z}}\right), \tag{8}$$

i.e., the dynamic index z which characterizes the energy scale of the critical fluctuations, $\omega \propto k^z$, can be related to a static index $\nu \approx 2/3$ which determines the variation in the correlation length, $\xi \propto \tau^{-\nu}$. For small deviations from the antiferromagnetic vector, the static susceptibility varies as $G_0(q) \propto \xi^{2-\eta}$. In the following discussion the Fisher index η, which characterizes the so-called anomalous dimensionality,[18] will be set equal to zero. This approximation is valid for three-dimensional systems.[18] It is necessary to introduce two scaling functions $\mathscr{F}_1$ and $\mathscr{F}_2$ to describe the fluctuation regions in an antiferromagnet:

$$\mathscr{K}(\mathbf{k},\omega) = G_0(\mathbf{k})\mathscr{F}_1\left(k\xi, \frac{\omega}{T_c\tau^{\nu z}}\right),$$

$$\mathscr{L}(\mathbf{q},\omega) = G_0(\mathbf{q})\mathscr{F}_2\left(q\xi, \frac{\omega}{T_c\tau^{\nu z}}\right). \tag{9}$$

Here, however, the kinetic coefficients D_0 and Γ_0 can, in turn, themselves be correlation lengths. Furthermore, as a renormalization group analysis shows,[14,19] the kinetic coefficients are singular in the fluctuation region of an antiferromagnet.

The theory developed in this paper is a variant of the interacting mode theory of Kawasaki.[20] We have tried to generalize the theory proposed by Maleev[16] for spin diffusion in ferromagnets to antiferromagnetic systems. In many regards, we follow the style and spirit of that paper. As noted before, our problem involves a study of the form of the scaling function F (see Eqs. (8) and (9)) and a determination of the frequency and momentum dependences of the kinetic coefficients in the fluctuation region, as well as establishing those approximations which must be made in a microscopic approach in order to satisfy the requirements of scaling invariance.

2. GENERALIZED KINETIC COEFFICIENTS

We therefore study the dynamic susceptibility of a cubic Heisenberg antiferromagnet located in zero magnetic field above the Néel temperature in the fluctuation region. Equations (6) and (7) can be rewritten in the more general form

$$K^R_{SS}(\mathbf{k},\omega) = \frac{i\gamma(\mathbf{k},\omega)}{\omega + iG_0^{-1}(\mathbf{k})\gamma(\mathbf{k},\omega)}, \tag{10}$$

while in the diffusion region

$$D_0 = \lim_{k\to 0}\lim_{\omega\to 0} k^{-2}\gamma(\mathbf{k},\omega)G_0^{-1}(\mathbf{k}), \tag{11}$$

and in the relaxation region the generalized kinetic coefficient $\gamma(\mathbf{k},\omega) = \Gamma(\mathbf{k},\omega)$. The limit of Eqs. (6) and (7) for $\mathbf{k}\to 0$ and $\omega\to 0$ depends strongly on the relationship between k and ω, similarly to the way it does in the theory of Fermi fluids.[21] In the following we shall be interested in the quasistatic limit, i.e. $k\to 0$ and $|\omega|/k^2 \to 0$.

As Maleev shows,[16] it is possible to go beyond the linear response theory and express the kinetic coefficients in terms of the Kubo function[22] of the operators S and $\dot{S}$ (the dot denotes differentiation with respect to time):

$$\gamma(\mathbf{k},\omega) = \frac{\Phi_{\dot{S}\dot{S}}(\mathbf{k},\omega)}{1 + G_0^{-1}(k)\Phi_{\dot{S}S}(\mathbf{k},\omega)}, \tag{12}$$

where

$$\Phi_{AB}(\mathbf{k},\omega)=\frac{1}{i\omega}\,[K^R_{AB}(\mathbf{k},\omega)-K^R_{AB}(\mathbf{k},0)],$$

$$K^R_{AB}(\mathbf{k},\omega)=i\int_0^\infty dt\; e^{i\omega t}\langle[A_{\mathbf{k}}(t),B_{-\mathbf{k}}(0)]\rangle.$$

Equation (12) is exact and accounts for the nonlinear nature of the relaxation forces. In the case of a purely exchange interaction in the long wavelength limit $\dot{S}_{\mathbf{k}}\sim k$, i.e., $\gamma=\Phi_{SS}(\mathbf{k},\omega)$, the denominator equals unity and Eq. (11) is the same as the result from the linear response theory. Generally speaking, however, the functions in the denominator cannot be neglected in a study of the frequency and momentum dependence of the kinetic coefficients.

It is easy to show that the retarded Green functions $K^R_{SS}(\mathbf{k},\omega)$, $K^R_{\dot{S}S}(\mathbf{k},\omega)$, and $K^R_{\dot{S}\dot{S}}(\mathbf{k},\omega)$ are related in the paramagnetic phase by simple formulas which follow from the dispersion relations:[23]

$$K^R_{SS}(\mathbf{k},\omega)=-i\omega K^R_{SS}(\mathbf{k},\omega),$$

$$K^R_{S\dot{S}}(\mathbf{k},\omega)=-K^R_{SS}(\mathbf{k},\omega)=i\omega K^R_{SS}(\mathbf{k},\omega),$$

$$\omega^2 K^R_{SS}(\mathbf{k},\omega)=[K^R_{\dot{S}\dot{S}}(\mathbf{k},\omega)-K^R_{\dot{S}\dot{S}}(\mathbf{k},0)]. \tag{13}$$

It is clear from these relations, in particular, that $K^R_{\dot{S}S}(\mathbf{k},\omega)$ is analogous to $K^R_{\dot{S}\dot{S}}(\mathbf{k},\omega)$ in its properties and symmetry.[16]

Combining Eqs. (11) and (13) with the equation of motion for the spin operators,

$$\dot{S}^\alpha_{\mathbf{k}}=-\frac{1}{\sqrt{N}}\sum_{\mathbf{p}}\,[V(\mathbf{p}+\mathbf{k})-V(\mathbf{p})]\epsilon_{\alpha\beta\gamma}S^\beta_{\mathbf{p}+\mathbf{k}}S^\gamma_{-\mathbf{p}} \tag{14}$$

(here $V(\mathbf{p})$ is the Fourier transform of the exchange integral) and transforming to ''imaginary'' time, we can obtain the relation between the Kubo functions and the correlators of the spin currents at the Matsubara frequencies:

$$K_{\dot{S}\dot{S}}(\mathbf{k},\omega_n)=\frac{(a^2T_c\alpha)^2}{6N}\int_0^{1/T}d\tau e^{i\omega_n\tau}\sum_{\mathbf{p}_1,\mathbf{p}_2}(\nabla V(\mathbf{p}_1)\mathbf{k})\times(\nabla V(\mathbf{p}_2)\mathbf{k})\times\langle T_\tau(S^\mu_{\mathbf{p}_1+\mathbf{k}}S^\rho_{-\mathbf{p}_1})_\tau(S^\mu_{-\mathbf{p}_2-\mathbf{k}}S^\rho_{\mathbf{p}_2})_0\rangle. \tag{15}$$

In retaining only the first gradients of the potentials, $\nabla V(\mathbf{p})\approx\mathbf{p}T_ca^2\alpha$, we limit ourselves to the lowest order terms in an expansion in ka, where a is the lattice constant; the constant $\alpha\approx1$. It will be clear from the following analysis that the corrections to the kinetic coefficients will be expressed in the form of series in powers of $k\xi$ and, since $\xi\gg a$, it is valid to neglect the higher derivatives of the exchange integral. Therefore, the problem of finding the kinetic coefficients has been reduced to calculating four-spin correlators with a current vertex. This problem can be solved by analytic continuation of the temperature diagrams with an upper semiaxis into the complex ω plane. A graphical expression for the current correlator is shown in Fig. 1.

The ''seed'' poles for the spin Green functions (6) and (7) lie on the imaginary axis, i.e., if we set up some fictitious quasiparticles to correspond to these poles, their energies will be purely imaginary. Introducing quasiparticles of this sort, e.g., ''diffusons'' and ''relaxons'', allows us to obtain closed expressions for the kinetic coefficients and to determine their scaling dimensionality.

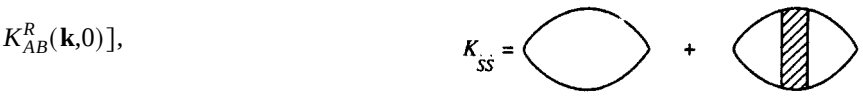

FIG. 1. Diagram series for the current correlator.

For the static susceptibility in the critical region we use the Ornstein–Zernike law:

$$G_0(\mathbf{q})=K^R_{SS}(\mathbf{q},0)=\frac{A}{T_c\tau^{2\nu}}\frac{1}{(q\xi)^2+1}, \tag{16}$$

where A is a constant ($A\sim1$) and $\tau\ll1$. In the diffusion region the static susceptibility has no singularities and $G_0\approx A/2T_c$.

The following sections are devoted to analyzing the diagram series for the spin current correlator in the fluctuation regions, finding the dynamic critical indices for the kinetic coefficients, and determining the momentum and frequency dependence of the spin diffusion coefficient and relaxation constant.

3. RELATIONSHIPS AMONG THE KINETIC COEFFICIENTS

To analyze the diagram series we introduce the concept of an irreducible self-energy part as a diagram which is continuous along one interaction line. Using the definition of γ and the properties of the functions K, we rewrite the expression for the generalized kinetic coefficient in terms of irreducible self-energy parts:

$$\gamma(\mathbf{k},\omega)=\frac{1}{i\omega}\left[\Sigma^R_{\dot{S}S}(\mathbf{k},\omega)-\Sigma^R_{\dot{S}\dot{S}}(\mathbf{k},0)+\frac{\mathscr{R}^R_{\dot{S}S}(\mathbf{k},\omega)\,\gamma(\mathbf{k},\omega)\,\mathscr{R}^R_{S\dot{S}}(\mathbf{k},\omega)}{-i\omega+G_0^{-1}(k)\,\gamma(\mathbf{k},\omega)}\right]\times\left[1+G_0^{-1}\frac{\mathscr{R}^R_{SS}(\mathbf{k},\omega)\,\gamma(\mathbf{k},\omega)}{i\omega(-i\omega+G_0^{-1}(k)\,\gamma(\mathbf{k},\omega))}\right]^{-1}. \tag{17}$$

Equation (17) can also be obtained by analyzing the diagram series for the spin current correlator,[16] as well as directly from the Larkin equation.[12,23] In the following we use the following notation:

$$K^R_{\dot{S}S}(\mathbf{k},\omega)=\mathscr{R}^R(\mathbf{k},\omega)K^R_{SS}(\mathbf{k},\omega);$$

and Σ^R_{AB} for the irreducible self-energy parts. The graphical expression for the irreducible part $\Sigma^R_{\dot{S}\dot{S}}$ corresponds to replacing a complete vertex in Fig. 1 by an irreducible vertex. Estimating $\mathscr{R}$ in self-consistent field theory[16,24] yields

$$\mathscr{R}\sim(k\xi)(ka)\ll(k\xi)^2. \tag{18}$$

In addition, its analytic properties imply that $\mathscr{R}^R\sim\omega$. We assume that the expression for $\mathscr{R}$ in the critical region also contains a term of order a/ξ in smallness, and for small ω we neglect this contribution. Thus, the generalized kinetic coef-

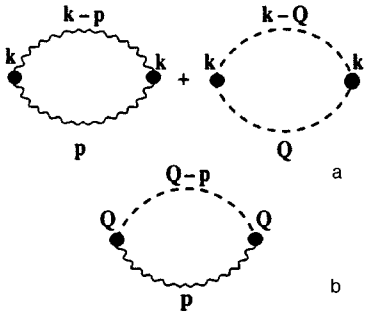

FIG. 2. Diagrams for the kinetic coefficients when two-particle intermediate states are included. A wavy line corresponds to the diffusion mode, a dashed line, to the relaxation mode. A dot denotes the vertex part of the static similarity theory.

ficient γ is defined only by the irreducible self-energy parts:

$$\gamma(\mathbf{k},\omega)=\frac{1}{i\omega}\,(\Sigma^R_{\dot S\dot S}(\mathbf{k},\omega)-\Sigma^R_{\dot S\dot S}(\mathbf{k},0)). \tag{19}$$

We now consider diagrams of a general form for the irreducible self-energy part Σ_{SS} at imaginary frequencies. These diagrams, in turn, can be classified in terms of the number of intermediate states. To begin with, we limit ourselves to diagrams with two-frequency intermediate states (Fig. 2a and b):

$$\begin{aligned}\Sigma^{(2)}_{\dot S\dot S}(\mathbf{k},i\omega)=&\frac{(T_c a^2\alpha)^2}{\sqrt{N}}\\ &\times T\sum_{\epsilon}\sum_{\mathbf{p}}\,(\mathbf{k}\Lambda^{(2)}(\mathbf{p},\mathbf{k},i\omega,i\epsilon,i(\omega-\epsilon)))\\ &\times(\mathbf{k}\Lambda^{(2)^\dagger}(\mathbf{p},\mathbf{k},i\epsilon,i(\omega-\epsilon),i\omega))\\ &\times K_{SS}(\mathbf{p},i\epsilon)K_{SS}(\mathbf{k}-\mathbf{p},i\omega-i\epsilon).\end{aligned} \tag{20}$$

In replacing the sum over the vectors $\mathbf{p}$ by an integral, we use $p\sim\xi^{-1}$ as an upper bound. Here the functions are integrated near the singularities (small $\mathbf{p}$ and $\mathbf{p}\sim\mathbf{q}+\mathbf{Q}$ in the neighborhood of the antiferromagnetic vector $\mathbf{Q}$).

The vertex parts Λ are analytic functions of all three frequencies, each of which has cuts along the real axis.[25] Vertex parts of this type have no other singularities in the complex ω planes.[25] Because of this property, the vertices can be resolved into a static part, which transforms into the vector vertex of static similarity theory, and a dynamic correction, which vanishes in the limit $\omega\to 0$. We now study the static part in more detail.

The static vertices in the diagrams (Fig. 2a) describe the long-wavelength processes of creating ''diffuson''–''diffuson'' and ''relaxon''–''relaxon'' pairs, i.e., identical modes interact. As we know, however, the static Green functions are independent of the direction of the momentum, i.e., diffuson and relaxon scattering processes contain the same vertex parts as do pair creation processes. This means that for these vertices, the Ward identity[18,21] holds (Fig. 3):

$$\Lambda^{(2)}(\mathbf{p},\mathbf{k},0)\sim\partial G_0^{-1}/\partial\mathbf{p}. \tag{21}$$

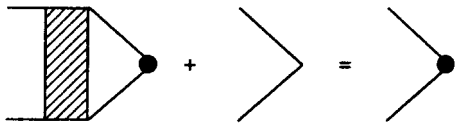

FIG. 3. The equations for a two-particle vertex part.

Here, in the second term the region of integration with respect to the momenta is concentrated near the points $\mathbf{p}\approx\mathbf{Q}$. The contribution of critical fluctuations to spin diffusion can be calculated by making the substitution $\mathbf{p}=\mathbf{q}+\mathbf{Q}$ and using the property $\partial G_0^{-1}/\partial\mathbf{p}=\partial G_0^{-1}/\partial\mathbf{q}$.

We now consider the diagram of Fig. 2b. Without loss of generality we can set the external momentum equal to the antiferromagnetic vector. In this case, we must consider two interacting modes of different kinds: a diffusion mode with short wave vectors and a relaxation mode with small deviations from the antiferromagnetism vector. Thus, the diagram of Fig. 2b describes ''diffuson''–''relaxon'' pair production. Thus, we cannot use the Ward identities for this vertex. However, the seed vertex (Fig. 3) has the scaling dimensionality

$$\Lambda_0^{(2)}(\mathbf{p},\mathbf{Q},0)\sim\partial V/\partial\mathbf{p}\sim\mathbf{p}.$$

It is also known that in the antiferromagnetic phase there is a doubling of the lattice, and the Brillouin zone of the ordered phase equals half the Brillouin zone of the disordered phase. This means that the points 0 and $\mathbf{Q}$ become equivalent in the antiferromagnetic phase. Given this fact, as well as the lack of a dependence on the direction of the momentum for the interacting modes, we may assume that rescattering by the static field does not change the scaling dimensionality of the static vertex at the antiferromagnetic vector, which can also be written in the form (21).[1)]

Continuing the diagrams shown in Fig. 2 analytically,[21] we obtain expressions for the kinetic coefficients:

$$\begin{aligned}D_0^{(2)}=&\widetilde{A}T_c\int_{-\infty}^{\infty}\frac{d\varepsilon}{2\pi}\coth\left(\frac{\varepsilon}{2T}\right)\sum_{\mathbf{p}}\,(\nabla G_0^{-1}(\mathbf{p}))^2\\ &\times\Big[\mathrm{Im}\,\mathscr{K}(\mathbf{p},\varepsilon)\,\frac{\partial}{\partial\varepsilon}\,\mathrm{Im}\,\mathscr{K}(\mathbf{p}-\mathbf{k},\varepsilon)\\ &+\mathrm{Im}\,\mathscr{L}(\mathbf{p},\varepsilon)\,\frac{\partial}{\partial\varepsilon}\,\mathrm{Im}\,\mathscr{L}(\mathbf{p}-\mathbf{k},\varepsilon)\Big],\end{aligned} \tag{22}$$

and

$$\begin{aligned}\Gamma_0^{(2)}=&\widetilde{B}\int_{-\infty}^{\infty}\frac{d\varepsilon}{2\pi}\coth\left(\frac{\varepsilon}{2T}\right)\sum_{\mathbf{p}}\,(\nabla G_0^{-1}(\mathbf{p})\mathbf{Q})^2\\ &\times\Big[\mathrm{Im}\,\mathscr{K}(\mathbf{p},\varepsilon)\,\frac{\partial}{\partial\varepsilon}\,\mathrm{Im}\,\mathscr{L}(\mathbf{p}-\mathbf{q},\varepsilon)\\ &+\mathrm{Im}\,\mathscr{L}(\mathbf{p},\varepsilon)\,\frac{\partial}{\partial\varepsilon}\,\mathrm{Im}\,\mathscr{K}(\mathbf{p}-\mathbf{q},\varepsilon)\Big].\end{aligned} \tag{23}$$

Here the index (2) indicates that only processes with two-particle intermediate states have been taken into account. For a ferromagnet it is necessary to restrict ourselves to just the

first term in Eq. (22), since a single-mode regime is involved. Equations (22) and (23) can be rewritten in a somewhat different form. Setting $\mathbf{k}=0$ and $\mathbf{q}=0$ in the integrands and integrating by parts, we obtain

$$D_0^{(2)}=\frac{\widetilde{A}}{4}\int_{-\infty}^{\infty}\frac{d\varepsilon}{2\pi}\sinh^{-2}\left(\frac{\varepsilon}{2T}\right)\sum_{\mathbf{p}}(\nabla G_0^{-1}(\mathbf{p}))^2 \times[(\mathrm{Im}\,\mathscr{K}(\mathbf{p},\varepsilon))^2+(\mathrm{Im}\,\mathscr{L}(\mathbf{p},\varepsilon))^2] \tag{24}$$

and

$$\Gamma_0^{(2)}=\frac{\widetilde{B}}{2T_c}\int_{-\infty}^{\infty}\frac{d\varepsilon}{2\pi}\sinh^{-2}\left(\frac{\varepsilon}{2T}\right)\sum_{\mathbf{p}}(\nabla G_0^{-1}(\mathbf{p})\mathbf{Q})^2 \times\mathrm{Im}\,\mathscr{K}(\mathbf{p},\varepsilon)\mathrm{Im}\,\mathscr{L}(\mathbf{p},\varepsilon). \tag{25}$$

These expressions can be regarded as a generalization of the equations obtained by Maleev[16] from the unitarity condition for the self-energy parts to the case of two interacting modes.

The region for integrating by parts is concentrated near the singular points of the scaling functions (9). Here because of the ''critical retardation'' in the neighborhood of the phase transition points, the characteristic energies of the fluctuations satisfy the condition $\omega^*\ll T_c$, which makes it possible to retain only the first term of the expansion of the hyperbolic tangent (Eqs. (22) and (23)) or hyperbolic sine (Eqs. (24) and (25)). Evaluating the integrals with respect to the frequencies and momenta in Eqs. (22) and (24) and separating out the scaling dimensionality, we obtain a relationship between the spin diffusion coefficient and the relaxation constant:

$$D_0=b_1T_c^2a^4\left(\frac{\xi}{a}\right)^{-3}\frac{1}{D_0}+b_2T_ca^2\left(\frac{\xi}{a}\right)\frac{1}{\Gamma_0}. \tag{26}$$

Note that in order to obtain Eq. (26), it suffices to substitute the retarded Green spin functions in the form of Eqs. (6) and (7) into Eqs. (22) and (24). After integrating with respect to the frequency, the remaining integrals over the momenta contain only the static correlator G_0. The first term is determined by a two-diffuson intermediate state, and the second by a two-relaxon intermediate state.

The integrals in Eqs. (23) and (25) can be calculated in similar fashion. The relaxation constant Γ_0 and the spin diffusion coefficient are related by the equation

$$\Gamma_0=c_1\left(\frac{\xi}{a}\right)\frac{1}{\Gamma_0}+c_2\left(\frac{\xi}{a}\right)\frac{D_0/T_ca^2}{\Gamma_0^2}. \tag{27}$$

The coefficients $b_{1,2}$, $c_{1,2}\sim 1$ in Eqs. (26) and (27) depend on the form of the dynamic and static scaling functions, and in general cannot be calculated using this approach. Solving the closed system of algebraic equations (26) and (27) yields the following scaling dimensionality for the kinetic coefficients:[2)]

$$D_0/T_ca^2\propto\Gamma_0\propto(\xi/a)^{-1/2}. \tag{28}$$

This sort of behavior is entirely consistent with that predicted by the dynamic scaling invariance hypothesis[14,15] and a renormalization group analysis.[15,19] Therefore, first, the kinetic coefficients for an antiferromagnet are singular in the fluctuation region, and second, spin diffusion is entirely determined by intermediate relaxation processes. The correction to the coefficient D_0 owing to self-diffusion is of smallness $\delta D_0/D_0\propto(\xi/a)^{-4}\propto\tau^{8/3}\ll 1$. That is, diffusion is not intrinsically a critical mode in an antiferromagnet. The dynamic critical index (see Eq. (8)) is $z=3/2$.

The simple physical considerations which will allow us to describe diffusion and relaxation in the fluctuation region are based on the idea that regions of size ξ with near ordering will develop as $T\to T_c$. In these regions the excitations are antiferromagnetic magnons with an acoustic dispersion character. Estimating the spin diffusion coefficient as $D_0\sim\xi^2/t_{\mathrm{diff}}$, where $t_{\mathrm{diff}}\sim\xi/c$ is the characteristic diffusion time and $c\sim\xi^{-1/2}$ is the ''sound'' speed,[14] we obtain $D_0\sim\xi^{1/2}$. Given the dynamic similarity hypothesis, according to which the dynamic critical index z, which determines the scale of the characteristic fluctuation energies, is invariant, we obtain $\Gamma_0\sim\xi^{1/2}$.

Despite the singularity of the kinetic coefficients, the relaxation time for the ordering parameter approaches infinity, which ensures the existence of macroscopic states corresponding to incomplete equilibrium.[27] The same applies to the characteristic spin diffusion times.

It should be noted that in introducing Eq. (26) we do not formally assume knowledge of the character of the excitations in the ordered phase. However, the conservation of the total moment and nonconservation of the ordering parameter actually determine the magnetic ordering properties in full.

4. FREQUENCY AND MOMENTUM DEPENDENCE OF THE KINETIC COEFFICIENTS

We shall now consider the generalized kinetic coefficients as functions of frequency and momentum. To do this we use the relationship between the retarded spin Green functions and the Kubo functions (see Eqs. (12) and (17)). Based on these equations, it is clear that the corrections associated with the frequency and momentum dependence of the kinetic coefficients are determined, first of all, by the frequency and momentum dependence of the irreducible self-energy parts, and second, by the nonlinear character of the relaxation forces. According to the estimate of Eq. (18), the momentum and frequency dependence of the kinetic coefficients can be studied in terms of the linear response theory, i.e., the nonlinearity of the relaxation forces can be neglected.

Let us first investigate the static renormalization of the kinetic coefficients. Equations (22) and (23) transform to the usual series expansion of the functions in the powers $(k\xi)^{2n}$ and $(q\xi)^{2n}$ from the static theory:

$$D^{(2)}(\mathbf{k},0)=D_0(0,0)[1+\alpha'(k\xi)^2+\ldots],$$

$$\Gamma^{(2)}(\mathbf{q},0)=\Gamma_0(0,0)[1+\beta'(q\xi)^2+\ldots].$$

This expansion is related to the existence of singularities in the correlators of the static theory at the points $k_i=-n^2\xi^{-2}$ (Ref. 26), where n is an integer. The coefficients α' and β' depend only on the form of the static correlation function.

We now proceed to analyze the energy dependence of the kinetic coefficients. Using Eq. (19), we obtain the following expressions for the real and imaginary parts of $\gamma(\mathbf{k},\omega)$:

$$\text{Re } \gamma(\mathbf{k},\omega)=\frac{\text{Im } \Sigma^R_{\dot S\dot S}(\mathbf{k},\omega)}{\omega},$$

$$\text{Im } \gamma(\mathbf{k},\omega)=-\frac{\text{Re } \Sigma^R_{\dot S\dot S}(\mathbf{k},\omega)-\text{Re } \Sigma^R_{\dot S\dot S}(\mathbf{k},0)}{\omega}. \tag{29}$$

Since Im γ is an odd function of ω and Re γ is an even function of ω, the regular expansion of the kinetic coefficients in powers of the frequency begins with ω^2.

We introduce an effective generalized kinetic coefficient γ^* according to the definition

$$\gamma^*=\frac{\dfrac{\partial}{\partial\omega}\,\text{Im } \Sigma^R_{\dot S\dot S}(\mathbf{k},\omega)\big|_{\omega=0}}{1+G_0^{-1}(\mathbf{k})\,\dfrac{\partial}{\partial\omega}\,\text{Re } \Sigma^R_{\dot S\dot S}(\mathbf{k},\omega)\big|_{\omega=0}}. \tag{30}$$

This expression for the effective generalized kinetic coefficient is analogous to the definition of effective mass in the theory of quantum liquids. The role of the Z factor is played by the renormalization constant on the mass shell:

$$Z=\frac{1}{1+G_0^{-1}(\mathbf{k})\,\dfrac{\partial}{\partial\omega}\,\text{Re } \Sigma^R_{\dot S\dot S}(\mathbf{k},\omega)\big|_{\omega=0}}.$$

Calculations of Z in the hydrodynamic and critical regions yield the following expressions for the renormalization constant:

$$Z(k\to 0)=\frac{1}{1+\epsilon'(k\xi)^2},$$

$$Z(q\to 0)=\frac{1}{1+\delta'+\delta''(q\xi)^2}, \tag{31}$$

where the constants ϵ', $\delta'\ll 1$ can also be expressed in terms of integrals of the static correlator G_0.

Extending the definition (30) to small but nonzero ω, we obtain an expansion for the real generalized spin diffusion coefficient D^* and the relaxation constant Γ^*:[3)]

$$D^{(2)*}(\mathbf{k},\omega)=D_0(0,0)[1+\alpha'(k\xi)^2+\alpha''_{k\xi}(\omega/\omega^*)^2+\ldots],$$

$$\Gamma^{(2)*}(\mathbf{q},\omega)=\Gamma_0(0,0)[\beta+\beta'(q\xi)^2+\beta''_{k\xi}(\omega/\omega^*)^2+\ldots]. \tag{32}$$

Here it must be noted that we do not claim to describe the behavior of the kinetic coefficients in the region $\omega\sim\omega^*$, $k,q\sim\xi^{-1}$. This range of frequencies and energies can scarcely be subject to detailed analysis at the present time. We therefore neglect the irregular corrections to the kinetic coefficients resulting from the generation in the higher orders of perturbation theory of an infinite sequence of poles in the retarded spin Green function, which contract to the real axis and cover the pole that produced them. We shall also not discuss the phenomena associated with the loss of a pole through a cut, etc.[16,17] All these corrections are small in the region of $\mathbf{k}$ and ω of interest to us and can be discarded.

We now consider the effect of the diagrams with many-particle ($m>2$) intermediate states. As noted above, we are only interested in the regular contribution:

$$\frac{\text{Im } \Sigma^{R(m)}_{\dot S\dot S}}{\omega}\sim(ka)^2\sum_{\mathbf{p}_1}\ldots\sum_{\mathbf{p}_m}\Lambda^{(m)}(\mathbf{k},\mathbf{p}_1,\ldots,\mathbf{p}_m)$$

$$\times\Lambda^{(m)\dagger}(\mathbf{k},\mathbf{p}_1,\ldots,\mathbf{p}_m)\,\delta(\mathbf{p}_1+\ldots p_m-\mathbf{k})\,\frac{1}{\pi^{m-1}}$$

$$\times\int_{-\infty}^{\infty}\ldots\int_{-\infty}^{\infty}\frac{d\varepsilon_1\ldots d\varepsilon_m\,\text{Im } K^R_{SS}(\mathbf{p}_1,\varepsilon_1)\ldots\text{Im } K^R_{SS}(\mathbf{p}_m,\varepsilon_m)}{\varepsilon_1\ldots\varepsilon_m}$$

$$\times\delta(\varepsilon_1+\ldots+\varepsilon_m-\omega), \tag{33}$$

where the functions K describe both the ''diffusons'' and the ''relaxons,'' and the integrals with respect to frequency are taken near the singular points of the scaling function. For $m=2$, Eq. (33) transforms into Eqs. (24) and (25).

As $k\to 0$, there are generalizations of Ward's identity[16] for the vertex parts $\Lambda^{(m)}$ analogous to Eq. (21), as a result of which the vertex can be expressed in terms of a sum of derivatives of the ordinary m-particle vertices of the static similarity theory. Using the ''dimensionality'' estimate for static vertices,[26] according to which $\Gamma_m\propto p^{3-m/2}$, in the limit $k\to 0$ we see that replacing the diagrams with two-particle intermediate states in the creation channel for ''diffusons'' and ''relaxons'' by diagrams with m-particle intermediate states does not change the scaling dimensionality of the irreducible self-energy parts. As for the behavior of the vertex parts at the antiferromagnetic vector, here the arguments advanced for diagrams with two-particle intermediate states are also valid. Thus, considering intermediate states with more than two particles does not change the scaling dimensionality of the kinetic coefficients, but only affects the values of the constants, which in any event cannot be calculated using the approach described here. The same can be said of the corrections associated with the energy dependence of the vertex parts.[16]

In conclusion, we note that the corrections associated with the frequency and momentum dependence of the kinetic coefficients can be investigated experimentally using neutron scattering, for which the scattering cross section is determined by the quantity $\text{Im } K^R_{SS}(\mathbf{k},\omega)/\omega$, where the imaginary part of the retarded spin Green function satisfies Eqs. (6) and (7) with the coefficients (32).

5. CONCLUSION

In this paper we have studied the scaling behavior of the generalized kinetic coefficients in a three-dimensional Heisenberg antiferromagnet. By means of an analysis based on a modified version of the interacting mode theory, we have found approximations in a microscopic approach for satisfying the requirements of the scaling invariance hypothesis. Specifically, it has been shown that in order to determine the scaling dimensionality of the kinetic coefficients, is sufficient to limit ourselves to processes with two-particle intermediate states, with the vertex parts being given by static similarity theory.

The regular frequency and momentum dependence of the spin diffusion coefficient and relaxation constant have been determined in a pole approximation. We have introduced the concept of effective kinetic coefficients, analogous to the definition of effective mass in the theory of quantum liquids. Including the renormalizations associated with multiple scattering of ''diffusons'' and ''relaxons'' has made it possible to write explicit series expressions for the scaling function in the frequency and momentum range $\omega \ll \omega^*$ and $k,q \ll \xi^{-1}$.

The static and dynamic similarity laws, as well as the assumed existence of just two modes (two singularities at low frequencies owing to the existence of the hydrodynamic and critical regimes), underlie the results obtained in this paper. The existence of diffusion and relaxation in an antiferromagnetic system is, in turn, related to the existence of a conserved quantity in the Heisenberg model and to the nonconservation of the ordering parameter in this model. Thus, all the formulas depend only to a small extent on the specific features of Heisenberg antiferromagnets and will be valid for any system with a nonconserved ordering parameter when an additional integral of the motion exists.

In more complicated physical systems, such as heavy Fermion compounds with integral filling of the f-shell (compounds based on Ce are an example of such materials) in the Kondo lattice model, for which the Heisenberg spin interaction is mediated by indirect exchange via conduction electrons, there may be a substantial deviation from the scaling behavior of Heisenberg magnets owing to the existence of additional modes that interact with paramagnons. Modes of this sort can develop, for example, as a result of spin-liquid correlations, which inhibit growth of the magnetic correlation length. In other words, a test for the existence of spin-liquid correlations may be to measure the generalized kinetic coefficients by neutron scattering. Other objects to which the methods described in this paper may be applied include systems with nearly zero or even negative temperatures of antiferromagnetic ordering,[6,28,29] anisotropic ferri-, and antiferrimagnets, and systems with dipole interactions.

The study of the kinetic coefficients near the Néel temperature carried out in this paper shows that diagram techniques for describing kinetic effects in antiferromagnets have many advantages over existing methods[14,15,20] and can be used to analyze unrenormalizable Hamiltonians, as well as for problems with nonlocal interacting modes.

In conclusion, we thank D. N. Aristov, Yu. M. Kagan, A. V. Lazuta, V. L. Pokrovskiĭ, and P. Pfeuty for valuable comments, constructive criticism, and interest in this work. We would like especially to thank S. V. Maleev for discussions which stimulated the writing of this article. This work was supported by the International Association INTAS (Projects 93-2834 and 83-285), the Netherlands Organization for the Support of Scientific Research NWO (Project 07-30-002), and the Russian Fund for Fundamental Research (Project 95-02-04250a).

[1)]Recall that the anomalous dimensionality index (Fisher index) is assumed equal to zero.

[2)]In a ferromagnet, the spin diffusion coefficient is not a singular function: $D_0/T_c a^2 \propto (\xi/a)^{-1/2}$.

[3)]$\omega^* \sim T_c \tau^{\nu z}$ is the characteristic energy of the fluctuations, with $z = 3/2$.

[1] S. Chakravarty, B. I. Halperin, and D. R. Nelson, Phys. Rev. B **39**, 2344 (1989).
[2] D. P. Arovas and A. Auerbach, Phys. Rev. B **38**, 316 (1988).
[3] A. Chubukov, Phys. Rev. B **44**, 392 (1991).
[4] H. Monien, D. Pines, and C. P. Slichter, Phys. Rev. B **44**, 120 (1990).
[5] D. M. Ginsberg (ed.), *Physical Properties of High-Temperature Superconductors II*, World Scientific, Singapore (1990).
[6] A. Millis, Phys. Rev. B **48**, 7183 (1993).
[7] S. Kambe *et al.*, J. Phys. Soc. Jpn. **65**, 3294 (1996).
[8] A. Rosch, A. Schröder, O. Stockert, and H. V. Löhneysen, submitted to Phys. Rev. B.
[9] P. W. Anderson, Mater. Res. Bull. **8**, 153 (1973).
[10] G. Baskaran, Z. Zou, and P. W. Anderson, Solid State Commun. **63**, 973 (1987).
[11] Yu. Kagan, K. A. Kikoin, and N. V. Prokof'ev, Physica B **182**, 201 (1992).
[12] K. A. Kikoin, M. N. Kiselev, and A. S. Mishchenko, JETP Lett. **60**, 600 (1994).
[13] K. A. Kikoin, M. N. Kiselev, and A. S. Mishchenko, Zh. Éksp. Teor. Fiz. **112**, 729 (1997) [JETP **85**, 399 (1997)].
[14] B. I. Halperin and P. C. Hohenberg, Phys. Rev. **177**, 952 (1969); Phys. Rev. **188**, 898 (1969); Rev. Mod. Phys. **49**, 435 (1977).
[15] B. I. Halperin, P. C. Hohenberg, and E. D. Siggia, Phys. Rev. B **13**, 1299 (1976).
[16] S. V. Maleev, Zh. Éksp. Teor. Fiz. **65**, 1237 (1973) [Sov. Phys. JETP **38**, 613 (1973)].
[17] S. V. Maleev, Zh. Éksp. Teor. Fiz. **66**, 889 (1974) [*sic*]; Preprints LIYaF/1038-1040 (1985); Sov. Sci. Rev. A **8**, 323 (1987).
[18] A. Z. Patashinskiĭ and V. L. Pokorovskiĭ, *Fluctuation Theory of Phase Transitions* [in Russian], Nauka, Moscow (1982).
[19] R. Freedman and G. F. Mazenko, Phys. Rev. Lett. **34**, 1571 (1975).
[20] K. Kawasaki, in *Phase Transitions and Critical Phenomena*, C. Domb and M. S. Green (eds.), Vol. 5a, Academic, New York (1976).
[21] A. A. Abrikosov, L. P. Gor'kov, and I. E. Dzyaloshinskiĭ, *Methods of Quantum Field Theory in Statistical Physics*, Dover, New York (1975).
[22] L. Kadanoff and P. Martin, Ann. Phys. **24**, 419 (1963).
[23] Yu. A. Izyumov and Yu. N. Skryabin, *Statistical Mechanics of Magnetically Ordered Systems* [in Russian], Nauka, Moscow (1987).
[24] V. G. Vaks, A. I. Larkin, and S. A. Pikin, Zh. Éksp. Teor. Fiz. **51**, 767 (1966) [*sic*]; Zh. Eksp. Teor. Fiz. **53**, 281 (1967) [Sov. Phys. JETP **26**, 188 (1967)].
[25] G. M. Eliashberg, Zh. Éksp. Teor. Fiz. **41**, 1241 (1961) [Sov. Phys. JETP **14**, 886 (1961)]; Zh. Éksp. Teor. Fiz. **42**, 1658 (1962) [Sov. Phys. JETP **15**, 1151 (1962)]; S. V. Maleev, TMF **4**, 86 (1970).
[26] A. A. Migdal, Zh. Éksp. Teor. Fiz. **55**, 1964 (1968) [Sov. Phys. JETP **28**, 1036 (1968)]; A. M. Polyakov, Zh. Éksp. Teor. Fiz. **57**, 2144 (1969) [Sov. Phys. JETP **30**, 1164 (1970)].
[27] E. M. Lifshitz and L. P. Pitaevskiĭ, *Physical Kinetics*, Pergamon Press, Oxford (1981).
[28] J. Hertz, Phys. Rev. B **14**, 1165 (1975).
[29] T. Moriya, *Spin Fluctuations in Itinerant Electron Magnetism*, Springer-Verlag, Berlin (1985).

Translated by D. H. McNeill

Paramagnetic labeling as a method for the soft spectroscopy of electronic states

M. N. Kiselev and A. S. Mishchenko*)

Kurchatov Institute Russian Scientific Center, 123182 Moscow, Russia
(Submitted 28 October 1997)
Zh. Éksp. Teor. Fiz. **113**, 1843–1865 (May 1998)

A self-consistent microscopic theory of the relaxation of the crystal-field levels of an impurity ion in a state with an integer valence implanted in a normal metal is devised. A microscopic approach based on the Coqblin–Schrieffer–Cooper approach, rather than the formal model of the sf exchange interaction, makes it possible to take into account the specific details of both the crystal-field states of the impurity ion and the electronic band spectrum of the metal. A new method for the soft spectroscopy of electronic states based on measurements of the temperature dependence of the width $\Gamma_{MM'}(T)$ of transitions between the crystal-field states $|M\rangle$ of a paramagnetic ion implanted in the compound being studied is proposed. To make specific use of this method in neutron and optical spectroscopy, a classification of the types of temperature dependence of the natural relaxation width $\gamma_M(T)$ of the levels is devised, and procedures for possible experimental methods are proposed. A nonzero value of the natural relaxation width $\gamma_G(T)$ of the crystal-field ground state $|G\rangle$ of an impurity ion at zero temperature is obtained within the proposed self-consistent model, but is beyond the scope of perturbation theory. It is shown that the widely accepted estimate of the characteristic temperature of Kondo systems $T^*=\Gamma_G(T=0)/2$ from the quasielastic scattering width at zero temperature $\Gamma_G(T=0)/2$ is incorrect in the case of strong relaxation in a system with soft crystal fields. The proposed model is applied to the quantitative analysis of the relaxation of the crystal-field levels of paramagnetic Pr^{3+} ions implanted in $CeAl_3$ and $LaAl_3$. The results of the calculations are in quantitative agreement with the experimental data. © *1998 American Institute of Physics.* [S1063-7761(98)02005-8]

1. INTRODUCTION

The methods that have been developed for studying electronic states in metals (angle-resolved photoemission spectroscopy;[1] quantum oscillations of the magnetic susceptibility,[2] conductivity,[3] magnetostriction,[4] and elastic moduli[5] associated with the de Haas–van Alphen effect; infrared spectroscopy;[6] Raman scattering;[7] etc.) provide complementary information regarding the structure of electron spectra. A comparison of the experimental data obtained by different methods with the results of band calculations of the electronic structure provides fairly reliable data on the properties of the compounds studied.

The methods for investigating electronic states can be divided into ''hard'' and ''soft'' methods. In the case of hard spectroscopy, the influence of the measurement process on the system exceeds the scales W^* of the characteristic interactions forming the electronic spectrum of the system (in Kondo systems W^* is of the order of the Kondo temperature T_K; in variable-valence systems W^* is of the order of the valence fluctuations). Therefore, compounds with strong electron correlations, which have low-energy modes in the spectrum of elementary excitations, can be investigated most effectively by soft spectroscopic methods, in which the measurement process does not destroy the eigenstates of the system being investigated. The conditions imposed on spectroscopic measurements by the softness of the elementary excitations in variable-valence and Kondo systems greatly restricts the set of methods that are applicable to the investigation of highly correlated systems. For example, the interpretation of photoemission measurements (because of the large energy transfers in the measurement process) and data from methods based on de Haas–van Alphen oscillations (because of the large magnetic fields, which can destroy the structure of soft excitations) requires a special investigation of the influence of the measurement process on the low-energy properties of the compound being studied. Therefore, the development of new soft spectroscopic methods for highly correlated electronic systems is an important undertaking.

This paper proposes a method for analyzing the electronic structure based on measurements of the temperature dependence of the relaxation of crystal-field levels of an impurity ion which has special properties (a paramagnetic label) and is implanted in the compound being investigated. A similar idea for investigating semiconductor compounds by an electron paramagnetic resonance technique was proposed back in Ref. 8. The method discussed in this paper relies on the technique of measuring the neutron or optical response of the system and is intended for studying metallic compounds. A spectroscopic procedure employing a paramagnetic label can be divided into two stages. In the first stage highly complete information on the energies and wave functions of the paramagnetic label P must be obtained. To this end a combined study (neutron scattering or Raman scattering measurements; magnetic susceptibility and specific heat mea-

surements) must be made of a reference single crystal of $P_l\{B\}$ ($\{B\}$ is the chemical formula without the paramagnetic label). In the second stage small quantities of the A ions in the compound $A_l\{B\}$ under investigation are replaced by the paramagnetic label P. Scrutiny of the temperature dependence of the relaxation of crystal-field levels of the paramagnetic label P in the compound $(A_{1-x}P_x)_l\{B\}$ can provide unique information regarding the electronic structure of the compound under investigation when several conditions are fulfilled. First, the inequality $x \ll 1$ is a necessary condition, which allows us to treat the relaxation of the crystal field at the paramagnetic label as a purely single-ion effect. Second, it must be shown that the structure of the crystal field of the paramagnetic label P in $(A_{1-x}P_x)_l\{B\}$ does not differ significantly from the structure of the crystal field in the pure reference crystal of $P_l\{B\}$. Fulfillment of the second condition has already been demonstrated for several compounds, in which the main contribution to the formation of the crystal field is made by the nearest neighbors from a formula unit of $\{B\}$, and hence the structures of the crystal fields of the paramagnetic label P in $P_l\{B\}$ and $(A_{1-x}P_x)_l\{B\}$ are practically identical. Examples of such compounds include RAl_3,[9–11] RNi_5,[12–14] and RNi[14–16] (R is a rare-earth ion).

It should be noted that the existing methods for calculating the temperature dependence of the relaxation of crystal-field states cannot be applied to the analysis of specific, highly correlated systems. Some of the methods employ the formal Hamiltonian, i.e., one which is not related in any way to the electronic structure, of the sf model.[17–19] Another deficiency of the previously developed methods is the use of nonself-consistent second-order perturbation theory,[17,18,20,21] which is inapplicable in the case of the large relaxation widths characteristic of highly correlated systems.

The goal of the present work is to devise a self-consistent theory for the relaxation of crystal-field levels, which can serve as a tool for studying the electronic structure of particular, highly correlated electronic systems with strong relaxation broadening. Section 2 presents the derivation of a microscopic interaction Hamiltonian, an analysis of the differences between it and the formal Hamiltonian of the sf model, and a discussion of the Coqblin–Schrieffer model. In Sec. 3 self-consistent equations are obtained for the natural relaxation widths of the crystal-field levels, and their influence on the cross section for magnetic inelastic neutron scattering is analyzed. In Sec. 4 qualitatively different types of temperature dependence of the relaxation width are classified. The effects associated with departure from the weak-relaxation approximation are analyzed in Sec. 5. In Sec. 6 the conditions which must be satisfied by the paramagnetic label are analyzed in detail, and experimental procedures which provide the most easily interpreted information are presented. The results of measurements of the relaxation widths of the crystal-field states of the paramagnetic label Pr^{3+} in the compounds $LaAl_3$ and $CeAl_3$ are considered in Sec. 7. The conclusions are presented in Sec. 8.

2. SPECIFIC DETAILS OF THE INTERACTION OF CRYSTAL-FIELD STATES WITH CONDUCTION ELECTRONS IN THE COQBLIN–SCHRIEFFER MODEL

The interpretation of the relaxation of a real paramagnetic label in a particular compound requires the formulation of a problem which takes into account both the specific details of the state of the impurity and the features of the electronic structure of the metal. Therefore, the sf exchange Hamiltonian, which is often employed to analyze the relaxation of crystal-field levels,[17–19]

$$\mathscr{H}_{sf}=\sum_{MM'}(f_M^{\dagger}\hat{\mathbf{J}}_{MM'}f_{M'})(c_{\alpha}^{\dagger}\boldsymbol{\sigma}_{\alpha\beta}c_{\beta}) \tag{1}$$

(where M and M' are the indices of the crystal-field states, α and β are the spin indices of the conduction electrons, $\hat{\mathbf{J}}$ is the total momentum operator, and $\boldsymbol{\sigma}$ denotes a Pauli matrix) is unsuitable for analyzing relaxation in a particular system, since it is a purely formal object, which is not related in any way to the features of the electronic structure of the metal or to the real character of the interaction of an impurity with conduction electrons.

The specific features of the relaxation occurring as a consequence of the interaction of an impurity with conduction electrons can be taken into account in the approaches[22–25] based on the Schrieffer–Wolff and Cornut–Coqblin formalisms.[26–28] A scheme permitting a first-principles calculation of the relaxation of a paramagnetic label can be devised within the method proposed in Refs. 22–25. The Anderson Hamiltonian describing an impurity ion[1)] with one f electron implanted in a metal is represented in the form of the sum

$$\mathscr{H}=\mathscr{H}_0+\mathscr{H}_1. \tag{2}$$

Here the first term

$$\mathscr{H}_0=\sum_{\theta\mathbf{k}\sigma}\epsilon_{\theta\mathbf{k}}c_{\theta\mathbf{k}\sigma}^{\dagger}c_{\theta\mathbf{k}\sigma}+\sum_M E_M f_M^{\dagger}f_M + \frac{U}{2}\sum_{MM'}^{M\neq M'} f_M^{\dagger}f_M f_{M'}^{\dagger}f_{M'} \tag{3}$$

describes the subsystem of delocalized conduction electrons with consideration of the single-particle potential of the f subshell (which is treated as a core state) and the subsystem of the crystal field of the f subshell in the single-particle potential created by the conduction electrons. The operator $c_{\theta\mathbf{k}\sigma}^{\dagger}$ ($c_{\theta\mathbf{k}\sigma}$) describes the creation (annihilation) of a conduction electron with the energy $\epsilon_{\theta\mathbf{k}}$, whose state is characterized by the Bloch wave

$$|\theta\mathbf{k}\sigma\rangle=u_{\theta\mathbf{k}}(\mathbf{r})e^{i\mathbf{kr}}|\sigma\rangle \tag{4}$$

with the wave vector $\mathbf{k}$, the band index θ, and the spin projection σ. The operator $f_M^{\dagger}$ (f_M) describes the creation (annihilation) of the crystal-field state $|M\rangle$ with the energy E_M. The wave functions $|M\rangle$ of the states of an f electron transform in accordance with the irreducible representation Υ_M of the point group of the site of the rare-earth impurity ion $\mathscr{G}_{\text{imp}}$:

$$|M\rangle = \sum_{m=-J_{\rm imp}}^{J_{\rm imp}} \Lambda^{M}_{m,J_{\rm imp}} |m\rangle. \tag{5}$$

Here the $|m\rangle$ are spherical harmonics, which describe the projections m of the total angular momentum of the impurity $J_{\rm imp}$, and U is the on-site Coulomb repulsion constant.

For a microscopic calculation procedure we must represent the many-particle interaction of the localized and delocalized subsystems in terms of the nomenclature for the band states of conduction electrons, rather than in the approximation of symmetrized partial waves.[27,28] In this nomenclature the interaction Hamiltonian

$$\mathscr{H}_1 = \sum_{\theta \mathbf{k}\sigma M} V^{M}_{\theta \mathbf{k}\sigma} f^{\dagger}_{M} c_{\theta \mathbf{k}\sigma} + \text{H.c.} \tag{6}$$

describes the mixing of the localized state $|M\rangle$ with the Bloch wave $|\theta \mathbf{k}\sigma\rangle$, and the hybridization parameter

$$V^{M}_{\theta \mathbf{k}\sigma} = \langle \theta \mathbf{k}\sigma | V_{\rm mix}(\mathbf{r}) | M\rangle \tag{7}$$

can be calculated by a band-calculation procedure. In the case of an impurity state with a nearly integer valence (the hybridization scale $|V^{M}_{\theta \mathbf{k}\sigma}|$ is considerably smaller than the distance from the E_M and $E_M + U$ levels to the Fermi energy ϵ_F), the Coqblin–Schrieffer transformation,[26,27] which eliminates the first order with respect to the hybridization from the Hamiltonian, is applicable. As a result, the interaction of the localized and delocalized subsystems is described by elastic and inelastic scattering processes of the conduction electrons on localized crystal-field states of the impurity:

$$\mathscr{H}_{\rm ex} = \sum_{MM'} \sum_{\theta \mathbf{k}\sigma} \sum_{\theta' \mathbf{k}'\sigma'} J^{MM'}_{\theta \mathbf{k}\sigma, \theta' \mathbf{k}'\sigma'} f^{\dagger}_{M} f_{M'} c^{\dagger}_{\theta \mathbf{k}\sigma} c_{\theta' \mathbf{k}'\sigma'}. \tag{8}$$

The interaction constants of the effective Hamiltonian are expressed in terms of quantities which can be determined by band-calculation methods:[22–25]

$$J^{MM'}_{\theta \mathbf{k}\sigma, \theta' \mathbf{k}'\sigma'} = \frac{V^{M'}_{\theta \mathbf{k}\sigma} (V^{M}_{\theta' \mathbf{k}'\sigma'})^{*}}{2} \left[\frac{1}{\epsilon_{\theta \mathbf{k}} - E_M} + \frac{1}{\epsilon_{\theta' \mathbf{k}'} - E_{M'}} \right]. \tag{9}$$

Although the nomenclature of the band states of conduction electrons is adequate in cases where the problem is a first-principles calculation of the parameters, the nomenclature of symmetrized partial waves, which permits the use of symmetry arguments, is more convenient for qualitative analysis. As a result of the standard transformation into the representations $|\theta k M\rangle$ of the partial waves[27,28]

$$c^{\dagger}_{\theta \mathbf{k}\sigma} = \sum_{kM''} \langle \theta \mathbf{k}\sigma | \theta k M''\rangle c^{\dagger}_{\theta k M''} \tag{10}$$

(here $c^{\dagger}_{\theta k M''}$ is the annihilation operator of a conduction electron in the state centered on the impurity ion with the wave number k, the total angular momentum $J_{\rm imp}$, and the angular dependence described by the irreducible representation $\Upsilon_{M''}$), the Hamiltonian of the exchange interaction can be represented in the form

$$\mathscr{H}_{\rm ex} = \sum_{MM'} f^{\dagger}_{M} f_{M'} \sum_{M''M'''} \sum_{kk'} \sum_{\theta\theta'} \Theta^{\theta' k' M'''}_{\theta k M''}(M, M') \times c^{\dagger}_{\theta k M''} c_{\theta' k' M'''}, \tag{11}$$

where

$$\Theta^{\theta' k' M'''}_{\theta k M''}(M, M') = \sum_{\mathbf{k}\mathbf{k}'} \sum_{\sigma\sigma'} \langle \theta \mathbf{k}\sigma | \theta k M''\rangle \times \langle \theta k' M''' | \theta \mathbf{k}'\sigma'\rangle J^{MM'}_{\theta \mathbf{k}\sigma, \theta' \mathbf{k}'_{\sigma}}. \tag{12}$$

The only restriction which is imposed on the symmetry of the exchange interaction is the condition that the interaction (11) have the symmetry of the point group of the impurity site.[31] Generally speaking, the seed basis of crystal-field states $\{|M\rangle\}$ obtained with consideration of only the single-particle crystal potential is not diagonal when the perturbation (11) is taken into account. In low-symmetry systems this perturbation can mix seed states of the crystal-field basis.[32] Therefore, in the general case the relation

$$\Theta^{\theta' k' M'''}_{\theta k M''}(M, M') = \tilde{J}^{MM'}_{\theta k, \theta' k'} \delta_{M''' M} \delta_{M'' M'}, \tag{13}$$

which reduces the exchange Hamiltonian to the standard Coqblin–Schrieffer expression in the partial-wave representation

$$\mathscr{H}_{\rm ex} = \sum_{MM'} f^{\dagger}_{M} f_{M'} \sum_{kk'} \sum_{\theta\theta'} \tilde{J}^{MM'}_{\theta k, \theta' k'} c^{\dagger}_{\theta k M'} c_{\theta' k' M}, \tag{14}$$

is an artefact of the simplifying assumption that the mixing potential has spherical symmetry in the vicinity of the impurity. Nevertheless, even in the simplest approximation, in which the band index θ and the dependence on the wave number k are neglected (i.e., the band system of the conduction electrons is replaced by an effective density of states), the approximate Hamiltonian

$$\mathscr{H}_{\rm ex} = \sum_{MM'} \bar{I}^{MM'} f^{\dagger}_{M} f_{M'} c^{\dagger}_{M'} c_{M}, \tag{15}$$

which faithfully takes into account the principal features of the symmetry of the states of the delocalized electrons, differs significantly from the formal sf exchange Hamiltonian (1). When the relaxation width is calculated, the sf exchange Hamiltonian (1) induces only transitions with a change in the projection of the total angular momentum of the impurity by unity or without any change in its projection. The relative values of the matrix elements specifying the transitions $|M'\rangle \to |M\rangle$ do not depend on the features of the electronic structure and are determined only by the properties of the Pauli matrices and the structure of the wave functions $|M\rangle$ of the localized states. Conversely, all the quantities appearing in the Hamiltonian (11) can be calculated for a specific impurity in a specific crystal, and the parameters of the approximate Hamiltonian (15) are obtained by averaging (11). Thus, in the general case the Hamiltonian (15) has nonzero matrix elements for the transition between any local states $|M\rangle$ and $|M'\rangle$, and the relations between the different matrix elements $\bar{I}^{MM'}$ are determined by the localized states of both the crystal field of the impurity and the band structure of the conduction electrons.

The calculation of the averaged parameters $\bar{I}^{MM'}$ can be performed by the methods described in Refs. 22–25 and is

beyond the scope of the present work. In this paper we wish to analyze which features of the temperature dependence of the relaxation widths of the crystal-field levels can be observed for various relations between the symmetrized exchange constants $\overline{I}^{MM'}$ of the Hamiltonian (15).

3. RELAXATION WIDTHS OF CRYSTAL-FIELD LEVELS AND THEIR INFLUENCE ON THE WIDTHS OF THE PEAKS FOR NEUTRON TRANSITIONS

The relaxation width Γ_{if} associated with the transition $|i\rangle \rightarrow |f\rangle$ is determined by the natural widths γ_i and γ_f of the initial $|i\rangle$ and final $|f\rangle$ states. It should be noted that the natural widths are determined not only by the mutual relaxation processes of the initial and final states $|i\rangle \leftrightarrow |f\rangle$, but also by the processes $|i\rangle \leftrightarrow |M\rangle$ ($|f\rangle \leftrightarrow |M\rangle$), which are associated with the interaction of the initial (final) states with all the other crystal-field states $\{|M\rangle\}$. In this case the natural width of the initial (final) state is determined by the set of parameters $\{\overline{I^{iM}}\}$ ($\{\overline{I^{fM}}\}$) of the Hamiltonian (15).

Let us consider the process responsible for the inelastic neutron transition $|i\rangle \rightarrow |f\rangle$ from the initial state $|i\rangle$ with the energy E_i to the final state with the energy $E_f = E_i + \Delta_{fi}$. We introduce the Matsubara Green's functions describing the crystal-field states of the impurity center j and the Green's functions of similar nature for Abrikosov pseudofermions,[33]

$$\mathcal{G}_\lambda = -\langle T_\tau f_{j,M}(\tau) f^\dagger_{j,M}(0)\rangle, \tag{16}$$

which have the following forms in the zeroth approximation (i.e., in the absence of relaxation):

$$\mathcal{G}_i^{(0)} = (i\omega - E_i + \mu)^{-1}, \tag{17}$$

$$\mathcal{G}_f^{(0)} = (i\omega - E_i - \Delta_{fi} + \mu)^{-1} \tag{18}$$

(in the notation adopted μ is the chemical potential of the pseudofermions, and in the final formulas it must be assumed that $\mu \rightarrow -\infty$).

The retarded Green's functions, which specify the spectral response of the system, can be obtained using the analytic continuation of the Matsubara Green's functions from the upper semiaxis onto the entire complex plane of ω. Passage to the retarded Green's functions in the zeroth-order Green's functions requires the replacement $i\omega \rightarrow \omega + i\delta$. The interactions of the crystal-field states with other subsystems of elementary excitations of the crystal lead to renormalization of the crystal-field energy and to the appearance of a frequency-dependent imaginary part in the denominator of the Green's function. The renormalizations of the crystal-field splittings can be included in the definition of the Green's functions (17) and (18) and will not be considered further. Let us next concentrate our attention on the temperature dependence of the relaxation width and take into account that the retarded Green's functions of the crystal-field levels can be written in the pole approximation in the form

$$\mathcal{G}_i^R(\omega) = [\omega - E_i + \mu + i\gamma_i(\omega)]^{-1}, \tag{19}$$

$$\mathcal{G}_f^R(\omega) = [\omega - E_i - \Delta_{fi} + \mu + i\gamma_f(\omega)]^{-1}. \tag{20}$$

The on-site susceptibility, which determines the magnetic neutron response of an impurity center, is expressed[33] in terms of the retarded Green's function

$$\chi_{if}^R(\tau) = -\langle T_\tau f_i^\dagger(\tau) f_f(\tau) f_f^\dagger(0) f_i(0)\rangle,$$

whose analytic continuation onto real frequencies has the following form:

$$\chi_{if}^{(0)R}(\Omega) = -|\Theta_{if}|^2 \int_{-\infty}^{\infty} \frac{d\epsilon}{2\pi} \tanh\left(\frac{\epsilon}{2T}\right) [\mathrm{Im}\ \mathcal{G}_i^R(\epsilon) \times \mathcal{G}_f^R(\epsilon+\Omega) + \mathrm{Im}\ \mathcal{G}_f^R(\epsilon)\mathcal{G}_i^A(\epsilon-\Omega)] \tag{21}$$

(here Θ_{if} is a matrix element, which depends on the wave functions of the initial and final crystal-field states and determines the intensity of the neutron scattering peak). Representing the resonant part of the susceptibility $\chi_{if}^R(\Omega)$ at $\Omega \approx \Delta_{fi}$ in the form

$$\chi_{if}^R(\Omega) = \frac{\Xi_0}{\Omega - \Delta_{fi} + i\Gamma_{if}}, \tag{22}$$

where Ξ_0 is the residue at the respective pole), we can obtain the dependence of Γ_{if} on the corresponding natural dampings of the pseudofermion Green's functions. In the limit $\gamma_{i,f} \ll \Delta_{fi}$ or $\gamma_{f,i} \ll T$ the relation between the relaxation constant Γ_{if} extracted from the results of magnetic inelastic neutron scattering experiments and the natural damping of the pseudofermion Green's functions acquires a simple form:

$$\Gamma_{if} = \gamma_i(\omega = E_i) + \gamma_f(\omega = E_f). \tag{23}$$

Thus, in the cases which are most interesting for a reliable experimental analysis (where the width of the inelastic transition is smaller than its energy) the problem of determining the temperature dependence of the width Γ_{if} of a transition reduces to a calculation of the natural widths of the initial and final states.

Let us consider the influence of conduction electrons on the natural width of crystal-field states in the Cornut–Coqblin model. For this purpose we use the effective Hamiltonian (15) obtained in the preceding section as the interaction Hamiltonian. The natural widths are calculated by standard Feynman-diagram techniques at finite temperatures. This allows us to partially sum diagram series and to obtain a closed system of self-consistent equations. The departure from perturbation theory is critical in the case of fairly strong relaxation, since the natural width $\gamma_M(\omega = E_M)$ of each crystal-field state $|M\rangle$ depends on the relaxation widths of the entire system of crystal-field levels and must, therefore, be found self-consistently. To illustrate this point, we consider the interaction between the states $|M\rangle$ and $|M'\rangle$ with the energies E_M and $E_{M'} = E_M + \Delta_{M'M}$, respectively. The simplest diagram which leads to relaxation of the crystal-field states is shown in Fig. 1a. The dashed line correspond to the Green's function of the conduction electron

$$G(\mathbf{r},\tau) = -\langle T_\tau \Psi_\xi(\mathbf{r},\tau)\Psi_\xi^\dagger(0,0)\rangle, \quad \xi = M, M' \tag{24}$$

(we neglect the difference between the Green's functions of the conduction electrons for different M). The diagrams corresponding to the vertex corrections can be classified in the following manner. The first are parquet diagrams, which are

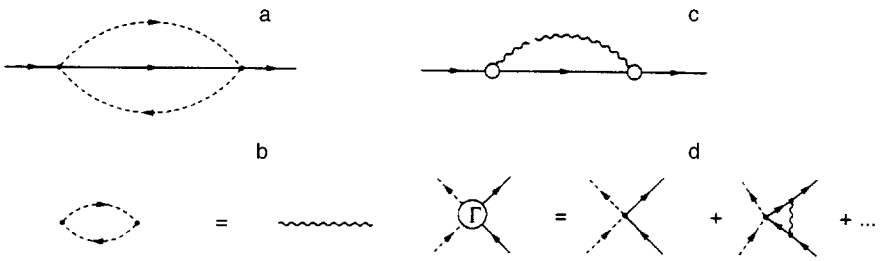

FIG. 1. Feynman diagrams: a—simple diagram describing the shift and damping of a crystal-field level (dashed line—conduction electron Green's function, solid line–crystal-field excitations); b—conduction electron polarization operator, which describes the electromagnetic interaction between crystal-field excitations; c—eigenenergy part of the crystal-field excitations with consideration of the vertex renormalization; d—skeletal diagrams for vertex corrections.

similar to the Abrikosov diagrams considered in the analysis of the Kondo effect in Ref. 33. Consideration of the contribution from the first nonvanishing term leads to the appearance of an interaction in the channel $\Gamma_{M=M'} \sim (I^2_{MM'}/W)\ln(W/\Delta_{MM'})$ and to the corrections $\delta\Gamma^{(3,p)}_{MM'} \sim (I^3_{MM'}/W^2)\ln^2(W/\Delta_{MM'})$ (W is the width of the conduction electron band). The second are nonparquet diagrams.[34] Consideration of the contribution from the first correction (Fig. 1d) leads to the additional contribution $\delta\Gamma^{(3,np)}_{MM'} \sim (I^3_{MM'}/W^2)\ln(W/\Delta_{MM'})$. We shall henceforth assume $I_{MM'}/W \ll 1$ and $(I_{MM'}/W)\ln(W/\Delta_{MM'}) \ll 1$ and neglect the vertex corrections in the perturbative approach. Under these circumstances

$$\sigma_M(i\omega_n) = [\overline{I}^{MM'}]^2 T^2 \sum_{\epsilon_1\epsilon_2} \frac{1}{\mathscr{N}^2} \sum_{\mathbf{p}_1,\mathbf{p}_2} G(\mathbf{p}_1,\epsilon_1)G(\mathbf{p}_2,\epsilon_2) \times \mathscr{G}_{M'(\neq M)}(\epsilon_1+\epsilon_2-\omega) \tag{25}$$

($\mathscr{N}$ is the total number of conduction electrons). Performing the analytic continuation of the expression (25) into the upper half-plane of the complex variable ω according to the usual rules,[35–37] we obtain the following expressions for the eigenenergy parts at real frequencies (the analogous equations for the sf exchange Hamiltonian were obtained by Maleev in a treatment of the relaxation of the crystal field in cubic metals[19]):

$$\gamma_M(\omega) = -\,\mathrm{Im}\ \sigma^R_M(\omega) = \frac{1}{\pi}[\overline{I}^{MM'}]^2 \int_{-\infty}^{\infty} dx \frac{1}{\mathscr{N}} \sum_{\mathbf{p}} [N(x)+n(x+\omega)]\,\mathrm{Im}\ \mathscr{G}^R_{M'(\neq M)}(x+\omega)\,\mathrm{Im}\ \Pi^R_{MM'}(\mathbf{p},x). \tag{26}$$

Here $N(x)=(e^{x/T}-1)^{-1}$, $n(x)=(e^{x/T}+1)^{-1}$, $\Pi(\mathbf{p},x)$ is the polarization operator of the conduction electrons (Fig. 1b), whose imaginary part describes the two-particle density of states:

$$\mathrm{Im}\,\frac{1}{\mathscr{N}}\sum_{\mathbf{p}} \Pi^R(\mathbf{p},x) = -\frac{\pi}{2}N_0^2 x, \tag{27}$$

where N_0 is the single-particle density of states of the conduction electrons at the Fermi level, in terms of which the dimensionless coupling constants $g_{MM'}$ are expressed:

$$g^2_{MM'} = \frac{1}{2}[I^{MM'}N_0]^2. \tag{28}$$

In the integrals (26) we perform the replacement $\omega+\mu=\tilde{\omega}$ corresponding to the displacement of the energy reference point. Allowing μ to tend to $-\infty$, we neglect the Fermi function on the right-hand side. This replacement has a simple physical meaning: the singularities of the functions $\mathscr{G}$ are determined by a far larger energy scale, and, therefore, the terms corresponding to consideration of the poles of the pseudofermion functions should be omitted.[38]

According to (23), the natural damping γ of the crystal-field states at the frequencies corresponding to the energies of the crystal-field levels must be calculated to determine the width of a neutron transition. Thus, in the case of the interaction of $|M\rangle$ and $|M'\rangle$, the quantities $\gamma_M(\omega=E_M)$ and $\gamma_{M'}(\omega=E_{M'})$ must be calculated. Determining the damping at the poles of the corresponding Green's functions, we obtain the system of coupled equations

$$\begin{cases} \gamma_M(\omega\to E_M) = \pi g^2_{MM'} \int_{-\infty}^{\infty} dx x N(x) P \times (x-\Delta_{M'M},\gamma_{M'}), \\ \gamma_{M'}(\omega\to E_M+\Delta_{M'M}) = \pi g^2_{MM'} \int_{-\infty}^{\infty} dx x N(x) \times P(x+\Delta_{M'M},\gamma_M), \end{cases} \tag{29}$$

where $P(x,\gamma)$ is the spectral function normalized to unity:

$$P(x,\gamma) = \frac{1}{\pi}\frac{\gamma}{x^2+\gamma^2}. \tag{30}$$

The expressions obtained are easily generalized to the case of an arbitrary set of constants in the Hamiltonian (15) ($\{\overline{I}^{MM'}\}$; $M,M'=1,\ldots,2J_{\mathrm{imp}}+1$) and an arbitrary system of crystal-field states with the energies E_M. Proceeding precisely as in the derivation of (25)–(29), we obtain the expressions for the frequency-dependent damping rates

$$\gamma^R_M(\omega) = -\,\mathrm{Im}\ \sigma^R_M(\omega) = \frac{1}{\pi}\sum_{M'=1}^{2J_{\mathrm{imp}}+1} \overline{I}^2_{MM'} \int_{-\infty}^{\infty} dx \frac{1}{\mathscr{N}} \sum_{\mathbf{p}} [N(x)+n(x+\omega)]\,\mathrm{Im}\ \mathscr{G}^R_{M'}(x+\omega)\,\mathrm{Im}\ \Pi^R_{MM'}(\mathbf{p},x),$$
$$M=1,\ldots,2J_{\mathrm{imp}}+1. \tag{31}$$

Neglecting the Fermi function on the right-hand side of (31), we obtain the system of self-consistent equations

$$\gamma_M(\omega)=-\sum_{M'=1}^{2J_{\rm imp}+1} g^2_{MM'}\int_{-\infty}^{\infty} dx x N(x)\,{\rm Im}\,\mathcal{G}^R_{M'}(x+\omega),$$

$$M=1,\ldots,2J_{\rm imp}+1. \tag{32}$$

Here the dimensionless coupling constants are expressed in terms of the parameters of the Hamiltonian (15):

$$g^2_{MM'}=g^2_{M'M}=\frac{1}{2}[\overline{I}^{MM'}N_0^{MM'}]^2, \tag{33}$$

where $N_0^{MM'}$ is the partial density of states of the conduction electrons corresponding to the $M\to M'$ transition.

The system of equations for finding the natural relaxation constants at the frequencies which determine the widths of the neutron transitions [see (23)] can be represented in the explicit form[2)]

$$\gamma_M(\omega\to E_M)=\int_{-\infty}^{\infty} dx x N(x) \times\sum_{M'=1}^{2J_{\rm imp}+1} g^2_{MM'}P(x-\Delta_{M'M},\gamma_{M'}),$$

$$M=1,\ldots,2J_{\rm imp}+1, \tag{34}$$

where

$$\Delta_{M'M}=E_{M'}-E_M.$$

4. CLASSIFICATION OF THE TEMPERATURE DEPENDENCE OF RELAXATION WIDTHS

The temperature dependence of the natural relaxation widths (and the widths of the neutron transitions determined by them) depends on the relationship between the different constants in the Hamiltonian (15) and on the energies of the crystal-field states. In this section we shall classify the types of temperature dependence for cases in which solutions of the self-consistent system of equations (34) can be obtained explicitly.

The simplest condition under which the system of equations (34) is decoupled is that the relaxation widths be small ($\gamma_M\to 0$). In this case, instead of the system of equations (32), we obtain the following expressions for the non-self-consistent widths of the levels $\gamma_M^{(0)}$:

$$\gamma_M^{(0)}=\pi\sum_{M'=1}^{L}\int_{-\infty}^{\infty} g^2_{MM'}xN(x)\,\delta(x-\Delta_{MM'}). \tag{35}$$

The calculation of (35) permits separation of the contributions to the temperature dependence of the natural width $\gamma_M(T)$ into three types:

$$\gamma_M(T)=\gamma_M^{(\rm eq)}(T)+\gamma_M^{\uparrow}(T)+\gamma_M^{\downarrow}(T). \tag{36}$$

The first type is associated with the relaxation caused by the interaction of the crystal-field state $|M\rangle$ with the levels $\{|M'\rangle\}$, whose energies $E_{M'}$ equal E_M:

$$\gamma_M^{(\rm eq)}(T)=\pi T\sum_{M'}^{E_{M'}=E_M} g^2_{MM'}. \tag{37}$$

The contributions to the natural relaxation width of the level $|M\rangle$ from higher-lying ($E_{M'}>E_M$) and lower-lying ($E_{M'}<E_M$) levels are given by the expressions

$$\gamma_M^{\uparrow}(T)=\pi\sum_{M'}^{E_{M'}>E_M} g^2_{MM'}\Delta_{M'M}N(\Delta_{M'M}) \tag{38}$$

and

$$\gamma_M^{\downarrow}(T)=\pi\sum_{M'}^{E_{M'}<E_M} g^2_{MM'}\Delta_{MM'}[N(\Delta_{MM'})+1], \tag{39}$$

respectively. In the limit of high temperatures, $T\gg\max(E_M)$, in accordance with the results in Refs. 17–21, the temperatures dependences of all three contributions to the relaxation are indistinguishable. All three contributions obey a Korringa law, and the expression for the natural relaxation width takes the form

$$\gamma_M(T)=\pi T\sum_{M'=1}^{2J_{\rm imp}+1} g^2_{MM'}. \tag{40}$$

At low temperatures the contributions of the higher-lying ($E_{M'}>E_M$) and lower-lying ($E_{M'}<E_M$) crystal-field levels differ significantly. In the limit $T\to 0$, $N(\Delta)$ is exponentially small, $N(\Delta)\to\exp(-\Delta/T)$, and (38)–(39) take the form

$$\gamma_M^{\uparrow}(T)=\pi\sum_{M'}^{E_{M'}>E_M} g^2_{MM'}\Delta_{M'M}\exp\left(-\frac{\Delta_{M'M}}{T}\right), \tag{41}$$

$$\gamma_M^{\downarrow}(T)=\pi\sum_{M'}^{E_{M'}<E_M} g^2_{MM'}\Delta_{MM'}. \tag{42}$$

Thus, as $T\to 0$, the contributions to the natural relaxation width from the higher-lying levels tend exponentially to zero, and the contributions from the lower-lying levels do not depend on the temperature.

Since the shape of the line for the neutron transition $|i\rangle\to|f\rangle$ is measured directly in an experiment, it would be interesting to analyze the temperature dependence of the width of the transition $\Gamma_{i\to f}(T)=\gamma_i(T)+\gamma_f(T)$ (see Fig. 2) for different relationships between the constants of the Hamiltonian (1). The diagonal interactions I^{ii} (I^{ff}) lead to a contribution $\sim\pi g_{ii}^2T$ ($\sim\pi g_{ff}^2T$), which is proportional to the temperature. In the case of the relaxation of only the initial (final) state as a result of interactions with the upper ($\uparrow$) levels, we have $[\Gamma^{\uparrow}_{i\to f}(T)]^{i(f)}\sim N(\Delta_{\uparrow i(f)})$, which leads to exponentially small damping, $\sim\exp(-\Delta_{\uparrow i(f)}/T)$, at low temperatures. When only the initial (final) state relaxes as a result of interactions with lower ($\downarrow$) levels, we have $[\Gamma^{\downarrow}_{i\to f}(T)]^{i(f)}\sim\Delta_{i(f)\downarrow}[N(\Delta_{i(f)\downarrow})+1]$, which can be described by a constant $\sim\Delta_{i(f)\downarrow}$ at low temperatures. The fourth special case is the one in which relaxation is mediated by the interaction between the initial and final states I^{if}. In this case $\Gamma^{if}_{i\to f}(T)\sim\Delta_{fi}[2N(\Delta_{fi})+1]=\Delta_{fi}\coth(\Delta_{fi}/2T)$.

If the special cases just described are realized in the system being studied, they are easily distinguished from one another even by qualitative visual inspection. The situation in which relaxation of the initial and final levels occurs only because of the influence of the higher-lying levels is easily distinguished (the dotted line in Fig. 3). In this case

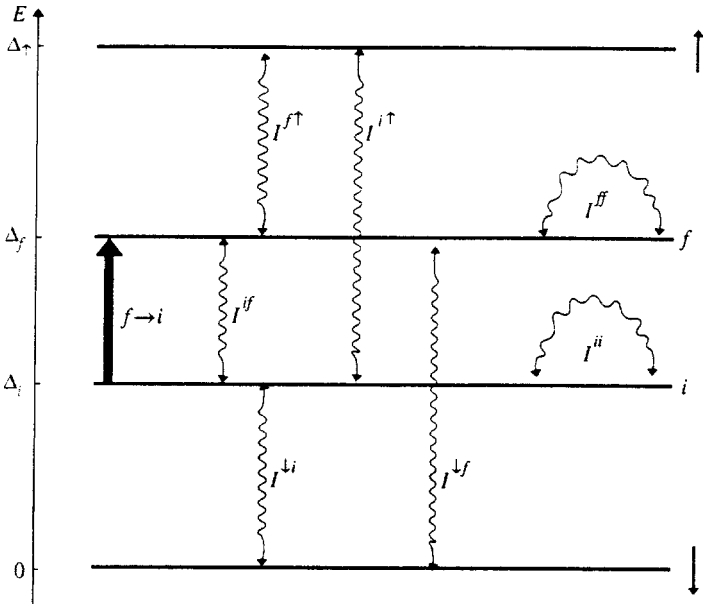

FIG. 2. General case of the classification of sources for the relaxation of the levels of the initial (i) and final (f) states of a transition (thick vertical arrow) due to interactions with lower-lying levels ($I^{\downarrow i}$ and $I^{\downarrow f}$) and higher-lying levels ($I^{\uparrow i}$ and $I^{\uparrow f}$) and due to mutual coupling of the initial and final states (I^{if}, wavy lines).

$\Gamma^{\uparrow}_{i\to f}(T\to 0)\to 0$. The mutual relaxation processes (the solid line in Fig. 3) are also visually distinguishable from the variants in which the broadening is a consequence of the interactions of the initial or final state with lower-lying levels (the dashed line in Fig. 3). The sharpness of the temperature dependence can serve as a criterion in these cases. In the former variant (see Fig. 3) we have $\Gamma^{if}_{i\to f}(T=2\Delta_{MM'})/\Gamma^{if}_{i\to f}(T=0)\approx 4$, and in the latter variant we have $\Gamma^{\downarrow}_{i\to f}(T=2\Delta_{MM'})/\Gamma^{\downarrow}_{i\to f}(T=0)\approx 2.5$.

5. CONSEQUENCES OF THE SELF-CONSISTENT PROCEDURE

Beside the obvious quantitative influence of the self-consistent procedure manifested as renormalization of the numerical values of the natural relaxation constants, there is a qualitative difference, which is expressed by the nonzero value of the relaxation width of the ground state $|G\rangle$ at zero temperature.

In the non-self-consistent procedure [see (41)] the width $\gamma^{(0)}_G(T\to 0)=\pi g^2_{GE}\Delta_{EG}\exp(-\Delta_{EG}/T)\to 0$ (E is the higher-lying level with the smallest value of Δ_{EG}). The solution of the system of self-consistent equations (29) (for $M=G$, $M'=E$) gives a nonzero width: $\gamma^{(sc)}_G(T=0)\neq 0$. Under the conditions $T\ll\gamma_{EG}$ and $T\ll\Delta_{EG}$ an explicit expression can be obtained for the width $\gamma^{(sc)}_G(T=0)$ of the level. Since at low temperatures the non-self-consistent natural width of the crystal-field excited level is $\gamma^{(0)}_E(T\to 0)=\pi g^2_{GE}\Delta_{EG}$, the weak corrections caused by the influence of the lower level can be neglected. Then the self-consistent width of the lower level is proportional to the square of the coupling constant:

$$\gamma^{(sc)}_G\approx\pi g^2_{GE}\gamma^{(0)}_E\ \ln\left(\frac{W}{\Delta_{GE}}\right) \tag{43}$$

(in the calculation we cut off the integral (29) at the width of the conduction electron band W). Substituting the expression for $\gamma^{(0)}_E$ into (43), we obtain[3)]

$$\gamma^{(sc)}_G\approx\pi^2 g^4_{GE}\Delta_{EG}\ \ln\left(\frac{W}{\Delta_{GE}}\right). \tag{44}$$

Since the corrections associated with the influence of the width of the lower level on the upper level contain an additional small factor $\sim g^2_{GE}$, (43) is the explicit solution of the system of self-consistent equations to within terms $\sim g^4_{GE}$ inclusively.

This result, which is unexpected from the standpoint of perturbation theory, can have a physical interpretation in the self-consistent theory. It should, first of all, be taken into account that $|G\rangle$ is the ground state of the system only when the interactions are disregarded. When the interaction with the delocalized conduction electrons is included, the nomenclature of the localized states is no longer the true quantum-mechanical basis, and $|G\rangle$ is not the true ground state.

A specific mechanism, which causes damping of the crystal-field state $|G\rangle$ at zero temperature, can be pointed out. The physical cause of the damping of $|G\rangle$ is the nonzero broadening of the excited state $|E\rangle$ (which also occurs in perturbation theory). Figure 4 presents the spectral functions of $|E\rangle$ [$P(x-1,\gamma^{(0)}_E=0.4)$] and $|G\rangle$ [$P(x,\gamma^{(0)}_G=0)=\delta(x)$] in the perturbative approximation. The width of $|G\rangle$ in the

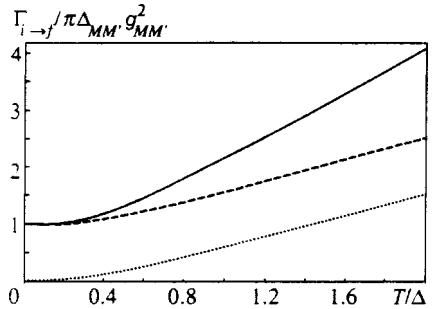

FIG. 3. Reduced temperature dependences of the total inelastic scattering width Γ_{if} due to relaxation processes with a higher-lying level (dotted line) and a lower-lying level (dashed line) and mutual processes (I^{if}, solid line).

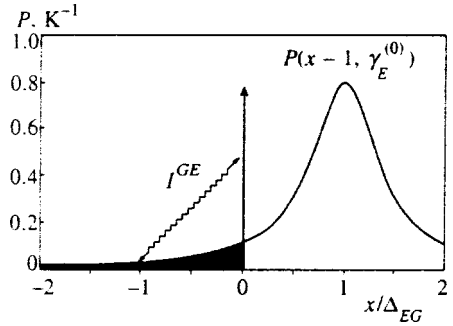

FIG. 4. Illustration of the origin of the finite width of the crystal-field ground state $|G\rangle$ (vertical arrow at $x/\Delta_{EG}=0$) due to relaxation processes (wavy lines with arrows) which couple the $|G\rangle$ level to the low-energy tail (darkened region) of the spectral function $P(x-1,\gamma_E^{(0)}\neq 0)$ of the upper $|E\rangle$ state.

self-consistent approach is nonzero ($\gamma_G^{(\mathrm{sc})}\neq 0$) because of the allowed transitions I^{GE} induced by the width of the upper level $|E\rangle$ to the low-energy tail (the darkened area in Fig. 4) of the Lorentzian contour of the upper level.

The result obtained, which attests to the nonzero contribution to the natural relaxation width of the ground-state level, calls for caution in approaching methods for estimating the characteristic temperature T^* in Kondo systems from the full width at half maximum (FWHM) of the quasielastic neutron scattering peak at zero temperature. According to the generally accepted approach,[39,40] the characteristic temperature is determined from the relation $T^*=\Gamma_{\mathrm{qe}}^{\mathrm{exp}}(T=0)/2$, where $\Gamma_{\mathrm{qe}}^{\mathrm{exp}}(T=0)$ is the experimentally observed quasielastic scattering width at zero temperature. In this procedure it is assumed that the width of the peak $\Gamma_{\mathrm{qe}}^{\mathrm{exp}}(T=0)$ is determined only by the anomalous width $\Gamma_K(T=0)$, which is associated with Kondo scattering processes on the lowest crystal-field state. However, the presence of the nonzero contribution $\gamma_G^{(\mathrm{sc})}(T=0)$ from the normal relaxation processes calls for additional refinement in the case of strong relaxation broadening in systems with soft crystal fields. In this situation, since the experimental width $\Gamma_{\mathrm{qe}}^{\mathrm{exp}}(T=0)$ is determined not only by the anomalous width $\Gamma_K(T=0)$, but also by the relaxation contribution $\gamma_G^{(\mathrm{sc})}(T=0)$, we have

$$\Gamma_{\mathrm{qe}}^{\mathrm{exp}}(T=0)=\Gamma_K(T=0)+2\gamma_G^{(\mathrm{sc})}(T=0), \tag{45}$$

and the standard relation should be rewritten in the form

$$T^*=\frac{\Gamma_{\mathrm{qe}}^{\mathrm{exp}}(T=0)-2\gamma_G^{(\mathrm{sc})}(T=0)}{2}. \tag{46}$$

Thus, when there is strong relaxation in systems with soft crystal fields, the determination of the characteristic temperature is complicated by the nonzero relaxation contribution at $T=0$. Nevertheless, the use of (46) and (44) provides an estimate in this case too. To analyze the contribution from the normal relaxation processes of a specific compound, we must determine the parameters (the crystal-field splitting $\Delta_{MM'}$ and the dimensionless relaxation constants $g_{MM'}$) which describe the relaxation in the particular material. The set of techniques discussed in the next section can be useful in solving this problem.

6. PARAMAGNETIC LABELING

Studying the electronic structure by measuring the relaxation of a paramagnetic label requires the observance of several conditions, which must be satisfied by the compound being studied $A_l\{B\}$ and the paramagnetic ion P. In this section we describe the most desirable general conditions, under which performing and interpreting paramagnetic labeling experiments are simplest, and we present some examples of compounds which satisfy these necessary conditions.

One necessary condition which must be satisfied by the compound $A_l\{B\}$ being studied is the existence of a reference compound $P_l\{B\}$ containing the paramagnetic label P. The reference compound must be a structural analog of the compound being studied. In the first stage the properties of the reference compound $P_l\{B\}$ must be investigated. The purpose of studying the reference compound is to obtain information on the crystal-field energies and wave functions of the paramagnetic label. This information can be obtained by analyzing experimental data from measurements of magnetic neutron scattering (or Raman scattering) and the thermodynamic properties (the magnetic susceptibility and specific heat). For neutron scattering experiments, which require a fairly large quantity of the material, it should be noted that a single-crystal sample is not required. This greatly facilitates implementation of the method, since magnetic susceptibility data suitable for reconstructing the crystal-field wave functions can be obtained from measurements on tiny single-crystal samples.

In the second stage, for which a polycrystalline sample suffices, inelastic neutron scattering experiments are performed on the compound $(A_{1-x}P_x)_l\{B\}$. The theoretical analysis requires information on the crystal-field states of the paramagnetic label P in $(A_{1-x}P_x)_l\{B\}$. The experimental neutron scattering data provide information on the energies of the crystal-field levels of the paramagnetic label in the compound being studied. Since it is impossible to study the crystal-field states of an ion of P in $(A_{1-x}P_x)_l\{B\}$ by thermodynamic methods, additional information on the crystal-field wave functions is needed. This information can be obtained by studying the trends in the variation of the crystal-field parameters of a family of compounds $R_l\{B\}$ (where R=A,P,...). There are presently several families of compounds for which such investigations have already been performed: RAl_3,[9–11] RNi_5,[12–14], and RNi[14–16] (R is a rare-earth ion). In these families the main contribution to the formation of the crystal field is made by the ions in the local environment and the conduction electrons. Therefore, the structures of the crystal-field wave functions of the paramagnetic label P in the reference compound and in the compound being studied are practically identical. Thus, the systems which are suitable for the proposed procedure are compounds in which the nearest neighbors of each ion of A that is replaced by the paramagnetic label are ions from an unsubstituted formula unit of {B}. The best systems for application of the method are materials in which the crystal-field parameters are determined predominantly by the nearest neighbors.

The next necessary condition is a small concentration of the ions of the paramagnetic label, $x\ll 1$, in $(A_{1-x}P_x)_l\{B\}$.

This condition permits consideration of the crystal fields and their relaxation as purely single-ion phenomena. A small value of x is also necessary to be sure that doping with the paramagnetic label did not lead to significant alteration of the electronic structure of the compound being studied.

An important desirable restriction imposed on the paramagnetic label is nondegeneracy of the crystal-field ground state of the ion. Fulfillment of this condition significantly simplifies the interpretation of the experimental data, since the natural width of the crystal-field ground state is specified by a simple exchange Hamiltonian of the form (15). A degenerate ground state $|G\rangle$ can lead to a Kondo effect, which results in the appearance of a specific temperature dependence of the quasielastic neutron scattering width: $\Gamma_{qe}(T) = 2\gamma_G(T) = a + b\sqrt{T}$.[40] The presence of a specific temperature dependence of the natural width of the crystal-field ground state greatly complicates the interpretation, since the width $\Gamma_{GM}(T) = \gamma_G(T) + \gamma_M(T)$ of any inelastic transition from the ground state contains this poorly studied component. This circumstance greatly complicates the analysis, since the theoretical treatment is simplest, if the temperature dependence of the natural widths $\gamma_M(T)$ of the levels is determined during the experiment. This dependence can be extracted from the solution of the system of equations

$$\Gamma_{MM'}(T) \approx \gamma_M(T) + \gamma_{M'}(T), \tag{47}$$

whose features must be analyzed separately for each specific case.

It is also noteworthy that one of the significant advantages of the method can be the possibility of regulating the selection rules by choosing different paramagnetic labels. It can easily be seen that different symmetries for the crystal-field states of the paramagnetic label will lead to different types of temperature dependence of the relaxation process. Therefore, significant information can be obtained by analyzing situations with different ions serving as the paramagnetic label in relaxation spectroscopy.

7. RELAXATION OF THE PARAMAGNETIC LABEL Pr^{3+} IN $Pr_{0.03}Ce_{0.97}Al_3$ AND $Pr_{0.03}La_{0.97}Al_3$

An example of a favorable combination of properties for the paramagnetic label and the compound being studied is the Pr^{3+} ion in the hexagonal compounds RAl_3 (R is a lanthanide). The crystal-field ground state (level 1 in Fig. 5) in pure $PrAl_3$ is the singlet $|\Gamma_1\rangle = |0\rangle$, and the only allowed transition at $T \to 0$ is the $|\Gamma_1\rangle \to |\Gamma_6\rangle$ transition to the $|\Gamma_6\rangle = |\pm 1\rangle$ state (level 2 in Fig. 5). The crystal fields of the praseodymium ion in $PrAl_3$ were studied in detail in Ref. 9 (see Fig. 5, in which the crystal-field levels are numbered from 1 to 6 in order of increasing energy). The singlet character of the ground state rules out both the Korringa relaxation channel $\sim |I^{11}|^2$ and the relaxation channel associated with Kondo processes.

The relaxation of the paramagnetic label Pr^{3+} was studied in $Pr_{0.03}Ce_{0.97}Al_3$ and $Pr_{0.03}La_{0.97}Al_3$. The crystal-field splitting energy of the praseodymium ion Δ_{21} in both $Pr_{0.03}Ce_{0.97}Al_3$ and $Pr_{0.03}La_{0.97}Al_3$ differs only slightly from the crystal-field energy $\Delta_{21}^R \approx 4.5$ meV in the reference compound $PrAl_3$. More specifically, in $Pr_{0.03}Ce_{0.97}Al_3$ $\Delta_{21} \approx 4.2$ meV, and in $Pr_{0.03}La_{0.97}Al_3$ $\Delta_{21} \approx 3.5$ meV. Therefore, in the simplest approximation the wave functions of the crystal-field states of the paramagnetic label in the compounds studied can be assumed to be only slightly altered from those in the reference. To describe the relaxation of the paramagnetic label in $CeAl_3$, we selected a system of levels which coincides with the crystal-field system in pure $PrAl_3$, and to analyze the relaxation in $LaAl_3$, we chose a system in which all the splitting energies are reduced by a factor of $3.2/4.5 \approx 0.711$ (see Fig. 5). The thoroughly studied laws governing the variation of the crystal field of the paramagnetic label in $Pr(La)Al_3$ (Refs. 9 and 10) can be used for a more exact calculation.

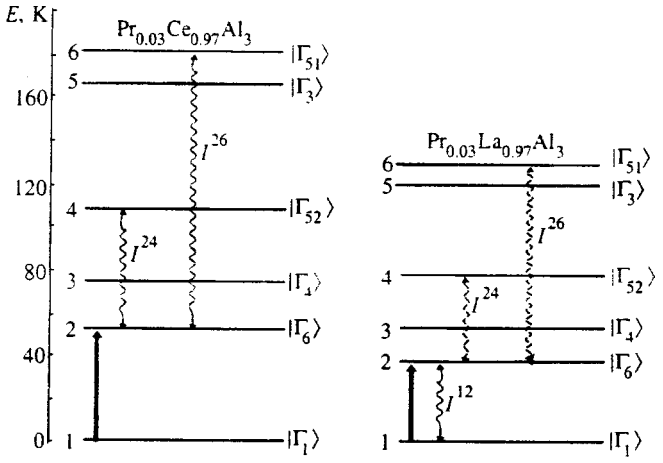

FIG. 5. Level scheme of the paramagnetic label Pr^{3+} in $CeAl_3$ (on the left) and $LaAl_3$ (on the right). Wave functions of the levels:[9] $|\Gamma_1\rangle = |0\rangle$; $|\Gamma_6\rangle = |\pm 1\rangle$; $|\Gamma_4\rangle = 2^{-1/2}|-3\rangle - 2^{-1/2}|-3\rangle$; $|\Gamma_{52}\rangle = a|\pm 4\rangle - \sqrt{1-a^2}|\mp 2\rangle$; $|\Gamma_3\rangle = 2^{-1/2}|3\rangle + 2^{-1/2}|-3\rangle$; $|\Gamma_{51}\rangle = \sqrt{1-a^2}|\pm 4\rangle + a|\mp 2\rangle$. The neutron transition studied in Ref. 9 is denoted by a vertical arrow. The postulated relaxation channels affecting the initial and final states are denoted by wavy lines with arrows.

In the experiments in Ref. 11 measurements of the temperature dependence of only the transition width $\Gamma_{12}(T)$ were performed (the FWHM of the Lorentzian, which corresponds to 2Γ in our notation, was measured in Ref. 11), while the natural relaxation widths $\gamma_1(T)$ and $\gamma_2(T)$ were not distinguished. Nevertheless, even in this case definite conclusions regarding the difference between the relaxation behavior of the paramagnetic label in $CeAl_3$ and $LaAl_3$ can be drawn.

Since level 1 of the paramagnetic label in $CeAl_3$ corresponds to the ground state, the relaxation of level 1 in interactions with lower-lying levels is impossible. Moreover, a visual comparison of the experimental data (Fig. 6) with the calculated dependences shown in Figs. 2 and 3 allows us to state that the mutual relaxation processes I^{12} are also absent. This conclusion can be drawn on the basis of a comparison of the widths at low and high temperatures: there is no temperature-dependent contribution at $T < 20$ K. Therefore, the only possible sources of natural relaxation broadening of levels 1 and 2 are the interactions of levels 1 and 2 with higher-lying levels 3, 4, 5, and 6.

Although the only quantum numbers in whose nomen-

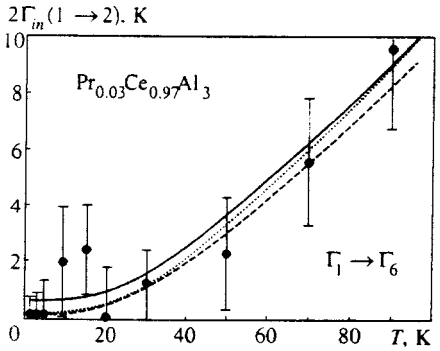

FIG. 6. Temperature dependence of the FWHM ($2\Gamma_{in}$) of the inelastic $|\Gamma_1\rangle \rightarrow |\Gamma_6\rangle$ transition in $CeAl_3$ for the paramagnetic label Pr using the level scheme in Fig. 5. Dotted line—best fitting in the non-self-consistent approximation for $g=g^{(0)}=0.115$. Solid line—best fitting in the self-consistent approximation for $g=g^{(sc)}=0.111$. Dashed line—non-self-consistent width for $g=g^{(sc)}=0.111$.

clature correct arguments can be advanced are the indices of the irreducible representations $M=\Gamma_1,\Gamma_3,\Gamma_4,\Gamma_6,\Gamma_{51}$, and Γ_{52}, we shall demonstrate that the nomenclature of the projections m of the spherical representation [see (5)] is also useful for a qualitative analysis of relaxation.

Using the known wave functions of the crystal-field states (see the caption to Fig. 5), we can rule out the transitions with $\delta m=\pm 1$ because of the lack of the $|\Gamma_1\rangle \leftrightarrow |\Gamma_6\rangle$ mutual relaxation channel. The transitions with $\delta m=\pm 2$ should lead to interactions of $|\Gamma_1\rangle$ with $|\Gamma_{51}\rangle$ and $|\Gamma_{52}\rangle$ and of $|\Gamma_6\rangle$ with $|\Gamma_4\rangle$ and $|\Gamma_3\rangle$. However, if the occurrence of transitions with $\delta m=\pm 2$ is assumed, the relaxation of $|\Gamma_6\rangle$ according to a Korringa law ($\propto T$) should be observed. Then (if it is assumed within a qualitative analysis that the interaction constants are identical for all the transitions with $\delta m=\pm 2$) the occurrence of relaxation according to a Korringa law does not correspond to the weak dependence of Γ_{12} on the temperature in the range $0<T<20$ K (see the experimental points in Fig. 6). Therefore, the occurrence of transitions with $\delta m=\pm 2$ should also be ruled out.

The next possible change in the spherical projection, $\delta m=\pm 3$, leads to interactions of $|\Gamma_1\rangle$ with $|\Gamma_4\rangle$ and $|\Gamma_3\rangle$ and of $|\Gamma_6\rangle$ with $|\Gamma_{52}\rangle$ and $|\Gamma_{51}\rangle$. These interactions do not lead to a contribution that is proportional to T to the widths of the levels of the initial state (γ_1) and the final state (γ_2) and do not contradict the weak temperature dependence of Γ_{12} at $T<20$ K. The energy splittings Δ_{42} and Δ_{62} corresponding to the interactions of the $|\Gamma_6\rangle$ level are smaller than the corresponding splittings Δ_{41} and Δ_{51} for the $|\Gamma_1\rangle$ level. Therefore, the contribution $\propto \exp(-\Delta/T)$ to the transition width Γ_{12} at $T<100$ K (under the assumption of approximately equal values of g for all $\delta m=\pm 3$) from the natural width $\gamma_2(T)$ of the $|\Gamma_6\rangle$ level can be considered the main contribution.

In the quantitative calculations presented below we took into account only the interaction constants I^{24} and I^{26}. In such an approximation the natural width of the crystal-field ground state is $\gamma_1(T)=0$, and, therefore, $\Gamma_{12}=\gamma_2(T)$. For simplicity, the values of I^{24} and I^{26} were set equal to one another (see Fig. 5). The conduction electron band was approximated by a constant density of states with a width of 2 eV. The best fit for the experimental data in the non-self-consistent approximation is achieved with the value of the dimensionless coupling constants $g^{(0)}=g^{(0)}_{|\Gamma_6\rangle|\Gamma_{52}\rangle}\equiv g^{(0)}_{|\Gamma_6\rangle|\Gamma_{51}\rangle}=0.115$. The self-consistent procedure gives the best results when $g^{(sc)}=g^{(sc)}_{|\Gamma_6\rangle|\Gamma_{52}\rangle}\equiv g^{(sc)}_{|\Gamma_6\rangle|\Gamma_{51}\rangle}=0.111$. It is noteworthy that the self-consistent value of the natural width $\gamma_{\Gamma_6}(T=0)$ obtained in the numerical calculation coincides to within a few percent with the results of the analytical formula (44). Figure 6 presents a comparison of the theoretical temperature dependences of the width of the $1\rightarrow 2$ inelastic neutron transition with experimental data. The theoretical data are presented in different approximations, viz., the self-consistent and non-self-consistent approximations. To illustrate the influence of the self-consistent approximation, the figure shows the temperature dependences of the self-consistent and non-self-consistent widths (the solid and dashed lines, respectively) calculated for the same dimensionless constant $g^{(sc)}=0.111$. It is seen from Fig. 6 that the self-consistent width is greater than the non-self-consistent width for the same value of the interaction constant. The effect of the self-consistent approximation, $\Gamma^{(sc)}_{12}/\Gamma^{(0)}_{12}\gg 1$, is most easily observed when the non-self-consistent width is small. Unfortunately, the instrumental errors of the neutron scattering method make it difficult to reliably isolate the effects of the self-consistent approximation. Therefore, the performance of Raman scattering experiments, whose experimental errors are considerably smaller, can provide important additional information.

A qualitative analysis of the experimental temperature dependence of the relaxation in $LaAl_3$ like the analysis performed above for $CeAl_3$ shows that the main relaxation channel corresponds to a change in the spherical projection $\delta m=\pm 1$. We note that this channel does not lead to Korringa relaxation for the initial state 1 or the final state 2. In this approximation relaxation of the initial state is possible only in the mutual I^{12} processes, and relaxation of the final state is possible both in the mutual I^{12} processes and in the I^{24} and I^{26} interactions with higher-lying levels (see the right-hand part of Fig. 5).

Since the non-self-consistent width is greater at all temperatures, it is difficult to observe the effects of the self-consistent approximation. Therefore, we calculated the transition width only in the non-self-consistent approximation (Fig. 7). It is noteworthy that the results of the fitting with consideration of only I^{12} are in better agreement with the experimental data than are the results of the calculations with consideration of equal values for all the interaction constants $I^{12}=I^{24}/\sqrt{1-a^2}=I^{26}/a$. These results are reminiscent of the qualitative character of the estimates based on the nomenclature of the spherical projections of the angular momentum m. A more rigorous approach would take into account, for example, that the contributions of the $m=0\leftrightarrow m=\pm 1$ and $m=\pm 1\leftrightarrow m=\pm 2$ transitions, which are both associated with a change in the spherical projection $\delta m=\pm 1$, can be significantly different in a lattice of fairly low symmetry.

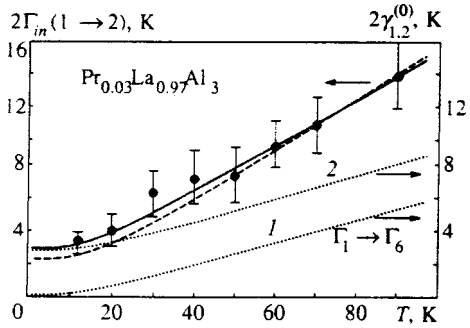

FIG. 7. Temperature dependence of the FWHM ($2\Gamma_{in}$) of the inelastic $|\Gamma_1\rangle \rightarrow |\Gamma_6\rangle$ transition in $LaAl_3$ for the paramagnetic label Pr in the non-self-consistent approximation using the level scheme in Fig. 5. Dashed line—model with $g_{12}=g_{24}/\sqrt{1-a^2}=g_{26}/a=0.094$; solid line—model with $g_{24}=g_{26}=0$, $g_{12}=0.108$. The dotted line *1* (*2*) corresponds to the natural relaxation width $\gamma_{\Gamma_1}(T)$ ($\gamma_{\Gamma_6}(T)$) of the levels.

8. CONCLUSIONS

The proposed self-consistent microscopic theory of the spectroscopy of the crystal-field levels of an impurity ion in a normal metal has several consequences, which can have a significant influence on our understanding of the relaxation processes in highly correlated systems.

Most importantly, the proposed approach, which is based on the Coqblin–Schrieffer–Cooper approach, rather than the formal sf exchange model, permits a first-principles microscopic calculation of the temperature dependence of the relaxation width of crystal-field states. A comparison of such calculations with experimental data, as well as the use of the conventional methods of infrared, Raman, and photoemission spectroscopy, makes it possible to test the faithfulness of the band calculations. Like the traditional methods, the proposed method permits the performance of a quick qualitative visual analysis of the experimental results obtained. An additional significant feature of the proposed spectroscopic method is the possibility of regulating the selection rules by choosing an appropriate paramagnetic label, which is impossible within the traditional methods.

The new soft spectroscopic method considered in this paper permits the investigation of the role of strong electron correlations in shaping the relaxation processes of crystal-field states. Since strong correlations can significantly alter the simple form of the effective Hamiltonian (15), relaxation features, whose characteristic temperatures are not related to the crystal-field splitting energies, can be observed in a highly correlated system. The observation of such features provides weighty evidence in support of the important role of strong correlations in the compound being studied. Moreover, the calculations performed in the self-consistent approach indicate that in the case of strong relaxation broadening the upper crystal-field levels have a significant influence on the experimentally measured characteristics, which, as was previously assumed, are determined only by the properties of the ground state of a highly correlated system. An example of the properties of the ground magnetic state of ions in highly correlated systems, which can be subject to a significant influence from crystal-field excited states, is the residual width of the magnetic quasielastic neutron scattering peak at zero temperature $\Gamma_G(T=0)$. In the case of soft crystal-field splittings, employment of the widely accepted phenomenological formula $T^*=\Gamma_G(T=0)/2$ to determine the characteristic temperature T^* of the Kondo system is in need of additional analysis.

In conclusion, we wish to note that the proposed approach should be useful in the case of the analysis of systems in which the crystal-field states transform into more complicated objects as a result of strong electron correlations. Such systems include concentrated Kondo systems, in which the rare-earth ions form a coherent lattice. In this case the localized crystal-field ground-state levels transform into a coherent continuum,[41] which has been termed a spin fluid. When there are sufficiently soft crystal-field splittings, a spin fluid undergoes strong interactions with localized excited states,[42] which should produce features in the relaxation of the magnetic states. Since crystal-field states are nothing more than well defined levels, this relaxation cannot be studied in a neutron scattering experiment within the proposed method. However, the relaxation in the magnetic subsystem should have a significant influence on the spectroscopic characteristics of the system that can be detected using resonance methods, such as muon spin rotation (μSR) and nuclear magnetic resonance. These processes can be studied experimentally and calculated theoretically after the proposed formalism is appropriately generalized.

We sincerely thank P. A. Alekseev, V. N. Lazukov, and S. V. Maleev for some critical discussions. This work was supported by the Russian Fund for Fundamental Research (Project 95-02-04250a), the International Association INTAS (Project 93-2834), and the Netherlands Organization for Scientific Research NWO (Nederlandse Organisatie voor Wetenschappelijk Onderzoek) (Project 07-30-002).

*)E-mail: andry@kurm.polyn.kiae.su

1)Below we shall consider a case which corresponds to the conditions of the proposed experimental method. In this situation the concentration of the paramagnetic label is chosen small enough that the interactions between the impurities can be neglected in each specific case.[29] For this reason, the influence of the impurity on the state of the conduction electrons can be neglected.[30]

2)All the expressions presented above were obtained without consideration of the vertex corrections (Fig. 1d),[37] which, however, are insignificant in the case of sufficiently small dimensionless interaction constants $g^2_{MM'} \ll 1$.

3)Consideration of the vertex corrections in the perturbative approach, unlike (44), leads to correction of the coefficient in front of the exponentially small natural width (41).

[1] J. P. Rice, B. G. Pazol, D. M. Ginsberg, T. J. Moran, and M. B. Weissman, J. Low Temp. Phys. **72**, 345 (1988).
[2] I. M. Lifshits and A. M. Kosevich, Zh. Eksp. Teor. Fiz. **29**, 739 (1955) [Sov. Phys. JETP **2**, 636 (1956)].
[3] E. N. Adams and T. D. Holstein, J. Phys. Chem. Solids **10**, 253 (1959).
[4] B. S. Chandrasekhar, Phys. Lett. **6**, 27 (1963).
[5] P. Thalmeier and B. Lüthi, in *Handbook on the Physics and Chemistry of Rare Earths*, K. A. Gschneider, Jr. and L. Eyring (eds.), Elsevier, Amsterdam (1991), Vol. 14, p. 225.
[6] V. L. Ginzburg and G. P. Motulevich, Usp. Fiz. Nauk **55**, 469 (1955).
[7] M. M. Sushchinsky, *Raman Spectra of Molecules and Crystals*, Israel Program for Scientific Translations, Jerusalem (1973).
[8] P. A. Aleksandrov and S. M. Yakubenya, in *Proceedings of the International Conference on the Science and Technology of Defect Control in*

Semiconductors, Yokohama, 1989, K. Sumino (ed.) (1990), Vol. **2, p.** 1605.
[9] P. A. Alekseev, I. P. Sadikov, Yu. L. Shitikov, E. M. Savitskii, O. D. Chistyakov, and J. K. Kjems, Phys. Status Solidi B **114**, 161 (1982).
[10] P. A. Alekseev, I. P. Sadikov, V. P. Kolyadin, A. V. Mirmel'shteĭn, and N. B. Kol'chugina, JETP Lett. **39**, 580 (1984).
[11] P. A. Alekseev, W. Bührer, V. N. Lazukov, E. V. Nefedova, I. P. Sadikov, O. D. Chistyakov, and M. Zolliker, Physica B **217**, 241 (1996).
[12] P. A. Alekseev, V. N. Lazukov, I. P. Sadikov, and A. Yu. Rumyantsev, JETP Lett. **43**, 758 (1986).
[13] P. A. Alekseev, V. N. Lazukov, I. P. Sadikov, and A. Yu. Rumyantsev, J. Magn. Magn. Mater. **75**, 323 (1988).
[14] P. A. Alekseev, E. S. Klement'ev, V. N. Lazukov, E. V. Nefedova, I. P. Sadikov, N. D. Efremova, L. D. Finkel'shteĭn, and N. B. Kol'chugina, Fiz. Met. Metalloved. **77**, 60 (1994).
[15] P. A. Alekseev, E. S. Klement'ev, V. N. Lazukov, I. P. Sadikov, M. N. Khlopkin, M. Adams, A. Yu. Muzychka, I. L. Sashin, N. B. Kol'chugina, and O. D. Chistyakov, JETP Lett. **63**, 1000 (1996).
[16] E. S. Clementyev, P. A. Alekseev, M. N. Khlopkin, V. N. Lazukov, I. P. Sadikov, W. Bührer, and A. Yu. Muzychka, Physica B **234–236**, 864 (1997).
[17] K. W. Becker, P. Fulde, and J. Keller, Z. Phys. B **28**, 9 (1977).
[18] K. Sugawara, Phys. Status Solidi B **92**, 317 (1979).
[19] S. V. Maleyev, Phys. Rev. B **50**, 302 (1994).
[20] L. C. Lopes and B. Coqblin, Phys. Rev. B **33**, 1804 (1986).
[21] L. C. Lopes and B. Coqblin, Phys. Rev. B **38**, 6807 (1988).
[22] J. M. Wills and B. R. Cooper, Phys. Rev. B **36**, 3809 (1987).
[23] N. Kiossus, J. M. Wills, and B. R. Cooper, J. Appl. Phys. **63**, 3683 (1988).
[24] N. Kiossus, J. M. Wills, and B. R. Cooper, Phys. Rev. B **44**, 10 003 (1991).
[25] Q. G. Sheng and B. R. Cooper, Phys. Rev. B **50**, 965 (1994).
[26] J. R. Schrieffer and P. A. Wolff, Phys. Rev. **149**, 491 (1966).
[27] B. Coqblin and J. R. Schrieffer, Phys. Rev. **185**, 847 (1969).
[28] B. Cornut and B. Coqblin, Phys. Rev. B **5**, 4541 (1972).
[29] A. A. Abrikosov, *Fundamentals of the Theory of Metals*, Elsevier, New York (1988).
[30] A. A. Abrikosov, L. P. Gor'kov, and I. E. Dzyaloshinskii, *Quantum Field Theoretical Methods in Statistical Physics*, Dover, New York (1963).
[31] B. R. Cooper, R. Siemann, D. Yang *et al.*, in *The Handbook on the Physics and Chemistry of the Actinides*, A. J. Freeman and G. H. Lander (eds.), North-Holland, Amsterdam (1985), Vol. 2 p. 435.
[32] A. S. Mishenko, JETP Lett. **66**, 487 (1997).
[33] A. A. Abrikosov, Physica (Amsterdam) **2**, 21 (1965).
[34] A. A. Abrikosov and A. A. Migdal, J. Low Temp. Phys. **3**, 519 (1970).
[35] G. M. Éliashberg, Zh. Éksp. Teor. Fiz. **41**, 1241 (1961) [Sov. Phys. JETP **14**, 886 (1962)].
[36] G. M. Éliashberg, Zh. Éksp. Teor. Fiz. **42**, 1658 (1962) [Sov. Phys. JETP **15**, 1151 (1962)].
[37] S. V. Maleev, Teor. Mat. Fiz. **4**, 86 (1970).
[38] S. V. Maleev, Zh. Éksp. Teor. Fiz. **79**, 1995 (1980) [Sov. Phys. JETP **52**, 1008 (1980)]; Zh. Éksp. Teor. Fiz. **84**, 260 (1983) [Sov. Phys. JETP **57**, 149 (1983)].
[39] N. Grewe and F. Steglich, in *Handbook on the Physics and Chemistry of Rare Earths*, K. A. Gschneider, Jr. and L. Eyring (eds.), Elsevier, Amsterdam (1991), Vol. 14, p. 343.
[40] P. Fulde and M. Loewenhaupt, Adv. Phys. **34**, 589 (1985).
[41] K. A. Kikoin, M. N. Kiselev, and A. S. Mishchenko, Zh. Éksp. Teor. Fiz. **112**, 729 (1997) [JETP **85**, 399 (1997)].
[42] Yu. Kagan, K. A. Kikoin, and A. S. Mishchenko, Phys. Rev. B **55**, 12 348 (1997).

Translated by P. Shelnitz

ELSEVIER

Physica B 259–261 (1999) 195–197

PHYSICA B

Effective action for the Kondo lattice model. New approach for $S = 1/2$

F. Bouis[a,*], M.N. Kiselev[a,b]

[a]*Laboratoire Léon Brillouin, CE-Saclay 91191, Gif-sur-Yvette, France*
[b]*Russian Research Center "Kurchatov Institute", 123 182 Moscow, Russia*

Abstract

In the partition function of the Kondo lattice (KL), spin matrices are exactly replaced by bilinear combinations of Fermi operators with the purely imaginary chemical potential $\lambda = -i\pi T/2$ (Popov representation). This new representation of spin operators allows one to introduce new Green's Functions (GF) with Matsubara frequencies $\omega_n = 2\pi T(n + \frac{1}{4})$ for $S = \frac{1}{2}$. A simple temperature diagram technique is constructed with the path integral method. This technique is standard and does not contain the complicated combinatoric rules characteristic of most of the known variants of the diagram techniques for spin systems. The effective action for the almost antiferromagnetic KL problem is derived. © 1999 Elsevier Science B.V. All rights reserved.

Keywords: Heavy fermions; Kondo lattice; Antiferromagnetism

Many systems in statistical physics are described by Hamiltonians containing spin matrices. Unfortunately, the diagrammatic perturbation theory for spin systems is complicated. Many variants are based on different representations of the spin matrices by Bose or Fermi operators. However, unphysical states always arise leading to constraints and complication of the Feynman codex. In this paper, we construct a simple diagrammatic technique (DT) for spin-$\frac{1}{2}$ that differs from the known techniques in the form of the GF, but which is standard in other respects, does not contain the complicated combinatoric rules characteristic of spin systems and permits one to take into account the constraints rigorously.

It is indeed possible to replace exactly spin-$\frac{1}{2}$ matrices by bilinear combinations of Fermi operators:

$$\sigma^z_{fi} \to S^z_{fi} = \tfrac{1}{2}(a^+_{i\uparrow}a_{i\uparrow} - a^+_{i\downarrow}a_{i\downarrow}),\ \sigma^+_{fi} \to S^+_{fi} = a^+_{i\uparrow}a_{i\downarrow},$$
$$\sigma^-_{fi} \to S^-_{fi} = a^+_{i\downarrow}a_{i\uparrow}, \tag{1}$$

by the basic formula shown in Ref. [1]

$$Z = \mathrm{Sp}\ \mathrm{e}^{-\beta H} = i^N \mathrm{Sp}\ \mathrm{e}^{-\beta(H_f + (i\pi/2\beta)N)}, \tag{2}$$

where H_f is obtained from H by replacement (1), and $N = \sum_{i\sigma} a^+_{i\sigma}a_{i\sigma}$. There is no constraint but the purely imaginary chemical potential of pseudofermions $\lambda = -i\pi T/2$ leads to the mutual cancellation of the unphysical states.

We analyze here the KL model which is a periodic lattice of magnetic atoms modeled by f-orbitals in a metallic background

$$\mathscr{H}_{KL} = -\sum_{ij,\sigma}(t_{ij} + \mu)\Psi^+_{i\sigma}\Psi_{j\sigma} + J_{sf}\sum_i \Psi^+_{i\sigma}\sigma\Psi_{i\sigma'}\boldsymbol{S}_{fi} + g\sum_i (H + h\mathrm{e}^{i\boldsymbol{R}_i\boldsymbol{Q}})S^z_{fi}. \tag{3}$$

We add a uniform (H) and a staggered (h) magnetic field ($g = \mu_B g_L$, where μ_B is the Bohr magneton and g_L is the Landé factor). We consider a simple cubic lattice with the notation $\boldsymbol{Q} = \boldsymbol{Q}_{AF} = (\pi,\pi,\pi)$. Using Popov representation of spins, the ratio of the partition function of the interacting system to the partition function of the corresponding free system can be represented in the form of functional

*Corresponding author. Tel.: 331-69-08-96-85; fax: 331-69-08-82-61; e-mail: bouis@llb.saclay.cea.fr.

0921-4526/99/$ – see front matter
PII: S0921-4526(98)01171-5

integrals as follows:

$$Z/Z_0 = \frac{\int Dv \exp[S - \frac{i\pi}{2\beta}\int_0^\beta d\tau \sum_i \bar{a}_{i,\alpha}(\tau)a_{i,\alpha}(\tau)]}{\int Dv \exp[S_0 - \frac{i\pi}{2\beta}\int_0^\beta d\tau \sum_i \bar{a}_{i,\alpha}(\tau)a_{i,\alpha}(\tau)]}, \quad (4)$$

where the Euclidean action for the KL model is

$$S = \int_0^\beta d\tau \left\{ \sum_i [\bar{\Psi}_{i,\sigma}\partial_\tau \Psi_{i,\sigma} + \bar{a}_{i,\alpha}\partial_\tau a_{i,\alpha}] - \mathscr{H}_{KL}(\tau) \right\}. \quad (5)$$

We note by Dv the integration over the anticommuting Grassmann variables Ψ_σ, a_α. By making the replacement $a_{i,\alpha}(\tau) \to a_i^\alpha(\tau)\exp((i\pi/2\beta)\tau)$, etc., which cancels the last term in both exponents in numerator and denominator of Eq. (4), we come to the following boundary conditions for Grassmann fields: $\Psi_\sigma(\beta) = -\Psi_\sigma(0), \bar{\Psi}_\sigma(\beta) = -\bar{\Psi}_\sigma(0)$, $\bar{a}^\alpha(\beta) = -i\bar{a}^\alpha(0), a^\alpha(\beta) = ia^\alpha(0)$. Going over to the momentum representation for all Grassmann variables and assuming $s_{sk} = \sum_p \bar{\Psi}_{p+k}\sigma\Psi_p$ we obtain

$$S = \sum_k \bar{\Psi}_{k,\sigma} G_0^{-1} \Psi_{k,\sigma} + \sum_p \bar{a}_p^\alpha \mathscr{G}_0^{-1} a_p^\alpha + J_{sf}\sum_k s_{sk} S_{f-k} + \tfrac{1}{2}hg\sum_k \bar{a}_k^\alpha \sigma^z a_{k+Q}^{\alpha'}, \quad (6)$$

where the inverse GF of Ψ-fields is $G_0^{-1} = i2\pi T(n + 1/2) - \varepsilon_k + \mu$ with dispersion $\varepsilon_k = -\sum_\delta t_{i,i+\delta} e^{i\delta k}$ and the inverse GF of a^α Grassmann fields is $\mathscr{G}_{0\alpha}^{-1} = i2\pi T(m + \tfrac{1}{4}) - \tfrac{1}{2}gH\sigma_{\alpha\alpha}^z$ with unusual Matsubara frequencies. Note that Popov representation can be used for spins $S = 1$ also. In this case the frequencies are shifted to $\omega_m = 2\pi T(m + 1/3)$. Moreover the method has been extended to arbitrary spin in Ref. [8].

We now confine ourselves to the limiting case $T_N \sim T_K \sim T_0$ [2] assuming the same energy scale for antiferromagnetic (AF) and Kondo correlations. It allows us to integrate over the fast Ψ fields with energies $\varepsilon \sim \mu \gg T_0$ using the bare electrons GF. We can also integrate over the fast fields a^α ($\omega \gg T_0$) taking into account one-site Kondo renormalization of vertices ($J_{sf} \to \mathscr{J}_{sf}$) and self-energy parts ($G_0 \to G$) [3]. As a result, a simple DT is constructed. Contrary to other DT (see, e.g. Refs. [4,5]) the constraint on the spin subsystem is taken into account exactly. The new action which is written in terms of slow Ψ and a^α variables contains an additional AF Heisenberg interaction between spins due to the indirect RKKY exchange [3,4]:

$$S_{eff} = \sum_k \bar{\Psi}_{k,\sigma}^{slow} G^{-1} \Psi_{k,\sigma}^{slow} + \sum_k \mathscr{J}_{sf} s_{sk}^{slow} S_{f-k} + S_H. \quad (7)$$

The last term in (7) can be analyzed separately and represented by auxiliary three-component Bose fields $\phi^\gamma(k)$ [1]

$$S_H = \sum_{k_1 k_2 \sigma} \bar{a}_{k_1}^\alpha [\mathscr{G}_0^{-1}\delta_{k_1,k_2} + \sigma^z h\delta_{k_1+Q,k_2}] a_{k_2}^\alpha - \sum_k [\tfrac{1}{2}\phi_k^3 S_{-k}^z + \eta_k^* S_k^- + \eta_k S_k^+] + S_0[\phi] \quad (8)$$

with the following notation: $S_0 = -\frac{1}{4}\sum_k (I_k^{RKKY})^{-1}\phi_k^\gamma \phi_{-k}^\gamma$, $\eta_k^* = (\eta_k)^*$ and $\eta_k = (\phi_k^1 - i\phi_k^2)/2$. In the case $T_K \ll T_N$ only magnetic terms in the effective action are important. We note by W the matrix of the quadratic form in a^α variables. Integrating over all a^α fields one can find the nonpolynomial action of the AF Heisenberg model in terms of Bose fields [6]:

$$S_H = S_0[\phi^3, \eta] + \log\det W[\phi^3, \eta]. \quad (9)$$

In the case considered, namely $T_N \sim T_K \sim T_0$ the procedure of derivation of the effective action is a little bit complicated. Taking into account the second term in Eq. (7) one has to replace $\phi^\gamma \to \phi^\gamma - 2\mathscr{J}_{sf} s_{s,k}^{\gamma slow}$ in Eq. (9). As a result, the effective action can be rewritten as follows:

$$S_{eff} = \sum_k \bar{\Psi}_{k,\sigma}^{slow} G^{-1} \Psi_{k,\sigma}^{slow} + S_0[\phi^3, \eta] + \log\det W[\phi_k^\gamma - 2\mathscr{J}_{sf} s_{sk}^{\gamma slow}]. \quad (10)$$

Eqs. (7)–(10) are the key result of the present work. This effective action describes the low-energy properties of the KL model. The last term in Eq. (9) takes into account the mutual influence of conduction electrons and spins. Magnetic instabilities of both kind of electrons could then be easily analyzed.

Let us concentrate on the former problem (8). The spin subsystem undergoes a phase transition with $T_c = T_0$ corresponding to the appearance of a nonzero staggered magnetization ρ as $h \to 0$. This problem is related to the Bose-condensation of the field $\phi_k^3 = \tilde{\phi}_k^3 + \rho(\beta N)^{1/2}\delta_{k,Q}\delta_\omega$ and in one-loop approximation results in the usual mean-field equation for AF order parameter [6] in the presence of Kondo-scattering processes [3]. Note that a magnetic transition in the localized system may induce a magnetic transition in the itinerant system.

Taking into account the compensation equation [3,6] and calculating the $\log\det W[\phi^3, \eta]$ approximately by the method of stationary phase the following expression for the spin subsystem effective action can be obtained:

$$S_H^{eff} = \sum_k \eta_k^* \chi_t^{-1} \eta_k + \sum_k \phi_k^{3*} \chi_\ell^{-1} \phi_{-k}^3 - 1/4 \sum_k (I_k^{RKKY})^{-1} \phi_k^\gamma \phi_{-k}^\gamma, \quad (11)$$

where χ_t and χ_ℓ are transverse and longitudinal susceptibilities, respectively. As usual, the transverse susceptibility describes the AF magnons excitations. At the temperature range $T > T_0$ when the condensate solution is absent the effective action has the same form except that the transverse and longitudinal susceptibilities describe the paramagnon excitations which can result in some untrivial effects in heavy-fermion compounds [7]. These excitations introduce a new energy scale corresponding to the critical behavior.

Summarizing, we constructed a simple diagrammatic technique which allows one to analyze the effective action of the KL model when the energy scales for AF and Kondo correlations are the same. This effective action describes the slow electron subsystem interacting with the spin fluctuations of either magnon or paramagnon type.

The support of the grant RFBR 98-02-16730 (MNK) is acknowledged.

References

[1] V.N. Popov, S.A. Fedotov, Sov. Phys. JETP 67 (1988) 535.
[2] S. Doniach, Phys. B 91 (1977) 231.
[3] K.A. Kikoin et al., Sov. Phys. JETP 85 (1997) 399.
[4] A.A. Abrikosov, Phys. 2 (1965) 21.
[5] D.M. Newns, N. Read, Adv. Phys. 36 (1987) 799.
[6] F. Bouis, M.N. Kiselev, to be published.
[7] A. Rosch et al., Phys. Rev. Lett. 79 (1997) 159.
[8] O. Veits, R. Oppermann, M. Binderberger, J. Stein, J. Phys. I France 4 (1994) 493.

Ginzburg-Landau functional for nearly antiferromagnetic perfect and disordered Kondo lattices

M. Kiselev,[1] K. Kikoin,[2] and R. Oppermann[1]
[1]*Institut für Theoretische Physik, Universität Würzburg, D-97074, Germany*
[2]*Ben-Gurion University of the Negev, Beer-Sheva 84105, Israel*
(Received 17 June 2001; revised manuscript received 28 November 2001; published 16 April 2002)

Interplay between Kondo effect and antiferromagnetic and spin glass ordering in perfect and disordered bipartite Kondo lattices is considered. The Ginzburg-Landau equation is derived from the microscopic effective action written in three mode representation (Kondo screening, antiferromagnetic correlations, and spin liquid correlations). The problem of the local constraint is resolved by means of the Popov-Fedotov representation of the localized spin operators. It is shown that the Kondo screening enhances the tendency to a spin-liquid crossover and partially suppresses antiferromagnetic ordering in perfect Kondo lattices and spin glass ordering in doped Kondo lattices. The modified Doniach diagram is constructed, and possibilities of going beyond the mean-field approximation are discussed.

DOI: 10.1103/PhysRevB.65.184410 PACS number(s): 75.20.Hr, 71.27.+a, 75.10.Nr, 75.30.Mb

I. INTRODUCTION

The Kondo lattice (KL) systems are famous for their unusual electronic and magnetic properties, including giant effective masses observed in thermodynamic and de Haas–van Alphen measurements,[1] unconventional superconductivity,[2] and a fascinating variety of magnetic properties.[3] The great majority of the metallic KL systems demonstrates antiferromagnetic (AFM) correlations and all types of the AFM order may be found in these compounds. There are localized spins in U_2Zn_{17}, UCd_{11}, $CeIn_3$,[3] quadrupole ordering in CeB_6,[4] interplay between localized and itinerant excitations in several U-and Ce-based compounds,[5] puzzling magnetic order of tiny moments in UPt_3, URu_2Si_2, UNi_2Al_3,[6] quantum phase transition in $CeCu_{6-x}Au_x$,[7] fluctuation-type dynamical ordering in $U(Pt_{1-x}Pd_x)_3$,[8] short-range magnetic correlations in the astonishingly wide temperature interval of critical behavior in $CeCu_6$ and $CeRu_2Si_2$.[9] This list is by no means exhaustive. The superconducting state in most cases coexists with antiferromagnetism, and, apparently, Cooper pairing itself is mediated by magnetic fluctuations.[2,10] The dominant contribution to the low-temperature thermodynamics is also given by spin degrees of freedom.[11,12]

On the other hand, all low-temperature characteristics of KL's are determined by a Kondo temperature T_K. These characteristics are Fermi-like, but the energy scale of the ''fermion'' spectrum is renormalized by a factor T_K/ε_F relative to a conventional electron Fermi liquid.[3] Apparently, the AFM correlations due to Ruderman-Kittel-Kasuya-Yosida (RKKY) interaction I partially suppressed by intrasite Kondo effect should be treated as a background for all unusual properties of Kondo lattices. The main theoretical challenge is to find a scenario of crossover from a high-temperature regime of weak interaction (scattering) between localized spins and conduction-electron Fermi liquid to a low-temperature strong-coupling regime where the spins lose their localized nature and are confined into an unconventional quantum liquid involving spin degrees of freedom of conduction electrons.

In the phase diagram of the disordered KL more exotic possibilities such as non-Fermi-liquid regimes arise, which were observed, for example, near the $T=0$ quantum critical point in $Y_{1-x}U_xPd_3$ (see, e.g., Ref. 13). In this family of ternary alloys the spin-glass (SG) behavior was discovered in a U concentration range $0.3<x<0.5$ with a freezing temperature T_f growing monotonically with x (see Ref. 14). Among other U-based heavy fermion compounds with SG behavior, URh_2Ge_2,[15] $U_2Rh_3Si_5$,[16] and U_2PdSi_3 (Ref. 17) should be mentioned. The effects of ''Kondo disorder'' were reported for $UCu_{5-x}Pd_x$ in Ref. 18. Later on the competition between RKKY and Kondo exchange for disordered Ce alloys was discovered experimentally (see Refs. 19–21). The magnetic phase diagram of $CeNi_{1-x}Cu_x$ exhibits change of magnetic ordering from AFM to ferromagnetic (FM) at $x=0.8$, whereas for $0.2<x<0.8$ the SG state appears only at high temperatures above the FM order. Apparently, the Kondo interaction could be considered as the mechanism leading to the reduction of magnetic moments because increasing Ni contents effectively reduces the strength of the indirect exchange interaction, and then, a larger temperature stability range of the SG phase appears (see Refs. 19 and 20).

The competition between the one-site Kondo-type correlations and the indirect intersite exchange is visualized in Doniach's diagram where possible phase transition and crossover energies are plotted as functions of a ''bare'' coupling parameter $\alpha=J/\varepsilon_F$ characterizing the exchange interaction between the spin and electron subsystems in KL's.[22] Only Kondo screening and RKKY coupling were competing in the original Doniach diagram. Later on it was noticed that the trend to spin liquid (SL) ordering is the third type of correlation which modifies essentially the magnetic phase diagram of KL's in a critical region $T_K \sim I$ of the Doniach diagram.[23–25]

In this paper we present a high-temperature mean-field description of transitions from a paramagnetic state to correlated spin states in KL's, which does not violate the local constraint for the spin-fermion operators. We use the Popov-Fedotov representation of spin operators[26] to construct the effective action for KL's. In this representation the local constraint is rigorously fulfilled. We consider the mutual influence of various order parameters (Kondo, AFM, SL, and SG correlation functions) and derive a Ginzburg-Landau functional (Sec. II). On the basis of this functional we construct generalized Doniach's diagrams that take into account all the

interplays. The Doniach diagram for a perfect KL is presented in Sec. III and the influence of Kondo screening on the SG diagram for a disordered KL is considered in Sec. IV.

All existing theories appeal to mean-field approximations that violate the local gauge invariance both in the Kondo and SL channels.[27] As a result, fictitious second-order phase transitions from a free spin (paramagnetic) state to a confined spin (Kondo singlet or resonating valence bond SL) state arise in spite of the fact that neither symmetry is violated by these transformations. A different approach allows us to get rid of the assumption of a Kondo-type ''condensate'' within the framework of a mean-field theory. To eliminate the fictitious phase transition to a SL state one should refrain from a mean-field approach to the SL mode. We offer a scenario of a continuous crossover from a paramagnetic state of localized spins to the SL state, where the interplay between critical AFM fluctuations and Kondo screening clouds in KL's results in ''Fermionization'' of spin excitations at low temperatures (Sec. V). In Sec. VI the interrelations between the theory and real heavy fermion systems is briefly discussed.

II. DERIVATION OF EFFECTIVE ACTION

The Hamiltonian of the KL model is given by

$$H=\sum_{k\sigma}\ \varepsilon_k c^{\dagger}_{k\sigma}c_{k\sigma}+J\sum_{j}\ \left(\mathbf{S}_j\mathbf{s}_j+\frac{1}{4}N_j n_j\right). \tag{1}$$

Here the local electron and spin-density operators for conduction electrons at site j are defined as

$$n_j=\sum_{j\sigma}\ c^{\dagger}_{j\sigma}c_{j\sigma},\qquad \mathbf{s}_j=\sum_{\sigma}\ \frac{1}{2}c^{\dagger}_{j\sigma}\hat{\tau}_{\sigma\sigma'}c_{j\sigma'}, \tag{2}$$

where $\hat{\tau}$ are the Pauli matrices and $c_{j\sigma}=\Sigma_k c_{k\sigma}\exp(ikj)$. The SG freezing is possible if an additional quenched randomness of the intersite exchange I_{jl} between the localized spins arises. This disorder is described by

$$H'=\sum_{jl}\ I_{jl}(\mathbf{S}_j\mathbf{S}_l). \tag{3}$$

We start with a perfect Kondo lattice. The spin correlations in KL's are characterized by two energy scales, i.e., $I\sim\ J^2/\varepsilon_F$, and $\Delta_K\sim\varepsilon_F\exp(-\varepsilon_F/J)$ (the intersite indirect exchange of the Ruderman-Kittel-Kasuya-Yosida (RKKY) type and the Kondo binding energy, respectively). At high enough temperatures the localized spins are weakly coupled with the electron Fermi sea having the Fermi energy ε_F, so that the magnetic response of a rare-earth sublattice of a KL is of paramagnetic Curie-Weiss type. With decreasing temperature either a crossover to a strong-coupling Kondo singlet regime occurs at $T\sim\Delta_K$ or the phase transition to an AFM state occurs at $T=T_N\sim zI$ where z is a coordination number in the KL. If $T_N\approx\Delta_K$ the interference between two trends results in the decrease of both characteristic temperatures or in suppressing one of them. As was noticed in Refs. 24 and 28, in this case the SL correlations with characteristic energies $\Delta_s\sim I$ may overcome the AFM correlations, and the spin subsystem of the KL can condense in a SL state yet in a region of weak Kondo coupling.

To describe all three modes in a unified way one should derive a free-energy functional $\mathcal{F}(T)$ in a region of $T>(T_N,\Delta_K,\Delta_s)$. First, we integrate out the highest energies $\sim\varepsilon_F$. Here and below we use the dimensionless coupling constants $J\to J/\varepsilon_F$, $I\to I/\varepsilon_F$, etc. Since we are still in a weak-coupling limit of Kondo-type scattering, we may restrict ourselves to the standard high-temperature renormalization of the one site coupling $J\to\tilde{J}(T)=1/\ln(T/\Delta_K)$ and the second-order equation of perturbation theory in J for RKKY interaction. As a result, one arrives at an effective Hamiltonian

$$\tilde{H}=\sum_{k\sigma}\ \varepsilon_k c^{\dagger}_{k\sigma}c_{k\sigma}+\tilde{J}\sum_{j}\ \mathbf{s}_j\mathbf{S}_i-I\sum_{jl}\ \mathbf{S}_j\mathbf{S}_l$$

$$+gh\sum_{i}\ (-1)^j S^z_j. \tag{4}$$

Here all energies are measured in $\varepsilon_F=1$ units, and an infinitesimal staggered magnetic field is introduced that respects the symmetry of the magnetic bipartite lattice in the AFM case (ε_F is restored in further calculations wherever it is necessary).

To calculate the spin part of the free energy $\mathcal{F}_s(T)=-T\ln\mathcal{Z}_s$ we represent the partition function $\mathcal{Z}$ in terms of a path integral. The spin subsystem is described by means of the Popov-Fedotov trick[26]

$$\mathcal{Z}_s=\mathrm{Tr}\ e^{-\beta H}=i^N\mathrm{Tr}\ e^{-\beta[H+i\pi N^f/(2\beta)]}. \tag{5}$$

Here $\beta=T^{-1}$, N is the number of unit cells, $N^f=\Sigma_j N^f_j$, and the spin $S=1/2$ operators are represented by bilinear combinations of fermion operators

$$S^z_j=(f^{\dagger}_{j\uparrow}f_{j\uparrow}-f^{\dagger}_{j\downarrow}f_{j\downarrow})/2,\ S^+_j=f^{\dagger}_{j\uparrow}f_{j\downarrow},\ S^-_j=f^{\dagger}_{j\downarrow}f_{j\uparrow}. \tag{6}$$

These operators obey the constraint

$$N^f_j=\sum_{\sigma}\ f^{\dagger}_{j\sigma}f_{j\sigma}=1. \tag{7}$$

In accordance with Ref. 26, the Lagrange term with a fixed imaginary chemical potential $-i\pi T/2$ is added to the Hamiltonian (1). We use the path-integral representation for the partition function,

$$\frac{\mathcal{Z}}{\mathcal{Z}^0}=\frac{\int D\bar{c}Dc D\bar{f}Df\exp\mathcal{A}}{\int D\bar{c}Dc D\bar{f}Df\exp\mathcal{A}_0}. \tag{8}$$

Then the Euclidean action for the KL is given by

$$\mathcal{A}=\mathcal{A}_0-\int_0^{\beta}d\tau\mathcal{H}_{int}(\tau),$$

$$\mathcal{A}_0=\mathcal{A}_0[c,f]=\int_0^{\beta}d\tau\sum_{j\sigma}\ \{\bar{c}_{j\sigma}(\tau)[\partial_\tau-\varepsilon(-i\nabla)+\mu]c_{j\sigma}(\tau)$$

$$+\bar{f}_{j\sigma}(\tau)(\partial_\tau-i\pi T/2)f_{j\sigma}(\tau)\}. \tag{9}$$

Following the Popov-Fedotov procedure, the imaginary chemical potential is included in discrete Matsubara frequencies for semifermion operators $f_{j\sigma}$. As a result the Matsubara frequencies are determined as $\omega_m = 2\pi T(m+1/4)$ for spin semifermions and $\epsilon_n = 2\pi T(n+1/2)$ for conduction electrons. In terms of the temperature Green's function the Euclidian action has the form

$$\begin{aligned}\mathcal{A} = \mathcal{A}_0 + \mathcal{A}_{int} &= \sum_{k\sigma} \overline{c}_{k\sigma} G_0^{-1}(k) c_{k\sigma} \\ &+ \sum_{j\sigma} \overline{f}_{j\sigma}(\omega_n) D_{0\sigma}^{-1}(\omega_n) f_{j\sigma}(\omega_n) \\ &+ \frac{\tilde{J}}{2} \sum_{j\sigma\sigma'} \sum_{\varepsilon_m,\omega_n} \overline{c}_{j\sigma}(\varepsilon_1) f_{j\sigma}(\omega_2) \overline{f}_{j,\sigma'}(\omega_1) c_{j,\sigma'}(\varepsilon_2) \\ &\times \delta_{\varepsilon_1-\varepsilon_2,\omega_1-\omega_2} + I \sum_{jl,\sigma\gamma} \sum_{\omega_n} \overline{f}_{j\sigma}(\omega_1) \\ &\times \hat{\tau}_{\sigma\sigma'} f_{j,\sigma'}(\omega_2) \overline{f}_{l,\gamma}(\omega_3) \hat{\tau}_{\gamma\gamma'} f_{l\gamma'}(\omega_4) \delta_{\omega_1-\omega_2,\omega_3-\omega_4}.\end{aligned} \tag{10}$$

Here the Green's functions (GF's) for bare quasiparticles are

$$G_0(k, i\epsilon_n) = \frac{1}{i\epsilon_n - \varepsilon_k + \mu}, D_{0\sigma}^{\nu}(i\omega_m) = \frac{1}{i\omega_m - \sigma g h^{\nu}/2} \tag{11}$$

(ν is the index of magnetic sublattice that defines the direction of the staggered magnetic field).

The first interaction term in this equation is responsible for *low-energy* Kondo correlations, and we will treat it in conventional manner.[29] In the RKKY term two modes should be considered, namely the local mode of AFM fluctuations[30,31] and the nonlocal spin liquid correlations.[31,32] For these modes we adopt the Néel-type antiferromagnetism and the resonating valence bond (RVB) type spin liquid state, respectively. In accordance with the general path-integral approach to KL's, we first integrate over fast (electron) degrees of freedom. Then in the sf-exchange contribution to the action (10) we are left with the auxiliary field ϕ with a statistics complementary to that of semifermions.[33] The spin correlations in the intersite RKKY term are treated in terms of vector Bose fields $\mathbf{Y}$ (AFM mode) and a scalar field W (spin liquid RVB mode). As a result, $\mathcal{A}_{int}$ is represented by the following expression:

$$\begin{aligned}\mathcal{A}_{int} = -\frac{2}{\tilde{J}} \mathrm{Tr} |\phi|^2 - \mathrm{Tr} \frac{1}{I_{\mathbf{q}}} \mathbf{Y}_{\mathbf{q}} \mathbf{Y}_{-\mathbf{q}} - \mathrm{Tr} \frac{1}{I_{\mathbf{q}_1-\mathbf{q}_2}} W_{\mathbf{P}\mathbf{q}_1} W_{\mathbf{P}\mathbf{q}_2} \\ - \mathrm{Tr} \overline{f}_{j\sigma} \phi_j G_0(\mathbf{r}) \overline{\phi}_l f_{l\sigma}.\end{aligned} \tag{12}$$

When making a Fourier transformation for nonlocal spin liquid correlations (the third term on the right hand side) we introduced the coordinates $\mathbf{R} = (\mathbf{R}_j + \mathbf{R}_l)/2$ and $\mathbf{r} = \mathbf{R}_j - \mathbf{R}_l$ for the RVB field, and $\mathbf{P}, \mathbf{q}$ are the corresponding momenta. Below we assume $\mathbf{P} = 0$ and omit it in notations for the SL mode, $W_{0\mathbf{q}} \equiv W_{\mathbf{q}}$.

A consequent mean-field approach demands the introduction of three "condensates," i.e., three time-independent c-fields for Kondo coupling, AFM coupling, and SL coupling, respectively, that arise as a consequence of a saddle-point approximation for all three modes. For example, the mean-field description of the interplay between the Kondo and RVB couplings was presented in Refs. 23 and 25. The undesirable consequence of this approximation is the violation of the electromagnetic U(1) gauge invariance, when the electrical charge is ascribed to an initially neutral spin fermion field f (see, e.g., Ref. 12). According to a scenario offered in Refs.[24] and 32, there is no necessity of introducing the mean-field saddle point for Kondo coupling because the transition to a correlated spin state occurs at $T > T_K$. In this case the one site Kondo correlations suppress the Néel phase transition (reduce $T_N^0 \to T_N$) in favor of the spin liquid state with a characteristic crossover temperature $T^* > T_N$. Therefore we refrain from using the saddle-point approximation for the field ϕ but still use it for the fields $\mathbf{Y}$ and W.

To condense the equation for the action $\mathcal{A}$ we introduce a spinor representation for semifermions

$$\overline{F}_{\mathbf{p}} = (\overline{f}_{\mathbf{p}\uparrow} \;\; \overline{f}_{\mathbf{p}\downarrow} \;\; \overline{f}_{\mathbf{p}+\mathbf{Q}\uparrow} \;\; \overline{f}_{\mathbf{p}+\mathbf{Q}\downarrow}),$$

and the following definition of the Fourier transform of the inverse semi-fermionic Green's function

$$D_m^{-1}(W_{\mathbf{p}}, \mathbf{Y}_{\mathbf{Q}}) = \begin{pmatrix} i\omega_m - W_{\mathbf{p}} & 0 & Y_{\mathbf{Q}}^z & Y_{\mathbf{Q}}^+ \\ 0 & i\omega_m - W_{\mathbf{p}} & Y_{\mathbf{Q}}^- & -Y_{\mathbf{Q}}^z \\ Y_{\mathbf{Q}}^z & Y_{\mathbf{Q}}^+ & i\omega_m - W_{\mathbf{p}+\mathbf{Q}} & 0 \\ Y_{\mathbf{Q}}^- & -Y_{\mathbf{Q}}^z & 0 & i\omega_m - W_{\mathbf{p}+\mathbf{Q}} \end{pmatrix}. \tag{13}$$

The same function in a lattice representation is presented in Appendix A. This operator arises as a result of the Hubbard-Stratonovich transformation decoupling the magnetic modes $\mathbf{Y}$ and the spin-liquid mode W. Then the effective action $\mathcal{A}_s$ acquires the form

$$\mathcal{A}_s = \mathrm{Tr}\, \overline{F} D_m^{-1} F + \mathcal{A}_{int}. \tag{14}$$

Now we integrate over semi-Fermionic fields and obtain the effective action for a KL model,

$$\mathcal{A}_s = \mathrm{Tr}\,\ln[D_m^{-1}(\mathbf{Y},W) + \phi_j G_0(\mathbf{r})\overline{\phi_l}] - \frac{2}{\tilde{J}}\mathrm{Tr}|\phi|^2$$

$$-\mathrm{Tr}\frac{1}{I_{\mathbf{q}}}\mathbf{Y}_{\mathbf{q}}\mathbf{Y}_{-\mathbf{q}} - \mathrm{Tr}\frac{1}{I_{\mathbf{q}_1-\mathbf{q}_2}}W_{\mathbf{q}_1}W_{\mathbf{q}_2}. \quad (15)$$

Here the argument $|\phi|^2$ appears in the Green's function D_m as a result of integration of the last term in Eq. (12) over the semi-Fermionic fields.

In a mean-field approximation for two independent modes (neglecting renormalization due to Kondo scattering) Eq. (15) results in a free energy with two local minima reflecting two possible instabilities of the high-temperature paramagnetic state relative to the Néel and SL states. To describe these instabilities one should pick out the classic part of the Néel field,

$$\mathbf{Y} = (\beta N)^{1/2}\frac{I_{\mathbf{q}}}{2}\mathcal{N}\delta_{\mathbf{q},\mathbf{Q}}\delta_{\omega,0}\mathbf{e}_z + \tilde{\mathbf{Y}}_{\mathbf{q}}, \quad (16)$$

and use the eikonal approximation for the SL field,

$$W_{\mathbf{R},\mathbf{r}} = I\Delta(\mathbf{r})\exp(i\theta). \quad (17)$$

Here $\mathcal{N}=\langle Y^z_{\mathbf{Q}}\rangle$ is the staggered magnetization, $\tilde{\mathbf{Y}}_{\mathbf{q}}$ are the fluctuations around the mean-field magnetization, $\mathbf{Q}$ is the AFM vector for a given bipartite lattice, $\mathbf{e}_z$ is the unit vector along the magnetization axis, $\Delta(\mathbf{r})$ is the modulus of RVB field, and $\theta=[\mathbf{r}\cdot\mathbf{A}(\mathbf{R})]$ is the phase of this field.

It is known for Heisenberg lattices dimensions $d>1$ that T_N is higher than the temperature T_{sl} of the crossover to the SL state, so that the ordered magnetic phase is the Neel phase. Due to Kondo fluctuations that screen dynamically local magnetic correlations and slightly enhance the intersite semi-Fermionic correlations, the balance between two modes is shifted towards the spin liquid phase in a critical region of Doniach's diagram, $T_K \sim I$. To show this we include in the free energy the corresponding corrections induced by the last term in Eq. (12). As was mentioned above we refrain from using the mean-field approach to the Kondo field, so that the interplay between the Kondo mode and two other modes is taken into account by including the Néel mean-field corrections to the semi-Fermionic Green's function. Then instead of Eq. (13) one has the following equation for D^{-1}:

$$D_m^{-1}(\mathcal{N},\Delta) = \begin{pmatrix} i\omega_m - \Delta I_{\mathbf{q}} & 0 & \mathcal{N}I_{\mathbf{Q}}/2 & 0 \\ 0 & i\omega_m - \Delta I_{\mathbf{q}} & 0 & -\mathcal{N}I_{\mathbf{Q}}/2 \\ \mathcal{N}I_{\mathbf{Q}}/2 & 0 & i\omega_m - \Delta I_{\mathbf{q}} & 0 \\ 0 & -\mathcal{N}I_{\mathbf{Q}}/2 & 0 & i\omega_m - \Delta I_{\mathbf{q}} \end{pmatrix}. \quad (18)$$

The next steps, i.e., calculation of fluctuation corrections to the stationary point mean-field solutions, can be performed by introducing the auxiliary self-energies,

$$M(\tilde{\mathbf{Y}},\theta) = D_m^{-1}(\mathbf{Y},W) - D_m^{-1}(\mathcal{N},\Delta)$$

$$K_\phi(\omega_{n_1},\omega_{n_2}) = -T\sum_{\Omega}\phi_j(\omega_{n_1}-\Omega)G_0(\mathbf{r},\Omega)\overline{\phi_l}(\omega_{n_2}-\Omega). \quad (19)$$

Then the effective action is approximated by the polynomial expansion

$$\mathrm{Tr}\ln[D_m^{-1}(\mathbf{Y},W)+K_\phi] = \mathrm{Tr}\ln D_m^{-1}(\mathcal{N},\Delta) + \mathrm{Tr}\sum_{n=1}^{\infty}\frac{(-1)^{n+1}}{n}\{D_m(\mathcal{N},\Delta) \times [M(\tilde{\mathbf{Y}},\theta)+K_\phi]\}^n \quad (20)$$

(the Fourier transform of the diagonal part of the Green's function K_ϕ is calculated in Appendix A).

Neglecting all fluctuations, i.e., retaining only the first term in the right hand side of Eq. (20) together with quadratic terms for the AFM and SL modes (15), one obtains the following expression for the free energy per lattice cell:

$$\beta\mathcal{F}(\mathcal{N},\Delta) = \frac{\beta z|I|\mathcal{N}^2}{4} - \ln[2\cosh(\beta z I\mathcal{N}/2)] + \frac{\beta z|I|\Delta^2}{2} - \sum_{\mathbf{q}}\ln[2\cosh(\beta I_{\mathbf{q}}\Delta)] \quad (21)$$

($I_{\mathbf{Q}}=-I$). The standard self-consistent mean-field equations for the order parameters are obtained from the condition of minima of the free energy. These are

$$\mathcal{N} = \tanh\left(\frac{I_{\mathbf{Q}}\mathcal{N}}{2T}\right) \quad (22)$$

for the Néel parameter and

$$\Delta = -\sum_{\mathbf{q}}\nu(\mathbf{q})\tanh\left(\frac{I_{\mathbf{q}}\Delta}{T}\right) \quad (23)$$

for the real part of the RVB order parameter. Here $\nu(\mathbf{q}) = I_{\mathbf{q}}/I_0$. The latter equation was first derived in Ref. 34.

Then making the high-temperature expansion of Eq. (21), one obtains a Ginzburg-Landau (GL) equation in the approximation of two independent modes:

$$\beta\mathcal{F}(\mathcal{N},\Delta) = \frac{\beta|I|z\mathcal{N}^2}{4}\tau_N + c_N\mathcal{N}^4 + \frac{\beta|I|z\Delta^2}{2}\tau_{sl} + c_{sl}\Delta^4 \quad (24)$$

where $\tau_N = 1 - T_N/T$ and $\tau_{sl} = 1 - T_{sl}/T$. The temperatures of two magnetic instabilities are determined as the temperatures of sign inversion in the coefficients in the quadratic terms of the GL expansion $T_N = z|I|/2$ and $T_{sl} = |I|$. The fourth-order GL coefficients c_N and c_{sl} are positive and depend only on temperature. Up to this point the theory is formulated for arbitrary dimension d. In fact, the dimensionality enters the RKKY coupling parameter (see below) and determines the number of nearest neighbors z. We consider zI as a universal parameter in further calculations.

III. DONIACH'S DIAGRAM REVISITED

To describe the contribution of Kondo scattering to the magnetic part of the Doniach's diagram one should integrate $\mathcal{A}$ over the auxiliary field ϕ and thus find the Kondo corrections to both the Néel and RVB instability points. One should

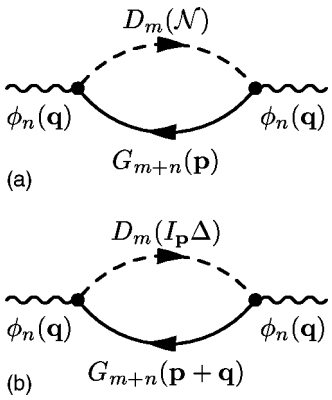

FIG. 1. Diagrams for the fluctuation contribution to the effective action responsible for Kondo screening corrections to magnetic (a) and spin liquid (b) correlations.

consider two cases: (i) $T_N > T_{sl}$ (Kondo corrections screen AFM magnetic moments), and (ii) $T_{sl} > T_N$ (Kondo corrections enhance nonlocal RVB correlations).

(i) *Kondo screening of AFM order*. In this case one takes $\Delta = 0$ in the Green's function (18). Then adding the last term of Eq. (12) to the effective action and integrating over the semi-Fermionic fields yields the correction to the effective action in a form of polarization operators given by the first diagram in Fig. 1(a).

Here the external wavy lines stand for the ''semi-Bosonic'' field ϕ describing Kondo correlations (see Ref. 33). These semi-Bosonic fields are still bosons from the point of view of the permutation relations, but unlike true Bosonic fields they do not satisfy symmetric boundary conditions, and cannot condense in a state with zero frequency and momentum. So the Popov-Fedotov formalism gives an adequate description of the fact that there is no broken symmetry corresponding to the Kondo temperature.[35] The polarization loop is formed by the conduction electron propagator G_0 (solid line) and local semi-Fermionic Green's function D_m given by Eq. (18) (see Appendix A for the explicit form of these Green's functions). As a result the modified effective action is

$$\mathcal{A}_\phi = 2\sum_{\mathbf{q},n}\left[\frac{1}{\tilde{J}} - \delta\Pi(\mathcal{N})\right]|\phi_n(\mathbf{q})|^2. \tag{25}$$

The logarithmic renormalization of the coupling constant is already taken into account in $\tilde{J}$. Therefore the dimensionless integral $\delta\Pi$ includes only contributions due to a nonzero magnetic molecular field,[36]

$$\delta\Pi(\mathcal{N}) = \left[\frac{\pi}{2}\left(\frac{1}{\cosh(\beta\mathcal{N})} - 1\right) + O\left(\frac{\mathcal{N}^2}{T\epsilon_F}\right)\right]. \tag{26}$$

(see Appendix B for detailed calculations). This correlation correction should be incorporated in the equation for the free energy, so that

$$\beta\mathcal{F}(\mathcal{N}) = \beta\mathcal{F}(\mathcal{N},0) + \mathrm{Tr}\,\ln\left[\frac{1}{\tilde{J}} - \delta\Pi(\mathcal{N})\right]. \tag{27}$$

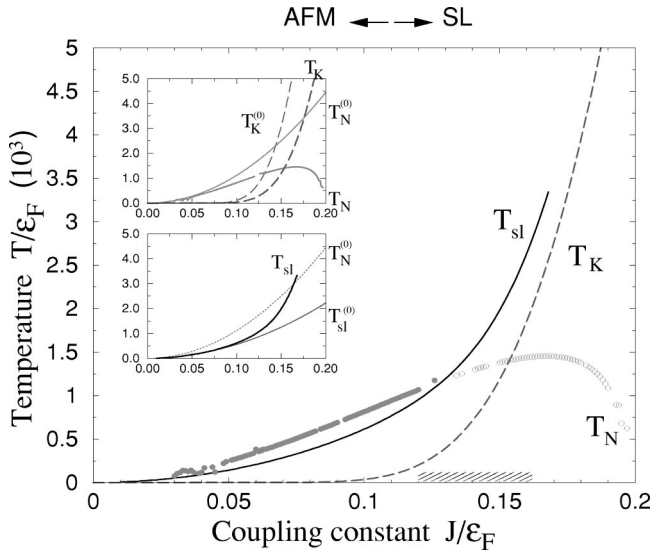

FIG. 2. Doniach's diagram with modifications due to Kondo screening (see text for explanation).

Then differentiation of Eq. (27) with respect to the Néel order parameter $\mathcal{N}$ gives the following self-consistent equation in the vicinity of the renormalized transition point,

$$\mathcal{N} = \tanh\left(\frac{I_\mathbf{Q}\mathcal{N}}{2T}\right)\left[1 - \frac{a_N}{\ln(T/T_K)}\,\frac{\cosh^2(\beta I_\mathbf{Q}\mathcal{N}/2)}{\cosh^2(\beta I_\mathbf{Q}\mathcal{N})}\right] \tag{28}$$

instead of Eq. (22). Here the Kondo temperature T_K is defined as the temperature where the coefficient in front of $|\phi_{n=0}|^2$ in Eq. (25), i.e., the function $\tilde{J}^{-1} - \delta\Pi(\mathcal{N})$, turns to zero. It is seen that the screening corrections near the Néel transition point are negative, $\delta\Pi(\mathcal{N}\to 0) = -a_N(\beta\mathcal{N})^2 < 0$, so that Kondo screening effectively increases the magnetic free energy, and eventually the logarithmic local-field corrections *reduce* the Néel temperature. The numerical solution of Eq. (28) is shown by the circles in Fig. 2. The top inset illustrates the reduction of T_N in comparison with the bare mean-field Néel temperature $T_N^0 = z\varepsilon_F\alpha^2/2$, where $\alpha = J/\varepsilon_F$ is the dimensionless coupling constant for the Doniach's diagram.

(ii) *Kondo enhancement of SL transition*. Now we assume $\mathcal{N} = 0$ in Eq. (21) and subsequent equations. Following the same lines as in the preceding subsection, one obtains the modified effective action

$$\mathcal{A}_\phi = 2\sum_{\mathbf{q},n}\left[\frac{1}{\tilde{J}} - \delta\Pi(I_\mathbf{q}\Delta)\right]|\phi_n(\mathbf{q})|^2 \tag{29}$$

instead of Eq. (25), and the polarization integral with the use of the diagram (b) from Fig. 1 is given by

$$\delta\Pi(I_\mathbf{q}\Delta) = \sum_\mathbf{k}\left[\frac{1}{\cosh\beta(I_\mathbf{k}\Delta)} - 1 + I_\mathbf{k}\Delta\tanh(\beta I_\mathbf{k}\Delta)\right] \times \frac{1}{\xi^2_{\mathbf{k}+q} + (\pi/2\beta)^2}, \tag{30}$$

instead of Eq. (26) (see Appendix B). Here $\xi_{\mathbf{p}}=\varepsilon_{\mathbf{p}}-\varepsilon_F$ is the dispersion law for conduction electrons near the Fermi surface. Inserting the corresponding corrections to the free energy,

$$\beta\mathcal{F}(\Delta)=\beta\mathcal{F}(0,\Delta)+\mathrm{Tr}\ln\left[\frac{1}{\tilde{J}}-\delta\Pi(I_{\mathbf{q}}\Delta)\right]. \qquad (31)$$

one obtains the corrected self-consistent equation for Δ. When deriving this equation, the spinon dispersion can be neglected since $\Delta\to 0$ in a critical point. Then one has

$$\Delta=-\sum_{\mathbf{q}}\ \nu(\mathbf{q})\left[\tanh\left(\frac{I(\mathbf{q})\Delta}{T}\right)+a_{sl}\frac{I_{\mathbf{q}}\Delta}{T\ln(T/T_K)}\right]. \qquad (32)$$

Here $a_{sl}\sim 1$ is a numerical coefficient. It is seen from Eq. (32) that unlike the case of local magnetic order, Kondo scattering favors transition to the SL state, because this scattering means in fact involvement of itinerant electron spin degrees of freedom into spinon dynamics. Mathematically, enhancement arises because $\delta\Pi(I_{\mathbf{q}}\Delta\to 0)=a_{sl}(\beta I_{\mathbf{q}}\Delta)^2>0$, so that Kondo ''antiscreening'' effectively decreases the magnetic free energy. The results of the numerical solution of Eqs. (31) and (32) are represented by circles in Fig. 2.

Here filled circles correspond to the region where the AFM order overcomes the SL phase, and the light circles show unphysical ''suppressed'' AFM solutions obtained beyond the region of validity of the mean-field equation (28). Two other characteristic temperatures, renormalized T_K and T_{sl}, are shown by dashed and solid lines, respectively. The effects of suppression of T_N (thin and thick solid lines for bare and renormalized temperatures) and T_K (thin and thick dotted lines) are illustrated by the upper and lower inset, respectively. As is seen from the modified Doniach's diagram, the interplay between three modes becomes significant in a critical region where the exchange coupling constant is close to the point $\alpha_c=0.13$ where $I=\Delta_K$ in the conventional Doniach's diagram. If the Kondo screening is not taken into account, then $T_{sl}^{(0)}(\alpha)<T_N^{(0)}(\alpha)$ (thin solid and dotted lines in the lower inset). The Kondo screening changes this picture radically, and as a result, a wide enough interval of the parameter α just to the right of the critical value α_c arises, where the enhanced transition temperature T_{sl} exceeds both the reduced Néel temperature T_N and the Kondo temperature T_K. The calculations of T_{sl} presented in Fig. 2 are performed for $d=2$. A similar picture exists for $d=3$, although the domain of the stable SL state is more narrow (for a given value of zI). This means that in this region the stable magnetic phase is, in fact, the spin liquid phase. If one descends from high temperatures in a hatched region of Doniach's diagram where $T_K\sim T_N$, the Kondo scattering suppresses the AFM correlations, but the SL correlations quench the Kondo processes at some temperature $T_{sl}>T_K$. As a result the Kondo-type saddle point is not realized in the free-energy functional in agreement with the assumption made above in our derivation of Ginzburg-Landau expansion. The preliminary version of this scenario was presented in Ref. 24. The more refined mean-field approach described here confirms and enhances this scenario, however, the SL liquid phase is still described in the mean-field approximation. Although the local constraint for spin operators is not violated in the Popov-Fedotov formalism, the gauge phase is still fixed,[27] so the next task is the consideration of fluctuation back flows described by the higher-order terms of the Ginzburg-Landau expansion.

IV. ISING SPIN GLASSES IN DONIACH'S DIAGRAM

In this section we consider the interplay between Kondo scattering and magnetic correlations in the case of a *random* RKKY interaction (3), where the randomness results in the formation of a spin-glass phase. We consider disorder induced by paramagnetic impurities in KL. As was shown in Ref. 37, elastic scattering results in the appearance of a random phase $\delta(r)$ in RKKY indirect exchange parameter,

$$I_{ij}\equiv I(r)\simeq-\left(\frac{J^2}{\varepsilon_F}\right)\frac{\cos\left[2p_Fr-\frac{\pi}{2}(d+1)+\delta(r)\right]}{(2p_Fr)^d}, \qquad (33)$$

where $r=|R_i-R_j|$ and d is the dimensionality of the KL. This form of random exchange predetermines two possible scenarios of SG ordering.

(i) Fluctuations take place around a node of the RKKY interaction (33). This asymptotic behavior is derived from the general equation for the RKKY exchange parameter,[38,39]

$$I_{ij}=-\frac{J^2}{\varepsilon_F}\frac{\pi}{d-1}\left(\frac{p_Fa_0^2}{2\pi r}\right)^d(p_Fr)^2[J_{d/2-1}(p_Fr)Y_{d/2-1}(p_Fr)+J_{d/2}(p_Fr)Y_{d/2}(p_Fr)].$$

[a_0 is the lattice spacing, $J_\nu(x)$ and $Y_\nu(x)$ are the Bessel functions of the first and second kind]. In this case FM and AFM bonds enter the partition function on equal footing, and quenched independent random variables I_{ij} can be described by a Gaussian distribution $P(I_{ij})\sim\exp[-I_{ij}^2N/(2I^2)]$.[40] The magnetic ordering effects also can be included in our approach by introducing a nonzero standard deviation $\Delta I\neq 0$ into the distribution $P(I_{ij})$ that, in turn, results in additional competition between SG and AFM (or, in some cases, FM) states. Recently, the competition between AFM and SG regimes was considered in Ref. 41.

(ii) RKKY exchange fluctuates around some negative value in the AFM domain of exchange parameters. In this case there is a competition between SG, SL, and AFM phases. The third possibility, i.e., fluctuations in the FM domain is somewhat trivial because in this case Kondo fluctuations cannot significantly change the freezing scenario.

We start with the case (i). To understand the situation qualitatively we make the following simplifying approximations. First, we consider only a Ising-like exchange in the Hamiltonian (3):

$$H'=-\sum_{\langle ij\rangle}I_{ij}S_i^zS_j^z. \qquad (34)$$

This is a usual approximation in the theory of spin glasses that allows one to forget about the quantum dynamics of the

spin variables.[42] In the original paper[43] the simplifying assumptions ($d=\infty$, separate electron bath for each localized spin) were made. Thus the form of the spin-spin correlator was predetermined, and these assumptions allowed the authors to obtain an exact solution in a framework of dynamical mean-field theory. We refrain from using these approximations. Second, we confine ourselves with the mean-field (replica symmetric) solution of the Edward-Anderson (EA) model.[44] This means that only a pairwise interaction of nearest neighbors is taken into account. The number z of nearest neighbors should be big enough ($z^{-1}\ll 1$) to justify the mean-field approximation. We consider the interplay between SG and Kondo-type correlations by means of the replica method. We use the approach developed in Ref. 45 for the Sherrington-Kirkpatrick model.[46] Both electron and semifermion variables are replicated ($c\to c^a, f\to f^a$, where $a=1,\ldots,n$), and the number of replicas is tended to zero, so that the free energy per cell is given by the limit $\mathcal{F}=\beta^{-1}\lim_{n\to 0}(1-\langle \mathcal{Z}^n\rangle_{av})/(nN)$. Here the replicated partition function is

$$\langle \mathcal{Z}^n\rangle_{av}=\prod \int dI_{ij}P(I_{ij})\prod D\{c^a_{i,\sigma}f^a_{i,\sigma}\} \times\exp\left(\mathcal{A}_0[c^a,f^a]-\int_0^\beta d\tau H_{int}(\tau)\right) \tag{35}$$

where $\mathcal{A}_0$ (10) corresponds to noninteracting fermions.

Averaging over disorder and integrating out high-energy electronic states by virtue of a replica-dependent Hubbard-Stratonovich transformation one arrives at the following equation

$$\langle \mathcal{Z}^n\rangle_{av}=\prod \int D\{c^a,f^a,\phi^a\}\exp\left(\mathcal{A}_0+\frac{zI^2}{4N}\mathrm{Tr}[X^2] +\int_0^\beta d\tau \mathrm{Tr}\left\{\phi^a\overline{c^a}f^a+\overline{\phi^a}\overline{f^a}c^a-\frac{2}{\tilde{J}}|\phi^a|^2\right\}\right) \tag{36}$$

with

$$X^{ab}(\tau,\tau')=\sum_i\sum_{\sigma,\sigma'}\overline{f^a_{i,\sigma}}(\tau)\sigma f^a_{i,\sigma}(\tau)\overline{f^b_{i,\sigma'}}(\tau')\sigma' f^b_{i,\sigma'}(\tau').$$

Then following the standard pattern of replica theory for spin glasses[45,47] one fixes the saddle point in spin space related to the EA order parameter q_{EA}. At this stage the initial problem is mapped onto a set of independent Kondo scatterers for low energy conduction electrons in external replica dependent effective magnetic field:

$$\langle Z^n\rangle_{av}=\exp\left(-\frac{1}{4}z(\beta I)^2N[n\tilde{q}^2+n(n-1)q^2] +\sum_i \ln\left[\prod\int D\{f^a,\phi^a\}\int_x^G\int_{y^a}^G \times\exp(\mathcal{A}\{f^a,\phi^a,y^a,x\})\right]\right) \tag{37}$$

where $\int_x^G f(x)$ denotes $\int_{-\infty}^{\infty}dx/\sqrt{2\pi}\exp(-x^2/2)f(x)$,

$$\mathcal{A}\{f^a,\psi^a,y^a,x\}=\sum_{a,\sigma}\overline{f^a_\sigma}[(D^{(a)}_m)^{-1}-\sigma h(y^a,x)]f^a_\sigma -\frac{2}{\tilde{J}}\sum_n|\phi^a_n|^2 \tag{38}$$

and $h(y^a,x)=I\sqrt{zq}x+I\sqrt{z(\tilde{q}-q)}y^a$ is an effective local magnetic field, which depends on the diagonal and off-diagonal elements of the Parisi matrix, $\tilde{q}=\langle S^a_i(0)S^a_i(t\to\infty)\rangle$ and $q=\langle S^a_i(0)S^b_i(t\to\infty)\rangle$ ($a\neq b$), respectively. The latter one is the EA order parameter $q_{EA}=q$. Neglecting all fluctuations and retaining only the first two terms in the exponent in Eq. (37), one comes to the EA mean-field equation for the free energy,

$$\beta\mathcal{F}=\frac{z(\beta I)^2}{4}[(1-\tilde{q})^2-(1-q)^2] -\int_x^G \ln[2\cosh(\beta Ix\sqrt{zq})]. \tag{39}$$

(see Ref. 47). Then making the high-temperature expansion, one obtains the Ginzburg-Landau equation in the vicinity of the SG transition,[48]

$$\beta\mathcal{F}_{sg}=\frac{z(\beta I)^2}{4}q^2\tau_{sg}-c_{sg}q^3+d_{sg}q^4, \tag{40}$$

where $\tau_{sg}=1-T_f/T$ and $T_f=\sqrt{z}I$ is a spin-glass freezing temperature.

Like in the previous case of the ordered KL we incorporate the static replica dependent magnetic field h in semi-Fermionic Green's functions. As a result, the modified effective action for the Kondo fields arises like in Eqs. (25) and (29),

$$\mathcal{A}[y^a,x]=\ln\{2\cosh[\beta h(y^a,x)]\} -\sum_n\left[\frac{1}{\tilde{J}}-\delta\Pi[h(y^a,x)]\right]|\phi^a_n|^2. \tag{41}$$

Here similarly to Eq. (26)

$$\delta\Pi(h)=\left[\frac{\pi}{2}\left(\frac{1}{\cosh(\beta h)}-1\right)+O\left(\frac{h^2}{T\epsilon_F}\right)\right]. \tag{42}$$

Finally, performing the Gaussian average over the ϕ fields and taking the limit $n\to 0$ one obtains the free energy

$$\beta\mathcal{F}(\tilde{q},q)=\frac{1}{4}z(\beta I)^2(\tilde{q}^2-q^2) -\int_x^G\ln\left(\int_y^G 2\cosh[\beta h(y,x)]/\{1 -J\Pi[0,h(y,x)]\}\right). \tag{43}$$

Corrected equations for q and $\tilde{q}$ are determined from the conditions $\partial\mathcal{F}(\tilde{q},q)/\partial\tilde{q}=0$, $\partial\mathcal{F}(\tilde{q},q)/\partial q=0$. These are

$$\frac{1}{2}z(\beta I)^2\tilde{q}=\int_x^G \frac{\partial \ln \mathcal{C}}{\partial \tilde{q}}, \qquad \frac{1}{2}z(\beta I)^2 q=-\int_x^G \frac{\partial \ln \mathcal{C}}{\partial q},$$

$$\mathcal{C}=\int_y^G 2\cosh[\beta h(y,x)]/\{1-J\Pi[0,h(y,x)]\}. \quad (44)$$

Under the condition $h(y,x)\leqslant 1$ a useful approximate equation for $\mathcal{C}$ is obtained:[45]

$$\ln[C\mathcal{C}(x,\tilde{q},q)]=-\frac{1}{2}\ln[1+\gamma u^2(\tilde{q}-q)] + \frac{u^2}{2}\frac{[\tilde{q}-q(1+\gamma x^2)]}{1+\gamma u^2(\tilde{q}-q)} + \ln\left[\cosh\left(\frac{ux\sqrt{q}}{1+\gamma u^2(\tilde{q}-q)}\right)\right]. \quad (45)$$

Here the following shorthand notations are used: $u=\beta I\sqrt{z}$, $C=J/\epsilon_F \ln(T/T_K)$ and $\gamma=2c/\ln(T/T_K)$ with $c=(\pi/4+2/\pi^2)\sim 1$. We note again that when $J=0$, which corresponds to the absence of Kondo interaction, $\mathcal{C}(x,\tilde{q},q)=2\exp[\frac{1}{2}z(\beta I)^2(\tilde{q}-q)]\cosh(\beta Ix\sqrt{zq})$, and Eq. (44) turns into the standard EA equation, providing, e.g., an exact identity $\tilde{q}=1$.

In the vicinity of the freezing point Eq. (44) acquires the form

$$\tilde{q}=1-\frac{2c}{\ln(T/T_K)}-O\left(\frac{1}{\ln^2(T/T_K)}\right),$$

$$q=\int_x^G \tanh^2\left(\frac{\beta Ix\sqrt{zq}}{1+2cz(\beta I)^2(\tilde{q}-q)/\ln(T/T_K)}\right) + O\left(\frac{q}{\ln^2(T/T_K)}\right). \quad (46)$$

As a result of the numerical solution of Eqs. (46) we obtain the analog of Doniach's diagram for a disordered KL where the spin-glass freezing temperatures without and with Kondo screening contributions are shown ($T_f^{(0)}$ and T_f, respectively).

Here $T_f^{(0)}$ is obtained from the GL equation (40) neglecting the Kondo screening effect, and T_f was defined from Eqs. (46) under additional condition $\partial^2 \mathcal{F}_{sg}/\partial q^2=0$. The influence of Kondo screening on the diagonal element of the Parisi matrix $\tilde{q}$ is illustrated by the inset of Fig. 3 (the bare value of $\tilde{q}=1$ is shown by the dashed line). Like in the case of a perfect KL, the screening effect is noticeable when $T_f^{(0)}\sim T_K^{(0)}$.

The influence of the SG transition on a Kondo temperature for a KL with SG freezing was studied recently in Ref. 49. Although the Kondo effect in this paper is considered in a mean-field approximation (i.e., Kondo screening is treated as a true phase transition) and a static ansatz was applied for SG, the authors obtained strong reduction of Kondo temperature in the same region $T_K\sim T_f^{(0)}$.

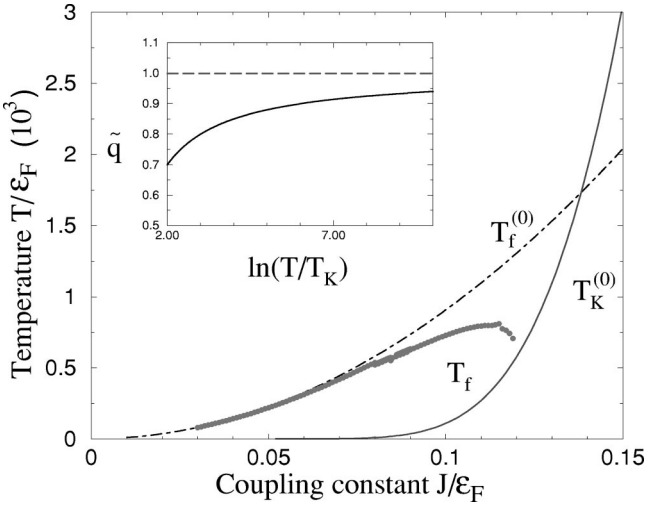

FIG. 3. Doniach's diagram for spin-glass transition in a disordered KL (see text for explanation).

V. CORRELATIONS IN THE KONDO LATTICE BEYOND THE MEAN FIELD

The mean-field Doniach's diagram even in its improved form oversimplifies enormously the real picture of the interplay between three competing modes in the effective action (12). First of all, the proximity of three characteristic temperatures, T_K, T_{sl}, and T_N means that even when one of them is dominant, i.e., determines the local minimum of the free energy, two others define the fluctuations around the saddle point. Second, it is clear physically that only the Néel temperature T_N is a temperature of a *real* phase transition, whereas T_{sl} and T_K are merely characteristic crossover temperatures. The main shortcoming of the mean-field approximation is that this approach treats all three modes on equal footing. The method described in the preceding section allows one to get rid of the artificial phase transition at $T=T_K$, however, the problems with the description of the SL phase still exist. Meanwhile, it is known that the mean-field approximation for the SL state violates the local gauge invariance[23,28,27,50] and fixes the phase θ of the SL mode W (17). The second-order phase transition from paramagnetic to the SL state[34] is an undesirable corollary of this crude approximation, and fluctuation corrections to the mean-field solution cannot improve this defect of the theory.

In this section we consider several scenarios of mode-mode correlations in a system described by the general equations (9) and (12) for the effective action $\mathcal{A}$. First, we offer the description of a *crossover* to a SL state, which allows one to bypass the mean-field saddle point (23). It will be demonstrated that the interplay between fluctuations of the fields ϕ and $\mathbf{Y_Q}$ can trigger the transformation of localized critical relaxation AFM modes into SL-type correlations without loss of criticality. The main idea of our scenarios is that the heavy fermion state of KL is, in fact, an unconventional AFM state with spin excitations changing their character from Bose-like

spin fluctuations or spin waves to Fermi-like spinon modes. Next, we consider the behavior of the Kondo mode below T_{sl} and describe the quenching of Kondo scattering by SL fluctuations in a hatched part of Doniach's diagram (Fig. 2) where the static molecular field is absent.

We demonstrated above that the Kondo screening enhances SL correlations on a level of the mean-field approximation. A similar effect should exist on a more refined level of interacting fluctuation modes. To find the corresponding mechanism we refrain from the use of the bilocal representation of the spin mode. Instead of introducing the mode W associated with the gauge noninvariant U(1) field described by the phase θ in Eq. (17), we consider the effect of interference of Kondo screening modes associated with spins located on different sites of the KL. In fact we consider the high-temperature precursors of the orthogonality catastrophe mentioned by Nozieres in his formulation of the ''exhaustion problem.''[51] In a revised scheme we start with the action determined by the Hamiltonian (1). Starting with the integration over ''fast'' electronic variables (with energies $\sim\varepsilon_F$), we obtain

$$\mathcal{A}_{int}=-\frac{2}{\tilde{J}}\mathrm{Tr}|\phi|^2-\mathrm{Tr}\frac{1}{I_{\mathbf{q}}}\mathbf{Y}_{\mathbf{q}}\mathbf{Y}_{-\mathbf{q}}-\mathrm{Tr}\ \overline{f}_{j\sigma}\phi_j G_0(\mathbf{r})\overline{\phi}_l f_{l\sigma}$$
$$-\mathrm{Tr}\ \overline{\phi}_j\phi_l\Pi_4\overline{\phi}_l\phi_j-\mathrm{Tr}\ \mathbf{Y}_j\overline{\phi}_j\phi_l\Pi_6\overline{\phi}_l\phi_j\mathbf{Y}_l. \quad (47)$$

Here instead of introducing the scalar mode W we retained higher-order terms in the Kondo screening fields. These terms are illustrated by the diagrams in Fig. 4.

The diagram in Fig. 4(a) describes the interference of Kondo clouds around the sites $\mathbf{R}_j$ and $\mathbf{R}_l$. Zigzag lines stand for the AFM vector mode. Like all screening diagrams in Fermi systems it contains a Friedel-like oscillating factor. To estimate the polarization operator we use the asymptotic form of the electron Green's function in d dimensions at large distances,[32,38]

$$G(r,\Omega)\sim\frac{1}{(p_F r)^{(d-1)/2}}\exp\left[-\frac{|\Omega|}{2\varepsilon_F}p_F r\right.$$
$$\left.+i\left(p_F r-\pi\frac{d+1}{4}\right)\mathrm{sgn}\ \Omega\right]. \quad (48)$$

Inserting this function in a four-tail diagram of Fig. 4(a), one comes to

$$\Pi_4\sim-\frac{1}{T\varepsilon_F^2}\frac{\cos\left[2p_F r-(d+1)\frac{\pi}{2}\right]}{(2p_F r)^{d-1}}+O\left(\frac{1}{\varepsilon_F^3}\ln\left[\frac{T}{\varepsilon_F}\right]\right). \quad (49)$$

Therefore we expect that this interference correlates with RKKY-type magnetic order, and the interaction between the corresponding modes represented by the diagram (b) in Fig. 4 influences the magnetic response in a ''critical'' region of the Doniach's diagram. This response is determined by the fluctuation corrections to Néel effective action,

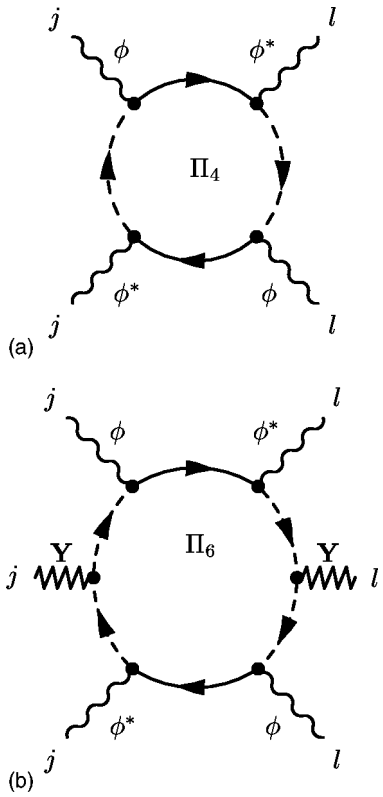

FIG. 4. Diagrams for fourth- and sixth-order polarization operators Π_4 (a) and Π_6 (b) in the effective action responsible for mode-mode coupling.

$$\delta\mathcal{A}_{eff}=\frac{1}{4}\sum_{\mathbf{q},\alpha,\omega_n}Y^{\alpha}(\mathbf{q},\omega_n)[I^{-1}(\mathbf{q})+\chi_0\delta_{n,0}]Y^{\alpha}(\mathbf{q},\omega_n). \quad (50)$$

Here α are Cartesian coordinates, $\chi_0=\beta/4$ is a static Curie susceptibility of an isolated spin $S=1/2$ [Fig. 5(a)]. The term in square brackets is, in fact, the inverse Ornstein-Zernicke correlator $\sim a_0^2(\mathbf{Q}-\mathbf{q})^2+\tau_N$ at $T\gtrsim T_N$ and $\mathbf{Q}-\mathbf{q}\to 0$. The first nonvanishing correction to χ_0 is given by Fig. 5(b). In this diagram the spins S_j and S_l are screened independently, (the wavy lines represent all parquet vertex insertions). In the mean-field approach the similar effects are de-

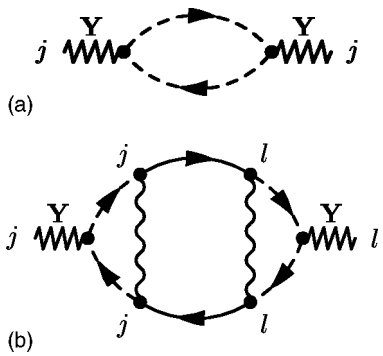

FIG. 5. Diagrams describing local (Curie-type) magnetic susceptibility χ_0 (a) and nonlocal correction taking into account Kondo screening of vertices (b).

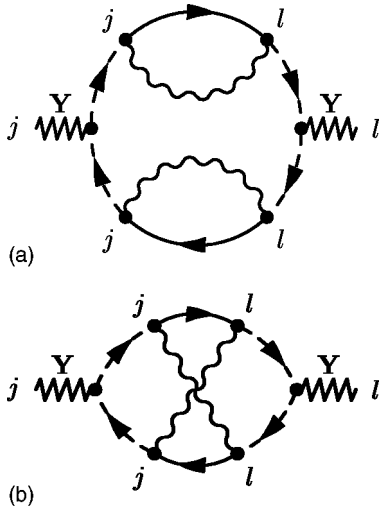

FIG. 6. Leading diagrams describing interference of Kondo clouds in magnetic susceptibility (see text for details).

scribed by Eq. (28). Indeed, each vertex correction $\Gamma_{i=j,l}(\omega,\epsilon)\sim\langle\phi(\epsilon)\bar{\phi}(\epsilon)\rangle$ gives the contribution $\sim 1/\ln(\epsilon/T_K)$, and integration over the internal frequency ϵ results in the $1/\ln(T_N^0/T_K)$ correction in Eq. (28).[24,32]

The effects essentially beyond mean field are described by those diagrams that cannot be cut along a pair of electron propagators (solid lines) [see Figs. 6 and 7(a)]. The first of these diagrams [Fig. 6(a)] can be treated as a nonlocal correction to the one site spin susceptibility [Fig. 5(a)] induced by interfering flow and counterflow of two Kondo clouds. As a result, the spin-fermion propagator becomes nonlocal without introducing the mean-field order parameter (17). The next diagram [Fig. 6(b)] is a kind of ''exchange'' by these clouds in the course of two-spinon propagation. Up to now we exploited the ''proximity'' effects $T\gtrsim T_K$. A critical AFM mode given by the Fourier transform of the diagram of Fig. 5(a) with the wave vector $\mathbf{q}\simeq\mathbf{Q}$ also exists in this temperature interval, and, moreover, this mode is dominant in the spin susceptibility at $T\gtrsim T_N$. This means that the nonlocal contributions of Fig. 6 should be taken also at these $\mathbf{q}$. Due to nonlocality, the temperature dependence of the spin polarization loop will be weaker than the Curie law $1/T$, and the inverse static susceptibility given by these diagrams is

$$\chi_{\mathbf{Q}}^{-1}(T)=\chi_0^{-1}(T)+\chi_{sl}^{-1}(T)+\tilde{I}_{\mathbf{Q}}. \tag{51}$$

This deviation from the Curie law results in a depression of the Néel phase transition or, in other words, in extension of critical regime to temperatures well below T_N^0 in accordance with the scenario described in Ref. 28. Magnetic instabilities that can emerge at $T\ll T_N^0$ will be the instabilities of the spin liquid phase. These instabilities have much in common with itinerant fluctuational magnetism considered, e.g., in Refs. 52 and 53.

Diagram (a) in Fig. 7 with bare spinon propagators gives only a local correction to the susceptibility, however at $T\ll T_N^0$ where the spinon lines are dressed by the self-energies shown in Fig. 6(a), this diagram also becomes nonlocal and, therefore contributes to the nonlocal term on the right-hand side of Eq. (51). The processes taken into account in diagram (b) of Fig. 7 describe the feedback influence of spin fluctuations on the Kondo screening. This diagram together with higher-order terms of the same type results in the dynamical suppression of T_K as a result of the appearance of spin fluctuation energy $\omega_{sf}\sim\xi^{-z}$ in the logarithmic Kondo contribution $\ln(\varepsilon_F/\max\{T,\omega_{sf}\})$. This mechanism is effective not too close to the real T_N where the magnetic correlation length ξ determining the short-range magnetic order is still comparable with the lattice spacing (here z is the dynamical critical exponent).

This schematic description is only a scenario of the theory of critical phenomena in KL's. The discussion of fluctuations around the SG transitions are beyond the scope of this paper. Some details of modulated replica symmetry breaking schemes, which combine treelike and wavelike structures in AFM SG may be found in Ref. 41. A more detailed calculation of the critical magnetic and spin-glass fluctuations in the spin liquid will be published separately.

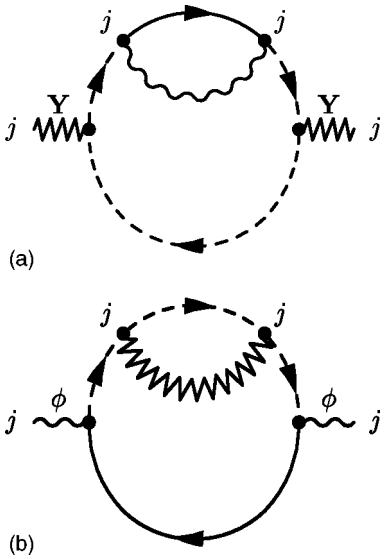

FIG. 7. (a) Next to parquet approximation for Kondo corrections to the magnetic susceptibility; (b) magnetic fluctuation correction to single-site Kondo scattering.

VI. CONCLUDING REMARKS

We derived in this paper the phase diagram for the Kondo lattice model, starting with a high-temperature expansion of the effective action. As a first step, we succeeded in getting rid of one of the fictitious saddle points, i.e., we avoided the introduction of ''Kondo-condensate'' averages $\langle c_{k\sigma}^{\dagger}f_{i\sigma}\rangle$ used in previous revisions of the Doniach's diagram.[23,25] In our modified Doniach's diagram (Fig. 3) the *renormalized* T_K is the lowest of all characteristic temperatures for all reasonable values of coupling constant α where one can neglect valence fluctuations. In fact, the mean-field calculations of Ref. 25 give a similar picture. The feedback of this result is that the strong Kondo regime is unachievable in a critical region of Doniach's diagram, and the real role of Kondo screening for small α where $T_N>T_{sl}>T_K$ is to reduce localized magnetic

moments and enhance the electronic density of states around ε_F. Thus the moderately heavy fermion systems with relatively big magnetic moments ordered antiferromagnetically arise ($CeIn_3$, $CeAl_2$ are possible examples).[54]

In a critical region of Doniach's diagram Kondo screening changes radically the behavior of KL. According to our mean-field results the conventional AFM order is suppressed at $T \sim T_{sl} \gtrsim T_N$. The SL phase that arises instead is, nevertheless, close to magnetic instability, and one can expect that the spin subsystem eventually orders magnetically. If the new transition temperature $\tilde{T}_N$ is finite the singlet spinon coupling is incomplete, so that RVB's have residual magnetic moments, and these moments are ordered at $T=\tilde{T}_N$ (we emphasize once more that T_N marked by light circles in a hatched region of the phase diagram of Fig. 3 is not a real transition temperature. It rather designates the temperature region where critical AFM fluctuations arise). Of course, the magnitude of these moments is extremely small, and one can qualify this type of magnetic order as intermediate between localized and itinerant AFM. In the temperature interval $\tilde{T}_N < T < T_N$ the critical AFM relaxation mode characterizes the magnetic response of the system. When $\tilde{T}_N = 0$, one deals with a quantum phase transition, and the case $\tilde{T}_N < 0$, apparently, corresponds to short-range correlations existing in a wide temperature interval $0 < T < T_N$. This picture describes in gross features the magnetic properties of magnetic KL's, but any kind of quantitative description will be possible only after realization of the scenarios for the critical behavior of spin liquid briefly sketched in Sec. V.

Now we turn to the discussion of conclusions that could be derived from our theory concerning the nature of the heavy fermion state. The most important one is that the separation of charge and spin degrees of freedom existing in KL at high temperatures takes place also in a strong-coupling regime at $T \ll T_K$. Indeed, at high T exceeding all characteristic temperatures in the KL the spin excitation spectrum is simple structureless peak of the width T around zero energy. This peak is manifested as Curie-type magnetic susceptibility and trivial high-temperature corrections $\sim 1/T^n$ to all thermodynamic quantities due to weak paramagnetic spin scattering of the conduction electrons, whose Fermi-liquid continuum exists as independent charge branch of the elementary excitations. Since all transformations of the spin subsystem occur at $T > T_K$ (at least in a region of $\alpha < 0.2$ where the valence fluctuations are still negligible), this central peak still exists in a strong-coupling regime. Below $T_{sl} \sim T_K$ this peak is formed by spin liquid excitations. The character of these excitations resembles relaxation modes in a picture of fluctuation itinerant magnetism[52,53] in a wide temperature interval down to T_{coh} where the coherent spin liquid regime of Fermi type is established. The interaction between the SL mode and the conduction electrons is the same exchange-type scattering as at high temperatures. This coupling constant $\tilde{J}$ is, however, enhanced by the Kondo effect [see Eq. (25)]. The electrons in a layer of the width T_K around the Fermi level interact nonadiabatically with spin fermions at low T. As a result the giant Migdal effect arises[55] which results in a strong electron mass enhancement. So, the heavy fermion state in accordance with this picture is a two-component Fermi liquid where the characteristic energies of the charge subsystem (slow electrons with $\epsilon < T_K$) and the spin subsystem (spinons with $\omega \sim T_{sl}$) are nearly the same.

An exponentially narrow low-energy peak of predominantly spin origin appears practically in all theories of strongly correlated electron systems. In the archetypal Hubbard model this peak arises on the dielectric side of Mott-Hubbard transition, and still exists on the metallic side, where the charge and spin degrees of freedom are already coupled. This is the point where the links between Hubbard and Anderson models arise at least on a level of dynamical mean-field theory (DMFT) valid at $d \to \infty$.[56] On the other hand, the mean-field solution that results in merged charge and spin degrees of freedom in a central peak becomes exact in the large-N theories for the $N=\infty$ saddle point.[57] Recent achievements in this direction are connected with confirmation of Noziere's prediction of a second scale in the Kondo lattice[51] in the limit of the exhaustion regime of small electron concentration. At this temperature the ''bachelor'' spins form a coherent Fermi liquid and lose their localized nature. This anticipation was confirmed by recent calculations within the mean-field slave boson approximation of $N \to \infty$ theory.[58] In our approach the regime of bachelor spins does not arise, because the Kondo coupling remains weak even at $T \ll T_K$ (see above), but the spin degrees of freedom become coherent at $T \sim T_{coh}$, so that the existence of two coherence scales is an intrinsic property of the model.

Another aspect of large N theories is the possibility of supersymmetric description that allows combined description of spin degrees of freedom in a mixed fermion-boson SU(N) representation.[59] This approach allowed the authors to retain intersite RKKY interaction in the limit of $N \to \infty$ in spite of $1/N^2$ effect of suppression of all intersite magnetic correlations in a standard large N approach. The use of the Popov-Fedotov representation allows the treatment of different magnetic modes described by these operators as semifermions or semibosons in different physical situations.[33] In this paper we appealed to SU(2) symmetry. The general recipe of generation of modes with intermediate statistics between Fermi and Bose limiting cases for the SU(N) algebra is offered in Ref. 60. In fact, the eventual transformation of the states with intermediate statistics into true fermions (bosons) occurs only at $T \to 0$. Thus this approach may be extremely useful for an adequate description of quantum phase transitions.[61]

In principle, other collective modes can modify the scenario of the AFM phase transition in KL's. In particular, the low-lying crystal-field excitations may intervene the magnetic phase transition in the same fashion as Kondo clouds in our theory. Probably the CeNiSn family of semimetallic Kondo lattices is an example of such an intervention.[62]

ACKNOWLEDGMENTS

Authors thank A. Mishchenko for fruitful collaboration in the early stages of this work, A. Luther, D.Aristov, and G. Khaliullin for valuable discussions, and A. Tsvelik for useful

remarks. The work was supported by SFB-410. M.K. acknowledges the support of the Alexander von Humboldt Foundation, K.K. is grateful to Israeli-USA BSF-1999354 for partial support and to the University of Würzburg for hospitality.

APPENDIX A:

To evaluate the contribution of the Kondo mode in the expansion (20) for the effective action, one needs the Fourier transform of the Green's function K_ϕ (19). This is

$$\begin{pmatrix} \bar{\phi}_n(\mathbf{k})G^0(\mathbf{q})\phi_n(\mathbf{k}) & 0 & \bar{\phi}_n(\mathbf{k})G^0(\mathbf{q})\phi_n(\mathbf{k}+\mathbf{Q}) & 0 \\ 0 & \bar{\phi}_n(\mathbf{k})G^0(\mathbf{q})\phi_n(\mathbf{k}) & 0 & \bar{\phi}_n(\mathbf{k})G^0(\mathbf{q})\phi_n(\mathbf{k}+\mathbf{Q}) \\ \bar{\phi}_n(\mathbf{k}+\mathbf{Q})G^0(\mathbf{q})\phi_n(\mathbf{k}) & 0 & \bar{\phi}_n(\mathbf{k}+\mathbf{Q})G^0(\mathbf{q})\phi_n(\mathbf{k}+\mathbf{Q}) & 0 \\ 0 & \bar{\phi}_n(\mathbf{k}+\mathbf{Q})G^0(\mathbf{q})\phi_n(\mathbf{k}) & 0 & \bar{\phi}_n(\mathbf{k}+\mathbf{Q})G^0(\mathbf{q})\phi_n(\mathbf{k}+\mathbf{Q}) \end{pmatrix} \tag{A1}$$

The components $D_{m\sigma}(\mathbf{q})$ of the semi-Fermionic Green's function D in Eq. (20) are determined by inverting the matrix (18). There are normal and anomalous components,

$$-\int_0^\beta d\tau e^{i\omega_m\tau}\langle T_\tau f_\sigma(\mathbf{q},\tau)\bar{f}_\sigma(\mathbf{q},0)\rangle = \frac{i\omega_m - W_\mathbf{q}}{(i\omega_m - W_\mathbf{q})^2 - Y^2} \tag{A2}$$

and

$$-\int_0^\beta d\tau e^{i\omega_m\tau}\langle T_\tau f_\sigma(\mathbf{q},\tau)\bar{f}_\sigma(\mathbf{q}+\mathbf{Q},0)\rangle = \frac{Y\hat{\tau}^z_{\sigma\sigma}}{(i\omega_m - W_\mathbf{q})^2 - Y^2}, \tag{A3}$$

respectively. Here $Y=\mathcal{N}I_\mathbf{Q}/2$ and $W_\mathbf{q}=I_\mathbf{q}\Delta$.

To perform calculations in real space, one should know the inverse Green's function (13) in coordinate representation:

$$D_m^{-1}(W,\mathbf{Y}) = \begin{pmatrix} i\omega_m + Y_j^z & Y_j^+ & W_{jl} & 0 \\ Y_j^- & i\omega_m - Y_j^z & 0 & W_{jl} \\ W_{lj} & 0 & i\omega_m - Y_l^z & Y_l^+ \\ 0 & W_{lj} & Y_l^- & i\omega_m + Y_l^z \end{pmatrix}. \tag{A4}$$

It should be noted that the nonlocal term W_{jl} in Eq. (A4) responsible for SL correlations transforms into diagonal term $W_\mathbf{q}$ in momentum representation (13), whereas the local staggered field $\mathbf{Y}_i$ has nondiagonal matrix elements in momentum space corresponding to AFM correlations at $\mathbf{q}=\mathbf{Q}$.

APPENDIX B:

The sum of polarization integrals presented in Fig. 1 is given by the following equation:

$$\Pi_n(Y,W_\mathbf{q}) = -T\sum_{m,\sigma,\mathbf{p}} D_{m\sigma}(\mathbf{p})G^0_{m+n}(\mathbf{p}+\mathbf{q}) \tag{B1}$$

Only the normal component (A2) survives in this equation as a result of spin summation. The Neel loop [Fig. 1(a)] after performing frequency summation acquires the form

$$\Pi(Y,0) = \sum_\mathbf{p} \left\{ \tanh\left(\frac{\xi_\mathbf{p}}{2T}\right)\left[\frac{\xi_\mathbf{p}-Y}{(\xi_p-Y)^2+\lambda^2} + \frac{\xi_\mathbf{p}+Y}{(\xi_\mathbf{p}+Y)^2+\lambda^2}\right] + \frac{\lambda}{\cosh(Y/T)}\left[\frac{1}{(\xi_\mathbf{p}-Y)^2+\lambda^2} + \frac{1}{(\xi_\mathbf{p}+Y)^2+\lambda^2}\right] - \tanh\left(\frac{Y}{T}\right)\left[\frac{\xi_\mathbf{p}-Y}{(\xi_\mathbf{p}-Y)^2+\lambda^2} - \frac{\xi_\mathbf{p}+Y}{(\xi_\mathbf{p}+Y)^2+\lambda^2}\right]\right\}. \tag{B2}$$

Here $\xi_p=\varepsilon_p-\varepsilon_F$, $\lambda=\pi T/2$. This integral is an even function of the order parameter, $\Pi(Y)=\Pi(-Y)$. Using the inequality $Y\ll\epsilon_F$, two last terms can be simplified, and introducing the integral over the electron band with constant density of states ρ_0, one has

$$\Pi(Y,0) = \frac{1}{4}\rho_0\int_{-\epsilon_F}^{\epsilon_F} d\xi\left\{\tanh\left(\frac{\xi_\mathbf{p}}{2T}\right) \times\left[\frac{\xi_\mathbf{p}-Y}{(\xi_\mathbf{p}-Y)^2+\lambda^2} + \frac{\xi_\mathbf{p}+Y}{(\xi_\mathbf{p}+Y)^2+\lambda^2}\right]\right\} + \frac{\pi\rho_0}{2\cosh(Y/T)} + \frac{\rho_0 Y}{\epsilon_F}\tanh\left(\frac{Y}{T}\right). \tag{B3}$$

Incorporating ρ_0 in dimensionless variables, one has in the vicinity of the Néel point where $Y\ll T$,

$$\Pi(Y,0)=\frac{1}{2}\left[\ln\left(\frac{\epsilon_F^2}{4T^2}\right)+\pi\right]-a_N\left(\frac{Y}{T}\right)^2+O\left(\frac{Y^2}{T\epsilon_F}\right). \tag{B4}$$

The logarithmic term is, in fact, included in the renormalized coupling constant $\tilde{J}$ in Eq. (25) for the effective action, and the remaining terms give Eq. (26) for $\delta\Pi$. Deeper in the magnetic phase where $Y\gg T$, the Kondo effect is quenched by the molecular field, so that

$$\Pi=\ln\left(\frac{\epsilon_F}{Y}\right)+b_N\left(\frac{T}{Y}\right)^2+O\left(\frac{T^2}{\epsilon_F^2}\right). \tag{B5}$$

The numerical coefficients a_N, b_N arising from approximate estimates of the integrals in Eq. (A3) are of the order of unity.

The SL loop [Fig. 1(b)] can be estimated for $\mathbf{q}=0$. After frequency summation it is presented by the following integral:

$$\Pi(0,\Delta)=\frac{1}{2}\sum_{\mathbf{p}}\frac{\xi_{\mathbf{p}}\tanh\left(\frac{\xi_{\mathbf{p}}}{2T}\right)+I_{\mathbf{p}}\Delta\tanh\left(\frac{I_{\mathbf{p}}\Delta}{T}\right)+\frac{\lambda}{2\cosh(I_{\mathbf{p}}\Delta/T)}}{\xi_{\mathbf{p}}^2+\lambda^2}. \tag{B6}$$

This function is also even, $\Pi(\Delta)=\Pi(-\Delta)$. Extracting from Eq. (B6) the logarithmic term $\ln(\varepsilon_F/2T)$, one comes to Eq. (30) for $\delta\Pi$. In a critical region of Doniach's diagram where $\Delta\ll T$, one has

$$\delta\Pi(0,\Delta)=a_{sl}\frac{\Delta^2}{2T^2}\sum_{\mathbf{p}}\frac{\nu_{\mathbf{p}}^2}{\xi_{\mathbf{p}}^2+\lambda^2},\quad a_{sl}\sim 1. \tag{B7}$$

[1] G.G. Lonzarich, J. Magn. Magn. Mater. **76-77**, 1 (1988); M. Springford, Physica B **171**, 151 (1990); Y. Onuki and A. Hasegawa, J. Magn. Magn. Mater. **108**, 19 (1992).

[2] M. Sigrist and K. Ueda, Rev. Mod. Phys. **63**, 239 (1991); R.H. Heffner and M.R. Norman, Comments Condens. Matter Phys. **17**, 361 (1996).

[3] U. Rauchschwalbe, Physica B **147**, 1 (1987); H. R. Ott, in *Progress in Low Temperature Physics*, edited by D. F. Brewer (Elsevier, Amsterdam, 1987) Vol. XI, p. 215; N. Grewe and F. Steglich, in *Handbook on the Physics and Chemistry of Rare Earths*, edited by K. A. Gschneider, Jr. and L. Eyring (Elsevier, Amsterdam, 1991), Vol. 14, p. 343.

[4] J.M. Effantin, J. Rossat-Mignod, P. Burlet, H. Bartholin, S. Kunii, and T. Kasuya, J. Magn. Magn. Mater. **47-48**, 145 (1985).

[5] A. Loidl, A. Krimmel, K. Knorr, G. Sparn, M. Lang, C. Geibel, S. Horn, A. Grauel, F. Steglich, B. Welslau, N. Grewe, H. Nakotte, F. de Boer, and A.P. Murani, Ann. Phys. (Leipzig) **1**, 78 (1992); A. Bernasconi, M. Mombelli, Z. Fisk, and H.R. Ott, Z. Phys. B: Condens. Matter **94**, 423 (1994).

[6] A. de Visser and J.J.M. France, J. Magn. Magn. Mater. **100**, 204 (1991).

[7] H. von Löhneysen, A. Neubert, T. Pietrus, A. Schröder, O. Stockert, U. Tutsch, M. Löwenhaupt, A. Rosch, and P. Wölfle, Eur. Phys. J. B **5**, 447 (1998).

[8] A. de Visser, M.J. Graf, P. Estrela, A. Amato, C. Baines, D. Andreica, F.N. Gygax, and A. Schenk, Phys. Rev. Lett. **85**, 3005 (2000).

[9] J. Rossat-Mignod, L.P. Regnauld, J.L. Jacoud, C. Vettier, P. Lejay, J. Flouquet, E. Walker, D. Jaccard, and A. Amato, J. Magn. Magn. Mater. **76&77**, 376 (1988).

[10] N.D. Mathur, F.M. Groschke, S.R. Julian, J.R. Walker, D.M. Freye, R.K.W. Haselwimmer, and G.G. Lonzarich, Nature (London) **394**, 39 (1998).

[11] C. M. Varma, in *Theory of Heavy Fermions and Valence Fluctuations*, Springer Series in Solid State Sciences Vol. 62, edited by T. Kasuya and T. Saso (Springer, Berlin, 1985), p. 277.

[12] Yu. Kagan, K.A. Kikoin, and N.V. Prokof'ev, Physica B **182**, 201 (1992).

[13] M.B. Maple, M.C. de Andrade, J. Herrmann, Y. Dalichaouch, D.A. Gajewski, C.L. Seaman, R. Chau, R. Movshovich, M.C. Aronson, and R. Osborn, J. Low Temp. Phys. **99**, 314 (1995).

[14] L.Z. Liu, J.W. Allen, C.L. Seaman, M.B. Maple, Y. Dalichaouch, J.S. Kang, M.S. Torikachvili, and M.A. Lopez de la Torre, Phys. Rev. Lett. **68**, 1034 (1992).

[15] S. Süllow, G.J. Nieuwenhuys, A.A. Menovsky, J.A. Mydosh, S.A.M. Mentink, T.E. Mason, and W.J.L. Buyers, Phys. Rev. Lett. **78**, 354 (1997).

[16] B. Becker, S. Ramakrishnan, A.A. Menovsky, G.J. Nieuwenhuys, and J.A. Mydosh, Phys. Rev. Lett. **78**, 1347 (1997).

[17] D.X. Li, Y. Shiokawa, Y. Homma, A. Uesawa, A. Dönni, T. Suzuki, Y. Haga, E. Yamamoto, T. Homma, and Y. Ōnuki, Phys. Rev. B **57**, 7434 (1998).

[18] O.O. Bernal, D.E. MacLaughlin, H.G. Lukefahr, and A. Andraka, Phys. Rev. Lett. **75**, 2023 (1995).

[19] J.C. Gomez Sal, J. Garcia Soldevilla, J.A. Blanco, J.I. Espeso, J. Rodriguez Fernandez, F. Luis, F. Bartolome, and J. Bartolome, Phys. Rev. B **56**, 11 747 (1997).

[20] J. Garcia Soldevilla, J.C. Gomez Sal, J.A. Blanco, J.I. Espeso, and J. Rodriguez Fernandez, Phys. Rev. B **61**, 6821 (2000).

[21] D. Eom, M. Ishikawa, J. Kitagawa, and N. Takeda, J. Phys. Soc. Jpn. **67**, 2495 (1998).

[22] S. Doniach, Physica B **91**, 231 (1977); C. Lacroix and M. Cyrot, Phys. Rev. B **20**, 1969 (1979).

[23] P. Coleman and N. Andrei, J. Phys.: Condens. Matter **1**, 4057 (1989).

[24] K.A. Kikoin, M.N. Kiselev, and A.S. Mishchenko, Pis'ma Zh. Eksp. Teor. Fiz. **60**, 583 (1994) [JETP Lett. **60**, 600 (1994)].

[25] J.R. Iglesias, C. Lacroix, and B. Coqblin, Phys. Rev. B **56**, 11 820 (1997); B.H. Bernhard, C. Lacroix, J.R. Iglesias, and B. Coqblin, *ibid.* **61**, 441 (2000).

[26] V.N. Popov and S.A. Fedotov, Zh. Eksp. Teor. Fiz. **94**, 183 (1988) [Sov. Phys. JETP **67**, 535 (1988)].

[27] L.B. Ioffe and A.I. Larkin, Phys. Rev. B **39**, 8988 (1989); P.A. Lee and N. Nagaosa, *ibid.* **46**, 5621 (1992).
[28] K.A. Kikoin, M.N. Kiselev, and A.S. Mishchenko, Physica B **230-232**, 490 (1997).
[29] N. Read and D.M. Newns, J. Phys. C **16**, 3273 (1983).
[30] F. Bouis and M.N. Kiselev, Physica B **259-261**, 195 (1999).
[31] M.N. Kiselev and R. Oppermann, Phys. Rev. Lett. **85**, 5631 (2000).
[32] K.A. Kikoin, M.N. Kiselev, and A.S. Mishchenko, Zh. Eksp. Teor. Fiz. **112**, 729 (1997) [Sov. Phys. JETP **85**, 490 (1997)].
[33] The specific feature of $S=1/2$ is that the set $2\pi T(m+1/4)$ can be interpreted both as a ''semi-Fermionic'' and a ''semi-Bosonic'' field. The complementary field ϕ which appears in the decoupling procedure for bi-Grassmann products in representation (8) will be referred to as a semi-Bosonic field for the physical reasons which are discussed below.
[34] G. Baskaran, Z. Zou, and P.W. Anderson, Solid State Commun. **63**, 973 (1987); A. Ruckenstein, P. Hirschfeld, and J. Appel, Phys. Rev. B **36**, 857 (1987).
[35] A.M. Tsvelik and P. Wiegmann, Adv. Phys. **32**, 483 (1983).
[36] A.A. Abrikosov and A.A. Migdal, J. Low Temp. Phys. **3**, 519 (1970).
[37] A.Yu. Zyuzin and B.Z. Spivak, Pis'ma Zh. Eksp. Teor. Fiz. **43**, 185 (1986) [JETP Lett. **43**, 234 (1986)]; L.N. Bulayevskii and S.V. Panyukov, *ibid.* **43**, 190 (1986) [*ibid.* **43**, 240 (1986)].
[38] D.N. Aristov, Phys. Rev. B **55**, 8064 (1996).
[39] J. Stein, Eur. Phys. J. B **12**, 5 (1999).
[40] S. Sachdev, N. Read, and R. Oppermann, Phys. Rev. B **52**, 10 286 (1995).
[41] R. Oppermann, D. Sherrington, and M. Kiselev, cond-mat/0106066 (unpublished).
[42] A mean-field solution of a fully connected quantum Heisenberg SG model in a large N limit that involves the quantum dynamics of spin variables was presented in A. Georges, O. Parcollet, and S. Sachdev, Phys. Rev. Lett. **85**, 840 (2000).
[43] A. Sengupta and A. Georges, Phys. Rev. B **52**, 10 295 (1995).
[44] S.F. Edwards and P.W. Anderson, J. Phys. F: **5**, 965 (1975).
[45] M.N. Kiselev and R. Oppermann, Pis'ma Zh. Eksp. Teor. Fiz. **71**, 359 (2000) [JETP Lett. **71**, 250 (2000)].
[46] D. Sherrington and S. Kirkpatrick, Phys. Rev. Lett. **35**, 1972 (1975).
[47] R. Oppermann and A. Muller-Groeling, Nucl. Phys. B **401**, 507 (1993).
[48] K. Binder and A.P. Young, Rev. Mod. Phys. **58**, 801 (1986).
[49] A. Theumann, B. Coqblin, S.G. Magalhães, and A.A. Schmidt, Phys. Rev. B **63**, 054409 (2001).
[50] I. Affleck, Z. Zou, T. Hsu, and P.W. Anderson, Phys. Rev. B **38**, 745 (1988).
[51] P. Nozieres, Ann. Phys. (Paris) **10**, 19 (1985); Eur. Phys. J. B **6**, 447 (1998).
[52] T. Moriya, *Spin Fluctuations in Itinerant Electron Magnetism* (Springer, Berlin, 1985).
[53] Y. Okuno and K. Miyake, J. Phys. Soc. Jpn. **67**, 3342 (1998).
[54] Metallic compounds containing U, apparently, should be described by the Anderson-lattice Hamiltonian because of the partially itinerant nature of the $5f$ electrons, so we refrain here from direct application of our model to U-based heavy fermion systems.
[55] K. Kikoin, J. Phys.: Condens. Matter **8**, 3601 (1996).
[56] A. Georges, G. Kotliar, W. Krauth, and M. Rozenberg, Rev. Mod. Phys. **68**, 13 (1996).
[57] P. Coleman, Phys. Rev. B **35**, 5072 (1987).
[58] S. Burdin, A. Georges, and D.R. Grempel, Phys. Rev. Lett. **85**, 1048 (2000).
[59] P. Coleman, C. Pepin, and A.M. Tsvelik, Phys. Rev. B **62**, 3852 (2000).
[60] M. N. Kiselev, H. Fedmann, and R. Oppermann, Eur. Phys. J. B **22**, 53 (2001).
[61] A. M. Tsvelik (private communication).
[62] Yu.M. Kagan, K.A. Kikoin, and A.S. Mishchenko, Phys. Rev. B **55**, 12 348 (1997); K.A. Kikoin, M.N. Kiselev, A.S. Mishchenko, and A. de Visser, *ibid.* **59**, 15 070 (1999).

Semi-fermions in quantum spin systems

Schwinger-Keldysh Semionic Approach for Quantum Spin Systems

M. N. Kiselev and R. Oppermann
Institut für Theoretische Physik, Universität Würzburg, D-97074 Würzburg, Germany
(Received 14 July 2000)

We derive a path-integral Schwinger-Keldysh approach for quantum spin systems. This is achieved by means of a semionic representation of spins as fermions with imaginary chemical potential. The major simplifying feature in comparison with other representations (Holstein-Primakoff, Dyson-Maleev, slave bosons/fermions, etc.) is that the local constraint is taken into account exactly. As a result, the standard diagram technique with the usual Feynman codex is constructed. We illustrate the application of this technique for the Néel and spin-liquid states of the antiferromagnetic Heisenberg model.

PACS numbers: 75.10.–b, 75.40.Gb, 71.10.Fd

For a long time [1] physicists have been aware of the fact that spin operators which commute on different sites and anticommute on the same site are neither Fermi nor Bose operators. Less convergent opinions exist on whether fermionizations or bosonizations or none of those should be used to take care of spin statistics in many body quantum theory. At least the answers appear to be linked to the type of physical problem considered. The widely accepted view is that path integral representations and diagrammatic expansions for spin systems are thus substantially more complicated than those of pure fermion/boson systems. Many variants of the diagram technique [2], which are based on different representation of spins such as Bose [1–4], Fermi [5–7], Majorana [8], supersymmetric [9], or Hubbard [10] operators, have been proposed. Another method to treat spin Hamiltonians is based on direct representation of coherent states for spins (nonlinear σ model, see, e.g., [8]). Some of these techniques [1–10], being applicable only at low temperatures or in large spin ($S \gg 1$) limit, nevertheless describe well the excitations in ordered magnets (ferromagnetic and antiferromagnetic magnons), but fail to provide rigorous calculations in strongly correlated systems such as Kondo lattices or quantum magnets. Other techniques, based on a successful choice for the hierarchy of coupling constants, are mainly restricted to equilibrium situations. The fundamental problem which is at the heart of the difficulty is the local constraint. On one hand, any representation of spin operators as a bilinear combination of Fermi or Bose quasiparticles makes the dimensionality of the Hilbert space, where these operators act, greater than the dimensionality of the Hilbert space for spin operators. As a result, the spurious unphysical states should be excluded from the consideration, resulting in substantial complication of corresponding rules of diagrammatical summation. On the other hand, there is no Wick theorem directly for spin operators but the Gaudin theorem [11] instead (see also [7,10]). It cannot, however, avoid complications in diagram techniques based on Hubbard operators, rendering the resummation of diagram series in many cases practically uncontrollable. The exclusion of double-occupied and empty states for impurity spins interacting with a conduction electron bath (single impurity Kondo problem) [6] is cured by an infinite chemical potential for Abrikosov pseudofermions. It works for dilute spin subsystems, where all spins can be considered independently. Unfortunately, attempts to generalize this technique to the lattice of spins result in the replacement of the local constraint (the number of particles on each site is fixed) by a so-called global constraint (in the saddle point approximation), where the number of particles is fixed only as an average value for the whole crystal. There is no reason to believe that such an approximation is a good starting point for the description of strongly correlated systems. Besides, it is very difficult to take into account the fluctuations related to the replacement of a local constraint by a global one.

An alternative approach for spin Hamiltonians free of the local constraint problem has been proposed in the pioneering paper of Popov and Fedotov (PF) [12]. Based on the exact fermionic representation for $S = 1/2$ and $S = 1$ operators, where fermions are treated as quasiparticles with imaginary chemical potential, these authors demonstrated the power and simplification of the corresponding Matsubara diagram technique. For these two special cases the Matsubara frequencies are $\omega_n = 2\pi T(n + 1/4)$ for $S = 1/2$ and $\omega_n = 2\pi T(n + 1/3)$ for $S = 1$, providing a rigorous description of (and restricted to) the equilibrium situation. The semionic representation used by PF is neither fermionic nor bosonic, but reflects the fundamental Pauli nature of spins. Later, the generalization of the PF technique for arbitrary spin [13] was derived by introducing proper chemical potentials for spin fermions. The goal of this paper is to derive a method for nonequilibrium systems, which allows one to treat quantum spin Hamiltonians on the same footing as Fermi or Bose systems.

A long time ago Keldysh [14] proposed a novel approach for the description of kinetic phenomena in metals. This approach was found especially fruitful for normal metals [15], and, in many recent applications, for superconductors [16] and for disordered interacting (normal or superconducting) electron liquids [17], for example. The previous application of the real-time formalism to the quantum theory of Bose-Einstein condensation (BEC) [18] allowed the derivation of a Fokker-Planck equation,

which describes both kinetic and coherent stages of BEC. Moreover, Ref. [19] developed the closed-time path integral formalism for aging effects in quantum disordered systems being in contact with an environment. The Keldysh formalism in application to disordered systems (see [20,21]) also attracted interest some time ago as an alternative approach to the replica technique. The main advantage of closed-time contour calculations is an automatic normalization (disorder independent) of the partition function. In this paper we derive the Keldysh formalism for quantum spin systems (e.g., Heisenberg clean and disordered magnets, Kondo systems [22,23]), which is based on PF ideas of semionic representation.

We reformulate the PF concept by adopting it to real-time formalism. As an example, we consider $S = 1/2$. As it was first shown in [12] (see also [24]), the partition function of a spin system with Hamiltonian H_S can be replaced by the partition function of an effective "fermionic" system with Hamiltonian H_F as follows

$$Z_S = \mathrm{Tr} e^{-\beta \hat{H}_S} = (\pm i)^N \mathrm{Tr} e^{-\beta(\hat{H}_F \pm i\pi \hat{N}_F/2\beta)}, \quad (1)$$

where $\beta = 1/T$, and the usual fermionic representation of spin similar to, e.g., Abrikosov pseudofermions [6] is used: $S^+ = f_\uparrow^\dagger f_\downarrow$, $S^- = f_\downarrow^\dagger f_\uparrow$, $S^z = \frac{1}{2}(f_\uparrow^\dagger f_\uparrow - f_\downarrow^\dagger f_\downarrow)$, and $N_F = f_\uparrow^\dagger f_\uparrow + f_\downarrow^\dagger f_\downarrow$.

Representing spins as bilinear combinations of Fermi operators, we enlarged by a factor of 2 the Hilbert space of the Hamiltonian. In addition to physical states $|1,0\rangle$ and $|0,1\rangle$ two unphysical states $|1,1\rangle$ and $|0,0\rangle$ are introduced. Nevertheless, in the average over all states, unphysical states cancel each other, since $\mathrm{Tr}_{\mathrm{unphys}}[\exp(\mp i\pi/2)]^{N_F} = (\mp i)^0 + (\mp i)^2 = 0$. This representation being of semionic origin results in the conventional Matsubara diagram technique with $\omega_n = 2\pi T(n + 1/4)$ or $\omega_n = 2\pi T(n + 3/4)$, depending on the sign in expressions (1). Besides, one can introduce the auxiliary distribution function for quasiparticles [25],

$$f^{(1/2)}(\epsilon) = T\sum_n \frac{e^{i\omega_n \tau}|_{+0}}{i\omega_n - \epsilon} = \frac{1}{e^{\pm i\pi/2}\exp(\beta\epsilon) + 1}, \quad (2)$$

where $(\pm)$ signs in the exponent (2) are the same as in (1). We note that, since auxiliary Fermi fields do not represent the true quasiparticles of the problem, helping only to treat properly the spin operators, the distribution function for these objects in general should not be a real function, e.g., $f^{(1/2)} = n(2\epsilon) \mp \frac{i}{2}\,\mathrm{sech}(\epsilon/T)$, where $n(x) = [\exp(x/T) + 1]^{-1}$ is the standard Fermi distribution function. As we shall see for $S = 1/2$ and $S = 1$, $1 - 2\,\mathrm{Re} f^{(S)}(\epsilon) = B_S(\epsilon/T)$ is expressed in terms of the Brillouin function $B_S(x) = (1 + \frac{1}{2S}) \times \coth[(1 + \frac{1}{2S})x] - \frac{1}{2S}\coth(\frac{x}{2S})$, e.g., for $S = 1/2$, $B_{1/2}(x) = \tanh(x)$. We also note that in the $T \to 0$ limit the imaginary part of $f^{(1/2)}$ satisfies the identity $\mathrm{Im} f^{(1/2)}(x) = \mp i\pi T\delta(x)/2$.

The spin correlation functions of any order can be expressed in terms of the two-component field $\psi^T = (f_\uparrow f_\downarrow)$:

$$\langle S_{i_1}^{\alpha_1}(t_1)\cdots S_{i_n}^{\alpha_n}(t_n)\rangle = \mathrm{Tr}[\rho_0(\psi^\dagger\sigma_{i_1}^{\alpha_1}\psi)_{t_1}\cdots(\psi^\dagger\sigma_{i_n}^{\alpha_n}\psi)_{t_n}],$$

where $\rho_0 = \exp(-\beta H_0)/\mathrm{Tr}\exp(-\beta H_0)$ is the density matrix and σ denotes Pauli matrices. We included the term $i\pi N_F/(2\beta)$ into the Hamiltonian $H_0 = -h\sum_i S_i^z \pm i\pi T/2\sum_i N_F^{(i)}$ of noninteracting spins in a uniform external magnetic field h, since it exists both in the numerator and denominator of ρ_0.

Following the standard route [26] we can express the partition function of the problem containing spin operators as a path integral over Grassmann variables $\bar{\psi}, \psi$

$$\mathcal{Z}/\mathcal{Z}_0 = \int D\bar{\psi}D\psi \exp(i\mathcal{A}) \Big/ \int D\bar{\psi}D\psi \exp(i\mathcal{A}_0), \quad (3)$$

where actions $\mathcal{A}$ and $\mathcal{A}_0$ are taken as an integral along the closed-time contour $C_t + C_\tau$ which is shown in Fig. 1. The contour is closed at $t = -\infty + i\tau$ since $\exp(-\beta H_0) = T_\tau \exp(-\int_0^\beta H_0\, d\tau)$. We denote the ψ fields on the upper and lower sides of the contour C_t as ψ_1 and ψ_2, respectively. The fields Ψ stand for the contour C_τ. These fields provide matching conditions for $\psi_{1,2}$ and are excluded from final expressions. Taking into account the semionic boundary conditions for generalized Grassmann fields $\Psi^\mu(\beta) = i\Psi^\mu(0)$, $\bar{\Psi}^\mu(\beta) = -i\bar{\Psi}^\mu(0)$, one gets the matching conditions for $\psi_{1,2}$ at $t = \pm\infty$,

$$\psi_1^\mu(-\infty) = i\psi_2^\mu(-\infty), \qquad \psi_1^\mu(+\infty) = \psi_2^\mu(+\infty). \quad (4)$$

The correlation functions can be represented as a functional derivation of the generating functional

$$Z[\eta] = \mathcal{Z}_0^{-1}\int D\bar{\psi}D\psi \times \exp\Big(i\mathcal{A} + i\oint_C dt\,(\bar{\eta}\sigma^z\psi + \bar{\psi}\sigma^z\eta)\Big),$$

where η represents sources and the σ^z matrix stands for "causal" and "anticausal" orderings along the contour.

The on-site Green's functions (GF's) which are matrices 4×4 with respect to both Keldysh (lower) and spin (upper) indices are given by

$$G_{\mu\nu}^{\alpha\beta}(t,t') = -i\frac{\delta}{i\delta\bar{\eta}_\mu^\alpha(t)}\frac{\delta}{i\delta\eta_\nu^\beta(t')}Z[\eta]|_{\bar{\eta},\eta\to 0}.$$

After a standard shift transformation [26] of fields ψ the Keldysh GF of free PF fermions assumes the form

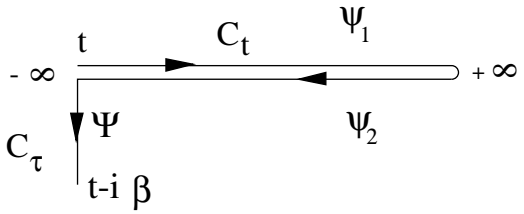

FIG. 1. Keldysh double side contour going along real-time axis $-\infty \to +\infty \to -\infty$ and "closed" in imaginary time.

$$G_0^{\alpha}(\epsilon) = G_0^{R,\alpha}\begin{pmatrix} 1 - f_\epsilon & -f_\epsilon \\ 1 - f_\epsilon & -f_\epsilon \end{pmatrix} - G_0^{A,\alpha}\begin{pmatrix} -f_\epsilon & -f_\epsilon \\ 1 - f_\epsilon & 1 - f_\epsilon \end{pmatrix},$$

where the retarded and advanced GF's are

$$G_0^{(R,A)\alpha}(\epsilon) = (\epsilon + \sigma^z_{\alpha\alpha} h/2 \pm i\delta)^{-1}, \qquad f_\epsilon = f^{(1/2)}(\epsilon). \tag{5}$$

The interdependence of matrix elements of the GF in Keldysh space is more transparent after rotation

$$\hat{G} \Rightarrow \frac{1 - i\sigma^y}{\sqrt{2}}\,\sigma^z G\,\frac{1 + i\sigma^y}{\sqrt{2}} = \begin{pmatrix} G^R & G^K \\ 0 & G^A \end{pmatrix}, \tag{6}$$

where $G_0^K = -i2\pi\delta(\epsilon \pm h/2)[B_{1/2}(\epsilon/T) \pm i\,\mathrm{sech}(\epsilon/T)]$. We emphasize that, unlike diagrammatic techniques for Fermi and Bose operators, the off-diagonal element (Keldysh component) in semionic representation is expressed in terms of a Brillouin function, containing correct information about occupied states. We recall that diagonal elements of the matrix (6) in "triangular" representation satisfy the Dyson equation providing the exact description of the system. The equation of motion for G^K generally constitutes the quantum-kinetic equation.

Let us illustrate the application of the Schwinger-Keldysh formalism for spin Hamiltonians. We consider the Heisenberg model with nearest neighbor interaction

$$H_{\mathrm{int}} = -\sum_{\langle ij\rangle} J_{ij}\left(\vec{S}_i\vec{S}_j - \frac{1}{4}\right) = \frac{1}{2}\sum_{\langle ij\rangle} J_{ij}\psi_i^\dagger\psi_j\psi_j^\dagger\psi_i\,.$$

We firstly discuss the *Néel solution* for the Heisenberg model with isotropic antiferromagnetic (AFM) exchange ($J < 0$). By applying the PF transformation to the partition function, one obtains the action as an integral along the closed-time Keldysh contour,

$$\mathcal{A} = \mathcal{A}_0 + \mathcal{A}_{\mathrm{int}} = \mathcal{A}_0 + \oint_C dt \sum_{\mathbf{q}} J(\mathbf{q})\vec{S}_{\mathbf{q}}(t)\vec{S}_{-\mathbf{q}}(t), \tag{7}$$

where $\mathcal{A}_0$ corresponds to noninteracting PF fermions

$$\mathcal{A}_0 = \oint_C dt \sum_i \bar{\psi}_i\begin{pmatrix} (G_0^{R,\alpha})^{-1} & 0 \\ 0 & (G_0^{A,\alpha})^{-1} \end{pmatrix}\psi_i\,. \tag{8}$$

We denote $J_{\mathbf{q}} = J\sum_{\langle\mathbf{l}\rangle} e^{i\mathbf{q}\mathbf{l}}$, $\nu_{\mathbf{q}} = J_{\mathbf{q}}/J_0$ and apply the eight-component PF representation with $\psi^T = (\tilde{\psi}_{\mathbf{k}}^T\tilde{\psi}_{\mathbf{k}+\mathbf{Q}}^T)$, where $\mathbf{Q} = (\pi, \ldots, \pi)$ for hypercubic lattice. To decouple the four-fermion term along the Keldysh contour with the help of the Hubbard-Stratonovich transformation we introduce the two-Keldysh-component *vector* (Bose) field $\vec{\Phi}^T = (\vec{\Phi}_1\vec{\Phi}_2)$. As a result we obtain

$$\mathcal{A}_{\mathrm{int}} = -\,\mathrm{Tr}(\vec{\Phi}_{\mathbf{q}}^T J_{\mathbf{q}}^{-1}\sigma^z\vec{\Phi}_{\mathbf{q}}) + \mathrm{Tr}(\bar{\psi}\vec{\Phi}_\mu\vec{\sigma}\gamma^\mu\psi)\,. \tag{9}$$

Now we integrate out ψ fields and express the effective action in terms of $\vec{\Phi}$ fields

$$\mathcal{A}_{\mathrm{eff}} = -\,\mathrm{Tr}(\vec{\Phi}_{\mathbf{q}}^T J_{\mathbf{q}}^{-1}\sigma^z\vec{\Phi}_{\mathbf{q}}) + \mathrm{Tr}\ln(G_0^{-1} + \vec{\Phi}_\mu\vec{\sigma}\gamma^\mu),$$

where $\gamma^\mu = (\sigma^z \pm 1)/2$ acts in Keldysh space. Since in general $\vec{\Phi}$ is a time- and space-dependent fluctuating field, the partition function (3) cannot be evaluated exactly. Nevertheless, when a magnetic instability occurs, we can represent the longitudinal component of this field as a superposition of a staggered time-independent part ("staggered condensate") and a fluctuating field

$$\Phi_\mu^z(\mathbf{q},\omega) = \tfrac{1}{2}\mathcal{N}J_{\mathbf{q}}\gamma^\mu\delta_{\mathbf{q},\mathbf{Q}}\delta(\omega) + \phi_\mu^z(\mathbf{q},\omega), \tag{10}$$

where $\mathcal{N}$ is a staggered magnetization and $\Phi_\mu^\pm(\mathbf{q},\omega) = \phi_\mu^\pm(\mathbf{q},\omega)$ with the matching conditions at $t = \pm\infty$,

$$\phi_1^\pm(-\infty) = \phi_2^\pm(-\infty), \qquad \phi_1^\pm(+\infty) = \phi_2^\pm(+\infty). \tag{11}$$

We expand $\mathrm{Tr}\ln(G_0^{-1} + \vec{\phi}_\mu\vec{\sigma}\gamma^\mu)$ in accordance with

$$\mathrm{Tr}\ln(\cdots) = \mathrm{Tr}\ln G_0^{-1} + \sum_{n=1}^{\infty}\frac{(-1)^{n+1}}{n}(G_0\vec{\phi}_\mu\vec{\sigma}\gamma^\mu)^n. \tag{12}$$

The spectrum of the excitations (AFM magnons) can be defined as poles of the transverse GF $D^{+-}_{\mathbf{x},t} = D(\mathbf{x},t) = -i\langle T_C\phi_1^+(\mathbf{x},t)\phi_1^-(0,0)\rangle$. The procedure of the calculation of this GF is similar to that for a fermionic GF. By introducing the sources and evaluating (12), one gets

$$D_0(\omega) = D_0^R\begin{pmatrix} 1 + N_\omega & N_\omega \\ 1 + N_\omega & N_\omega \end{pmatrix} - D_0^A\begin{pmatrix} N_\omega & N_\omega \\ 1 + N_\omega & 1 + N_\omega \end{pmatrix},$$

where the retarded and advanced magnon GF's are

$$D_0^{R,A}(\mathbf{q},\omega) = [\omega - \omega(\mathbf{q}) \pm i\delta]^{-1}, \qquad N_\omega = [\exp(\beta\omega) - 1]^{-1}.$$

The magnon spectrum $\omega_{\mathbf{q}}$ is determined by the zeros of the expression $J_{\mathbf{q}}^{-1} - \Pi_2^{+-}(\omega)$ (see Fig. 2a) in equilibrium

$$\omega_{\mathbf{q}} = |J_0|\mathcal{N}\sqrt{1 - \nu_{\mathbf{q}}^2} \Rightarrow c|\mathbf{q}|\,, \qquad \mathcal{N} = \tanh\left(\frac{J_{\mathbf{Q}}\mathcal{N}}{2T}\right). \tag{13}$$

The magnon damping is defined by four-magnon processes Π_4^{+-+-}, shown in Fig. 2b. The derivation of the kinetic equation and calculation of magnon damping is reserved here for a detailed publication. The results (13) (and similar for quantum FM) are in full agreement with the spin-wave theory (see, for example, Refs. [2] and [3,7]).

The second possibility to decouple the four-fermion term in the Heisenberg model is provided by the bilocal *scalar* bosonic field Λ_{ij} depending on two sites. By introducing new coordinates $\vec{R} = (\vec{R}_i + \vec{R}_j)/2$, $\vec{\rho} = \vec{R}_i - \vec{R}_j$

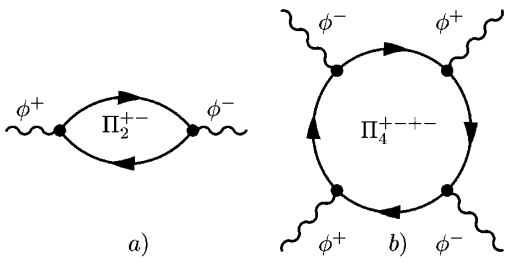

FIG. 2. Feynman diagrams contributing to dispersion (a) and damping (b) of magnons. The solid line denotes PF fermions.

and applying a Fourier transformation, we obtain the effective action

$$\mathcal{A}_{\text{eff}} = -\tfrac{1}{2}\,\mathrm{Tr}(\Lambda^T_{Pq_1} J^{-1}_{\mathbf{q_1}-\mathbf{q_2}} \sigma^z \Lambda_{Pq_2}) + \mathrm{Tr}\ln(G_0^{-1} - \Lambda_\mu \gamma^\mu)\,.$$

This effective action describes the nonequilibrium quantum spin liquid (SL). We confine ourselves to consider the uniform phase [27] of *resonant valence bonds* (RVB) in 2D antiferromagnets. It is suitable to rewrite the functional in new variables, namely, the amplitude Δ and the phase $\Theta = \vec{p}\vec{A}(\vec{R})$, according to formula

$$\Lambda_\mu^{\langle ij\rangle}(\vec{R},\vec{p}) = \Delta(\vec{p}) J \gamma^\mu \exp[i\vec{p}\vec{A}_\mu(\vec{R})]\,. \qquad (14)$$

The exponent in (14) stands for gauge fluctuations to be taken in eikonal approximation. The spectrum of excitations in the uniform SL is defined by the zeros of $\pi^{R,\alpha\beta}_{q,\omega} = \mathrm{Tr}[\,p^\alpha p^\beta (G^R_{p+q} G^K_p + G^K_{p+q} G^A_p) + \delta_{\alpha\beta} f(J_{\mathbf{p}}\Delta)]$ in equilibrium [28] and is purely diffusive (see, e.g., [27])

$$\omega_{\mathbf{q}} = iJ\Delta|\mathbf{q}|^3, \qquad \Delta = -\sum_{\mathbf{q}} \nu(\mathbf{q}) \tanh\!\left(\frac{J_{\mathbf{q}}\Delta}{T}\right). \qquad (15)$$

The quantum kinetic equation for nonequilibrium spin RVB liquids can be obtained by taking into account the higher order diagrams similar to Fig. 2b with currentlike vertices and will be presented elsewhere.

We discuss finally the Schwinger-Keldysh formalism for spins $S > 1/2$. As shown by Popov and Fedotov for $S = 1$, it is possible to eliminate the unphysical states by introducing three-component fermions $\psi^T = (f_\uparrow f_0 f_\downarrow)$ with imaginary chemical potential $\lambda = -i\pi T/3$. The boundary conditions for Ψ on the imaginary part of the contour C_τ read as follows: $\Psi^\mu(\beta) = e^{i\pi/3}\Psi^\mu(0)$, $\bar{\Psi}^\mu(\beta) = e^{-i\pi/3}\bar{\Psi}^\mu(0)$. As a result, the distribution function in equilibrium is $f^{(1)}(\epsilon) = 1/[e^{\pm i\pi/3}\exp(\epsilon/T) + 1]$. Thus, the Schwinger-Keldysh formalism with 6×6 matrices for GF (6) and $f_\epsilon = f^{(1)}(\epsilon)$ in equilibrium is obtained. The off-diagonal Keldysh component is given by

$$G_0^K = -i2\pi\delta(\epsilon \pm h) \times \left[B_1(\epsilon/T) \pm i\sqrt{3}\sinh\!\left(\frac{\epsilon}{2T}\right) \Big/ \sinh\!\left(\frac{3\epsilon}{2T}\right)\right].$$

For arbitrary spin values $S > 1$ there is no unique imaginary chemical potential for $2S + 1$ component PF fermions, but instead they are distributed on each lattice site j according to

$$P(\lambda_j) = \sum_{l=0}^{[S-1/2]} a_l \delta(\lambda_j - \lambda_l)\,,$$

$$a_l = \frac{2i}{2S+1} \sin\!\left(\pi\,\frac{2l+1}{2S+1}\right),$$

where $\lambda_l = i\pi T(2l+1)/(2S+1)$ [13]. Thus, the Schwinger-Keldysh approach can be generalized for arbitrary spin values in the same fashion as for $S = 1/2$ and $S = 1$.

In summary, we derived the technique applicable for nonequilibrium dynamics of quantum spin systems. Unlike other techniques this approach takes into account the constraint rigorously and allows one to treat spins on the same footing as Fermi and Bose systems. The method derived can be applied especially to problems where the local constraint becomes important, e.g., quantum phase transition in clean and disordered magnets, spin glasses, Kondo lattices, nonequilibrium Kondo systems, etc.

We acknowledge useful discussions with L. V. Keldysh and many helpful conversations with H. Feldmann and K. Kikoin. This work is supported by the SFB410 (II-VI semiconductors). M. N. K. expresses his gratitude to the Alexander von Humboldt Foundation for support of his research.

[1] T. Holstein and H. Primakoff, Phys. Rev. **58**, 1098 (1940); F. Dyson, Phys. Rev. **102**, 1217 (1956); S. V. Maleev, Sov. Phys. JETP **6**, 776 (1958).
[2] A. Auerbach, *Interacting Electrons and Quantum Magnetism* (Springer-Verlag, Berlin, 1994).
[3] D. Arovas and A. Auerbach, Phys. Rev. B **38**, 316 (1988).
[4] A. Chubukov, Phys. Rev. B **44**, 12 318 (1991).
[5] I. Affleck and J. B. Marston, Phys. Rev. B **37**, 3774 (1988).
[6] A. A. Abrikosov, Physics **2**, 5 (1965).
[7] V. G. Vaks, A. I. Larkin, and S. A. Pikin, Sov. Phys. JETP **26**, 188 (1968); **26**, 647 (1968).
[8] A. M. Tsvelik, *Quantum Field Theory in Condensed Matter Physics* (Cambridge University Press, Cambridge, UK, 1995).
[9] P. Coleman, C. Pepin, and A. M. Tsvelik, Phys. Rev. B **62**, 3852 (2000).
[10] J. Hubbard, Proc. R. Soc. London. A **285**, 542 (1965).
[11] M. Gaudin, Nucl. Phys. **15**, 89 (1960).
[12] V. N. Popov and S. A. Fedotov, Sov. Phys. JETP **67**, 535 (1988).
[13] O. Veits *et al.,* J. Phys. I (France) **4**, 493 (1994).
[14] L. V. Keldysh, Sov. Phys. JETP **20**, 1018 (1965); J. Schwinger, J. Math. Phys. **2**, 407 (1961).
[15] J. Rammer and H. Smith, Rev. Mod. Phys. **58**, 323 (1986).
[16] M. V. Feigel'man, A. I. Larkin, and M. A. Skvortsov, Phys. Rev. B **61**, 12 361 (2000), cond-mat/0008463.
[17] A. Kamenev and A. Andreev, Phys. Rev. B **60**, 2218 (1999); C. Chamon, A. Ludwig, and C. Nayak, Phys. Rev. B **60**, 2239 (1999).
[18] H. T. C. Stoof, Phys. Rev. Lett. **78**, 768 (1997).
[19] L. Cugliandolo and G. Lozano, Phys. Rev. B **59**, 915 (1999).
[20] R. Kree, Z. Phys. B **65**, 505 (1987).
[21] H. Sompolinsky and A. Zippelius, Phys. Rev. Lett. **47**, 359 (1981).
[22] V. Barzykin and I. Affleck, Phys. Rev. B **57**, 432 (1997).
[23] M. Kiselev and R. Oppermann, JETP Lett. **71**, 250 (2000).
[24] C. Gros and M. D. Johnson, Physica (Amsterdam) **165B–166B**, 985 (1990).
[25] J. Stein and R. Oppermann, Z. Phys. B **83**, 333 (1991).
[26] V. S. Babichenko and A. N. Kozlov, Solid State Commun. **59**, 39 (1986).
[27] L. B. Ioffe and A. I. Larkin, Phys. Rev. B **39**, 8988 (1989); P. A. Lee and N. Nagaosa, Phys. Rev. B **46**, 5621 (1992).
[28] M. Reizer, Phys. Rev. B **39**, 1602 (1989).

JETP Letters, Vol. 71, No. 6, 2000, pp. 250–254. From Pis'ma v Zhurnal Éksperimental'noĭ i Teoreticheskoĭ Fiziki, Vol. 71, No. 6, 2000, pp. 359–365.

CONDENSED MATTER

Spin-Glass Transition in a Kondo Lattice with Quenched Disorder[1]

M. N. Kiselev*, ** and R. Oppermann*, ***

** Institüt für Theoretische Physik, Universität Würzburg, D-97074 Würzburg, Germany*

*** Russian Research Center Kurchatov Institute, pl. Kurchatova 1, Moscow, 123182 Russia*

**** University of Oxford, Department of Physics, OX1 3NP Oxford, UK*

Received January 24, 2000; in final form, February 18, 2000

We use the Popov–Fedotov representation of spin operators to construct an effective action for a Kondo lattice model with quenched disorder at finite temperatures. We study the competition between the Kondo effect and frozen spin order in Ising-like spin glass. We present the derivation of new mean-field equations for the spin-glass order parameter and analyze the effects of screening of localized spins by conduction electrons on the spin-glass phase transition. © *2000 MAIK "Nauka/Interperiodica".*

PACS numbers: 75.20.Hr; 75.10.Nr; 75.30.Mb

One of the most interesting questions of physics of heavy-fermion compounds is the competition between Kondo screening of localized spins by conduction electrons (CE) and ordering of these spins due to Ruderman–Kittel–Kasuya–Yosida (RKKY) interaction (see, e.g., [1]). The screening is attributed to the Kondo effect, viz., the resonance scattering of an electron on a magnetic atom with simultaneous change of the spin projection. In dilute alloys such scattering results in a sharp resonance at the Fermi level with characteristic energy width $\epsilon \sim T_K \sim \epsilon_F \exp(-\alpha^{-1})$, where T_K is the Kondo temperature, J is the coupling constant, ρ is the density of states of CE at the Fermi level, and $\alpha = \rho J$. As was recently discussed (see, e.g., [2, 3]), such competition can be responsible for the non-Fermi-liquid behavior observed in some heavy-fermion compounds. Most of such materials share two characteristics: proximity to the magnetic region of an appropriate phase diagram (usually temperature vs. pressure or chemical composition) and disorder due to chemical substitution. In many respects, the concentrated Kondo systems, e.g., the lattice of magnetic atoms interacting with CE "bath" [Kondo lattice (KL)], show striking similarities to dilute Kondo systems. The Kondo temperature in these systems is a characteristic crossover temperature at which spins transform their local properties to some itinerant Fermi-liquid behavior determining the low-temperature regime of heavy-fermion compounds. Non-Fermi-liquid behavior in a heavy-fermion system is then mainly attributed to reducing the Kondo temperature and possibly even suppressing it to zero. In turn, the magnetic or spin glass (SG) transition can also be suppressed due to the interplay between Kondo scattering and spin–spin interaction. Thus, such an interplay can result in a quantum phase transition [2] when both Kondo and magnetic temperatures are equal to zero at some finite doping. The role of chemical substitution in this case is to "tune" the Fermi level of a metallic system providing sharp Kondo resonance.

The problem of competition between the RKKY and Kondo interactions in a clean system was studied for the first time by Doniach [4] in the "Kondo necklace" model. The transition typically takes place between a paramagnetic metal and a magnetic (usually AFM) metal. In this case, there are two possibilities: the compound will have long-range magnetic order when the RKKY interaction is sufficiently large compared with the Kondo interaction, or the compound will be paramagnetic due to the quenching of magnetic moments of the rare earth atoms and the ground state has the features of a Kondo-singlet state. Nevertheless, in the region $T^M_{\mathrm{RKKY}} \sim T_K$ the competition between magnetic and Kondo interactions results in a dramatic change in the "naive" Doniach diagram (see [5]). Namely, both Kondo and magnetic temperatures are strongly suppressed and a spin-liquid state (e.g., of resonance valence bond type [6]) occurs.

The goal of this letter is to present some results concerning the competition between the Kondo effect and Ising-like SG transition, which is in many aspects similar to the magnetic instability. We study mechanisms of suppressing the SG transition and effects of screening in a disordered environment. In this paper, we consider the high-temperature regime of the KL model. We leave aside the issue of the ground-state properties and especially the question whether the non-Fermi-liquid behavior is a generic feature of vicinity to a quantum phase transition for a future publication.

[1] This article was submitted by the authors in English.

The Hamiltonian of the KL model with additional quenched randomness of exchange interaction between localized spins is given by

$$H_{KL} = \sum_{k\sigma}\varepsilon_k c^\dagger_{k\sigma}c_{k\sigma} + J\sum_i\left(\mathbf{s}_i\mathbf{S}_i + \frac{1}{4}n_iN_i\right) - \sum_{ij}I_{ij}(S^z_iS^z_j + \lambda S^+_iS^-_j). \quad (1)$$

The system under consideration is a periodic lattice of magnetic atoms modeled by f orbitals interacting with metallic background spin density operator $\mathbf{s}_i = \frac{1}{2}c^\dagger_{i\alpha}\boldsymbol{\sigma}_{\alpha\alpha'}c_{i\alpha'}$. The first term in Hamiltonian (1) describes the kinetic energy of CE, and the second stands for the Kondo coupling ($J > 0$). We denote $n_i = \sum_\sigma c^\dagger_{i,\sigma}c_{i,\sigma}$ as the CE density operator. The identity $N_i = 1$ describes the half-filled f-electron shell. Quenched independent random variables I_{ij} with distribution $P(I_{ij}) \sim \exp(-I^2_{ij}N/2I^2)$ stand for direct spin–spin interaction [7]. We assume that this random interaction is of RKKY origin,[2] namely, for d-dimensional system $I \sim \alpha^2\epsilon_F l^{-d}$, where l is the lattice constant in the magnetic sublattice. The magnetic effects can also be included in our approach by introducing the nonzero standard deviation $\Delta I = \bar{I}_{\mathrm{RKKY}}$ into the distribution $P(I_{ij})$, which, in turn, can result in additional competition between SG and AFM (or, rarely, FM) states. For simplicity, we neglect these effects in this letter and concentrate on the interplay between the Kondo interaction and the effects of bond disorder. Since the indirect RKKY interaction through CE is mostly determined by "fast" electrons with characteristic energies $\epsilon \sim \epsilon_F \gg T_K$, we also neglect the Kondo renormalizations of RKKY exchange.

As has been well known for a long time, the spin $S = 1/2$ matrices can be exactly replaced by bilinear combination of Fermi operators

$$S^z_i = \frac{1}{2}(f^\dagger_{i\uparrow}f_{i\uparrow} - f^\dagger_{i\downarrow}f_{i\downarrow}),$$

$$S^+_i = f^\dagger_{i\uparrow}f_{i\downarrow}, \quad S^-_i = f^\dagger_{i\downarrow}f_{i\uparrow}.$$

Nevertheless, most fermionic representations of spin are not free of constraint problem. For this reason, the dimensionality of space in which these operators act is always greater than the dimensionality of the spin matrices. Elimination of unphysical states is a serious problem which makes the diagrammatic techniques quite complicated. Moreover, in most cases, the analytic continuation of Feynman diagrams becomes extremely difficult. To avoid the main difficulties related to constraint, the new representation for spin operators was proposed in the long-forgotten paper of Popov and Fedotov [9]. In this representation the partition function of the problem containing spin operators (H_S) can be easily expressed in terms of new fermions with imaginary chemical potential (H^f_S):

$$Z_S = \mathrm{Tr}e^{-\beta H_S} = i^N\mathrm{Tr}\exp\{-\beta(H^f_S + i\pi N_f/2\beta)\},$$

$$N_f = \sum_{i\sigma}f^\dagger_{i\sigma}f_{i\sigma}, \quad \beta = 1/T.$$

As a result, there is no constraint, the unphysical states are eliminated, and the standard Matsubara–Abrikosov–Gor'kov diagrammatic technique is obtained [9–11].

We sketch our derivation of the effective action and of resulting mean-field equations for the KL model in order to make explicit the approximations adopted and the physics underlying these approximations. To construct the path-integral representation for the partition function, the new Grassmann variables $c^\dagger_{i\alpha} \longrightarrow \bar{\Psi}_{i\sigma}$, $c_{i\sigma} \longrightarrow \Psi_{i\sigma}$ for CE with chemical potential μ and $f^\dagger_{i\alpha} \longrightarrow \bar{a}_{i\sigma}$, $f_{i\alpha} \longrightarrow a_{i\alpha}$ for Popov–Fedotov spin operators ($S = 1/2$) are introduced. The Euclidean action for the KL model is given by

$$\mathcal{A} = \int_0^\beta d\tau\left(\sum_{i\alpha}[\bar{\Psi}_{i\alpha}(\tau)(\partial_\tau + \mu)\Psi_{i\alpha}(\tau) + \bar{a}_{i\alpha}(\tau)(\partial_\tau - i\pi T/2)a_{i\alpha}(\tau)] - H_{int}(\tau)\right), \quad (2)$$

where the generalized Grassmann fields satisfy the following boundary conditions: $\Psi_{i\alpha}(\beta) = -\Psi_{i\alpha}(0)$, $\bar{\Psi}_{i\alpha}(\beta) = -\bar{\Psi}_{i\alpha}(0)$, $a_{i\alpha}(\beta) = ia_{i\alpha}(0)$, $\bar{a}_{i\alpha}(\beta) = -i\bar{a}_{i\alpha}(0)$.

In this paper, we consider $\lambda = 0$, which corresponds to the Sherrington–Kirkpatrik [12] spin-glass model. Such an anisotropy of RKKY interaction can be associated, e.g., with lattice geometry. In the case of the Ising-like model, the dynamical fluctuations in the spin subsystem appear only due to the interaction with conduction electrons and, in the high temperature regime $T \sim T_{\mathrm{SG}}$, can be neglected. To study the influence of Kondo scattering on the SG transition temperature T_{SG}, we use standard replica trick $\Psi_i(\tau) \longrightarrow v^a_i(\tau)$, $a_i(\tau) \longrightarrow \varphi^a_i(\tau)$, $a = 1, \ldots, n$. Then the free energy of the model

[2] It has been pointed out in [8] that the presence of nonmagnetic impurities makes the RKKY interaction a random interaction even in the case of regular arrangement of magnetic moments.

can be calculated (see, e.g., [13]) by taking the formal limit $n \longrightarrow 0$ in

$$\langle Z^n \rangle_{av} = \prod \int dI_{ij} P(I_{ij}) \prod D[\varphi^a_{i,\sigma} \nu^a_{i,\sigma}] \times \exp\left(\mathcal{A}_0[\nu^a, \varphi^a] - \int_0^\beta d\tau H_{int}(\tau) \right), \quad (3)$$

where $\mathcal{A}_0$ corresponds to noninteracting fermions.

As we already mentioned, to consider the competition between the Kondo scattering and the trend of disorder, we assume that the magnetic temperature $T^M_{\mathrm{RKKY}} \ll T^*$, where T^* stands for a characteristic temperature corresponding to the Kondo temperature in the lattice. This assumption allows one to decouple the Kondo interaction term $H^K_i = -\frac{J}{2} \bar{\nu}^a_{i,\sigma} \varphi^a_{i,\sigma} \bar{\varphi}^a_{i,\sigma'} \nu^a_{i,\sigma'}$ in each site by the replica-dependent Hubbard–Stratonovich field ψ^a_i [14]. Performing the average over the random potential in (3) results in

$$\langle Z^n \rangle_{av} = \prod \int D[\nu^a, \varphi^a, \psi^a] \exp\left(\mathcal{A}_0 + \frac{I^2}{4N} \mathrm{Tr}[X^2] + \int_0^\beta d\tau \sum_{i,a,\sigma} \left\{ \psi^a_i \bar{\nu}^a_{i\sigma} \varphi^a_{i\sigma} + \psi^{a*}_i \bar{\varphi}^a_{i\sigma} \nu^a_{i\sigma} - \frac{2}{J} |\psi^a_i|^2 \right\} \right) \quad (4)$$

with

$$X^{ab}(\tau, \tau') = \sum_i \sum_{\sigma,\sigma'} \bar{\varphi}^a_{i,\sigma}(\tau) \sigma \varphi^a_{i,\sigma}(\tau) \bar{\varphi}^b_{i,\sigma'}(\tau') \sigma' \varphi^b_{i,\sigma'}(\tau').$$

The next step is to perform the Gaussian integration over the replica-dependent Grassmann field ν^a describing CE and to decouple the eight-fermion term $\mathrm{Tr}[X^2]$ with the help of Q matrices (see details in [10]). As a result, the partition function is given by

$$\langle Z^n \rangle_{av} = \int D[Q] \exp\left(-\frac{1}{4} (\beta I)^2 N \mathrm{Tr}[Q^2] + \sum_i \ln \left\{ \prod \int D[\varphi^a, \psi^a] \times \exp\left[\sum_a \sum_{\{\omega\}} \bar{\varphi}^a_{i,\sigma} \mathcal{G}^{-1}_a \varphi^a_{i\sigma} + \frac{1}{2} (\beta I)^2 \mathrm{Tr}[QX] \right] \right\} \right), \quad (5)$$

where $\mathcal{G}^{-1}$ is the inverse Green's function for Popov–Fedotov fermions depending on Matsubara frequencies $\omega_n = 2\pi T(n + 1/4)$ (see details in [9]),

$$\mathcal{G}^{-1}_a = i\omega_{n_1} \delta_{\omega_{n_1}, \omega_{n_2}} - T \sum_\epsilon \psi^{a*}_i(\epsilon_l + \omega_{n_1}) \times G_0(-i\nabla_i, \epsilon_l) \psi^a_i(\epsilon_l + \omega_{n_2}), \quad (6)$$

and $G_0(-i\nabla, \epsilon_l) = (i\epsilon_l - \varepsilon(-i\nabla) + \mu)^{-1}$ stands for the CE Green's function $\epsilon_l = 2\pi T(l + 1/2)$.

We are still left with a term of fourth order residing in $\mathrm{Tr}[QX]$ and cannot evaluate the Grassmann integral directly. Consequently, a second decoupling is needed. To perform it, we stress that we do not intend to deal with dynamical behavior here and confine ourselves by high temperature regime in the vicinity of the SG transition such that the lowest Matsubara frequency is sufficient. Assuming this and recalling that the spatial fluctuations are suppressed by the choice of infinite-range interaction [12], one can consider Q as a constant saddle-point matrix under condition $Q = Q^T$. The elements of this matrix will later be determined self-consistently from the saddle-point condition. Assuming that the elements of Q are $Q^{aa}_{SP} = \tilde{q}$ and $Q^{a \neq b}_{SP} = q$, one can decouple the $\mathrm{Tr}[QX]$ term by introducing replica-independent z and replica-dependent y^a fields and map the KL problem with disorder onto an effective one-site interacting spin system coupled to an external local replica-dependent magnetic field:

$$\langle Z^n \rangle_{av} = \exp\left(-\frac{1}{4} (\beta I)^2 N (n\tilde{q}^2 + n(n-1)q^2) + \sum_i \ln \left[\prod \int D[\varphi^a, \psi^a] \int_z^G \int_{y^a}^G \exp(\mathcal{A}[\varphi^a, \psi^a, y^a, z]) \right] \right), \quad (7)$$

where $\int_z^G f(z)$ denotes $\int_{-\infty}^{\infty} dz/\sqrt{2\pi} \exp(-z^2/2) f(z)$,

$$\mathcal{A}[\varphi^a, \psi^a, y^a, z] = \sum_{a,\sigma} \bar{\varphi}^a_\sigma [\mathcal{G}^{-1}_a - \sigma H(y^a, z)] \varphi^a_\sigma - \frac{2}{J} \sum_\omega |\psi^a(\omega)|^2 \quad (8)$$

and $H(y^a, z) = I\sqrt{q}\, z + I\sqrt{\tilde{q} - q}\, y^a$ is the effective local magnetic field. Note that the variable $q = \langle S^a_i S^b_i \rangle$ corresponds to the Edwards–Anderson SG order parameter when the limit $n \longrightarrow 0$ is taken. Nevertheless, the diagonal element $\tilde{q}$ can be set to neither zero nor one, in contrast to the classical Ising glass theory, because of dynamical effects due to the interaction with the CE bath. To take into account this interaction, we include a replica-dependent magnetic field into the bare Green's function $\mathcal{G}^a_{0\sigma} = (i\omega_n - \sigma H(y^a, z))^{-1}$ and perform the inte-

gration over Popov–Fedotov Grassmann variables with the help of the expression

$$\mathrm{Tr}\ln(\mathcal{G}_a^{-1} - \sigma H) = \ln(2\cosh(\beta H)) + \mathrm{Tr}\sum_{m=1}^{\infty}\frac{(-1)^{m+1}}{m}(\mathcal{G}^a_{0\sigma}(H)\Sigma(\psi^a))^m, \quad (9)$$

where $\Sigma(\psi^a) = -T\sum_{\epsilon}\psi_i^{a*}(\epsilon + \omega_{n_1})G_0(-i\nabla_i, \epsilon)\psi_i^a(\epsilon + \omega_{n_2})$ depends on the variable ψ "responsible" for Kondo interaction. Calculating the first term in expansion (9), one gets the following expression for the effective "bosonic" action in the one-loop approximation:

$$\mathcal{A}[\psi^a, H] = \ln(2\cosh(\beta H(y^a, z))) - \frac{2}{J}\sum_n [1 - J\Pi(i\Omega_n, H(y^a, z))]|\psi^a|^2 - O(|\psi^a|^4). \quad (10)$$

The polarization operator Π in the limit $T, H \ll \epsilon_F$ is given by

$$\Pi(i\Omega_n, H) = -\beta^{-1}\sum_{n,\mathbf{k},\sigma} G_0(\mathbf{k}, i\epsilon_n + i\Omega_n)\mathcal{G}_{0\sigma}(i\epsilon_n, H) \xrightarrow{\Omega_n = 0} \rho(0)\left[\ln\left(\frac{\epsilon_F}{\sqrt{H^2 + \pi^2\beta^{-2}/4}}\right) + \frac{\pi}{2\cosh(\beta H)} + O\left(\frac{H^2}{\epsilon_F^2}\right)\right]. \quad (11)$$

When $H = 0$, the coefficient in front of $|\psi^a|^2$ in Eq. (10) changes its sign at $T^* \sim \epsilon_F\exp(-\alpha^{-1})$. This is a manifestation of the single-impurity Kondo effect (see, e.g., [14, 15]).

One can now perform the Gaussian integration over ψ^a fields in Eq. (7) by the stationary phase method:

$$\int D[\psi^a]\exp(\delta\mathcal{A}[\psi^a]) = \exp(-\mathrm{Tr}\ln[1 - J\Pi(i\Omega_n, H(y^a, z))]).$$

After the last step, namely, integration over replica-dependent field y^a, the limit $n \longrightarrow 0$ can be taken. The free energy per site $f = \beta^{-1}\lim_{n\to 0}(1 - \langle Z^n\rangle_{av})/nN$ is given by

$$\beta f(\tilde q, q) = \frac{1}{4}(\beta I)^2(\tilde q^2 - q^2) - \int_z^G \ln\left(\int_y^G \frac{2\cosh(\beta H(y, z))}{1 - J\Pi(0, H(y, z))}\right). \quad (12)$$

New equations for q, $\tilde q$ are determined by conditions $\partial f(\tilde q, q)/\partial\tilde q = 0$, $\partial f(\tilde q, q)/\partial q = 0$:

$$\frac{1}{2}(\beta I)^2\tilde q = \int_z^G \frac{\partial\ln\mathcal{F}}{\partial\tilde q}, \quad \frac{1}{2}(\beta I)^2 q = -\int_z^G \frac{\partial\ln\mathcal{F}}{\partial q}, \quad \mathcal{F} = \int_y^G \frac{2\cosh(\beta H(y, z))}{1 - J\Pi(0, H(y, z))}. \quad (13)$$

Eqs. (12), (13) contain the key result of the paper. They represent the solution of the KL problem with quenched disorder on a replica symmetrical level. To demonstrate some interesting physical effects described by these equations, let us consider the case $T \sim T_{SG} \geq T^*$ (Kondo high-temperature limit). Since $H(y^a, z)$ is a dynamical variable, we break the parametrical region of H to several pieces. First, when $H \gg T, T^*$, the logarithm in Eq. (11) is cut by H and there are no temperature-dependent Kondo corrections to the mean field equations. This corresponds to the limit $T^* \ll I$ providing frozen spins and preventing them from resonance scattering.[3] Nevertheless, when $T^* \sim I$, the region $H \leq T$ becomes very important. We calculate $\mathcal{F}$ expanding the rhs of Eq. (12) up to $(H/T)^2$:

$$\ln(C\mathcal{F}_{z,\tilde q,q}) = -\frac{1}{2}\ln(1 + \gamma u^2 r^2) + \frac{u^2}{2}\frac{r^2 - q\gamma z^2}{1 + \gamma u^2 r^2} + \ln\left[\cosh\left(\frac{uz\sqrt{q}}{1 + \gamma u^2 r^2}\right)\right]. \quad (14)$$

We use the following shorthand notations: $u = \beta I$, $\gamma = 2c/\ln(T/T^*)$, $r^2 = \tilde q - q$, and $C = 2c\alpha/\gamma$ with $c = \pi/4 + 2/\pi^2 \sim 1$. We note again that when $J = 0$, which corresponds to the absence of Kondo interaction,

$$\mathcal{F}(z, \tilde q, q) = \exp\left(\frac{1}{2}(\beta I)^2(\tilde q - q)\right)\cosh(\beta I z\sqrt{q})$$

and the standard Sherrington–Kirkpatrik equation [12] takes place, providing, e.g., an exact identity $\tilde q = 1$.

In the vicinity of the phase-transition point, Eq. (13) reads

$$\tilde q = 1 - \frac{2c}{\ln(T/T^*)} + O\left(\frac{1}{\ln^2(T/T^*)}\right), \quad q = \int_z^G \tanh^2\left(\frac{\beta I z\sqrt{q}}{1 + 2c(\beta I)^2(\tilde q - q)/\ln(T/T^*)}\right) + O\left(\frac{q}{\ln^2(T/T^*)}\right). \quad (15)$$

[3] We also note that when $T^* \gg I$ the SG transition does not happen.

These equations describe a second-order transition in an SG Ising-like Sherrington–Kirkpatrik[4] system coupled with a CE bath in the presence of Kondo scattering. Taking the limit $q \longrightarrow 0$, we estimate the temperature of SG transition $(T_{SG}/I)^2 = 1 - 4c/\ln(T_{SG}/T^*) - \ldots < 1$. Thus, the Kondo-scattering resonance results in depression of the SG-transition temperature due to the screening effects in the same way as magnetic moments and one-site susceptibility are screened in the single-impurity Eq. Kondo problem [15]. This screening shows up at large time scale $t \geq 1/T^*$ and affects both diagonal and nondiagonal elements of the Q matrix. Moreover, $\tilde{q}$ becomes partially screened well above the SG transition point. Recalling that $H \sim Iy\sqrt{\tilde{q}}$, one can see that our assumption $H/T \leq 1$ is consistent with Eq. (15) even if $T \sim T_{SG}$. It is necessary to note that a growing SG order parameter in Eqs. (10)–(11) suppresses the Kondo effect and also provides a broader validity domain for Eq. (15). We leave the self-consistent analysis of Eqs. (12), (15) for a future detailed publication.

In conclusion, we have considered the Kondo high-temperature limit (in a sense of $T > T^*$) of a KL model with quenched disorder. We derived new mean field equations for the SG transition in the presence of strong Kondo scattering and have shown that the partial screening of both diagonal and nondiagonal elements of the Q matrix takes place. As a result, the temperature of SG transition is strongly suppressed when Ising and Kondo interactions are of the same order of magnitude.

We thank F. Bouis, B. Coqblin, K. Kikoin, and P. Pfeuty for useful discussions. This work is supported by the SFB410 (II-VI semiconductors). One of us (MNK) is grateful to the Alexander von Humboldt Foundation for support during his stay in Germany.

[4] When an Ising system described by Eq. (1) with nearest neighbor interaction is treated with the mean-field theory, equations identical to Eq. (13) are obtained with $\sqrt{Z}\,I$ replacing I, where Z is the average number of neighbors.

REFERENCES

1. N. Grewe and F. Steglich, in *Handbook of the Physics and Chemistry of Rare Earths*, Ed. by K. A. Gschneider, Jr., and L. Eyring (Elsevier, Amsterdam, 1991), Vol. 14, p. 343.
2. A. Rosch, A. Schröder, O. Stockert, and H. V. Löhneysen, Phys. Rev. Lett. **79**, 159 (1997).
3. A. Schröder, G. Aeppli, E. Bucher, *et al.*, Phys. Rev. Lett. **80**, 5623 (1998).
4. S. Doniach, Physica B (Amsterdam) **91**, 231 (1977).
5. K. A. Kikoin, M. N. Kiselev, and A. S. Mishchenko, Pis'ma Zh. Éksp. Teor. Fiz. **60**, 583 (1994) [JETP Lett. **60**, 600 (1994)]; Zh. Éksp. Teor. Fiz. **112**, 729 (1997) [JETP **85**, 399 (1997)]; J. R. Iglesias, C. Lacroix, and B. Coqblin, Phys. Rev. B **56**, 11820 (1997).
6. P. Coleman and N. Andrei, J. Phys.: Condens. Matter **1**, 4057 (1989).
7. S. Sachdev, N. Read, and R. Oppermann, Phys. Rev. B **52**, 10286 (1995); A. Sengupta and A. Georges, *ibid.* **52**, 10295 (1995).
8. A. Yu. Zyuzin and B. Z. Spivak, Pis'ma Zh. Éksp. Teor. Fiz. **43**, 185 (1986) [JETP Lett. **43**, 234 (1986)]; L. N. Bulaevskiĭ and S. V. Panyukov, Pis'ma Zh. Éksp. Teor. Fiz. **43**, 190 (1986) [JETP Lett. **43**, 240 (1986)].
9. V. N. Popov and S. A. Fedotov, Zh. Éksp. Teor. Fiz. **94**, 193 (1988) [Sov. Phys. JETP **67**, 535 (1988)].
10. R. Oppermann and A. Muller-Groeling, Nucl. Phys. B **401**, 507 (1993).
11. F. Bouis and M. Kiselev, Physica B (Amsterdam) **259**–**261**, 195 (1999).
12. D. Sherrington and S. Kirkpatrik, Phys. Rev. Lett. **35**, 1972 (1975).
13. K. Binder and A. P. Young, Rev. Mod. Phys. **58**, 801 (1986).
14. N. Read and D. M. Newns, J. Phys. C **16**, 3273 (1983).
15. A. M. Tsvelik and P. B. Wiegmann, Adv. Phys. **32**, 453 (1983).

Eur. Phys. J. B **22**, 53–63 (2001)

THE EUROPEAN PHYSICAL JOURNAL B

EDP Sciences

Semi-fermionic representation of SU(N) Hamiltonians

M.N. Kiselev[1,2,a], H. Feldmann[1], and R. Oppermann[1]

[1] Institut für Theoretische Physik, Universität Würzburg, 97074 Würzburg, Germany
[2] Russian Research Center "Kurchatov Institute", 123 182 Moscow, Russia

Received 26 February 2001 and Received in final form 25 April 2001

Abstract. We represent the generators of the SU(N) algebra as bilinear combinations of Fermi operators with imaginary chemical potential. The distribution function, consisting of a minimal set of discrete imaginary chemical potentials, is introduced to satisfy the local constraints. This representation leads to the conventional temperature diagram technique with standard Feynman codex, except that the Matsubara frequencies are determined by neither integer nor half-integer numbers. The real-time Schwinger-Keldysh formalism is formulated in the framework of complex equilibrium distribution functions for auxiliary semi-fermionic fields. We discuss the continuous large N and SU(2) large spin limits. We illustrate the application of this technique for magnetic and spin-liquid states of the Heisenberg model.

PACS. 75.10.-b General theory and models of magnetic ordering – 75.10.Jm Quantized spin models – 75.40.Gb Dynamic properties (dynamic susceptibility, spin waves, spin diffusion, dynamic scaling, etc.) – 71.10.Fd Lattice fermion models (Hubbard model, etc.)

Several approaches have been proposed for the description of spin systems in statistical physics. Methods of functional integration based on various representation of spin operators such as Fermi, Bose, Majorana, supersymmetric or Hubbard operators [1–11] have been applied to many problems involving quantum spins and pseudospins [12–23]. The difficulty with the representation of spin operators is connected with the fact that spins possess neither Fermi nor Bose statistics. The commutation relations for spins are determined by the SU(2) algebra, leading to the absence of a Wick theorem for SU(2) generators. The Gaudin [24] theorem existing instead makes it impossible to construct a simple diagram technique directly for spin operators. To resolve this problem, various representations [2–11] have been introduced. Nevertheless, the representation of spins as a bilinear combination of Fermi/Bose operators enlarges the dimensionality of Hilbert space where these operators act. Thus, the spurious (unphysical) states should be excluded from the consideration resulting in a constraint requirement. Basically, different representations cure the constraint problem in a different way. Nevertheless, the usual price for simplicity is the replacement of the local constraint on each point containing the spins by a so-called global constraint, so that the restriction is fulfilled only in the average over all sites. It is known that such a replacement results in uncontrollable approximations for quantum spins (especially in low dimensions). Although the use of a global constraint is questionable for SU(2) systems, it becomes more reasonable for higher SU(N) groups, especially in the "large N limit". The corresponding approach is known as "$1/N$ expansion", [17–21] successfully describing the strong coupling limits of the Kondo impurity [12], Anderson lattice [13–15] and Hubbard [16] models and also SU(N) Heisenberg antiferromagnets on a square lattice [17–22] shedding light on the mechanism of high T_c superconductivity in cuprate compounds. Although SU($N = 2$) models are of primary physical interest, the SU($N \neq 2$) models can be considered as "approximate models" where an "exact solution" can be gained in contrast to "exact models" where the "approximate solution" is hard to obtain [20,21]. The simplification arises due to expansion in the inverse number of "flavors" $1/N$, making it possible to start with mean-field solution and systematically find corrections to it.

The goal of this paper is to consider a semi-fermionic representation for SU(N) generators for arbitrary (not necessary large) N, applying a different idea of constraint realization. This idea is know as Popov-Fedotov [25] representation being initially proposed for $S = 1/2$ and $S = 1$ spins. Based on an exact representation of spin operators as fermions with imaginary chemical potential, this representation resulted in the conventional Feynman temperature diagram technique, nevertheless providing a rigorous treatment of the local constraint [26–31]. In this paper we give a generalization of this method to SU(N) and we also construct the real-time formalism for the semi-fermionic spin representation.

The SU(N) algebra is determined by the generators obeying the following commutational relations:

$$[\hat{S}^{\beta}_{\alpha,i}\hat{S}^{\rho}_{\sigma j}] = \delta_{ij}(\delta^{\rho}_{\alpha}\hat{S}^{\beta}_{\sigma i} - \delta^{\beta}_{\sigma}\hat{S}^{\rho}_{\alpha i}) \quad (1)$$

[a] e-mail: kiselev@physik.uni-wuerzburg.de

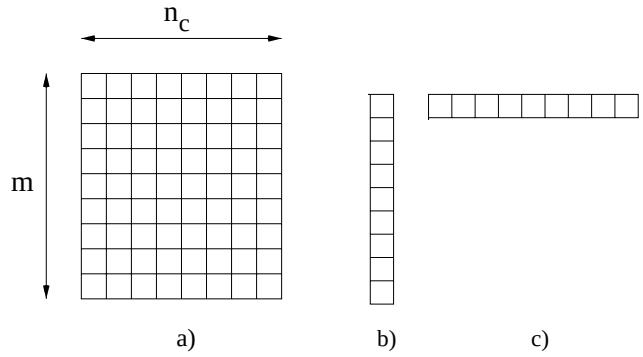

Fig. 1. (a) Rectangular Young tableau to denote a SU(N) representation, (b) single column tableau corresponding to $n_c = 1$ and (c) single row tableau standing for spin $S = n_c/2$ representation of SU(2) group.

where $\alpha, \beta = 1, ..., N$. We adopt the definition of the Cartan algebra [32] of the SU(N) group $\{H_\alpha\} = S^\alpha_\alpha$ similar to the one used in [17], noting that the diagonal generators S^α_α are not traceless. To ensure a vanishing trace, the diagonal generators should only appear in combinations

$$\sum_{\alpha=1}^{N} s_\alpha S^\alpha_\alpha \quad \text{with} \quad \sum_{\alpha=1}^{N} s_\alpha = 0 \tag{2}$$

which effectively reduces the number of independent diagonal generators to $N-1$ and the total number of SU(N) generators to N^2-1.

For SU(2) one recognizes the usual spin operators

$$S^2_1 = S^+, \quad S^1_2 = S^-, \quad S^2_2 - S^1_1 = 2S^z \tag{3}$$

with the usual commutation relations [33] and the Pauli matrices as generators of the SU(2) group. We shall not confine ourself to some special type of Hamiltonian. Nevertheless, it's worthwhile to mention that the SU(N) generalization of the Heisenberg model is given by the following expression [17,20,21]

$$H = \frac{J}{N} \sum_{\langle ij \rangle} \sum_{\alpha\beta} \hat{S}^\beta_\alpha(i) \hat{S}^\alpha_\beta(j). \tag{4}$$

On each site, there may exist many particles, whose symmetry properties define a specific representation of SU(N). The most transparent way to visualize an irreducible SU(N) representation are Young tableaux [34,35]. Instead of the general Young tableau, specified by $N-1$ integers, for example the lengths of the rows, we restrict us for the main part of the paper to rectangular tableaux, with $1 \leq m \leq N$ rows and $n_c \geq 1$ columns, illustrated in Figure 1.

The familiar spin is given by $N = 2$, $m = 1$, $n_c = 2S$, so the Young tableau contains one row of $2S$ length, with only one box for $S = 1/2$. Also of special importance are the tableaux with $n_c = 1$, giving the $N-1$ fundamental representations of SU(N).

The $\hat{S}^\alpha_\beta$ generator may be written as biquadratic form in terms of Schwinger boson operators [22,33]:

$$\hat{S}^\alpha_\beta = b^\dagger_{\alpha p} b^{\beta p} \tag{5}$$

and a constraint as follows

$$\sum_{\alpha=1}^{N} b^\dagger_{\alpha p} b^{\alpha q} = \delta^q_p n_c \tag{6}$$

where $p = 1, ..., m$ is the number of "colors".

The equivalent fermionic representation of the generators of SU(N)[17] is given by

$$\hat{S}^\alpha_\beta = \sum_a c^\dagger_{\alpha a} c^{\beta a} \tag{7}$$

where the "color" index $a, b = 1, ..., n_c$ and the $n_c(n_c+1)/2$ constraints

$$\sum_{\alpha=1}^{N} c^\dagger_{\alpha a} c^{\alpha b} = \delta^b_a m \tag{8}$$

restrict the Hilbert space to the states with $m * n_c$ particles and ensure the characteristic symmetry in the color index a. The antisymmetric behavior with respect to α is a direct consequence of the fermionic representation.

Let us consider the partition function for the Hamiltonian, expressed in terms of SU(N) generators

$$Z_S = \mathrm{Tr} \exp(-\beta H_S). \tag{9}$$

For SU(2) $S = 1/2$ and $S = 1$ it is possible to map the spin partition function onto a fermionic partition function where the chemical potential of fermions is purely imaginary [25]

$$Z_S = A \, \mathrm{Tr} \exp\left(-\beta(H_\mathrm{F} - \mu N_\mathrm{F})\right) = A Z_\mathrm{F} \tag{10}$$

with $\mu = -\mathrm{i}\pi T/2$ and $A = \mathrm{i}^{n_\mathrm{site}}$ for $S = 1/2$ and $\mu = -\mathrm{i}\pi T/3$ and $A = (\mathrm{i}/\sqrt{3})^{n_\mathrm{site}}$ for $S = 1$, n_site denotes the number of sites in a lattice. This results in usual Feynman-like diagram technique built up with the help of auxiliary Fermi (Grassmann) fields. The corresponding Matsubara frequencies for Popov-Fedotov (PF) fermions after applying the generalized Grassmann boundary conditions [25] read as $\omega_n = 2\pi T(n + 1/4)$ for $S = 1/2$ and $\omega_n = 2\pi T(n+1/3)$ for $S = 1$. The imaginary chemical potentials are important for the realization of an exclusion principle providing the fulfillment of the general identity

$$Z_S = \mathrm{Tr} \exp(-\beta H_S) = \mathrm{Tr} \exp(-\beta H_\mathrm{F}) \delta_{n_\mathrm{F},1}. \tag{11}$$

The Popov-Fedotov representation has been generalized for arbitrary values of spin S for the SU(2) group in [36] by introducing the distribution of discrete chemical potentials $\mu(j)$, with j being the site index, for PF fermions:

$$Z_S = \prod_j \int \mathrm{d}\mu(j) P(\mu(j)) Z_\mathrm{F}(\mu(j)). \tag{12}$$

For the SU(N) algebra we shall try to find the partition function in a similar manner

$$Z_S = \int \prod_j \mathrm{d}\mu(j) P(\mu(j)) \mathrm{Tr} \exp\left(-\beta(H_\mathrm{F} - \mu(j) n_\mathrm{F})\right) = \int \prod_j \mathrm{d}\mu(j) P(\mu(j)) Z_\mathrm{F}(\mu(j)). \tag{13}$$

We use the path integral representation of the partition function

$$Z_S/Z_S^0 = \int \prod_j \mathrm{d}\mu(j) P(\mu(j)) \exp(\mathcal{A}) / \int \prod_j \mathrm{d}\mu(j) P(\mu(j)) \exp(\mathcal{A}_0) \tag{14}$$

where the action $\mathcal{A}$ and $\mathcal{A}_0$ are determined by

$$\mathcal{A} = \mathcal{A}_0 - \int_0^\beta \mathrm{d}\tau H_\mathrm{F}(\tau),$$
$$\mathcal{A}_0 = \sum_j \sum_{k=1}^N \int_0^\beta \mathrm{d}\tau \bar{a}_k(j,\tau)(\partial_\tau + \mu(j)) a_k(j,\tau) \tag{15}$$

and the fermionic representation of SU(N) generators (7) is applied.

To begin with we confine ourselves to two particular cases of SU(N) with $n_\mathrm{c} = 1$ (corresponding to an effective "spin size" $S = 1/2$ and in the language of Young tableaux described by one column) and SU(2) for arbitrary value of $n_\mathrm{c} = 2S$ (one row Young tableau).

Let us first consider $n_\mathrm{c} = 1$. We denote the corresponding distribution by $P_{N,m}(\mu(j))$, where m is the number of particles in the SU(N) orbital, or in other words, $1 \leq m < N$ labels the different fundamental representations of SU(N).

$$n_j = \sum_{k=1}^N \bar{a}_k(j) a_k(j) = m. \tag{16}$$

To satisfy this requirement, the minimal set of chemical potentials and the corresponding form of $P_{N,m}(\mu(j))$ are to be derived.

Let us classify the states in Fock and spin spaces. We note that the dimension of the Fock space is $dim H_\mathrm{F} = 2^N$ and spurious states should be excluded. Thus, there are $\nu(N,m) = C_N^m = N!/(m!(N-m)!)$ physical states which can be obtained from the vacuum state $\Phi_0 = \underbrace{|0,...,0\rangle}_{N}$ as follows

$$\Phi_\mathrm{phys}^{\{\nu\}} = (\prod_{l=1}^m a_l^\dagger)\Phi_0 \tag{17}$$

or from the $|\underbrace{1,...,1}_{m},\underbrace{0,...,0}_{N-m}\rangle$ state by transferring the occupied states from left to the right side using the group generators.

To derive the distribution function we use the following identity for constraint (16) expressed in terms of Grassmann variables

$$\delta_{n_j,m} = \frac{1}{N} \sin\left(\pi(n_j - m)\right) / \sin\left(\frac{\pi(n_j - m)}{N}\right). \tag{18}$$

Substituting this identity into (11) and comparing with (12) on gets

$$P_{N,m}(\mu(j)) = \frac{1}{N} \sum_{k=1}^N \exp\left(\frac{\mathrm{i}\pi m}{N}(2k-1)\right) \delta(\mu(j) - \mu_k) \tag{19}$$

where

$$\mu_k = -\frac{\mathrm{i}\pi T}{N}(2k-1). \tag{20}$$

Since the Hamiltonian is symmetric under exchange of particles and holes if the sign of the chemical potential is changed simultaneously, we can simplify (19) to

$$P_{N,m}(\mu(j)) = \frac{2\mathrm{i}}{N} \sum_{k=1}^{\lfloor N/2 \rfloor} \sin\left(\pi m \frac{2k-1}{N}\right) \delta(\mu(j) - \mu_k) \tag{21}$$

where $\lfloor N/2 \rfloor$ denotes the integer part of $N/2$. As the discussion below will show, this is the minimal representation of the distribution function corresponding to the minimal set of the discrete imaginary chemical potentials. Another distributions function different from (21) can be constructed when the sum is taken from $k = N/2 + 1$ to N. Nevertheless, this DF is different from (21) only by the sign of imaginary chemical potentials $\tilde{\mu}_k = \mu_k^* = -\mu_k$ and thus is supplementary to (21).

Particularly interesting for even N is the case when the SU(N) orbital is half-filled, $m = N/2$. Then all chemical potentials are weighted with equal weight

$$P_{N,N/2}(\mu(j)) = \frac{2\mathrm{i}}{N} \sum_{k=1}^{N/2} (-1)^{k+1} \delta(\mu(j) - \mu_k). \tag{22}$$

Taking the limit $N \to \infty$ one may replace the summation in expression (22) in a suitable way by integration. Note, that taking $N \to \infty$ and $m \to \infty$ we nevertheless keep the ratio $m/N = 1/2$ fixed. Then, the following limiting distribution function can be obtained:

$$P_{N,N/2}(\mu(j)) \overset{N\to\infty}{\longrightarrow} \frac{\beta}{2\pi\mathrm{i}} \exp\left(-\beta\mu(j)\frac{N}{2}\right) \tag{23}$$

resulting in the usual continuous representation of the local constraint for the simplest case $n_\mathrm{c} = 1$ (compare it with (11))

$$Z_S = \mathrm{Tr}(\exp\left(-\beta H_\mathrm{F}\right) \delta(n_j - \frac{N}{2})). \tag{24}$$

We note the obvious similarity of the limiting DF (23) with the *Gibbs canonical distribution* provided that the

Wick rotation from the imaginary axis of the chemical potential μ to the real axis of energies E is performed and thus $\mu(j)N/2$ has a meaning of energy.

Up to now the representation we discussed was purely fermionic and expressed in terms of usual Grassmann variables when the path integral formalism is applied. The only difference from slave fermionic approach is that imaginary chemical potentials are introduced to fulfill the constraint. Nevertheless, by making the replacement

$$\begin{aligned} a_k(j,\tau)) &\rightarrow a_k(j,\tau)\exp\left(\frac{\mathrm{i}\pi\tau}{\beta}\frac{2k-1}{N}\right) \\ \bar{a}_k(j,\tau) &\rightarrow \bar{a}_k(j,\tau)\exp\left(-\frac{\mathrm{i}\pi\tau}{\beta}\frac{2k-1}{N}\right) \end{aligned} \tag{25}$$

we are coming to generalized Grassmann (semi-fermionic) boundary conditions

$$\begin{aligned} a_k(j,\beta) &= a_k(j,0)\exp\left(\mathrm{i}\pi\tfrac{2k-1}{N}\right) \\ \bar{a}_k(j,\beta) &= \bar{a}_k(j,0)\exp\left(-\mathrm{i}\pi\tfrac{2k-1}{N}\right)\cdot \end{aligned} \tag{26}$$

This leads to a temperature diagram technique for Green functions

$$\mathcal{G}^{\alpha\beta}(j,\tau) = -\langle T_\tau a_\alpha(j,\tau)\bar{a}_\beta(j,0)\rangle \tag{27}$$

of semi-fermions with Matsubara frequencies different from both Fermi and Bose representations.

The minimal set of Matsubara frequencies $\omega_n/(2\pi T)$ forms for SU(N) with even N the triangle table shown in Figure 2.

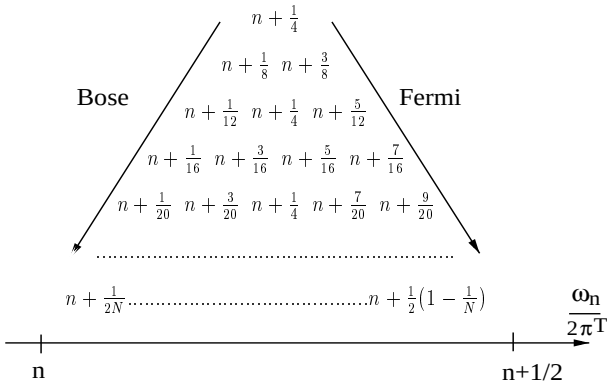

Fig. 2. The minimal set of Matsubara frequencies for SU(N) representation with even N.

The exclusion principle for this case is illustrated on Figure 3, where the first two groups SU(2) and SU(4) are shown. The first point to observe is that the spin Hamiltonian does not distinguish the n particle and the n hole (or $N-n$ particle) subspace. Due to equation (20) the two phase factors $\exp(\beta\mu n)$ and $\exp(\beta\mu(N-n))$ accompanying these subspaces in equation (21) add up to a purely imaginary value within the same chemical potential, and the empty and the fully occupied states are always canceled.

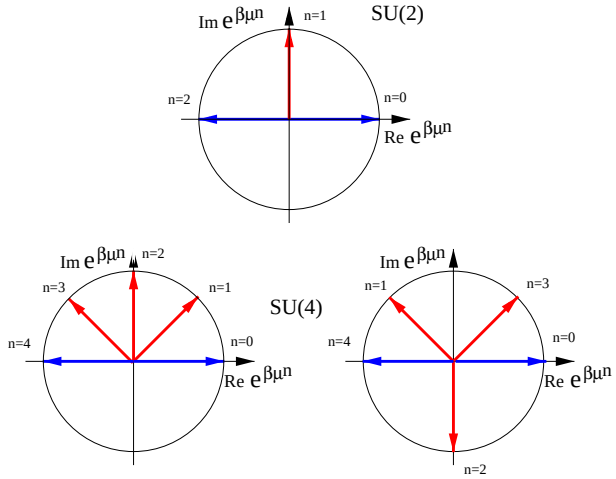

Fig. 3. Graphical representation of exclusion principle for SU(N) semi-fermionic representation with even N, $n_c = 1$ (we use $\mu = \mathrm{i}\pi T/2$ for SU(2) and $\mu_1 = \mathrm{i}\pi T/4$, $\mu_2 = 3\mathrm{i}\pi T/4$ for SU(4)).

In the case of $N \geq 4$, where we have multiple chemical potentials, the distribution function $P(\mu)$ linearly combines these imaginary prefactors to select out the desired physical subspace with particle number $n = m$.

In Figure 3, we note that on each picture the empty and fully occupied states are canceled in their own unit circle. For SU(2) there is a unique chemical potential $\mu = \pm\mathrm{i}\pi T/2$ which results in the survival of single occupied states. For SU(4) there are two chemical potentials (see also Fig. 2). The cancellation of single and triple occupied states is achieved with the help of proper weights for these states in the distribution function whereas the states with the occupation number 2 are doubled according to the expression (22). In general, for SU(N) group with $n_c = 1$ there exists $N/2$ circles providing the realization of the exclusion principle.

We consider now the generalization of the SU(2) algebra for the case of a large moment S with $2S+1$ projections. Here, the most convenient fermionic representation is constructed with the help of a $2S+1$ component Fermi field $a_k(j)$ provided that the generators of SU(2) satisfy the following equations

$$\begin{aligned} S^+ &= \sum_{k=-S}^{S-1}\sqrt{S(S+1)-k(k+1)}a^\dagger_{k+1}(j)a_k(j) \\ S^- &= \sum_{k=-S+1}^{S}\sqrt{S(S+1)-k(k-1)}a^\dagger_{k-1}(j)a_k(j) \\ S^z &= \sum_{k=-S}^{S} k a^\dagger_k(j)a_k(j) \end{aligned} \tag{28}$$

such that $dim H_{\rm F} = 2^{2S+1}$ whereas the constraint reads as follows

$$n_j = \sum_{k=-S}^{k=S} a_k^{\dagger}(j) a_k(j) = l = 1. \tag{29}$$

We consider the distribution function for arbitrary l for the sake of generality. It describes the orbital part of an atomic subshell with orbital quantum number S, with l particles present. We denote the corresponding distribution function of the chemical potential by $P_{2S+1,l}(\mu(j))$. Following the same routine as for SU(N) generators and using the occupancy condition to have l (or $2S+1-l$) states from the $2S+1$ states filled, one gets the following distribution function, after using the particle-hole symmetry of H_S:

$$P_{2S+1,l}(\mu(j)) = \frac{2\mathrm{i}}{2S+1} \times \sum_{k=1}^{\lfloor S+1/2 \rfloor} \sin\left(\pi l \frac{2k-1}{2S+1}\right) \delta(\mu(j) - \mu_k) \tag{30}$$

where the chemical potentials are $\mu_k = -\mathrm{i}\pi T(2k-1)/(2S+1)$ and $k = 1, ..., \lfloor S+1/2 \rfloor$, similarly to equation (20).

In the particular case of the SU(2) model with $l = 1$ for some chosen values of spin S the distribution functions are determined by the following expressions

$$P_{2,1}(\mu(j)) = \mathrm{i}\ \delta(\mu(j) + \frac{\mathrm{i}\pi T}{2}) \tag{31}$$

for $S = 1/2$

$$P_{3,1}(\mu(j)) = P_{3,2}(\mu(j)) = \frac{\mathrm{i}}{\sqrt{3}}\ \delta(\mu(j) + \frac{\mathrm{i}\pi T}{3}) \tag{32}$$

for $S = 1$.

This result corresponds to the original Popov-Fedotov description restricted to the $S = 1/2$ and $S = 1$ cases. We present as an example some other distribution functions obtained according to general scheme considered above:

$$P_{4,1}(\mu) = P_{4,3}(\mu) = \frac{\mathrm{i}\sqrt{2}}{4}\left(\delta(\mu + \frac{\mathrm{i}\pi T}{4}) + \delta(\mu + \frac{3\mathrm{i}\pi T}{4}\right) \tag{33}$$

for $S = 3/2$, SU(2) and

$$P_{4,2}(\mu) = \frac{\mathrm{i}}{2}\left(\delta(\mu + \frac{\mathrm{i}\pi T}{4}) - \delta(\mu + \frac{3\mathrm{i}\pi T}{4})\right) \tag{34}$$

for effective spin "$S = 1/2$", SU(4),

$$P_{5,1}(\mu) = P_{5,4}(\mu) = \frac{\mathrm{i}}{\sqrt{10}}\left(\sqrt{1 - \frac{1}{\sqrt{5}}}\delta(\mu + \frac{\mathrm{i}\pi T}{5}) + \sqrt{1 + \frac{1}{\sqrt{5}}}\delta(\mu + \frac{3\mathrm{i}\pi T}{5})\right) \tag{35}$$

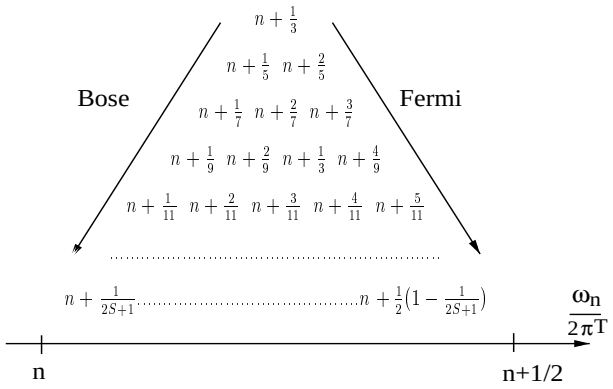

Fig. 4. The minimal set of Matsubara frequencies for SU(2) representation for integer values of the spin and $l = 1$.

for $S = 2$, $SU(2)$ etc.

A limiting distribution function corresponding to equation (23) for the constraint condition with arbitrary l is given by

$$P_{\infty,l}(\mu(j)) \stackrel{S\to\infty}{\longrightarrow} \frac{\beta}{2\pi\mathrm{i}} \exp(-\beta l \mu(j)). \tag{36}$$

For the case $l = m = N/2 \to \infty$ and $S = (N-1)/2 \to \infty$ the expression for the limiting DF $P_{\infty,l}(\mu(j))$ coincides with (23). We note that in $S \to \infty$ (or $N \to \infty$) limit continuum chemical potentials play role of additional U(1) fluctuating field whereas for finite S and N they are characterized by fixed and discrete values.

When S assumes integer values, the minimal fundamental set of Matsubara frequencies is given by the table in Figure 4.

The exclusion principle for SU(2) in the large spin limit can be also understood with the help of Figure 3 and Figure 5. One can see that empty and fully occupied states are canceled in each given circle similarly to even-N SU(N) algebra. The particle-hole (PH) symmetry of the representation results in an equivalence of single occupied and $2S$ occupied states whereas all the other states are canceled due to proper weights in the distribution function (30). In accordance with PH symmetry being preserved for each value of the chemical potential all circle diagrams (see Fig. 3, Fig. 5) are invariant with respect to simultaneous change $\mu \leftrightarrow -\mu$ and $n_{\rm particle} \leftrightarrow n_{\rm holes}$.

Let us make few comments concerning the general rectangular Young tableau of size $n_{\rm c} * m$. The fermionic representation (7) is characterized by an $N * n_{\rm c}$ component field with $n_{\rm c}$ identical diagonal constraints and $n_{\rm c}(n_{\rm c}-1)/2$ off-diagonal constraints (8). The effective "filling" determining the number of fermions on each site is $mn_{\rm c}$. However, not all of these $(n_{\rm c}N)!/((n_{\rm c}m)!((N-m)n_{\rm c})!)$ states are representing proper physical states. One should take into account the constraints equation (8) to obtain the complete set. The number of physical states of a rectangular

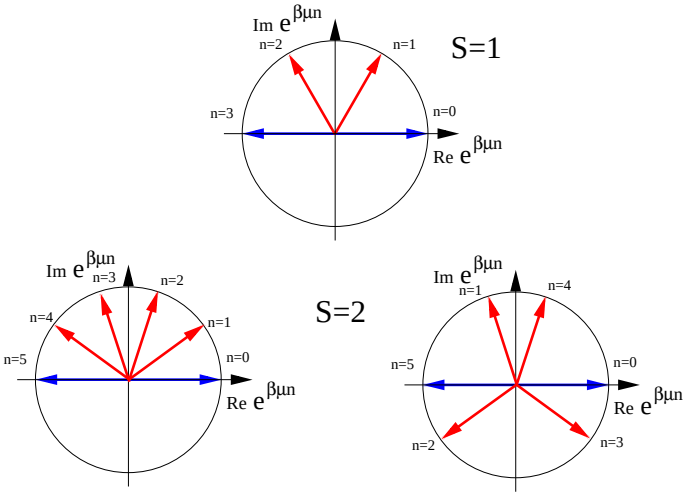

Fig. 5. Graphical representation of exclusion principle for SU(2) semi-fermionic representation for $S = 1$ and $S = 2$. For any arbitrary integer value of spin there exists S circle diagrams corresponding to the S different chemical potentials and providing the realization of the exclusion principle.

Young tableau is given by the expression:

$$\nu(N,m,n_{\rm c}) = \frac{\overbrace{C^m_{N+n_{\rm c}-1}C^m_{N+n_{\rm c}-2}\ldots C^m_{m+n_{\rm c}}}^{N-m}}{\underbrace{C^m_{N-1}C^m_{N-2}\ldots C^m_m}_{N-m}} = \frac{\overbrace{C^m_{N+n_{\rm c}-1}C^m_{N+n_{\rm c}-2}\ldots C^m_N}^{n_{\rm c}}}{\underbrace{C^m_{m+n_{\rm c}-1}C^m_{m+n_{\rm c}-2}\ldots C^m_m}_{n_{\rm c}}}\cdot \qquad (37)$$

While the diagonal part of equation (8) could be satisfied with color-dependent chemical potentials $\mu_a(j)$, coupling only to $\sum_\alpha c^\dagger_{\alpha a}c^{\alpha a}$, an exclusion procedure for the off-diagonal constraints needs either projection operators or an a priori restriction on the trace, using *e.g.* coherent states [17].

Another generalization is applicable for a broader range of cases. The general Young tableau (not necessarily rectangular), representing any irreducible representation (p), can be described in the context of our approach in the following way. The generators $S^{(p)}_m$ are expressed as matrices

$$(S^{(p)}_m)_{\beta\alpha} = \langle\psi^{(p)}_\beta|T^{(k)\times(l)}_m|\psi^{(p)}_\alpha\rangle \qquad (38)$$

with $T^{(k)\times(l)}_m = T^{(k)}_m + T^{(l)}_m$ being the generators in a suitable direct product of representations (k) and (l) and the states $|\psi^{(p)}_\alpha\rangle$ are obtained in terms of Clebsch-Gordon coefficients

$$|\psi^{(p)}_\alpha\rangle = \sum_{\mu,\nu}(k,l;\mu,\nu|p;\alpha)|\psi^{(k)}_\mu\rangle\times|\psi^{(l)}_\nu\rangle\,. \qquad (39)$$

This procedure can be iterated until (k) and (l) are fundamental irreducible representations of SU(N). The size of the matrices $S^{(p)}_m$ is equal to the dimension of the representation, $\nu^{(p)}$. The trace is now easily expressed in terms of $\nu^{(p)}$ fermionic fields, enforcing the constraint $\delta_{n_j,1}$ with the distribution of chemical potentials (see Eq. (21))

$$P_{\nu^{(p)},1}(\mu(j)) = \frac{2{\rm i}}{\nu^{(p)}}\sum_{k=1}^{\lfloor\nu^{(p)}/2\rfloor}\sin\left(\pi\frac{2k-1}{\nu^{(p)}}\right)\delta(\mu(j)-\mu_k). \qquad (40)$$

For the simple case of SU(2), which yields only single-row tableaux, this procedure gives the fermionic representation described in equations (28–30). In the case of single-column tableaux for SU(N), however, and in the general case of mixed symmetry, it does not fully use the fermionic commutation properties. Therefore, it is in general not the representation with the minimal number of fermions and the minimal number of chemical potentials in $P(\mu)$.

We discuss finally the real-time formalism based on the semi-fermionic representation of SU(N) generators. This approach is necessary for treating the systems being out of equilibrium, especially for many component systems describing Fermi (Bose) quasiparticles interacting with spins. The real time formalism is also an alternative approach for the analytical continuation method for equilibrium problems allowing direct calculations of correlators whose analytical properties as function of many complex arguments can be quite cumbersome.

A long time ago Keldysh [38] and Schwinger [39] have proposed a novel approach for the description of kinetic phenomena in metals. This approach was found especially fruitful for normal metals [40], and, in many recent applications, for superconductors [41], for disordered interacting (normal or superconducting) electron liquids [42] for example. The previous application of the real-time formalism to the quantum theory of Bose-Einstein condensation (BEC) [45] allowed the derivation of a Fokker-Planck equation, which describes both kinetic and coherent stages of BEC. Moreover [46] developed the closed-time path integral formalism for aging effects in quantum disordered systems being in contact with an environment. The Keldysh technique in application to disordered systems (see [42–44] and [47,48]) has also been recently applied to develop a field theory alternative to the previously used replica technique.

To derive the real-time formalism for SU(N) generators we use the path integral representation along the closed time Keldysh contour (see Fig. 6). Following the standard route [49] we can express the partition function of the problem containing SU(N) generators as a path integral over Grassmann variables $\psi_l = (a_{l,1}(j),\ldots,a_{l,N}(j))^T$ where $l = 1,2$ stands for upper and lower parts of the Keldysh contour, respectively,

$$\mathcal{Z}/\mathcal{Z}_0 = \int {\rm D}\bar\psi{\rm D}\psi\exp({\rm i}\mathcal{A})/\int {\rm D}\bar\psi{\rm D}\psi\exp({\rm i}\mathcal{A}_0) \qquad (41)$$

where the actions $\mathcal{A}$ and $\mathcal{A}_0$ are taken as an integral along the closed-time contour $C_t + C_\tau$ which is shown

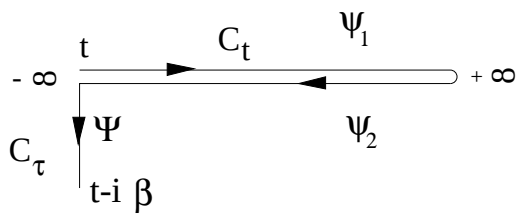

Fig. 6. The Keldysh contour going from $-\infty \to \infty \to -\infty$ in real time. The boundary conditions on the imaginary time segment determine the generalized distribution functions for quasiparticles.

in Figure 6. The contour is closed at $t = -\infty + \mathrm{i}\tau$ since $\exp(-\beta H_0) = T_\tau \exp\left(-\int_0^\beta H_0 \mathrm{d}\tau\right)$. We denote the ψ fields on upper and lower sides of the contour C_t as ψ_1 and ψ_2 respectively. The fields Ψ stand for the contour C_τ. These fields provide matching conditions for $\psi_{1,2}$ and are excluded from final expressions. Taking into account the semi-fermionic boundary conditions for generalized Grassmann fields (26) one gets the matching conditions for $\psi_{1,2}$ at $t = \pm\infty$,

$$\begin{aligned}\psi^\mu_{1,\alpha}|_k(-\infty) &= \exp\left(\mathrm{i}\pi\frac{2k-1}{N}\right)\psi^\mu_{2,\alpha}|_k(-\infty)\\ \psi^\mu_{1,\alpha}|_k(+\infty) &= \psi^\mu_{2,\alpha}|_k(+\infty)\end{aligned} \tag{42}$$

for $k = 1, ..., \lfloor N/2 \rfloor$ and $\alpha = 1, ..., N$. The correlation functions can be represented as functional derivatives of the generating functional

$$Z[\eta] = \mathcal{Z}_0^{-1}\int \mathrm{D}\bar\psi\mathrm{D}\psi \exp\left(\mathrm{i}\mathcal{A} + \mathrm{i}\oint_C \mathrm{d}t(\bar\eta\sigma^z\psi + \bar\psi\sigma^z\eta)\right) \tag{43}$$

where η represents sources and the σ^z matrix stands for "causal" and "anti-causal" orderings along the contour.

The on-site Green's functions (GF) which are matrices of size $2N \times 2N$ with respect to both Keldysh (lower) and spin-color (upper) indices are given by

$$G^{\alpha\beta}_{\mu\nu}(t,t') = -\mathrm{i}\frac{\delta}{\mathrm{i}\delta\bar\eta^\alpha_\mu(t)}\frac{\delta}{\mathrm{i}\delta\eta^\beta_\nu(t')}Z[\eta]|_{\bar\eta,\eta\to 0}. \tag{44}$$

To distinguish between imaginary-time (27) and real-time (44) GF's we use different notations for Green's functions in these representations.

After a standard shift-transformation [49] of fields ψ the Keldysh GF of free semi-fermions assumes the form

$$G^\alpha_0(\epsilon) = G^{R,\alpha}_0\begin{pmatrix}1-f_\epsilon & -f_\epsilon\\ 1-f_\epsilon & -f_\epsilon\end{pmatrix} - G^{A,\alpha}_0\begin{pmatrix}-f_\epsilon & -f_\epsilon\\ 1-f_\epsilon & 1-f_\epsilon\end{pmatrix}$$

where the retarded and advanced GF's are

$$G^{(R,A)\alpha}_0(\epsilon) = (\epsilon \pm \mathrm{i}\delta)^{-1}, \quad f_\epsilon = f^{(N,k)}(\epsilon) \tag{45}$$

with equilibrium distribution functions

$$f^{(N,k)}(\epsilon) = T\sum_n \frac{\mathrm{e}^{\mathrm{i}\omega_{n_k}\tau|_{+0}}}{\mathrm{i}\omega_{n_k}-\epsilon} = \frac{1}{\mathrm{e}^{\mathrm{i}\pi(2k-1)/N}\exp(\beta\epsilon)+1}\,. \tag{46}$$

A straightforward calculation of $f^{(N,k)}$ for the case of even N leads to the following expression

$$f^{(N,k)}(\epsilon) = \frac{\sum_{l=1}^{N}(-1)^{l-1}\exp\left(\beta\epsilon(N-l)\right)\exp\left(-\dfrac{\mathrm{i}\pi l(2k-1)}{N}\right)}{\exp(N\beta\epsilon)+1}, \tag{47}$$

where $k = 1, ..., N/2$.

The equilibrium distribution functions (EDF) $f^{(2S+1,k)}$ for the auxiliary Fermi-fields representing arbitrary S for $SU(2)$ algebra are given by

$$f^{(2S+1,k)}(\epsilon) = \frac{\sum_{l=1}^{2S+1}(-1)^{l-1}\exp\left(\beta\epsilon(2S+1-l)\right)\exp\left(-\dfrac{\mathrm{i}\pi(2k-1)}{2S+1}\right)}{\exp((2S+1)\beta\epsilon)+(-1)^{2S+1}} \tag{48}$$

for $k = 1, ..., \lfloor S + 1/2 \rfloor$. Particularly simple are the cases of $S = 1/2$ and $S = 1$,

$$\begin{aligned}f^{(2,1)}(\epsilon) &= n_{\mathrm{F}}(2\epsilon) - \mathrm{i}\frac{1}{2\cosh(\beta\epsilon)}\\ f^{(3,1)}(\epsilon) &= \frac{1}{2}n_{\mathrm{B}}(\epsilon) - \frac{3}{2}n_{\mathrm{B}}(3\epsilon) - \mathrm{i}\sqrt{3}\frac{\sinh(\beta\epsilon/2)}{\sinh(3\beta\epsilon/2)}\,.\end{aligned} \tag{49}$$

Here, standard notations for Fermi/Bose distribution functions $n_{\mathrm{F/B}}(\epsilon) = [\exp(\beta\epsilon) \pm 1]^{-1}$ are used.

In general the EDF for half-integer and integer spins can be expressed in terms of Fermi and Bose EDF respectively. We note that since auxiliary Fermi fields introduced for the representation of SU(N) generators do not represent the true quasiparticles of the problem, helping only to treat properly the constraint condition, the distribution functions for these objects in general do not have to be real functions. Nevertheless, one can prove that the imaginary part of the EDF does not affect the physical correlators and can be eliminated by introducing an infinitesimally small real part for the chemical potential. In spin problems, a uniform/staggered magnetic field usually plays the role of such real chemical potential for semi-fermions.

Let us illustrate the application of the semi-fermionic formalism for spin Hamiltonians. As an example we consider the SU(2) Heisenberg model for $S = 1/2$ with the nearest neighbor interaction

$$H_{\mathrm{int}} = -\sum_{\langle ij\rangle} J_{ij}\boldsymbol{S}_i\boldsymbol{S}_j. \tag{50}$$

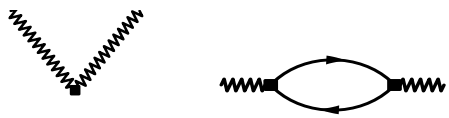

Fig. 7. First few graphs for the free energy expanded with respect to local molecular magnetic field. Solid line stands for semi-fermions. Zig-zag line denotes the "condensate" field.

We start with imaginary-time semi-fermionic description of the ferromagnetic (FM) state of the Heisenberg model ($J > 0$). We follow the standard procedure developed in the original paper of Popov and Fedotov [25]. After applying the Hubbard-Stratonovich transformation to decouple the four-semi-fermion term in (50) by the *local vector* field $\boldsymbol{\Phi}_i(\tau)$ the effective action is obtained:

$$\mathcal{A}_{\rm eff}^{\rm FM}[\psi,\Phi] = \tilde{\mathcal{A}}_0[\psi,\Phi] - \frac{1}{4}\int_0^\beta \mathrm{d}\tau \sum_{\boldsymbol{q}} (I_{\rm FM}(\boldsymbol{q}))^{-1}\boldsymbol{\Phi}_q(\tau)\boldsymbol{\Phi}_q(\tau) \quad (51)$$

where $\psi^T = (\psi_\uparrow \psi_\downarrow)$ - fields denoting the semi-fermions in SU(2) representation of the $S = 1/2$ spin operators,

$$I(q) = I_{\rm FM}(q) = \frac{1}{N}\sum_{r_{ij}} I_{\rm FM}(\boldsymbol{r}_{ij})\mathrm{e}^{\mathrm{i}\boldsymbol{qr}} \quad (52)$$

and $I(0) = ZJ > 0$ for the FM instability (here Z denotes the number of the nearest neighbors, N stands for the number of unit cells). The FM phase transition corresponds to appearance at $T = T_{\rm c}$ of the nonzero average $\langle\Phi^z(0,0)\rangle$ which stands for nonzero uniform magnetization, or by another words, corresponds to the Bose condensation of the field Φ^z.

Splitting the field Φ^z on the time-independent spatially homogeneous (*uniform*) part and the fluctuating filed $\tilde{\Phi}^z$

$$\Phi^z(\boldsymbol{k},\omega) = \mathcal{M}(\beta N)^{1/2}\delta_{\boldsymbol{k},0}\delta_{\omega,0} + \tilde{\Phi}^z(\boldsymbol{k},\omega) \quad (53)$$

make it possible to integrate over all semi-fermionic fields. As a result, the nonpolynomial effective action can be derived for the FM Heisenberg model

$$\mathcal{A}_{\rm eff} = \mathcal{A}_0[\Phi] + \mathtt{Tr}\ln\left(\mathcal{G}_\sigma^{-1}(\Phi^z,\Phi^\pm)\right) \quad (54)$$

where $\mathcal{G}_\sigma = -\langle T_\tau \psi_\sigma(\boldsymbol{j},\tau)\bar{\psi}_\sigma(\boldsymbol{j},0)\rangle$ stands for the local Green's function of semi-fermions. The expansion of the $\mathrm{Tr}\ln\mathcal{G}_\sigma^{-1}$ with respect to Φ fields results in standard Ginzburg-Landau functional (see Fig. 7). The effects of molecular field are included into zero approximation for GF:

$$\mathcal{G}_\sigma^0(\mathrm{i}\omega_n) = [\mathrm{i}\omega_n + \sigma^z_{\sigma\sigma}\mathcal{M}/2]^{-1}.$$

In one loop approximation the standard molecular field equation can be reproduced

$$\mathcal{M} = I_{\rm FM}(0)\tanh(\beta\mathcal{M}/2). \quad (55)$$

The saddle point (mean-field) effective action is given by well-known expression

$$\mathcal{A}_0[\mathcal{M}] = -N\left[\frac{\beta\mathcal{M}^2}{4I_{\rm M}(0)} - \ln\left(2\cosh\left(\frac{\beta\mathcal{M}}{2}\right)\right)\right] \quad (56)$$

and the free energy per spin f_0 (see Fig. 7) is determined by standard equation:

$$\beta f_0 = -\ln Z_S = \frac{\beta\mathcal{M}^2}{4I_{\rm M}(0)} - \ln\left(2\cosh\left(\frac{\beta\mathcal{M}}{2}\right)\right)\cdot \quad (57)$$

Calculation of the second variation of $\mathcal{A}_{\rm eff}$ gives rise to the following expression

$$\begin{aligned}\delta\mathcal{A}_{\rm eff} = &-\frac{1}{4}\sum_{\boldsymbol{k}}\Phi^z(\boldsymbol{k},0)\left[I_{\rm M}^{-1}(\boldsymbol{k}) - \frac{\beta}{2\cosh^2(\beta\Omega)}\right]\Phi^z(\boldsymbol{k},0)\\ &-\frac{1}{4}\sum_{\boldsymbol{k},\omega\neq 0} I_{\rm M}^{-1}(\boldsymbol{k})\Phi^z(\boldsymbol{k},\omega)\Phi^z(\boldsymbol{k},\omega)\\ &-\sum_{\boldsymbol{k},\omega}\Phi^+(\boldsymbol{k},\omega)\left[I_{\rm M}^{-1}(\boldsymbol{k}) - \frac{\tanh(\beta\Omega)}{2\Omega - \mathrm{i}\omega}\right]\Phi^-(\boldsymbol{k},\omega)\end{aligned} \quad (58)$$

where $\Omega = (g\mu_{\rm B}H + \mathcal{M})/2$. For $T > T_{\rm c}$ one easily obtains the effective static spin-spin interaction equivalent to those given by the Random Phase Approximation (RPA)

$$\Gamma(\boldsymbol{q},0) = \langle\boldsymbol{\Phi}(\boldsymbol{q},0)\boldsymbol{\Phi}(-\boldsymbol{q},0)\rangle = 2I(\boldsymbol{q})/(1 - 2\chi_0 I(\boldsymbol{q})),$$

where $\chi_0^{+-}(\boldsymbol{q},0) = 2\chi_0^{zz}(\boldsymbol{q},0) = 2\chi_0 = 2S(S+1)\beta/3$ stands for the on-site spin susceptibility in paramagnetic state.

Let us now consider the Heisenberg model with antiferromagnetic (AFM) sign of the exchange integral ($J < 0$).

$$\mathcal{A}_{\rm eff}^{\rm AFM}[\psi,\Phi] = \tilde{\mathcal{A}}_0[\psi,\Phi] + \frac{1}{4}\int_0^\beta \mathrm{d}\tau\sum_{\boldsymbol{q}}(I_{\rm AFM}(\boldsymbol{q}))^{-1}\boldsymbol{\Phi}_q(\tau)\boldsymbol{\Phi}_q(\tau) \quad (59)$$

and $I(\boldsymbol{Q}) = ZJ < 0$ for the AFM instability corresponding to vector $\mathbf{Q} = (\pi,...,\pi)$ (we consider the hypercubic lattice for simplicity). In contrast to the FM case, we can now represent the longitudinal component of the field Φ^z as a superposition of the *staggered* time-independent part ("staggered condensate") and a fluctuating field

$$\Phi^z(\boldsymbol{k},\omega) = \mathcal{N}(\beta N)^{1/2}\delta_{\boldsymbol{k},\boldsymbol{Q}}\delta_{\omega,0} + \tilde{\Phi}^z(\boldsymbol{k},\omega). \quad (60)$$

As a result, the integration over semi-fermionic fields can be done explicitly. Introducing two sublattices for ψ fields one gets 4×4 matrix structure for the semi-fermionic Green's functions. Since the AFM instability is associated with appearance of a nonzero staggered magnetization $\mathcal{N}$, it is necessary to take into account both "normal" and

"anomalous" GF determined as follows:

$$\mathcal{G}^0_\sigma(\mathrm{i}\omega_n) = -\int_0^\beta \mathrm{d}\tau \mathrm{e}^{\mathrm{i}\omega_n\tau}\langle T_\tau \psi_\sigma(\boldsymbol{k},\tau)\bar{\psi}_\sigma(\boldsymbol{k},0)\rangle = -\frac{\mathrm{i}\omega_n}{\omega_n^2+\tilde{\Omega}^2} \quad (61)$$

$$\mathcal{F}^0_\sigma(\mathrm{i}\omega_n) = -\int_0^\beta \mathrm{d}\tau \mathrm{e}^{\mathrm{i}\omega_n\tau}\langle T_\tau \psi_\sigma(\boldsymbol{k},\tau)\bar{\psi}_\sigma(\boldsymbol{k}+\boldsymbol{Q},0)\rangle = -\frac{\tilde{\Omega}\sigma^z_{\sigma\sigma}}{\omega_n^2+\tilde{\Omega}^2}\cdot \quad (62)$$

where $\tilde{\Omega} = (\mathcal{N} + g\mu_\mathrm{B}h)/2$. Integrating over all semi-fermions one obtains the mean-field equation for the staggered magnetization:

$$\mathcal{N} = -I_\mathrm{AFM}(Q)\tanh(\beta\mathcal{N}/2) \quad (63)$$

and

$$\mathcal{A}_0[\mathcal{N}] = N\left[\frac{\beta\mathcal{N}^2}{4I_\mathrm{M}(Q)} + \ln\left(2\cosh\left(\frac{\beta\mathcal{N}}{2}\right)\right)\right]\cdot \quad (64)$$

After taking into account the second variation of $\mathcal{A}_\mathrm{eff}$ the following expression for the effective action is obtained (see *e.g.* [56,57]):

$$\begin{aligned}\delta\mathcal{A}_\mathrm{eff} = {} & \frac{1}{4}\sum_{\boldsymbol{k}} \Phi^z(\boldsymbol{k},0)\left[I^{-1}_\mathrm{M}(\boldsymbol{k}) + \frac{\beta}{2\cosh^2(\beta\tilde{\Omega})}\right]\Phi^z(\boldsymbol{k},0) \\ & + \frac{1}{4}\sum_{\boldsymbol{k},\omega\neq 0} I^{-1}_\mathrm{M}(\boldsymbol{k})\Phi^z(\boldsymbol{k},\omega)\Phi^z(\boldsymbol{k},\omega) \\ & + \sum_{\boldsymbol{k},\omega}\Phi^+(\boldsymbol{k},\omega)\left[I^{-1}_\mathrm{M}(\boldsymbol{k}) + \frac{2\tilde{\Omega}\tanh(\beta\tilde{\Omega})}{4\tilde{\Omega}^2+\omega^2}\right]\Phi^-(\boldsymbol{k},\omega) \\ & - \sum_{\boldsymbol{k},\omega}\Phi^+(\boldsymbol{k}+\boldsymbol{Q},\omega)\frac{\mathrm{i}\omega}{4\tilde{\Omega}^2+\omega^2}\Phi^-(\boldsymbol{k},\omega). \end{aligned} \quad (65)$$

The application of the Schwinger-Keldysh formalism for the Heisenberg model is straightforward. Applying the semi-fermionic transformation to the partition function one obtains the action as an integral along the closed-time Keldysh-contour

$$\mathcal{A} = \mathcal{A}_0 + \mathcal{A}_\mathrm{int} = \mathcal{A}_0 + \oint_C \mathrm{d}t \sum_{\mathbf{q}} J(\mathbf{q})\boldsymbol{S}_{\mathbf{q}}(t)\boldsymbol{S}_{-\mathbf{q}}(t) \quad (66)$$

where $\mathcal{A}_0$ corresponds to noninteracting semi-fermions

$$\mathcal{A}_0 = \oint_C \mathrm{d}t \sum_i \bar{\psi}_i \begin{pmatrix} (G_0^{R,\alpha})^{-1} & 0 \\ 0 & (G_0^{A,\alpha})^{-1}\end{pmatrix}\psi_i. \quad (67)$$

We denote $J_\mathbf{q}{=}J\sum_{\langle \mathbf{l}\rangle}\mathrm{e}^{\mathrm{i}\mathbf{q}\mathbf{l}}$, $\nu_\mathbf{q}{=}J_\mathbf{q}/J_0$ and apply four-component semi-fermionic representation for FM case and eight-component representation with $\psi^T{=}(\tilde{\psi}^T_\mathbf{k}\tilde{\psi}^T_{\mathbf{k}+\mathbf{Q}})$ for the AFM case. Performing the standard Hubbard-Stratonovich transformation along the Keldysh contour

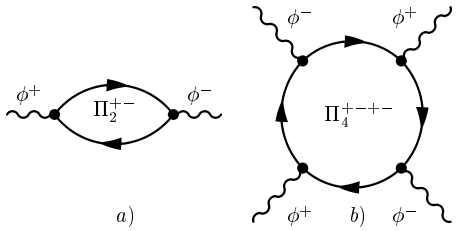

Fig. 8. Feynman diagrams contributing to dispersion (a) and damping (b) of magnons. Solid line denotes semi-fermions.

with the help of the two-Keldysh-component *vector* (Bose) field Φ, one gets

$$\mathcal{A}_\mathrm{int} = -\frac{1}{2}\mathrm{Tr}(\boldsymbol{\Phi}^T_\mathbf{q}J^{-1}_\mathbf{q}\sigma^z\boldsymbol{\Phi}_\mathbf{q}) + \mathrm{Tr}(\bar{\psi}\boldsymbol{\Phi}_\mu\boldsymbol{\sigma}\gamma^\mu\psi). \quad (68)$$

Now we integrate out ψ fields and express the effective action in terms of $\boldsymbol{\Phi}$ fields

$$\mathcal{A}_\mathrm{eff} = -\frac{1}{2}\mathrm{Tr}(\boldsymbol{\Phi}^T_\mathbf{q}J^{-1}_\mathbf{q}\sigma^z\boldsymbol{\Phi}_\mathbf{q}) + \mathrm{Tr}\ln\left(G_0^{-1} + \boldsymbol{\Phi}_\mu\boldsymbol{\sigma}\gamma^\mu\right)$$

where $\gamma^\mu{=}(\sigma^z \pm 1)/2$ acts in Keldysh space. Since in general $\boldsymbol{\Phi}$ is a time- and space-dependent fluctuating field the partition function (41) cannot be evaluated exactly. Nevertheless, when a magnetic instability occurs, we can represent the longitudinal component of this field as a superposition of a uniform (FM) or staggered (AFM) time-independent part and a fluctuating field

$$\Phi^z_\mu(\mathbf{q},\omega) = \textit{condensate} \; + \; \phi^z_\mu(\mathbf{q},\omega), \quad (69)$$

where $\Phi^\pm_\mu(\mathbf{q},\omega) = \phi^\pm_\mu(\mathbf{q},\omega)$ with the matching conditions at $t = \pm\infty$

$$\phi^\alpha_1(-\infty) = \phi^\alpha_2(-\infty), \;\; \phi^\alpha_1(+\infty) = \phi^\alpha_2(+\infty). \quad (70)$$

We expand $\mathrm{Tr}\ln(G_0^{-1} + \boldsymbol{\phi}_\mu\boldsymbol{\sigma}\gamma^\mu)$ in accordance with

$$\mathrm{Tr}\ln(...) = \mathrm{Tr}\ln G_0^{-1} + Tr\sum_{n=1}^{\infty}\frac{(-1)^{n+1}}{n}(G_0\boldsymbol{\phi}_\mu\boldsymbol{\sigma}\gamma^\mu)^n. \quad (71)$$

The spectrum of the excitations (FM or AFM magnons) can be defined as poles of the transverse GF

$$D^{+-}_{\mathbf{x},t} = D(\mathbf{x},t) = -\mathrm{i}\langle T_C\phi^+_1(\mathbf{x},t)\phi^-_1(0,0)\rangle\cdot$$

The procedure of the calculation of this GF is similar to that for a "fermionic" GF. Introducing the sources and evaluating (71) one gets

$$D_0(\omega) = D_0^R\begin{pmatrix}1+N_\omega & N_\omega \\ 1+N_\omega & N_\omega\end{pmatrix} - D_0^A\begin{pmatrix}N_\omega & N_\omega \\ 1+N_\omega & 1+N_\omega\end{pmatrix}$$

where the retarded and advanced magnons GF's are

$$D^{R,A}(\mathbf{q},\omega) = (\omega - \omega(\mathbf{q}) \pm \mathrm{i}\delta)^{-1}, \;\; N_\omega = (\exp(\beta\omega)-1)^{-1}.$$

The magnon spectrum is determined by the zeros of the determinant of $J_{\mathbf{q}}^{-1} - \Pi_2^{+-}(\omega)$ (see Fig. 8a) in equilibrium

$$\omega_{\mathbf{q}} = J_0 \mathcal{M}(1 - \nu_{\mathbf{q}}) \Rightarrow \lambda \mathbf{q}^2, \tag{72}$$

for FM magnons and

$$\omega_{\mathbf{q}} = |J_0| \mathcal{N} \sqrt{1 - \nu_{\mathbf{q}}^2} \Rightarrow c|\mathbf{q}|, \tag{73}$$

for AFM magnons. The uniform and staggered magnetization are given by equations (55) and (63) correspondingly.

The magnon damping is defined by four-magnon processes Π_4^{+-+-}, shown in Figure 8b. The derivation of the kinetic equation and calculation of magnon damping is reserved here for a detailed publication.

We consider now the second possibility to decouple the four-fermion term in the Heisenberg model with the antiferromagnetic sign of spin-spin interaction which can be written in a form equivalent to (50):

$$H_{\rm int} = \frac{1}{2} \sum_{\langle ij \rangle} J_{ij} \psi_i^\dagger \psi_j \psi_j^\dagger \psi_i + \frac{1}{4} \sum_{\langle ij \rangle} J_{ij} \rho_i \rho_j. \tag{74}$$

Last term in the Hamiltonian (74) describes the fluctuations of semi-fermionic density $\rho_i = \psi_i^\dagger \psi_i$ and therefore is irrelevant for our calculations. In contrast to description of the local correlations achieved with the help of the local *vector* bosonic field we introduce now the bi-local *scalar* bosonic field Λ_{ij} depending on two sites and responsible for inter-site semi-fermionic correlations. Defining new coordinates $\boldsymbol{R}{=}(\boldsymbol{R}_i{+}\boldsymbol{R}_j)/2$, $\boldsymbol{r}{=}\boldsymbol{R}_i{-}\boldsymbol{R}_j$ and applying a Fourier transformation we obtain the effective action

$$\mathcal{A}_{\rm eff} = -\frac{1}{2} \mathrm{Tr}(\Lambda_{Pq_1}^T J_{\mathbf{q_1}-\mathbf{q_2}}^{-1} \sigma^z \Lambda_{Pq_2}) + \mathrm{Tr} \ln \left(G_0^{-1} - \Lambda_\mu \gamma^\mu \right).$$

This effective action describes the nonequilibrium quantum spin-liquid (SL). We confine ourselves to consider the uniform phase [50,51,54,55] of *Resonant Valence Bonds* (RVB) in 2D antiferromagnets. It is suitable to rewrite the functional in new variables, namely the amplitude Δ and the phase $\Theta = \boldsymbol{r}\boldsymbol{A}(\boldsymbol{R})$, according to formula

$$\Lambda_\mu^{\langle ij \rangle}(\boldsymbol{R},\ \boldsymbol{r}) = \Delta(\boldsymbol{r}) J \gamma^\mu \exp\left(\mathrm{i} \boldsymbol{r} \boldsymbol{A}_\mu(\boldsymbol{R})\right). \tag{75}$$

The exponent in (75) stands for gauge fluctuations to be taken in eikonal approximation. As a result, the effective action can be written in continuum limit in terms of the gauge fields A_α as follows:

$$\mathcal{A}_{\rm eff} = \oint_C \mathrm{d}t \int \mathrm{d}\boldsymbol{k} A_\alpha(\boldsymbol{k}, t) \pi^{\alpha\beta} A_\beta(\boldsymbol{k}, t). \tag{76}$$

The spectrum of excitations in the uniform SL is defined by the zeros of current-current correlation function [30]

$$\pi_{q,\omega}^{R,\alpha\beta} = \mathrm{Tr}(p^\alpha p^\beta (G_{p+q}^R G_p^K + G_{p+q}^K G_p^A) + \delta_{\alpha\beta} f(J_{\mathbf{p}} \Delta))$$

in equilibrium [52,53] and is purely diffusive (see *e.g.* [50])

$$\omega = \mathrm{i} J \Delta |\mathbf{q}|^3, \quad \Delta = -\sum_{\mathbf{q}} \nu(\mathbf{q}) \tanh\left(\frac{J_{\mathbf{q}} \Delta}{T}\right). \tag{77}$$

We denote G^K an off-diagonal element (Keldysh component) of semi-fermionic GF in triangular representation, provided that

$$G_0^K(\epsilon) = -\mathrm{i} 2\pi \delta(\epsilon \pm h)[B_{1/2}(\beta\epsilon) \pm \mathrm{i}\,\mathrm{sech}(\beta\epsilon)]$$

is expressed in terms of a Brillouin function $B_{1/2}$ containing correct information about occupied states. The equation of motion for G^K generally constitutes the quantum kinetic equation.

The quantum kinetic equation for nonequilibrium spin RVB-liquids can be obtained by taking into account the higher order diagrams similarly to Figure 8b with current-like vertices and will be presented elsewhere.

We discuss now briefly some possible applications of the imaginary-time and real-time Schwinger-Keldysh semi-fermionic formalism developed for SU(N) Hamiltonians for solution of the condensed matter physics problems. The Keldysh technique in application to disordered systems attracts a constant interest (see [42–46]) as an alternative approach to the replica technique. The main advantage of the closed-time contour calculations is an automatic normalization (disorder independent) of the partition function (see [42]). The application of real-time Schwinger-Keldysh approach allows one to study the quantum dynamics of disordered systems being out of equilibrium. We note, that the formalism developed in the present paper is also a very promising tool for description of a quantum phase transitions (magnetic, spin-glass etc.) in SU(N) models (see [58,59]) Another possible application of the semi-fermionic SU(N) representation is the description of paramagnet-(ferro) antiferromagnet or paramagnet-spin liquid transitions in equilibrium and nonequilibrium strongly correlated electron systems (see [60,61]). The nonlinear spin waves in strongly correlated local-itinerant magnets and the kinetic properties of the nonequilibrium spin liquid are also possible problems to be considered with the method proposed. The third interesting example of the application of the semi-fermionic formalism is the Kondo systems [62], for example the Kondo lattice model usually used for interpretation of an exotic properties of heavy-fermion compounds or the nonequilibrium Kondo-systems in semiconducting hetero-structures (see *e.g.* [63–66]). The main advantage of the semi-fermionic representation in applications to the strongly correlated systems in comparison with another methods is that the local constraint is taken into account exactly and the usual Feynman diagrammatic codex for the composite itinerant-local compound is applicable.

Summarizing, we constructed a general scheme for the semi-fermionic representation for generators of the SU(N) algebra. A representation for the partition function is found both in imaginary and real time. The approach developed leads to the standard diagram technique for Fermi operators, although the constraint is taken into account rigorously. The method proposed allows to treat SU(N) generators on the same footing as Fermi and Bose systems. The technique derived can be helpful for the description of quantum systems in the vicinity of a quantum phase transition point and for nonequilibrium systems.

This work was started on the workshop "Strongly correlated systems" in the ICTP in Trieste. One of the authors (MNK) is grateful to many participants of this workshop and especially N. Andrei, A. Tsvelik and A. Protogenov for fruitful discussions. We thank also D. Aristov and A. Luther for valuable comments and interest to our work. The work is supported by the DFG under SFB 410, by the Evangelisches Studienwerk Villigst (HF) and by an Alexander von Humboldt fellowship (MNK).

References

1. T. Holstein, H. Primakoff, Phys. Rev. B **58**, 1098 (1940).
2. F. Dyson, Phys. Rev. **102**, 1217 (1956).
3. S.V. Maleyev, Sov. Phys. JETP **6**, 776 (1958).
4. A.A. Abrikosov, Physics **2**, 5 (1965).
5. A.A. Abrikosov, Sov. Phys. JETP **26**, 641 (1967).
6. V.G. Vaks, A.I. Larkin, S.A. Pikin, Sov. Phys. JETP **26**, 188 (1968).
7. V.G. Vaks, A.I. Larkin, S.A. Pikin, Sov. Phys. JETP **26**, 647 (1968).
8. J. Hubbard, Proc. R. Soc. London A **285**, 542 (1965).
9. P. Coleman, C. Pepin, A.M. Tsvelik, Phys. Rev. B **62**, 3852 (2000).
10. P. Coleman, C. Pepin, A.M. Tsvelik, Nucl. Phys. B **586**, 641 (2000).
11. P. Coleman, J. Hopkinson, C. Pepin, Phys. Rev. B **63**, 140411R (2001).
12. N. Read, D.M. Newns, J. Phys. C **16**, 3273 (1983).
13. A. Auerbach, K. Levin, Phys. Rev. Lett. **57**, 877 (1986).
14. A.J. Millis, P.A. Lee, Phys. Rev. B **35**, 3394 (1987).
15. N.E. Bicker, Rev. Mod. Phys. **59**, 845 (1987).
16. G. Kotliar, A.E. Ruckenstein, Phys. Rev. Lett. **57**, 1362 (1986).
17. N. Read, S. Sachdev, Nuc. Phys. B **316**, 609 (1989).
18. N. Read, S. Sachdev, Phys. Rev. Lett. **62**, 1694 (1989).
19. N. Read, S. Sachdev, Phys. Rev. B **42**, 4568 (1990).
20. I. Affleck, J.B. Marston, Phys. Rev. B **37**, 3774 (1988).
21. J.B. Marston, I. Affleck, Phys. Rev. B **39**, 11538 (1989).
22. D.P. Arovas, A. Auerbach, Phys. Rev. B **38**, 316 (1988).
23. A. Chubukov, Phys. Rev. B **44**, 12318 (1991).
24. M. Gaudin, Nuc. Phys. **15**, 89 (1960).
25. V.N. Popov, S.A. Fedotov, Zh. Eksp. Teor. Fiz. **94**, 183 (1988) [Sov. Phys. JETP **67**, 535 (1988)].
26. J. Stein, R. Oppermann, Z. Phys. B **83**, 333 (1991).
27. C. Gros, M. D. Johnson, Physica B **165-166**, 985 (1990).
28. F. Bouis, M.N. Kiselev, Physica B **259-261**, 195 (1999).
29. M.N. Kiselev, R. Oppermann, JETP Lett. **71**, 250 (2000).
30. M.N. Kiselev, R. Oppermann, Phys. Rev. Lett. **85**, 5631 (2000).
31. H. Feldmann, R. Oppermann, J. Phys. A **33**, 1325 (2000).
32. E. Cartan, *Leçons sur la theorie des spineurs* (Hermann, Paris, 1938).
33. A. Auerbach, *Interacting electrons and quantum magnetism* (Springer, New York, 1994).
34. J.-Q. Chen, *Group representation theory for physicists* (World Scientific, Singapore, 1989).
35. D.B. Lichtenberg, *Unitary Symmetry and Elementary Particles* (Academic Press, New York, 1970).
36. O. Veits, R. Oppermann, M. Binderberger, J. Stein, J. Phys. I France **4**, 493 (1994).
37. F.D.M. Haldane, Phys. Rev. Lett. **67**, 937 (1991).
38. L.V. Keldysh. Sov. Phys. JETP **20**, 1018 (1965).
39. J. Schwinger, J. Math. Phys. **2**, 407 (1961).
40. J.Rammer, H. Smith, Rev. Mod. Phys. **58**, 323 (1986).
41. M.V. Feigel'man, A.I. Larkin, M.A. Skvortsov, Phys. Rev. B **61**, 12 361 (2000).
42. A. Kamenev, A. Andreev, Phys. Rev. B **60**, 2218 (1999).
43. C. Chamon, A. Ludwig, C. Nayak, Phys. Rev. B **60**, 2239 (1999).
44. A. Altland, A. Kamenev, Phys. Rev. Lett. **85**, 5615 (2000).
45. H.T.C. Stoof, Phys. Rev. Lett. **78**, 768 (1997).
46. L. Cugliandolo, G. Lozano, Phys. Rev. B **59**, 915 (1999).
47. R. Kree, Z. Phys. B **65**, 505 (1987).
48. H. Sompolinsky, Phys. Rev. Lett. **47**, 935 (1981), H. Sompolinski, A. Zippelius, Phys. Rev. Lett. **47**, 359 (1981).
49. V.S. Babichenko, A.N. Kozlov. Sol. State Comm. **59**, 39 (1986).
50. L.B. Ioffe, A.I. Larkin. Phys. Rev. B **39**, 8988 (1989).
51. P.A. Lee, N. Nagaosa, Phys. Rev. B **46**, 5621 (1992).
52. M. Reizer, Phys. Rev. B **39**, 1602 (1989).
53. M. Reizer, Phys. Rev. B **40**, 11571 (1989).
54. G. Baskaran, P.W. Anderson, Phys. Rev. B **37**, 580 (1988).
55. G. Baskaran, Z. Zou, P.W. Anderson, Sol. State Commun. **63**, 973 (1987).
56. F. Bouis, *Thèse de doctorat de l'école polytechnique*, Paris (1999).
57. S. Azakov, M. Dilaver, A.M. Oztas, Int. J. Mod. Phys. B **14**, 13 (2000), `cond-mat/9903379`.
58. A. Georges, O. Parcolet, S. Sachdev, Phys. Rev. Lett. **85**, 840 (2000).
59. A. Georges, O. Parcolet, S. Sachdev, Phys. Rev. B **63**, 134406 (2001).
60. M. Kiselev, R. Oppermann (unpublished).
61. M. Kiselev, K. Kikoin, R. Oppermann, Physica B (to be published).
62. V. Barzykin, I. Affleck, Phys. Rev. B **57**, 432 (1997).
63. M. Pustilnik, Y. Avishai, K. Kikoin, Phys. Rev. Lett. **84**, 1756 (2000).
64. A. Kaminski, Yu.V. Nazarov, L.I. Glazman, Phys. Rev. Lett. **83**, 384 (1999).
65. L.I. Glazman, F.W.J. Hekking, A.I. Larkin, Phys. Rev. Lett. **83**, 1830 (1999).
66. K. Kikoin, Y. Avishai, Phys. Rev. Lett. **86**, 2090 (2001).

Resonance Kondo tunneling through a double quantum dot at finite bias

M. N. Kiselev,[1] K. Kikoin,[2] and L. W. Molenkamp[3]
[1]*Institut für Theoretische Physik, Universität Würzburg, D-97074 Würzburg, Germany*
[2]*Ben-Gurion University of the Negev, Beer-Sheva 84105, Israel*
[3]*Physikalisches Institut (EP 3), Universität Würzburg, D-97074 Würzburg, Germany*
(Received 23 January 2003; revised manuscript received 15 May 2003; published 23 October 2003)

It is shown that the resonance Kondo tunneling through a double quantum dot (DQD) with *even* occupation and *singlet* ground state may arise at a strong bias, which compensates the energy of singlet/triplet excitation. Using the renormalization group technique we derive scaling equations and calculate the differential conductance as a function of an auxiliary dc bias for parallel DQD described by SO(4) symmetry. We analyze the decoherence effects associated with the triplet/singlet relaxation in DQD and discuss the shape of differential conductance line as a function of dc bias and temperature.

DOI: 10.1103/PhysRevB.68.155323 PACS number(s): 72.10.Fk, 05.10.Cc, 72.15.Qm

I. INTRODUCTION

Many fascinating collective effects, which exist in strongly correlated electron systems (metallic compounds containing transition and rare-earth elements) may be observed also in artificial nanosize devices (quantum wells, quantum dots, etc.). Moreover, fabricated nanoobjects provide unique possibility to create such conditions for observation of many-particle phenomena, which by no means may be reached in ''natural'' conditions. Kondo effect (KE) is one of such phenomena. It was found theoretically[1,2] and observed experimentally[3–5] that the charge-spin separation in low-energy excitation spectrum of quantum dots under strong Coulomb blockade manifests itself as a resonance Kondo-type tunneling through a dot with odd electron occupation $\mathcal{N}$ (one unpaired spin $S=1/2$). This resonance tunneling through a quantum dot connecting two metallic reservoirs (leads) is an analog of resonance spin scattering in metals with magnetic impurities. A Kondo-type tunneling arises under conditions which do not exist in conventional metallic compounds. The KE emerges as a dynamical phenomenon in strong time dependent electric field,[6–10] it may arise at finite frequency under light illumination.[11–13] Even the net zero spin of isolated quantum dot (even $\mathcal{N}$) is not an obstacle for the resonance Kondo tunneling. In this case it may be observed in double quantum dots (DQD) arranged in parallel geometry,[14] in T-shaped DQD,[14–16] in two-level single dots[17,18] or induced by strong magnetic field[19–22] whereas in conventional metals magnetic field only suppresses the Kondo scattering. The latter effect was also discovered experimentally.[23–25]

One of the most challenging options in Kondo physics of quantum dots is the possibility of controlling the Kondo effect by creating the nonequilibrium reservoir of fermionic excitations by means of strong bias $eV \gg T_K$ applied between the leads[26] (T_K is the equilibrium Kondo temperature which determines the energy scale of low-energy spin excitations in a quantum dot). However, in this case the decoherence effects may prevent the formation of a full scale Kondo resonance (see, e.g., discussion in Refs. 27–29). It was argued in recent disputes that the processes, associated with the finite current through a dot with odd $\mathcal{N}$ may destroy the coherence on an energy scale $\Gamma \gg T_K$ and thus prevent formation of a ground state Kondo singlet, so that only the weak coupling Kondo regime is possible in strongly nonequilibrium conditions.

In the present paper we discuss Kondo tunneling through DQD with even $\mathcal{N}$, whose ground state is a spin singlet $|S\rangle$. It will be shown that the Kondo tunneling through *excited* triplet state $|T\rangle$ arises at finite eV. In this case the ground state is stable against any kind of spin-flip processes induced by external current, the decoherence effects develop only in the intermediate (virtual) triplet state, and the estimates of decoherence rate should be revisited.

As was noticed in Ref. 15, quantum dots with even $\mathcal{N}$ possess the dynamical symmetry $SO(4)$ of *spin rotator* in the Kondo tunneling regime, provided the low-energy part of excitation spectrum is formed by a singlet-triplet (ST) pair, and all other excitations are separated from the ST manifold by a gap noticeably exceeding the tunneling rate γ. A DQD with even $\mathcal{N}$ in a side-bound (T-shape) configuration where two wells are coupled by the tunneling v and only one of them (say, l) is coupled to metallic leads (L,R) is a simplest system satisfying this condition.[15] Such system was realized experimentally in Ref. 30. Novel features introduced by the dynamical symmetry in Kondo tunneling are connected with the fact that unlike the case of conventional $SU(2)$ symmetry of spin vector **S**, the $SO(4)$ group possesses two generators **S** and **P**. The latter vector describes transitions between singlet and triplet states of spin manifold (this vector is an analog of Runge-Lenz vector describing the hidden symmetry of hydrogen atom). As was shown in Ref. 14, this vector alone is responsible for Kondo tunneling through quantum dot with even $\mathcal{N}$ induced by external magnetic field.

Another manifestation of dynamical symmetry peculiar to DQDs with even $\mathcal{N}$ is revealed in this paper. It is shown that in the case when the ground state is singlet $|S\rangle$ and the S/T gap $\delta \gg T_K$, a Kondo resonance channel arises under a strong bias eV comparable with δ. The channel opens at $|eV-\delta| < T_K$, and the tunneling is determined by the *nondiagonal* component $J_{ST}=\langle T|J|S\rangle$ of effective exchange induced by the electron tunneling through DQD [see Fig. 1 (right panel)].

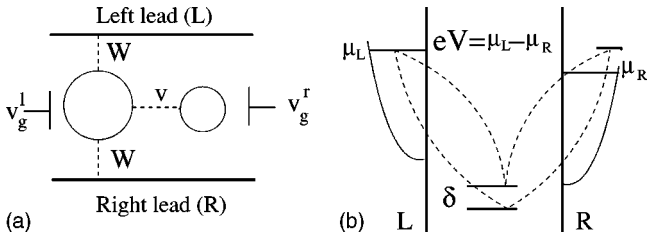

FIG. 1. Left panel: Double quantum dot in a side-bound configuration. Right panel: cotunneling processes in biased DQD responsible for the resonance Kondo tunneling.

II. COTUNNELING HAMILTONIAN OF T-SHAPED DQD

The basic properties of symmetric DQD occupied by even number of electrons $\mathcal{N}=2n$ under strong Coulomb blockade in each well are manifested already in the simplest case $n=1$, which is considered below. Such DQD is an artificial analog of a hydrogen molecule H_2. If the interwell Coulomb blockade Q is strong enough, one has $\mathcal{N}=n_l+n_r$, $n_l=n_r=1$, the lowest states of DQD are singlet and triplet and the next levels are separated from ST pair by a charge transfer gap $\sim Q$. We assume that both wells are neutral at $n_{l,r}=1$. Then the effective interwell exchange I responsible for the singlet-triplet splitting arises because of tunneling v between two wells, $I=v^2/Q=\delta$. It is convenient to write the effective spin Hamiltonian of isolated DQD in the form

$$H_d=E_S\left|S\right\rangle\left\langle S\right|+\sum_{\eta} E_T\left|T\eta\right\rangle\left\langle T\eta\right|\equiv\sum_{\Lambda=S,T\eta} E_\Lambda X^{\Lambda\Lambda}, \tag{1}$$

where $X^{\Lambda\Lambda'}=|\Lambda\rangle\langle\Lambda'|$ is a Hubbard configuration change operator (see, e.g., Ref. 31), $E_T=E_S+\delta$, $\eta=\pm,0$ are three projections of $S=1$ vector. Two other terms completing the Anderson Hamiltonian, which describes the system shown in Fig. 1 (left panel), are

$$H_b+H_t=\sum_{k\alpha\sigma}\epsilon_{k\alpha}c^\dagger_{k\alpha\sigma}c_{k\alpha\sigma}+\sum_{\Lambda\lambda}\sum_{k\alpha\sigma}(W^{\Lambda\lambda}_\sigma c^\dagger_{k\alpha\sigma}X^{\lambda\Lambda}+\text{H.c.}). \tag{2}$$

The first term describes metallic electrons in the leads and the second one stands for tunneling between the leads and the DQD. Here $\alpha=L,R$ marks electrons in the left and right lead, respectively, the bias eV is applied to the left lead, so that the chemical potentials are $\mu_{FL}=\mu_{FR}+eV$, $W^{\Lambda\lambda}_\sigma$ is the tunneling amplitude for the well l (left), $|\lambda\rangle$ are one-electron states of DQD, which arises after escape of an electron with spin projection σ from DQD in a state $|\Lambda\rangle$.

We solve the problem in a Schrieffer-Wolff (SW) limit,[31] when the activation energies $|E_\Lambda-E_\lambda-\mu_{F\alpha}|$ and Coulomb blockade energy Q are essentially larger then the tunneling rate γ, and charge fluctuations are completely suppressed both in the ground and excited state of DQD. In this limit one may start with the SW transformation, which projects out charge excitations. We confine ourselves with the bias $eV\lesssim\delta\ll D$, where D is the width of the electrons in the leads, so the leads are considered in the SW transformation as two independent quasi equilibrium reservoirs (see Refs. 8,9). As is shown in Ref. 15, the SW transformation being applied to a spin rotator results in the following effective spin Hamiltonian

$$H_{\text{int}}=\sum_{\alpha\alpha'}[(J^{TT}_{\alpha\alpha'}\mathbf{S}+J^{ST}_{\alpha\alpha'}\mathbf{P})\cdot\mathbf{s}_{\alpha\alpha'}+J^{SS}_{\alpha\alpha'}X^{SS}n_{\alpha\alpha'}]. \tag{3}$$

Here $\mathbf{s}_{\alpha\alpha'}=\Sigma_{kk'}c^\dagger_{k\alpha\sigma}\hat{\tau}c_{k'\alpha'\sigma'}$, $n_{\alpha\alpha'}=\Sigma_{kk'}c^\dagger_{k\alpha\sigma}\hat{1}c_{k'\alpha'\sigma}$, $\hat{\tau}$, $\hat{1}$ are the Pauli matrices and unity matrix, respectively. The effective exchange constants are

$$J^{\Lambda\Lambda'}_{\alpha\alpha'}\approx\frac{W^{\Lambda\lambda}_\sigma W^{*\lambda\Lambda'}_\sigma}{2}\left(\frac{1}{\epsilon_{F\alpha}-E_S/2}+\frac{1}{\epsilon_{F\alpha'}-E_S/2}\right).$$

In this approximation the small differences between singlet and triplet states are neglected. In addition, $J^{\Lambda\Lambda'}_{\alpha\alpha'}\sim I$ in real DQD.

Two vectors **S** and **P** with spherical components

$$S^+=\sqrt{2}(X^{10}+X^{0-1}),\quad S^-=\sqrt{2}(X^{01}+X^{-10}),$$

$$S^z=X^{11}-X^{-1-1},\quad P^z=-(X^{0S}+X^{S0}),$$

$$P^+=\sqrt{2}(X^{1S}-X^{S-1}),\quad P^-=\sqrt{2}(X^{S1}-X^{-1S}) \tag{4}$$

obey the commutation relations of o_4 algebra

$$[S_j,S_k]=ie_{jkl}S_l,\quad [P_j,P_k]=ie_{jkl}S_l,\quad [P_j,S_k]=ie_{jkl}P_l$$

(j,k,l are Cartesian coordinates and e_{jkl} is a Levi-Civita tensor). These vectors are orthogonal, $\mathbf{S}\cdot\mathbf{P}=0$, and the Casimir operator is $\mathbf{S}^2+\mathbf{P}^2=3$. Thus, the singlet state is involved in spin scattering via the components of the vector **P**.

We use $SU(2)$-like semifermionic representation for S operators[32–34]

$$S^+=\sqrt{2}(f^\dagger_0f_{-1}+f^\dagger_1f_0),\quad S^-=\sqrt{2}(f^\dagger_{-1}f_0+f^\dagger_0f_1),$$

$$S^z=f^\dagger_1f_1-f^\dagger_{-1}f_{-1}, \tag{5}$$

where $f^\dagger_{\pm1}$ are creation operators for fermions with spin "up" and "down," respectively, whereas f_0 stands for spinless fermion.[32,33] This representation can be generalized for $SO(4)$ group by introducing another spinless fermion f_s to take into consideration the singlet state. As a result, the P operators are given by the following equations:

$$P^+=\sqrt{2}(f^\dagger_1f_s-f^\dagger_sf_{-1}),\quad P^-=\sqrt{2}(f^\dagger_sf_1-f^\dagger_{-1}f_s),$$

$$P^z=-(f^\dagger_0f_s+f^\dagger_sf_0). \tag{6}$$

The Casimir operator $\mathbf{S}^2+\mathbf{P}^2=3$ transforms to the local constraint

$$\sum_{\Lambda=\pm,0,s}f^\dagger_\Lambda f_\Lambda=1.$$

The final form of the spin cotunneling Hamiltonian is

$$H_{\rm int}=\sum_{kk',\alpha\alpha'=L,R} J^S_{\alpha\alpha'} f_s^\dagger f_s c^\dagger_{k\alpha\sigma} c_{k'\alpha'\sigma} + \sum_{kk',\alpha\alpha'\Lambda\Lambda'} (J^T_{\alpha\alpha'}\hat{S}^d_{\Lambda\Lambda'} + J^{ST}_{\alpha\alpha'}\hat{P}^d_{\Lambda\Lambda'}) \times \tau^d_{\sigma\sigma'} c^\dagger_{k\alpha\sigma} c_{k'\alpha'\sigma'} f^\dagger_\Lambda f_{\Lambda'}, \quad (7)$$

where $\hat{S}^d$ and $\hat{P}^d (d=x,y,z)$ are 4×4 matrices defined by relations (4)–(6) and $J^S=J^{SS}$, $J^T=J^{TT}$, and J^{ST} are singlet, triplet, and singlet-triplet coupling SW constants, respectively.

The cotunneling in the ground singlet state is described by the first term of the Hamiltonian (7), and no spin flip processes accompanying the electron transfer between the leads emerge in this state. However, the last term in Eq. (7) links the singlet ground state with the excited triplet and opens a Kondo channel. In equilibrium this channel is ineffective, because the incident electron should have the energy δ to be able to initiate spin-flip processes. We will show in the next section that the situation changes radically, when strong enough external bias is applied.

III. KONDO SINGULARITY IN TUNNELING THROUGH DQD AT FINITE BIAS

We deal with the case, which was not met in the previous studies of non-equilibrium Kondo tunneling. The ground state of the system is singlet, and the Kondo tunneling in equilibrium is quenched at $T\sim\delta$. Thus, the elastic Kondo tunneling arises only provided $T_K \gg \delta$ in accordance with the theory of two-impurity Kondo effect.[15,35,36] However, the energy necessary for spin flip may be donated by external electric field eV applied to the left lead, and in the opposite limit $T_K \ll \delta$ the elastic channel emerges at $eV\approx\delta$. The processes responsible for resonance Kondo cotunneling at finite bias are shown in Fig. 1 (left panel).

In conventional spin $S=1/2$ quantum dots the Kondo regime out of equilibrium is affected by spin relaxation and decoherence processes, which emerge at $eV \gg T_K$ (see, e.g., Refs. 9,27–29). These processes appear in the same order as Kondo cotunneling itself, and one should use the nonequilibrium perturbation theory (e.g., Keldysh technique) to take them into account in a proper way. In our case these effects are expected to be weaker, because the nonzero spin state is involved in Kondo tunneling only as an intermediate virtual state arising due to S/T transitions induced by the second term in the Hamiltonian (3), which contains vector **P**. The nonequilibrium repopulation effects in DQD are weak as well (see next section, where the nonequilibrium effects are discussed in more details).

Having this in mind, we describe Kondo tunneling through DQD at finite $eV \lesssim \delta$ within the quasiequilibrium perturbation theory in a weak coupling regime (see the quasiequilibrium approach to description of decoherence rate at large eV in Ref. 27). To develop the perturbative approach for $T>T_K$ we introduce the temperature Green's functions (GF) for electrons in a dot, $\mathcal{G}_\Lambda(\tau)=-\langle T_\tau f_\Lambda(\tau) f^\dagger_\Lambda(0)\rangle$, and GF for the electrons in the left (L) and right (R) lead,

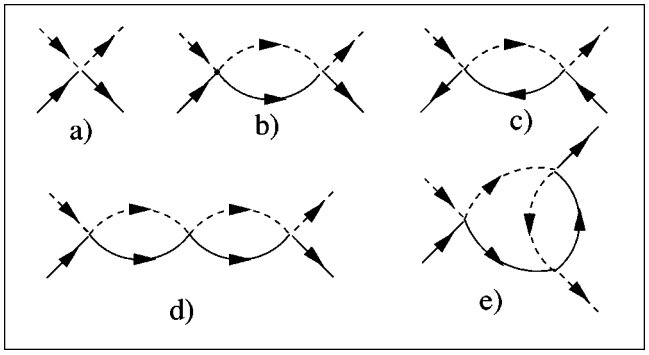

FIG. 2. Leading (b),(d) and next to leading (c),(e) parquet diagrams determining renormalization of J^S (a). Solid lines denote electrons in the leads. Dashed lines stand for electrons in the dot.

$G_{L,R}(k,\tau)=-\langle T_\tau c_{L,R\sigma}(k,\tau) c^\dagger_{L,R\sigma}(k,0)\rangle$. Performing a Fourier transformation in imaginary time for bare GF's, we come to following expressions:

$$G^0_{k\alpha}(\epsilon_n)=(i\epsilon_n-\epsilon_{k\alpha}+\mu_{L,R})^{-1},$$

$$\mathcal{G}^0_\eta(\omega_m)=(i\omega_m-E_T)^{-1}, \quad \eta=-1,0,1,$$

$$\mathcal{G}^0_s(\epsilon_n)=(i\epsilon_n-E_S)^{-1}, \quad (8)$$

with $\epsilon_n=2\pi T(n+1/2)$ and $\omega_m=2\pi T(m+1/3)$.[32,33] The first leading and next to leading parquet diagrams are shown on Fig. 2.

Corrections to the singlet vertex $\Gamma(\omega,0;\omega',0)$ are calculated using an analytical continuation of GF's to the real axis ω and taking into account the shift of the chemical potential in the left lead. Since the electron from the left lead tunnels into the empty state in the right lead separated by the energy eV, we have to put $\omega=eV$, $\omega'=0$ in the final expression for $\Gamma(\omega,0;\omega',0)$. Thus, unlike conventional Kondo effect we deal with the vertex at finite frequency ω similarly to the problem considered in Ref. 27. We assume that the leads remain in equilibrium under applied bias and neglect the relaxation processes in the leads (''hot'' leads). In a weak coupling regime $T>T_K$ the leading non-Born contributions to the tunnel current are determined by the diagrams of Figs. 2(b)–2(e).

The effective vertex shown in Fig. 2(b) is given by the following equation:

$$\Gamma^{(2b)}_{LR}(\omega)=J^{ST}_{LL}J^{TS}_{LR}\sum_{\mathbf{k}}\frac{1-f(\epsilon_{kL}-eV)}{\omega-\epsilon_{kL}+\mu_L-\delta}. \quad (9)$$

Changing the variable ϵ_{kL} for $\epsilon_{kL}-eV$ one finds that

$$\Gamma^{(2b)}_{LR}(\omega=eV)\sim J^{ST}_{LL}J^{TS}_{LR}\nu\ln(D/\max\{(eV-\delta),T\}).$$

Here $D\sim\varepsilon_F$ is a cutoff energy determining effective bandwidth, ν is a density of states on a Fermi level and $f(\varepsilon)$ is the Fermi function. Therefore, under condition $|eV-\delta| \ll \max[eV,\delta]$ this correction does not depend on eV and becomes quasielastic.

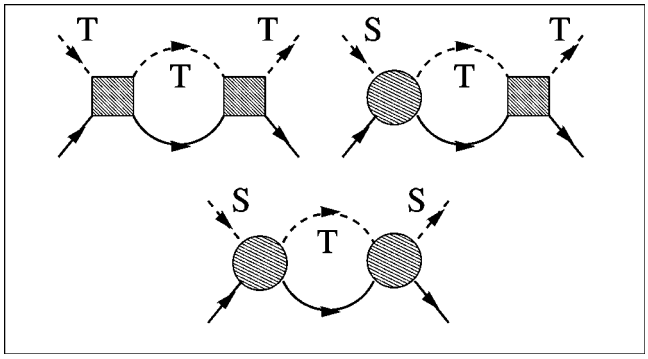

FIG. 3. Irreducible diagrams contributing to RG equations. Hatched boxes and circles stand for triplet-triplet and singlet-triplet vertices respectively. Notations for lines are the same as in Fig. 2.

Unlike the diagram Fig. 2(b), its ''parquet counterpart'' term Fig. 2(c) contains $eV+\delta$ in the argument of the Kondo logarithm:

$$\Gamma_{LR}^{(2c)}(\omega)=J_{LL}^{ST}J_{LR}^{TS}\sum_{\mathbf{k}}\frac{f(\epsilon_{kL}-eV)}{\omega-\epsilon_{kL}+\mu_L+\delta}. \tag{10}$$

At $eV\sim\delta\gg T$ this contribution is estimated as

$$\Gamma_{LR}^{(2c)}(eV)\sim J_{LL}^{ST}J_{LR}^{TS}\nu\ln(D/(eV+\delta))\ll\Gamma_{LR}^{(2b)}(eV).$$

Similar estimates for Figs. 2(d) and 2(e) give

$$\Gamma_{LR}^{(2d)}(\omega)\sim J_{LL}^{ST}J_{LL}^{T}J_{LR}^{TS}\nu^2\ln^2(D/\max\{\omega,(eV-\delta),T\}),$$

$$\Gamma_{LR}^{(2e)}(\omega)\sim J_{LL}^{ST}J_{LL}^{T}J_{LR}^{TS}\nu^2\ln(D/\max\{\omega,(eV-\delta),T\})\times\ln(D/\max\{\omega,eV,T\}. \tag{11}$$

Then $\Gamma_{LR}^{(2e)}(\omega)\ll\Gamma_{LR}^{(2d)}(\omega)$ at $eV\to\delta$.

Thus, the Kondo singularity is restored in nonequilibrium conditions where the electrons in the left lead acquire additional energy in external electric field, which compensates the energy loss δ in a singlet-triplet excitation. The leading sequence of most divergent diagrams degenerates in this case from a parquet to a ladder series.

Following the poor man's scaling approach, we derive the system of coupled renormalization group (RG) equations for Eq. (7). The equations for LL cotunneling are

$$\frac{dJ_{LL}^{T}}{d\ln D}=-\nu(J_{LL}^{T})^2,\quad \frac{dJ_{LL}^{ST}}{d\ln D}=-\nu J_{LL}^{ST}J_{LL}^{T}. \tag{12}$$

The scaling equations for J_{LR}^{Λ} are as follows:

$$\frac{dJ_{LR}^{T}}{d\ln D}=-\nu J_{LL}^{T}J_{LR}^{T},\quad \frac{dJ_{LR}^{ST}}{d\ln D}=-\nu J_{LL}^{ST}J_{LR}^{T},$$

$$\frac{dJ_{LR}^{S}}{d\ln D}=\frac{1}{2}\nu\left(J_{LL,+}^{ST}J_{LR,-}^{TS}+\frac{1}{2}J_{LL,z}^{ST}J_{LR,z}^{TS}\right). \tag{13}$$

One-loop diagrams corresponding to the poor man's scaling procedure are shown in Fig. 3. To derive these equations we collected only terms $\sim(J^T)^n\ln^{n+1}(D/T)$ neglecting contributions containing $\ln[D/(eV)]$. The analysis of RG equations beyond the one loop approximation will be published elsewhere.

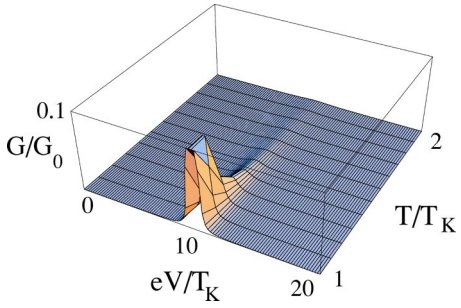

FIG. 4. The Kondo conductance as a function of dc-bias eV/T_K and T/T_K. The singlet-triplet splitting $\delta/T_K=10$.

The solution of the system (13) reads as follows:

$$J_{\alpha,\alpha'}^{T}=\frac{J_0^T}{1-\nu J_0^T\ln(D/T)},\quad J_{\alpha,\alpha'}^{ST}=\frac{J_0^{ST}}{1-\nu J_0^T\ln(D/T)},$$

$$J_{LR}^{S}=J_0^S-\frac{3}{4}\nu(J_0^{ST})^2\frac{\ln(D/T)}{1-\nu J_0^T\ln(D/T)}. \tag{14}$$

Here $\alpha=L$, $\alpha'=L,R$. One should note that the Kondo temperature is determined by triplet-triplet processes only in spite of the fact that the ground state is singlet. One finds from Eq. (14) that $T_K=D\exp[-1/(\nu J_0^T)]$. This temperature is noticeably smaller than the ''equilibrium'' Kondo temperature T_{K0}, which emerges in tunneling through triplet channel in the ground state, namely, $T_K\approx T_{K0}^2/D$. The reason for this difference is the reduction of usual parquet equations for T_K to a simple ladder series. In this respect our case differs also from conventional Kondo effect at strong bias,[27] where the nonequilibrium Kondo temperature $T^*\approx T_{K0}^2/eV$ arises. In our model the finite bias does not enter T_K because of the compensation $eV\approx\delta$ in spite of the fact that we take the argument $\omega=eV$ in the vertex (9).

The differential conductance $G(eV,T)/G_0\sim|J_{LR}^{ST}|^2$ (see Ref. 37) is the universal function of two parameters T/T_K and eV/T_K, $G_0=e^2/\pi\hbar$:

$$G/G_0\sim\ln^{-2}(\max[(eV-\delta),T]/T_K). \tag{15}$$

Its behavior as a function of bias and temperature is shown in Fig. 4. It is seen from this picture that the resonance tunneling ''flashes'' at $eV\sim\delta$ and dies away out of this resonance. In this picture the decoherence effects are not taken into account, and it stability against various non-equilibrium corrections should be checked.

IV. DECOHERENCE EFFECTS

We analyze now the decoherence rate $\hbar/\tau_d$ associated with T/S transition relaxation induced by cotunneling. The calculations are performed in the same order of the perturbation theory as it has been done for the vertex renormalization

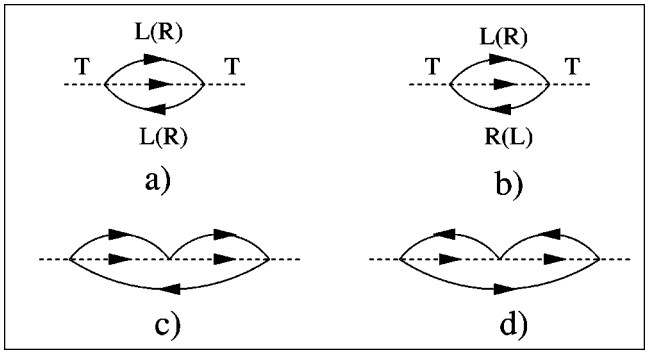

FIG. 5. Leading diagrams (a)–(d) for $\hbar/\tau_d$ (see text). Dashed line in the self-energy part stands for the singlet state of a two-electron configuration in the dot.

(see Figs. 2 and 3). The details of the calculation scheme are presented in the Appendix.

To estimate the decoherence effects, one should calculate the decay of the triplet state or in other terms to find the imaginary part of the retarded self-energy of triplet semifermion propagators at actual frequency [see discussion before Eq. (9)], $\hbar/\tau_d = -2\,\mathrm{Im}\,\Sigma_T^R(\omega)$. The second and third order diagrams determining $\hbar/\tau_d$ are shown in Figs. 5(a)–5(d). Two leading terms given by the diagrams of Figs. 5(a), 5(b) describe the damping of triplet excitation due to its inelastic relaxation to the ground singlet state. These terms are calculated in Appendix [see Eqs. (A8), (A10)]. One finds from these equations that the relaxation rate associated with ST transition is

$$1/\tau_d^{ST} \sim (J^{ST}/D)^2 \max[eV, \omega, T_K]. \tag{16}$$

It should be noted that for corrections associated with LL (RR) diagrams [Fig. 5(a)], describing cotunneling processes on a left (right) lead, the use of quasiequilibrium technique is fully justified when the leads themselves are in thermal equilibrium. We are interested in the zero frequency damping at resonance $eV \approx \delta$. Neglecting the small difference between J^T and J^{ST} (see Ref. 15), we also take $J^T \approx J^{ST} = J$. Thus the $T \to S$ spin relaxation effect (16) does not contain logarithmic enhancement factor in the lowest order. It is estimated as

$$1/\tau_d^{ST} \sim (eV)(J/D)^2 \approx J^3/D^2. \tag{17}$$

The repopulation of triplet state as a function of external bias is controlled by the occupation number for triplet state modified by the bias eV. The latter, in turn, depends on the modified exchange splitting δ^* given by solution of the equation

$$\delta^* - \delta = \mathrm{Re}\,\Sigma^R(\delta^*, eV, T). \tag{18}$$

The $\mathrm{Re}\,\Sigma^R$ [Figs. 5(a), 5(b)] is given by

$$\mathrm{Re}\,\Sigma_{TST}^{R(2)}(\omega, eV, T) = -a_2 \left(\frac{J}{D}\right)^2 \omega \ln\left(\frac{D}{\max[\omega, eV, T]}\right), \tag{19}$$

where $a_2 \sim 1$ is a numerical coefficient. As it is seen, the perturbative equation for $\mathrm{Re}\,\Sigma^R$ is beyond the scope of leading-log approximation. As a result, $\delta^*(eV) - \delta \ll \delta$ and repopulation of the triplet state is exponentially small. The corresponding factor in the occupation number is

$$P_t(eV) = \exp[-\delta^*(eV)/T]. \tag{20}$$

The effects of repopulation become important only at $eV \gg \delta$ when $|\delta^* - \delta| \sim \delta$. In that case the quasiequilibrium approach is not applicable and one should start with the Keldysh formalism.[27,28] This regime is definitely not realized in conditions considered above.

Next second order contribution is the damping of triplet state itself given by Eqs. (A12), (A14). It is seen from these equations that this damping is of threshold character

$$1/\tau_d^{TT} \sim (J/D)^2 (\omega - \delta)\,\theta(\omega - \delta), \tag{21}$$

where $\theta(\omega)$ is a Heaviside step function. These processes emerge only at $\omega > \delta$, so unlike the conventional case[27] they are not dangerous.

Corresponding contribution to $\mathrm{Re}\,\Sigma^R$ casts the form

$$\mathrm{Re}\,\Sigma_{TTT}^{R(2)} = -b_2 \left(\frac{J}{D}\right)^2 (\delta - \omega) \ln\left|\frac{D}{\max[(\delta - \omega), T]}\right|, \tag{22}$$

where $b_2 \sim 1$.

Next, one has to check whether the higher order logarithmic corrections modify the estimate (17). These corrections start with the third order terms shown in Figs. 5(c), 5(d). Straightforward calculations lead to $eV(J/D)^3 \ln(D/eV)$ correction [see the first term Eq. (A23)]. This leading term like the second order term originates from $T \to S$ spin relaxation processes. All other contributions are either of threshold character, or vanish at $\omega \to 0$. As a result, the estimate

$$\hbar/\tau_d \sim eV(J_0^{ST}/D)^2 \{1 + O[\nu J \ln(D/(eV))]\}$$

holds. The topological structure (sequence of intermediate singlet and triplet states and cotunneling processes in the left and right lead) in perturbative corrections for the triplet self-energy part is different from those for the singlet-singlet vertex (see Appendix). Namely, the leading (ladder) diagrams for the vertex contain maximal possible number of intermediate triplet states, whereas the higher order nonthreshold log-diagrams for the self-energy part must contain at least one intermediate singlet state. As it is seen from the Appendix [Eqs. (A18)–(A23)], the higher order contributions to $\mathrm{Im}\,\Sigma_T(\omega)$ are not universal and the coefficients in front of log have sophisticated frequency dependence. As a result, the perturbative series for triplet self-energy part cannot be collected in parquet structures and remain beyond the leading-log approximation discussed in the Sec. III. There is no strong enhancement of the second order term in SO(4) spin rotator model in contrast to SU(2) case discussed in Ref. 27. As was pointed out above, the main reason for differences in estimates of coherence rate is that in case of QD with odd $\mathcal{N}$, the Kondo singlet develops in the ground state of the dot, and decoherence frustrate this ground state. In DQD with even $\mathcal{N}$ the triplet spin state arises only as a virtual state in cotunneling processes, and our calculations demonstrate explicitly that decoherence effects in this case are essentially weaker.

The third order correction to $\mathrm{Re}\,\Sigma$ is given by

$$\mathrm{Re}\,\Sigma^{R(3)}(\omega)\sim\left(\frac{J}{D}\right)^3\omega\ln^2\left(\frac{D}{\omega}\right) \tag{23}$$

(see Appendix). This correction also remains beyond the leading-log approximation.

Thus we conclude that the decoherence effects are not destructive for Kondo tunneling through T-shaped DQD, i.e., the $T_K\gg\hbar/\tau_d$ is valid provided

$$\delta(\delta/D)^2\ll T_K\ll\delta. \tag{24}$$

This interval is wide enough because $\delta/D\ll 1$ in the Anderson model.

The same calculation procedure may be repeated in Keldysh technique. It is seen immediately that in the leading-log approximation the off-diagonal terms in Keldysh matrix are not changed in comparison with equilibrium distribution functions because of the same threshold character of repopulation processes, so in the leading approximation the key diagram Fig. 5(b) (determining L-R current through the dot) calculated in Keldysh technique remains the same as Eqs. (A8)–(A10).

In fact, repopulation effects result in asymmetry of the Kondo-peak similar to that in Ref. 28 due to the threshold character of $\mathrm{Im}\,\Sigma_{TTT}$ (see Appendix). This asymmetry becomes noticeable at $eV\gg\delta$, where our quasiequilibrium approach fails, but this region is beyond our interest, because the bias-induced Kondo tunneling is negligible at large biases (see Fig. 4).

V. CONCLUDING REMARKS

We have shown in this paper that the tunneling through DQD with even $\mathcal{N}$ with singlet ground state and triplet excitation divided by the energy gap $\delta\gg T_K$ from the singlet state exhibits a peak in differential conductance at $eV\approx\delta$ (Fig. 4). This result is in striking contrast with the zero bias anomaly (ZBA) at $eV\approx 0$ which arises in the opposite limit $\delta<T_K$. In the latter case the Kondo screening is quenched at energies less than δ, so the ZBA has a form of a dip in the Kondo peak (see Ref. 18 for a detailed explanation of this effect).

In this case strong external bias initiates the Kondo effect in DQD, whereas in a conventional situation (QD with odd $\mathcal{N}$ spin 1/2 in the ground state) strong enough bias is destructive for Kondo tunneling. We have shown that the principal features of Kondo effect in this specific situation may be captured within a quasiequilibrium approach. The scaling equations (13), (14) can also be derived in Schwinger-Keldysh formalism (see Refs. 28,33) by applying the ''poor man's scaling'' approach directly to the dot conductance.[8]

Of course, our RG approach is valid only in the weak coupling regime. Although in our case the limitations imposed by decoherence effects are more liberal than those existing in conventional QD, they apparently prevent the full formation of the Kondo resonance. To clarify this point one has to use a genuine non-equilibrium approach, and we hope to do it in forthcoming publications.

One should mention yet another possible experimental realization of resonance Kondo tunneling driven by external electric field. Applying the alternate field $V=V_{\mathrm{ac}}\cos(\omega t)$ to the parallel DQD, one takes into consideration two effects, namely, (i) enhancement of Kondo conductance by tuning the amplitude of ac voltage to satisfy the condition $|eV_{\mathrm{ac}}-\delta|\ll T_K$ and (ii) spin decoherence effects due to finite decoherence rate.[8] One can expect that if the decoherence rate $\hbar/\tau\gg T_K$,

$$G_{\mathrm{peak}}/G_0\sim\ln^{-2}(\hbar/\tau T_K), \tag{25}$$

whereas in the opposite limit $\hbar/\tau\ll T_K$,

$$G_{\mathrm{peak}}=\overline{G(V_{ac}\cos[\omega t])} \tag{26}$$

is averaged over a period of variation of ac bias. In this case the estimate (15) is also valid.

In conclusion, we have provided an example of Kondo effect, which exists *only* in non-equilibrium conditions. It is driven by external electric field in tunneling through a quantum dot with even number of electrons, when the low-lying states are those of spin rotator. This is not too exotic situation because as a rule, a singlet ground state implies a triplet excitation. If the ST pair is separated by a gap from other excitons, then tuning the dc bias in such a way that applied voltage compensates the energy of triplet excitation, one reaches the regime of Kondo peak in conductance. This theoretically predicted effect can be observed in dc- and ac-biased double quantum dots in parallel geometry.

ACKNOWLEDGMENTS

This work was partially supported (MK) by the European Commission under LF project: Access to the Weizmann Institute Submicron Center (Contract No. HPRI-CT-1999-00069). The authors are grateful to Y. Avishai, A. Finkel'stein, A. Rosch, and M. Heiblum for numerous discussions. The financial support of the Deutsche Forschungsgemeinschaft (SFB-410) is acknowledged. The work of K.K. was supported by ISF grant.

APPENDIX

We calculate perturbative corrections for $\Sigma(\omega)$ by performing analytical continuation of $\Sigma(i\omega_n)$ into upper half plane of ω. The parameter of perturbation theory is $\nu J\ll 1$ where ν denotes the density of states for conduction electrons at the Fermi surface.

The second order self-energies have the following structure (the indices T and ST in exchange vertices are temporarily omitted):

$$\Sigma^{(2)}(i\omega_n)\sim J^2T^2\sum_{\omega_1\omega_2}\sum_{\mathbf{k_1},\mathbf{k_2}}G^0(-i\omega_1,-\mathbf{k}_1)\times G^0(i\omega_2,\mathbf{k}_2)\mathcal{G}^0(i\omega_n+i\omega_1+i\omega_2). \tag{A1}$$

The Green functions (GF) are defined in Eq. (8). Performing summation over Matsubara frequencies ω_1,ω_2 and replacing

the summation over $\mathbf{k_1},\mathbf{k_2}$ by integration over ξ_1,ξ_2 in accordance with standard procedure, we come to following expression:

$$\Sigma^{(2)}(i\omega_n)\sim\frac{1}{2}(J\nu)^2\int_{-D}^{D}d\xi_1\int_{-D}^{D}d\xi_2\frac{\left[\tanh\left(\frac{\lambda}{2T}\right)-\tanh\left(\frac{\xi_2}{2T}\right)\right]\left[\tanh\left(\frac{\xi_1}{2T}\right)-\tanh\left(\frac{\xi_2-\lambda}{2T}\right)\right]}{i\omega_n+\xi_2-\xi_1-\lambda_{S,T}}. \tag{A2}$$

Here we assumed that conduction electron's band has a width $W=2D$, $\epsilon_F\sim D$ and $\nu=1/D$ in order to simplify our calculations. This assumption is sufficient for log-accuracy of our theory. The Lagrange multipliers $\lambda_{S,T}$ are different for singlet (triplet) GF, namely, $\lambda_S=E_S$ and $\lambda_T=E_T+i\pi T/3$.

To account for decoherence effects in the same order of perturbation theory as we have done for the vertex corrections, we focus on the self-energy (SE) part of triplet GF. This SE has to be plugged in back to a semifermionic propagator to provide a self-consistent treatment of the problem. We denote the self-energy parts associated with singlet/triplet and triplet/triplet transitions as Σ_{TST} and Σ_{TTT}, respectively.

To prevent double occupancy of singlet/triplet states we take the limit $\mathrm{Re}[\lambda_{S,T}]\gg T$ in the numerator of Eq. (A2). As a result, Eq. (A2) casts the form

$$\Sigma^{(2)}(i\omega_n)\sim(J\nu)^2\int_{-D}^{D}d\xi_1\int_{-D}^{D}d\xi_2\frac{n(\xi_2)[1-n(\xi_1)]}{i\omega_n+\xi_2-\xi_1-\lambda_{S,T}}. \tag{A3}$$

Since all spurious states are ''frozen out'' we can put $\tilde{\lambda}_S=0$ and $\tilde{\lambda}_T=\delta=E_T-E_S$ in denominator (in the latter case we perform a shift $\tilde{\lambda}_T=\lambda_T-i\pi T/3$) and proceed with the analytical continuation $i\omega_n\to\omega+i0^+$. Without loss of generality we assume $\omega>0$. As a result, we get for retarded (R) self-energies

$$\mathrm{Im}\,\Sigma^{(2)R}_{TST}(\omega)\sim(J^{ST}\nu)^2\int_{-D}^{D}d\xi_1\int_{-D}^{D}d\xi_2 n(\xi_2)\times[1-n(\xi_1)]\delta(\omega+\xi_2-\xi_1), \tag{A4}$$

$$\mathrm{Re}\,\Sigma^{(2)R}_{TST}(\omega)\sim(J^{ST}\nu)^2\int_{-D}^{D}d\xi_1\int_{-D}^{D}d\xi_2 n(\xi_2)\times[1-n(\xi_1)]P\frac{1}{\omega+\xi_2-\xi_1}, \tag{A5}$$

$$\mathrm{Im}\,\Sigma^{(2)R}_{TTT}(\omega)\sim(J^{T}\nu)^2\int_{-D}^{D}d\xi_1\int_{-D}^{D}d\xi_2 n(\xi_2)[1-n(\xi_1)]\times\delta(\omega+\xi_2-\xi_1-\delta), \tag{A6}$$

$$\mathrm{Re}\,\Sigma^{(2)R}_{TTT}(\omega)\sim(J^{T}\nu)^2\int_{-D}^{D}d\xi_1\int_{-D}^{D}d\xi_2 n(\xi_2)\times[1-n(\xi_1)]P\frac{1}{\omega+\xi_2-\xi_1-\delta}, \tag{A7}$$

where P denotes the principal value of the integral.

We start with discussion of self-energy parts determining the spin relaxation due to $T\to S$ transitions shown in Figs. 5(a), 5(b). Assuming $T\ll D$ and neglecting temperature corrections at low temperatures $\omega\gg T$, we get

$$\mathrm{Im}\,\Sigma^{(2)R}_{TST}(\omega)\sim(J^{ST}\nu)^2\int_{0}^{D}d\xi_1\int_{-D}^{0}d\xi_2\delta(\omega+\xi_2-\xi_1)\sim[J^{ST}\nu(0)]^2\int_{0}^{\omega}d\xi\sim(J^{ST}\nu)^2\omega, \tag{A8}$$

$$\mathrm{Re}\,\Sigma^{(2)R}_{TST}(\omega)\sim(J^{ST}\nu)^2\int_{0}^{D}d\xi_1\int_{-D}^{0}d\xi_2 P\frac{1}{\omega+\xi_2-\xi_1}\sim(J^{ST}\nu)^2\omega\ln\left(\frac{D}{\omega}\right). \tag{A9}$$

In the opposite limit $T\gg\omega$

$$\mathrm{Im}\,\Sigma^{(2)R}_{TST}(\omega)\sim(J^{ST}\nu)^2 T, \tag{A10}$$

$$\mathrm{Re}\,\Sigma^{(2)R}_{TST}(\omega)\sim(J^{ST}\nu)^2\omega\ln\left(\frac{D\gamma}{2\pi T}\right), \tag{A11}$$

where $\ln\gamma=C=0.577\cdots$ is the Euler constant.

Next we turn to calculation of the triplet level damping due to TT relaxation processes [Figs. 5(a), 5(b)]. According to the Feynman codex, we can put $E_S=0$ at the first stage since the population of triplet excited state is controlled by finite level splitting δ. The contribution from diagram Fig. 5(a) is given by

$$\mathrm{Im}\,\Sigma^{(2LL)}_{TTT}=\mathrm{Im}\,\Sigma^{(2RR)}_{TTT}\sim(J^T_0\nu)^2(\omega-\delta)\ \theta(\omega-\delta), \tag{A12}$$

$$\mathrm{Re}\,\Sigma^{(2LL)}_{TTT}=\mathrm{Re}\,\Sigma^{(2RR)}_{TTT}\sim(J^T_0\nu)^2(\omega-\delta)\ \ln\left|\frac{D}{\omega-\delta}\right|. \tag{A13}$$

Similarly for Fig. 5(b),

$$\mathrm{Im}\,\Sigma^{(2LR)}_{TTT}=\mathrm{Im}\,\Sigma^{(2RL)}_{TTT}\sim(J^T_0\nu)^2(\omega-\delta)\ \theta(\omega-\delta) \tag{A14}$$

and, with logarithmic accuracy

$$\mathrm{Re}\,\Sigma^{(2LR)}_{TTT}=\mathrm{Re}\,\Sigma^{(2RL)}_{TTT}\sim(J^T_0\nu)^2(\omega-\delta)\ \ln\left|\frac{D}{\omega-\delta}\right|. \tag{A15}$$

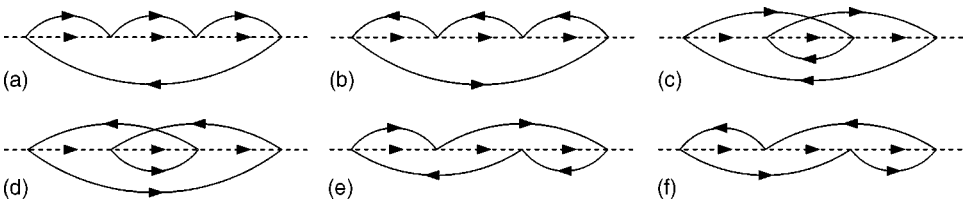

FIG. 6. Fourth order leading diagrams (a)–(f) for triplet self-energy part.

The threshold character of relaxation determined by the Fermi golden rule is the source of asymmetry in broadening of triplet line (see the text).

Now we turn to calculation of the third order diagrams $\Sigma^{(3)}$ shown in Figs. 5(c), 5(d).

$$\Sigma^{(3c)}(i\omega_n)\sim J^3T^3\sum_{\omega_{1,2,3}}\sum_{\mathbf{k_{1,2,3}}} G^0(-i\omega_1,-\mathbf{k}_1) \times G^0(i\omega_2,\mathbf{k}_2)G^0(-i\omega_3,-\mathbf{k}_3) \times\mathcal{G}^0(i\omega_n+i\omega_1+i\omega_2)\mathcal{G}^0(i\omega_n+i\omega_2+i\omega_3),$$

$$\Sigma^{(3d)}(i\omega_n)\sim J^3T^3\sum_{\omega_{1,2,3}}\sum_{\mathbf{k_{1,2,3}}} G^0(i\omega_1,\mathbf{k}_1) \times G^0(-i\omega_2,-\mathbf{k}_2)G^0(i\omega_3,\mathbf{k}_3) \times\mathcal{G}^0(i\omega_n+i\omega_1+i\omega_2)\mathcal{G}^0(i\omega_n+i\omega_2+i\omega_3).$$

Evaluation of Matsubara sums gives

$$\Sigma^{(3c)}(i\omega_n)\sim(J\nu)^3\int_{-D}^{D}d\xi_1\int_{-D}^{D}d\xi_2\int_{-D}^{D}d\xi_3 \times\frac{n(\xi_2)[1-n(\xi_1)][1-n(\xi_3)]}{(i\omega_n+\xi_2-\xi_3-\lambda_1)(i\omega_n+\xi_2-\xi_1-\lambda_2)}, \tag{A16}$$

$$\Sigma^{(3d)}(i\omega_n)\sim(J\nu)^3\int_{-D}^{D}d\xi_1\int_{-D}^{D}d\xi_2\int_{-D}^{D}d\xi_3 \times\frac{n(\xi_1)n(\xi_3)[1-n(\xi_2)]}{(i\omega_n+\xi_3-\xi_2-\lambda_1)(i\omega_n+\xi_1-\xi_2-\lambda_2)}. \tag{A17}$$

Let us consider first the case $\lambda_1=\lambda_2=\lambda_S=0$ which corresponds to two singlet fermionic lines inserted in self-energy part. Analytical continuation leads to following expression for $\Sigma^{(3)}=\Sigma^{(3b)}+\Sigma^{(3c)}$ at $T\ll\omega$

$$\mathrm{Im}\,\Sigma^{(3)}_{TSST}(\omega)\sim(J^{ST}\nu)^3\frac{J^S}{J^{ST}}\left[\omega\ln\left(\frac{D}{\omega}\right)-\omega\right], \tag{A18}$$

$$\mathrm{Re}\,\Sigma^{(3)}_{TSST}(\omega)\sim(J^{ST}\nu)^3\frac{J^S}{J^{ST}}\omega\mathrm{Re}\left[Li_2\left(-\frac{D}{\omega}\right)\right] \sim\left(\frac{J}{D}\right)^3\omega\ln^2\left(\frac{D}{\omega}\right), \tag{A19}$$

where $Li_2(x)$ is a dilogarithm function.[40] As we already noticed, the first log correction to $\mathrm{Im}\,\Sigma$ appears only in third order of the perturbation theory. Thus,

$$\mathrm{Im}\,\Sigma_{TSST}(\omega)\sim(J^{ST}\nu)^2\omega\left[1+a(J^S\nu)\ln\left(\frac{D}{\omega}\right)+\cdots\right], \tag{A20}$$

$$\mathrm{Re}\,\Sigma_{TSST}(\omega)\sim(J^{ST}\nu)^2\left[\omega\ln\left|\frac{D}{\omega}\right|\left\{1+b(J^S\nu)\ln\left|\frac{D}{\omega}\right|+\cdots\right\} +c(\omega-\delta)\ln\left|\frac{D}{\omega-\delta}\right|\left\{1+d(J^S\nu)\ln\left|\frac{D}{\omega-\delta}\right| +\cdots\right\}\right] \tag{A21}$$

with coefficient $a,b,c,d\sim1$. These results are consistent with the Abrikosov-Migdal theory[38,39] for SU(2) Kondo model.

We assume now that $\lambda_1=\lambda_2=\lambda_T=\delta$. It corresponds to the situation when both internal semifermionic GF correspond to different components of the triplet. Following the same routine as for calculation of $\Sigma^{(2)}$ we find

$$\mathrm{Im}\,\Sigma^{(3)}_{TTTT}(\omega)\sim(J^T\nu)^3\left[(\omega-\delta)\ln\left|\frac{D}{\omega-\delta}\right|-(\omega-\delta)\right] \times\theta(\omega-\delta). \tag{A22}$$

Thus, the corrections to the relaxation rate associated with transitions between different components of the triplet have a threshold character determined by the energy conservation.

Finally, we consider a possibility when two internal semifermionic GF correspond to different states, e.g., $\lambda_1=\lambda_S=0$, whereas $\lambda_2=\lambda_T=\delta$. Performing the calculations, one finds

$$\mathrm{Im}\,\Sigma^{(3)}_{TSTT}(\omega)\sim(J^{ST}\nu)^3\frac{J^T}{J^{ST}}\left(\left[\delta\ln\left|\frac{D}{\delta}\right|-(\delta-\omega)\ln\left|\frac{D}{\delta-\omega}\right| -\omega\right]+\left[\delta\ln\left|\frac{D}{\delta}\right|-\omega\ln\left|\frac{D}{\omega}\right|-(\delta-\omega)\right] \times\theta(\omega-\delta)\right). \tag{A23}$$

A similar expression can be derived for $\mathrm{Im}\,\Sigma^{(3)}_{TTST}(\omega)$.

Any insertion of the triplet line in diagrams Figs. 5(a)–

5(d) results in additional suppression of corresponding contribution for $\omega < eV$, which, in turn, prevents the effective renormalization of the vertex J^S in contrast to the processes shown in Fig. 3. The leading corrections in the fourth order of perturbation theory are shown in Figs. 6(a)–6(f). We point out that all corrections to $\mathrm{Im}\,\Sigma^{(n\geqslant 2)} \sim \omega \ln^{n-2}(D/\omega)$, $\mathrm{Re}\,\Sigma^{(n\geqslant 2)} \sim \omega \ln^{n-1}(D/\omega)$, and contain an additional power of the small parameter $\delta/D \ll 1$ as $\omega \to \delta$.

[1] L.I. Glazman and M.E. Raikh, JETP Lett. **47**, 452 (1988).
[2] T.K. Ng and P.A. Lee, Phys. Rev. Lett. **61**, 1768 (1988).
[3] D. Goldhaber-Gordon, J. Göres, M.A. Kastner, H. Shtrikman, D. Mahalu, and U. Meirav, Phys. Rev. Lett. **81**, 5225 (1998).
[4] S.M. Cronenwett, T.H. Oosterkamp, and L.P. Kouwenhoven, Science **281**, 540 (1998).
[5] F. Simmel, R.H. Blick, J.P. Kotthaus, W. Wegscheider, and M. Bichler, Phys. Rev. Lett. **83**, 804 (1999).
[6] T.K. Ng, Phys. Rev. Lett. **76**, 487 (1996).
[7] M.H. Hettler, J. Kroha, and S. Hershfield, Phys. Rev. B **58**, 5649 (1998).
[8] Y. Goldin and Y. Avishai, Phys. Rev. Lett. **81**, 5394 (1998); Phys. Rev. B **61**, 16 750 (2000).
[9] A. Kaminski, Yu.V. Nazarov, and L.I. Glazman, Phys. Rev. B **62**, 8154 (2000).
[10] R. López, R. Aguado, G. Platero, and C. Tejedor, Phys. Rev. B **64**, 075319 (2001).
[11] K. Kikoin and Y. Avishai, Phys. Rev. B **62**, 4647 (2000).
[12] T.V. Shahbazyan, I.E. Perakis, and M.E. Raikh, Phys. Rev. Lett. **84**, 5896 (2000).
[13] T. Fujii and N. Kawakami, Phys. Rev. B **63**, 064414 (2001).
[14] K. Kikoin and Y. Avishai, Phys. Rev. B **65**, 115329 (2002).
[15] K. Kikoin and Y. Avishai, Phys. Rev. Lett. **86**, 2090 (2001).
[16] Y. Takazawa, Y. Imai, and N. Kawakami, J. Phys. Soc. Jpn. **71**, 2234 (2002).
[17] W. Izumida, O. Sakai, and Y. Shimizu, J. Phys. Soc. Jpn. **67**, 2444 (1998).
[18] W. Hofstetter and H. Schoeller, Phys. Rev. Lett. **88**, 016803 (2002).
[19] M. Pustilnik, Y. Avishai, and K. Kikoin, Phys. Rev. Lett. **84**, 1756 (2000).
[20] M. Eto and Yu. Nazarov, Phys. Rev. Lett. **85**, 1306 (2000); Phys. Rev. B **64**, 085322 (2001).
[21] D. Giuliano, B. Jouault, and A. Tagliacozzo, Phys. Rev. B **63**, 125318 (2001).
[22] M. Pustilnik and L.I. Glazman, Phys. Rev. Lett. **85**, 2993 (2000); Phys. Rev. B **64**, 045328 (2001).
[23] S. Sasaki, S. De Franceschi, J.M. Elzerman, W.G. van der Wiel, M. Eto, S. Tarucha, and L.P. Kouwenhoven, Nature (London) **405**, 764 (2000).
[24] J. Nygård, D.H. Cobden, and P.E. Lindelof, Nature (London) **408**, 342 (2000).
[25] W.G. van der Wiel, S. De Franceschi, J.M. Elzerman, S. Tarucha, L.P. Kouwenhoven, J. Motohisa, F. Nakajima, and T. Fukui, Phys. Rev. Lett. **88**, 126803 (2002).
[26] Y. Meir and N.S. Wingreen, Phys. Rev. Lett. **68**, 2512 (1992); Phys. Rev. B **49**, 11 040 (1994).
[27] A. Rosch, J. Kroha, and P. Wölfle, Phys. Rev. Lett. **87**, 156802 (2001).
[28] A. Rosch, J. Paaske, J. Kroha, and P. Wölfle, Phys. Rev. Lett. **90**, 076804 (2003).
[29] O. Parcollet and C. Hooley, Phys. Rev. B **66**, 085315 (2002); P. Coleman and W. Mao, cond-mat/0203001 (unpublished); cond-mat/205004, Phys. Rev. B (to be published).
[30] L.W. Molenkamp, K. Flensberg, and M. Kemerink, Phys. Rev. Lett. **75**, 4282 (1995).
[31] A.C. Hewson, *The Kondo Problem to Heavy Fermions* (Cambridge University Press, Cambridge, 1993).
[32] V.N. Popov and S.A. Fedotov, Sov. Phys. JETP **67**, 535 (1988).
[33] M.N. Kiselev and R. Oppermann, Phys. Rev. Lett. **85**, 5631 (2000).
[34] M.N. Kiselev, H. Feldmann, and R. Oppermann, Eur. Phys. J. B **22**, 53 (2001).
[35] B.A. Jones and C.M. Varma, Phys. Rev. B **40**, 324 (1989).
[36] Possibility of additional Kondo peaks at $eV \gg T_K$ in strong magnetic field was noticed also in papers of Refs. 18,21.
[37] A. Kaminski, Yu.V. Nazarov, and L.I. Glazman, Phys. Rev. Lett. **83**, 384 (1999).
[38] A. Abrikosov, Physics **2**, 21 (1965).
[39] A.A. Abrikosov and A.A. Migdal, J. Low Temp. Phys. **5**, 519 (1970).
[40] M. Abramowitz and I. Stegun, *Handbook of Mathematical Functions* (Dover Publications, New York, 1965).

Proceedings TH2002 Supplement (2003) 155 – 180

1424-0637/03/040155-26 $1.50+0.20/0

Proceedings TH2002

Semi-Fermionic Approach for Quantum Spin Systems*

M. Kiselev

Abstract. We present a general derivation of semi-fermionic representation for generators of $SU(N)$ group as a bilinear combination of Fermi operators. The constraints are fulfilled by means of imaginary Lagrange multipliers. The important case of $SU(2)$ group is discussed. We demonstrate how the idea of semi-fermionic representation might be extended to the groups possessing dynamic symmetries. As an example, $SO(4)$ group is considered. We illustrate the application of semi-fermionic representations for various problems of strongly correlated physics.

PACS numbers: 71.27.+a, 75.20.Hr

Introduction

It is known that spin operators satisfy neither Fermi nor Bose commutation relations. For example, the Pauli matrices for $S = 1/2$ operator commute on different sites and anticommute on the same site. The commutation relations for spins are determined by $SU(2)$ algebra, leading to the absence of a Wick theorem for the generators. To avoid this difficulty and construct a diagrammatic technique and path integral representation for spin systems various approaches have been used. The first class of approaches is based on representation of spins as bilinear combination of Fermi or Bose operators [1]-[6], whereas the representations belonging to the second class deal with more complex objects like, e.g. the Hubbard [7] and supersymmetric [8] operators, the nonlinear sigma model [9] etc. However, in all cases the fundamental problem which is at the heart of the difficulty is the local constraint problem. To illustrate it, let's consider e.g., first class of representations. Introducing the auxiliary Fermi or Bose fields makes the dimensionality of the Hilbert space, where these operators act, greater than the dimensionality of the Hilbert space for the spin operators. As a result, the spurious unphysical states should be excluded from the consideration which leads in turn to some restrictions (constraints) on bilinear combinations of Fermi/Bose operators, resulting in substantial complication of corresponding rules of the diagrammatic technique. The representations from the second class suffer from the same kind of problem, transformed either into a high nonlinearity of resulting model (non-linear sigma model) or hierarchical structure of perturbation series in the absence of Wick theorem (Hubbard operators). The exclusion of double occupied and empty states

*Extended version of the talk given at TH-2002 conference, Paris, July 22-27, 2002

for a $S = 1/2$ impurity interacting with conduction electron bath (single impurity Kondo model), is controlled by fictitious chemical potential (Lagrange multiplier) of Abrikosov pseudofermions [4]. At the end of calculations this "chemical potential" λ should be put $\lambda \to -\infty$ to "freeze out" all unphysical states. In other words, there exists an additional $U(1)$ gauge field which freezes the charge fluctuations associated with this representation. The method works for dilute systems where all the spins can be considered independently. Unfortunately, attempts to generalize this technique to the lattice of spins results in the replacement of the local constraint (the number of particles on each site is fixed) by the so-called global constraint where the number of particles is fixed only on an average for the whole crystal. There is no reason to believe that such an approximation is a good starting point for the description of the strongly correlated systems. Another possibility to treat the local constraint rigorously is based on Majorana fermion representation. In this case fermions are "real" and corresponding gauge symmetry is Z_2. The difficulty with this representation is mostly related to the physical regularization of the fluctuations associated with the discrete symmetry group.

An alternative approach for spin Hamiltonians, free from local constraint problem, has been proposed in the pioneering paper of Popov and Fedotov [10]. Based on the exact fermionic representation for $S = 1/2$ and $S = 1$ operators, where the constraint is controlled by purely imaginary Lagrange multipliers, these authors demonstrated the power and simplification of the corresponding Matsubara diagram technique. The semi-fermionic representation (we discuss the meaning of this definition in the course of our paper) used by Popov and Fedotov is neither fermionic, nor bosonic, but reflects the fundamental Pauli nature of spins. The goal of this paper is to give a brief introduction to a semi-fermionic (SF) approach. A reader can find many useful technical details, discussion of mathematical aspects of semi-fermionic representation and its application to various problems in the original papers [10]-[21]. However, we reproduce the key steps of important derivations contained in [18],[19] in order to make the reader's job easier.

The manuscript is organized as follows: in Section I, the general concept of semi-fermions is introduced. We begin with the construction of the SF formalism for the fully antisymmetric representation of $SU(N)$ group and the fully symmetric SF representation of $SU(2)$ group using the imaginary-time (Matsubara) representation. We show a "bridge" between different representations using the simplest example of $S = 1$ in $SU(2)$ and discuss the SF approach for $SO(4)$ group. Finally, we show how to work with semi-fermions in real-time formalism and construct the Schwinger-Keldysh technique for SF. In this section, we will mostly follow original papers by the author [11], [18]. The reader acquainted with semi-fermionic technique can easily skip this section. In Section II, we illustrate the applications of SF formalism for various problems of condensed matter physics, such as ferromagnetic (FM), antiferromagnetic (AFM) and resonance valence bond (RVB) instabilities in the Heisenberg model, competition between local and non-local correlations in Kondo lattices in the vicinity of magnetic and spin glass critical points and the Kondo effect in quantum dots. In the Epilogue, we discuss some open questions

and perspectives.

1 Semi-fermionic representation

To begin with, we briefly reproduce the arguments contained in the original paper of Popov and Fedotov. Let's assume first $S = 1/2$. We denote as H_σ the Hamiltonian of spin system. The standard Pauli matrices can be represented as bilinear combination of Fermi operators as follows:

$$\sigma_j^z \to a_j^\dagger a_j - b_j^\dagger b_j, \qquad \sigma_j^+ \to 2a_j^\dagger b_j, \qquad \sigma_j^- \to 2b_j^\dagger a_j. \tag{1}$$

on each site i of the lattice. The partition function of the spin problem Z_σ is given by

$$Z_\sigma = Tr \exp(-\beta \hat{H}_\sigma) = i^N Tr \exp(-\beta(\hat{H}_F + i\pi \hat{N}_F/(2\beta)) \tag{2}$$

where $\hat{H}_F$ is the operator obtained from $\hat{H}_\sigma$ by the replacement (1) and

$$\hat{N} = \sum_{j=1}^{N} (a_j^\dagger a_j + b_j^\dagger b_j) \tag{3}$$

(N is the number of sites in the system and $\beta = 1/T$ is inverse temperature). To prove equation (2) we note that the trace over the nonphysical states of the i-th site vanishes

$$Tr_{unphys} \exp(-\beta(\hat{H}_F + i\pi \hat{N}_F/(2\beta)) = (-i)^0 + (-i)^2 = 0 \tag{4}$$

Thus, the identity (2) holds. The constraint of fixed number of fermions $\hat{N}_j = 1$, is achieved by means of the purely imaginary Lagrange multipliers $\mu = -i\pi/(2\beta)$ playing the role of imaginary chemical potentials of fermions. As a result, the Green's function

$$G = (i\omega_F - \epsilon)^{-1} \tag{5}$$

is expressed in terms of Matsubara frequencies $\omega_F = 2\pi T(n + 1/4)$ corresponding neither Fermi nor Bose statistics.

For $S = 1$ we adopt the representation of $\hat{H}_\sigma$ in terms of the 3-component Fermi field:

$$\sigma_j^z \to a_j^\dagger a - b_j^\dagger b, \quad \sigma_j^+ \to \sqrt{2}(a_j^\dagger c_j + c_j^\dagger b_j), \quad \sigma_j^- \to \sqrt{2}(c_j^\dagger a_j + b_j^\dagger c_j). \tag{6}$$

The partition function Z_σ is given by

$$Z_\sigma = Tr(-\beta \hat{H}_\sigma) = \left(\frac{i}{\sqrt{3}}\right)^N Tr \exp(-\beta(\hat{H}_F + i\pi \hat{N}_F/(3\beta)). \tag{7}$$

It is easy to note that the states with occupation numbers 0 and 3 cancel each other, whereas states with occupation 1 and 2 are equivalent due to the particle-hole symmetry and thus can be taken into account on an equal footing by proper

normalization of the partition function. As a result, the Green's function in the imaginary time representation is expressed in terms of $\omega_F = 2\pi T(n + 1/3)$ frequencies.

In this section, we show how semi-fermionic (Popov-Fedotov) representation can be derived using the mapping of partition function of the spin problem onto the corresponding partition function of the fermionic problem. The cases of arbitrary N (even) for SU(N) groups and arbitrary S for SU(2) group are discussed.

1.1 SU(N) group

We begin with the derivation of SF representation for SU(N) group. The SU(N) algebra is determined by the generators obeying the following commutation relations:

$$[\hat{S}^{\beta}_{\alpha,i}\hat{S}^{\rho}_{\sigma j}] = \delta_{ij}(\delta^{\rho}_{\alpha}\hat{S}^{\beta}_{\sigma i} - \delta^{\beta}_{\sigma}\hat{S}^{\rho}_{\alpha i}), \tag{8}$$

where $\alpha, \beta = 1, ..., N$. We adopt the definition of the Cartan algebra [22] of the SU(N) group $\{H_\alpha\} = S^{\alpha}_{\alpha}$ similar to the one used in [23], noting that the diagonal generators S^{α}_{α} are not traceless. To ensure a vanishing trace, the diagonal generators should only appear in combinations

$$\sum_{\alpha=1}^{N} s_\alpha S^{\alpha}_{\alpha} \quad \text{with} \quad \sum_{\alpha=1}^{N} s_\alpha = 0, \tag{9}$$

which effectively reduce the number of independent diagonal generators to $N - 1$ and the total number of SU(N) generators to $N^2 - 1$.

In this paper we discuss the representations of SU(N) group determined by rectangular Young Tableau (YT) (see [23] and [18] for details) and mostly concentrate on two important cases of the fully asymmetric (one column) YT and the fully symmetric (one row) YT.

The generator $\hat{S}^{\alpha}_{\beta}$ may be written as biquadratic form in terms of the Fermi-operators

$$\hat{S}^{\alpha}_{\beta} = \sum_{\gamma} a^{\dagger}_{\alpha\gamma} a^{\beta\gamma} \tag{10}$$

where the "color" index $\gamma = 1, ..., n_c$ and the $n_c(n_c + 1)/2$ constraints

$$\sum_{\alpha=1}^{N} a^{\dagger}_{\alpha\gamma_1} a^{\alpha\gamma_2} = \delta^{\gamma_2}_{\gamma_1} m \tag{11}$$

restrict the Hilbert space to the states with $m * n_c$ particles and ensure the characteristic symmetry in the color index a. Here m corresponds to the number of rows in rectangular Young Tableau whereas n_c stands for the number of columns. The antisymmetric behavior with respect to α is a direct consequence of the fermionic representation.

Let us consider the partition function for the Hamiltonian, expressed in terms of SU(N) generators

$$Z_S = Tr \exp(-\beta H_S) = Tr' \exp(-\beta H_F) \tag{12}$$

where Tr' denotes the trace taken with constraints (11). As it is shown in [18], the partition function of $SU(N)$ model is related to partition function of corresponding fermion model through the following equation:

$$Z_S = \int \prod_j d\mu(j) P(\mu(j)) Tr \exp\left(-\beta(H_F - \mu(j) n_F)\right) = \int \prod_j d\mu(j) P(\mu(j)) Z_F(\mu(j)) \tag{13}$$

here $P(\mu_j)$ is a distribution function of imaginary Lagrange multipliers. We calculate $P(\mu_j)$ explicitely using constraints (11).

We use the path integral representation of the partition function

$$Z_S / Z_S^0 = \int \prod_j d\mu(j) P(\mu(j)) \exp(\mathcal{A}) / \int \prod_j d\mu(j) P(\mu(j)) \exp(\mathcal{A}_0) \tag{14}$$

where the actions $\mathcal{A}$ and $\mathcal{A}_0$ are determined by

$$\mathcal{A} = \mathcal{A}_0 - \int_0^\beta d\tau H_F(\tau), \quad \mathcal{A}_0 = \sum_j \sum_{k=1}^N \int_0^\beta d\tau \bar{a}_k(j,\tau)(\partial_\tau + \mu(j)) a_k(j,\tau) \tag{15}$$

and the fermionic representation of SU(N) generators (10) is applied.

Let us first consider the case $n_c = 1$. We denote the corresponding distribution by $P_{N,m}(\mu(j))$, where m is the number of particles in the SU(N) orbital, or in other words, $1 \leq m < N$ labels the different fundamental representations of SU(N).

$$n_j = \sum_{k=1}^N \bar{a}_k(j) a_k(j) = m \tag{16}$$

To satisfy this requirement, the minimal set of chemical potentials and the corresponding form of $P_{N,m}(\mu(j))$ are to be derived.

To derive the distribution function, we use the following identity for the constraint (16) expressed in terms of Grassmann variables

$$\delta_{n_j,m} = \frac{1}{N} \sin\left(\pi(n_j - m)\right) / \sin\left(\frac{\pi(n_j - m)}{N}\right) \tag{17}$$

Substituting this identity into (12) and comparing with (14) one gets

$$P_{N,m}(\mu(j)) = \frac{1}{N} \sum_{k=1}^N \exp\left(\frac{i\pi m}{N}(2k-1)\right) \delta(\mu(j) - \mu_k), \tag{18}$$

where

$$\mu_k = -\frac{i\pi T}{N}(2k-1). \tag{19}$$

Since the Hamiltonian is symmetric under the exchange of particles and holes when the sign of the Lagrange multiplier is also changed simultaneously, we can simplify (18) to

$$P_{N,m}(\mu(j)) = \frac{2i}{N}\sum_{k=1}^{\lfloor N/2\rfloor}\sin\left(\pi m\frac{2k-1}{N}\right)\delta(\mu(j)-\mu_k) \tag{20}$$

where $\lfloor N/2\rfloor$ denotes the integer part of $N/2$. As shown below, this is the minimal representation of the distribution function corresponding to the minimal set of the discrete imaginary Lagrange multipliers. Another distributions function different from (20) can be constructed when the sum is taken from $k = N/2+1$ to N. Nevertheless, this DF is different from (20) only by the sign of imaginary Lagrange multipliers $\tilde{\mu}_k = \mu_k^* = -\mu_k$ and thus is supplementary to (20).

Particularly interesting for even N is the case when the SU(N) orbital is half–filled, $m = N/2$. Then all Lagrange multipliers carry equal weight

$$P_{N,N/2}(\mu(j)) = \frac{2i}{N}\sum_{k=1}^{N/2}(-1)^{k+1}\delta\left(\mu(j)-\mu_k\right). \tag{21}$$

Taking the limit $N\to\infty$ one may replace the summation in expression (21) in a suitable way by integration. Note, that while taking $N\to\infty$ and $m\to\infty$ limits, we nevertheless keep the ratio $m/N = 1/2$ fixed. Then, the following limiting distribution function can be obtained:

$$P_{N,N/2}(\mu(j)) \overset{N\to\infty}{\longrightarrow} \frac{\beta}{2\pi i}\exp\left(-\beta\mu(j)\frac{N}{2}\right) \tag{22}$$

resulting in the usual continuous representation of the local constraint for the simplest case $n_c = 1$

$$Z_S = Tr(\exp\left(-\beta H_F\right)\delta\left(n_j - \frac{N}{2}\right)) \tag{23}$$

We note the obvious similarity of the limiting DF (22) with the *Gibbs canonical distribution* provided that the Wick rotation from the imaginary axis of the Lagrange multipliers μ to the real axis of energies E is performed and thus $\mu(j)N/2$ has a meaning of energy.

Up to now, the representation we discussed was purely fermionic and expressed in terms of usual Grassmann variables when the path integral formalism is applied. The only difference from slave fermionic approach is that imaginary Lagrange multipliers are introduced to fulfill the constraint. Nevertheless, by making

the replacement

$$a_k(j,\tau)) \to a_k(j,\tau)\exp\left(\frac{i\pi\tau}{\beta}\frac{2k-1}{N}\right), \quad \bar{a}_k(j,\tau) \to \bar{a}_k(j,\tau)\exp\left(-\frac{i\pi\tau}{\beta}\frac{2k-1}{N}\right) \tag{24}$$

we arrive at the generalized Grassmann (semi-fermionic) boundary conditions

$$a_k(j,\beta) = a_k(j,0)\exp\left(i\pi\frac{2k-1}{N}\right), \quad \bar{a}_k(j,\beta) = \bar{a}_k(j,0)\exp\left(-i\pi\frac{2k-1}{N}\right) \tag{25}$$

This leads to a temperature diagram technique for the Green's functions

$$\mathcal{G}^{\alpha\beta}(j,\tau) = -\langle T_\tau a_\alpha(j,\tau)\bar{a}_\beta(j,0)\rangle \tag{26}$$

of semi-fermions with Matsubara frequencies different from both Fermi and Bose representations (see Fig.2).

The exclusion principle for this case is illustrated on Fig.1, where the $S = 1/2$ representation for the first two groups SU(2) and SU(4) are shown. The first point to observe is that the spin Hamiltonian does not distinguish the n particle and the n hole (or $N-n$ particle) subspace. Eq. (19) shows that the two phase factors $\exp(\beta\mu n)$ and $\exp(\beta\mu(N-n))$ accompanying these subspaces in Eq. (20) add up to a purely imaginary value within the same Lagrange multiplier, and the empty and the fully occupied states are always canceled. In the case of $N \geq 4$, where we have multiple Lagrange multipliers, the distribution function $P(\mu)$ linearly combines these imaginary prefactors to select out the desired physical subspace with particle number $n = m$.

In Fig.1, we note that on each picture, the empty and fully occupied states are canceled in their own unit circle. For SU(2) there is a unique chemical potential $\mu = \pm i\pi T/2$ which results in the survival of single occupied states. For SU(4) there are two chemical potentials (see also Fig.2). The cancellation of single and triple occupied states is achieved with the help of proper weights for these states in the distribution function whereas the states with the occupation number 2 are doubled according to the expression (21). In general, for SU(N) group with $n_c = 1$ there exists $N/2$ circles providing the realization of the exclusion principle.

1.2 SU(2) group

We consider now the generalization of the SU(2) algebra for the case of spin S. Here, the most convenient fermionic representation is constructed with the help of a $2S+1$ component Fermi field $a_k(j)$ provided that the generators of SU(2) satisfy the following equations:

$$S^+ = \sum_{k=-S}^{S-1} \sqrt{S(S+1) - k(k+1)}\, a^\dagger_{k+1}(j)a_k(j),$$

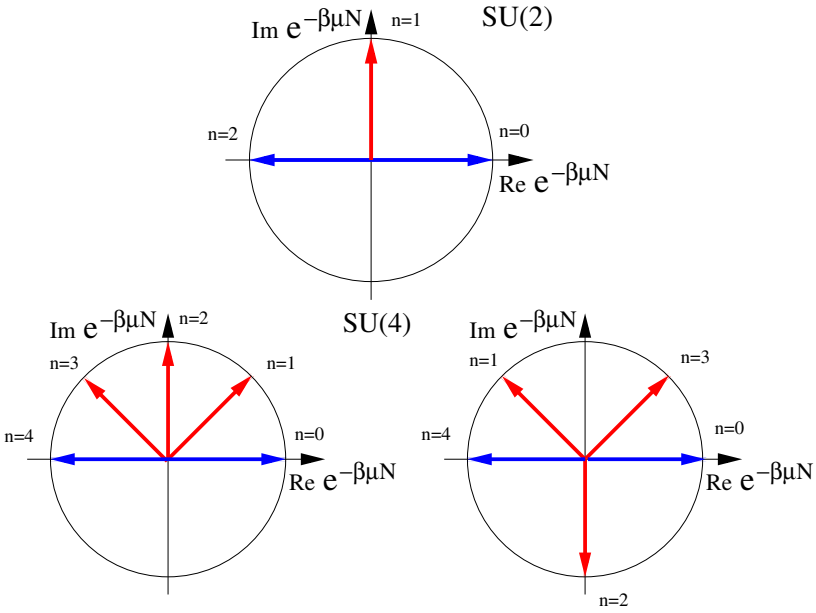

Figure 1: Graphical representation of exclusion principle for SU(N) semi-fermionic representation with even N, $n_c = 1$ (we use $\mu = i\pi T/2$ for SU(2) and $\mu_1 = i\pi T/4$, $\mu_2 = 3i\pi T/4$ for SU(4)).

$$S^- = \sum_{k=-S+1}^{S} \sqrt{S(S+1) - k(k-1)}\, a_{k-1}^\dagger(j) a_k(j),$$

$$S^z = \sum_{k=-S}^{S} k a_k^\dagger(j) a_k(j) \tag{27}$$

such that $dim H_F = 2^{2S+1}$ whereas the constraint reads as follows

$$n_j = \sum_{k=-S}^{k=S} a_k^\dagger(j) a_k(j) = l = 1 \tag{28}$$

Following the same routine as for SU(N) generators and using the occupancy condition to have $l = 1$ (or $2S$) states of the $(2S + 1)$ states filled, one gets the following distribution function, after using the particle–hole symmetry of the Hamiltonian H_S:

$$P_{2S+1,1}(\mu(j)) = \frac{2i}{2S+1} \sum_{k=1}^{\lfloor S+1/2 \rfloor} \sin\left(\pi \frac{2k-1}{2S+1}\right) \delta(\mu(j) - \mu_k) \tag{29}$$

where the Lagrange multipliers are $\mu_k = -i\pi T(2k-1)/(2S+1)$ and $k = 1, ..., \lfloor S + 1/2 \rfloor$, similarly to Eq.(19). In the particular case of the SU(2) model for some chosen values of spin S the distribution functions are given by the following expressions

$$P_{2,1}(\mu(j)) = i\, \delta\left(\mu(j) + \frac{i\pi T}{2}\right)$$

for $S = 1/2$

$$P_{3,1}(\mu(j)) = P_{3,2}(\mu(j)) = \frac{i}{\sqrt{3}}\, \delta\left(\mu(j) + \frac{i\pi T}{3}\right)$$

for $S = 1$.

This result corresponds to the original Popov-Fedotov description restricted to the $S = 1/2$ and $S = 1$ cases. A limiting distribution function corresponding to Eq. (22) for the constraint condition with arbitrary l is found to be

$$P_{\infty,l}(\mu(j)) \stackrel{S\to\infty}{\longrightarrow} \frac{\beta}{2\pi i} \exp(-\beta l \mu(j)). \tag{30}$$

For the case $l = m = N/2 \to \infty$ and $S = (N-1)/2 \to \infty$ the expression for the limiting DF $P_{\infty,l}(\mu(j))$ coincides with (23). We note that in $S \to \infty$ (or $N \to \infty$) limit, the continuum "chemical potentials" play the role of additional U(1) fluctuating field whereas for finite S and N they are characterized by fixed and discrete values.

When S assumes integer values, the minimal fundamental set of Matsubara frequencies is given by the table in Fig.2.

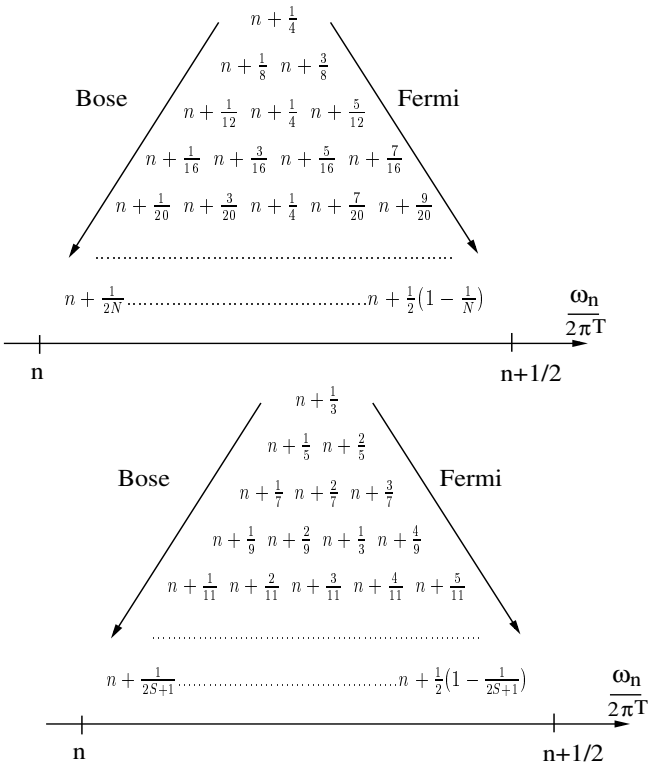

Figure 2: The minimal set of Matsubara frequencies for a) $SU(N)$ representation with even N/ $SU(2)$ representation for half-integer value of the spin. b) $SU(2)$ representation for integer values of the spin and $l = 1$.

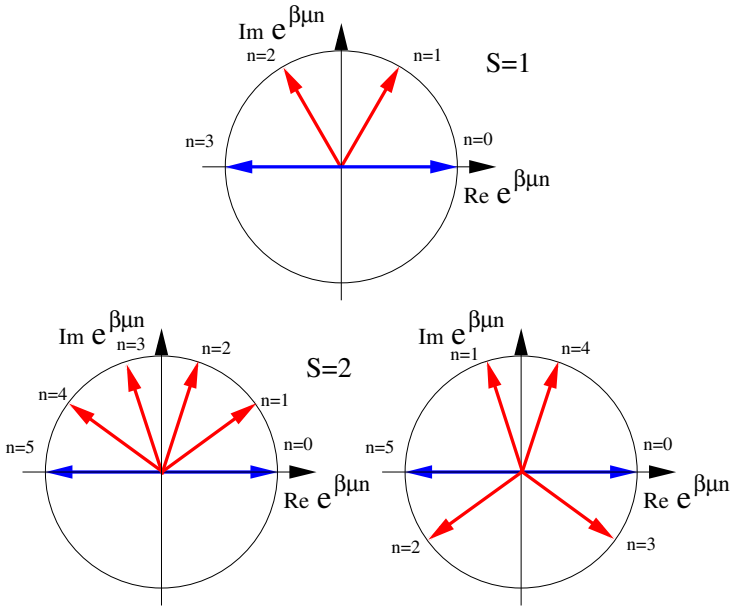

Figure 3: Graphical representation of exclusion principle for SU(2) semi-fermionic representation for $S = 1$ and $S = 2$. For any arbitrary integer value of spin there exists S circle diagrams corresponding to the S different chemical potentials and providing the realization of the exclusion principle.

The exclusion principle for SU(2) in the large spin limit can be also understood with the help of Fig.1 and Fig.3. One can see that the empty and the fully occupied states are canceled in each given circle similarly to even-N SU(N) algebra. The particle-hole (PH) symmetry of the representation results in an equivalence of single occupied and $2S$ occupied states whereas all the other states are canceled due to proper weights in the distribution function (29). In accordance with PH symmetry being preserved for each value of the chemical potential all circle diagrams (see Fig.3, Fig.5) are invariant with respect to simultaneous change $\mu \leftrightarrow -\mu$ and $n_{particle} \leftrightarrow n_{holes}$.

1.3 From SU(2) to SO(4)

We have shown that the general rectangular Young Tableau of size $n_c * m$ is represented by $N * n_c$ component fermionic field with n_c diagonal constraints and $n_c(n_c-1)/2$ off-diagonal constraints. However, the fully symmetric representation (one row) requires only $n_c + 1 = 2S + 1$ component field. The general scheme of projected representation for SU(N) group is given in [18]. We illustrate this idea on a simple example of $S = 1$.

We start with $2 * n_c = 4$ - field representation

$$(a_{11},\ a_{12},\ a_{21},\ a_{22}) \tag{31}$$

There are two diagonal and two off-diagonal constraints which read as follows:

$$a^\dagger_{11}a_{11} + a^\dagger_{21}a_{21} = 1, \quad a^\dagger_{12}a_{12} + a^\dagger_{22}a_{22} = 1. \tag{32}$$

$$a^\dagger_{11}a_{12} + a^\dagger_{21}a_{22} = 0, \quad a^\dagger_{12}a_{11} + a^\dagger_{22}a_{21} = 0 \tag{33}$$

and generators of $SU(2)$ group are given by

$$S^- = S^1_2 = a^\dagger_{11}a_{21} + a^\dagger_{12}a_{22}, \quad S^+ = S^2_1 = a^\dagger_{21}a_{11} + a^\dagger_{22}a_{12}$$

$$2S^z = S^2_2 - S^1_1 = a^\dagger_{21}a_{21} + a^\dagger_{22}a_{22} - a^\dagger_{11}a_{11} - a^\dagger_{12}a_{12} \tag{34}$$

Combining definition (34) with constraint (33) we reach the following equations:

$$\begin{aligned} S^- &= a^\dagger_{11}(a_{21} + a_{12}) + (a^\dagger_{12} + a^\dagger_{21})a_{22}, \\ S^+ &= (a^\dagger_{21} + a^\dagger_{12})a_{11} + a^\dagger_{22}(a_{12} + a_{21}), \\ S^z &= a^\dagger_{22}a_{22} - a^\dagger_{11}a_{11} \end{aligned} \tag{35}$$

Therefore, we conclude that the antisymmetric (singlet) combination $a_{12} - a_{21}$ does not enter the expression for spin $S = 1$ operators. Thus, three (out of four) component Fermi-field is sufficient for the description of $S = 1$ $SU(2)$ representation. Defining new fields as follows

$$a_{11} = f_{-1}, \quad a_{22} = f_1, \quad \frac{1}{\sqrt{2}}(a_{12} + a_{21}) = f_0, \quad \frac{1}{\sqrt{2}}(a_{12} - a_{21}) = s. \tag{36}$$

where fermions f_1, f_0, f_{-1} stand for $S^z = 1, 0 - 1$ projections of the triplet state and fermion s determines the singlet state, we come to standard $S = 1$ $SU(2)$ representation (c.f 6)

$$S^+ = \sqrt{2}(f_0^\dagger f_{-1} + f_1^\dagger f_0), \quad S^- = \sqrt{2}(f_{-1}^\dagger f_0 + f_0^\dagger f_1), \quad S_z = f_1^\dagger f_1 - f_{-1}^\dagger f_{-1}, \tag{37}$$

with the constraint

$$n_1 + n_0 + n_{-1} + n_s = 2 \tag{38}$$

where $n_\alpha = f_\alpha^\dagger f_\alpha$.

Nevertheless, the constraint (38) transforms to a standard SU(2) $S = 1$ constraint in both cases $n_s = 0$ and $n_s = 1$ since there is no singlet/triplet mixing allowed by SU(2) algebra.

To demonstrate the transformation of the local constraint let's first consider the case $n_s = 0$. The constraint reads as follows

$$n_1 + n_0 + n_{-1} = 2S \qquad \Longleftrightarrow \qquad \mathbf{S}^2 = S(S+1). \tag{39}$$

On the other hand, the the states with $2S$ occupation are equivalent to the states with single occupation due to particle-hole symmetry. Thus, the constraint (38) might be written as

$$\tilde{n}_1 + \tilde{n}_0 + \tilde{n}_{-1} = 1 \tag{40}$$

where $\tilde{n}_\alpha = 1 - n_\alpha$. The latter case corresponds to $n_s = 1$.

We start now with definition of $SO(4)$ group obeying the following commutation relations

$$[S_j, S_k] = ie_{jkl}S_l, \qquad [P_j, P_k] = ie_{jkl}S_l, \qquad [P_j, S_k] = ie_{jkl}P_l \tag{41}$$

where 6 generators of SO(4) group, namely vectors $\mathbf{S}$ and $\mathbf{P}$ are represented by the matrices

$$S^+ = \sqrt{2}\begin{pmatrix} 0 & 1 & 0 & 0 \\ 0 & 0 & 1 & 0 \\ 0 & 0 & 0 & 0 \\ 0 & 0 & 0 & 0 \end{pmatrix}, \quad S^- = \sqrt{2}\begin{pmatrix} 0 & 0 & 0 & 0 \\ 1 & 0 & 0 & 0 \\ 0 & 1 & 0 & 0 \\ 0 & 0 & 0 & 0 \end{pmatrix},$$

$$S^z = \begin{pmatrix} 1 & 0 & 0 & 0 \\ 0 & 0 & 0 & 0 \\ 0 & 0 & -1 & 0 \\ 0 & 0 & 0 & 0 \end{pmatrix}, \quad P^+ = \sqrt{2}\begin{pmatrix} 0 & 0 & 0 & 1 \\ 0 & 0 & 0 & 0 \\ 0 & 0 & 0 & 0 \\ 0 & 0 & -1 & 0 \end{pmatrix},$$

$$P^- = \sqrt{2}\begin{pmatrix} 0 & 0 & 0 & 0 \\ 0 & 0 & 0 & 0 \\ 0 & 0 & 0 & -1 \\ 1 & 0 & 0 & 0 \end{pmatrix}, \quad P^z = \begin{pmatrix} 0 & 0 & 0 & 0 \\ 0 & 0 & 0 & -1 \\ 0 & 0 & 0 & 0 \\ 0 & -1 & 0 & 0 \end{pmatrix}. \tag{42}$$

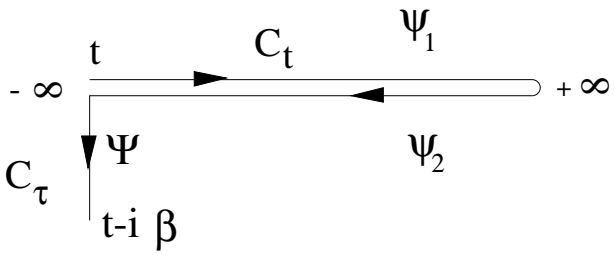

Figure 4: The Keldysh contour going from $-\infty \to \infty \to -\infty$ in real time. The boundary conditions on the imaginary time segment determine the generalized distribution functions for quasiparticles.

With the Casimir operator

$$\mathbf{S} \cdot \mathbf{P} = 0, \qquad \mathbf{S}^2 + \mathbf{P}^2 = 3.$$

Unlike SU(2) group, the singlet/triplet transitions are allowed in SO(4) group and determined by $\mathbf{P}$ operators. Using the definition of singlet/triplet fermions one comes to following representation

$$S^+ = \sqrt{2}(f_0^\dagger f_{-1} + f_1^\dagger f_0), \quad S^- = \sqrt{2}(f_{-1}^\dagger f_0 + f_0^\dagger f_1), \quad S_z = f_1^\dagger f_1 - f_{-1}^\dagger f_{-1}, \tag{43}$$

$$P^+ = \sqrt{2}(f_1^\dagger s - s^\dagger f_{-1}), \quad P^- = \sqrt{2}(s^\dagger f_1 - f_{-1}^\dagger s), \quad P_z = -(f_0^\dagger s + s^\dagger f_0). \tag{44}$$

with the only constraint

$$n_1 + n_0 + n_{-1} + n_s = 1$$

whereas the orthogonality condition is fulfilled automatically.

1.4 Real-time formalism

We discuss finally the real-time formalism based on the semi-fermionic representation of SU(N) generators. This approach is necessary for treating the systems out of equilibrium, especially for many component systems describing Fermi (Bose) quasiparticles interacting with spins. The real time formalism [24], [25] provides an alternative approach for the analytical continuation method for equilibrium problems allowing direct calculations of correlators whose analytical properties as function of many complex arguments can be quite cumbersome.

To derive the real-time formalism for SU(N) generators we use the path integral representation along the closed time Keldysh contour (see Fig.4). Following the standard route [26], we can express the partition function of the problem containing SU(N) generators as a path integral over Grassmann variables $\psi_l =$

$(a_{l,1}(j),...,a_{l,N}(j))^T$ where $l=1,2$ stands for upper and lower parts of the Keldysh contour, respectively,

$$\mathcal{Z}/\mathcal{Z}_0 = \int D\bar{\psi}D\psi \exp(i\mathcal{A})/\int D\bar{\psi}D\psi \exp(i\mathcal{A}_0) \tag{45}$$

where the actions $\mathcal{A}$ and $\mathcal{A}_0$ are taken as an integral along the closed-time contour $C_t + C_\tau$ which is shown in Fig.4. The contour is closed at $t = -\infty + i\tau$ since $\exp(-\beta H_0) = T_\tau \exp\left(-\int_0^\beta H_0 d\tau\right)$. We denote the ψ fields on upper and lower sides of the contour C_t as ψ_1 and ψ_2 respectively. The fields Ψ stand for the contour C_τ. These fields provide the matching conditions for $\psi_{1,2}$ and are excluded from the final expressions. Taking into account the semi-fermionic boundary conditions for generalized Grassmann fields (25) one gets the matching conditions for $\psi_{1,2}$ at $t = \pm\infty$,

$$\psi^\mu_{1,\alpha}|_k(-\infty) = \exp\left(i\pi\frac{2k-1}{N}\right)\psi^\mu_{2,\alpha}|_k(-\infty),$$
$$\psi^\mu_{1,\alpha}|_k(+\infty) = \psi^\mu_{2,\alpha}|_k(+\infty) \tag{46}$$

for $k = 1,...,\lfloor N/2 \rfloor$ and $\alpha = 1,...,N$. The correlation functions can be represented as functional derivatives of the generating functional

$$Z[\eta] = \mathcal{Z}_0^{-1}\int D\bar{\psi}D\psi \exp\left(i\mathcal{A} + i\oint_C dt(\bar{\eta}\sigma^z\psi + \bar{\psi}\sigma^z\eta)\right) \tag{47}$$

where η represents sources and the σ^z matrix stands for "causal" and "anti-causal" orderings along the contour.

The on-site Green's functions (GF) which are matrices of size $2N\times 2N$ with respect to both Keldysh (lower) and spin-color (upper) indices are given by

$$G^{\alpha\beta}_{\mu\nu}(t,t') = -i\frac{\delta}{i\delta\bar{\eta}^\alpha_\mu(t)}\frac{\delta}{i\delta\eta^\beta_\nu(t')}Z[\eta]|_{\bar{\eta},\eta\to 0}. \tag{48}$$

To distinguish between imaginary-time (26) and real-time (48) GF's, we use different notations for Green's functions in these representations.

After a standard shift-transformation [26] of the fields ψ the Keldysh GF of free semi-fermions assumes the form

$$G^\alpha_0(\epsilon) = G^{R,\alpha}_0\begin{pmatrix} 1-f_\epsilon & -f_\epsilon \\ 1-f_\epsilon & -f_\epsilon \end{pmatrix} - G^{A,\alpha}_0\begin{pmatrix} -f_\epsilon & -f_\epsilon \\ 1-f_\epsilon & 1-f_\epsilon \end{pmatrix},$$

where the retarded and advanced GF's are

$$G^{(R,A)\alpha}_0(\epsilon) = (\epsilon \pm i\delta)^{-1}, \quad f_\epsilon = f^{(N,k)}(\epsilon), \tag{49}$$

with equilibrium distribution functions

$$f^{(N,k)}(\epsilon) = T\sum_n \frac{e^{i\omega_{n_k}\tau|_{+0}}}{i\omega_{n_k}-\epsilon} = \frac{1}{e^{i\pi(2k-1)/N}\exp(\beta\epsilon)+1}. \tag{50}$$

A straightforward calculation of $f^{(N,k)}$ for the case of even N leads to the following expression

$$f^{(N,k)}(\epsilon) = \frac{\sum_{l=1}^{N}(-1)^{l-1}\exp\left(\beta\epsilon(N-l)\right)\exp\left(-\frac{i\pi l(2k-1)}{N}\right)}{\exp(N\beta\epsilon)+1}, \qquad (51)$$

where $k = 1, ..., N/2$. The equilibrium distribution functions (EDF) $f^{(2S+1,k)}$ for the auxiliary Fermi-fields representing arbitrary S for $SU(2)$ algebra are given by

$$f^{(2S+1,k)}(\epsilon) = \frac{\sum_{l=1}^{2S+1}(-1)^{l-1}\exp\left(\beta\epsilon(2S+1-l)\right)\exp\left(-\frac{i\pi(2k-1)}{2S+1})\right)}{\exp((2S+1)\beta\epsilon)+(-1)^{2S+1}} \qquad (52)$$

for $k = 1, ..., \lfloor S+1/2 \rfloor$. Particularly simple are the cases of $S = 1/2$ and $S = 1$,

$$f^{(2,1)}(\epsilon) = n_F(2\epsilon) - i\frac{1}{2\cosh(\beta\epsilon)}$$

$$f^{(3,1)}(\epsilon) = \frac{1}{2}n_B(\epsilon) - \frac{3}{2}n_B(3\epsilon) - i\sqrt{3}\frac{\sinh(\beta\epsilon/2)}{\sinh(3\beta\epsilon/2)} \qquad (53)$$

Here, the standard notations for Fermi/Bose distribution functions $n_{F/B}(\epsilon) = [\exp(\beta\epsilon) \pm 1]^{-1}$ are used. For $S = 1/2$ the semi-fermionic EDF satisfies the obvious identity $|f^{(2,1)}(\epsilon)|^2 = n_F(2\epsilon)$.

In general the EDF for half-integer and integer spins can be expressed in terms of Fermi and Bose EDF respectively. We note that since auxiliary Fermi fields introduced for the representation of SU(N) generators do not represent the true quasiparticles of the problem, helping only to treat properly the constraint condition, the distribution functions for these objects in general do not have to be real functions. Nevertheless, one can prove that the imaginary part of the EDF does not affect the physical correlators and can be eliminated by introducing an infinitesimally small real part for the chemical potential. In spin problems, a uniform/staggered magnetic field usually plays the role of such real chemical potential for semi-fermions.

2 Application of semi-fermionic representation

In this section we illustrate some of the applications of SF representation for various problems of strongly correlated physics.

2.1 Heisenberg model: FM, AFM and RVB

The effective nonpolynomial action for Heisenberg model with ferromagnetic (FM) coupling has been investigated in [10]. The model with antiferromagnetic (AFM)

interaction has been considered by means of semi-fermionic representation in [16] and [17] (magnon spectra) and in [11] for resonance valence bond (RVB) excitations. The Hamiltonian considered is given as

$$H_{int} = -\sum_{<ij>} J_{ij} \left(\vec{S}_i \vec{S}_j - \frac{1}{4} \right) \tag{54}$$

- Ferromagnetic coupling $J = I_{FM} > 0$

The exchange $\vec{S}_i \vec{S}_j$ is represented as four-semi-fermion interaction. Applying the Hubbard-Stratonovich transformation by the *local vector* field $\vec{\Phi}_i(\tau)$ the effective nonpolynomial action is obtained in terms of vector c-field. The FM phase transition corresponds to the appearance at $T \leq T_c$ of the nonzero average $\langle \Phi^z(q=0,0) \rangle$ which stands for the nonzero magnetization, or in other words, corresponds to the Bose condensation of the field Φ^z.

$$\Phi^z(\vec{k},\omega) = \mathcal{M}(\beta N)^{1/2} \delta_{\vec{k},0} \delta_{\omega,0} + \tilde{\Phi}^z(\vec{k},\omega). \tag{55}$$

In one loop approximation the standard molecular field equation can be reproduced

$$\mathcal{M} = I_{FM}(0) \tanh(\beta \mathcal{M}/2). \tag{56}$$

The saddle point (mean-field) effective action is given by well-known expression

$$\mathcal{A}_0[\mathcal{M}] = -N \left[\frac{\beta \mathcal{M}^2}{4 I_M(0)} - \ln \left(2 \cosh \left(\frac{\beta \mathcal{M}}{2} \right) \right) \right], \tag{57}$$

and the free energy per spin f_0 is determined by the standard equation:

$$\beta f_0 = -\ln Z_S = \frac{\beta \mathcal{M}^2}{4 I_M(0)} - \ln \left(2 \cosh \left(\frac{\beta \mathcal{M}}{2} \right) \right) \tag{58}$$

Calculation of the second variation of $\mathcal{A}_{eff}$ gives rise to the following expression

$$\begin{aligned} \delta \mathcal{A}_{eff} = & -\frac{1}{4} \sum_{\vec{k}} \Phi^z(\vec{k},0) \left[I_M^{-1}(\vec{k}) - \frac{\beta}{2 \cosh^2(\beta \Omega)} \right] \Phi^z(\vec{k},0) \\ & - \frac{1}{4} \sum_{\vec{k},\omega \neq 0} I_M^{-1}(\vec{k}) \Phi^z(\vec{k},\omega) \Phi^z(\vec{k},\omega) - \sum_{\vec{k},\omega} \Phi^+(\vec{k},\omega) \left[I_M^{-1}(\vec{k}) - \frac{\tanh(\beta\Omega)}{2\Omega - i\omega} \right] \Phi^-(\vec{k},\omega) \end{aligned} \tag{59}$$

where $\Omega = (g \mu_B H + \mathcal{M})/2$. The magnon spectrum ($T \leq T_c$) is determined by the poles of $\langle \Phi^+ \Phi^- \rangle$ correlator, $\omega = \lambda \mathbf{k}^2$.

- Antiferromagnetic coupling $J = I_{AFM} < 0$. *Néel solution*

The AFM transition corresponds to formation of the staggered condensate

$$\Phi^z(\vec{k},\omega) = \mathcal{N}(\beta N)^{1/2}\delta_{\vec{k},\vec{Q}}\delta_{\omega,0} + \tilde{\Phi}^z(\vec{k},\omega) \tag{60}$$

The one-loop approximation leads to standard mean-field equations for the staggered magnetization

$$\mathcal{N} = -I_{AFM}(Q)\tanh(\beta\mathcal{N}/2),$$
$$\mathcal{A}_0[\mathcal{N}] = N\left[\frac{\beta\mathcal{N}^2}{4I_{AFM}(Q)} + \ln\left(2\cosh\left(\frac{\beta\mathcal{N}}{2}\right)\right)\right]. \tag{61}$$

After taking into account the second variation of $\mathcal{A}_{eff}$, the following expression for the effective action is obtained [(see e.g. [16],[17]):

$$\delta\mathcal{A}_{eff} = \frac{1}{4}\sum_{\vec{k}}\Phi^z(\vec{k},0)\left[I^{-1}_{AFM}(\vec{k}) + \frac{\beta}{2\cosh^2(\beta\tilde{\Omega})}\right]\Phi^z(\vec{k},0)$$
$$+\frac{1}{4}\sum_{\vec{k},\omega\neq 0} I^{-1}_{AFM}(\vec{k})\Phi^z(\vec{k},\omega)\Phi^z(\vec{k},\omega)$$
$$+\sum_{\vec{k},\omega}\Phi^+(\vec{k},\omega)\left[I^{-1}_{AFM}(\vec{k}) + \frac{2\tilde{\Omega}\tanh(\beta\tilde{\Omega})}{4\tilde{\Omega}^2+\omega^2}\right]\Phi^-(\vec{k},\omega)$$
$$-\sum_{\vec{k},\omega}\Phi^+(\vec{k}+\vec{Q},\omega)\frac{i\omega}{4\tilde{\Omega}^2+\omega^2}\Phi^-(\vec{k},\omega). \tag{62}$$

The AFM magnon spectrum $\omega = c|\mathbf{k}|$.

- Antiferromagnetic coupling. *Resonance Valence Bond solution*

The four-semi-fermion term in (54) is decoupled by *bilocal scalar* field Λ_{ij}. The RVB spin liquid (SL) instability in 2D Heisenberg model corresponds to Bose-condensation of exciton-like [27] pairs of semi-fermions:

$$\Delta_0 = -\sum_{\mathbf{q}}\frac{I_{\mathbf{q}}}{I_0}\tanh\left(\frac{I_{\mathbf{q}}\Delta_0}{T}\right), \quad \mathcal{A}_0 = \frac{\beta|I|\Delta_0^2}{2} - \sum_{\mathbf{q}}\ln\left[2\cosh(\beta I_{\mathbf{q}}\Delta_0)\right] \tag{63}$$

where $\Delta_0 = \Delta(\mathbf{q}=0)$ is determined by the modulus of Λ_{ij} field

$$\Lambda_{<ij>}(\vec{R},\ \vec{r}) = \Delta(\vec{r})\exp\left(i\vec{r}\vec{A}(\vec{R})\right) \tag{64}$$

whereas the second variation of $\delta\mathcal{A}_{eff}$ describes the fluctuations of phase Λ_{ij}

$$\mathcal{A}_{eff} = \sum_{\mathbf{k},\omega} A_\alpha(\mathbf{k},\omega)\pi^{\alpha\beta}_{\mathbf{k},\omega}A_\beta(\mathbf{k},\omega),$$
$$\pi^{\alpha\beta}_{\mathbf{k},\omega} = Tr(p^\alpha p^\beta(G_{p+k}G_p + G_{p+k}G_p) + \delta_{\alpha\beta}f(I_{\mathbf{p}}\Delta_0)) \tag{65}$$

The spectrum of excitation in uniform SL is determined by zeros of π^R and is purely diffusive [28]-[29].

2.2 Kondo lattices: competition between magnetic and Kondo correlations

The problem of competition between Ruderman-Kittel-Kasuya-Yosida (RKKY) magnetic exchange and Kondo correlations is one of the most interesting problem of the heavy fermion physics. The recent experiments unambiguously show, that such a competition is responsible for many unusual properties of the integer valent heavy fermion compounds e.g. quantum critical behavior, unusual antiferromagnetism and superconductivity (see references in [19]). We address the reader to the review [30] for details of complex physics of Kondo effect in heavy fermion compounds. In this section we discuss the influence of Kondo effect on the competition between local (magnetic, spin glass) and non-local (RVB) correlations. The Ginzburg-Landau theory for nearly antiferromagnetic Kondo lattices has been constructed in [19] using the semi-fermion approach. We discuss the key results of this theory.

The Hamiltonian of the Kondo lattice (KL) model is given by

$$H = \sum_{k\sigma} \varepsilon_k c^\dagger_{k\sigma} c_{k\sigma} + J \sum_j \left(\mathbf{S}_j \mathbf{s}_j + \frac{1}{4} N_j n_j \right) \tag{66}$$

Here the local electron and spin density operators for conduction electrons at site j are defined as

$$n_j = \sum_{j\sigma} c^\dagger_{j\sigma} c_{j\sigma}, \quad \mathbf{s}_j = \sum_{\sigma} \frac{1}{2} c^\dagger_{j\sigma} \hat{\tau}_{\sigma\sigma'} c_{j\sigma'}, \tag{67}$$

where $\hat{\tau}$ are the Pauli matrices and $c_{j\sigma} = \sum_k c_{k\sigma} \exp(ikj)$. The spin glass (SG) freezing is possible if an additional quenched randomness of the inter-site exchange I_{jl} between the localized spins arises. This disorder is described by

$$H' = \sum_{jl} I_{jl} (\mathbf{S}_j \mathbf{S}_l). \tag{68}$$

We start with a perfect Kondo lattice. The spin correlations in KL are characterized by two energy scales, i.e., $I \sim J^2/\varepsilon_F$, and $\Delta_K \sim \varepsilon_F \exp(-\varepsilon_F/J)$ (the inter-site indirect exchange of the RKKY type and the Kondo binding energy, respectively). At high enough temperature, the localized spins are weakly coupled with the electron Fermi sea having the Fermi energy ε_F, so that the magnetic response of a rare-earth sublattice of KL is of paramagnetic Curie-Weiss type. With decreasing temperature either a crossover to a strong-coupling Kondo singlet regime occurs at $T \sim \Delta_K$ or the phase transition to an AFM state occurs at $T = T_N \sim zI$ where z is a coordination number in KL. If $T_N \approx \Delta_K$ the interference between two trends results in the decrease of both characteristic temperatures or in suppressing one of them. The mechanism of suppression is based on the screening effect due to Kondo interaction. As we will show, the Kondo correlations screen the local order parameter, but leave nonlocal correlations intact. The mechanism

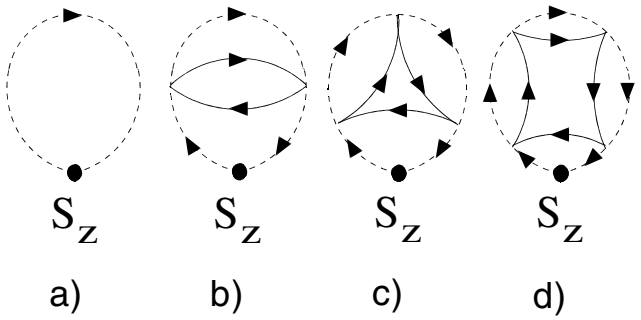

Figure 5: Kondo-screening of local moment by conduction electrons (solid line).

of Kondo screening for single-impurity Kondo problem is illustrated on Fig.5. The magnetization of local impurity in the presence of Kondo effect is given by:

$$\mathcal{M}(H) = S(g\mu_B)T\sum_{\omega}\left(\mathcal{G}_{\uparrow}(\omega) - \mathcal{G}_{\downarrow}(\omega)\right) = S(g\mu_B)\tanh\left(\frac{H\beta}{2}\right)\left[1 - \frac{1}{\ln(T/T_K)} - \frac{\ln(\ln(T/T_K))}{2\ln^2(T/T_K)} + ...\right]. \quad (69)$$

To take into account the screening effect in the lattice model we apply the semi-fermionic representation of spin operators. In accordance with the general path-integral approach to KL's, we first integrate over fast (electron) degrees of freedom. The Kondo exchange interaction is decoupled by auxiliary field ϕ [32] with statistics complementary to that of semi-fermions which prevents this field from Bose condensation except at $T = 0$. As a result, we are left with an effective bosonic action describing low-energy properties of KL model at high $T > T_K$ temperatures.

- Kondo screening of the Néel order

To analyze the influence of Kondo screening on formation of AFM order, we adopt the decoupling scheme for the Heisenberg model discussed in Section II.A. Taking into account the classic part of Néel field, we calculate the Kondo-contribution to the effective action which depends on magnetic order parameter $\mathcal{N}$:

$$\mathcal{A}_{\phi} = 2\sum_{\mathbf{q},n}\left[\frac{1}{\widetilde{J}} - \Pi(\mathcal{N})\right]|\phi_n(\mathbf{q})|^2. \quad (70)$$

where a polarization operator $\Pi(\mathcal{N})$ casts the form

$$\Pi(\mathcal{N}) = \rho(0)\ln\left(\frac{\epsilon_F}{T}\right) + \left[\frac{\pi}{2}\left(\frac{1}{\cosh(\beta\mathcal{N})} - 1\right) + O\left(\frac{\mathcal{N}^2}{T\epsilon_F}\right)\right], \quad (71)$$

where $\rho(0)$ is the density of states of conduction electrons at the Fermi level and the Kondo temperature $T_K = \epsilon_F \exp(-1/(\rho(0)J))$. Minimizing the effective action $\mathcal{A}(\phi, \mathcal{N})$ with respect to classic field $\mathcal{N}$, the mean field equation for Néel transition is obtained (c.f. with (56))

$$\mathcal{N} = \tanh\left(\frac{I_{\mathbf{Q}}\mathcal{N}}{2T}\right)\left[1 - \frac{a_N}{\ln(T/T_K)}\frac{\cosh^2(\beta I_{\mathbf{Q}}\mathcal{N}/2)}{\cosh^2(\beta I_{\mathbf{Q}}\mathcal{N})}\right]. \tag{72}$$

As a result, Kondo corrections to the molecular field equation reduce the Néel temperature

- Kondo enhancement of RVB correlations

Applying the similar procedure to nonlocal RVB correlations, we take into account the influence of Kondo effect on RVB correlations

$$\Pi(I_{\mathbf{q}}\Delta) = \rho(0)\ln\left(\frac{\epsilon_F}{T}\right) + \sum_{\mathbf{k}}\left[\frac{1}{\cosh\beta(I_{\mathbf{k}}\Delta)} - 1 + I_{\mathbf{k}}\Delta\tanh(\beta I_{\mathbf{k}}\Delta)\right]\frac{1}{\xi^2_{\mathbf{k}+\mathbf{q}} + (\pi/2\beta)^2}\,. \tag{73}$$

Here $\xi_k = \epsilon(\mathbf{k}) - \epsilon_F$. Minimizing the effective action with respect to Δ we obtain new self-consistent equation to determine the non-local semi-fermion correlator.

$$\Delta = -\sum_{\mathbf{q}}\frac{I_{\mathbf{q}}}{I_0}\left[\tanh\left(\frac{I_{\mathbf{q}}\Delta}{T}\right) + a_{sl}\frac{I_{\mathbf{q}}\Delta}{T\ln(T/T_K)}\right]. \tag{74}$$

It is seen that unlike the case of local magnetic order, the Kondo scattering favors transition into the spin-liquid state, because the scattering means the involvement of the itinerant electron degrees of freedom into the spinon dynamics.

- Kondo effect and quenched disorder

Let's assume that the RKKY interactions are random (e.g. due to the presence of non-magnetic impurities resulting in appearance of random phase in the RKKY indirect exchange). In this case the spin glass phase should be considered. As it has been shown in [15] and [19], the influence of static disorder on Kondo effect in models with Ising exchange on fully connected lattices (Sherrington-Kirkpatrick model) can be taken into account by the mapping KL model with quenched disorder onto the single impurity Kondo model in random (depending on replicas) magnetic field. It allows for the self-consistent determination of the Edwards-Anderson q_{EA}order parameter given by the following set of self-consistent equations

$$\tilde{q} = 1 - \frac{2c}{\ln(T/T_K)} - O\left(\frac{1}{\ln^2(T/T_K)}\right),$$

$$q = \int_x^G \tanh^2\left(\frac{\beta I x\sqrt{q}}{1 + 2c(\beta I)^2(\tilde{q} - q)/\ln(T/T_K)}\right) + O\left(\frac{q}{\ln^2(T/T_K)}\right). \tag{75}$$

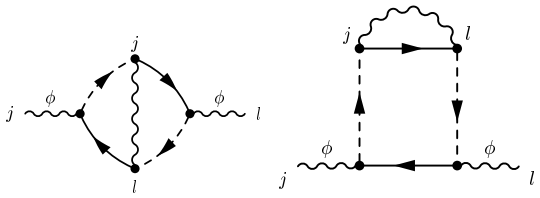

Figure 6: Feynman diagrams for nonlocal excitations associated with the overlap of Kondo clouds.

Here $q = q_{EA}$ and $\tilde{q}$ are nondiagonal and diagonal elements of Parisi matrix respectively. Therefore, the Kondo-scattering results in the depression of the freezing temperature due to the screening effects in the same way as the magnetic moments and the one-site susceptibility are screened in the single-impurity Kondo problem (c.f. Fig.5) when Ising and Kondo interactions are of the same order of magnitude. Let's now briefly discuss the fluctuation effects in Kondo lattices. The natural way to construct the fluctuation theory is to consider the non-local dynamical Kondo correlations described by the field $\phi(\mathbf{q}, \omega)$ (see Fig.6). In fact, the non-locality of the "semi-Bosonic" field is associated with an overlap of Kondo clouds [19] and responsible for a crossover from the localized magnetism to the itinerant-like fluctuational spin-liquid magnetism. The temperature dependence of static magnetic susceptibility becomes nonuniversal in spite of the fact that we are in a region of critical AFM fluctuations which is consistent with recent experimental observations.

2.3 Kondo effect in quantum dots

The single electron tunneling through the quantum dot [33] has been studied in great details during the recent decade. Among many interesting phenomena behind the unusual transport properties of mesoscopic systems, the Kondo effect in quantum dots, recently observed experimentally, continues to attract an attention both of experimental and theoretical communities. The modern nanoscience technologies allow one to produce the highly controllable systems based on quantum dot devices and possessing many of properties of strongly correlated electron systems. The quantum dot in a semiconductor planar heterostructure is a confined few-electron system (see Fig.7) contacted by sheets of two-dimensional gas (leads). Junctions between dot and leeds produce the exchange interaction between the spins of the dot and spins of itinerant 2D electron gas. Measuring the dc $I - V$ characteristics, one can investigate the Kondo effect in quantum dots under various conditions.

Various realizations of Kondo effect in quantum dots were proposed both

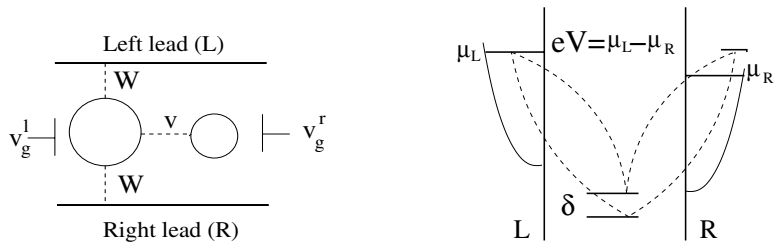

Figure 7: (a) Double quantum dot in a side-bound configuration (b) co-tunneling processes in biased DQD responsible for the resonance Kondo tunneling.

theoretically and experimentally in recent publications (see e.g. [34] for review). In order to illustrate the application of semi-fermionic approach we discuss briefly electric field induced Kondo tunneling in double quantum dot (DQD). As was noticed in [35], quantum dots with even $\mathcal{N}$ possess the dynamical symmetry $SO(4)$ of spin rotator in the Kondo tunneling regime, provided the low-energy part of its spectrum is formed by a singlet-triplet (ST) pair, and all other excitations are separated from the ST manifold by a gap noticeably exceeding the tunneling rate γ. A DQD with even $\mathcal{N}$ in a side-bound configuration where two wells are coupled by the tunneling v and only one of them (say, l) is coupled to metallic leads (L, R) is a simplest system satisfying this condition [35]. Such system was realized experimentally in Ref.[36]. As it was shown in [20] the Shrieffer-Wolff (SW) transformation, when applied to a spin rotator results in the following effective spin Hamiltonian

$$H_{int} = \sum_{kk',\alpha\alpha'=L,R} J^S_{\alpha\alpha'} f_s^\dagger f_s c^\dagger_{k\alpha\sigma} c_{k'\alpha'\sigma} + \sum_{kk',\alpha\alpha'\Lambda\Lambda'} \left(J^T_{\alpha\alpha'} \hat{S}^d_{\Lambda\Lambda'} + J^{ST}_{\alpha\alpha'} \hat{P}^d_{\Lambda\Lambda'} \right) \tau^d_{\sigma\sigma'} c^\dagger_{k\alpha\sigma} c_{k'\alpha'\sigma'} f^\dagger_\Lambda f_{\Lambda'} \quad (76)$$

where the c-operators describe the electrons in the leads and f-operators stand for the electrons in the dot. The matrices $\hat{S}^d$ and $\hat{P}^d$ (d=x,y,z) are 4×4 matrices defined by relations (41) (see Section I.C) and $J^S = J^{SS}$, $J^T = J^{TT}$ and J^{ST} are singlet, triplet and singlet-triplet coupling SW constants, respectively.

Applying the semi-fermionic representation of SO(4) group introduced in Section I.C we started with perturbation theory results analyzing the most divergent Feynman diagrams for spin-rotator model [20]. Following the "poor man's scaling" approach we derive the system of coupled renormalization group equations for effective couplings responsible for the transport through DQD. As a result, the differential conductance $G(eV, T)/G_0 \sim |J^{ST}_{LR}|^2$ is shown to be the universal

function of two parameters T/T_K and V/T_K, $G_0 = e^2/\pi\hbar$:

$$G/G_0 \sim \ln^{-2}\left(\max[(eV-\delta), T]/T_K\right) \tag{77}$$

Thus, the tunneling through singlet DQDs with $\delta = E_T - E_S \gg T_K$ exhibits a peak in differential conductance at $eV \approx \delta$ instead of the usual zero bias Kondo anomaly which arises in the opposite limit, $\delta < T_K$. Therefore, in this case the Kondo effect in DQD is induced by a strong external bias. The scaling equations can also be derived in Schwinger-Keldysh formalism (see [11] and also [18]) by applying the "poor man's scaling" approach directly to the dot conductance. The detailed analysis of the model (76) in a real-time formalism is a subject for a separate publication.

3 Epilogue and perspectives

In this paper, we demonstrated several examples of the applications of semi-fermionic representation to various problems of condensed matter physics. The list of these applications is not exhaustive. We did not discuss, e.g., the interesting development of SF approach for the Hubbard model with repulsive [14] and attractive [13] interaction, Dicke model, 2D Ising model in transverse magnetic field, application of SF formalism to mesoscopic physics [21] etc. Nevertheless, we would like to point out some problems of strongly correlated physics where the application of SF representation might be a promising alternative to existing field-theoretical methods.

Heavy Fermions

- Crossover from localized to itinerant magnetism in Kondo lattices
- Quantum critical phenomena associated with competition between local and nonlocal correlations
- Nonequilibrium spin liquids
- Effects of spin impurities and defects in spin liquids
- Crystalline Electric Field excitations in spin liquids
- Dynamic theory of screening effects in Kondo spin glasses.

Mesoscopic systems

- Nonequilibrium Kondo effect in Quantum Dots
- Two-channel Kondo in complex multiple dots
- Spin chains, rings and ladders

- Nonequilibrium spin transport in wires

Summarizing, we constructed a general concept of semi-fermionic representation for SU(N) groups. The main advantage of this representation in application to the strongly correlated systems in comparison with another methods is that the local constraint is taken into account exactly and the usual Feynman diagrammatic codex is applicable. The method proposed allows us to treat spins on the same footing as Fermi and Bose systems. The semi-fermionic approach can be helpful for the description of the quantum systems in the vicinity of a quantum phase transition point and for the nonequilibrium spin systems.

Acknowledgments

I am grateful to my colleagues F.Bouis, H.Feldmann, K.Kikoin and R.Oppermann for fruitful collaboration on different stages of SF project. I am thankful to Alexander von Humboldt Foundation for financial support. The support of Deutsche Forschungsgemeinschaft (SFB-410 project) is gratefully acknowledged. My special thank to participants of Strongly Correlated Workshops in Trieste and especially to A.Protogenov for many inspiring discussions. My particular thank to A.Dutta for careful reading of this manuscript and useful suggestions.

References

[1] T. Holstein and H. Primakoff, Phys. Rev. B **58**, 1098 (1940).

[2] F. Dyson, Phys. Rev. **102**, 1217 (1956).

[3] S. V. Maleyev, Sov. Phys. JETP **6**, 776 (1958).

[4] A. A. Abrikosov, Physics **2**, 5 (1965).

[5] V. G. Vaks, A. I. Larkin, and S. A. Pikin, Sov. Phys. JETP **26**, 188 (1968).

[6] V. G. Vaks, A. I. Larkin, and S. A. Pikin, Sov. Phys. JETP **26**, 647 (1968).

[7] J. Hubbard, Proc. R. Soc. London A **285**, 542 (1965).

[8] P. Coleman, C. Pepin, and A. M. Tsvelik, Phys. Rev. B **62**, 3852 (2000).

[9] A.M.Tsvelik, *Quantum field theory in condensed matter physics.* Cambridge (1995)

[10] V. N. Popov and S. A. Fedotov, Zh. Eksp. Teor. Fiz. **94**, 183 (1988), [Sov. Phys. JETP **67**, 535 (1988)].

[11] M. N. Kiselev and R. Oppermann, Phys.Rev.Lett **85**, 5631 (2000).

[12] O. Veits, R. Oppermann, M. Binderberger, and J. Stein, J. Phys. I France **4**, 493 (1994).

[13] J. Stein and R. Oppermann, Z. Phys. B **83**, 333 (1991).

[14] C. Gros and M. D. Johnson, Physica B **165-166**, 985 (1990).

[15] M. N. Kiselev and R. Oppermann, JETP Lett. **71**, 250 (2000).

[16] F. Bouis and M. N. Kiselev, Physica B **259-261**, 195 (1999).

[17] S.Azakov, M.Dilaver, A.M.Oztas. Int. Journal of Modern Phys. **B 14**, 13 (2000).

[18] M.N.Kiselev, H.Feldmann and R.Oppermann, Eur.Phys. J **B 22**, 53 (2001)

[19] M.N.Kiselev, K.Kikoin and R.Oppermann, Phys. Rev. **B 65**, 184410 (2002)

[20] M.N.Kiselev, K.Kikoin and L.W.Molenkamp cond-mat/0206503.

[21] P.Coleman and W.Mao cond-mat/0203001,cond-mat/0205004.

[22] E. Cartan, *Leçons sur la theorie des spineurs* (Hermann, Paris, 1938).

[23] N. Read and S. Sachdev, Nuc. Phys. B **316**, 609 (1989).

[24] L.V.Keldysh. Sov. Phys. JETP **20**, 1018 (1965)

[25] J.Schwinger. J.Math.Phys. **2**, 407 (1961)

[26] V. S. Babichenko and A. N. Kozlov. Sol. St. Comm. **59**, 39 (1986).

[27] For simplicity we consider *uniform* RVB state.

[28] L.B.Ioffe, A.I.Larkin. Phys.Rev. **B 39**, 8988 (1989).

[29] P.A.Lee, N.Nagaosa. *ibid*, **B 46**, 5621 (1992).

[30] P.Coleman, cond-mat/0206003.

[31] A.Tsvelik and P.B.Wiegmann, Adv.Phys. **32**, 453 (1983).

[32] N. Read and D. M. Newns, J. Phys. C **16**, 3273 (1983).

[33] I.Aleiner, P.Brouwer, and L.Glazman, Phys. Rep. **358**, 309 (2002).

[34] K.Kikoin and Y.Avishai, Phys.Rev. **B65**, 115329 (2002).

[35] K.Kikoin and Y.Avishai, Phys.Rev.Lett. **86**, 2090 (2001).

[36] L.W.Molenkamp *et al.*, Phys. Rev. Lett. **75**, 4282 (1995)

M.Kiselev
Institut für Theoretische Physik
Universität Würzburg
D-97074 Würzburg, Germany